M-29-64-1 • 4 OCTOBER 1964

M-29-64-1

FINAL REPORT

MARINER MARS 1969 ORBITER STUDY

CONTRACT NO. JPL 950877

FACILITY FORM 602

N65-21458 (ACCESSION NUMBER)

460 (PAGES)

CR-62193 (NASA CR OR TMX OR AD NUMBER)

1 (THRU)

31 (CODE)

(CATEGORY)

GPO PRICE $ _____

OTS PRICE(S) $ _____

Hard copy (HC) $7.00

Microfiche (MF) $2.25

RE-ORDER NO. 64-825

M-29-64-1 • 4 OCTOBER 1964

M-29-64-1

FINAL REPORT

MARINER MARS 1969 ORBITER STUDY

CONTRACT NO. JPL 950877

This work was performed for the Jet Propulsion Laboratory, California Institute of Technology, sponsored by the National Aeronautics and Space Administration under Contract NAS7-100.

Prepared by

LOCKHEED MISSILES AND SPACE COMPANY

SUNNYVALE, CALIFORNIA

Prepared for

CALIFORNIA INSTITUTE OF TECHNOLOGY, JET PROPULSION LABORATORIES

PASADENA, CALIFORNIA

Lockheed

MISSILES & SPACE COMPANY

A GROUP DIVISION OF LOCKHEED AIRCRAFT CORPORATION

SUNNYVALE, CALIFORNIA

1 of 459

FOREWORD

This report was prepared by the Lockheed Missiles & Space Company, Sunnyvale, California, and contains the results of a study performed for the California Institute of Technology/Jet Propulsion Laboratory under Contract No. 950877, Mariner Mars 1969 Orbiter Study.

ABSTRACT

21458

The study of a Mariner Mars 1969 Orbiter, based on the Flox Atlas-Centaur launch system, was performed by Lockheed Missiles & Space Company under JPL Contract No. 950877. The objective was to determine the feasibility of performing orbiter and orbiter/capsule missions to Mars and Venus during the 1969–1971 time period with emphasis on a 1969 Mars mission. Mission and performance tradeoffs were made and a conceptual design developed.

A preliminary program plan and preliminary cost estimate was made for a Mars 1969 and a follow-on Mars 1971 mission.

The study results indicate that a Mariner Mars orbiter is feasible in 1969 or 1971 and that this orbiter could readily carry an entry capsule. The 1969 orbiter could be modified for a 1970 Venus orbiter mission. The concept lends itself to conservative design approaches and extensive use of Mariner C technology and hardware.

A heat sterilized atmospheric capsule that does not survive landing on the surface of Mars appears quite feasible.

A heat sterilized biological capsule, which must survive landing on Mars and perform a biological experiment, does not appear feasible in 1969 when designed to cope with a surface environment of 11 mb atmospheric pressure, 200 ft/sec winds and rough terrain.

CONTENTS

Section		Page
	FOREWORD	iii
	ABSTRACT	v
	ILLUSTRATIONS	xi
	TABLES	xvii
1	INTRODUCTION	1-1
	1.1 Study Scope and Objectives	1-1
	1.2 Study Ground Rules and Input Data	1-2
	1.3 Mission Prime Objectives – Mars	1-3
	1.4 Mission Concepts	1-3
2	SUMMARY AND CONCLUSIONS	2-1
	2.1 Principal Results	2-1
	2.2 Conclusions	2-6
3	MISSION AND PERFORMANCE ANALYSIS	3-1
	3.1 Basic Ground Rules and Input Data	3-2
	3.2 Interplanetary Mission Considerations	3-6
	3.2.1 Typical Mission Profile	3-6
	3.2.2 Guidance and Communication Geometry	3-6
	3.2.3 Interplanetary Transfer Characteristics	3-15
	3.3 Orbital Operation Criteria	3-23
	3.3.1 Orbit Selection	3-23
	3.3.2 Lifetime Characteristics	3-27
	3.3.3 Experimental Considerations	3-28
	3.3.4 Orbit Variations	3-30
	3.4 Orbiter Injection Maneuver	3-31
	3.4.1 Orbiter Approach Geometry	3-33
	3.4.2 Performance Requirements	3-33

CONTENTS (Cont.)

Section		Page
	3.4.3 Maneuver Loss Evaluation	3-35
	3.4.4 Trajectory Changes and Dispersions	3-39
	3.5 Entry Systems	3-42
	3.5.1 Entry Trajectory Criteria	3-48
	3.5.2 Entry Dynamics	3-53
	3.5.3 Separation Maneuver and Attitude Control	3-58
	3.5.4 Entry From Orbit Considerations	3-62
4	SYSTEM DESIGN	4-1
	4.1 Spacecraft Concept Selection	4-1
	4.2 Description of Basic Orbiter (Configuration 4) Without Capsule	4-12
	4.3 Description of Basic Orbiter (Configuration 4) With Capsule	4-24
	4.4 Capsule Design	4-25
	4.5 Centaur Adapter Structure	4-33
	4.6 Capsule/Spacecraft Adapter Structure	4-34
	4.7 Structural Analysis	4-35
	4.8 Material Selection	4-37
	4.9 Weight and Balance	4-40
5	SUBSYSTEM DESCRIPTION	5-1
	5.1 Guidance and Control	5-1
	5.1.1 Attitude Control	5-1
	5.1.2 Guidance	5-9
	5.2 Experimental Techniques and Instrumentation	5-24
	5.2.1 Scientific Objectives	5-24
	5.2.2 Initial Selection of Scientific Payloads	5-25
	5.2.3 Orbiter Capabilities	5-25
	5.2.4 The Orbiter Television System	5-58
	5.2.5 Other Orbiter Experiments	5-62
	5.2.6 Capsule Capabilities	5-64

CONTENTS (Cont.)

Section		Page
	5.2.7 Recommended Instrumentation for Mars 1969 Mission	5-64
	5.2.8 Mars 1971 and Venus 1970 Missions	5-67
5.3	Electronic Subsystems	5-68
	5.3.1 Mission Requirements	5-69
	5.3.2 System Tradeoffs	5-93
	5.3.3 Electronic System Design	5-121
	5.3.4 System Weight and Volume Summary	5-188
	5.3.5 Long Lead Time Development Items	5-188
5.4	Propulsion	5-190
	5.4.1 Primary Propulsion System	5-191
	5.4.2 Details of the Selected Primary Propulsion System	5-194
	5.4.3 Reaction Control System	5-202
	5.4.4 Capsule Guidance Propulsion System Selection	5-205
	5.4.5 Capsule Spin Motors Selection	5-207
5.5	Thermodynamic Analysis	5-208
	5.5.1 Prelaunch and Ascent	5-208
	5.5.2 Transfer Orbit	5-209
	5.5.3 Mars Orbit	5-216
	5.5.4 Venus Mission	5-218
5.6	Aerothermal Environment	5-219
	5.6.1 Atmospheric Characteristics	5-219
	5.6.2 Entry Trajectory	5-220
	5.6.3 Shock Layer Flow	5-220
	5.6.4 Heat Transfer	5-224
	5.6.5 Thermal Protection	5-240
	5.6.6 Conclusions	5-252
5.7	Parachute Descent System	5-253
	5.7.1 Approach Design	5-255
	5.7.2 Note on Parachute Textile Materials	5-256

CONTENTS (Cont.)

Section		Page
	5.7.3 Final Descent Parachute for a Biocapsule	5-256
	5.7.4 Drag Parachute	5-257
	5.7.5 Recovery System Sequencing	5-260
	5.7.6 Development Test Program	5-262
	5.7.7 Summary of Design Data	5-264
	5.7.8 Tradeoffs	5-265
	5.8 Sterilization	5-267
	5.8.1 Sterilization Concept	5-267
	5.8.2 Problem Areas	5-268
	5.8.3 Support Equipment	5-270
6	DEVELOPMENT PROGRAM PLAN	6-1
	6.1 Development Program	6-1
	6.2 Integrated Test Plan	6-11
	6.3 Reliability Program	6-21
	6.4 Program Manufacturing Plan	6-30
	6.5 Facilities Plan	6-37
	6.6 Launch Operations Plan	6-40
7	PROGRAM COSTS	7-1
	7.1 Summary of Costs	7-1
	7.2 Distribution of Costs by Time	7-3
8	REFERENCES	8-1

ILLUSTRATIONS

Figure		Page
3-1	Launch System Earth Escape Payload	3-3
3-2	Model Atmospheres for Mars	3-4
3-3	Typical Transfer Profile – Mars 1969	3-7
3-4	Typical Transfer Profile – Mars 1971	3-8
3-5	Typical Transfer Profile – Venus 1970	3-8
3-6	Midcourse Communications and Guidance Geometry – Mars 1969 and Mars 1971	3-13
3-7	Midcourse Communications and Guidance Geometry – Venus 1970	3-14
3-8	Variation of Transfer Characteristics With Launch Date – Mars 1969	3-16
3-9	Variation of Transfer Characteristics With Launch Date – Mars 1971	3-17
3-10	Variation of Transfer Characteristics With Launch Date – Venus 1970	3-18
3-11	Mars 1969 Performance Capability	3-20
3-12	Mars 1971 Performance Capability	3-21
3-13	Venus 1970 Performance Capability	3-22
3-14	Weight in Orbit Capability, I_{SP} = 302 sec – Mars	3-25
3-15	Weight in Orbit Capability, I_{SP} = 302 sec – Venus	3-26
3-16	Mars Orbit Characteristics	3-29
3-17	Mars Orbit Variations Due to Oblateness	3-32
3-18	Orbiter Approach and Injection Geometry – Mars 1969	3-34
3-19	Mass Ratio Requirements for Constant-Thrust Continuous Burn Into Mars Orbit at Constant Inertial Attitude (ξ_I)	3-36
3-20	Injection Maneuver Penalties – Mars 1969	3-37

Figure		Page
3-21	Orbiter Nozzle-Angle Requirements – Mars 1969	3-38
3-22	Orbiter Nozzle-Angle Requirements – Mars 1971	3-40
3-23	Orbiter Injection Maneuver Ignition Time Requirements	3-41
3-24	Orbiter Injection Altitude Variations – Mars 1969 and 1971	3-43
3-25	Orbiter Injection Position Variations – Mars 1969 and 1971 (1800 km Orbit Periapsis Altitude)	3-44
3-26	Orbiter Injection Maneuver Dispersions – Mars 1969 and 1971	3-45
3-27	Capsule Entry Weight and Size – Mars	3-47
3-28	Maximum Acceleration Environment for Ballistic Entry at Mars	3-49
3-29	Variation of Convective Heat Load With Entry Path Angle – Mars	3-51
3-30	Ballistic Descent Profile – Mars Entry Velocity, V_E = 21,000 ft/sec, Entry Altitude, h_E = 800,000 ft	3-52
3-31	Parachute Deployment Environment – Mars	3-54
3-32	Wind Effect on Capsule Velocity – Mars	3-55
3-33	Capsule Angle of Attack Convergence	3-57
3-34	Mars Approach Geometry	3-60
3-35	Capsule Separation Velocity Requirements	3-61
3-36	Orbiter-Capsule Approach Geometry Variations With Guidance Tolerances – Mars	3-63
3-37	Capsule Entry Attitude	3-64
3-38	Impulse Requirements for Entry From Orbit – Mars	3-66
3-39	Retromaneuver Requirements for Entry From Orbit – Mars	3-67
3-40	Orbiter Capsule Communications Geometry – Mars Entry From Orbit	3-69
4-1	Mars 1969 Orbiter Alternate Configurations	4-3
4-2	Mariner Mars 1969 Orbiter (With Capsule) Configuration 2	4-7
4-3	Mariner Mars Orbiter (Without Capsule) Configuration 2	4-9
4-4	Mariner Mars 1969 Orbiter Configuration 3	4-13
4-5	Mars 1969 Orbiter (Without Capsule) Configuration 4	4-15
4-6	Mars 1969 Orbiter (With Capsule) Configuration 4	4-17
4-7	Revised Engine and Tank Installation for 1971 Mission	4-23

Figure		Page
4-8	Capsule Assembly (Atmospheric)	4-27
4-9	Capsule Assembly (Biological)	4-31
4-10	Summary of Mass Moments of Inertia	4-39
4-11	Alternate Launch Shroud and Spacecraft Concepts	4-51
5-1	Mariner Orbiter Attitude Control Reference System	5-3
5-2	Dispersion of Impact Parameter After First Correction – Mars 1969	5-15
5-3	Dispersion of Impact Parameter After second Correction – Mars 1969	5-16
5-4	Orbit Dispersion – Mars 1969	5-19
5-5	Nominal Approach Conditions – Mars 1969	5-20
5-6	Dispersion of Apoapsis – Mars 1969	5-21
5-7	Earth Occultation – Mars 1969	5-22
5-8	Refraction by Mars Atmosphere	5-33
5-9	Effect of Atmospheric Refraction on the Radio Occultation Point	5-37
5-10	1969 Mariner – Earth Occultation Zone for Mars Orbits	5-39
5-11	Relation Between True and Apparent Radii Measurements for an Oblate Ellipsoid	5-43
5-12	Effect of Atmospheric Refraction on Angular Diameter Measurement	5-44
5-13	Determination of Mars Radius With Television Data	5-49
5-14	Antenna Look Angle Parameters – 1969 Mission	5-81
5-15	Antenna Look Angle Parameters – 1971 Mission	5-82
5-16	Required Antenna Look Angles Referenced to Look Angle at Encounter – 1969 Mission	5-83
5-17	Required Antenna Look Angles Referenced to Look Angle at Encounter – 1971 Mission	5-84
5-18	Spacecraft-Earth Communication Range – 1969 and 1971 Missions	5-85
5-19	Solar Constant – 1969 and 1971 Missions	5-86
5-20	Fixed Antenna Beamwidth Required vs. Mission Designed Lifetime	5-97

Figure		Page
5-21	Antenna Gain at Encounter vs. Mission Design Orbit Lifetime – 1969 Mission	5-98
5-22	Antenna Gain at Encounter vs. Mission Design Lifetime – 1971 Mission	5-99
5-23	Data Rate Penalty of Limited Freedom Antennas vs. Time in Orbit – 1969 Mission	5-100
5-24	Data Rate Penalty of Limited Freedom Antennas vs. Time in Orbit – 1971 Mission	5-103
5-25	Antenna Gain at Encounter vs. Mission Design Lifetime – 1969 and 1971 Missions	5-104
5-26	Solar Array Characteristics Using Mariner C Panels – 1969 Mission	5-107
5-27	LMSC Flex-Rib Unfurlable-Steerable Antenna – Weight vs. Diameter of Parabolic Reflector	5-108
5-28	LMSC Flex-Rib Unfurlable Reflector – Furled Diameter and Volume vs. Reflector Diameter	5-109
5-29	Electronics Systems Weight Variation vs. Time in Orbit and Data Rate	5-110
5-30	Electronics System Functional Block Diagram	5-123
5-31	Orbiter-Only Power Profile – 1969 Mission	5-155
5-32	Orbiter Power System	5-160
5-33	Solar Array Output for Mariner – 1969 Mission	5-163
5-34	Solar Array Panel Temperature for Mariner C	5-164
5-35	Solar Photovoltaic System Power Output for Mariner C	5-165
5-36	Functional Block Diagram of Atmospheric Capsule System	5-167
5-37	Atmospheric Capsule Data Handling (Capsule)	5-168
5-38	Atmospheric Capsule Data Handling (Orbiter)	5-169
5-39	Atmospheric Capsule Power System	5-176
5-40	Functional Block Diagram Biological Capsule System	5-179
5-41	Biocapsule Electronics	5-180
5-42	Orbiter Receiver for Support of Biocapsule	5-181
5-43	Biocapsule Power System	5-187

Figure		Page
5-44	Thrust Chamber Performance (N_2O_4/MMH)	5-193
5-45	Thrust Chamber Optimization (N_2O_4/MMH)	5-195
5-46	Primary Propulsion System Schematic	5-196
5-47	Primary Propulsion System Thrust Chamber	5-199
5-48	Cold Gas Attitude Control System Nozzle Optimization	5-204
5-49	Reaction Control System Schematic – Cold Gas	5-206
5-50	Solar Constant, Earth-Mars 1969 Trajectory	5-210
5-51	Orbiter Temperatures vs. α/ϵ Ratio	5-211
5-52	Degradation of White Paints, Surface Normal to Sun, Earth-Mars 1969 Trajectory	5-213
5-53	Orbiter Temperatures, Earth-Mars 1969 Trajectory	5-214
5-54	Solar Panel Temperatures, Earth-Mars 1969 Trajectory	5-215
5-55	Absorbed Fluxes on Typical Solar Panel	5-217
5-56	High Temperature Radiance of Several N_2, CO_2, A Gas Mixtures at 1.0 Atmosphere of Pressure	5-221
5-57	Heat Shield Design Trajectory for Mariner Capsule	5-222
5-58	Shock Layer Thermodynamic Conditions	5-223
5-59	Lander Vehicle Surface Pressure Distribution	5-225
5-60	Lander Vehicle Shock Standoff Distance	5-226
5-61	Forebody Convective Heat Transfer Distribution	5-229
5-62	Momentum Thickness Reynolds Number Distribution of Forebody	5-231
5-63	Radiative Heat Transfer Distribution Over Capsule Forebody	5-235
5-64	Influence of Angle of Attack on Afterbody and Aerodynamic Stabilizer Convective Heat Transfer Level	5-238
5-65	Influence of Atmosphere and Trajectory Uncertainties on Stagnation Point Heating	5-239
5-66	Estimated Angle of Attack History During Entry	5-241
5-67	Afterbody Heating Histories	5-242
5-68	Beryllium Heat Shield Temperature Response at Forebody Geometric Center	5-244
5-69	Beryllium Shield Thickness Requirements	5-245
5-70	Nylon-Phenolic Heat Shield Temperature Response at Forebody Geometric Center	5-247

Figure		Page
5-71	Influence of Injection on Convective Heat Transfer History	5-249
5-72	Heat Shielding Requirements at Stagnation Point	5-250
5-73	Afterbody Temperature Histories	5-251
5-74	Envelope of Entry Trajectories	5-254
5-75	Parachute Design	5-259
5-76	Capsule Entry Time History	5-261
5-77	Capsule Subsonic Descent Time History	5-266
6-1	Program Master Schedule - 1969 Mission	6-5
6-2	Program Master Schedule - 1971 Mission	6-7
6-3	Program Test Schedule - by Mission	6-16
6-4	Reliability Data Acquisition and Reduction	6-25
6-5	Computer Program for Reliability	6-26
6-6	Manufacturing Schedule	6-33
6-7	Orbiter Product Flow Plan	6-35
6-8	Capsule Product Flow Plan	6-36
7-1	Program Cost Distribution	7-4
7-2	Program Cost Distribution for Development, Manufacturing and Testing	7-5

TABLES

Table		Page
2-1	Payload Capability – 1969 Mars Mission	2-2
3-1	Mars Model Atmospheres	3-5
3-2	1969 Mars Transfer Trajectory Data	3-10
3-3	1971 Mars Transfer Trajectory Data	3-11
3-4	1970 Venus Transfer Trajectory Data	3-12
3-5	Summary of Burnout Weight in Orbit	3-24
3-6	Mars Orbiter Lifetime	3-24
4-1	Preliminary Weight Comparison – Basic Spacecraft	4-5
4-2	Additional Equipment Added to Basic Orbiter When a 61-in. Diameter Capsule is Installed	4-25
4-3	Energy Absorption Capability of Various Materials and Systems	4-33
4-4	Strength Analysis Summary	4-36
4-5	Material Candidates – Orbiter	4-38
4-6	Weight Summary – Configuration 4, Empty	4-41
4-7	Detailed Subsystem Weight Breakdown – Basic Orbiter	4-41
4-8	Weight Summary – Configuration 4 (No Capsule) – Loaded	4-45
4-9	Weight Summary – Configuration 4 (With 61-in Diameter Atmospheric Capsule) – Loaded	4-46
4-10	Weight Summary – Atmospheric Capsule	4-47
4-11	Weight Summary – Biological Capsule	4-48
5-1	Experimental Instrument Shopping List	5-26
5-2	Determination of Mars Radius	5-29
5-3	Atmospheric Data for Mars	5-34
5-4	Resolving Power of the Orbiter TV System	5-61
5-5	Recommended Experimental Instrumentation	5-65

Table		Page
5-6	Sequence of Events – Orbiter Only	5-70
5-7	Sequence of Events – Orbiter Plus Biocapsule	5-87
5-8	Biocapsule Communication Constraints	5-92
5-9	Summary of Antenna Trade-Offs	5-102
5-10	Transmitters for 2.3G Telemetry	5-106
5-11	Biocapsule-to-Earth Link Calculation	5-114
5-12	Earth-to-Biocapsule Link Calculation	5-116
5-13	Biocapsule-to-Orbiter Link Calculation (Coherent PSK)	5-118
5-14	Orbiter Command Link Calculation	5-127
5-15	DSIF-to-Orbiter Link Calculation	5-129
5-16	Orbiter-to-DSIF Link Calculation	5-132
5-17	Cruise Phase Orbiter-to-Earth Link Calculations	5-134
5-18	Mobile Tracking Station-to-Orbiter Link	5-136
5-19	Orbiter-to-Mobile Tracking Station Link	5-138
5-20	System Commands	5-141
5-21	Sequence Timer Requirements	5-147
5-22	Mars Orbiter Tape Recorder	5-152
5-23	Channel Repetition Rate	5-153
5-24	Estimated Orbiter-Only Power Requirements – 1969 Mission	5-156
5-25	Power Source Requirements (Unregulated)	5-159
5-26	Mission Power System Equipment – 1969	6-162
5-27	Atmospheric Capsule – Orbiter Link (Separation Phase)	5-172
5-28	Atmospheric Capsule – Orbiter Link (Entry Phase)	5-173
5-29	Estimated Atmospheric Capsule Power/Energy Requirements	5-175
5-30	Atmospheric Capsule Power System Components	5-174
5-31	Biocapsule-to-Orbiter Entry Link	5-183
5-32	Estimated Biocapsule Power/Energy Requirements	5-186
5-33	Electronics Weight and Volume Summary	5-189
5-34	Orbiter Primary Propulsion System Characteristics	5-197
5-35	Primary Propulsion System Weight Breakdown	5-198

Table		Page
5-36	Nitrogen Cold Gas System Weight Breakdown	5-203
5-37	Preliminary Development Test Program – Parachute	5-263
6-1	Integrated Test Plan – 1971 Mission Orbiter and Capsule	6-12
6-2	1971 Mission Sequence of Events	6-23
7-1	Summary – Program Costs	7-2

Section 1
INTRODUCTION

1.1 STUDY SCOPE AND OBJECTIVES

This report presents the results of work performed by the Lockheed Missiles & Space Company for the Jet Propulsion Laboratories under JPL Contract No. 950877 during the period May 4, 1964 to September 4, 1964.

The prime objective of this study was the conceptual design of an unmanned spacecraft, launched by a Flox Atlas/Centaur, to perform scientific orbiter and orbiter/capsule missions to the planet Mars during the launch opportunities of 1969 and 1971. An additional objective was the definition of capability for a 1970 mission to Venus.

System candidates were selected and tradeoffs of missions, systems and subsystems performed to arrive at a feasible, conservative concept for the 1969 mission. This concept was then refined and the impact of using the same basic design for missions to Mars in 1971 and to Venus in 1970 was evaluated.

The basic launch system was a 20 percent Flox Atlas-Centaur and performance capability effects of varying the Flox to extremes of 30 percent and 0 percent were determined.

A development plan and cost analysis (exclusive of the launch system) of the selected concept is presented for Mars missions in 1969 and 1971.

Critical long leadtime items are identified.

The contract statement of work is contained in Ref. 1, LMSC document No. A304797-1, "Proposal for Mariner Mars Orbiter 1969-1971," Volume 1, dated 21 February 1964.

1.2 STUDY GROUND RULES AND INPUT DATA

The ground rules and input data for the study are shown in Refs. 1 and 2. These ground rules include.

- Orbiter and orbiter/capsule missions to Mars in 1969 and 1971.
- Orbiter mission to Venus in 1970.
- The nominal Earth-escape capability is that of the 20 percent Flox Atlas-Cantaur with variations of Flox to 30 percent and 0 percent.
- Spacecraft designed to limits of Surveyer launch shroud and adapted to Centaur stage.
- Design to quasi steady-state accelerations at the launch separation plane of 6 g axial and 0.4 g lateral.
- Two identical spacecraft will be launched within a 30-day launch window for each mission.
- Planetary environment data as provided by JPL, including JPL Martian model atmospheres G through K and 200 ft/sec gusts.
- 210 ft. dish DSIF (Deep Space Instrumentation Facility) network available, all three stations.
- The DSIF is available during launch. The system will be available 24 hours a day during maneuver and transfer periods and for the last week of planet approach. The DSIF is available 24 hours a day for thirty days after planet contact and for 8 hours each day thereafter until the mission is completed.
- The probability of landing a single viable Earth organism on Mars must be less than one in 10,000 and on Venus must be less than one in 100.
- Orbiters are designed for six months of operation after planet contact.
- The RMS value of a midcourse maneuver to correct for injection errors at 20 hours after injection is 10 meters/second, one sigma.
- Components and subystems developed for Mariner C will be utilized where feasible.

1.3 MISSION PRIME OBJECTIVES – MARS

The mission prime objectives, in order of priority, of a Mars mission were provided by JPL in Ref. 2 as follows:

- "Demonstrate orbiting capability and tracking for an extended period including the use of the orbiter in determining planet size and shape.
- Demonstrate capability of successful landing and survival for several hours.
- Successful performance of a television mission on the orbiter."

A "preferred list" of scientific instruments was provided by JPL in Ref. 2 for use in the selection of instruments for a mission.

1.4 MISSION CONCEPTS

Mission concepts included in the study were:

Mars 1969

- An orbiter alone.
- An orbiter carrying an atmospheric (non-surviving) capsule released before orbit.
- An orbiter carrying a bio (surviving) capsule released before orbit.

Mars 1971

- An orbiter alone.
- An orbiter carrying a bio-capsule released before orbit.
- An orbiter carrying a bio-capsule released from orbit.

Venus 1970

- An orbiter alone

All capsules perform atmospheric experiments during entry.

Section 2
SUMMARY AND CONCLUSIONS

2.1 PRINCIPAL RESULTS

The Mariner Mars Orbiter study results presented in this report show that a single basic spacecraft design, launched by the Flox Atlas-Centaur, can meet the Mars 1969 and 1971 orbiter mission objectives. This spacecraft can have provisions for carrying an entry capsule if desired. The escape weight capability of the Atlas Centaur launch system is quite marginal for the Mars 1969 mission without the addition of Fluorine to the Atlas oxidizer (Flox). Fluorine would not be necessary for a Mars 1971 mission, unless a sizable entry capsule is desired on the mission.

An entry capsule, designed to make measurements in the Martian atmosphere but not survive landing, could be carried by the 1969 or 1971 Mars orbiters. Attempts to design a capsule to survive entry and perform a biological experiment on the surface of Mars for the 1969 mission were not successful within the constraints of launch system capability, heat sterilization requirements, and the severe atmosphere, wind and terrain specified for the study. A biological capsule may be feasible for the 1971 Mars mission.

The basic concept is that of an orbiter injected into a 1,800 × 36,000 km orbit about Mars. This orbiter has the provisions and capability, at a weight penalty of about 10 lb, to carry a 61 in dia ballistic entry capsule that is separated from the orbiter about two days prior to planet encounter. A unique feature of this concept is the ability to perform the orbit injection function from the cruise condition without an attitude maneuver.

The 1969 Mars orbiter mission can be achieved with a program go-ahead in FY 1966. No new breakthroughs are required and Mariner C technology and hardware can be used extensively.

A brief description of the principal results in major areas of study follows.

2.1.1 Payload Capability

The various combinations of percent Flox in the Atlas and launch year provide payloads that vary from inadequate to generous. The net scientific payload in orbit about Mars in 1969 or in an entry capsule is shown, by percent Flox, in Table 2-1. The 1971 Mars mission opportunity provides additional weights in orbit for science, science support, redundancy and contingency of 280, 355, and 565 lb for 0, 20, and 30 percent Flox respectively.

Table 2-1

PAYLOAD CAPABILITY – 1969 MARS MISSION

	Weight in lb for Percent Flox in Atlas		
	0%	20%	30%
Orbiter Only			
Scientific Payload	18	132	132
Redundancy and Contingency	38	104	216
Orbiter Plus Atmospheric Capsule			
Scientific Payload – Orbiter	18	88	88
Scientific Payload – Capsule	18	18	18
Redundancy and Contingency	82	28	140

2.1.2 Design Concepts

The orbiter vehicle is common to all missions and acts as a communications relay for the atmospheric capsule. The selected design concept consists of a spacecraft comprising four major assemblies:

- The Surveyer launch shroud.
- The support structure which adapts the spacecraft to the Centaur.

- The orbiter which consists of the propulsion module and equipment module, and provisions for carrying a capsule.
- The entry capsule which is sealed in a sterilization shroud.

2.1.3 Guidance and Control

The vehicle attitude is normally space-oriented with the roll axis and solar panels pointed toward the Sun. Attitude information is obtained from a Sun sensor and a Canopus tracker and processed by the on-board Computer and Controller. Attitude control is provided by the nitrogen gas jets. An initial reference is used for all maneuvers. DSIF tracking data are provided for all trajectory corrections, through the on-board computer. To provide a 4σ probability that the orbiter does not approach closer than 300 km to the surface of Mars, the final orbit periapsis nominal aim point is not less than 1500 km.

Vehicle cameras and antennas are directed by the on-board Computer and Controller.

2.1.4 Experiments

Scientific payloads were chosen to accomplish the primary mission objectives and to take full advantages of mission payload capability.

The experiments were designed to make measurements during interplanetary flight, during orbit about the planet and while entering the planet atmosphere.

Both high resolution (15 m) and low resolution (150 m) TV data would be obtained to aid in defining the nature of the surface of Mars.

2.1.5 Electronics System

The selected communication system is basically that of the Mariner C and is designed to operate with the planned three station 210 ft dish DSIF network. The orbiter-Earth

link uses a coherent PSK modulation system in connection with an omni-directional antenna and a 4-ft parabolic antenna. The system provides for transmission rates of up to 300 bits per second for communication to Earth from Mars orbit.

The orbiter-atmospheric capsule entry link employs a crossed dipole antenna on the orbiter and a whip antenna on the capsule. Operating frequency is 250 Mc with PCM-FM modulation. Data rate is 50 bits per second at a maximum range of 10,000 km.

Primary electrical power is supplied by the Mariner C solar panels at a minimum of 310 watts. Secondary power for the orbiter is provided by batteries. Primary batteries are used for power on the capsule.

2.1.6 Propulsion System

State-of-the-art propulsion systems technology was found to satisfy the requirements for trajectory corrections, orbit injection and attitude control. The main propulsion system is used both for midcourse guidance corrections and for orbit injection and requires development of a new engine. The engine uses N_2O_4 – MMH propellants and develops a thrust of 750 lb delivering an I_{sp} of 302 sec. Guidance and spinup of the capsule are performed by small, solid-propellant motors. Orbiter attitude control is provided by nitrogen gas jets.

2.1.7 Thermal Control

The thermodynamic analyses were limited to parametric studies and general energy balances to determine steady state temperature levels of the spacecraft.

Most of the temperature control requirements will be met by means such as specific surface finishes, insulation, isolators, heat sinks and selective arrangement of equipment. If limited active temperature control becomes necessary this could probably be provided by controllable shutters and by electric heaters.

2.1.8 Entry Systems

The entry systems proposed for the Mariner Mars capsule include a high drag entry body similar to the Apollo Command module configurations, protected by an ablative or a heat sink heat shield. Parachutes would be used for the final deceleration system.

2.1.9 Spacecraft Sterilization

Sterilization ground rules require that the probability of contamination of Mars must not exceed one in ten thousand. This is met by:

- Guidance accuracy with a 4σ probability of entry into the Martian atmosphere in less than 50 years after encounter.
- Clean room techniques to keep contamination of the vehicle to a minimum.
- Final heat sterilization of the capsule in a sterilization shroud.
- Retention of the capsule in the sealed sterilization shroud until after separation from the orbiter.
- Separation of the shroud prior to capsule entry guidance maneuver.

2.1.10 Development Program Plan

The development program plan was prepared in order to outline program requirements and to provide sufficient data to support a rough order of magnitude program cost estimate. The plan describes program requirements for spacecraft development, integrated testing, reliability, manufacturing, facilities and ground support, launch operations and data processing.

A program go-ahead in September 1965 for Phase II design and hardware would meet the schedule requirements for a 1969 Mars mission.

2.1.11 Program Cost

Cost estimates by major areas are presented for a 1969 Mars mission and for a 1971 follow-on Mars mission. A bare minimum program is estimated to cost a total of 110.7 million dollars for a 1969 mission (orbiter only) and a 1971 mission (orbiter plus capsule).

Excluded from the estimates is the cost associated with:

- Launch vehicles
- NASA launch center operations
- DSIF or other tracking units and data acquisition operations
- Launch pad systems operations

2.2 CONCLUSIONS

The principal conclusions that can be drawn from the results of this study are:

- Orbiter and atmospheric capsule missions to Mars are feasible in the 1969 and 1971 launch opportunities using a Flox Atlas-Centaur launch system.
- Biological capsules, designed within the framework and ground rules of the study, cannot be readily provided for the 1969 mission.
- Entry into orbit without a spacecraft attitude maneuver prior to engine burn can be accomplished in both 1969 and 1971 missions.
- A single basic modular design can be developed which can accomplish both Mars and Venus missions and which can carry a capsule if desired.
- Current technology is adequate, and extensive use of Mariner C hardware contributes to the adequacy of a conservative design.
- A program start in FY 1966 is required to accomplish a 1969 Mars mission.

Section 3
MISSION AND PERFORMANCE ANALYSIS

The primary objective of the mission and performance analysis effort was the definition of mission capabilities for a Mars orbiter launched by a Flox Atlas-Centaur. Major emphasis was placed on the 1969 Mars orbiter, with and without an entry capsule, with secondary attention to the 1971 Mars and 1970 Venus mission opportunities. Thirty-day launch windows were selected to yield the maximum burnout weight in orbit about the target plant.

The analyses conducted in the area of mission and performance analysis were divided into three broad categories:

- Interplanetary transfer
- Orbiter approach, injection into orbit, and operation in orbit
- Capsule entry performance

The division is somewhat arbitrary in that the mode of operation, trajectory geometry, performance capability, and vehicle design requirements are intimately related and interdependent. The techniques for calculation and analysis determine the definition of each category. Also, the principal criteria and predominant parameters can be more easily demonstrated.

The objectives of this portion of the Mariner orbiter study were to:

a. Establish orbiter performance requirements and capability.
b. Determine weight capability in Mars and Venus orbits.
c. Define thirty-day launch windows for the 1969 and 1971 Mars and the 1970 Venus missions.
d. Establish communication and guidance geometry.
e. Define nominal design trajectories and orbits.
f. Establish orbiter and capsule vehicle design requirements.

The results of these analysis are presented in this section including data from previous LMSC studies such as the Voyager (Ref. 3) where applicable. The main emphasis was placed upon the Mars orbiter requirements and concept. The analysis of the entry system was limited to applying and refining previous study results and establishing detail trajectories for heat shield, parachute, and structural design. However, the development of the entry system concepts, techniques, and design requirements is presented in sufficient detail to demonstrate the entry capsule feasibility, to indicate principal limitations, and to illustrate the implications upon the orbiter vehicle concept and design.

The examination of individual trajectory maneuvers from the viewpoint of the complete mission profile led to one important concept vitally affecting the orbiter design arrangement. This concept was for performing the orbit injection maneuver while maintaining the interplanetary cruise attitude with fixed thrust nozzle angle. The consequence was a lighter weight, more compact design yielding increased reliability by elimination of one orientation maneuver. The development of this mode is traced in detail in a later section.

3.1 BASIC GROUND RULES AND INPUT DATA

The basic ground rules and input data for mission analysis and launch window selection included the following:

- The Earth-escape capability of the Flox Atlas-Centaur launch system as shown in Fig. 3-1. 20 percent Flox in the Atlas is the nominal system.
- The declination of the departure asymptote from Earth was limited to angles between -28 and +33 deg.
- Mass discarded or consumed enroute to Mars includes: support structure 50 lb. ; midcourse propellant 30 lb. ; attitude control gas 4 lb.
- Interplanetary trajectory data was obtained from Refs. 4, 5, and 6.
- Model atmospheres for Mars as specified by JPL and shown in Table 3-1 and Fig. 3-2 (Ref. 2) with surface gusts of 200 ft/sec.
- The orbiter primary propulsion system I_{sp} is 302 sec.

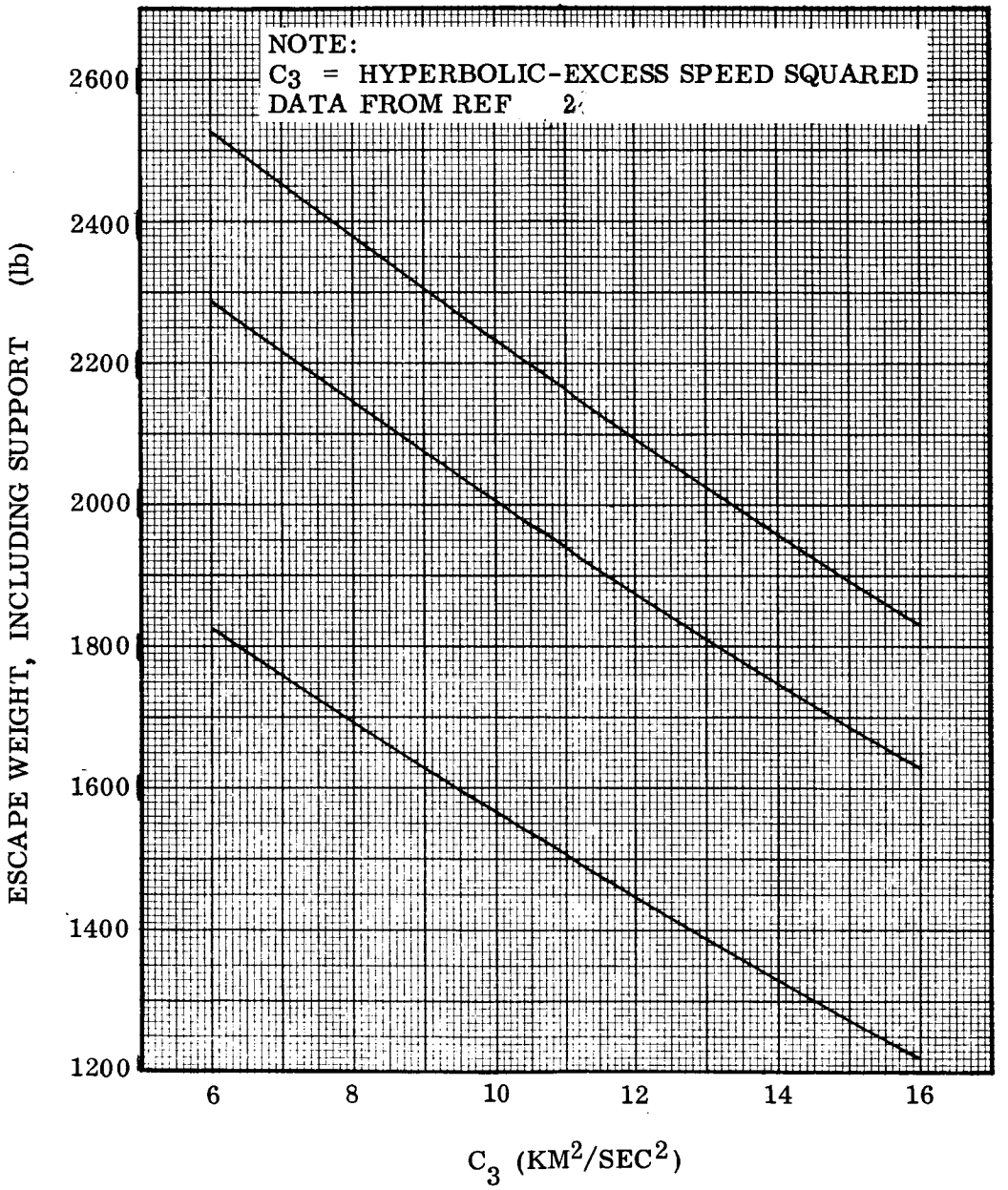


Fig. 3-1 Launch System Earth Escape Payload

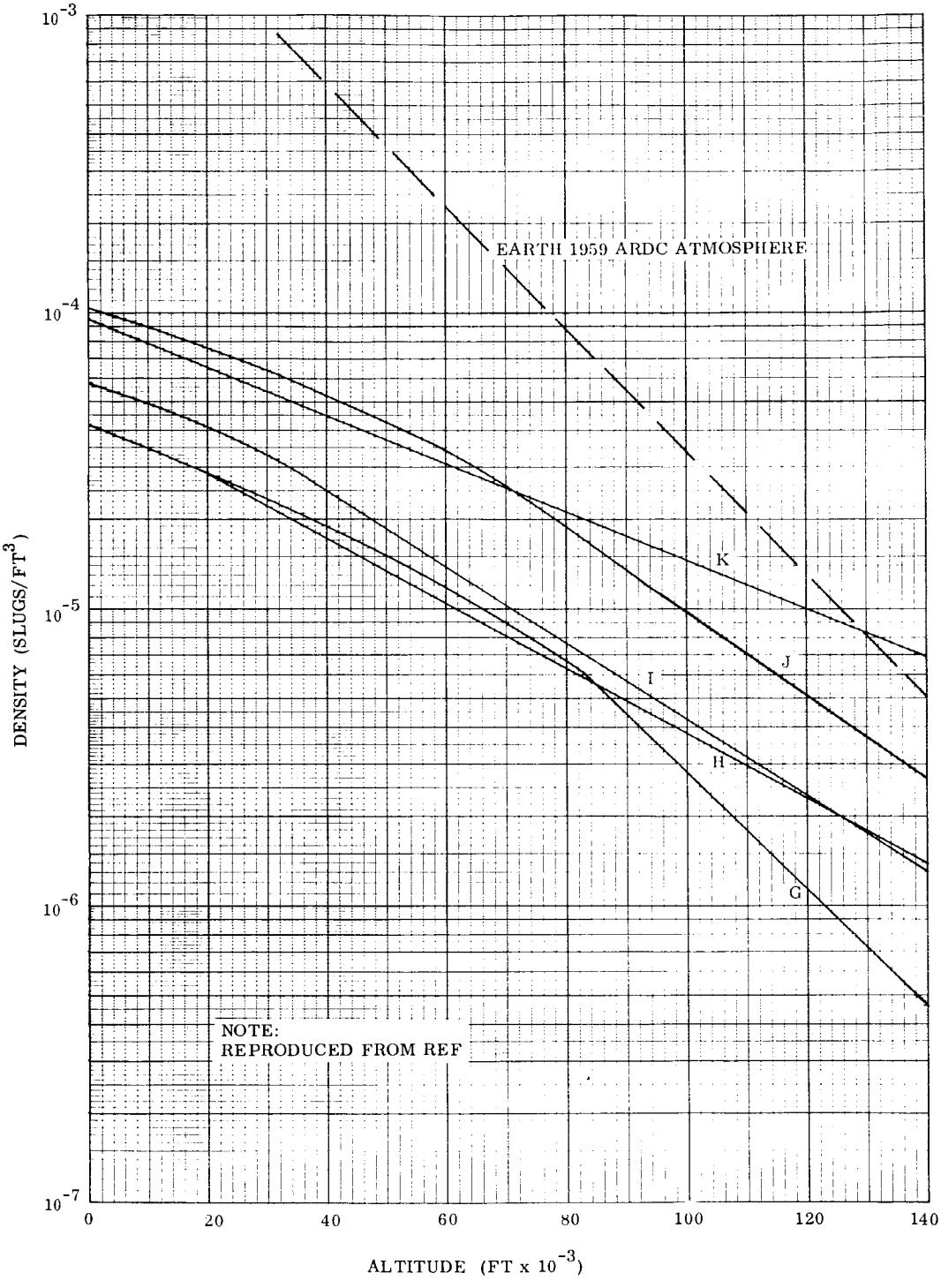


Fig. 3-2 Model Atmospheres for Mars

Table 3-1

MARS MODEL ATMOSPHERES

(Interim low Pressure Models With 13.3 gm/cm^2 Argon)

Property	Symbol	Dimensions	G	H	I	J	K
Surface pressure	P_o	mb	11	11	15	30	30
		lb/ft^2	23.0	23.0	31.3	62.6	62.6
Stratosphere temperature	Ts	°K	130	230	180	130	230
		°R	234	414	324	234	414
Surface temperature	To	°K	260	260	230	210	230
		°R	468	468	414	378	414
Acceleration of gravity at surface	g	cm/sec^2	375	375	375	375	375
		ft/sec^2	12.3	12.3	12.3	12.3	12.3
Composition (volume)		%					
CO_2			64.8	64.8	43.3	10.5	10.5
A			35.2	35.2	32.2	13.0	13.0
N_2			0	0	24.5	76.5	76.3
Molecular weight	M	mol^{-1}	42.6	42.6	38.8	31.3	31.3
Specific heat ratio	γ		1.37	1.37	1.39	1.40	1.40
Adiabatic temp. lapse rate	Γ	°K/km	5.18	5.18	4.91	4.05	0
		°R/ft $\times 10^3$	2.84	2.84	2.69	2.22	
Tropopause altitude	h_T	km	25.09	5.79	10.19	19.75	0
		ft	82300	19000	33400	64800	
Inverse scale height (stratosphere)	β	km^{-1}	.1478	.0835	.0972	.1085	.0613
		ft$^{-1} \times 10^5$	4.506	2.546	2.963	3.308	1.869
Surface density	ρ_o	(gm/cm^3)10^5	2.17	2.17	3.04	5.37	4.91
		(sl/ft^3)10^5	4.21	4.21	5.90	10.42	9.54
Artificial surface density	ρ_o'	(gm/cm^3)10^5	13.60	2.52	4.35	14.20	
		(sl/ft^3)10^5	26.40	4.89	8.44	27.55	
Density at tropopause	ρ_t	(gm/cm^3)10^5	0.332	1.55	1.62	1.66	4.91
		(sl/ft^3)10^5	0.643	3.02	3.14	3.23	9.54

Reproduced from Ref. 2

3.2 INTERPLANETARY MISSION CONSIDERATIONS

3.2.1 Typical Mission Profile

In order to place the missions in proper perspective, typical transfer orbit characteristics are illustrated in Fig. 3-3 for the 1969 Mars opportunity. Launch occurs on January 29, 1969 with arrival at Mars on October 26, 1969. The relative position of the spacecraft with Mars and Earth is shown at 40 day intervals. The Type II trajectory was selected to provide maximum weight in orbit at Mars within the launch constraints at the Florida launch site. A transfer angle of about 206 deg results with the spacecraft first passing inside Earth's orbit and then slightly outside the orbit of Mars. Conjunction of Earth and Sun is seen to occur after about 120 days although the spacecraft is out of the plane of the ecliptic. Note that the look angle geometry between Earth-spacecraft-Sun remains essentially constant near encounter and varies only moderately during the six months orbiting lifetime. The variation of Earth's position at launch, and Mars and Earth positions at encounter over the thirty-day launch window indicate that the relative geometry varies only slightly. The 1971 Mars and 1970 Venus missions exhibit similar characteristics as illustrated in Figs. 3-4 and 3-5.

These exact trajectories were computed with the Interplanetary Trajectory Program (Reference 7) including the gravitational influence of Earth and Mars (or Venus) perturbations due to the other planets. Tables 3-2, 3-3 and 3-4 list longitude, latitude, and distances of the Sun, Earth, and Mars (or Venus) as viewed from the spacecraft from Earth escape injection to Mars (or Venus) periapsis passage.

3.2.2 Guidance and Communication Geometry

The communication and guidance geometry for the three missions is illustrated in Figs. 3-6 and 3-7, in terms of the spacecraft look angles between Earth and Sun, Sun and Canopus, and the relative inclination of the planes containing these angles. This geometry is depicted by the sketch in Fig. 3-6. Large variations occur in these angles

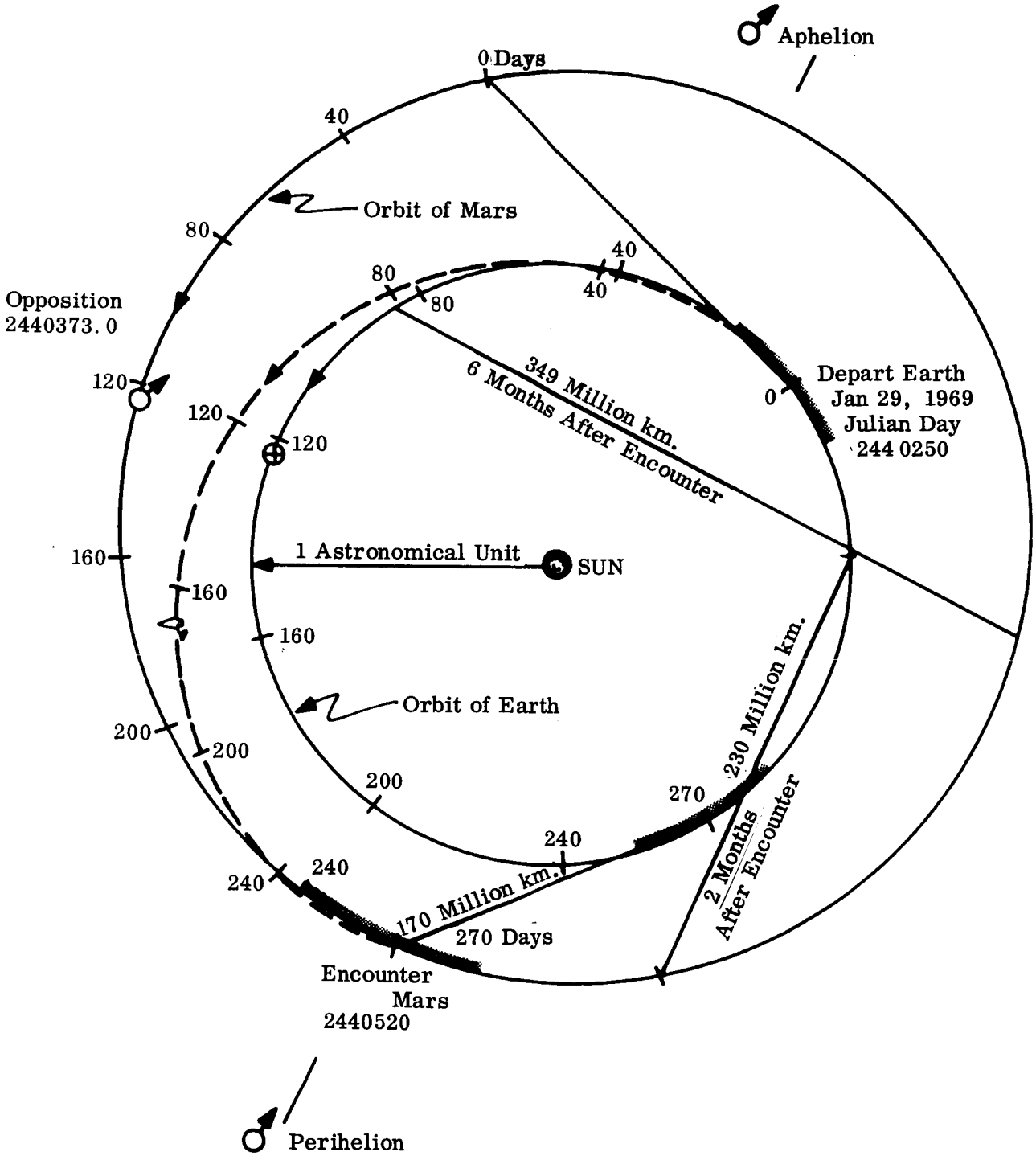


Fig. 3-3 Typical Transfer Profile – Mars 1969

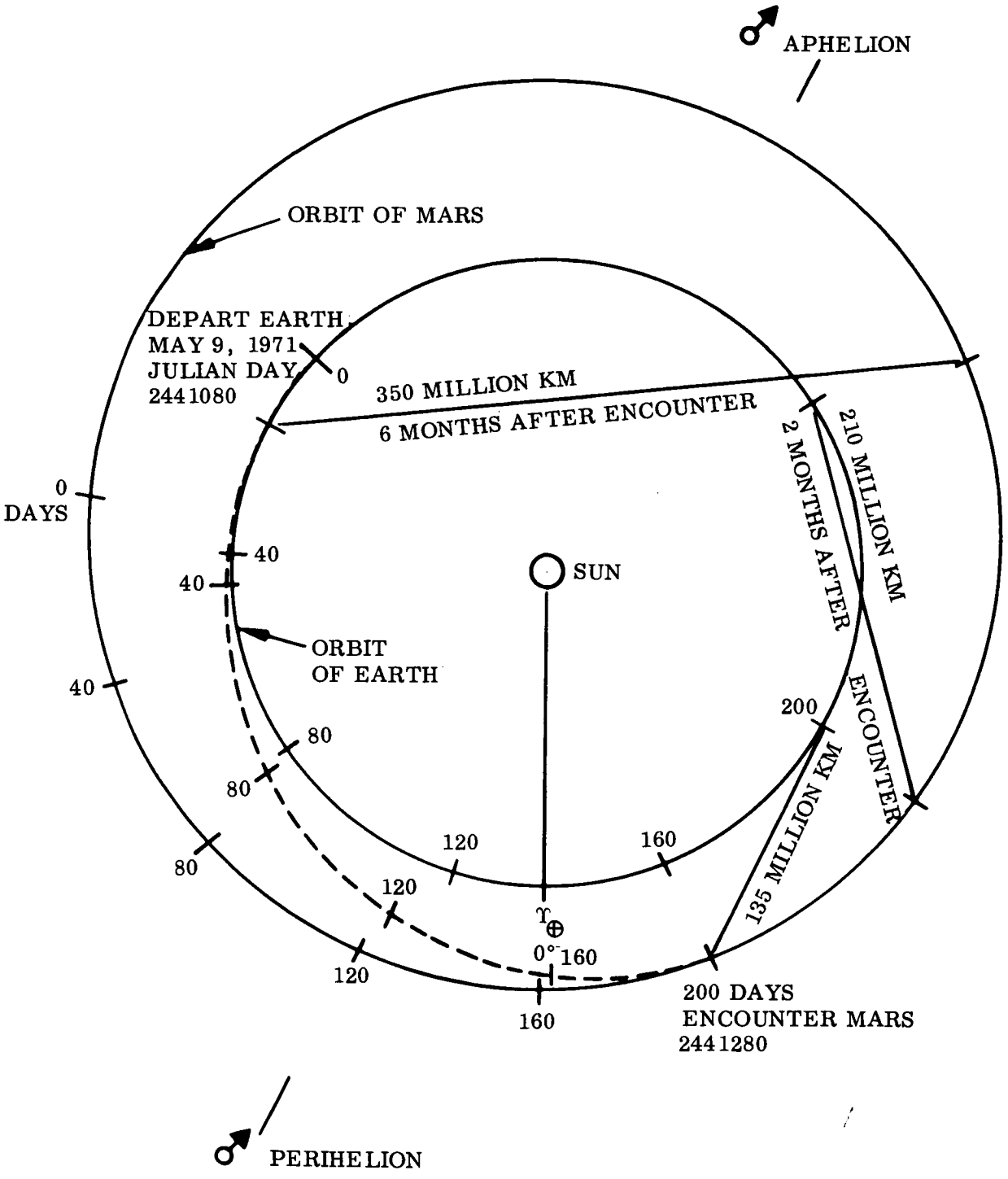


Fig. 3-4 Typical Transfer Profile – Mars 1971

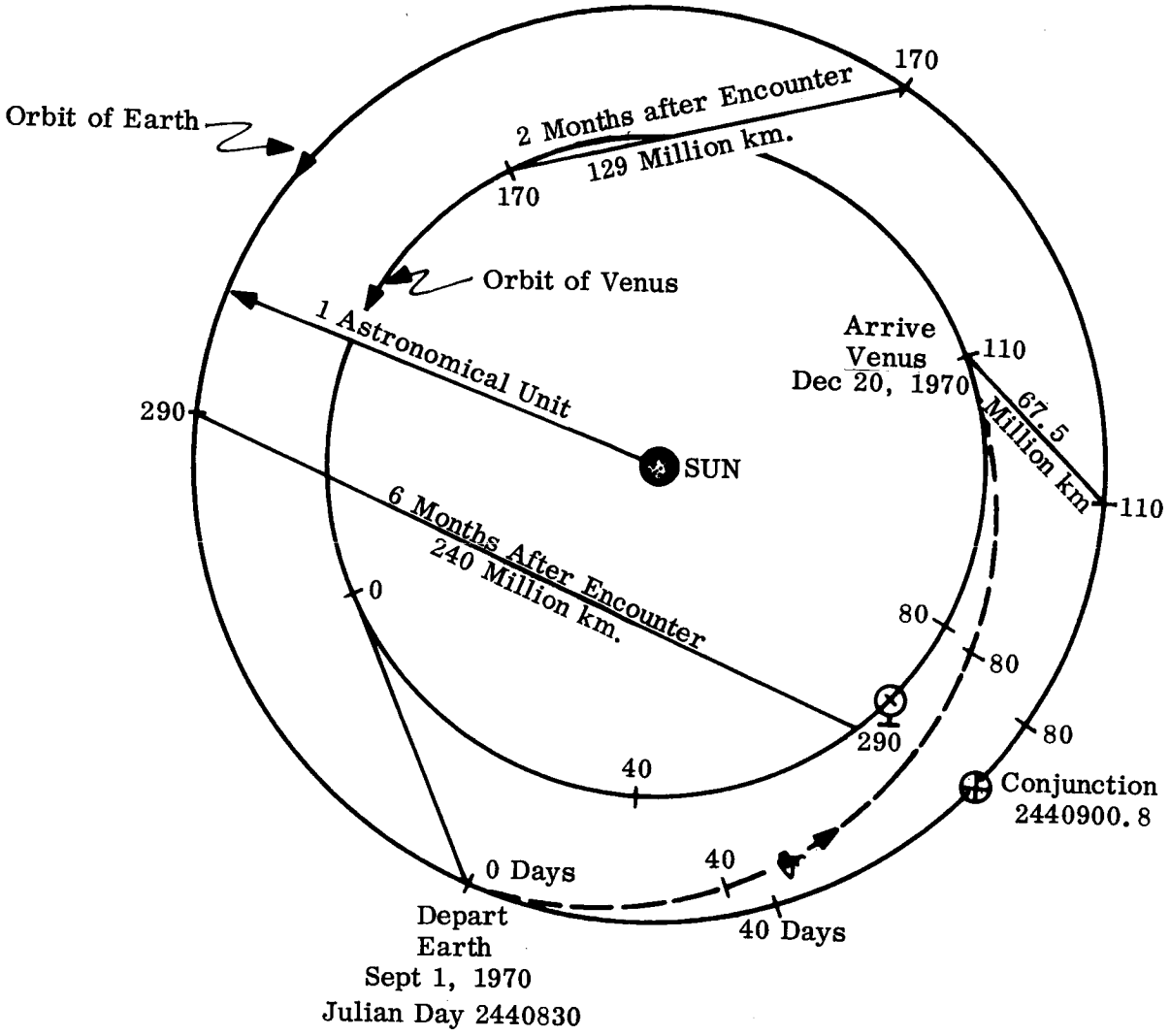


Fig. 3-5 Typical Transfer Profile – Venus 1970

Table 3-2

1969 MARS TRANSFER TRAJECTORY DATA

		Sun			Earth			Mars		
Point No.	Flight Time (Days)	Long. (Deg.)	Lat. (Deg.)	$\times 10^6$ Distance (Km)	Long. (Deg.)	Lat. (Deg.)	$\times 10^6$ Distance (Km)	Long. (Deg.)	Lat. (Deg.)	$\times 10^6$ Distance (Km)
0*	0	308.103	+.003	147.274	292.277	17.963	.006579	225.998	1.336	216.755
1	.25	308.388	-.025	147.228	68.431	-38.049	.112	226.119	1.316	216.289
2	.50	308.663	-.045	147.186	73.419	-36.853	.200	226.240	1.302	215.847
3	.75	308.937	-.064	147.146	75.356	-36.319	.284	226.361	1.289	215.408
4	1.0	309.211	-.082	147.108	76.411	-36.011	.365	226.483	1.276	214.971
8	2.0	310.305	-.152	146.966	78.161	-35.467	.680	226.969	1.224	213.227
16	4.0	312.494	-.288	146.714	79.370	-35.005	1.295	227.937	1.121	209.743
24	6.0	314.688	-.423	146.498	79.818	-34.904	1.898	228.900	1.016	206.254
32	8.0	316.887	-.557	146.316	80.128	-34.826	2.498	229.855	.907	202.760
36	10.0	319.090	-.690	146.166	80.396	-34.753	3.094	230.803	.796	199.261
50	20.0	330.148	-1.334	145.907	81.808	-34.366	6.022	235.402	.183	181.757
70	40.0	352.088	-2.438	147.794	85.279	-33.627	11.354	243.685	-1.354	147.540
74	52.0	4.844	-2.924	150.334	86.913	-33.319	13.962	247.871	-2.511	128.213
78	64.0	17.112	-3.256	153.750	87.310	-33.051	16.008	251.311	-3.873	110.271
82	90.0	41.642	-3.464	163.233	80.676	-31.056	19.110	255.555	-7.630	77.444
86	130.0	73.839	-2.798	179.715	60.940	-17.045	29.902	251.608	-15.129	44.944
90	170.0	100.780	-1.560	194.095	63.072	-5.151	58.808	239.660	-20.648	29.378
94	210.0	124.494	- .179	203.646	79.101	- .361	100.495	232.692	-21.954	18.804
98	229.0	135.137	+.466	206.113	88.820	+ .785	122.369	231.913	-22.022	13.291
102	241.0	131.757	.860	206.940	95.396	1.305	136.330	231.903	-22.005	9.550
110	259.0	151.636	1.426	207.105	105.778	1.880	156.953	232.189	-22.011	3.671
126	268.0	156.585	1.694	206.702	111.176	2.097	166.938	232.746	-21.929	0.668
130	269.0	157.136	1.724	206.636	111.784	2.119	168.029	233.345	-21.816	0.332
132	269.50	157.549	1.746	207.482	112.088	2.129	168.574	234.566	-21.581	0.163
P**	269.963							340.944	+18.230	0.004336

*29 Jan 1969

**P = Pericenter, 10 Oct 1969

Table 3-3

1971 MARS TRANSFER TRAJECTORY DATA

Point No.		Flight Time (Days)	Sun Long. (Deg.)	Sun Lat. (Deg.)	Sun $\times 10^6$ Distance (Km)	Earth Long. (Deg.)	Earth Lat. (Deg.)	Earth $\times 10^6$ Distance (Km)	Mars Long. (Deg.)	Mars Lat. (Deg.)	Mars $\times 10^6$ Distance (Km)
27 May 1971	0	0	65.611	-0.003	151.526	353.678	-10.866	.006579	311.050	-2.596	104.487
	1	0.25	65.890	+0.004	151.570	133.044	+9.539	.104818	311.150	-2.601	104.111
	2	0.5	66.158	0.009	151.598	137.838	9.966	.183619	311.245	-2.609	103.769
	3	0.75	66.425	0.014	151.614	139.813	10.122	.256737	311.339	-2.616	103.432
	4	1	66.690	0.019	151.636	140.922	10.204	.327015	311.434	-2.264	103.099
	8	2	67.747	0.038	151.722	142.817	10.334	.596013	311.810	-2.657	101.783
	16	4	69.848	0.073	151.915	143.970	7.464	1.547	312.550	-2.727	99.195
	24	6	71.939	0.107	152.136	144.392	10.379	1.620	313.272	-2.799	96.645
	32	8	74.022	0.141	152.388	144.572	10.393	2.118	313.975	-2.873	94.131
	36	10	76.097	0.174	152.668	144.635	10.398	2.611	314.656	-2.950	91.651
	44	14	80.220	0.239	153.316	144.555	10.394	3.587	315.952	-3.110	86.796
	52	22	88.346	0.363	154.942	143.826	10.332	5.509	318.251	-3.460	77.536
	60	30	96.279	0.476	156.975	142.441	10.178	7.419	320.114	-3.852	68.926
	72	46	111.461	0.665	162.060	138.070	9.458	11.485	322.327	-4.773	53.854
	80	70	132.319	0.846	171.430	131.123	7.321	19.905	321.387	-6.451	36.864
	84	110	162.169	0.910	188.422	131.842	3.709	46.236	311.471	-8.948	20.997
	88	150	187.260	0.775	203.359	145.931	1.771	88.857	303.728	-9.732	11.759
	96	164	200.771	0.639	210.258	157.526	1.117	119.986	302.381	-9.778	6.276
	100	186	207.228	0.561	213.002	163.833	0.873	136.428	302.286	-9.771	3.409
	104	190	209.344	0.534	213.807	165.994	0.802	141.979	302.326	-9.764	2.440
	112	194.5	211.707	0.503	214.644	168.457	0.726	148.248	302.479	-9.743	1.344
	126	198.25	213.662	0.477	215.286	170.533	0.666	153.484	303.230	-9.647	0.425
	130	199.25	214.180	0.470	215.449	171.089	0.651	154.882	304.750	-9.445	0.178
	132	199.75	214.438	0.467	215.529	171.366	0.644	155.584	311.251	-8.506	0.049
13 Dec 1971 Pericenter		199.92							64.546	+11.491	0.004336

Table 3-4

1970 VENUS TRANSFER TRAJECTORY DATA

			Sun			Earth			Venus		
Point No.		Flight Time (Days)	Long. (Deg.)	Lat. (Deg.)	$\times 10^6$ Distance (Km)	Long. (Deg.)	Lat. (Deg.)	$\times 10^6$ Distance (Km)	Long. (Deg.)	Lat. (Deg.)	$\times 10^6$ Distance (Km)
31 Aug 1970	0	0	157.623	-0.000	150.919	153.265	+14.906	0.006579	203.732	-2.268	102.277
	1	0.25	157.833	-0.018	150.851	30.030	-24.961	0.109	203.965	-2.323	101.881
	2	0.5	158.049	-0.031	150.806	34.840	-24.461	0.192	204.194	-2.370	101.513
	3	0.75	158.266	-0.043	150.764	36.765	-24.215	0.271	204.423	-2.415	101.150
	4	1	158.485	-0.055	150.722	37.828	-24.068	0.347	204.652	-2.461	100.789
	6	1.5	158.923	-0.077	150.640	38.982	-23.897	0.496	205.111	-2.551	100.070
	8	2	159.364	-0.099	150.556	39.602	-23.800	0.641	205.569	-2.641	99.354
	16	4	161.133	-0.185	150.209	40.662	-23.739	1.204	207.396	-3.006	96.502
	24	6	162.914	-0.270	149.835	40.873	-23.647	1.760	209.209	-3.382	93.660
	32	8	164.705	-0.355	149.433	40.914	-23.682	2.312	211.009	-3.771	90.827
	36	10	166.507	-0.439	149.002	40.866	-23.522	2.861	212.794	-4.173	88.004
	48	18	173.835	-0.775	146.992	40.108	-23.216	5.044	219.770	-5.927	76.862
	60	30	185.275	-1.269	143.150	37.740	-22.249	8.378	229.635	-9.068	60.892
	72	44	199.545	-1.811	137.538	33.887	-19.942	12.754	239.850	-13.706	44.069
	80	60	217.519	-2.330	129.968	30.307	-15.774	19.458	248.749	-20.574	28.152
	88	76	237.850	-2.641	121.791	30.328	-11.008	29.422	252.809	-28.759	16.276
	100	90	257.998	-2.624	114.921	34.254	-7.261	41.687	251.569	-35.058	8.724
9 Dec 1970	111	100	173.831	-2.384	110.698	39.193	-5.030	52.591	249.351	-37.549	4.250
	116	102.5	177.969	-2.289	109.783	40.678	-4.532	55.581	248.869	-37.828	3.180
	120	104.5	281.328	-2.204	109.099	41.932	-4.152	58.042	248.522	-37.930	2.330
	124	106.25	284.300	-2.121	108.538	43.076	-3.830	60.245	248.222	-37.889	1.586
	132	108.25	287.735	-2.017	107.940	44.436	-3.474	62.819	247.664	-37.411	0.733
	134	109	289.033	-1.975	107.727	44.960	-3.342	63.800	247.013	-36.621	0.410
	135	109.5	289.903	-1.944	107.586	45.315	-3.253	64.462	245.466	-34.558	0.190
19 Dec 1970 Pericenter		109.885							142.109	-64.998	0.007177

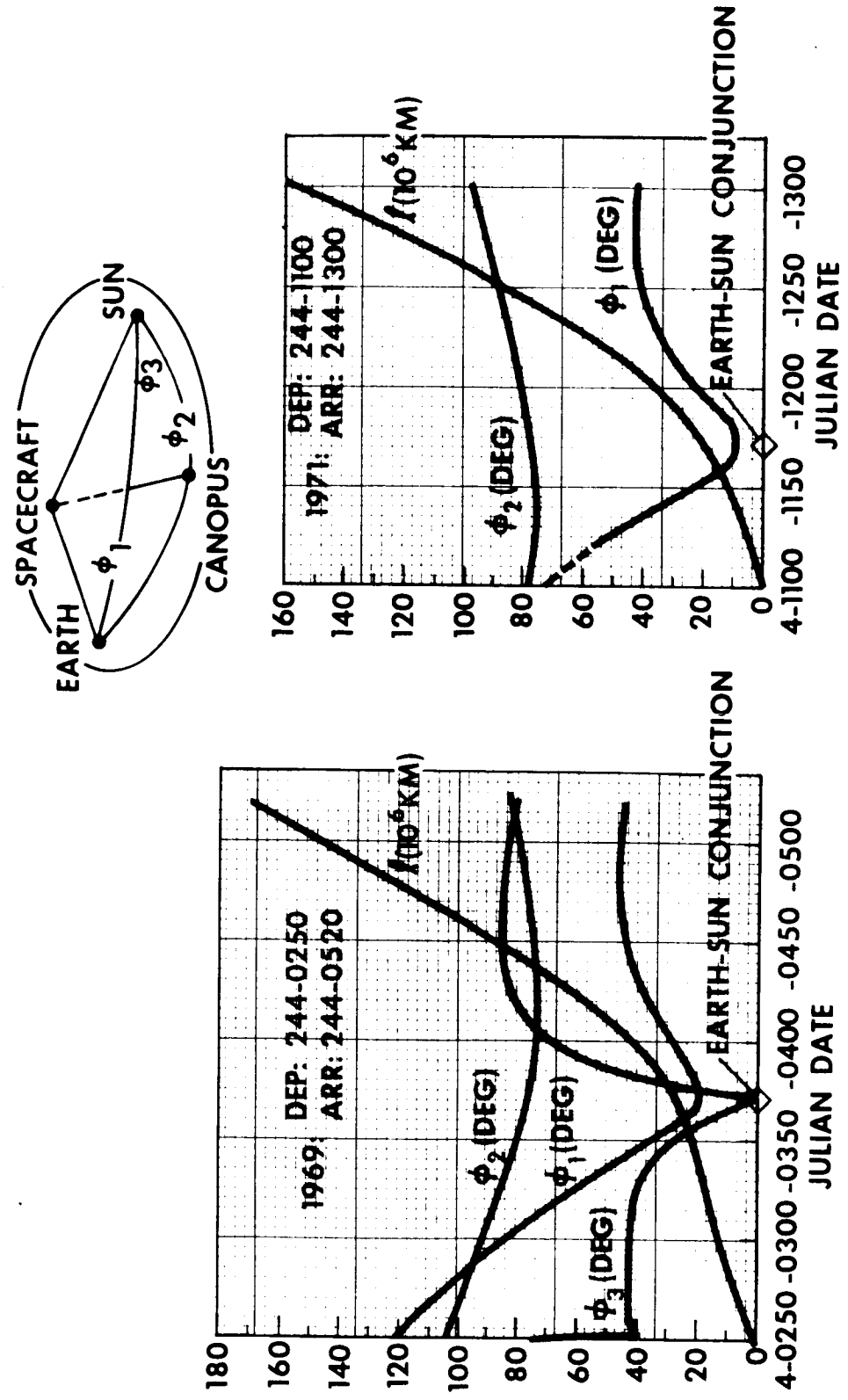


Fig. 3-6 Midcourse Communications and Guidance Geometry – Mars 1969 and Mars 1971

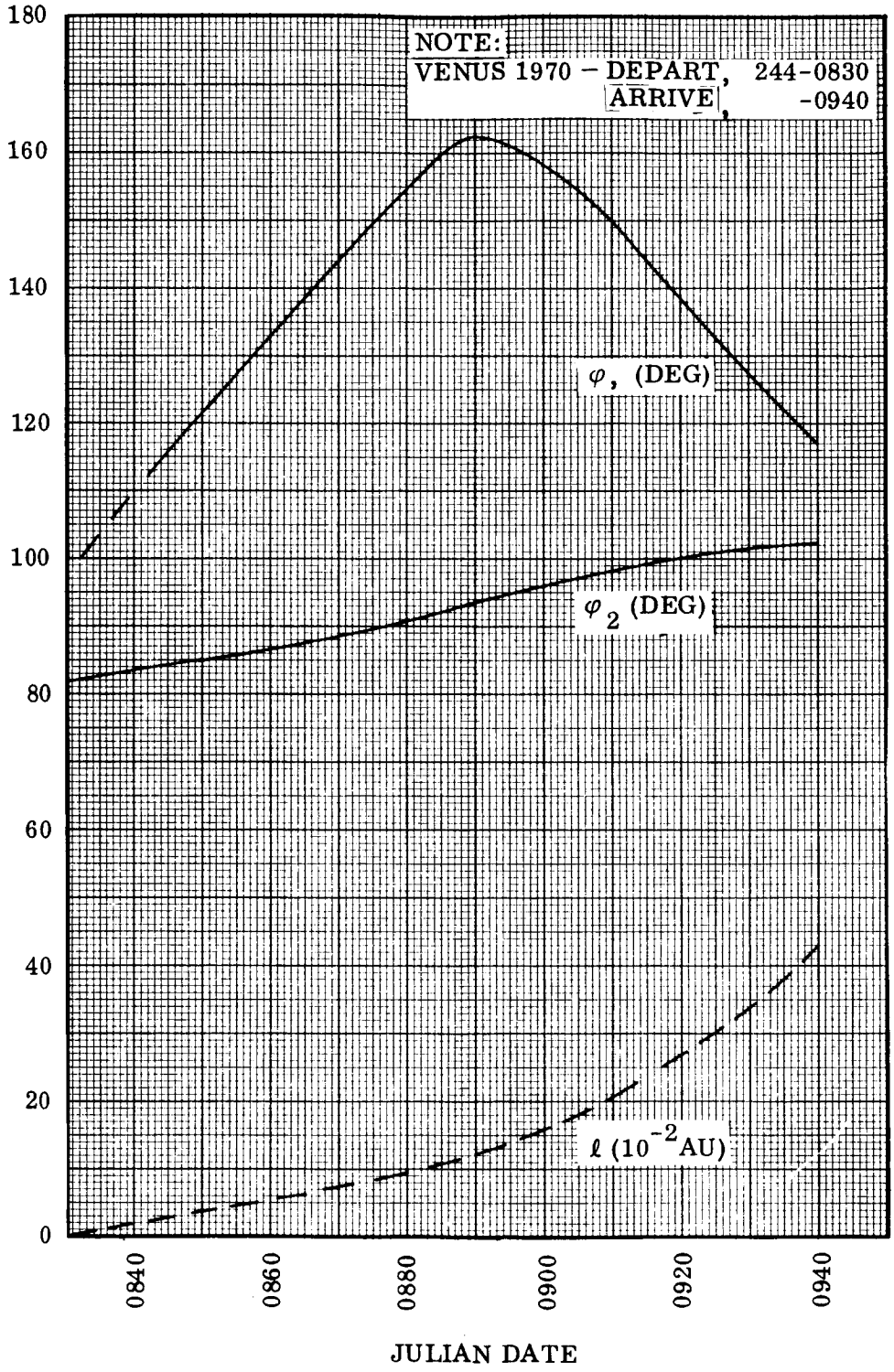


Fig. 3-7 Midcourse Communications and Guidance Geometry – Venus 1970

throughout the transfer period as implied by Figs. 3-3 to 3-5. In the 1969 Mars transfer, the Earth-spacecraft-Sun angle (ϕ_1) exhibits a 100 deg change, whereas the Sun-spacecraft-Canopus angle (ϕ_2) changes about 30 deg. The relative roll orientation (ϕ_3) of Earth and Canopus about the spacecraft-Sun axis changes rapidly near Earth and rapidly near conjunction, but remains nearly constant for 100 days before encounter. (The negative portion has been plotted positively for convenience.) These geometrical characteristics establish the antenna and star tracker gimballing requirements (See Section 5.3). Communication distance (ℓ) increases gradually until conjunction since the transfer orbit remains near Earth's orbit. A more rapid increase after conjunction results in a distance near 170 million km at encounter. The communication distance becomes about 260 million km after 3 mo in orbit about Mars, increasing to 350 million km after 6 mo in orbit (see Fig. 3-3). Even after 6 mo in orbit, good communication characteristics can be expected since the Sun is displaced about 20 deg from the spacecraft-Earth direction.

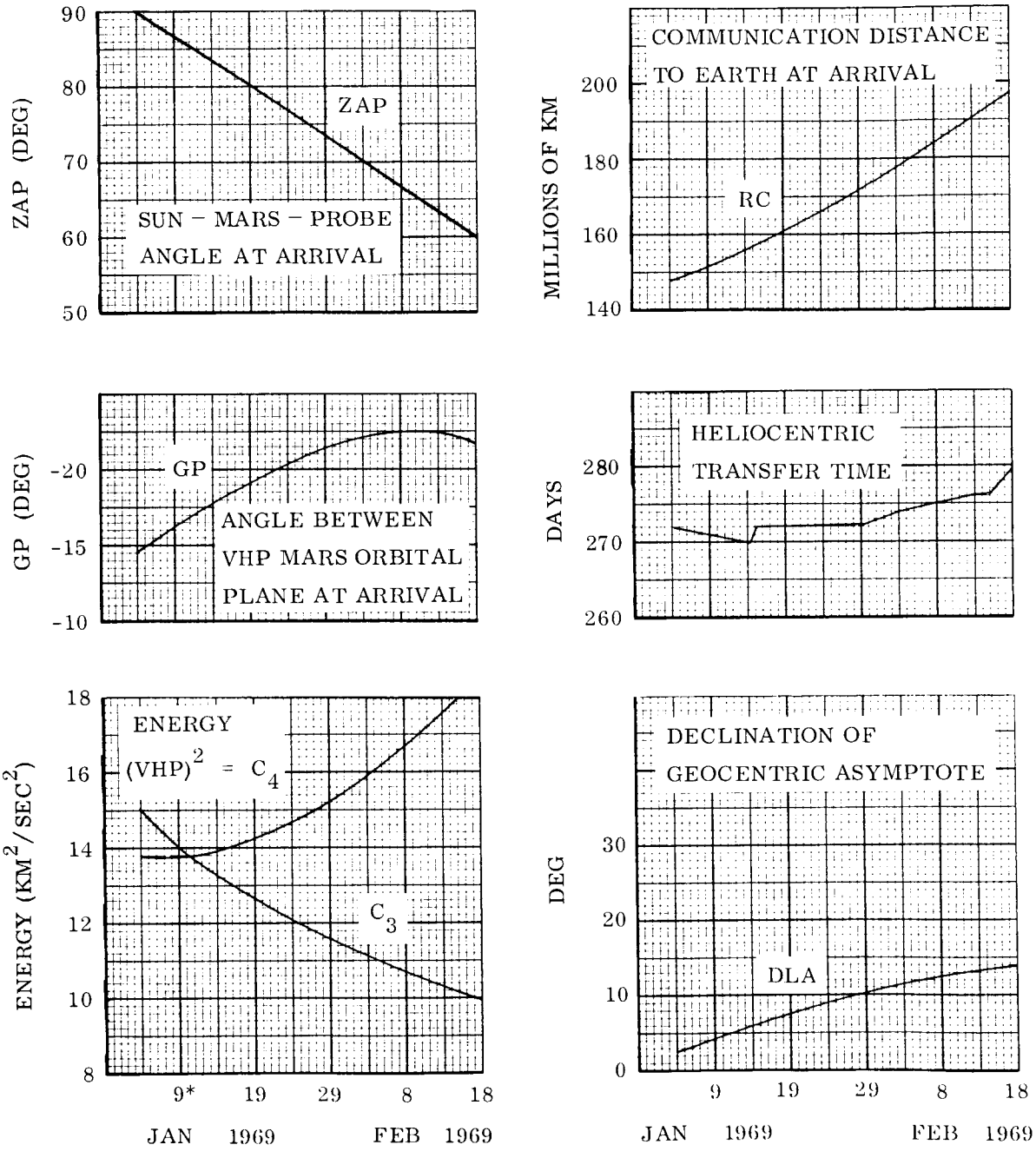
Smaller variations in the communication and guidance angles are encountered during the 1971 Mars mission as seen in Fig. 3-6. The 1970 Venus mission (Fig. 3-7) shows the comparable characteristics, except that the direction of change is inverted because of transfer to a smaller orbit than Earth's.

3.2.3 Interplanetary Transfer Characteristics

The variations of the principal transfer characteristics throughout the 30-day launch window are presented in Figs. 3-8, 3-9 and 3-10, as obtained from Refs. 4 and 5. The balance between departure excess energy, C_3 and arrival excess energy, C_4 is of primary importance in obtaining the maximum spacecraft weight in orbit about the target planet.

The launch windows shown for Mars 1969 and Venus 1970 were selected to provide maximum weight in orbit. The opening day of the launch window shown for Mars 1971 was determined by the requirement to restrict the declination of the geocentric asymptote to limits of -28 deg and +33 deg.

NOTE:
LAUNCH WINDOW CHOSEN FOR MAXIMUM WEIGHT IN ORBIT
C_3 = DEPARTURE HYPERBOLIC-EXCESS SPEED SQUARED
VHP = ARRIVAL HYPERBOLIC-EXCESS SPEED
TERMS AND DATA ARE FROM REF 5 , JPL – M 33-100



*JULIAN DAY 2440230

Fig. 3-8 Variation of Transfer Characteristics With Launch Date – Mars 1969

NOTE:
LAUNCH WINDOW CHOSEN FOR MAXIMUM WEIGHT IN ORBIT
C_3 = DEPARTURE HYPERBOLIC-EXCESS SPEED SQUARED
VHP = ARRIVAL HYPERBOLIC-EXCESS SPEED
TERMS AND DATA ARE FROM REF. 5, JPL TM 33-100

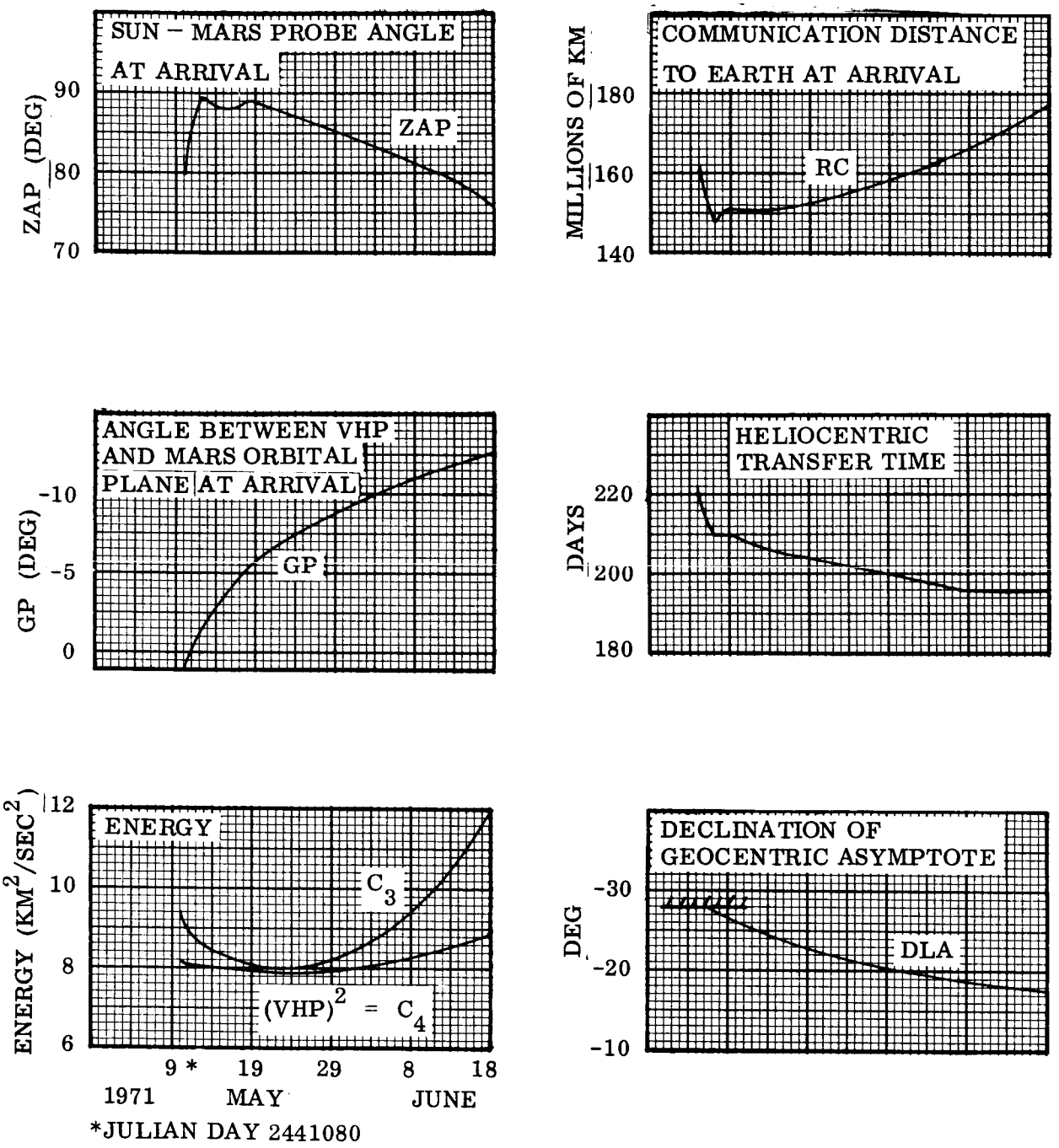
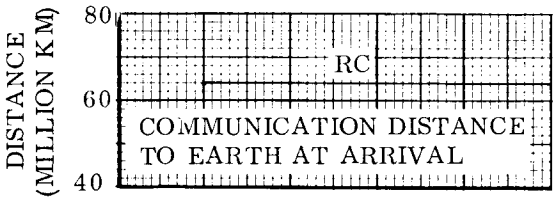
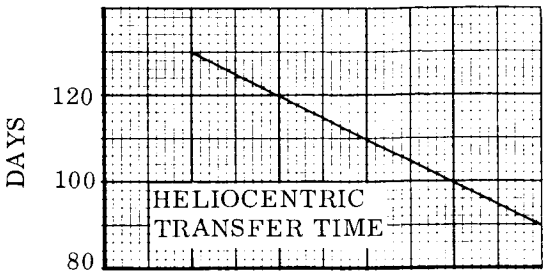
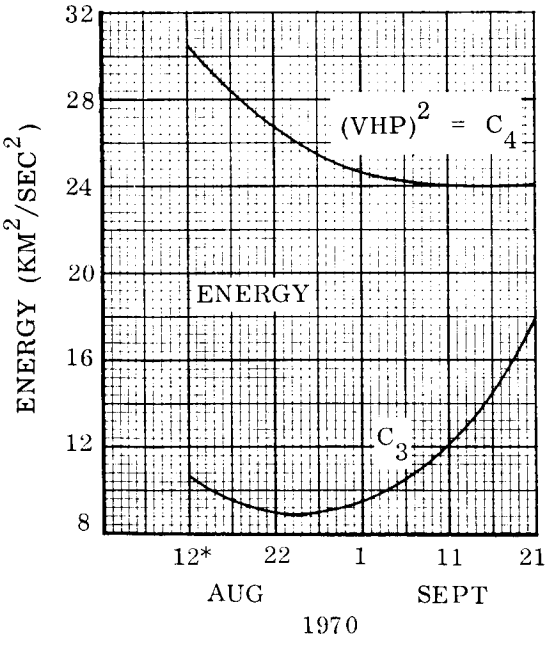


Fig. 3-9 Variation of Transfer Characteristics With Launch Date – Mars 1971

NOTE:
LAUNCH WINDOW CHOSEN FOR MAXIMUM WEIGHT IN ORBIT
C_3 = DEPARTURE HYPERBOLIC-EXCESS SPEED SQUARED
VHP = ARRIVAL HYPERBOLIC-EXCESS SPEED
TERMS ARE FROM REF 5
DATA FROM REF 4







*JULIAN DAY 2440810

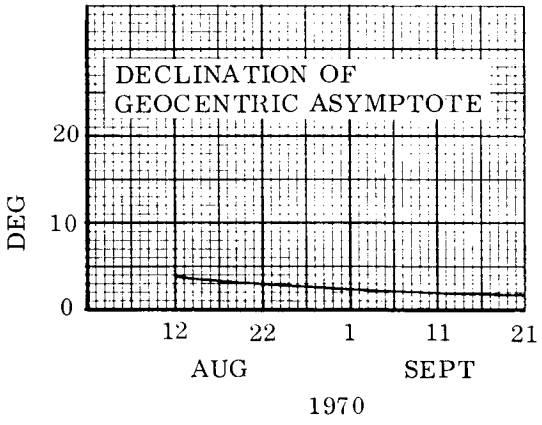


Fig. 3-10 Variation of Transfer Characteristics With Launch Date – Venus 1970

3.2.4 Performance Capability and Launch Window Selection

The escape weight at Earth and the burnout weight in orbit about Mars and Venus are shown in Figs. 3-11, 3-12 and 3-13 for the launch windows selected.

The escape weights for the nominal 20 percent Flox Atlas-Centaur are shown to be around 2000 lb (1800 to 2145 lb) for all missions considered. Examination of the 0 percent and 30 percent Flox curves shows that for each 1 percent addition of Fluorine to the Atlas oxidizer, the escape weight is increased by 21 to 22 lb.

Approximately 85 lb of mass is dropped or consumed between the time of departure at Earth and arrival at the target planet. This mass consists of the spacecraft support structure (50 lb) midcourse guidance propellant (30 lb) and attitude control gas (4 lb).

The orbit injection propulsion system was assumed to have an I_{sp} of 302 sec.

A nominal orbit of 1,800 km periapsis and 36,000 km apoapsis was assumed for Mars. This orbit decreased the injection energy requirement to a near minimum while insuring a 50 yr orbital lifetime within the tolerance of the guidance system. The burnout weight in Mars orbit is shown by the lower curves of Figs. 3-11 and 3-12, assuming no injection losses. Allowance for gravity and trajectory shaping losses for the constant thrust attitude during injection is obtained from Fig. 3-20 as discussed later. On-loading of orbit injection propellant throughout the launch window is assumed for the 1969 Mars mission.

The nominal burnout weight in orbit for the 1969 Mars mission with no capsule is then 960 lb. This represents about 50 percent of the arrival weight. For each pound of capsule separated before start of orbit inject, the orbital weight is decreased about 0.5 lb. The burnout weight varies from the nominal 960 lb for 20 percent Flox to 730 lb for no Flox and 1180 lb for 30 percent Flox.

NOTE:
LAUNCH WINDOW CHOSEN FOR MAXIMUM WEIGHT IN 1800 × 36000 KM ORBIT
NO CAPSULE CARRIED
WEIGHT DROPPED OR CONSUMED DURING HELIOCENTRIC
TRANSFER = 85 LB
NO THRUST ANGLE OR GRAVITY BURN TIME LOSSES DURING ORBIT INJECT
I_{SP} = 302 SEC

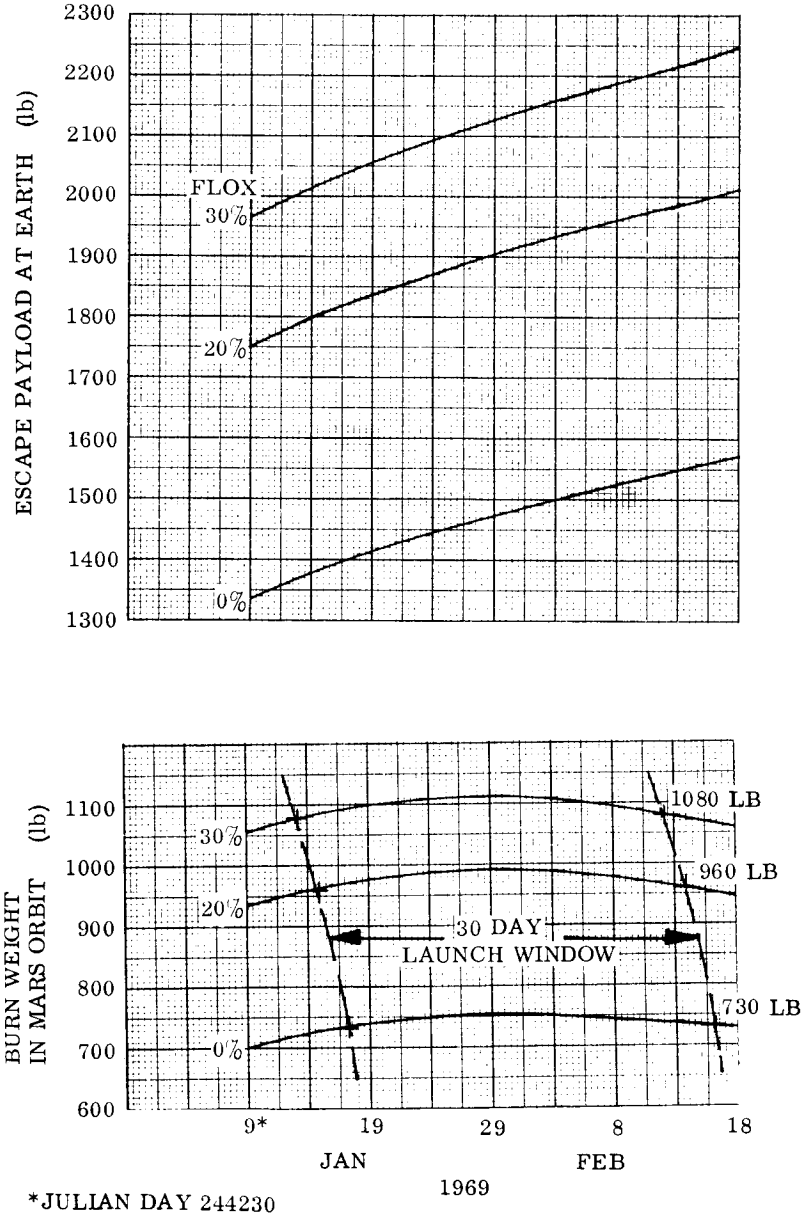


Fig. 3-11 Mars 1969 Performance Capability

NOTE:

LAUNCH WINDOW CHOSEN FOR MAXIMUM WEIGHT IN 1800 × 36,000 KM ORBIT
NO CAPSULE CARRIED
WEIGHT DROPPED OR CONSUMED DURING HELIOCENTRIC
TRANSFER = 85 LB
NO THRUST ANGLE OR GRAVITY BURN TIME LOSSES
DURING ORBIT INJECT
I_{SP} = 302 SEC

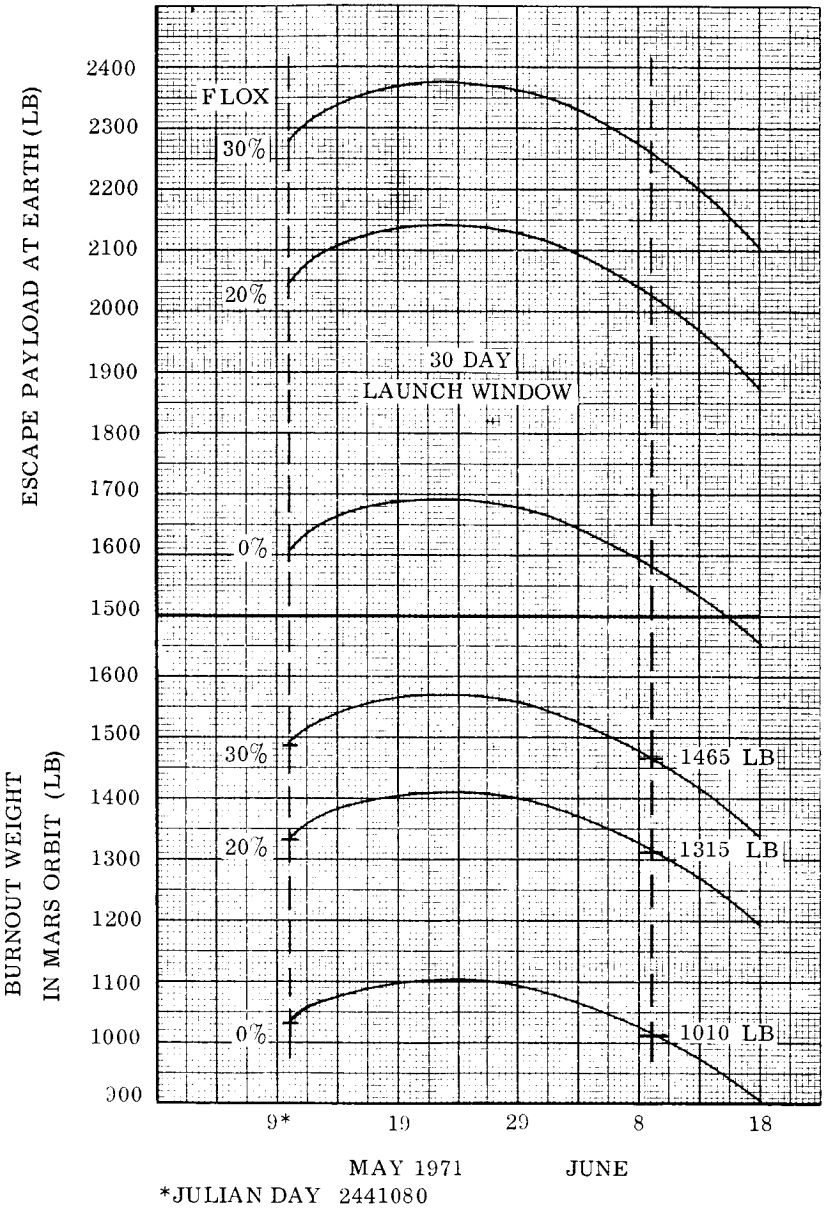


Fig. 3-12 Mars 1971 Performance Capability

NOTE:

LAUNCH WINDOW CHOSEN FOR MAXIMUM WEIGHT IN 1000 x 100,000 KM ORBIT
NO CAPSULE CARRIED
WEIGHT DROPPED OR CONSUMED DURING HELIOCENTRIC
TRANSFER = 85 LB
NO THRUST ANGLE OR GRAVITY BURN TIME LOSSES
DURING ORBIT INJECT
I_{SP} = 302 SEC

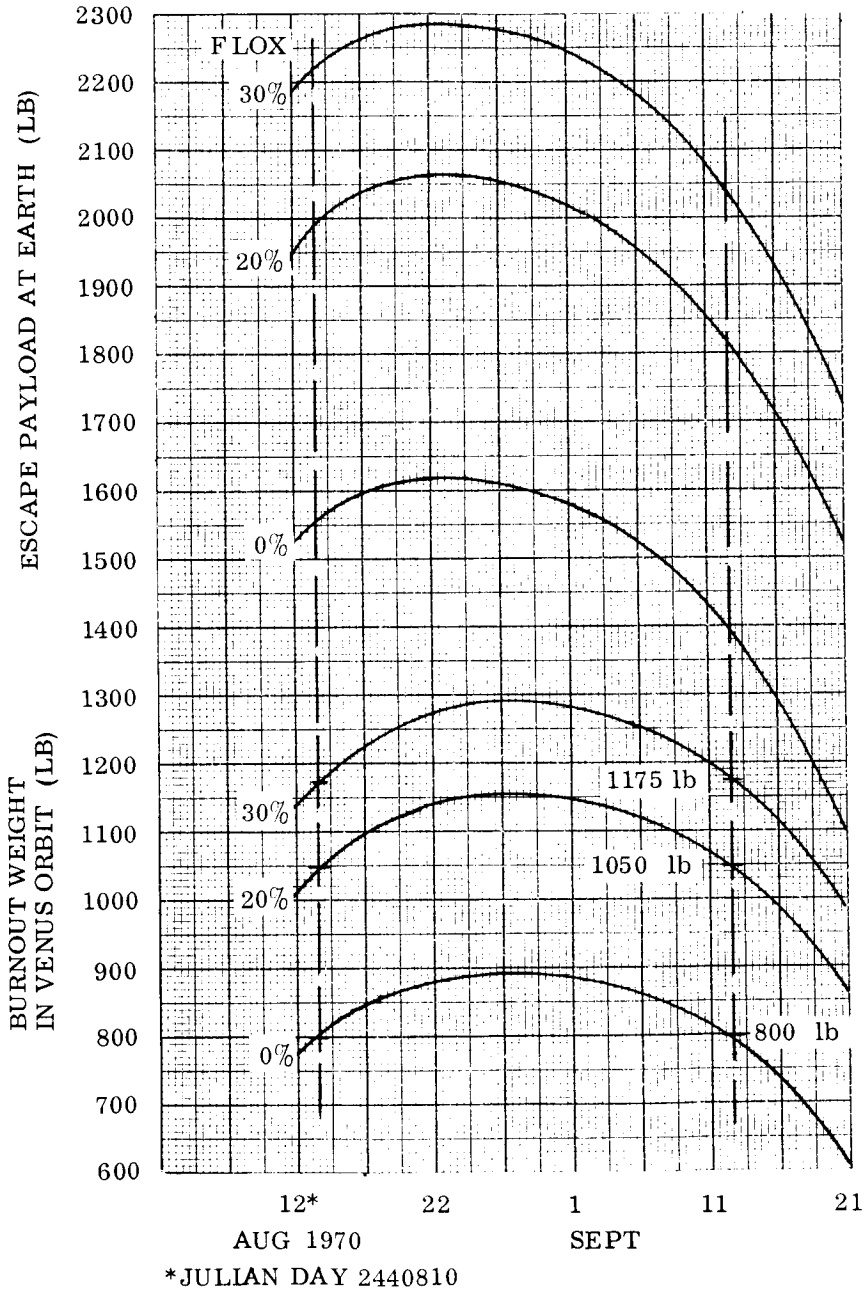


Fig. 3-13 Venus 1970 Performance Capability

The corresponding weights in orbit for the 1971 Mars mission are: nominal 1315 lb, no Flox 1010 lb and 30 percent Flox 1465 lb. The propellant loading can remain constant throughout the launch window.

A nominal orbit of 1,000 km by 100,000 km was chosen for Venus performance calculations. The burnout weights in this orbit for the 1970 mission, shown on Fig. 3-13 and assuming impulsive burn, are: nominal 1050 lb, no Flox 800 lb, and 30 percent Flox 1175 lb.

The orbital weights for the three missions is summarized in Table 3-5.

3.3 ORBITAL OPERATION CRITERIA

3.3.1 Orbit Selection

The nominal design orbit was selected to minimize the injection energy requirements, yield a minimum 50-yr lifetime, provide the geometry necessary for the primary experiments and to simplify communications, guidance and operational requirements.

The fraction of the approach weight which can be placed in orbit is influenced profoundly by the orbit geometry and significantly by the mission period. This is illustrated in Fig. 3-14 and 3-15 in terms of the planet approach energy C_4 for several combinations of the orbit periapsis and apoapsis altitudes. An effective I_{sp} of 302 sec for the propulsion system was used. The 1969 Mars mission results in the most severe orbit inject energy requirement. Between 0.50 to 0.56 of the approach weight can be placed in the nominal $1800 \times 36,000$ km orbit in 1969, whereas in 1971 at Mars a weight fraction of 0.67 - 0.68 can be achieved. For Venus, the corresponding capability for a nominal $1000 \times 100,000$ km orbit is 0.55 to 0.60 during the 1970 mission.

The 1800 by 36,000 km orbit was selected as the nominal geometry early in the study based on the estimated approach guidance tolerances, orbit lifetime requirements, and minimizing injection energy requirements. The large eccentricity and low periapsis

Table 3-5

SUMMARY OF BURNOUT WEIGHT IN ORBIT

Mission	*Burnout Weight in Orbit (lb)		
	Flox		
	0%	20% (Nominal)	30%
Mars – 1969 1,800 × 36,000 km orbit	730	960	1080
Mars – 1971 1,800 × 36,000 km orbit	1010	1315	1465
Venus – 1970 1,000 × 100,000 km orbit	800	1050	1175

*No thrust angle or gravity losses included

Table 3-6

MARS ORBITAL LIFETIME

$m/C_DA = 6.25\ km/m^2$

Altitude km	Lifetime – Years		
	K Atmos	H Atmos	K Atmos + Chamberlain
200	-	1.6×10^{-4}	-
300	0.5×10^{-3}	0.53	-
400	0.22	2240	-
500	202.0	8.93×10^{6}	-
1,800	2.8×10^{36}	5102×10^{43}	50
2,300	5.1×10^{44}	7.02×10^{67}	50
1,800 × 18,000	-	-	

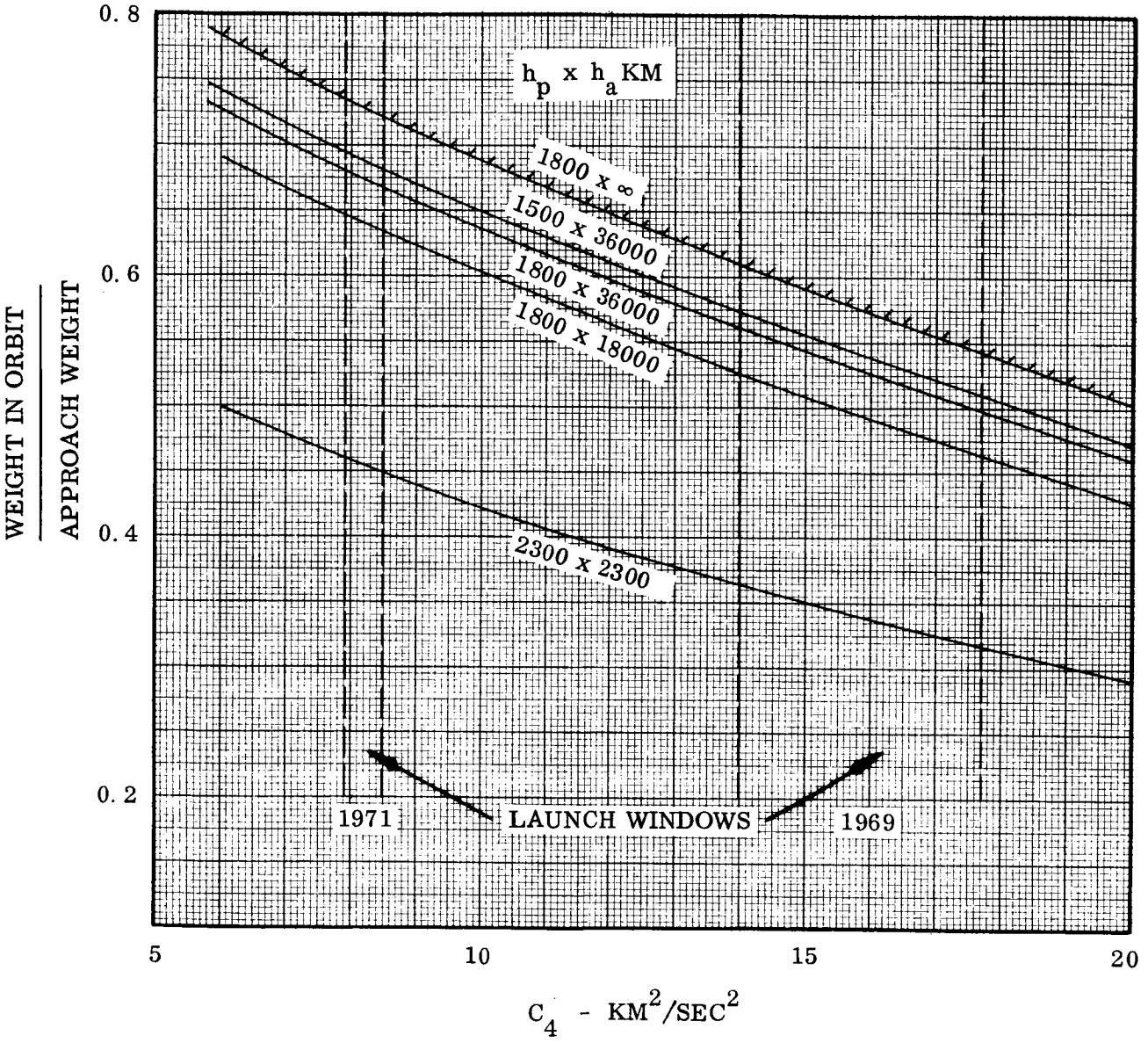


Fig. 3-14 Weight in Orbit Capability, I_{SP} = 302 SEC – Mars

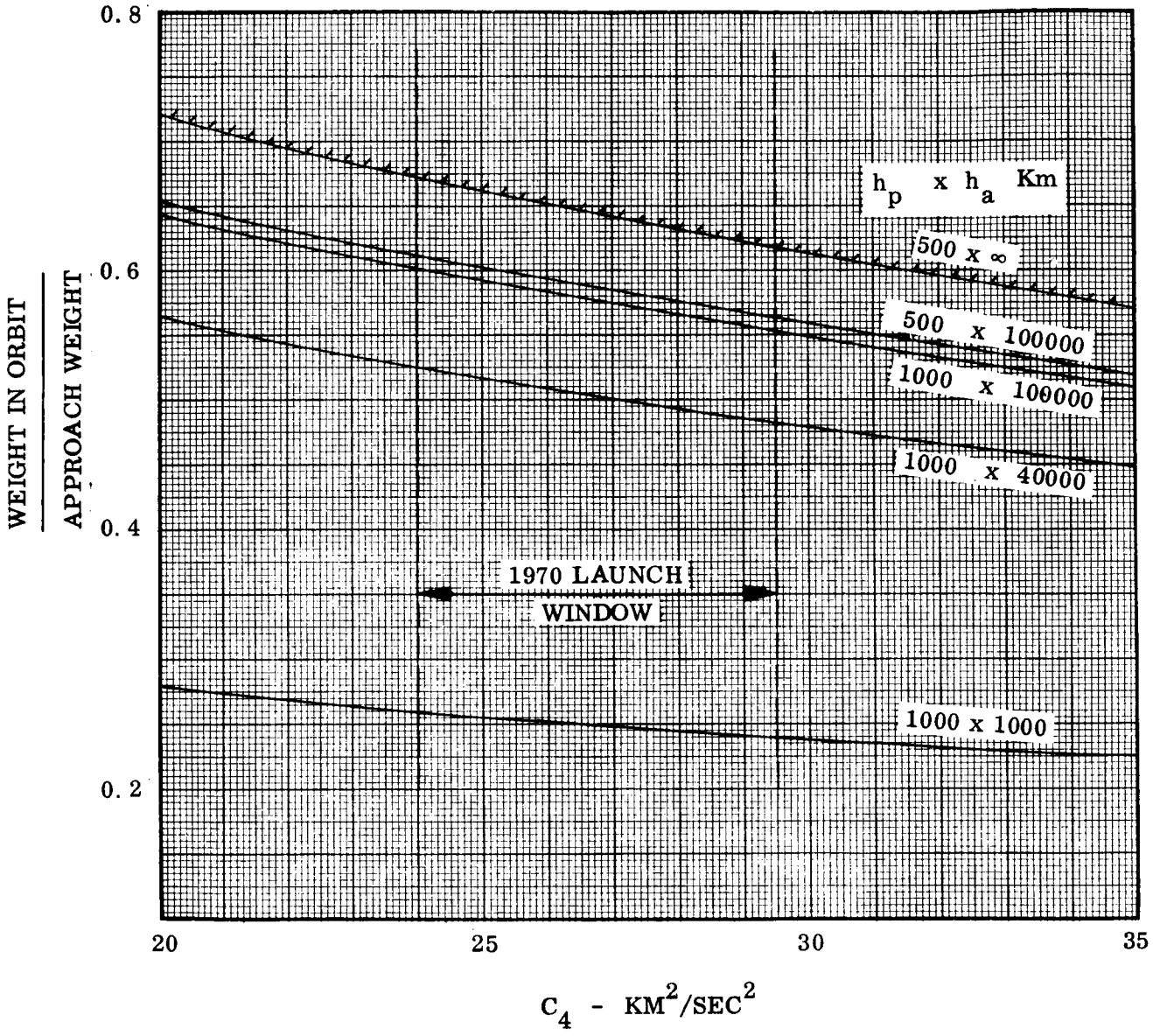


Fig. 3-15 Weight in Orbit Capability, I_{SP} = 302 SEC – Venus

altitude reduce the injection energy requirements as is apparent from Fig. 3-14. More detailed analysis of the guidance capability (Section 5. 1) indicate that a 1500 km periapsis altitude is feasible. This would yield about a 15 lb increase in the weight in orbit capability at Mars. The nominal capability is within 6 percent of the maximum limit defined by the escape condition for the 1800 km periapsis. Decreasing eccentricity or apoapsis is quite costly as indicated by the 1800 × 18,000 km curve for which 6 percent decrease in weight fraction occurs. Providing a circular orbit is so expensive that the mission is essentially wiped out. The 1970 Venus mission also yields greater weight fractions for similarly large eccentricity and low periapsis orbits, as shown in Fig. 3-15.

3.3.2 Lifetime Characteristics

For this study, the minimum orbit altitude was determined upon the basis of a circular orbit and exponential extensions of the specified Mars atmospheric models (JPL G-K). These assumptions would yield sufficiently conservative lifetimes to account for variations in the orbit due to approach guidance and orbit inject maneuver tolerances. The JPL model K atmosphere (yielding the highest densities at high altitudes) indicated that a 300 km orbit altitude is sufficient to provide a 50-yr lifetime for an equivalent drag area of 50 sq m.

The effects of orbit geometry and atmospheric model on orbit lifetime are shown in Table 3-6. The significant difference between these results and the minimum orbits suggested by JPL for the Voyager study arises from JPL's fairing the density profile through a singular density point at 1500 km altitude defined by Chamberlain (Ref. 8). In view of the extremely low densities from the surface to 250 km of the model atmospheres specified for the study, use of the Chamberlain data appears unnecessarily conservative. Better determination of the high altitude density profile for purposes of orbit lifetime control appears to be a pertinent experiment for presently programmed flyby missions.

Very significant increase of lifetime results from the higher eccentricity of the nominal design orbit as shown by Table 3-6 for the nominal design orbit of 1800 × 36,000 km.

3.3.3 Experimental Considerations

A nominal Mars orbit period of 25 hr was considered desirable to provide overlapping TV ground coverage and to allow communication with the lander capsule near the end of the first orbit. The periapsis altitude and desired period then determine the retro energy requirements as shown in Fig. 3-16 for the range of approach energy levels encountered during the 1969 and 1971 Mars missions. For fixed injection ΔV, the period varies radically with periapsis altitude as indicated by the cross hatched area about the nominal point. For example, a ± 800 km change in periapsis altitude causes a period variation of about +21 hr and -12 hr, respectively, for the end of the 1969 Mars window. The variation is limited to about +10 and -8 hr for the 1971 Mars missions. Approach periapsis altitude tolerances on the order of ± 800 km will result from Earth based tracking and guidance.

Acceptance of these wide orbit period variations will have important implications upon the biological capsule communications system (see Section 5.3) and the capsule design requirements (Section 4). The 50 year lifetime contour on Fig. 3-16 shows that the lifetime constraints will not be exceeded for the latest estimates of the density profile.

One method of reducing the period variations (at the cost of increased ΔV) is to set the maximum period and injection impulse for the maximum periapsis altitude tolerance. This is illustrated in Fig. 3-16 for C_4 of 18 km^2/sec^2 by the lower curve where the nominal 18 hour period varies between about 11 and 30 hr for the example ± 800 km altitude dispersion. The period variation is always less than 30 hr which allows the orbit to "catch up" to the landed capsule within 1-1/2 days after impact. This mode requires balancing out lander impact location tolerance and the orbit inclination, period and periapsis position.

The second method is to provide on-board guidance to control the retro velocity cutoff, depending upon the measured altitude. The added complexity for providing additional equipment or utilizing appropriate scientific instrumentation would tend to reduce overall reliability.

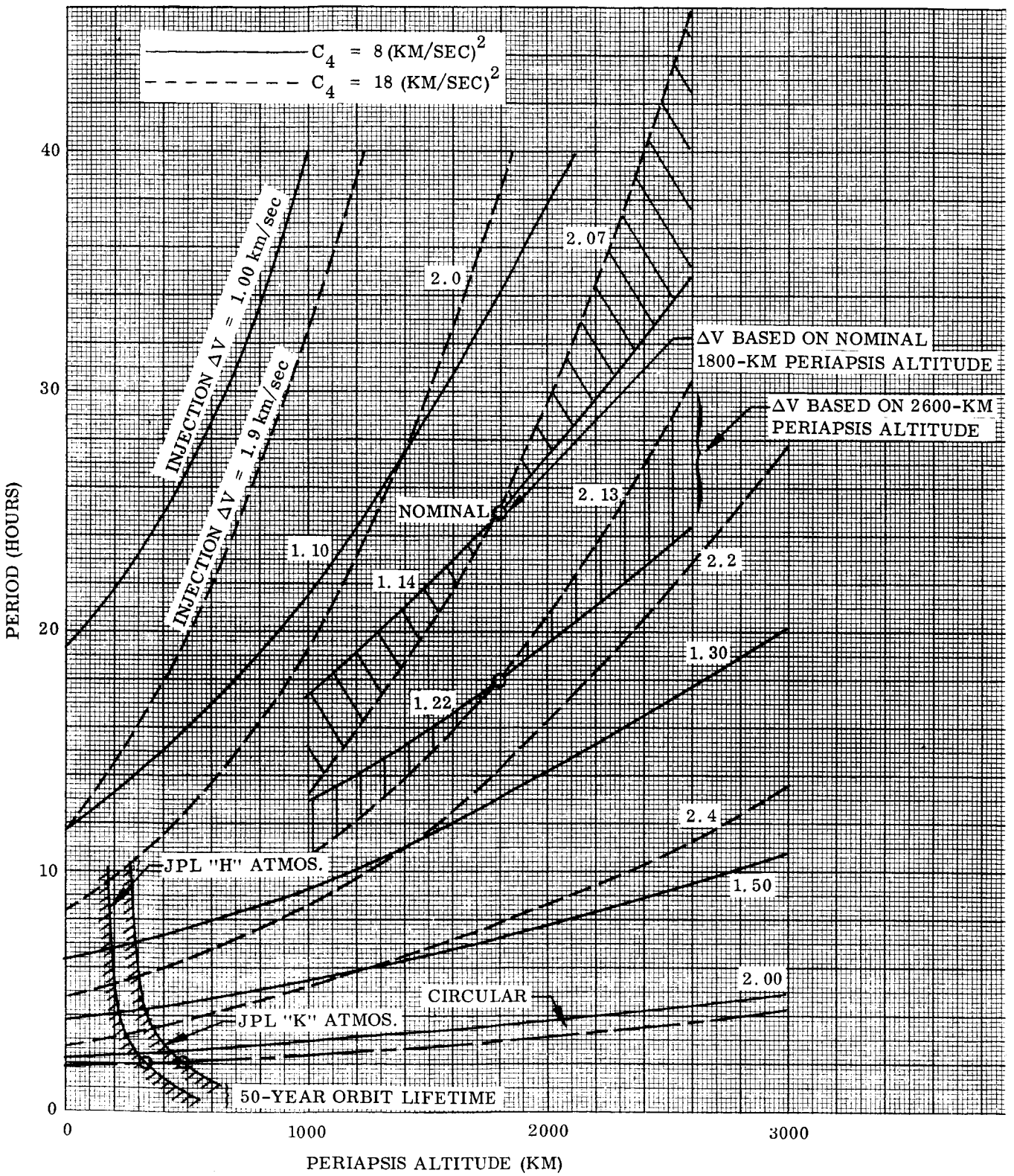


Fig. 3-16 Mars Orbit Characteristics

A third method might be to adjust the orbit period after injection. For the nominal orbit, about 0.3 m/sec. per km initial periapsis error would be required. Since the orbit period is highly sensitive to periapsis altitude, post facto measurement of the approach periapsis by period determination appears practical. The orbit period adjustment is relatively expensive, namely about 13 m/sec/hr of period change. For example, with a 500-m periapsis error, about 40 lb of propellant is required to adjust the period to a nominal 25 hr.

The orientation of the nominal design orbit was selected to satisfy the second major objective of the mission (i.e., to measure Mars diameter), to maintain solar cell power, and to keep Canopus reference in view. An orientation was chosen at Mars encounter to provide the greatest probability of planet occultation for diameter measurements. The highly eccentric orbit allows continuous viewing of both the Sun and Canopus. The periapsis is placed on the sunlit side and yields a relatively high inclination to the Mars equator. The encounter inclination of the orbit was selected at 24.6 deg, and 13.2 deg and 115.3 deg to the ecliptic for 1969 Mars, 1971 Mars, and 1970 Venus, respectively. Initially, the Earth view of the orbit is edge on. This view rotates to become more normal to the orbit plane during the orbital operational lifetime. After six months, the orbit is inclined about 135 deg to the Earth-Mars line-of-sight.

3.3.4 Orbit Variations

Only minor variations in orbit parameters will occur during the six month orbital mission duration. Perturbations to the orbit from Mars oblateness were estimated from currently accepted values based on observations of the moons, Phobos and Deimos. The secular perturbations due to oblateness are given by:

$$d\Omega/d\theta = -J \frac{R^2}{p^2} \cos i \qquad \text{(regression of nodes)}$$

$$d\omega/d\theta = J \frac{R^2}{p^2} \left(2 - \frac{5}{2} \sin i\right) \qquad \text{(rotation of apsides)}$$

The magnitude of these effects was evaluated through the factor $J(R^2/p^2)(d\theta/dt)$ presented in Fig. 3-17 as a function of the semi-major axis of the orbit. The variation in this factor is slight over a range of periapsis altitude from 500 to 2000 km. For a 25 hr orbit period with an 1800 km periapsis altitude, the perturbations will be on the order of 0.1 deg/day. Such a variation in the regression of nodes will not affect the measurements of planet diameter during the occultation period. Over a period of 6 mo, the shift may be sufficient to improve the presently accepted value of J.

3.4 ORBITER INJECTION MANEUVER

The weight in orbit capability presented in Figs. 3-11 and 3-12 was determined for no injection losses. In this Section losses are determined for an injection burn performed in the cruise attitude, that is, with the roll axis oriented toward the sun and the star tracker locked on Canopus. Incorporating this fixed attitude concept into the vehicle design accrues several distinct advantages:

- One attitude maneuver is eliminated at a critical time with a consequent increase in reliability.
- Solar cell power is maintained, permitting use of all electronics during orbit inject without additional battery weight.
- The side-mounted engine design yields a more compact and lighter vehicle and allows a larger maximum capsule diameter.
- The high gain antenna remains pointed toward Earth allowing data transmission during orbit inject.

Propulsion losses, attitude requirements and performance capability were evaluated for three maneuver modes; gravity turn, constant inertial attitude and optimum programmed attitude. The results demonstrated that for any given launch day the constant attitude maneuver is considerably more efficient than the gravity turn and negligible gain is achieved with optimal attitude programming. Furthermore, only moderate propulsion penalty accrues from using a fixed attitude with respect to the Sun, throughout the launch window. The considerations leading to the recommendation of orbit injection from the cruise attitude are developed in the following paragraphs.

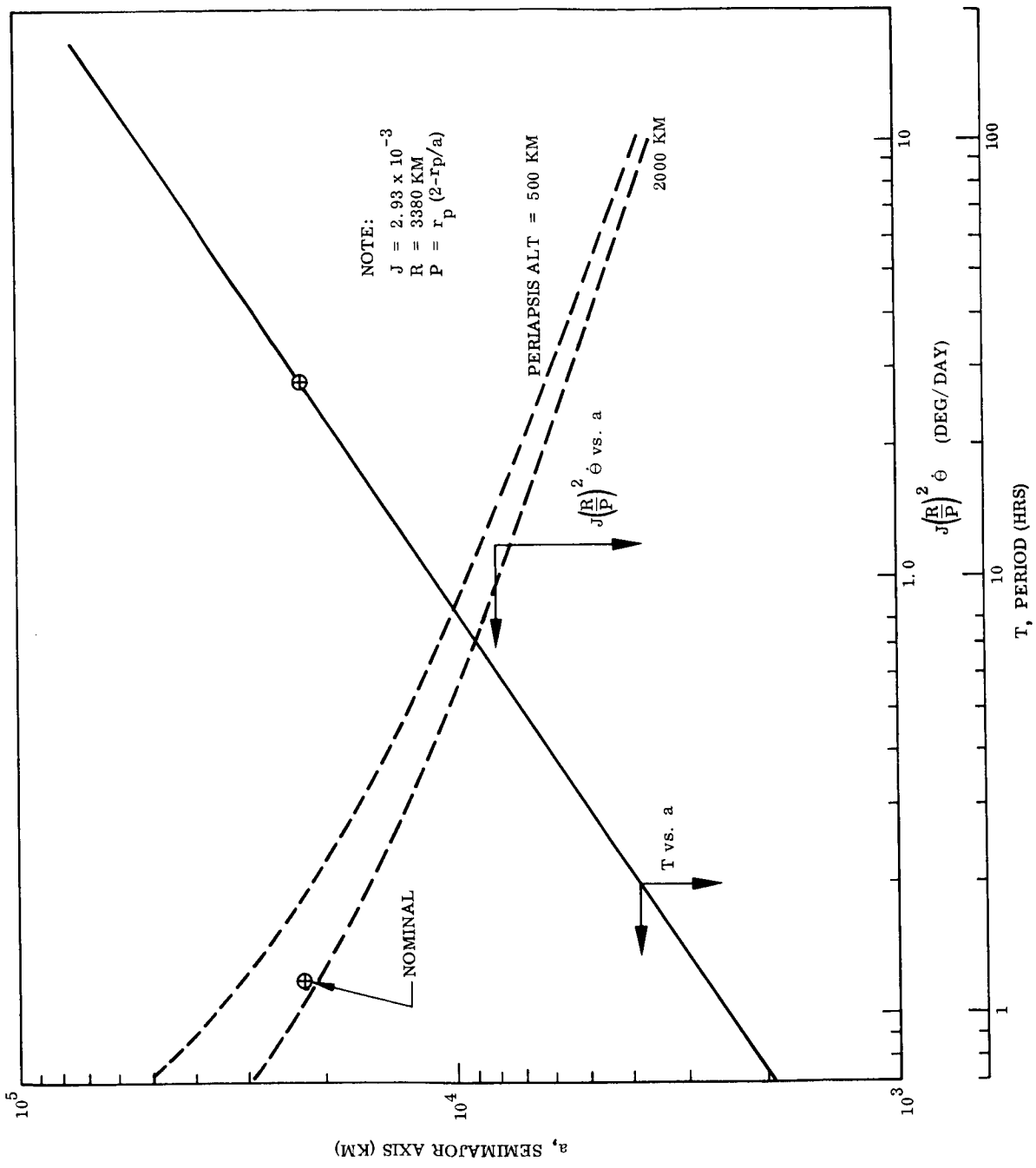


Fig. 3-17 Mars Orbit Variations Due to Oblateness

3.4.1 Orbiter Approach Geometry

The orbiter approach geometry during the Mars 1969 launch window is illustrated in Fig. 3-18 for a periapsis altitude of 1800 km. The direction of the Sun and Earth in the plane of the approach asymptote are depicted for the nominal mission of January 29, 1969 along with the position of the approach hyperbola periapsis for an approach hyperbolic excess velocity, V_H = 4 km/sec (C_4 = 16 km^2/sec^2). The variation and direction of change throughout the thirty-day launch window are shown by the shaded segments and arrows. The corresponding positions and variations of the orbit inject maneuver ignition and burnout are illustrated in a similar manner for the side-mounted engine configuration with a nozzle angle of 89 deg to the spacecraft-Sun line operating in the cruise attitude.

Note that the path of the hyperbola is nearly normal to the direction of the Sun in the region of thrusting and that the trajectory during thrusting deviates only slightly from the vacuum hyperbola. Thus, for a gravity turn, the thrust axis is essentially perpendicular to the Sun direction. This immediately suggested maintaining cruise attitude during thrusting.

3.4.2 Performance Requirements

For this analysis, the inertial thrust attitude angle, ξ, was defined with respect to the local horizontal at burnout (see Fig. 3-18) at the Mars orbit periapsis. Propellant requirements and trajectory characteristics were generated with a 5-D point mass trajectory program incorporating two degrees of attitude programming. The computation was initiated at the burnout point (the 1800 × 36,000 km orbit periapsis) and proceeded "backwards" with increasing mass to a specified hyperbolic energy. Thrust to weight ratios (T/W) between 0.2 and 1.0 at burnout and attitude angles, ξ, between +10 deg and -25 deg were evaluated for a propulsion system effective I_{sp} of 310 sec. Change of I_{sp} to 302 sec will have only slight effect upon these data.

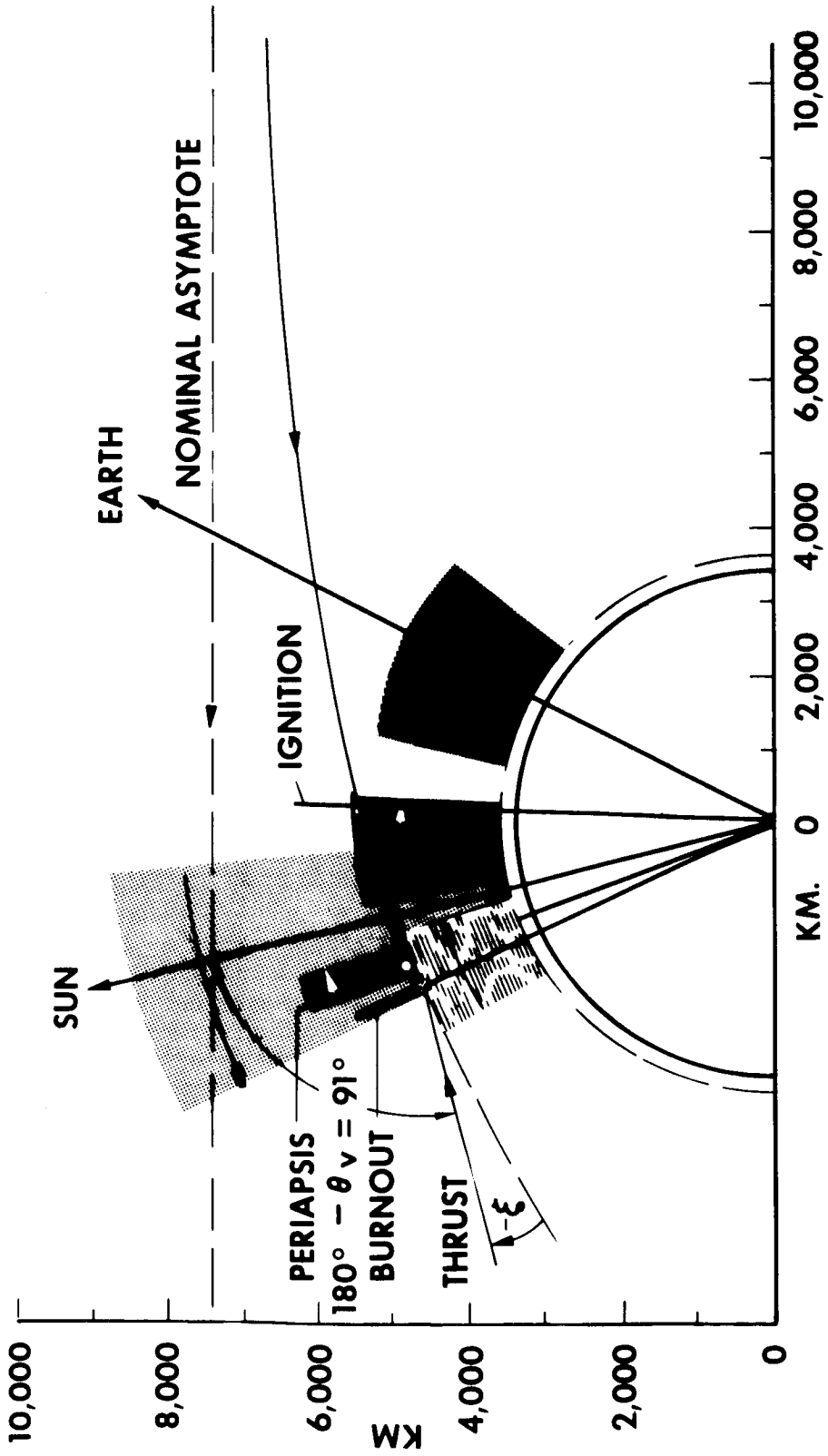


Fig. 3-18 Orbiter Approach and Injection Geometry – Mars 1969

The mass ratio requirements (weight at start of burn/weight at burnout) are seen in Fig. 3-19 to be a function primarily of the approach energy level with lesser effects from final T/W and attitude angle. Mass ratio varies between about 1.75 and 2.0 for the 1969 mission and from about 1.45 to 1.55 in 1971. A final T/W ratio greater than 0.5 appears sufficient to minimize gravity losses.

3.4.3 Maneuver Loss Evaluation

Moderate losses occur for the large variation in thrust attitude angles required as shown in Fig. 3-20 for an 0.6 final T/W ratio throughout the 1969 launch window. The propulsion penalty is presented as a fraction of the impulsive burn mass ratio for each approach energy level. Minimum losses between 0.4 percent to 0.8 percent accrue by employing an attitude maneuver to yield an angle ξ between the thrust vector and the velocity vector at burnout of between 2 deg and 4 deg throughout the thirty day window as indicated by the cross-hatched area. These losses represent a significant performance improvement over the corresponding gravity turn losses of 1.2 percent and 1.8 percent.

The maximum penalty for using a fixed nozzle angle (θ_V) of 89 deg to the spacecraft-Sun line is seen to be about 3 percent. This corresponds to about 22 lb less burnout weight in orbit than for the attitude maneuvering case.

The selection of a fixed nozzle angle for orbit inject in the cruise orientation is more clearly demonstrated in Fig. 3-21. The variation of the angle (θ_V) between the thrust vector and the Sun direction is presented as a function of the angle ξ, with approach speed as the parameter. Contours of maneuver losses are overlaid. The constant thrust angle (θ_V = 89 degrees, for example) is adjusted until the same loss contour is encountered for values of velocity corresponding to the maximum variation over the 1969 launch window (C_4 = 14 to 18 Km^2/sec^2).

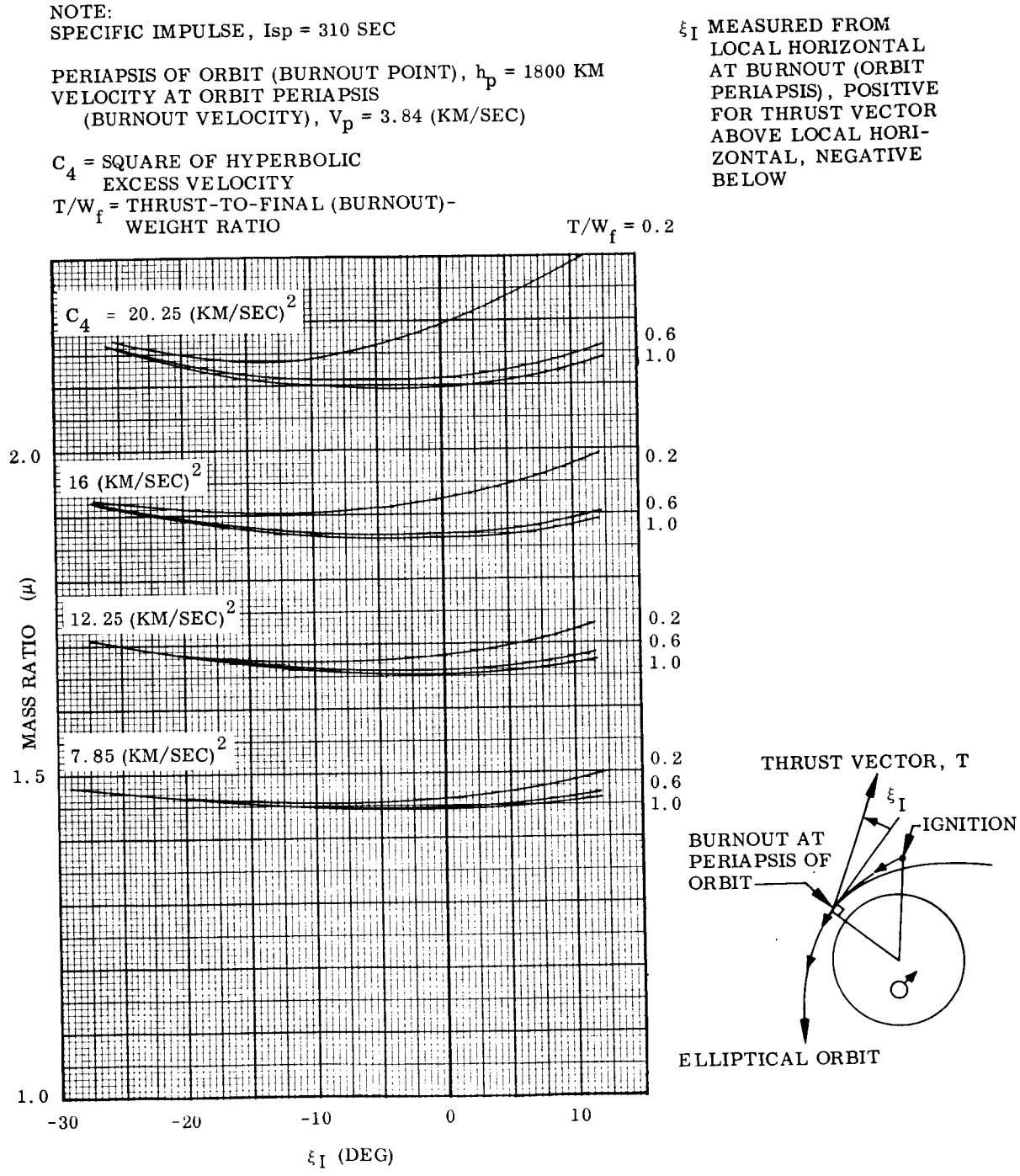


Fig. 3-19 Mass Ratio Requirements for Constant-Thrust Continuous Burn Into Mars Orbit at Constant Inertial Attitude (ξ_I)

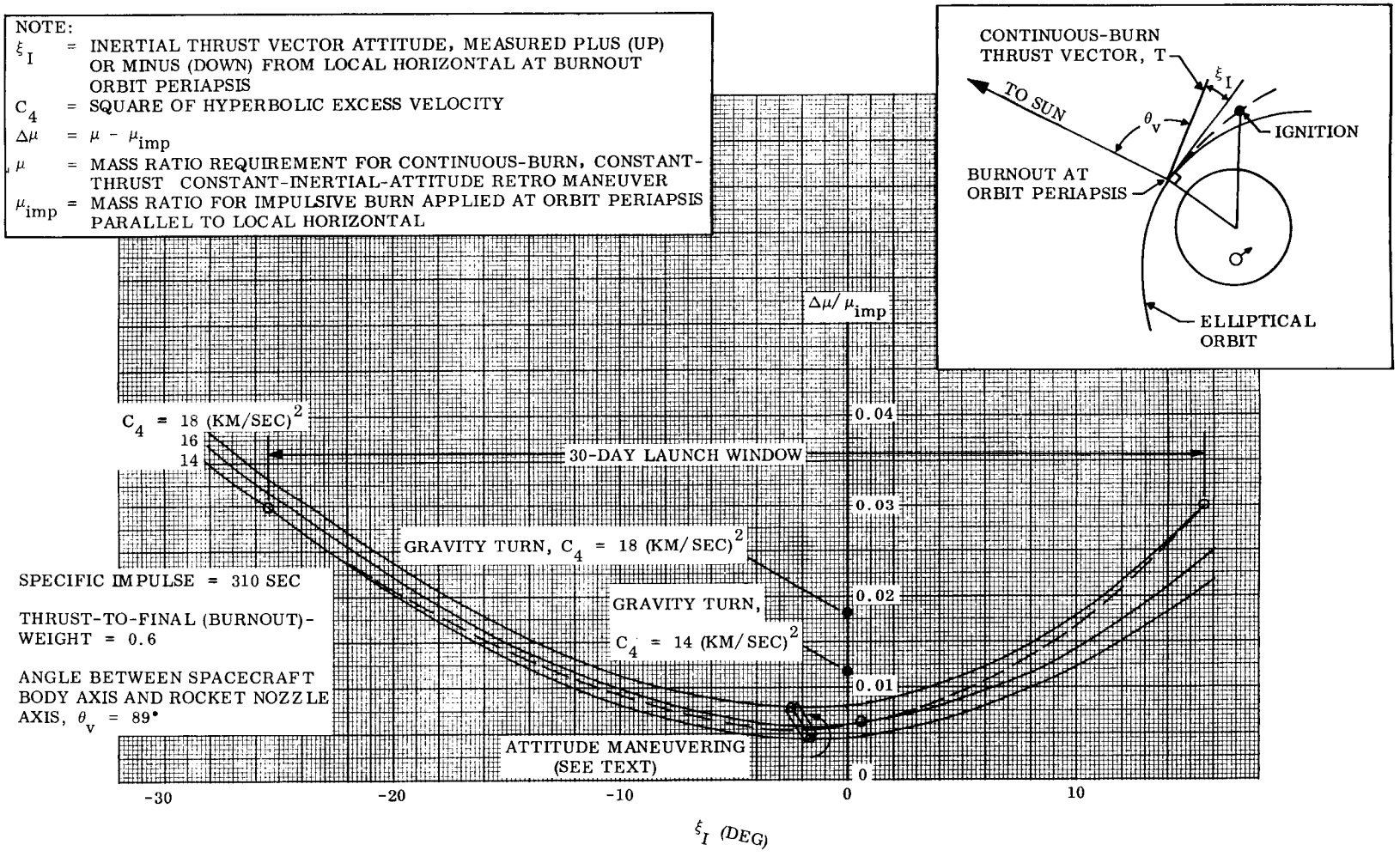


Fig. 3-20 Injection Maneuver Penalties – Mars 1969

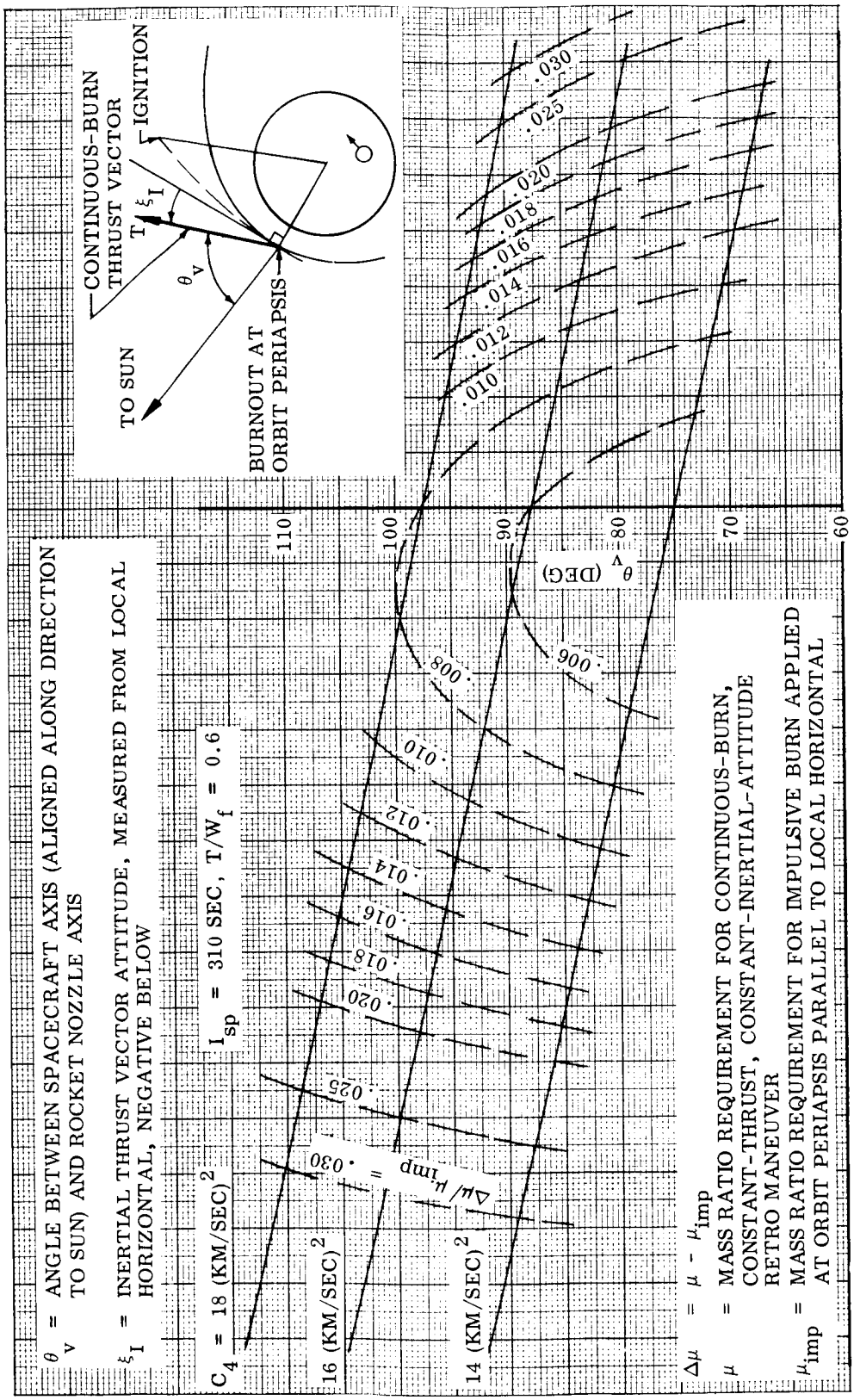


Fig. 3-21 Orbiter Nozzle-Angle Requirements – Mars 1969

In 1971 the approach energy range shifts to C_4 = 7.9 to 8.3 Km^2/sec^2. The selection of a fixed nozzle angle for the 1971 mission is made through use of Fig. 3-22. Here it is shown that the minimum penalty of 0.225 percent or about 3 lb will occur with a thrust angle, θ_V, of 64.5 deg. If the 1969 mission optimum θ_V of 89 deg were retained for the 1971 mission, the resulting penalty would be about 9.5 percent. This corresponds to about 125 lb less burnout weight in orbit than for the optimum angle case. It appears, therefore, that either the engine mounting angle should be changed for the 1971 mission or the concept of injection from the cruise attitude abandoned and an attitude maneuver performed.

3.4.4 Trajectory Changes and Dispersions

Ignition time defined with respect to the time of hyperbolic periapsis passage is shown in Fig. 3-23 to be dependent primarily on approach energy and final thrust to weight ratio. Thrust attitude effects are small.

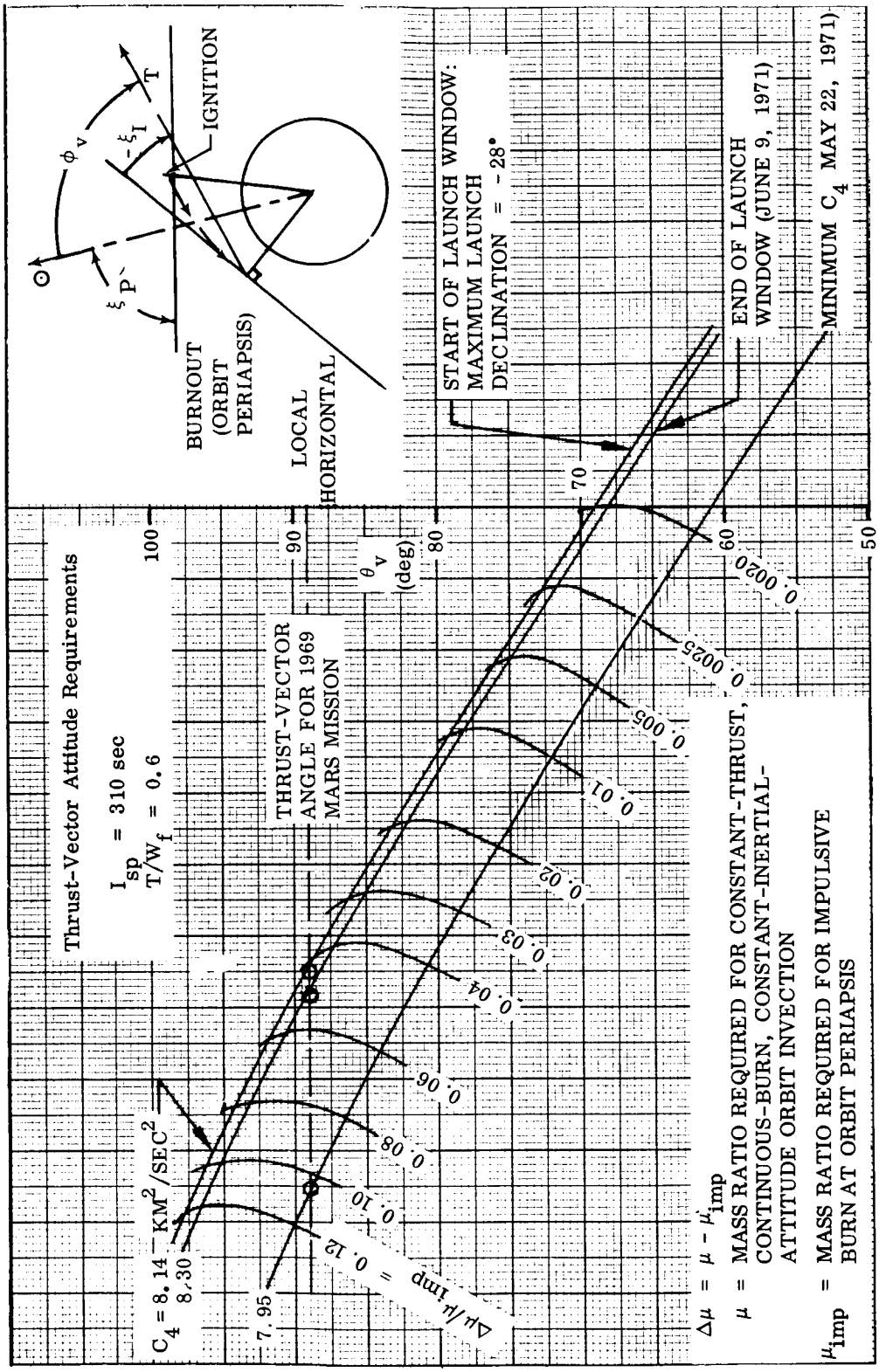


Fig. 3-22 Orbiter Nozzle-Angle Requirements – Mars 1971

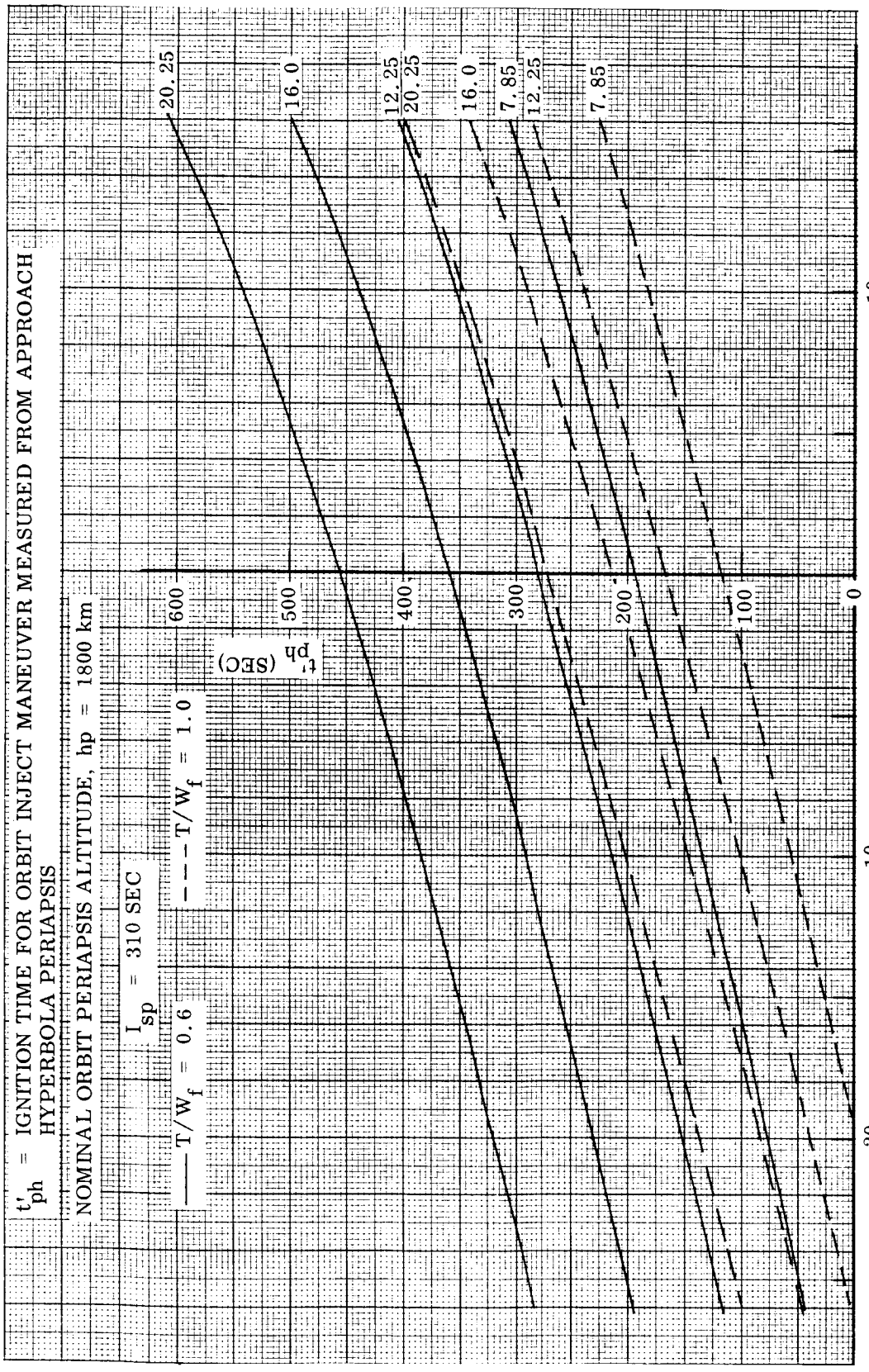


Fig. 3-23 Orbiter Injection Maneuver Ignition Time Requirements

The change in orbit periapsis altitude from the approach (flyby) periapsis altitude is given in Fig. 3-24. The maximum variation for the 1969 Mars orbiter concept selected is about -40 km.

The angular position shift of burnout periapsis is indicated in Fig. 3-25. The variation in true anomaly from the approach periapsis position varies linearly with thrust attitude angle over a maximum range of about +12 deg to -4 deg.

Dispersions of orbit characteristics resulting from injection maneuver and propulsion system errors are significantly smaller than those due to approach guidance tolerances. Figure 3-26 illustrates the effects of in-plane ($\Delta\xi$) and normal ($\Delta\epsilon$) attitude, and propulsion system performance (ΔI_{sp}), on orbit inclination, period and periapsis attitude. Orbit inclination and altitude errors are seen to be essentially negligible. The period errors are moderate when compared to the 12 to 24 hr variation noted in Fig. 3-16.

3.5 ENTRY SYSTEMS

While the main emphasis of the study was placed upon the conceptual design of the orbiter vehicle, the entry system concepts and requirements can exert a major influence. The philosophy adopted in the definition of the entry system was to minimize the requirements imposed upon the orbiter design and operation and to establish the most rugged and least sensitive entry system possible for the environment encountered.

The ballistic blunt body mode of atmospheric entry provides the simplest and most reliable system for unmanned vehicles. The principal restrictions result from the acceleration limits of the scientific instrumentation and structure, from the guidance tolerances to ensure capture by the planetary atmosphere, and from terminal velocity conditions at surface impact. The atmospheric uncertainties encountered at Mars influence the acceleration and guidance restrictions to a moderate degree and exhibit a profound influence upon the terminal velocity condition.

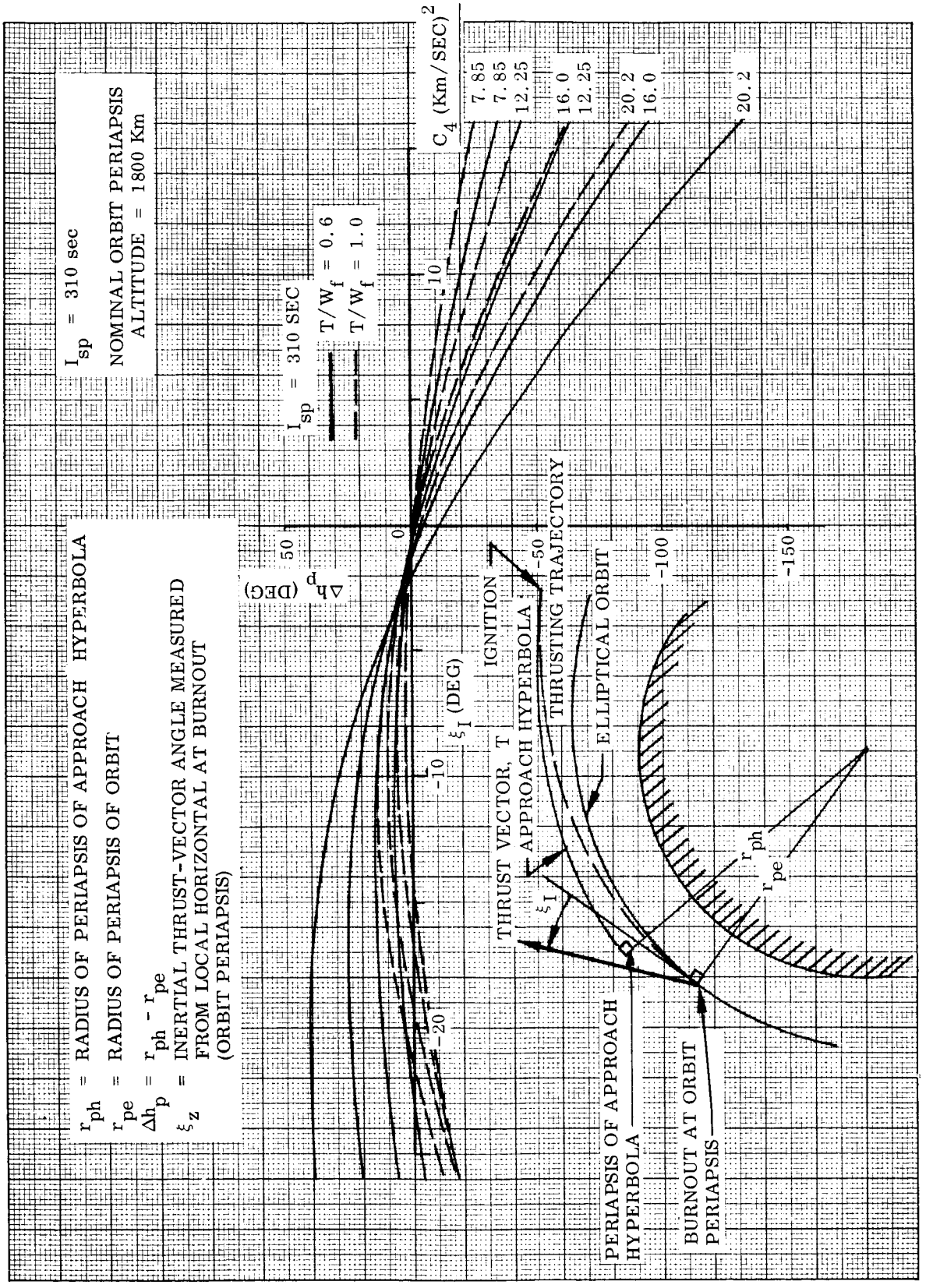


Fig. 3-24 Orbiter Injection Altitude Variations, Mars 1969 and 1971

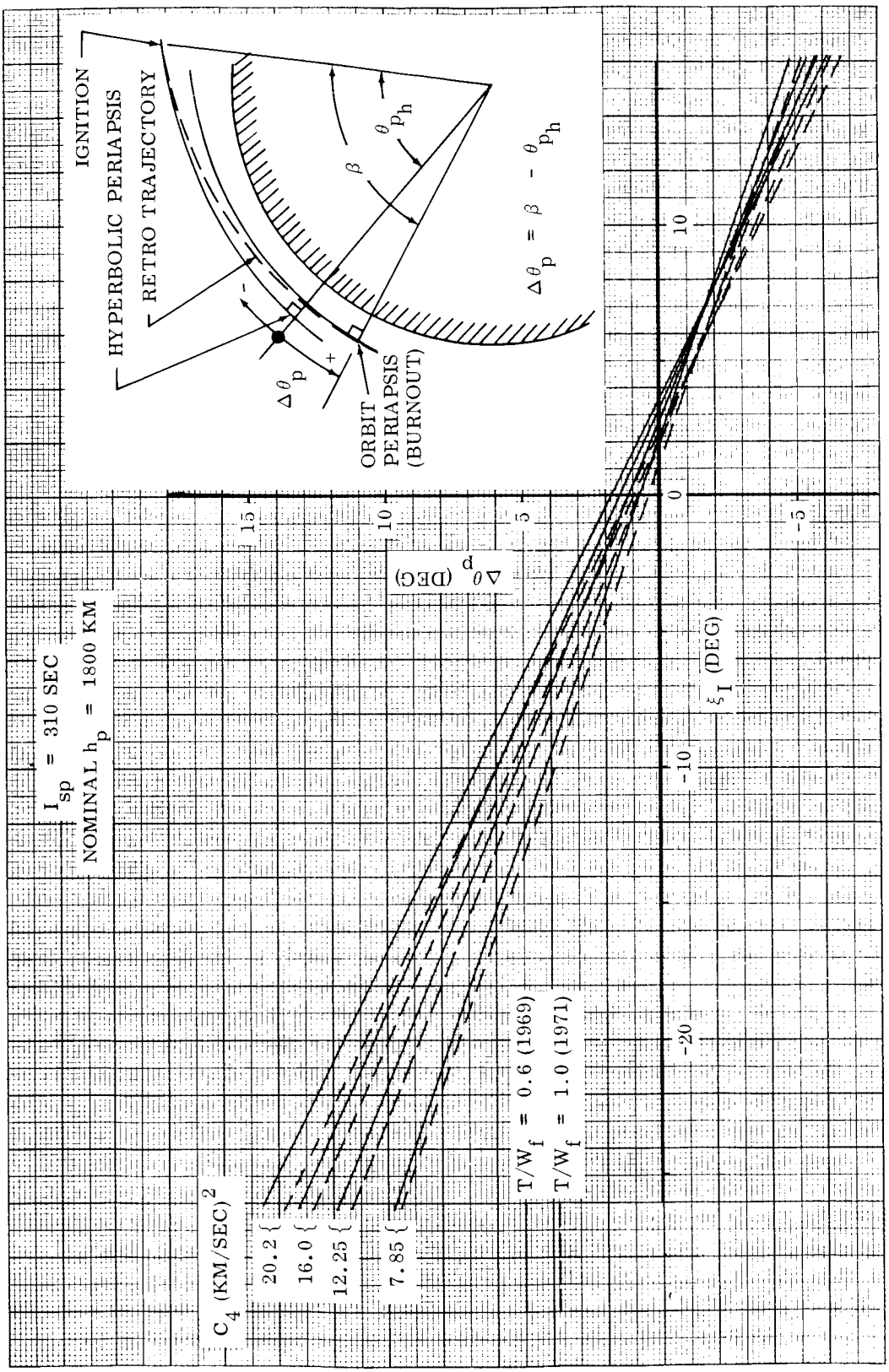


Fig. 3-25 Orbiter Injection Position Variations – Mars 1969 and 1971 (1800 km Orbit Periapsis Altitude)

$\Delta\epsilon$ = THRUST MISALIGNMENT ANGLE, MEASURED NORMAL TO PLANE OF APPROACH HYPERBOLA

$\Delta\xi_I$ = VARIATION IN INERTIAL THRUST-VECTOR ATTITUDE ANGLE

ΔI_{sp} = VARIATION IN SPECIFIC IMPULSE

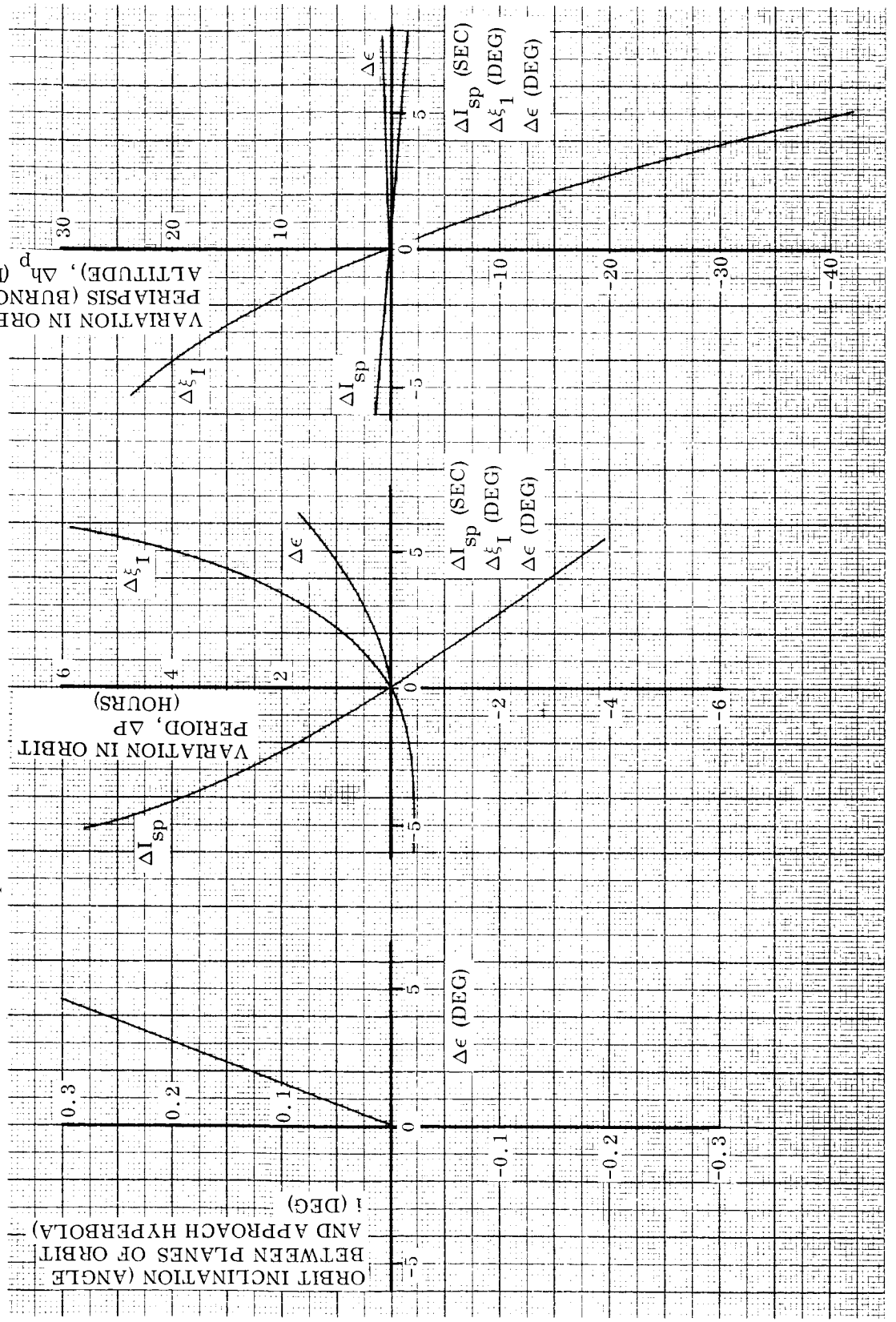


Fig. 3-26 Orbiter Injection Maneuver Dispersions – Mars 1969 and 1971

Within volume and arrangement constraints, the minimum entry vehicle weight will be obtained by the configuration with the highest drag per unit area with minimum heat shield area. A configuration with these attributes and for which aerodynamic and heat transfer data is available is the current Apollo command module configuration. This compact shape lends itself to efficient internal arrangement, provides good stability characteristics, exhibits high drag per unit area, and has a blunt stagnation region shape conducive to reducing the magnitude of the heat transfer rate. Consequently, this configuration was adapted to the Mariner Mars entry capsule with one modification, namely, reducing the length by removing as much of the aft cone apex as possible.

The ground rules for the study included consideration of a heat sterilizable capsule to survive impact, perform biological experiments and communicate data within a period of one day. The requirement for heat sterilization plus the imposition of 200 fps winds near the surface essentially caused elimination of the biological capsule because of excess weight. Utilization of sterile assembly techniques combined with no wind can provide a feasible lander with biological experiments. These conclusions are summarized in Fig. 3-27. The capsule entry weight variation with size is illustrated for sterile assembly and no winds, with scientific instrumentation weighing 9 and 17 lb, respectively. Comparison with the weight-diameter contours for ballistic parameters from 5 to 7 lb/ft^2 indicate a minimum diameter of 57.5 in. and 52 in. for the 17 lb and 9 lb science packages, respectively. The maximum capsule diameter of 76 in. is set by the launch shroud dimensions. A nominal design point of 61-in. diameter was selected for the study on this basis. A W/C_DA of 7 lb/ft^2 represents the maximum entry ballistic parameter yielding subsonic impact and parachute deployment conditions below Mach 2 and above a minimum 15,000-ft altitude. The nominal design point yields an entry weight of 188 lb. Accounting for heat sterilization, 200 fps surface winds and impact against a hard vertical surface yield weighs which are off the figure. By assuming a wind profile similar to Earth's surface winds, as explained later, the crush structure is reduced sufficiently to yield a weight of about 295 lb for the 61-in. diameter capsule. Even projecting this weight to the maximum size yields ballistic factors larger than 7 psf. Hence, the heat sterilizable biological capsule does not appear feasible when the specified wind criteria is imposed. A non-surviving atmosphere

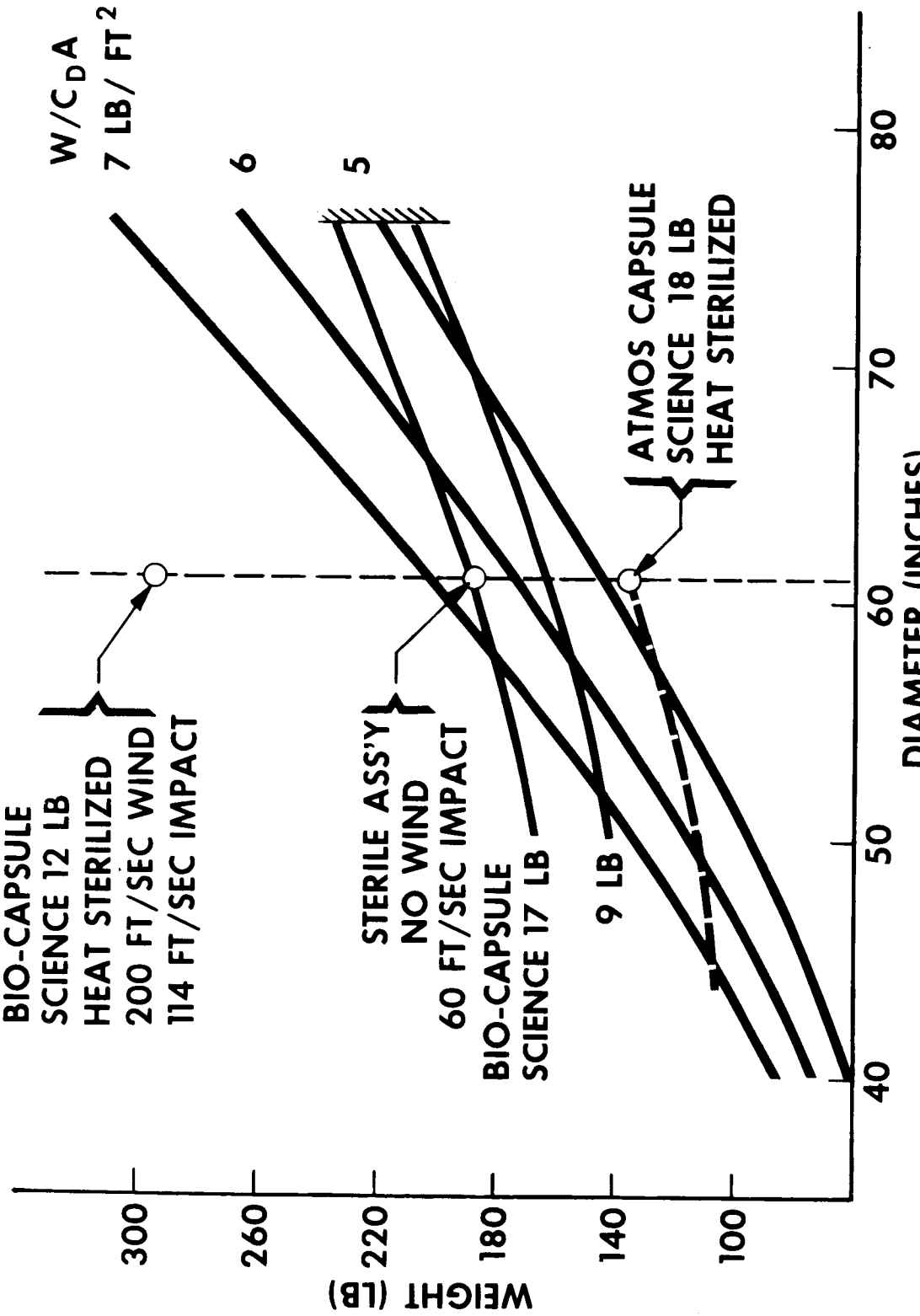


Fig. 3-27 Capsule Entry Weight and Size

72

experiment capsule carrying eighteen pounds of instruments appears practical even with heat sterilization as indicated by the nominal point at 136 pounds entry weight. This is extrapolated to 108 lb for a 45 in. diameter capsule with $W/C_D A = 7$ psf.

The entry system criteria, vehicle selection configuration, design requirements and operational considerations leading to these conclusions are described in the following sections.

3.5.1 Entry Trajectory Criteria

With the specified atmosphere models, the entry problem reduces primarily to slowing the entry capsule to a reasonable touchdown velocity for a survivable biological experiment or providing adequate subsonic flight time for measuring atmospheric properties and data communication to the orbiter. The JPL atmosphere models "G" through "K" characteristics are listed in Table 3-1 and the density profile is given in Fig. 3-2. With limited weight available on the Mariner orbiter mission for addition of an entry system, the cost in terms of heat protection, supporting structure, and parachute system and impact absorption material weight for delivering a given equipment weight to the desired terminal conditions assumes critical importance.

The specified model atmospheres for Mars yield acceleration loadings as shown in Fig. 3-28 for vertical entry at the maximum entry speed for the 1969 mission. The maximum acceleration magnitude is seen to be proportional to the representative scale heights illustrated here. For the extremes of the atmosphere model designated, the maximum acceleration encountered for vertical entry is about 115 Earth G's. This is about one-third of the maximum acceleration for Earth vertical re-entry at orbital speed. The maximum magnitude can vary by a factor of two from the "G" to "K" model atmospheres. Note that the Allen-Eggers analytic solution is in excellent agreement with digitally computed trajectory data shown. Hence, the analytic solutions are useful for demonstrating the influence of the atmospheric parameters upon the environment and design requirement. Furthermore, the Allen-Eggers analytic model is

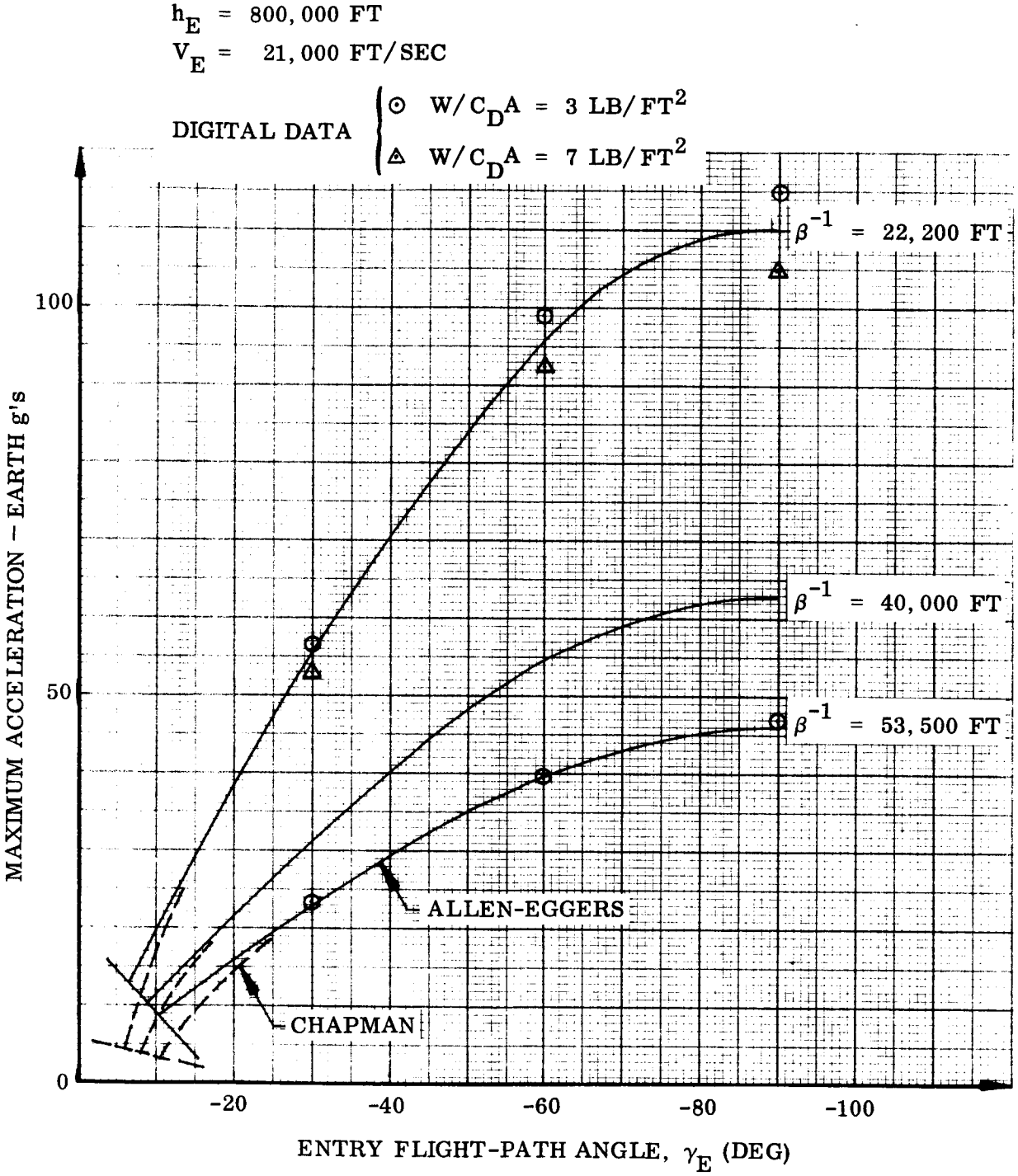


Fig. 3-28 Maximum Acceleration Environment for Ballistic Entry at Mars

especially useful in designing experiments for and interpreting data from an atmosphere capsule.

The minimum entry flight path angle for single pass entry varies between about six to twelve degrees which defines the upper entry corridor boundary. Although the maximum acceleration level is low on the skip-out boundary, a minimum design acceleration of 12 G's is required due to the uncertainties of the atmosphere model. The lower limit (i.e., minimum density gradient, β) of the atmosphere model also defines the upper limit of the entry corridor. The lower limit of the entry corridor is then set by the maximum allowable acceleration tolerance. However, the types of experiments which can be accomplished within a small size and weight capsule and limited data handling capability will require simply and easily defined entry trajectory characteristics. These properties can be best achieved with steep angle trajectories. For Mars, steep entry implies flight path angles greater than thirty degrees.

A significant advantage is gained with steep entry angles by the corresponding reduction in the heating environment encountered. This is demonstrated in Fig. 3-29 where the total convective heat load at a given entry path angle is compared to that for vertical entry. For the example cited, a five-fold increase in the heat load occurs between the skip limit and vertical entry. Since the heat shield weight is proportional to the heat load, a significant reduction in heat shield weight will result for steep entries. With the reduced guidance tolerance, the variation across the design entry corridor is reduced to less than a factor of 1.4. Furthermore, the influence of the atmosphere model uncertainties are slight (about ± 12 percent).

The terminal environment will depend not only upon the density near the surface but on the drag capability of the entry capsule during high speed flight at higher altitudes. This is illustrated in Fig. 3-30 for the model atmosphere extremes with entry at 21,000 fps. Almost 7/8 of the atmosphere is traversed before appreciable deceleration occurs. With shallow entry path, subsonic velocities can be achieved since deceleration occurs at higher altitudes. Velocities representing state-of-the-art parachute deployment capability are reached at relative low altitudes as indicated by the contours on the left side of the figure.

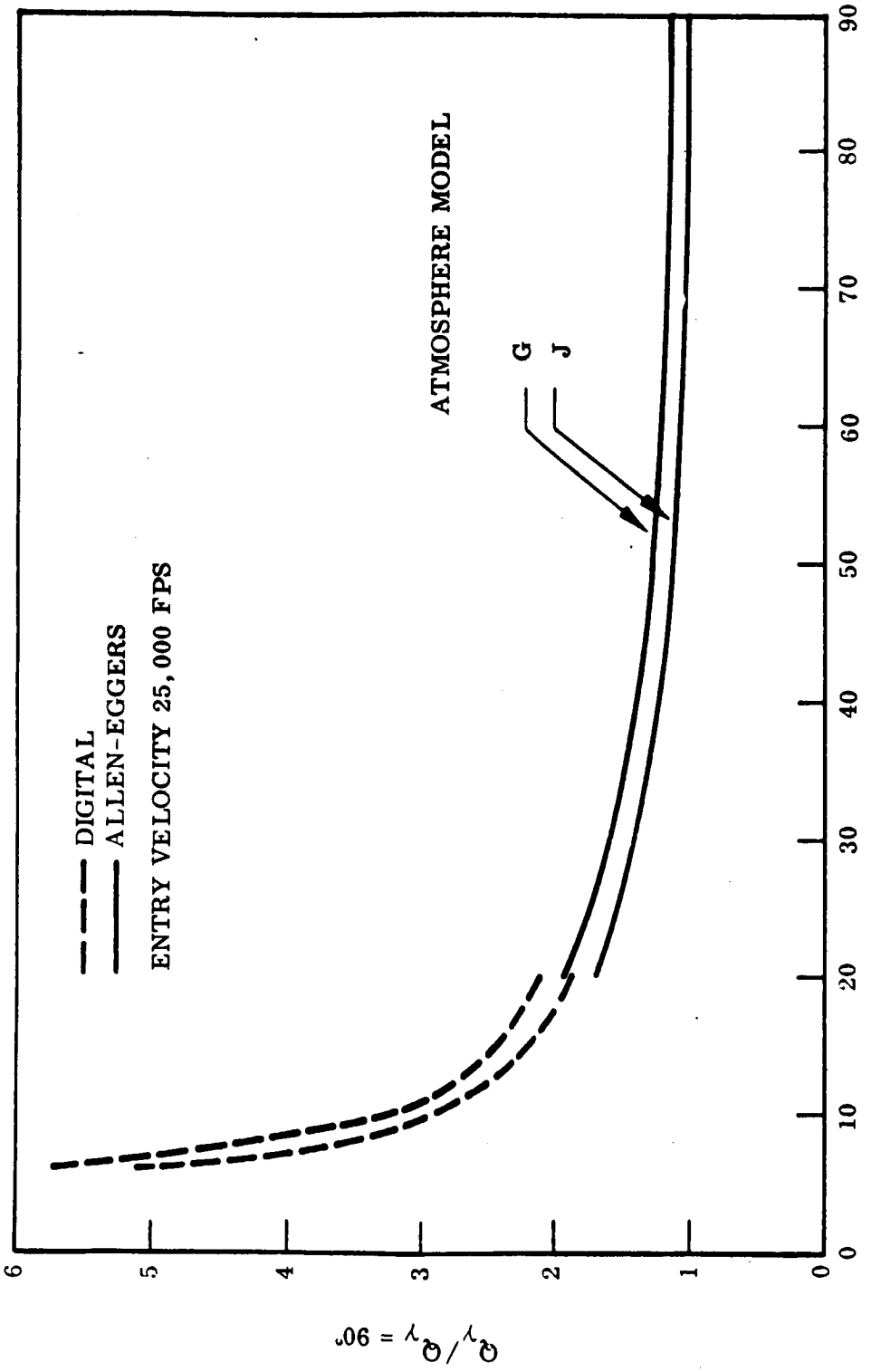


Fig. 3-29 Variation of Convection Heat Load With Entry Path Angle – Mars

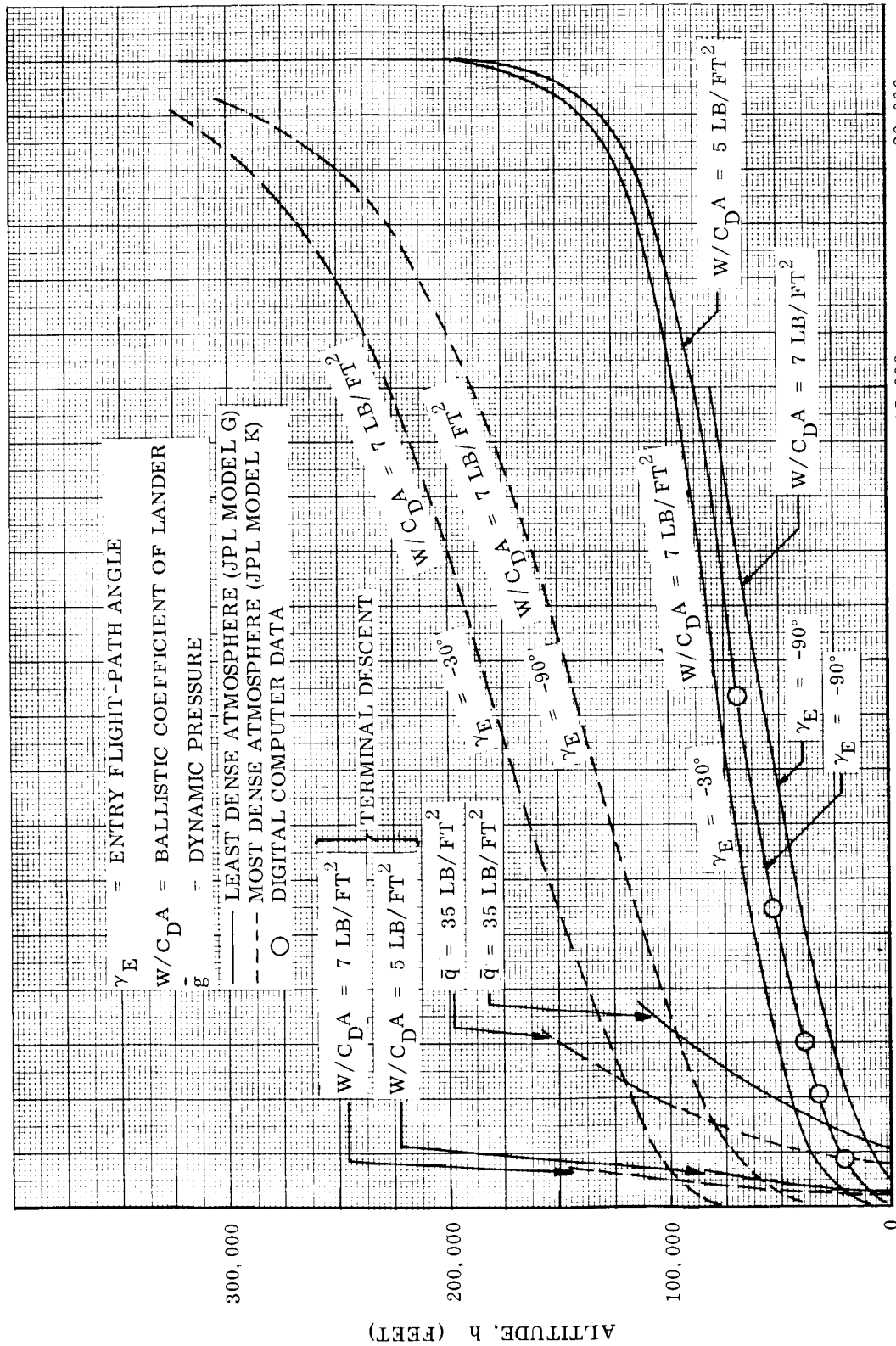


Fig. 3-30 Ballistic Descent Profile – Mars (Entry Velocity, V_E = 21,000 ft/sec
Entry Altitude, h_E = 800,00 ft)

The parachute deployment requirements are presented in Fig. 3-31 in terms of Mach number, ballistic parameter and entry path angle. These data are taken from digital computation incorporating the specified density altitude profile and drag variations with Mach number. The altitude for chute deployment within current state-of-the-art ($M < 2.5$) is seen to be less than 30,000 ft for the steepest entry path in the corridor and a ballistic parameter of 7 lb/ft^2. This represents the most severe design case for the parachute system. In order to increase both chute deployment altitudes and subsonic descent time the entry corridor was chosen between limits of 30 deg and 60 deg. This was just within the tolerance of the guidance system.

The most severe criteria affecting the design requirements for the survivable lander was the 200 fps surface wind coupled with impact against a hard, vertical surface. Also, a parachute designed for a maximum twenty degree angular oscillation amplitude was assumed. These conditions then determine the amount and distribution of the impact attentuation structure for the instrument package. As mentioned previously, the 200 fps wind at the surface required an impractical amount of crushable structure. An interpretation of the wind criteria was developed which led to the wind profile shown in Fig. 3-32. Assuming a surface roughness corresponding to 5 ft diameter boulders and a viscosity similar to Earth's atmosphere resulted in a reduction in the magnitude of the horizontal velocity of the capsule to about 114 fps at a height of 100 ft above the surface. Interpreting the wind criteria in this manner reduces the capsule weight requirements significantly. It is apparent that surface winds may constitute a serious obstacle to performing surface biological experiments.

3.5.2 Entry Dynamics

The allowable entry vehicle guidance thrust attitude, separation rate, and attitude tolerances, and spin rate during entry are governed by the angle of attack permissible at the time of data collection and during certain critical events. The two principal angle-of-attack limitations arise during the period of maximum heating and at parachute deployment. Minimizing the heating of the afterbody requires angle-of-attack covergence to less than 20 deg by the time the altitude of maximum heating is reached. This will

ENTRY ALTITUDE, h_E = 800,000 FT
ENTRY VELOCITY, V_E = 21,000 FT/SEC
JPL MODEL "G" ATMOSPHERE

h = ALTITUDE
$\bar{q}$ = DYNAMIC PRESSURE AT ALTITUDE h
γ_E = ENTRY FLIGHT-PATH ANGLE
M = FREE-STREAM MACH NUMBER AT ALTITUDE h
W/C_DA = BALLISTIC COEFFICIENT OF LANDER

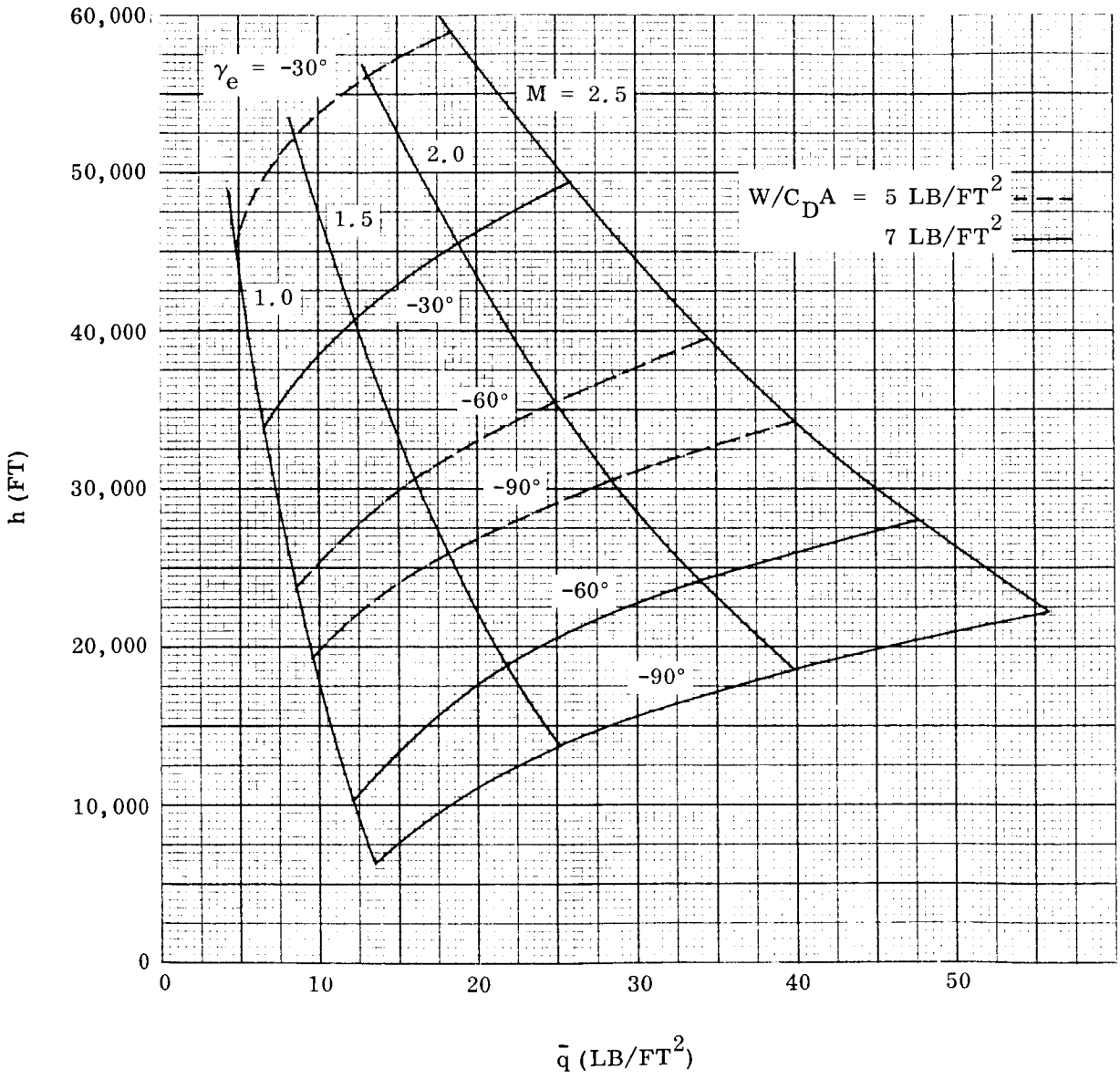


Fig. 3-31 Parachute Deployment Environment – Mars

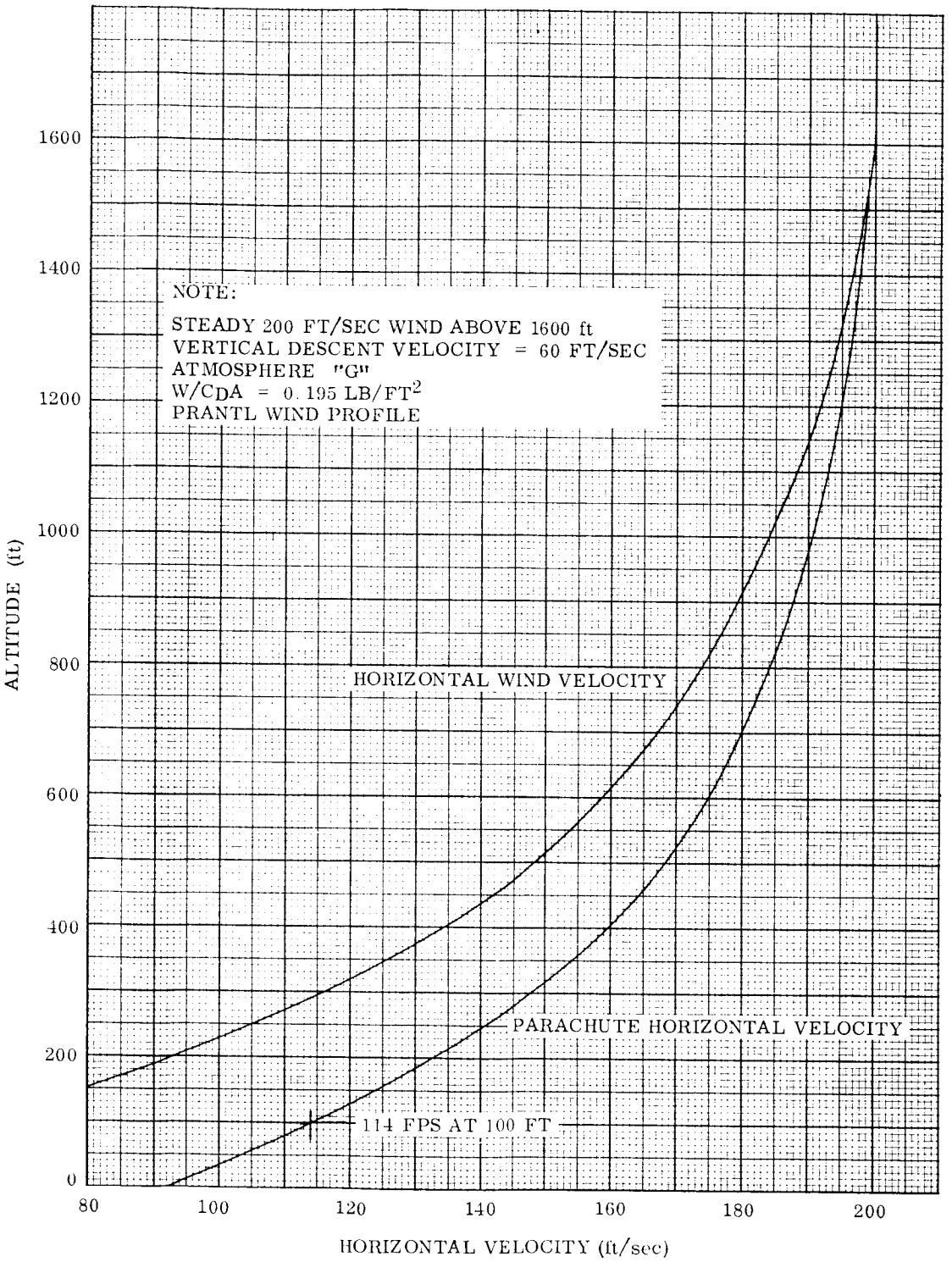


Fig. 3-32 Wind Effect on Capsule Velocity – Mars

ensure a stagnation region on the main heat shield. A similar angle-of-attack limitation (about 45 deg) is required for successful chute deployment.

The angle of attack at these critical times stems from the following:

- Attitude and angular rates of the vehicle at separation
- Thrust misalignment during guidance motor burning
- Trim asymmetries; for blunt configurations, primarily the lateral center of gravity tolerances
- Capsule inertial characteristics

The trim asymmetry effect is best controlled by setting an adequate static restoring moment (C_m/α). The attitude and angular rate allowance are governed by the degree of angle-of-attack convergence by the time of interest. The thrust misalignment effects require either an active attitude control system or spin.

An active control system is costly in weight and complexity and was not considered.

The results of the dynamics evaluation are illustrated in Fig. 3-33 assuming the least dense of the atmosphere models and vertical entry at 25,000 fps. These assumptions impose the most severe conditions upon the angle-of-attack convergence control. An example of the effects of spin and of a change in moment of inertia are shown.

These data show that for the indicated range of inertial characteristics of the capsule, excellent angle-of-attack convergence is possible with no spin. The critical points are designated by the appropriate symbols. For example, with an entry angle-of-attack of 90 deg (but no angular rates), the angle-of-attack is reduced to 8 deg at the maximum heating point and to 6 deg at the altitude of maximum dynamic pressure. Because of the high magnitude of damping parameter for the capsule configuration, the angle-of-attack continues to decrease to about 4 deg at parachute deployment. However, the damping parameter is critically dependent upon the balance between the moment of inertia properties of the capsule and the aerodynamic damping characteristics of the

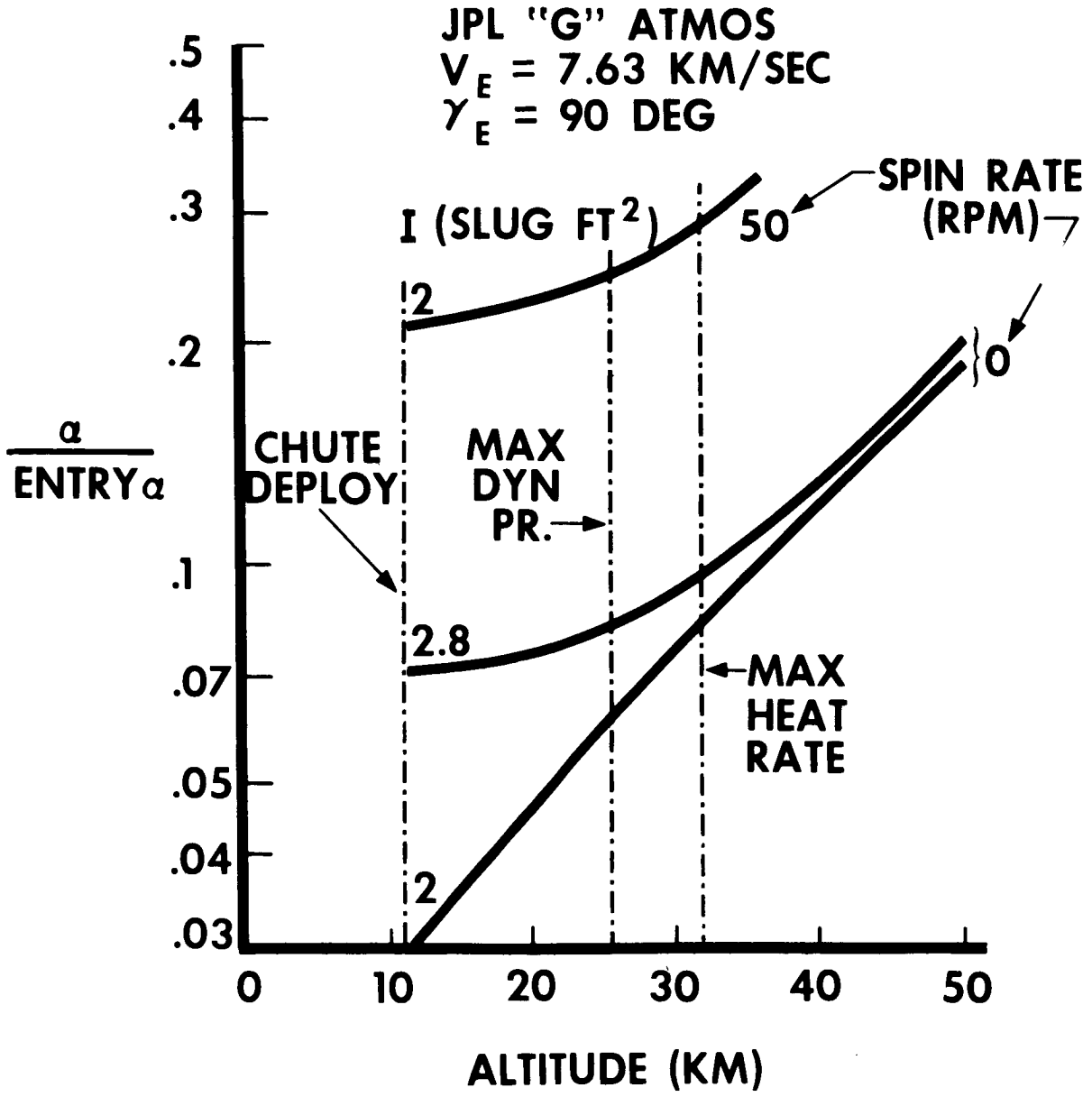


Fig. 3-33 Capsule Angle of Attack Convergence

configuration geometry. The curve labeled with I = 2.8 illustrates that even a change in the damping parameter by a factor of two provides excellent convergence beyond maximum dynamic pressure. The influence of spin is seen to be powerful in resisting the convergence due to the increase in gyroscopic stability. The spin rate of 60 rpm (selected for thrust vector control during guidance rocket thrusting) increases the angle of attack by a factor over three as compared to the no-spin case, when coupled with the worst atmosphere. In this case, the angle limitation during heating cannot be met for large entry angles of attack.

Four solutions are possible to restore the stability necessary: (1) de-spin (2) reduce the spin rate (3) increase aerodynamic stability and (4) reduce entry angle of attack. A de-spin requirement leads to increased weight and complexity and hence reduced reliability. Selection of a lower spin rate is desirable if separation and retro requirements can be satisfied. Increased aerodynamic stability appears to be an effective means of reducing the angle of attack. An increase in C_m/α to 1.6 will provide an improvement by a factor of two. However, this would require adding an extendable aerodynamic surface to the back end of the capsule with a consequent increase in complexity. The afterbody of the Apollo shape adopted for the entry capsule resulted from booster integration and abort requirements. Although sufficient aerodynamic forces are available, the pressure distribution of this aft cone yields a destablizing moment at high angles of attack for any practical center-of-gravity location. This effect is reduced by removing as much of the aft cone as practical. Addition of an aerodynamic sleeve does not appear necessary after considering the efficacy of the fourth listed solution.

The best method is to reduce the initial entry angle of attack by proper application of the separation and guidance maneuver. This was indeed possible as discussed in the following section.

3.5.3 Separation Maneuver and Attitude Control

The selection of the separation point and maneuver requirements depends upon nominal entry trajectory selection, the capsule descent, experiment and data transmission time,

and the proximity of the orbiter injection maneuver and timing requirements. The orbiter and capsule approach geometry presented in Fig. 3-34 illustrates the interaction of these considerations. A typical orbiter approach trajectory for the nominal mission profile (January 29, 1969 launch date) with an approach energy level of 16 km^2/sec^2 and periapsis altitude of 1800 km was selected for this example. Entry trajectories are shown for the extremes of the entry corridor resulting from separation at two days before periapsis. A forward velocity increment of 26 m/sec was applied to provide impact (through the K model atmosphere with parachute) prior to orbiter injection maneuver ignition. The lines of sight at entry and at impact indicate that adquate communication time for atmosphere experiments is attained. The most stringent condition results for shallow entry path angles. For the case illustrated about six minutes between impact and ignition results for a thirty degree entry path, increasing to about sixteen minutes for the sixty degree entry. The line of sight variations indicated by the time indices provide a measure of the orbiter antenna gimbal requirements. With the capsule spin maintaining orientation along the direction of the applied separation velocity, the angle ϵ varies $\pm$ 31 deg throughout shallow entry and about $\pm$ 40 deg for steep entry. Note also that the entry angle of attack is reduced significantly by the additional forward velocity component.

The separation performance requirements are small as demonstrated in Fig. 3-35, for the example cited above. From the curves on the left side, a normal (to the approach asymptote) velocity of less than 50 m/sec will yield entry for separation one day out or greater. This corresponds to about five pounds of propellant for a 200 lb capsule. A two day separation time was selected for the nominal design requirements, yielding a normal velocity component of about 30 m/sec for the selected entry path angle of 45 deg. Differences in the nominal periapsis altitude and approach energy are accounted for by changing the separation time appropriately.

The curves on the right side of Fig. 3-35 show the forward velocity requirements to provide a time increment between capsule impact and orbiter ignition. The case illustrated in Fig. 3-34 is noted in Fig. 3-35 by the dashed lines. Selection of a

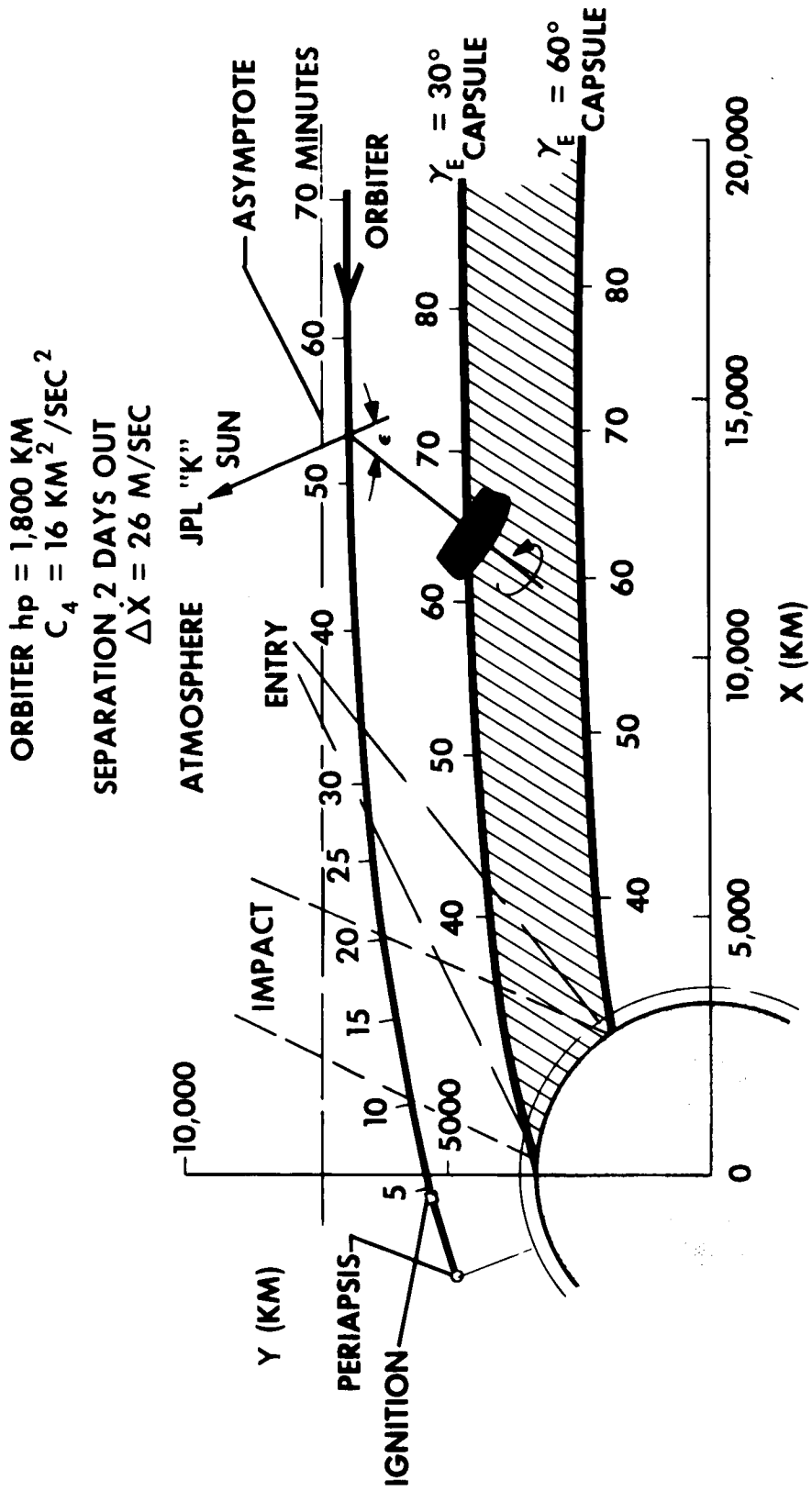


Fig. 3-34 Mars Approach Geometry

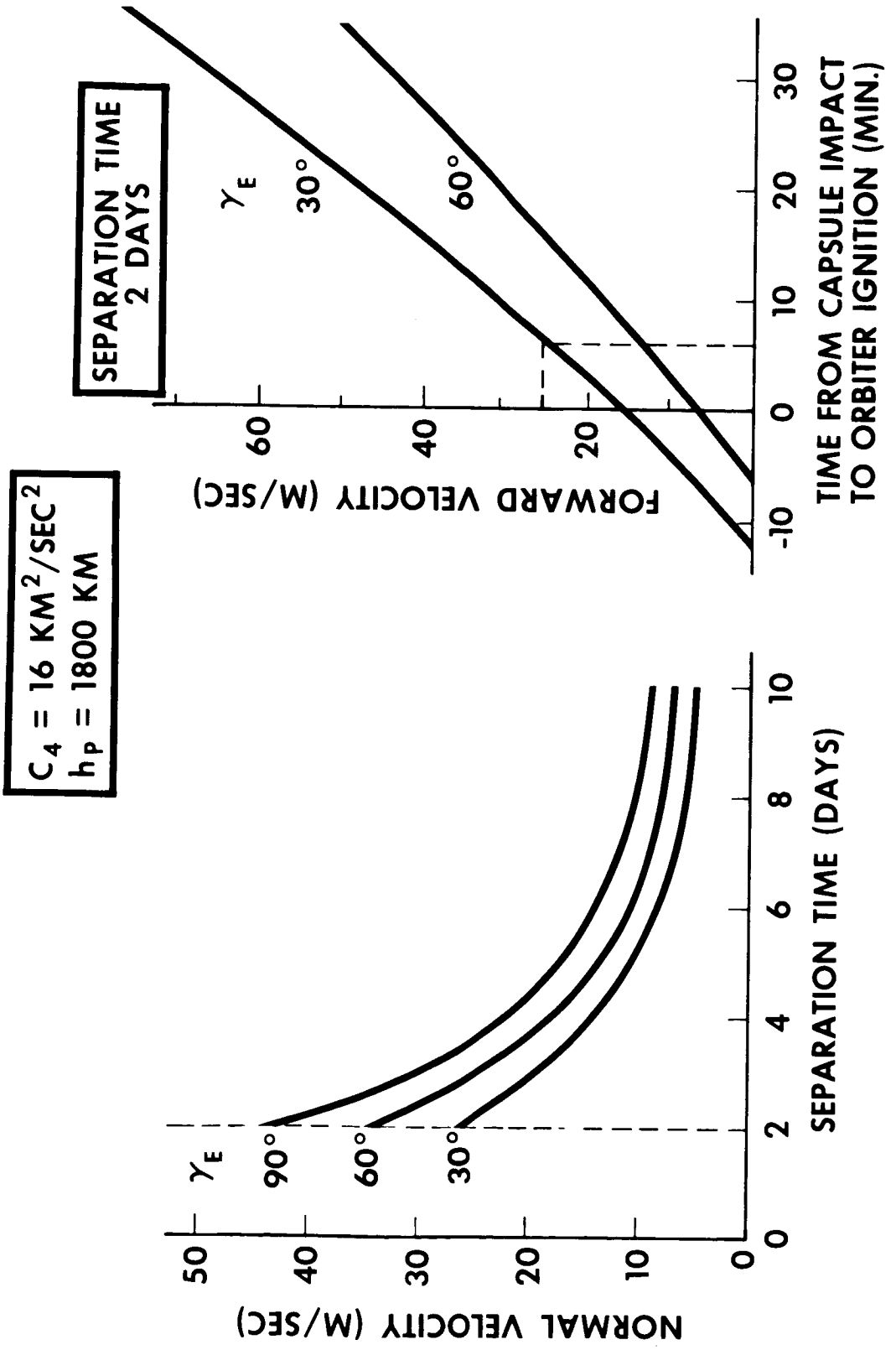


Fig. 3-35 Capsule Separation Velocity Requirements

50 m/sec separation capability for the nominal 45 deg entry angle allows application of 40 m/sec to the forward velocity component. This yields a minimum time increment of 15 min between capsule impact and orbiter ignition for the shallow entry tolerance.

The consequence of approach guidance tolerance upon the orbiter-capsule communication geometry is illustrated in Fig. 3-36 for 50 m/sec separation velocity increment. The minimum time increment of about 17 min occurs for the higher periapsis tolerence of +600 km. The look angle geometry is approximately the same as in Fig. 3-34. The periapsis altitude tolerance increases the antenna angle range by about 1-1/2 deg at entry and 2-1/2 deg at impact. Note again that the entry angle-of-attack is reduced (to about 20 deg).

The influence of the forward velocity addition upon entry angle-of-attack is more succinctly demonstrated in Fig. 3-37. The maximum entry angle-of-attack is less than 30 deg for the most steep trajectory within the corridor. Even for vertical entry, the initial angle-of-attack is only 45 deg. Thus, the angle of attack convergence within the atmosphere is greatly enhanced by adding the forward velocity increment and by the increased approach guidance capability in lowering the periapsis altitude.

A direct consequence of this improved entry attitude control is the elimination of the necessity for capsule de-spin to provide adequate angle-of-attack convergence. Hence, one sequence and operation can be eliminated, simplifying the design and enhancing reliability.

3.5.4 Entry from Orbit Considerations

The possibility of carrying the entry capsule into Mars orbit was suggested as a possible mode for later missions where greater payload capability existed. A few results taken from the LMSC in-house Voyager study (Ref. 3) will serve to illustrate the pertinent considerations.

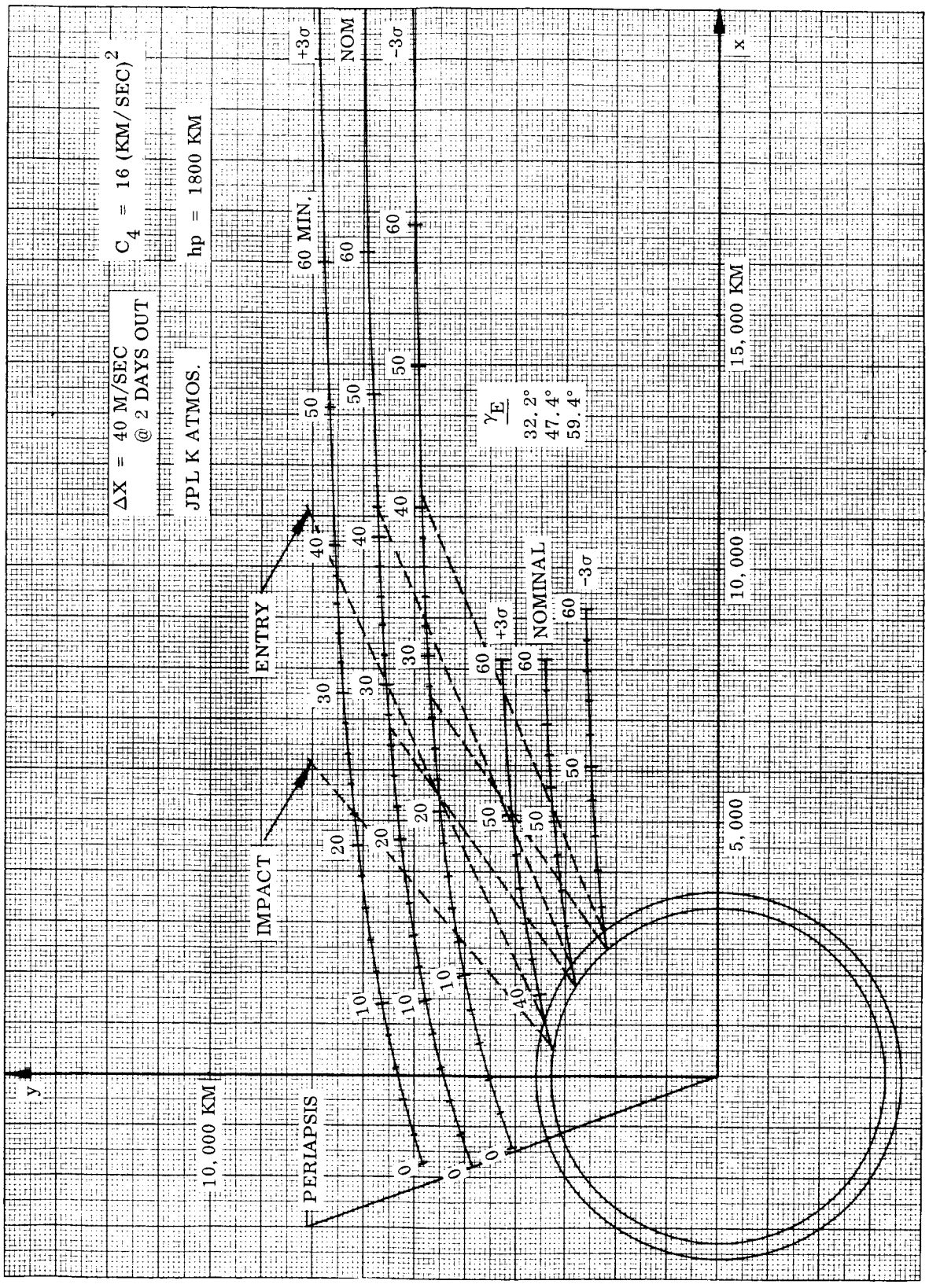


Fig. 3-36 Orbiter-Capsule Approach Geometry Variations With Guidance Tolerances – Mars

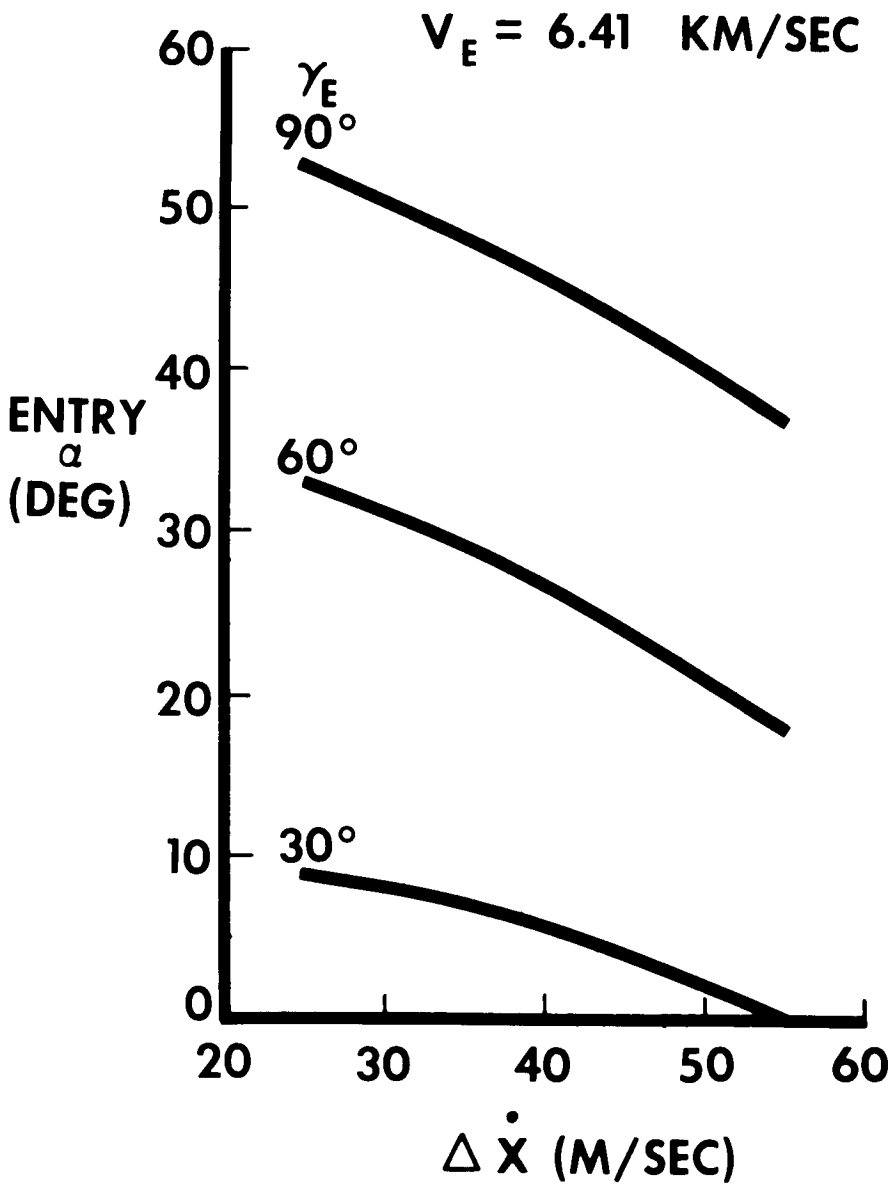


Fig. 3-37 Capsule Entry Attitude

The effect of orbit variations on capsule retro requirements is shown in Fig. 3-38. It is evident that the retro ΔV requirements to obtain a given entry path angle do not vary significantly for wide variations in the orbit periapsis altitude. Further, the sensitivity to retro errors can be essentially eliminated by selecting an entry path angle of 37.5 deg. The corresponding ΔV of 285 m/sec (about twice the minimum) must be reconciled with the increased propulsion system weight. However, the additional propulsion capability yields a greater flexibility in orbit retro maneuver operation.

The retro requirements for landing-point control from the nominal orbit are indicated in Fig. 3-38. The range angle θ is measured from apoapsis. Hence, the landing is fixed by the choice of ΔV and the orbit orientation. The cost of landing-point control is seen to be high for this technique.

The variation of the retropropulsion requirements with orbit position in the nominal Mars orbit are illustrated in Fig. 3-39. While the entry path angle varies significantly, the entry velocity variation is slight. The minimum possible ΔV of 132 m/sec is set by the skip-out boundary and retro exactly at apoapsis. This condition is obviously unrealistic due to guidance and mechanization tolerances. A moderate increase in ΔV to 152 m/sec is seen to provide an orbit position tolerance $\Delta\Phi$ of ± 18 deg. In view of the heat shield weight savings obtained for entry angles greater than 20 deg, the maximum ΔV possible consistent with the propulsion weight increase should be selected.

Thrust vector control of the retro maneuver as considered for the capsule entry is most simply and reliably handled by imparting a suitable spin to the entry vehicle after separation. Separation attitude changes and rate can be held to acceptable levels by current LMSC design techniques, utilized for such vehicles as the Discoverer reentry capsule. The spin rate is selected to provide a "large" number of turns (say ten) during the thrusting period, depending on the expected thrust misalignment and the allowable path deviation. Quite large retro ΔV or deviations appear tolerable

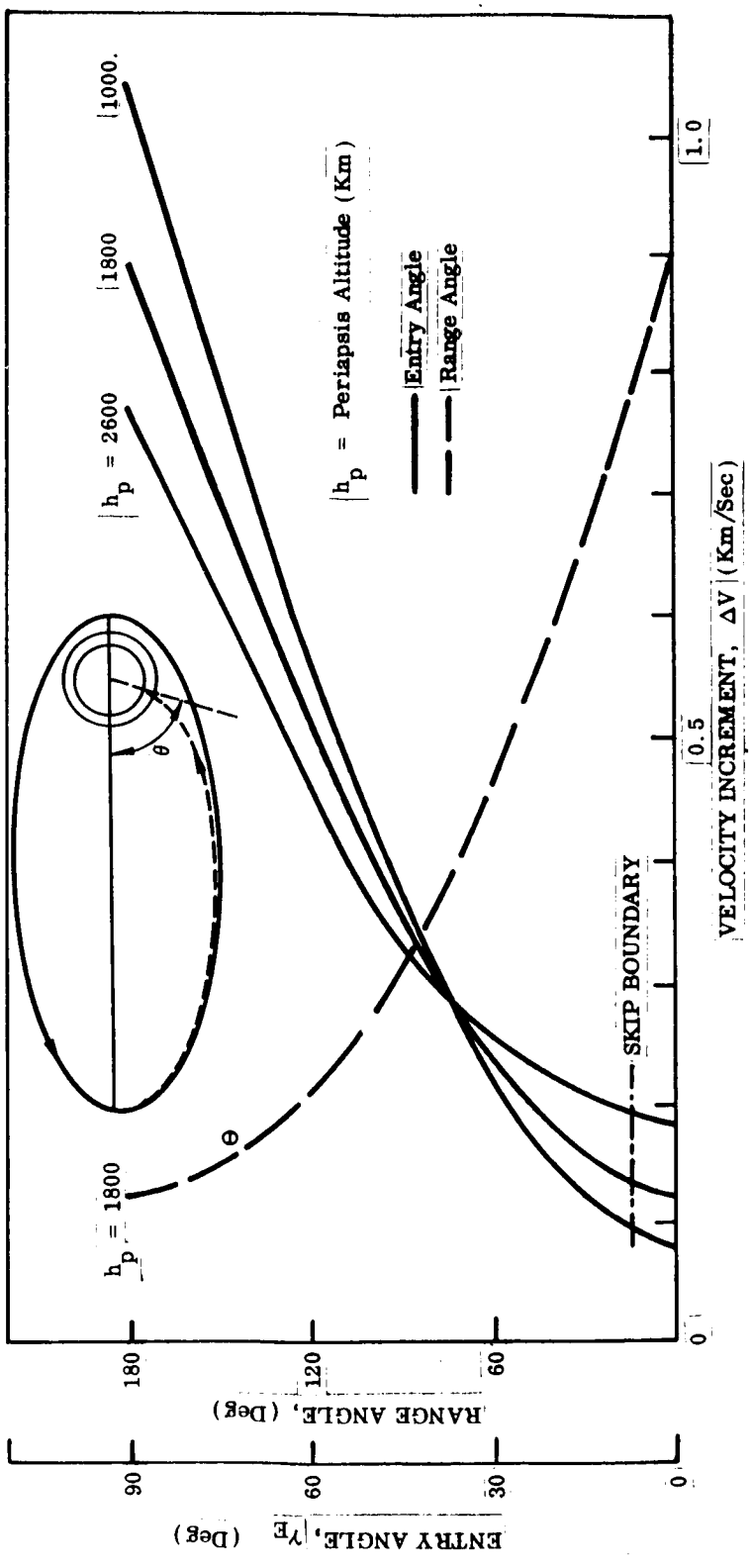


Fig. 3-38 Impulse Requirements for Entry From Orbit – Mars

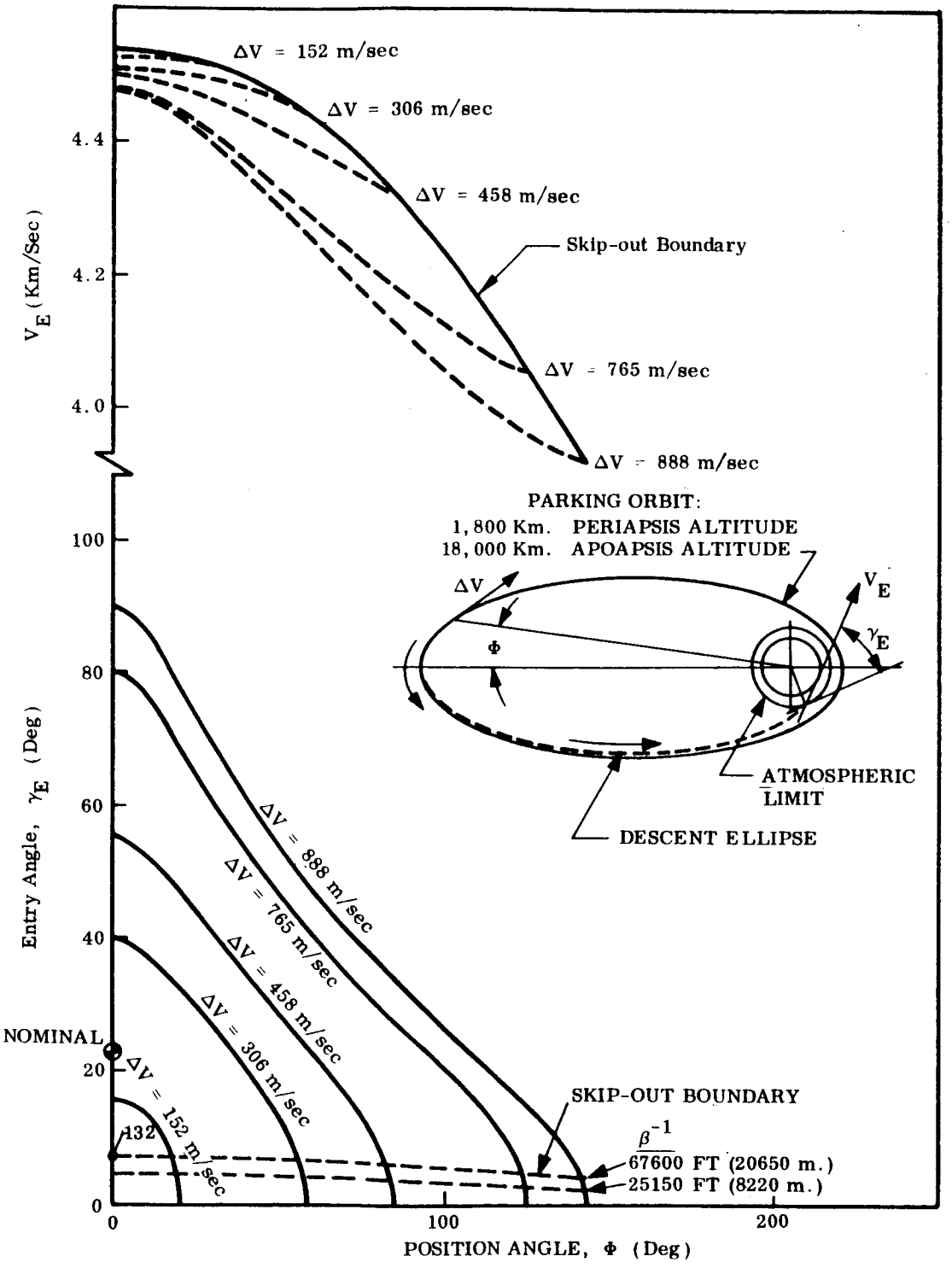


Fig. 3-39 Retromaneuver Requirements for Entry From Orbit – Mars

for the design approach adopted for the entry vehicle in conjunction with the impulse requirements shown in Figs. 3-38 and 3-39.

Good communication between the orbiter and the entry vehicle is maintained for retro in the vicinity of apoapsis, as demonstrated in Fig. 3-40 for any entry path angle. The sighting angles vary over a range of 9 to 30 deg, which will tend to minimize antenna orientation requirements. The geometry illustrated is representative of the range of orbit characteristics shown in Fig. 3-38 and hence such variations will present no communication orientation problem.

The principal differences between entry from orbit and entry from the approach hyperbola are a reduced acceleration and heating environment, and a much larger separation ΔV requirement for the latter. The weight saving on heat shield and structure appears to be considerably less than the penalty for increased ΔV. In addition, the complete entry system must be carried into orbit at a propellant cost equal to the weight of the capsule. Hence, this mode does not appear to be a practical approach for limited payload capability launch vehicles. It may be attractive for a 1971 Mars mission.

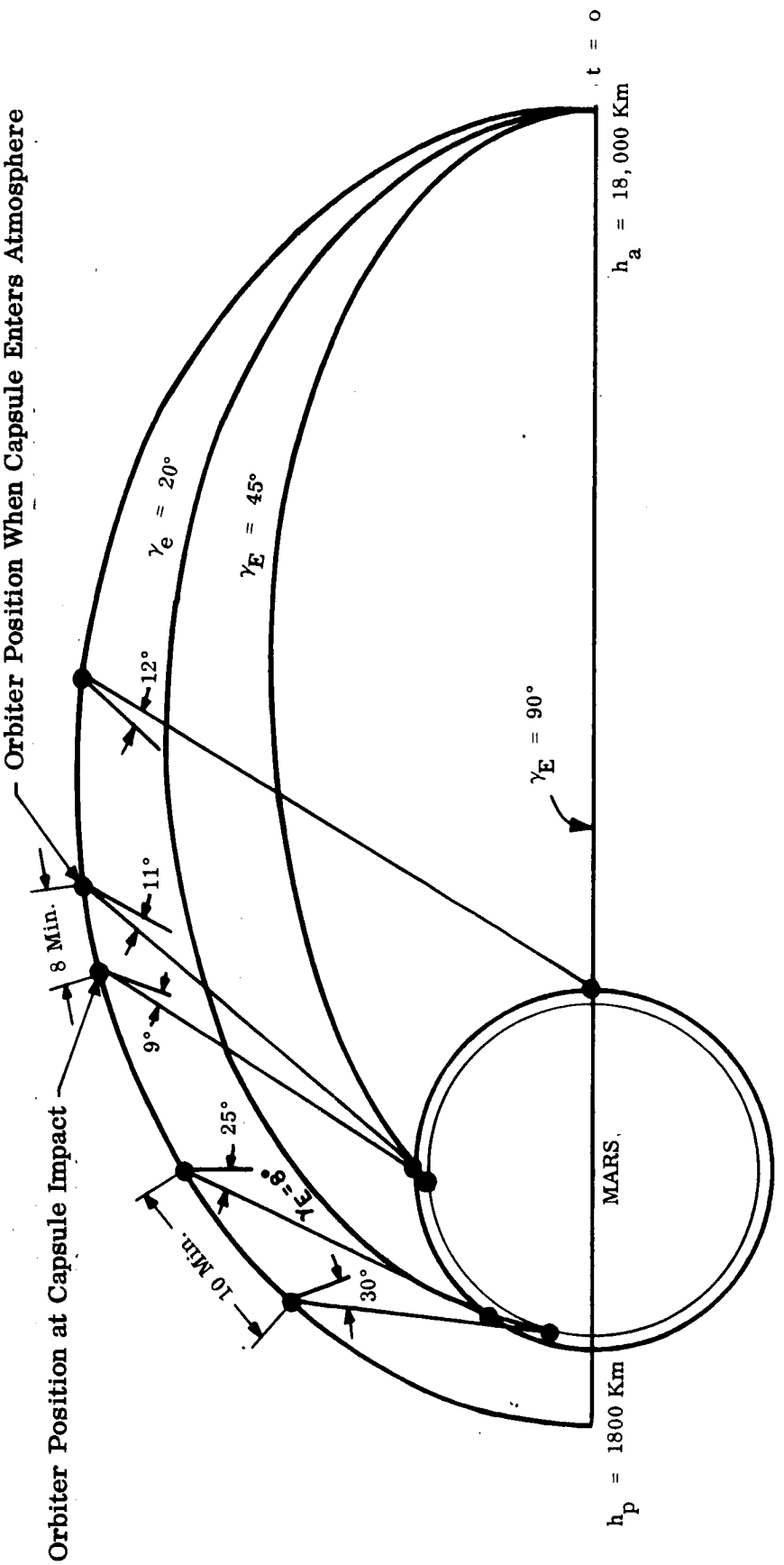


Fig. 3-40 Orbiter Capsule Communications Geometry – Mars Entry From Orbit

Section 4
SYSTEM DESIGN

The approach to design of the Mariner spacecraft was governed by the scientific payload requirements, by the sterilization and reliability requirements, and by the objective to perform all missions with a single spacecraft design.

The scientific payloads as described in Section 5.2 consist of the following main packages:

- Interplanetary experiments
- Mars orbital experiments
- Mars entry and surface experiments

The weight, volume, power, sequencing, and installation requirements for these experimental packages were a primary influence in the design selection.

4.1 SPACECRAFT CONCEPT SELECTION

During the initial phase of the study several spacecraft configurations were investigated and alternate equipment, propulsion and science platform locations were compared. From these early configurations the four most promising designs were selected for further study and analysis. These four configurations are shown in Fig. 4-1.

At the conclusion of the first phase (2 mos) of the study, the selection of a single preferred concept was made from the four basic configurations, and the remaining portion of the study (approximately two months) was spent in refining the preferred concept, Configuration 4.

In each of the configurations the existing static and dynamic payload envelope data provided by JPL in Ref. 2 were used as basic design criteria. These restraints were

used in conjunction with the existing Surveyor shroud geometry and the 57.50 in. diameter interface ring attached to the forward bulkhead of the Centaur.

All of the conceptual designs described in the following paragraphs will require the on-loading of fuel and oxidizer during the Mars 1969 launch window. This will be necessary to take maximum advantage of the launch system payload capability. Existing flight proven hardware, particularly Mariner C components have been used wherever possible. With the exception of Configuration 1, all of the concepts have been designed in such a manner that a capsule can be installed without major modification to the basic orbiter spacecraft.

The selection of a single preferred concept, with emphasis on the hardware requirements this early in the 1969 Mars orbiter program, has been done with the intent of obtaining a sound, representative vehicle into which has been integrated all of the performance and hardware requirements necessary for the mission. The spacecraft weight estimates are therefore considered in greater detail than would have been possible if only parametric data had been used.

At the conclusion of the first phase of the study, a comparison of the weights of Configurations 2, 3, and 4 was made and is presented on Table 4-1.

A summary description of the four basic configurations examined during the study is contained in the following paragraphs and are followed by a detailed description of the preferred concept (Configuration 4).

4.1.1 Configuration 1

This concept is an early design in which the installation of a capsule is not considered. The centrally located propellant tank provides the basic structural element around which are located the electronic and scientific equipment, with the solar panels attached to the lower section of the outer structural ring. The antenna is mounted directly to the oxidizer tank and is enclosed during the launch phase by the booster adapter structure. The main propulsion engine is attached to a gimbal ring supported on a short conical structure attached to the fuel tank.

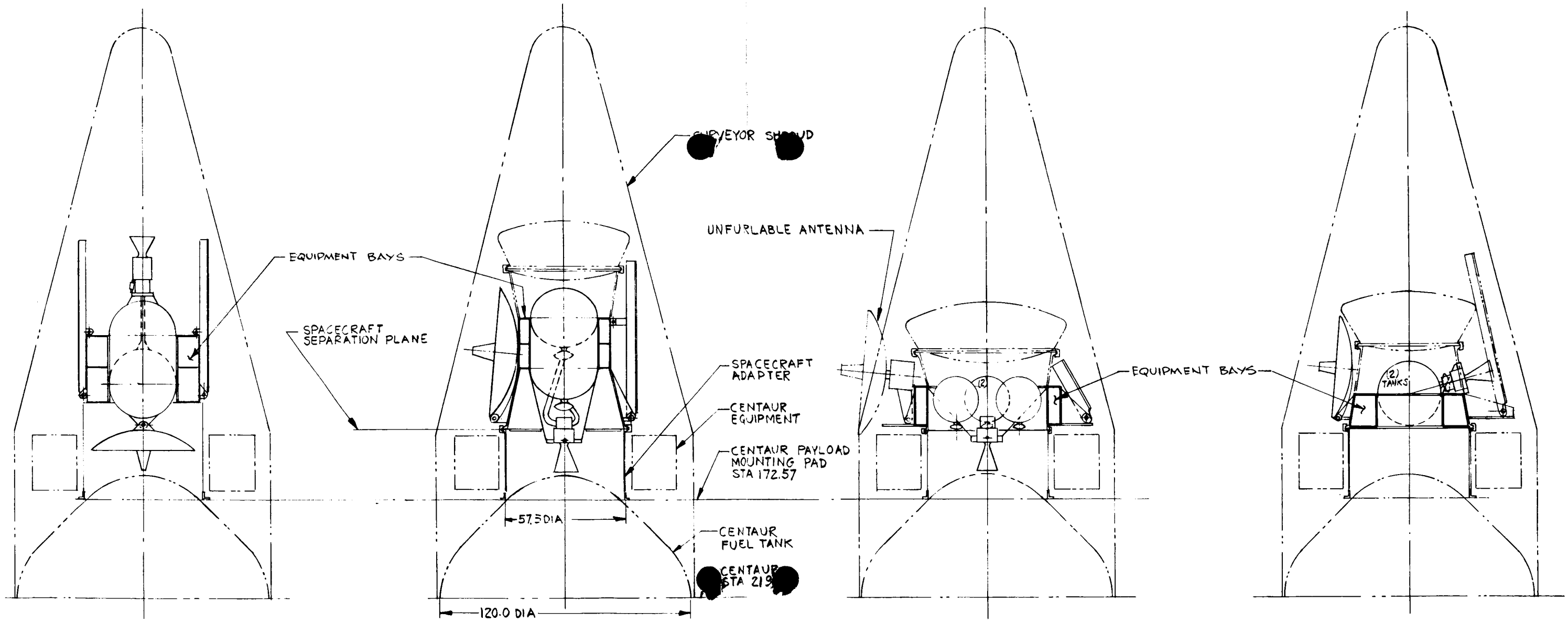


Fig. 4-1 Mars 1969 Orbiter Alternate Configurations

Table 4-1

PRELIMINARY WEIGHT COMPARISON
(BASIC SPACECRAFT)

	Configuration 2	Configuration 3	Configuration 4
Structure	85	80	79
Actuators and Pin Pullers	15	15	15
Insulation and Thermal Cont.	15	14	15
Guidance (100 percent Redundancy)	65	65	65
Engine	20	20	20
Valves and Mtg. Brkts.	10	15	10
Propellant Tanks	50*	25*	25*
Plumbing	10	20*	10
Batteries, Wiring	116	116	116
Solar Panels (51 ft^2 minimum)	51	51	51
Electronics (26 lb Redundancy)	123	123	123
Attitude Control Gas (N_2)	20*	40*	33*
Attitude Control Gas Tanks	25*	45*	38*
Pressurization Gas (He)	4	4	4
Pressurization Gas Tank	21	21	21
TOTAL	630 lbs	654 lbs	625 lbs

*Denotes major differences.

Although this concept results in a very compact design it was dropped early in the study because major modifications would be required to install a capsule, and it would have only a slight weight advantage over Configuration 2. In addition it was found that with the antenna mounted below the solar panels, the required look angles could not be achieved. During separation of the spacecraft from the Centaur, extreme care would be necessary to ensure that the antenna edge ring does not impinge upon the Centaur adapter structure.

4.1.2 Configuration 2

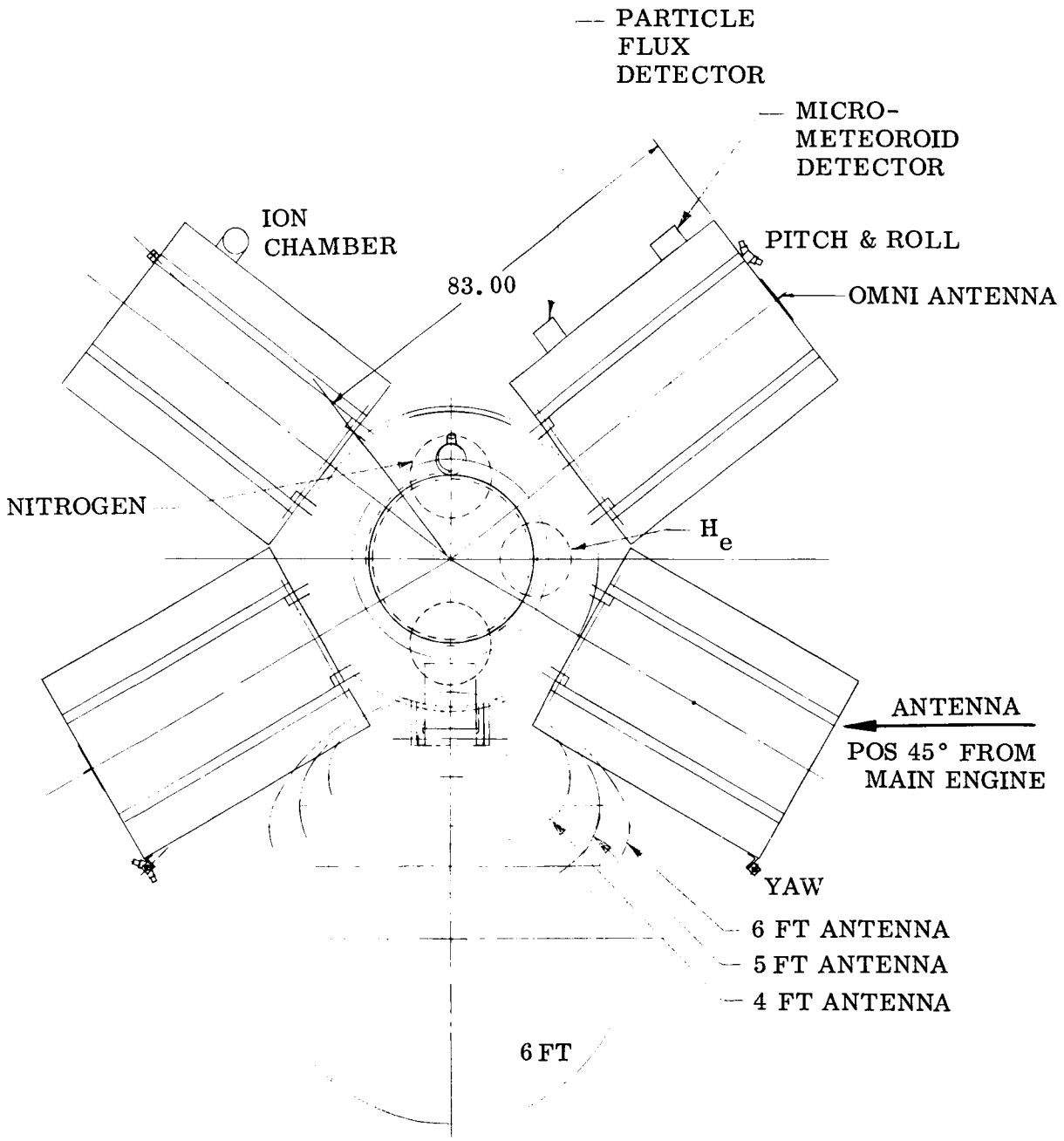
This is a combined orbiter/capsule concept utilizing the same tank arrangement as Configuration 1, but with the tankage reversed and the propulsion unit installed on the aft dome of the tanks on the centerline of the vehicle. This arrangement permits a shorter length booster adapter and better clearances for spacecraft/booster separation.

Inboard profiles of Configuration 2 with and without a capsule are shown on Fig. 4-2 and Fig. 4-3, respectively. Both of these drawings show unfurlable antennas with diameters ranging from 4 ft to 6 ft; however a rigid antenna of 4 ft diameter could be installed on either design.

The major features of this concept are:

- Accepts 61-in. diameter capsule.
- Utilizes Mariner C solar panels.
- Center of Gravity shift during engine burn is along thrust axis, reducing engine gimbal angles.
- Single, compartmented propellant tank.
- Long overall length gives least moment of inertia in the roll axis, requiring less attitude control gas than the shorter vehicles.
- Requires large structural support cone between Centaur adapter and spacecraft equipment bay.
- Scientific equipment mounted on forward end of equipment bay is well clear of any possible impingement from the exhaust plume of the main propulsion unit.
- Antenna look angles (these became more severe after the layouts were made) will be difficult to achieve because of the engine nozzle protrusion.

The propellant tank is a single welded pressure vessel with a central, integral bulkhead separating the fuel from the oxidizer. To obtain a minimum length tank, elliptical domes have been used, the ellipsoids have a semimajor to semiminor axes ratio of $\sqrt{2}$:1 to eliminate the possibility of compressive stresses in the domes.



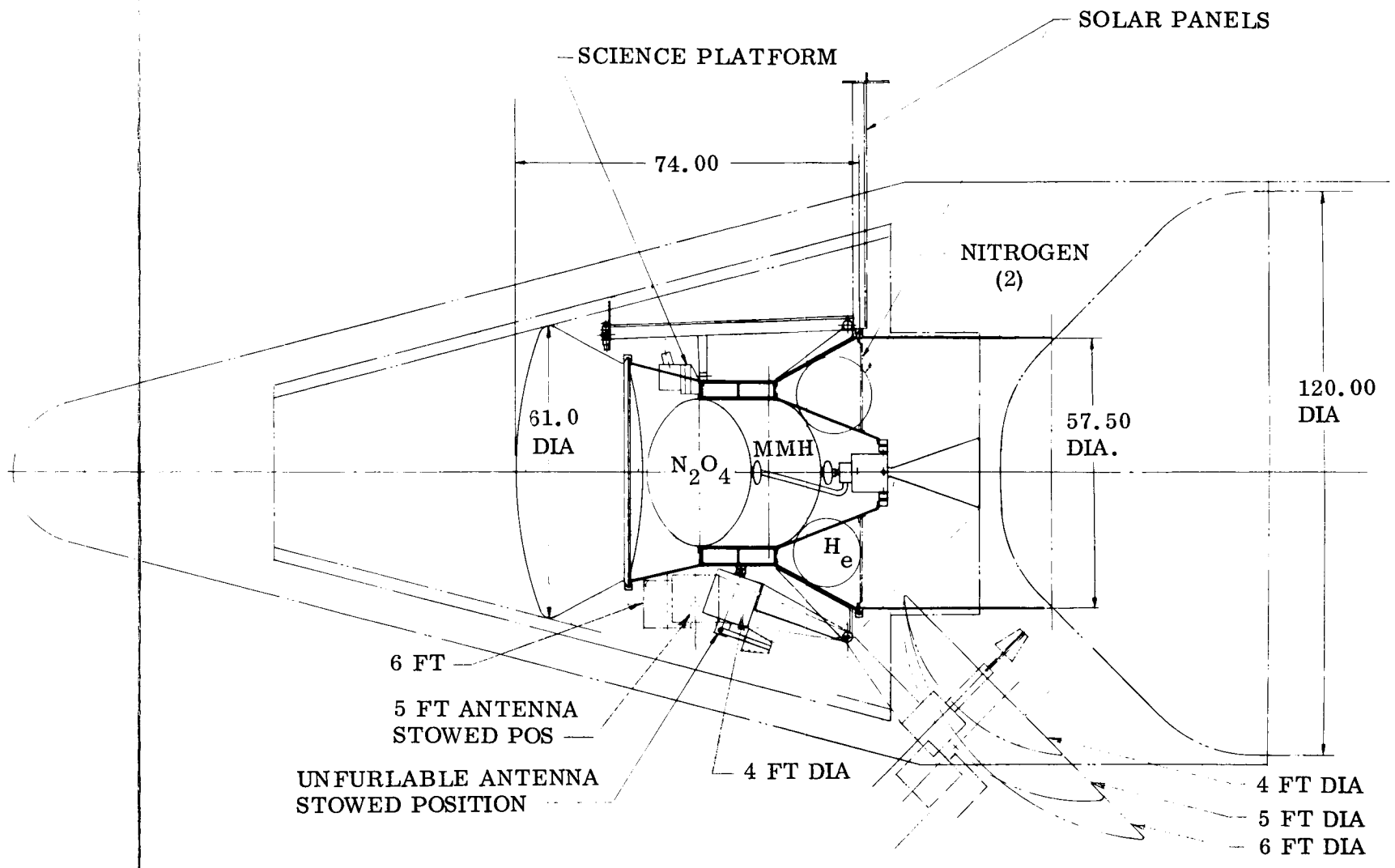
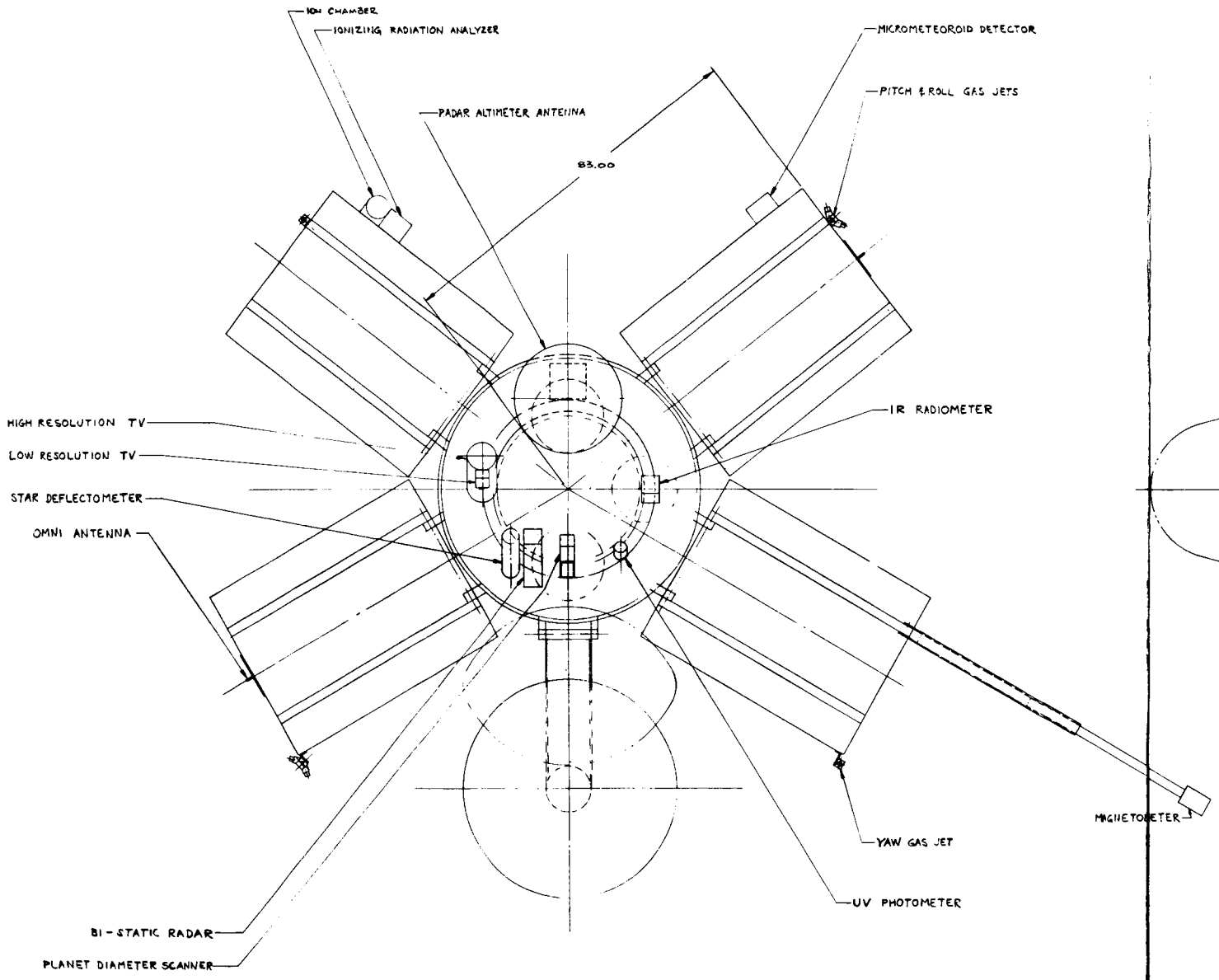


Fig. 4-2 Mariner Mars 1969 Orbiter (With Capsule) Configuration 2



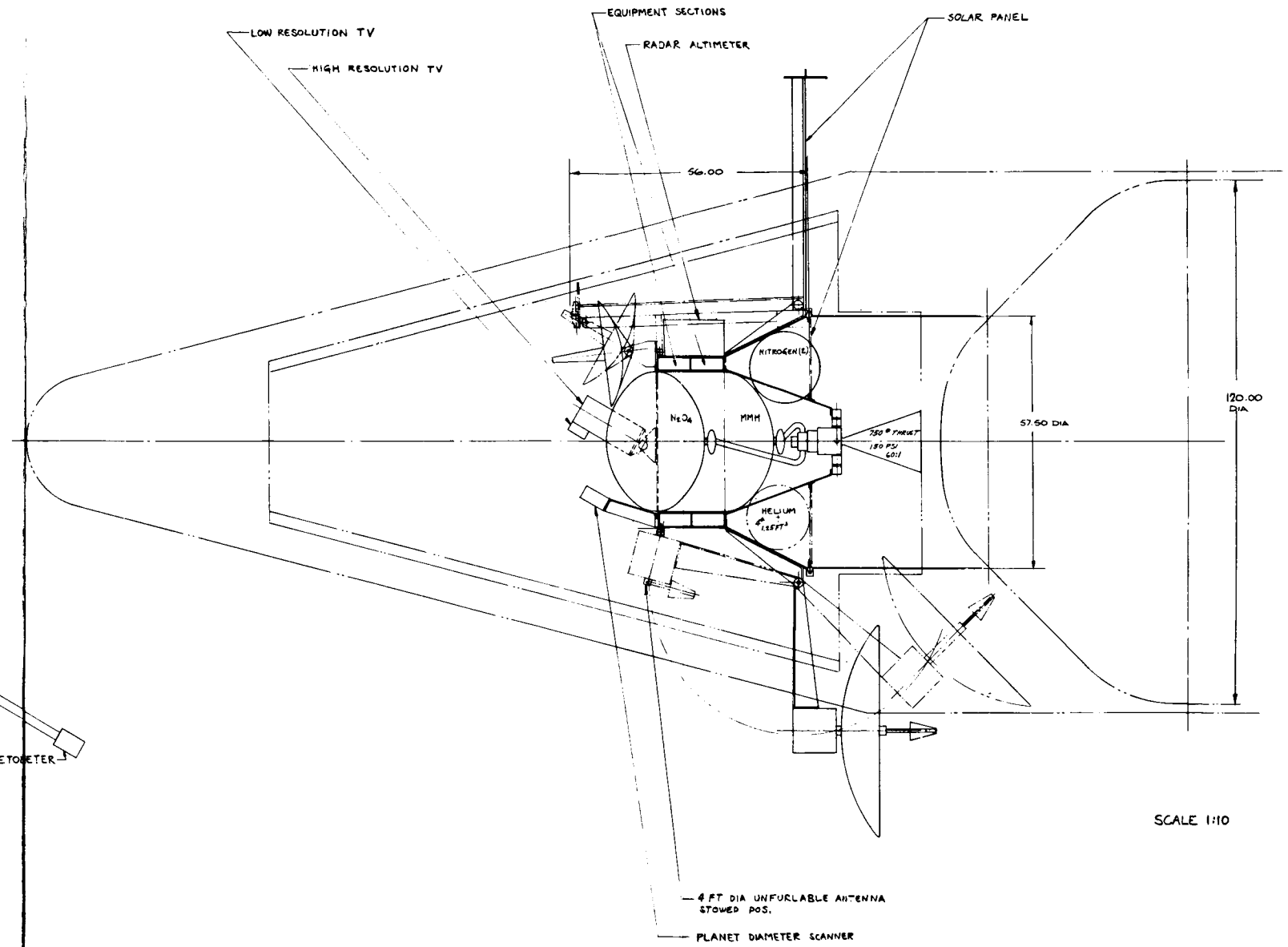


Fig. 4-3 Mariner Mars Orbiter (Without Capsule) Configuration 2

4.1.3 Configuration 3

In this concept the basic philosophy was to determine the maximum capsule diameter possible within the restraints of the surveyor shroud geometry. The design is illustrated on Fig. 4-4.

The large diameter capsule (77 in.) precludes the use of a rigid parabolic antenna and therefore two alternative antenna arrangements are shown. The first is an unfurlable parabolic design that is stowed in a canister secured to the spacecraft during launch. This design, called "FLEX-RIB," has been completely developed on a current LMSC project and will soon be flight tested on an Agena mission. The second alternative antenna that was briefly investigated is of the helical type; although such a design would have the advantage of a small area with respect to solar pressure (permitting a symmetrical distribution of the solar panels around the spacecraft centerline) it is felt that the very long, slender design would prove impractical to manufacture to the very close tolerances necessary for antenna performance. As with Configuration 2 the antenna look angles will be restricted somewhat by the engine nozzle protrusion. If the mission is flown without a capsule, a rigid parabolic antenna of conventional design could be installed.

To minimize vehicle length, and to reduce center of gravity shift as much as possible the propellants are contained in four separate spherical tanks, with the combustion chamber of the main propulsion unit nesting between them. This system would require complicated manifolding, plumbing, and valving to ensure proper fuel utilization.

Other major features of this concept are:

- Accepts 77-in. diameter capsule.
- Mariner C solar panels could not be installed.
- Short length vehicle, gives highest roll moment of inertia requiring greater amount of attitude control gas than longer vehicles.

4.1.4 Configuration 4

This configuration was selected as the preferred concept and has been examined in more detail than the other designs. A detailed description of the configuration is contained elsewhere in this report, therefore only a brief summary of the design follows.

The main feature of this concept is the side-mounted engine. The advantages of such an arrangement are:

- Cruise orientation can be maintained during orbit injection, eliminating a maneuver at a critical time in the mission
- Solar power can be maintained throughout the mission, except at midcourse correction
- Communication with Earth can be maintained at orbit injection
- Scientific instrumentation and data readout equipment can be operable during orbit inject
- Accepts 71-in. diameter capsule
- Two simple spherical propellant tanks are used
- Short-length primary structure
- Light weight
- Look angles for antenna are readily obtained

Inboard profiles of Configuration 4 without and with capsules are shown on Fig. 4-5 and Fig. 4-6, respectively.

4.2 DESCRIPTION OF BASIC ORBITER (CONFIGURATION 4) WITHOUT CAPSULE

The orbiter assembly is made up of the following major subsystems.

- Scientific Instrumentation
- Structure
- Propulsion
- Power supply

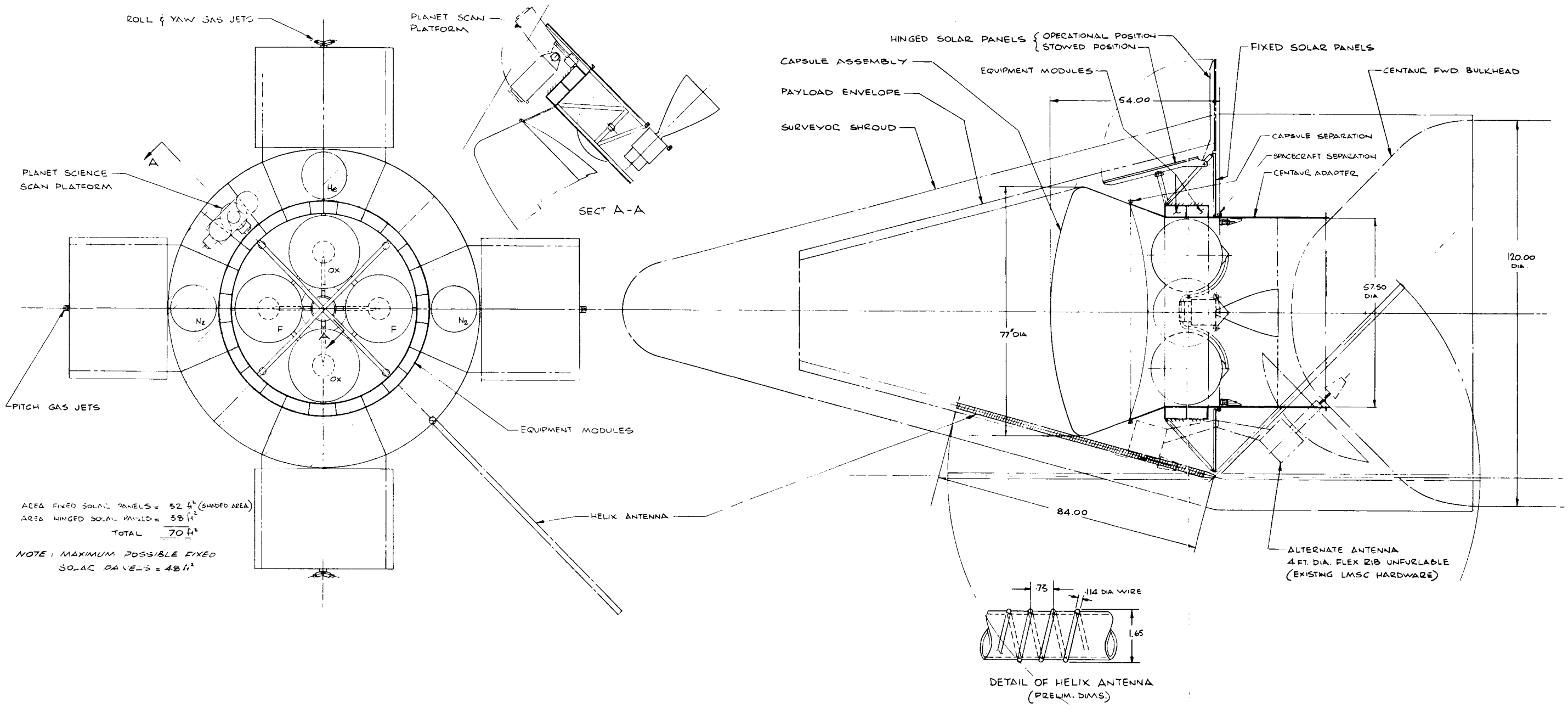
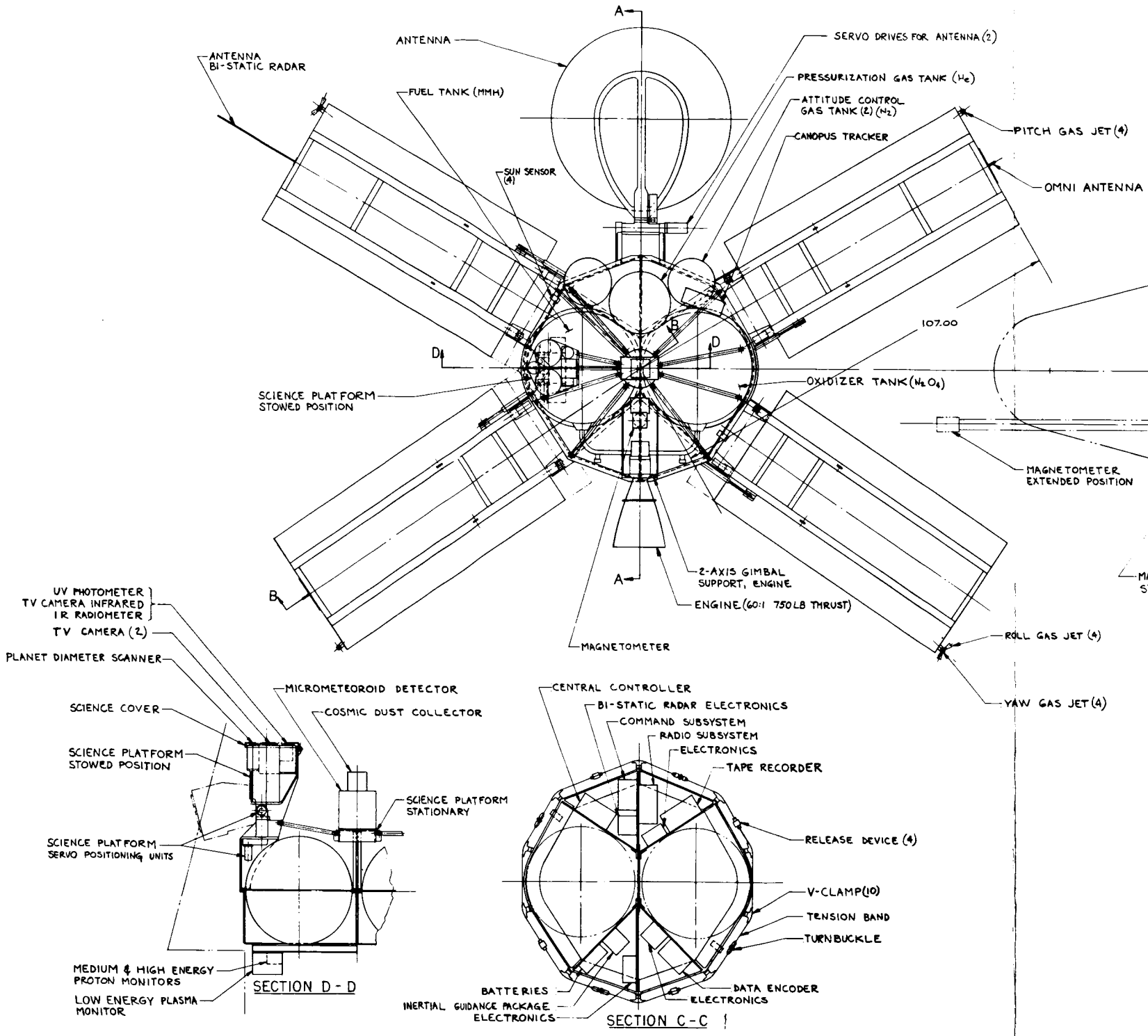


Fig. 4-4 Mariner Mars 1969 Orbiter Configuration 3



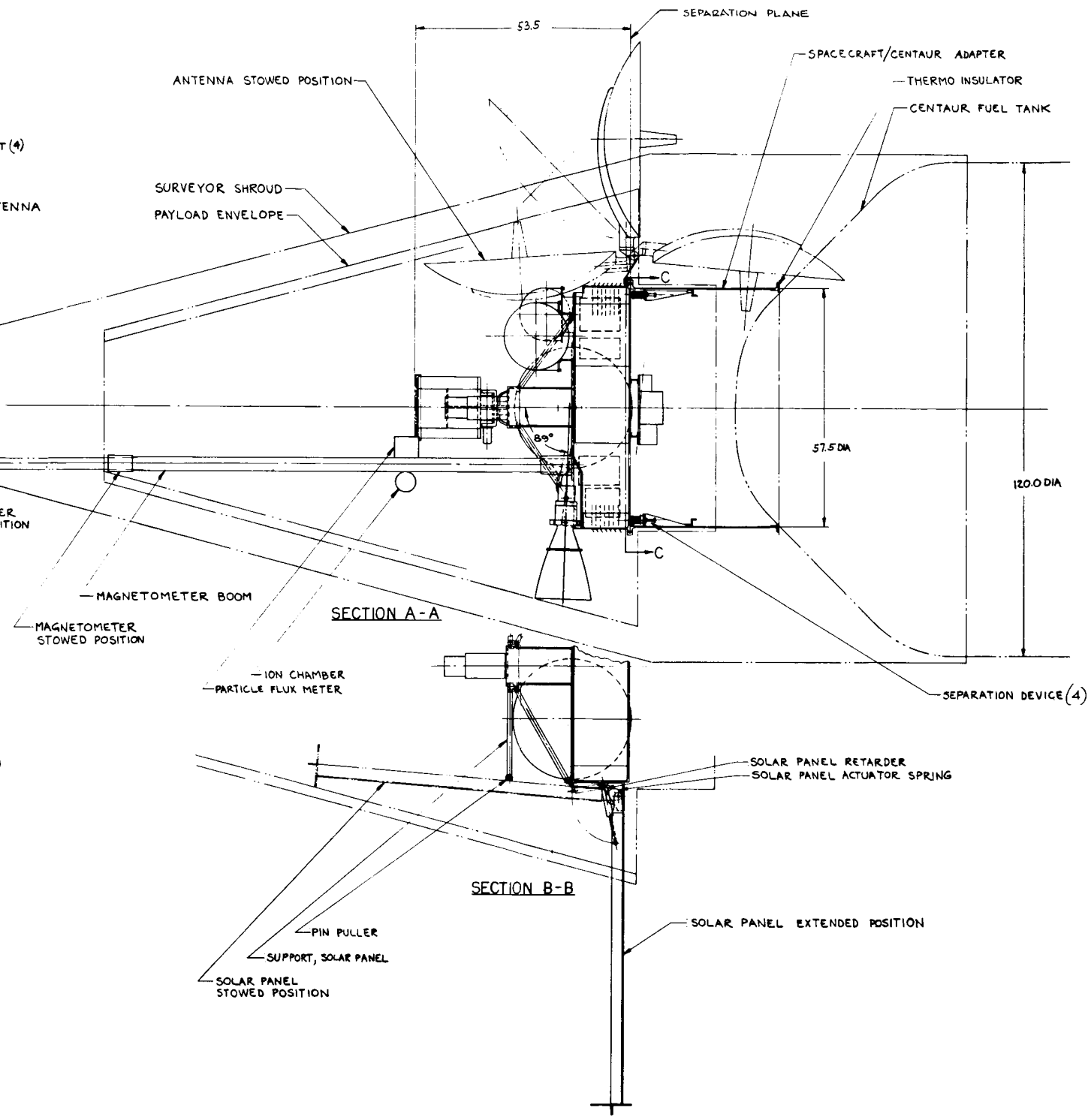


Fig. 4-5 Mars 1969 Orbiter (Without Capsule) Configuration

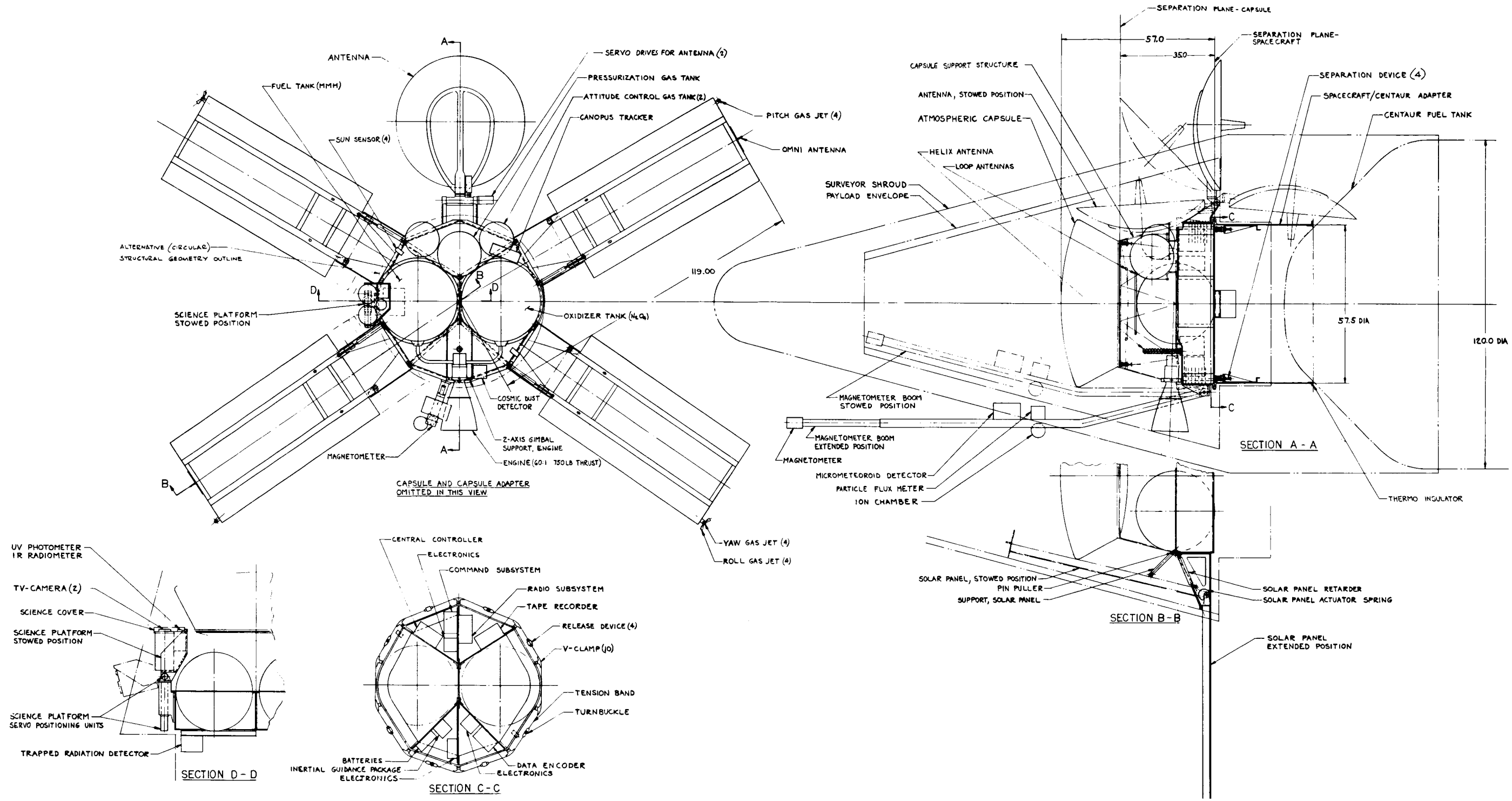


Fig. 4-6 Mars 1969 Orbiter (With Capsule) Configuration

- Electronics
- Thermal control
- Guidance
- Attitude control

4.2.1 Scientific Instrumentation Installation

The scientific instrumentation has been either independently mounted on the spacecraft or mounted on a planet science scan platform. The planet science scan platform will be gimballed by the use of two electric servo motors, each of which will be programmed to provide maximum possible planet coverage.

The science platform has been mounted on the same side of the spacecraft as the fuel tanks to help maintain the spacecraft center of gravity at the vehicle center line. This location provides sufficient clearance for the look angles of the camera's other equipment. The platform will be protected during the coast phase by a retractable protective cover and by thermal insulation.

Scientific instrumentation assumed for design purposes to be carried on the platform consists of:

- Visual TV (2 cameras)
- Infrared TV
- Ultraviolet photometer
- Infrared radiometer
- Planet diameter scanner

The independently mounted scientific equipment has been distributed at various locations on the spacecraft as shown on Fig. 4-5.

A complete list of all recommended scientific instrumentation is shown in Section 5.2.

4.2.2 Structure

The basic structure consists of an octagonal outer frame to which is attached a series of beams. The beams support the propellant tanks and the majority of the electronic equipment; strong points located at the intersections of the beams and the outer framework will serve as the attachment points for the solar panel assemblies. Additional strong points are provided in the outer framework to support the propulsion unit, communications antenna, and the science platform. These same strong points could be utilized to attach the capsule adapter support truss.

Two spherical propellant tanks are installed side-by-side within the octagonal framework. A conical sump at the tank outlets houses a multiple screen arrangement that is designed to ensure fuel entrapment at engine ignition.

The equipment bays are located within the octagonal frame on either side of the fuel tanks. Top and bottom closures are provided by stiffened panels attaching to the outer ring and the beam caps. The flat sides of the outer frame will have a series of louvers built into them, if necessary, to provide an active thermal control system for the internal equipment.

4.2.3 Main Propulsion Engine Installation

For the 1969 mission the main engine is installed at approximately 89 deg to the spacecraft center line on the forward face of the basic structural shell as shown on Fig. 4-5.

The gimbal ring at the throat of the engine is attached to the upper ring of the octagonal framework by a pair of stiffened brackets that extend inward to the upper flanges of two of the internal diagonal beams. The engine actuator loads will be reacted at integral fittings built into the beam structures. The propellant tank pressure vessel, containing helium, is installed directly in line with the main engine and is also mounted on the forward face of the structural shell.

For the 1971 mission, the basic orbiter will require considerably less propellant than is necessary for the 1969 mission; approximately 670 lb against 990 lb. Although this smaller amount of fuel could be carried in the 1969 orbiter tanks, with a large ullage space, a better approach would be to install new smaller tanks which can readily be attached to the same strong points on the basic spaceframe. The smaller tanks would be lighter and would permit better propellant orientation within the tank and tank pump. The engine installation may also require modification in order to align the engine to the optimum angle for orbit injection from the cruise attitude. For the 1961 mission, this angle is approximately 60 deg as compared to 89 deg for the 1969 mission. This can be done by building a thrust structure above the forward face of the octagonal structure as shown on Fig. 4-7.

The structural weight penalty for new tanks and 60 deg thrust angle is estimated to be 6 lb. If the 1969 tanks are retained while the thrust angle is changed to 60 deg, the structural weight penalty is estimated to be 9 lb.

4.2.4 Power Supply Installation

With the exception of the solar array all of the power supply subsystem is installed within the main equipment bays. The solar array, which is the same as that used on Mariner C vehicles is attached at the lower end of the octagonal structure.

To maintain the center of solar pressure as close as possible to the spacecraft center line, the solar panels have been installed slightly offset from the normally 90 deg square pattern used on Mariner C. In determining this location, the 4 ft diameter antenna dish was assumed to have a 25 deg effective pressure area in the same plane as the solar panels. The offset location permits easy installation of a rigid type antenna and also the main propulsion engine. The exhaust plume impingement on the solar panels was examined and found to be of only minor significance.

4.2.5 Electronics Installation

The majority of the electronic components have been installed within the two main equipment bays, although there is also some space available for additional equipment on the front and rear faces of the basic structure. The equipment bays shown on Figs. 4-5 and 4-6 are 14 in. high; detailed examination may show that this will need to be increased to obtain more internal volume. If high-density integral packaging techniques are developed, these equipment bays should provide more than adequate volume.

4.2.6 Thermal Control

A discussion of thermal control techniques is presented in Section 5.5 of this report. Thermal painted surfaces in addition to louvers, heaters, small local heat sinks, and thermal insulation blankets and covers will all be used.

4.2.7 Guidance Components Installation

The inertial guidance system will be installed within the main equipment bay enclosure.

4.2.8 Attitude Control System Installation

To obtain the required view angles, the Canopus tracker has been installed on the forward end of the octagonal frame. Sun sensors are installed on both front and rear faces of the spacecraft.

The attitude control system is basically the same as that used on Mariner C spacecraft, with 100 degrees redundancy in the hardware components. The attitude control gas (N_2) is contained within two identical spherical pressure vessels mounted on either side of the thrust axis. The reaction jet nozzles are located on the extreme outboard ends of the solar panels in a similar manner to Mariner C except that the attachment points will be offset from the center lines of the panels. This has been done to avoid building separate outriggers onto the panels which would be necessary to obtain a symmetrical 90 deg square pattern between nozzle assemblies in the plan view.

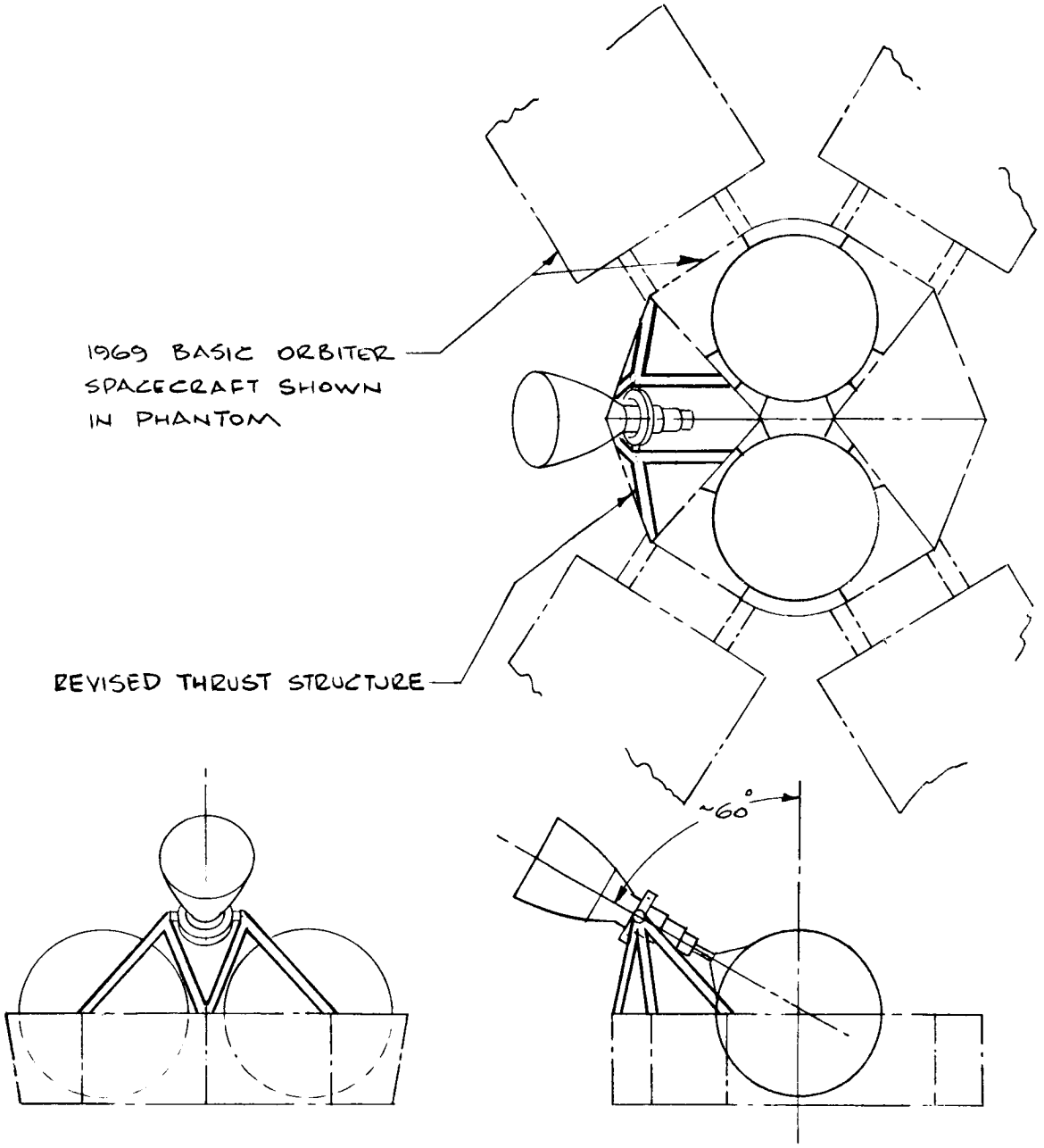


Fig. 4-7 Revised Engine and Tank Installation for 1971 Mission

4.2.9 Antenna Installation

A rigid 4-ft diameter parabolic communication antenna is installed opposite the main propulsion engine and is attached to the lower basic framework by a pair of cantilevered brackets. The hinge point extends slightly below the spacecraft separation plane to provide clearance for the maximum antenna look angle. The antenna is provided with a two-axis gimbal system.

4.2.10 Science Instrumentation Installation

With the installation of a capsule the centrally located, independently mounted science equipment must be relocated. In addition, the infrared TV and the planet diameter scanner are deleted from the gimballed platform. A description of science instruments is presented in Section 5.2.

4.3 DESCRIPTION OF BASIC ORBITER (CONFIGURATION 4) WITH CAPSULE

The basic orbiter spacecraft discussed in the preceding paragraphs will require only a minimum amount of modification to allow a capsule to be installed. For a 61 in. diameter capsule (the nominal diameter used in the study) the major change would be to install outrigger structures at the base of the octagonal framework to support the Mariner C solar panels; such a vehicle is shown in Fig. 4-6. The maximum diameter capsule that can be installed without using outriggers is 48 in. An alternative to using outriggers would be to use shorter length solar panels and to attach fixed solar panels to the underside of the spacecraft equipment bays. The use of shorter solar panels has the disadvantage of reducing the moment arm of the attitude control reaction jets mounted on the outer edge of the panels, thereby requiring an increase in attitude control gas. The upper supports for the solar panel attachments would require repositioning.

The structural weight penalty on the basic spacecraft for installing a 61 in. diameter capsule has been estimated at 10 lb. A detailed breakdown of the additional equipment required on the basic spacecraft when fitted with either an atmospheric or biological capsule is shown on Table 4-2.

Table 4-2

ADDITIONAL EQUIPMENT ADDED TO BASIC ORBITER WHEN A 61 IN. DIAMETER CAPSULE IS INSTALLED

Description	Atmospheric Capsule (lb)	Biological Capsule (lb)
Electronics		
Crossed Dipole Antenna	1	–
Receiver	4	–
Command and Sequence Timer Equipment	2	2
Buffer Storage	3	3
Miscellaneous (Relays, etc.)	3	3
Structure		
Solar Panel Outriggers	8	8
Miscellaneous Fittings	2	2
TOTAL	23	18

4.4 CAPSULE DESIGN

Two basic types of capsules were examined during the study; an atmospheric capsule which does not survive after impact and a biological capsule which would survive impact.

For both types of capsule a high drag, blunt forebody/conical aftbody, Apollo-type entrybody was selected as the most efficient shape. The entire heat shield and its supporting structure are jettisoned prior to parachute deployment.

4.4.1 Atmospheric Capsule

The atmospheric capsule is shown on Fig. 4-8 and is made up of the following major subassemblies.

- Sterility shroud
- Entry body (including heat shield)
- Payload compartment

- Descent system (described in section 5.7)
- Guidance rocket system (described in Section 5.4)

Sterility Shroud. The sterility shroud completely envelopes the atmospheric capsule and remains on the capsule until after separation of the capsule assembly from the spacecraft 2 days prior to planet encounter. The shroud consists of two highly polished aluminum subassemblies welded together at the maximum diameter adjacent to the circumferential shroud separation plane. Separation of the shroud from the capsule is achieved by firing the prima-cord charge around the periphery of the welded flanges of the two halves of the shroud; the separation force is obtained from a series of small springs between the entry body and the shroud. A debris shield and shock absorber would be installed on the inner surface of the shroud adjacent to the separation plane. The shroud will be vented during the boost phase of the flight, an internal pressure of approximately 1.0 psi being maintained throughout the flight.

The hardpoints are integral with the shroud at the spin rockets and a snubbing device will transmit spin loads to the capsule structure. A two-stage electrical disconnect and the vent valve are installed on the aft dome of the shroud; also attached to the outside of the aft dome is the loop antenna required for communication with the orbiter.

Hardpoints are provided on the aft ring of the sterility shroud to which will be attached taper pins that form a part of the pin-puller separation mechanism.

Entry Body. The entry body consists of the forebody heatshield, aft body heatshield, and internal supporting structure.

The forebody heat shield depicted in Fig. 4-8 is a microballoon construction nylon phenolic ablator bonded to a waffle pattern back-up structure made from HM -21A-T81 magnesium thorium alloy; however, severe dimensional stability problems can be anticipated with the nylon phenolic during the heat sterilization cycle, and a silicon ablator or a heat sink of beryllium should be used if the heat sterilization technique remains a design ground rule. The forebody geometry is a shallow spherical dome with an outside diameter of 61 in. The transition from the forebody to the aftbody

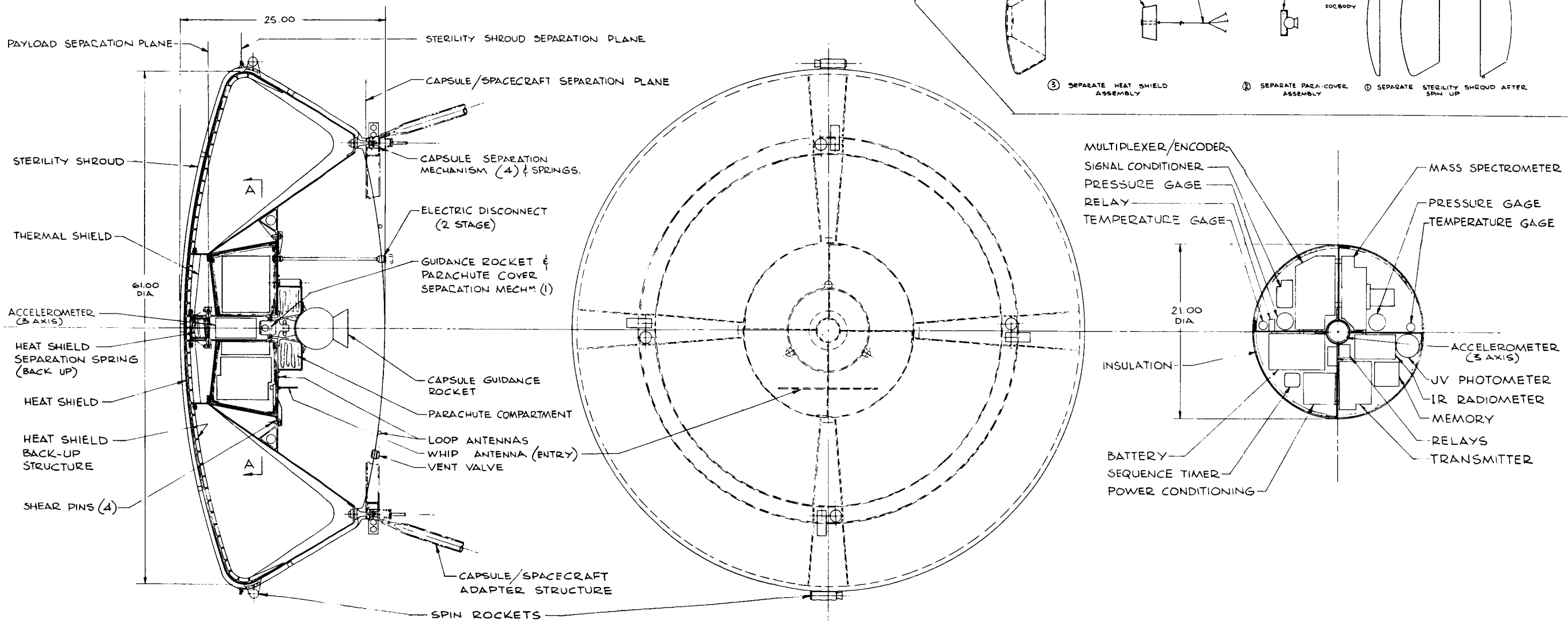


Fig. 4-8 Capsule Assembly (Atmospheric)

115

4.4.2 Biological Capsule Assembly

The biological capsule, shown on Fig. 4-9, differs from the atmospheric capsule primarily because provision must be made to survive impact on the Martian surface.

The biocapsule consists of the following major components:

- Sterility shroud
- Entry body
- Lander capsule

The sterility shroud and entrybody are basically the same as the atmospheric capsule.

Lander Capsule. The lander capsule houses the scientific experiments, the communications and power supply, the parachute system and the guidance rocket. The primary instrument, a life experiment, is housed in a central compartment to which are attached the pickup devices to obtain a sample of surface material. The structural webs that support the majority of the capsule equipment are also attached to the central column.

Two recessed monopole antennas are installed on opposite surfaces of the science housing, either one of which will be activated by a gravity switch depending on the final attitude the capsule adopts after impact.

The science housing is surrounded on sides and bottom by a spherical balsa wood impact structure designed to absorb impact at velocities of 114 ft/sec without exceeding an acceleration of 900 Earth g's.

A preliminary analysis of several energy absorption systems was made. The energy absorption capabilities of these systems are listed on Table 4-3. It is seen that the crushable balsa wood system has the greatest potential efficiency, followed by metal honeycomb. Although balsa wood was selected primarily for its energy absorption capacity a secondary advantage is that its dielectric properties permit the use of flush mounted antennas on the internal back-up structure. If aluminum (or other metal) were used a pop-out antenna device would be necessary.

cone is formed by an annular section with a radius of approximately 2.50 in. Weight estimates are shown in Section 4.9 both for asceptic assembly using a Nylon Phenolic heat shield and for heat sterilization using a beryllium heat sink.

The heatshield aftbody forms the external conical surface of the entry body and has a ring attached to the aft end to which are secured hard points for the capsule/orbiter attachments. The internal support structural cone is also attached to the aft ring. The stiffened aftbody cone is constructed from beryllium.

The internal supporting structure consists of a stiffened conical shell extending from the aft ring of the aftbody heat shield to a ring located at the base of the instrument capsule. Four fittings attached to the stiffeners on the internal cone are provided to give stability to the aft face of the payload compartment. All of the internal structure is constructed of magnesium alloys ZK60A-T81 and HK31A-H24.

Payload Compartment. The payload compartment houses the scientific experiments, the communications and power supply, the parachute system, and the capsule guidance system. The payload capsule is attached to the entrybody by a small Marmon clamp at the lower end of a central support tube. This tube is also used to attach the equipment support webs and the parachute swivel attachment. Separation of the instrument probe from the entry body is achieved by releasing the small Marmon clamp immediately prior to parachute deployment.

The capsule guidance rocket is attached to the parachute compartment cover and is jettisoned by actuating a pin puller device installed in the aft end of the central tube; three ejection pistons equally spaced around the periphery of the parachute cover provide the separation force.

A loop antenna is provided on the aft face of the payload compartment for communication with the orbiter during capsule separation. A whip antenna is located on the aft face of the capsule instrument compartment for communication with the orbiter during the entry phase.

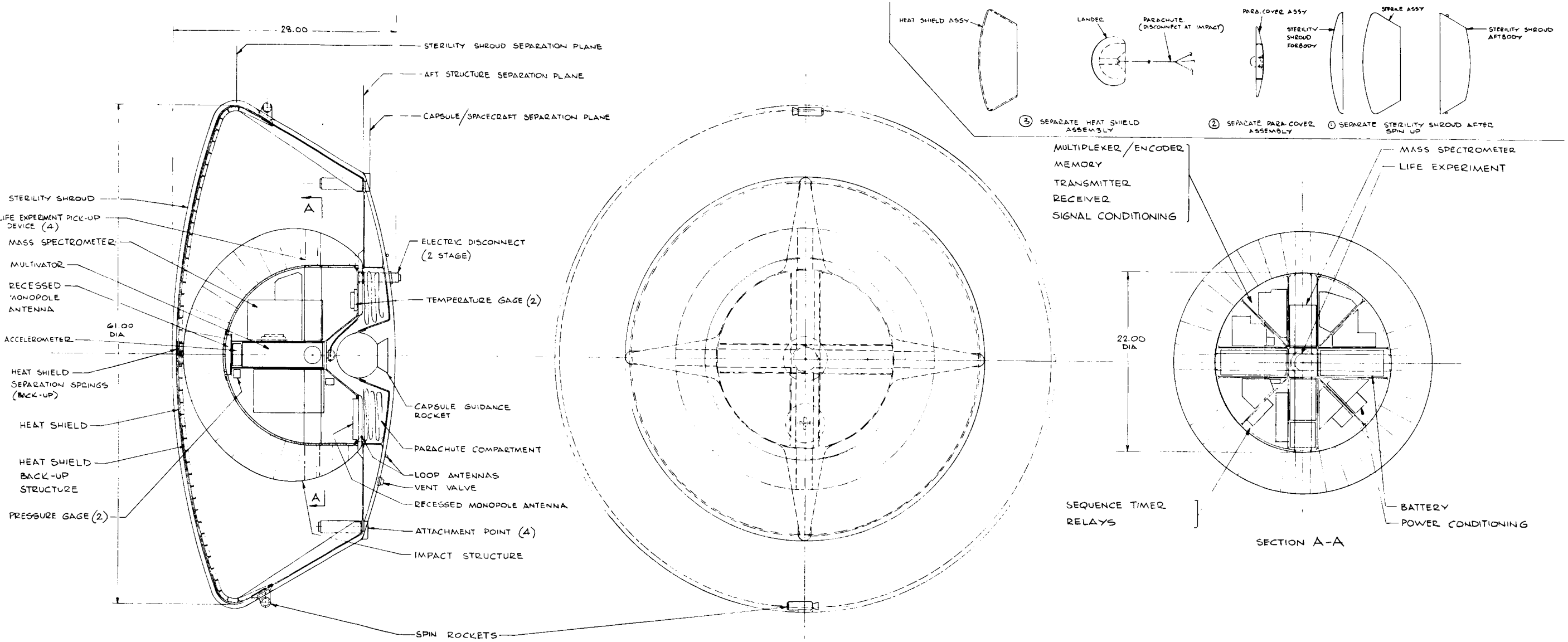


Fig. 4-9 Capsule Assembly (Biological)

The lander capsule assembly is attached to the entry body through a spider beam assembly on the aft face. The spider beam has a conical structure to support the guidance rocket and a short cylindrical section which forms a protecting cover for the parachute compartment. The spent guidance rocket is released from the entry body, together with the spider beam assembly, by releasing the separation mechanisms on the outside ends of the spider beams.

Table 4-3

ENERGY-ABSORPTION CAPACITY OF VARIOUS MATERIALS AND SYSTEMS*

System/Material	Range Energy Absorbed ft-lb/lb
Crushable/balsa	9,000 – 24,000
Crushable/plastics	1,000 – 4,500
Crushable/paper honeycomb	800 – 2,500
Crushable/metal honeycomb	2,000 – 11,000
Gas bag/metal	8,000 – 11,000
Gas bag/fabric	1,000 – 6,000

*Ref: NASA TN D-1308 Energy absorption devices for soft landing of space vehicles.

4.5 CENTAUR ADAPTER STRUCTURE

The adapter structure shown on Figs. 4-5 and 4-6 is of the orthodox ring/skin/stringer design with access holes for separation mechanism adjustments, etc. The aft end attaches rigidly and uniformly to the payload interface ring (57.50 in. diameter) on the forward bulkhead of the Centaur LH_2 tank. The forward section attaches to the spacecraft interface ring.

A brief strength analysis of the adapter structure was made in order to obtain a preliminary weight estimate. Two load transfer theories were considered: (1) uniform load contacts around the periphery of the shell, and (2) concentrated loads at ten

points of attachment to local stiffeners which distribute the loads uniformly throughout the shell. The weight difference is only 2.7 lb as discussed in Section 4.7.

Thermal isolators may be necessary at the lower end of the adapter at the Centaur bulkhead and some local beef-up of the adapter shell has been included in the adapter weight estimate to allow for the extremely low temperatures that can be expected from the Centaur LH_2 tank.

The interface ring provided at the base of the spacecraft octagonal structure transfers all loads into the Centaur adapter structure and also forms the separation plane.

Separation of the spacecraft from the Centaur adapter is achieved by releasing a tension band and allowing the closely aligned spring assemblies to impart the required separation velocity to the spacecraft. This system is the same as that employed on Mariner C. An alternative method would be to use pin pullers (as used on Ranger flights) in place of the tension band arrangement.

4.6 CAPSULE/SPACECRAFT ADAPTER STRUCTURE

The capsule assembly described in the previous paragraphs is attached to the orbiter by a truss-type structure designed to transmit capsule loads to strong points built into the basic orbiter structure. The tubular cross-bracing assemblies would be arranged in such a manner that they do not interfere with the scan envelopes of the scientific instruments on the science scan platform. They will also have to clear the fixed equipment, H_e and N_2 bottles, engine, magnetometer boom, etc., installed on the forward face of the orbiter.

The capsule separation mechanism is installed on the forward ring of the adapter structure and consists of four pin pullers and closely aligned compression spring assemblies. Tipoff rates will be critical during capsule separation and extreme care will be necessary during detail design phases to ensure a clean flat separation.

4.7 STRUCTURAL ANALYSIS

A preliminary structural analysis of the spacecraft has been made and is summarized in this section.

The main components considered were:

- Solar panel supports (for orbiter with capsule)
- Fuel tankage and supports
- Equipment support beams
- Spacecraft/Centaur adapter structure

The analysis considered only two flight-load conditions: (1) Booster acceleration, and (2) spaceflight. The booster acceleration condition (specified in Ref. 2) was a maximum quasi-steady state acceleration at the separation plane of 6-g axial and 0.4-g lateral. All critical loads occur during the boost phase of the flight.

Several materials and types of fabrication were considered for the various components, as shown in the Strength Analysis Summary, Table 4-4. In most case, magnesium alloy appears to be the most practical.

The solar panel support structure required for the orbiter/capsule configuration becomes impractical to fabricate when attempting to design the structure for zero margin, and the gage selection was therefore based on minimum handling requirements. The magnesium alloy proved to be the most efficient choice of material. The dynamics of the structure has not been studied and final analysis may prove that stiffness requirements are more critical than strength requirements.

The propellant tanks were designed for internal pressures existing during flight. The tanks are pressurized to 250 psia. For design, this value is increased by the increment due to hydrostatic head caused by booster acceleration. Fuel-oxidizer proportions were selected to yield balanced tank volumes together with optimum engine operation.

Table 4-4

STRENGTH ANALYSIS SUMMARY

Item	Material	Weight (lb)	Margin of Safety	Alternate	Weight	M.S.
Solar Panel Support Frames	HK31A-H24	6.00	High	None	–	–
Solar Panel Support Struts	2K60A-T5	1.06	High	None	–	–
Fuel Tankage	AL 2219-T87	24.8	0	None	–	–
Equipment Support Panels	Mag Sandwich Panels	7.3	High	Mag Skin & Stringer	13.5	+.58
Equipment Section Ring Frames	7075-T6	9.4	+.60	2K60A-T5	9.9	+.09
Equipment Section Outer Shell	HK31A Shell w/2K 60A-T5 Strs.	9.9	+.19	Mag Longeron & Shear Web	8.9	+.31
Adapter – Orbiter/ Centaur	HK31A Shell	31.0	0	Shell/Stiff**	33.7	0

**Alternate configuration considers concentrated loads being reacted at forward section by tapered stiffeners.

The tanks were designed to have an ullage space for a volume of approximately 5 lb per tank. Aluminum alloy 2219-T87 was selected as the most suitable material because of its good strength to weight ratio and its excellent weldability. The spherical tanks are identical, consisting of two hemispheres. The hemispheres would be spun from 2219 aluminum sheets and chem-milled to reduce membrane areas to required thickness (approximately half the thickness of the equator and polar areas where welding reduces the unit strength). Flanges are welded to the hemispheres to provide both continuous attachment and external support.

The equipment support beams provide for the internal support of the propellant tanks as well as the support of all the equipment and engine thrust structure. Two types of fabrication were considered for analysis: (1) the common aircraft type of shear web with zee stiffeners using magnesium alloy and (2) thin magnesium sandwich panels with aluminum honeycomb core. As can be seen from the strength summary, Table 4-4 the honeycomb sandwich panels are much lighter, inherently provide much greater lateral stiffness, and have a very high margin of safety. As in the case of the solar panel supports, final analysis may prove that stiffness requirements are more critical than strength; therefore, no attempt was made to optimize the sandwich configuration.

The forward and aft rings are designed to resist the "kick" loads caused by the shear panels. Analysis has shown that both aluminum alloy 7075-T6 and Magnesium alloy HM 31A-T5 are satisfactory. The aluminum ring will be lighter, but the weight variation is small.

The equipment section outer shell is presently designed as a partial octagon where most of the outer panels are flat. The lightest design for this type of configuration is to have eight main longerons carrying the loads directly to the interstage structure. Light, stiffened shear panels are installed between the longerons to give the structure torsional and shear stability and strength. This type of fabrication lends itself nicely to accessability of equipment since nonstructural circular doors may be installed in the shear webs.

Mass moments of inertia were calculated for an orbiter alone and for an orbiter with capsule. A summary of the results is presented in Fig. 4-10.

4.8 MATERIAL SELECTION

Several material candidates have been considered for each of the major structural components; these are shown in Table 4-5.

Table 4-5

MATERIAL CANDIDATES – ORBITER

Primary Structure

- Aluminum 7075-T6
- Beryllium/Alum Alloy (Lockalloy)
- * Magnesium HK 31A-H24 (Sheet and Plate)
  ZK 60A-T5 (Extrusions and forgings)
  HM 21A-T8 (High Temperature)

Propellant Tanks

- Filament Wound Fiberglass
- Titanium
- Stainless Steel
- * Aluminum 2219-T87 (7106 and 7039)

Helium and Nitrogen Pressure Tanks

- * Titanium 6AL4V (Existing hardware)

Spacecraft/Centaur Adapter

- Beryllium
- Lockalloy
- Aluminum 7075-T6
- * Magnesium HK 31A-T4
  ZK 60A-T5

*Indicates material selected for use in calculating structural weight.

The material selection has been based on the conservative approach where only currently available material, state-of-the-art manufacturing techniques, and well established material mechanical properties are considered. However, further evaluation of other materials such as beryllium, Lockalloy (B_e/Al), and Mag/Lithium should be made in an effort to reduce the structural weight of the spacecraft.

LOADED CONDITION (INCLUDED 900 LBS PROPELLANTS AND 220 LB CAPSULE)

$\bar{X}$ = 17.81 IN.

$\bar{Y}$ = 0.55 IN.

$\bar{Z}$ = -1.13 IN.

I_X = 338 SLUG FT^2

I_Y = 240 SLUG FT^2

I_Z = 318 SLUG FT^2

EMPTY CONDITION (NO PROPELLANTS, NO CAPSULE)

$\bar{X}$ = 14.01 IN.

$\bar{Y}$ = -3.31 IN.

$\bar{Z}$ = -2.98 IN.

I_X = 265 SLUG FT^2

I_Y = 177 SLUG FT^2

I_Z = 203 SLUG FT^2

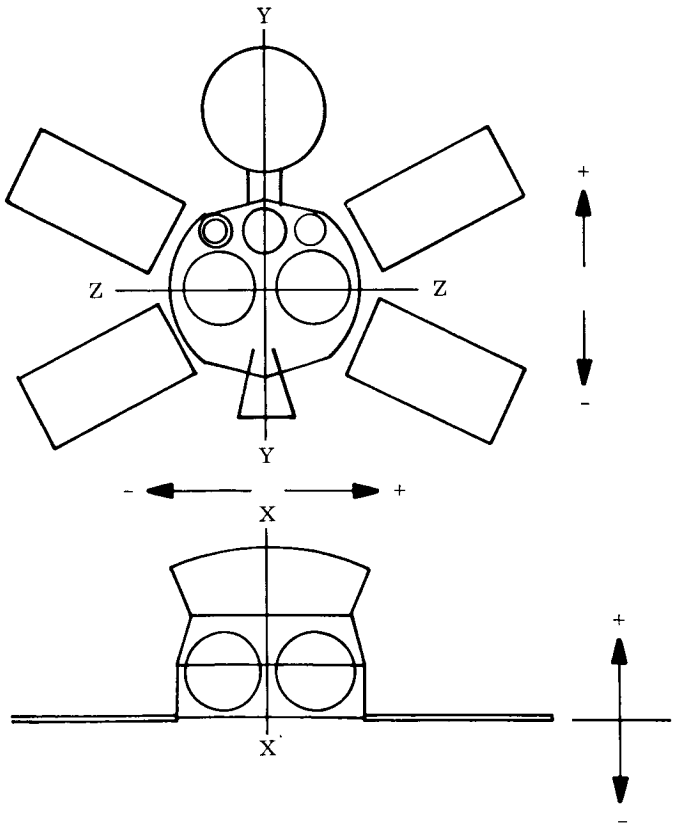


Fig. 4-10 Summary of Mass Moments of Inertia

4.9 WEIGHT AND BALANCE

A weight summary for the basic orbiter is shown in Table 4-6. A detailed weight breakdown for each subsystem on the basic orbiter is shown in Table 4-7.

Tables 4-8 and 4-9 present the overall vehicle weights for the orbiter alone and the orbiter with capsule, respectively, and indicate the weight capabilities for 0 deg, 20 deg and 30 deg Flox Atlas-Centaur boosters. The 20 deg flox vehicle has been considered the nominal vehicle throughout the study. As can be seen from the tables the 0 deg flox vehicle has very marginal performance even without a capsule and a negative margin when the 61 in. diameter capsule is added. Propellant weight for orbit injection is computed on the basis of thrusting from the cruise attitude as discussed in Section 3. The penalty for this method of orbit injection is a 3 percent increase in mass ratio for the 1969 Mars Mission as shown in Fig. 3-20. This result is about a 3 percent (29 lb) reduction in burnout weight in orbit.

An equipment list and the weight estimates for an atmospheric capsule are shown in Table 4-10. The weight advantages to be obtained by using an asceptic assembly technique rather than heat sterilization can be seen from this table. Included in the table is the weight estimate for a 45-in. diameter capsule, discussed in Section 3.

An equipment list and weight estimates for a biocapsule are shown in Table 4-11. Here again a weight advantage for asceptic assembly is shown.

Table 4-6

WEIGHT SUMMARY – CONFIGURATION 4 (FIG. 4-5) – EMPTY
(BASIC ORBITER LESS IMPULSE PROPELLANTS AND PAYLOAD)

Subsystem	Weight (lb)
Structure	99
Propulsion	112
Power Supply	189
Electronics	166
*Guidance	26
*Attitude Control	88
Thermal Control	15
	695

*Includes 100 percent redundancy on components, and 200 percent redundancy on control gas.

Table 4-7

DETAILED SUBSYSTEM WEIGHT BREAKDOWN – BASIC ORBITER

Structure	Weight (lb)
Top Ring	5
Bottom Ring	9
Equipment Beams	14
Top Closure	3
Bottom Closure	3
Outer Skin	10
Inner Skin	2
Beef-up at Engine	4
Solar Panel Attachments	8
S/C Separation Fittings	1
N_2 + H_e Tank Supports	4
Longerons and Stiffeners	5
Miscellaneous Brackets	5
Science Support Structure	6
Scan Platform Actuators	5
Umbilical Attachments	2
Hardware (Bolts, etc.)	3
Magnetometer boom	7
Miscellaneous	3
Total	99 lb

Table 4-7 (Cont.)

Propulsion	Weight (lb)
Engine Assembly (Inc. Gimbal Ring)	21.8
*Propellant Tanks	31.0
Fill Valves	0.5
Lines and Fittings	4.3
H_e Tank	23.7
H_e Gas	3.4
H_e Fill Valve	0.2
H_e Tank Support	2.0
Pressure Regulator	1.0
Gas Filter	0.5
Check Valves (2)	0.2
Relief Valves (2)	2.0
Thrust Structure	3.0
Residual Propellants	10.0
Gimbal Actuator System	7.0
Start Valve	1.5
TOTAL	112.1

*The fuel and oxidizer tank weight is made up as follows:

Tank Shell	10.6
Weld Lands	0.6
Attach. Flange	1.2
Sump	1.3
Slosh + Vortex Baffles	1.8
Total	15.5 lb per tank assembly

Thermal Control	
Louver Assemblies (4)	8
Heaters	2
Local Heat Sinks	3
Paint, Misc.	2
TOTAL	15

Table 4-7 (Cont.)

Power Supply		
Solar Panel Assemblies		75
Booster Regulator		42
Power Synchronizer		2
Battery Charger		3
2400 CPS Inverter		5
400 Cps 1 ϕ Inverter		2
400 Cps 3 ϕ Inverter		7
Secondary Battery		23
Wiring, Misc. etc.		30
	Total	189
Attitude Control System		
Nitrogen Gas		19.0
Nitrogen Gas Tanks (2)		24.0
4 Jet Manifold Assemblys (2)		2.5
2 Jet Manifold Assemblys (2)		1.5
Plumbing and Line Fittings		4.0
Gas Regulators		2.0
Sun Sensors		3.0
Electronics		9.0
Canopus Tracker		20.0
Misc. Wiring, etc.		3.0
	Total	88.0
Guidance Subsystem		
Inertial Unit		18
Electronics		6
Miscellaneous Wiring, etc.		2
	Total	26

Table 4-7 (Cont.)

Electronics		
Radio Systems		
4 ft dia. parabolic antenna (including mechanisms and supt. brkts.)		22
Omni antennas (2)		4
Receiver		6.5
Exciter		3.5
Power Amplifier		2
DC to DC Converter		3
Circulators, etc.		5
Misc. Brkts, wiring, etc.		8
	Sub-Total	54 lb
Data Encoder		
PN Generator		2
Modulator, Amplifier, etc.		2
Power Supply		1
Event Counters		2
Misc. (switching, wiring, etc.)		4
	Sub-Total	11 lb
Central Controller		
Experiment Support Electronics		15
Command Programmer		5
Command Sub-system		9
Sequence Timer		5
Clock and Countdown		3
Multiplexer/Encoder		12
Tape Recorder		36
Misc. (wiring, relays, etc.)		6
	Sub-Total	91 lb
Status Instrumentation	Sub-Total	10 lb
	Electronics Total	166 lb

Table 4-7 (Cont.)

Centaur Adapter Structure	Weight (lb)
End Rings + Doors	9
Skin	22
Spring Assemblies	4
Separation Mechm. Supports	4
Local Beef-up at Centaur	4
Insulator Ring	2
Insulation Blankets	6
Tension Band Assembly	5
Total	56

Table 4-8

WEIGHT SUMMARY – CONFIGURATION 4 (NO CAPSULE) – LOADED

	0% Flox	20% Flox	30% Flox
Basic Spacecraft	652	695	700
Science Payload	18	132	132
Orbit Injection Weight Required	670	827	832
Redundancy and Contingency	38	104	216
Orbit Injection Weight Capability	708	931	1,048
Impulse Propellant	787	998	1,102
Centaur Adapter	50	56	60
Total Vehicle Weight (lb)	1,545	1,985	2,210

Table 4-9

WEIGHT SUMMARY – CONFIGURATION 4 (WITH 61-IN. DIAMETER ATMOSPHERE CAPSULE) – LOADED

	0% Flox	20% Flox	30% Flox
Basic Spacecraft	675	718	723
Science Payload on Basic Spacecraft	18	88	88
Capsule Adapter and Separation Mechanism	18	18	18
Orbit Injection Weight Required	711	824	829
Redundancy and Contingency	-82	28	140
Orbit Injection Weight Capability	629	852	969
Capsule Complete (18 lb Science)	158	158	158
Impulse Propellant	708	919	1,023
Centaur Adapter	50	56	60
Total Vehicle Weight (lb)	1,545	1,985	2,210

Table 4-10

WEIGHT SUMMARY – ATMOSPHERIC CAPSULE

	Asceptic Assembly (lb) 61 in. Dia	Heat Sterilized (lb)	
		61 in. Dia	45 in. Dia
Scientific Instruments	18	18	18
Sterility Shroud	22	24	13
Heat Shield	22 (N)	33 (B)	18 (B)
Heat Shield Back-up Structure	14	0	0
Entrybody Internal Structure	14	19	10
Guidance Rocket Assembly	10	11	8
Payload Compartment Structure	11	12	12
Electronics	20	20	20
Battery & Inverter	7	15	15
Insulation	2	2	2
Parachute System	3	4	4
Total Capsule Weight	143	158	120
Total Weight at Entry	118	130	104
Weight on Parachute (Including Parachute)	61	71	71

N = Nylon Phenolic (Micro balloon)
B = Beryllium

Table 4-11

WEIGHT SUMMARY – BIOLOGICAL CAPSULE
(61 in. Dia.)

	Asceptic Assembly (lb)	Heat Sterilized (lb)	
Scientific Instruments	12	12	5
Sterility Shroud Assembly	22	24	24
Heat Shield	33 (N)	33 (B)	33 (B)
Heat Shield Back-up Structure	18	20	20
Guidance Rocket Assembly	20	24	22
Payload Compartment Structure	20	22	22
Crush Structure (Balsa)*	28	50	31
Electronics	43	43	43
Batteries & Inverter	30	84	49
Insulation	2	2	2
Parachute System	21	37	23
Total Capsule Weight	249	351	274
Total Weight at Entry	222	320	244
Weight on Parachute (Incl. Parachute)	156	248	175

N = Nylon Phenolic (micro balloon)

B = Beryllium

*Assumes 114 ft/sec impact velocity and maximum deceleration of 900 g's.

4.10 ALTERNATIVE LAUNCH SHROUD AND SPACECRAFT CONCEPTS

Although the existing Surveyor shroud has been used in the vehicle configuration studies, there are many alternate shroud geometries possible. Two of these alternatives are compared with the surveyor shroud on Fig. 4-11 and are briefly described here.

The tangent ogive shroud shown on Fig. 4-11 indicates that approximately 4 ft 6 in can be reduced from the length of the overall vehicle, and by reducing aerodynamic drag forces results in less structural loading in the lower booster stages. As can be seen from the sketch the amount of unused volume can be decreased considerably.

The double conical shape depicted in Fig. 4-11 has the advantage of utilizing the full 120 in diameter of the Centaur. Other advantages are that very large diameter capsules could be accommodated and a fixed solar panel area of 78 ft^2 can be used. Also in such a design the fuel and ozidizer tanks of the orbiter can be placed on the thrust line of the engine thus reducing cg travel at engine burn. In this design all of the orbiter equipment is installed around the periphery of the vehicle and is readily accessible for adjustment and checkout on the launch pad. The Centaur equipment bay has been rearranged to utilize the full 120 in. diameter.

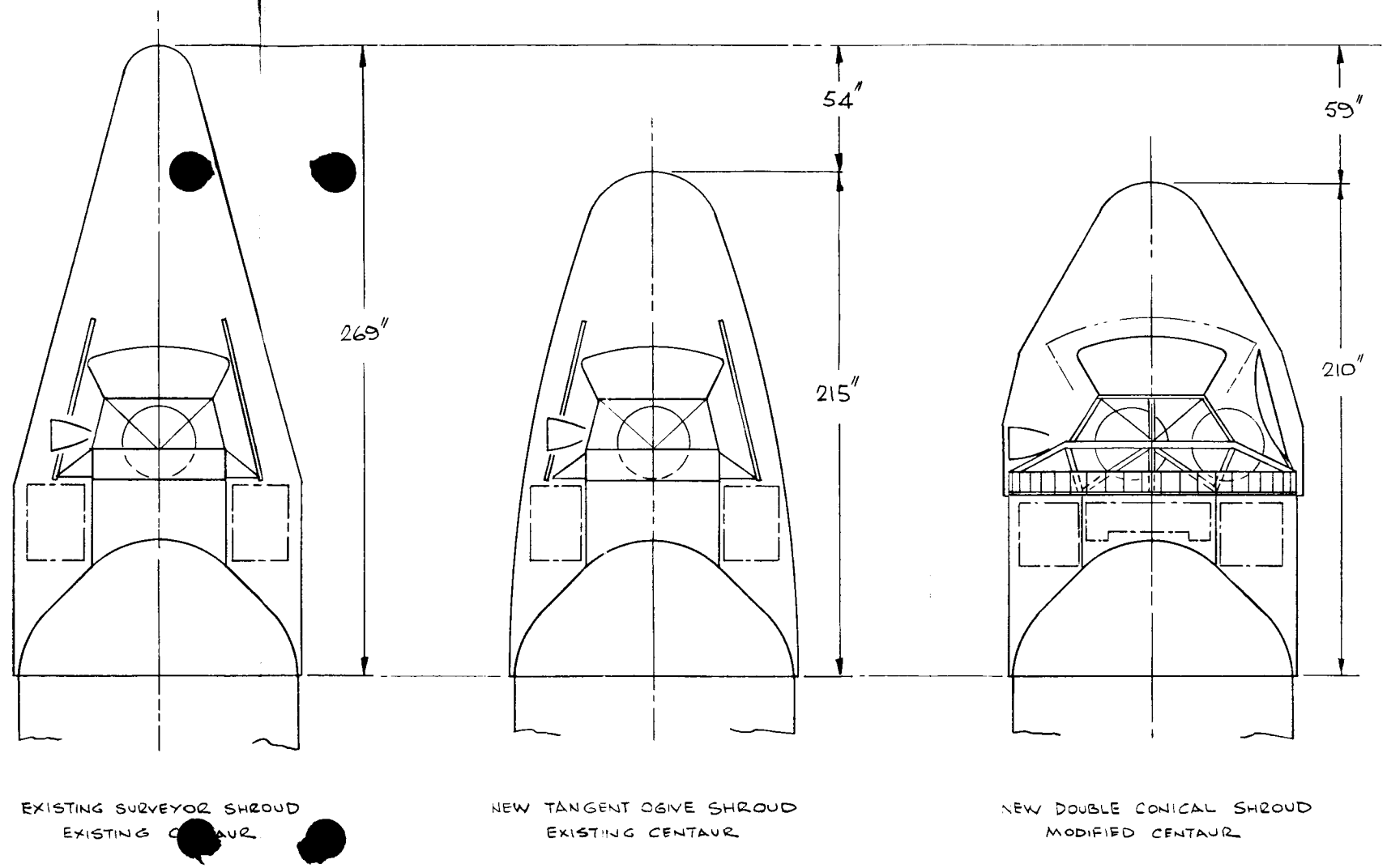


Fig. 4-11 Alternate Launch Shroud and Spacecraft Concepts

Section 5
SUBSYSTEM DESCRIPTION

5.1 GUIDANCE AND CONTROL

5.1.1 Attitude Control

The function of the attitude control system is to stabilize the spacecraft so that its solar panels face the Sun. This permits orientation of the communication antenna toward Earth. Requirements for Attitude Control exist both during the transfer from Earth to Mars and during the vehicle's life on orbit at Mars. In addition, the attitude control system provides a reference system of coordinates within which orientation and thrust vector control for guidance maneuvers are accomplished.

For the Mars missions two maneuvers are anticipated to correct the course of the spacecraft, and for vehicles which include a direct-entry capsule an additional orientation maneuver is required for release of the capsule. The vehicle design with a side-mounted engine permits injection into orbit about Mars in 1969 and 1971 without changing the in-flight orientation. If the same vehicle is used on a Venus mission, a maneuver for injection into orbit is required.

After the vehicle is in a planetary orbit, its attitude will remain fixed provided the planetary scan subsystem remains operative. In the event that this unit fails, it would be possible to direct the scientific instruments for short periods of time by reorienting the vehicle upon a command from Earth.

5.1.1.1 Description

Control System Operation. The attitude control system that is considered most appropriate for these missions is similar to that used on Mariner C. It operates in a primary mode in which the attitude is fixed during most of its lifetime and in a secondary mode for short intervals when a special orientation is required.

In the primary mode the longitudinal axis points toward the Sun, and roll about this axis is stabilized with reference to Canopus (Fig. 5-1). A sun sensor directed forward in the spacecraft senses the deviation from the direction of the Sun in the pitch and yaw axes and energizes the reaction control jets on these axes to rotate the vehicle opposite to the deviation. A star tracker directed toward the south celestial pole detects the direction of Canopus relative to the vehicle and actuates reaction control jets on the roll axis to keep Canopus in the center of the field of view.

A stabilization accuracy of one degree is required for pointing the high-gain antenna. This is also adequate for directing the solar panels and/or orientation for guidance maneuvers. Consequently, in the absence of disturbances, each axis of the control system is designed to operate with a two-degree deadband, centered about the null position. To achieve optimum utilization of the specific impulse of the propellant a minimum on-time for the reaction jets is designed into the controller. Twenty milliseconds is considered to be a practical value. The vehicle's attitude will then limit cycle within the bounds of the deadband at a rate determined by the thrust of the jets.

In the secondary mode, the required orientation may be such that the Sun sensor and star tracker are not directed at the Sun and Canopus. For example, the orientation required at the time of the first guidance correction is dependent on the random dispersion of the errors incurred at launch. For this purpose, three gyroscopes with mutually perpendicular input axes are mounted on the vehicle. Before reorienting the vehicle, the gyroscopes are energized with their spin vectors caged through their torquers. Actuation signals to the controller are transferred from the Sun sensor and star tracker to the output signals from the gyros.

In the caged mode, the gyros measure the vehicle rates so that the spacecraft can be commanded to assume an angular rate by applying currents to the torquers. To rotate through a specified angle, the currents are applied for a fixed duration and then removed. After thrusting, or any other function of the maneuver, the rotation is made again in the opposite direction to return to the primary orientation. At this time, control is transferred back to the primary attitude references.

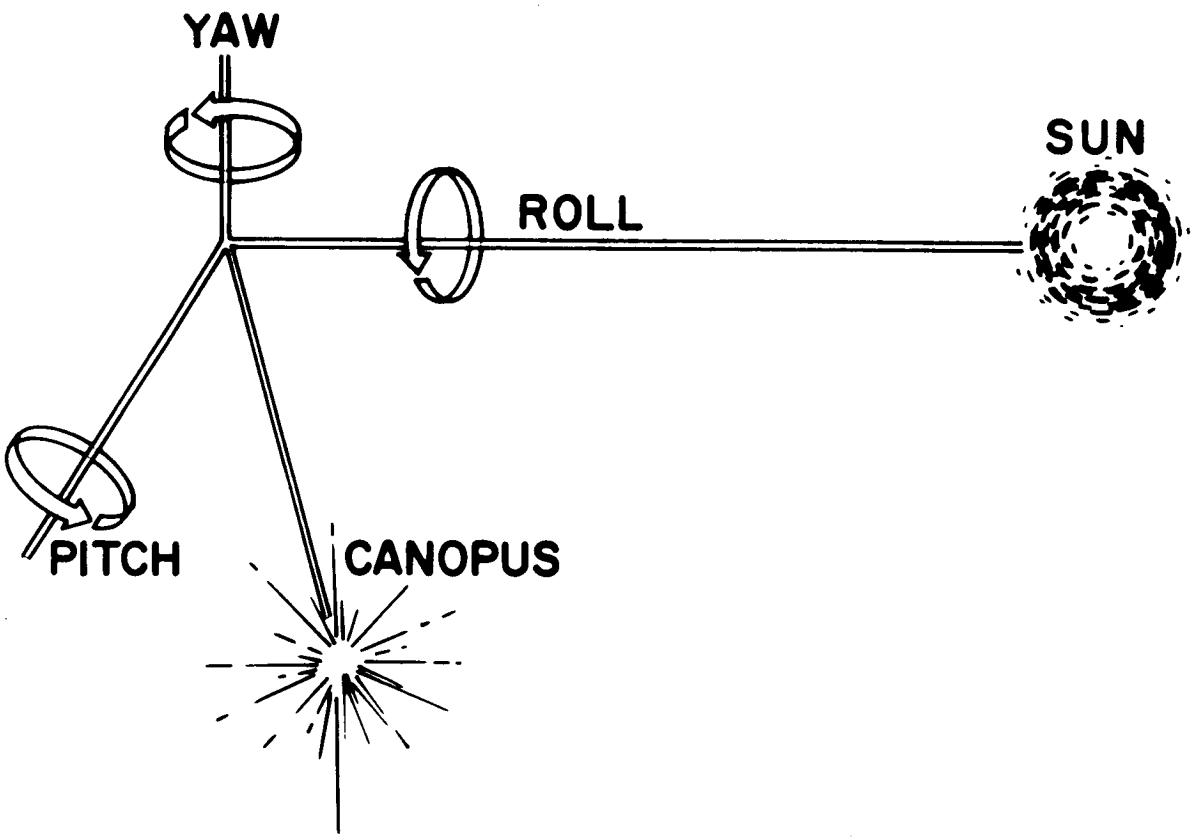


Fig. 5-1 Mariner Orbiter Attitude Control Reference System

Thus to perform a maneuver, the magnitudes and durations of the currents to be applied are transmitted to the spacecraft and stored in the computer. At the selected time, a computer program will execute the maneuver and return the vehicle to its primary mode of operation.

To establish the primary reference initially and to reestablish it if it is lost for any reason, an acquisition sequence is followed. With the gyros energized, the pitch and yaw axes will drive until the sun sensor is nulled. A secondary sun sensor directed backward in the vehicle provides a reference when the orientation is more than 180 deg from the Sun.

When the signals from the sun sensor fall below a prescribed level, indicating Sun acquisition, a roll rate is commanded. As the star tracker passes over Canopus, the roll axis locks onto the signal from the tracker and stops the rotation. After acquisition is accomplished, the gyros are deenergized and damping of vehicle motion is accomplished by derived rate circuits in the controller. In the event of a false acquisition in roll, as evidenced by lack of communication through the high-gain antenna, an override signal which causes the vehicle to continue to roll can be commanded through the omnidirectional antenna. Although the data rate at large distances is very low in this mode, sufficient communication is possible to convey the override command.

Thrust Vector Control. For midcourse and injection maneuvers, the rocket engine is fired until a specified velocity increment is acquired by the spacecraft. To control the direction of the increment of velocity, the vehicle is rotated until the rocket engine points opposite to the desired velocity vector. The engine is mounted on two gimbals which permit it to rotate relative to the pitch and yaw axes of the vehicle. Before firing the engine, the gyros are uncaged, causing them to measure the angles of deviation rather than the rates. Signals from these gyros continue to drive the attitude controller and they are also used to drive the thrust vector controller which energized the actuators on the engine's gimbals. When the engine is fired, the gimbals move to maintain the vehicle's attitude, thereby causing the thrust vector to pass through the center of gravity.

Due to the release of the capsule and to the use of propellant during injection the center-of-gravity of the vehicle shifts, causing a deviation in the direction of the velocity vector that this system produces. However, the shift when the capsule is released will be known with fair accuracy, and the direction of the thrust vector for orbit injection is not critical. For the two guidance corrections, the location of the center of gravity will be known precisely from a measurement made before launch, and its uncertainty will contribute little to the error in the direction of the velocity vector. Net errors in the direction of the velocity due to sensors, gyro drift, and cg uncertainties are estimated to be 0.6 deg rms.

To control the magnitude of the incremental velocity, an accelerometer oriented along the direction of thrust is provided. Its output is integrated in the computer counting the number of pulses required to restore its test mass. When this number exceeds a specified value, a signal is derived which shuts off the engine. Errors in the magnitude of incremental velocity are caused primarily by uncertainties in the thrust profile during shutdown. These are estimated to produce an rms uncertainty of 0.1 m/sec.

Equipment. The sun sensors, gyros, and star tracker can be the same as those used on Mariner C. The star tracker is gimballed and has a field of view of 30 deg by 4 deg. Since Canopus lies about 15 deg off the south celestial pole, this permits it to be seen with the vehicle-to-sun line in any direction in the ecliptic if the 30-deg field is mounted along the longitudinal axis with its center toward the south pole. Developments in the area of optical sensors make it appear likely that a solid-state sensor having the same performance as the Canopus tracker for Mariner C will be available before 1969. If so, it should have some advantages in reliability and in the required operating voltage levels.

At present, cold gas jets with nitrogen as a propellant are preferred for the actuators. The use of solar vane actuators is not considered advantageous for the Mars orbiter mission in view of the magnitude of solar pressure at the radius of Mars and the disturbing influence that the albedo of Mars would exert during the time in orbit. Alternate

methods of actuation have been considered and are discussed in this report under the subject of propulsion.

Flight-control electronics for the Mariner orbiter consist primarily of the control and derived rate circuits for transferring attitude reference signals from the sensors to the actuators and the circuits required for thrust vector control. These are conventional semiconductor circuits which may be designed as modules or as integrated circuits. To increase the reliability, they will be provided in redundant sets with failure-monitoring and self-repairing capability.

The accelerometer for measuring thrust level is a standard type using a magnetically constrained test mass in a pulse rebalance circuit. Linearity and bias errors on the order of 5×10^{-4} g give adequate accuracy.

5.1.1.2 Impulse Requirements

Disturbances. Possible sources of torques tending to disturb the vehicle's attitude are micrometeroite impacts, solar radiation and, in orbit about a planet, the gradient of the gravitational field. To evaluate the effects of meteorites, the flux density at Mars is assumed to be the same as at Earth, 7×10^{-9} gm/m^2/sec at a velocity of 30 km/sec, and the spacecraft is approximated by a sphere 10 ft in diameter. The expected impulse derived from this is only 0.3 lb-ft-sec/mo, which could be overcome by a neglibible amount of cold gas propellant.

The effect of solar pressure acting on the 100 sq ft of frontal area of the spacecraft produces an impulse of 38 lb-ft-sec/mo if the center of pressure and center of gravity are offset by one ft. This effect does not add to the gas requirement for this system acting in a limit cycle mode, since the minimum impulse is considerably larger than that required to overcome the solar pressure disturbance.

With different principal moments of inertia, disturbing torques are exerted on the vehicle in orbit as a result of the gravitational field. With the nominal orbit considered

for the Mariner orbiter and a difference of 55 slug-ft^2 in the moments of inertia, the disturbance amounts to 1 lb-ft-sec/mo.

It is concluded that solar pressure is the dominant disturbance on the spacecraft, whether it is in heliocentric or planetocentric orbit. The meteorite flux at Mars may exceed that at Earth, but it would have to increase by two orders of magnitude before its effects become comparable to those due to solar radiation.

Limit Cycle. The majority of the impulse required to stabilize the vehicle is consumed by operation of the limit cycle. It is desirable to make its period as long as possible; however, for practical implementation with reliable and simple equipment the period is limited to about 2000 sec. If this is the period of the limit cycle corresponding to the largest moment of inertia (338 slug-ft^2), the impulse expenditure for this axis is 6.13 lb-sec/mo with the reaction jets mounted 10 ft from the cg. The remaining axes are estimated to have moments of 318 and 240 slug-ft^2 during transfer. With identical reaction jets on all axes, the impulse requirement is 21.5 lb-sec/mo. The thrust level on each axis is 0.13 lb.

After the capsule is released and the vehicle is injected into orbit its principal moments of inertia are reduced to 265, 203, and 177 slug-ft^2. With the same reaction control system, the periods of the limit cycles will decrease and the rate of impulse expenditure will be greater. Under these assumptions, the requirement for on-orbit operation becomes 29.8 lb-sec/mo.

The overall limit cycle requirement for a 9-month transfer phase and 6 months on orbit is 373 lb-sec exclusive of whatever amount of propellant is dissipated through leakage. If a specific impulse of 60 can be realized, the weight of the propellant is 6.2 lb. With a sustained disturbance due to solar pressure, this requirement remains essentially the same. A large meteorite impact would cause a higher rate of expenditure, but these should occur so infrequently that their net contribution is negligible.

Acquisitions and Maneuvers. The propellant used for maneuvering is a function of the rate with which it is desired to reorient the spacecraft. Reorientation can proceed as

slowly as it is practicable to torque the gyros, since no maneuver is required for which the time for performing it is critical. A typical maneuver is considered to be one in which the vehicle is turned 90 deg in 30 min. This operation, plus return to the original orientation, requires 3.6 lb-sec in addition to that used to maintain the limit cycles. The three maneuvers anticipated for the mission would then require 10.8 lb-sec of impulse. Additional propellant for 10 maneuvers will be carried as a backup for possible failures of the planetary scan system.

Acquisition or reacquisition of the references involves a rotation of the vehicle under gyro control in the same manner as for a maneuver. Because three axes are involved and the possibility of false acquisitions exists, the expected impulse required for an acquisition may be considerably larger than for a maneuver. It is estimated that 12 lb-sec are needed and that acquisition will occur twice during a typical mission.

Total Impulse. To summarize the preceding estimation of impulse for a 1969 orbiter/capsule mission of 9-month transfer duration and 6 months on orbit, the expected value of attitude control impulse is about 435 lb-sec exclusive of leakage and redundancy requirements. For an orbiter that does not carry a capsule, it is proposed to shorten the control jet moment arms from 10 ft to 9 ft, thus increasing impulse requirements to about 475 lb-sec.

5.1.1.3 Redundancy

The overall reliability of the attitude control system as described above is relatively low, and since the success of any part of the mission is critically dependent upon its operation every component is to be provided in redundant pairs. Each sun sensor and the star tracker is supplied in duplicate. All units are operative and comparators at their outputs detect failures. A diagnostic routine isolates the unit that has failed and removes it from the circuit.

The flight control electronic circuits will be designed in a self-monitoring and self-repairing unit which will make optimum use of the components carried as spares.

Since it contains three identical sets of circuitry for the three axes, provision will be made for applying each redundant circuit to whichever axis encounters a failure. By applying existing techniques in self-organization the electronic circuits can be made sufficiently reliable that the dominant mode of failure will exist in the sensors or the actuation system.

Duplicate sets of reaction jets and propellant supply systems will operate in parallel. In the event that a jet fails to open, the alternate jet will maintain operation in a limit cycle of longer duration. If a jet fails to close, it will exhaust its propellant supply as well as that of the other jets fed by that supply. The disbalance this situation incurs will be counteracted in part by jets fed from the other supply. Consequently an amount of propellant equal to three times that which is required without failures will be carried on the spacecraft. Thus an impulse capability of 1305 lb-sec is to be supplied for a 1969 orbiter carrying a capsule. For a 1969 orbiter without a capsule, the total impulse capability to be supplied is 1425 lb-sec. No additional allowance is made for leakage, since a leakage allowance is automatically provided in all circumstances except that of a valve stuck open very early in the mission.

5.1.2 Guidance

A nominal trajectory from Earth to Mars for each day within the selected 1969 launch window has been established. The purpose of the spacecraft guidance function is to provide means of following these trajectories as closely as possible by making periodic observations of the course and suitable corrections to the flight path.

For the missions considered here, the only means of navigation will be by radio tracking through the DSIF network. Alternate possibilities involving optical sensing of the stars and/or the destination planet have been rejected because of the considerably greater weight that would have to be carried in the form of instrumentation. Furthermore, instruments adequate for this purpose are not available and would have to be developed.

Changes in the flight path will be accomplished by placing the vehicle in a gyro-referenced mode, rotating it to a selected attitude, and firing the rocket engine until the velocity

increment required to achieve the new flight path is attained. During firing, the direction of the thrust vector is maintained by an autopilot, referenced to the gyroscopes and controlling the engine's gimbal angles.

Primary emphasis in this study has been placed on the guidance requirements for the 1969 Mars orbiter. The 1971 Mars mission and the 1970 Venus mission are expected to have requirements sufficiently similar to cause no changes in the design or performance of the vehicle.

5.1.2.1 Error Sources

Uncertainties in the physical model of the solar system and dispersions in the tracking data received through the DSIF network are the principal sources of navigation errors in determining the course of the spacecraft. Additional deviations from the nominal trajectory are caused by errors in pointing the thrust vector during maneuvers and in controlling the magnitude of the velocity increment it produces.

Physical Model. Distances measured relative to bodies in the solar system are uncertain to the extent that the Astronomical Unit (AU) is in error. That is, the absolute range of a spacecraft from Mars is indeterminate because the distance to Mars is not known precisely.

Determination of the AU by radar returns from Venus has reduced this uncertainty to within a standard deviation of 250 km. Inaccuracy in the measurement is due in part to the uncertainty in the velocity of propagation of radio waves and partly due to the fact that the particular area of the surface from which the energy was received is not known. The probable error in velocity of propagation, currently estimated at 200 m/sec, results in a standard deviation in the AU of 150 km. An error of 200 km is attributed to the reflecting surface and electronic equipment.

The ephemerides of the planets are established optically to within the resolving power of the telescope used for measurement. The standard deviation in their estimation

is currently about 0.05 sec of arc. The ratios of the distances between planetary orbits is known with extreme accuracy from observations of their orbital periods, and any error is considered neglibible compared to the other errors in the model.

At the time of arrival of the 1969 orbiter, Mars will be approximately 170 million kilometers distant from Earth. If the spacecraft were tracked with absolute precision relative to Earth its position relative to Mars would be in error by 43 kilometers in directions normal to the line of sight because of the uncertainty in the ephemeris of Mars. The error in Mars' position in the direction of the line of sight would be 283 kilometers if the full deviation of 250 km in the AU is used. However, since the method of tracking also involves the velocity of propagation of radio waves, this contribution to the error in the AU is cancelled for relative measurements and the line of sight error becomes 227 km.

These errors have an effect on the dispersion of the impact parameter. This is the location of the arrival asymptote relative to the center of the destination planet in a plane normal to the asymptote. For the nominal launch and arrival dates, January 29 and October 26, 1969, the ellipse of 1σ dispersions due to errors in the physical model is 324 kilometers long and 86 km wide in this plane.

DSIF Tracking. For several days after launch the vehicle is tracked continuously from the DSIF stations, and its course is determined within certain tolerances. After that, it is tracked periodically throughout the transit time. Both range tracking, by means of the time between the transmission of a signal and its return, and range-rate tracking, by means of the doppler shift in the carrier, are used.

A complete evaluation of the accuracies of orbit determination by this method is beyond this study. Here it is assumed that for near-earth tracking there is a standard deviation of 0.1 m/sec in the velocity in any direction between the trajectory that is determined by tracking and a trajectory that actually achieves the required position and arrival time of the asymptote upon arrival at Mars.

It is assumed that, as a result of correlation of the tracking data during the rest of the trip, the standard deviation in the position of the vehicle on the arrival asymptote is 10 km in the direction of the line of sight and 220 km in directions normal to the line of sight. The line of sight range at arrival can be derived almost entirely from ranging on the vehicle in the vicinity of Mars whereas the normal errors are strongly dependent upon near-earth tracking and periodic samples along the trajectory.

Solar Pressure. The uncertainty in the effects of solar pressure on the vehicle will produce a large deviation between the actual trajectory which the spacecraft follows and the one which is predicted. However, this deviation is measured as a result of DSIF tracking along the course and its contribution to the error in determination of the vehicle's position after tracking is expected to be small.

Maneuver Execution. During any thrusting maneuver, there is a deviation in the direction of the velocity increment given to the vehicle which is caused by errors in the attitude references to which the gyroscopes are aligned, drift in the gyros during the maneuver, and errors in controlling the thrust vector to the gyro reference. There is an error in the magnitude of the velocity increment caused by inaccuracies in measuring and integrating the vehicle's acceleration and in cutting off the rocket engine thrust at the correct time. The error in direction is estimated to have a standard deviation of 0.6 deg and the error in magnitude to have a standard deviation of 0.1 m/sec. Thus, with an expected value of 10 m/sec for the first correction, the 1σ error distribution in velocity is 0.1 m/sec in any direction. The 3σ value for computing propellant requirements is 30 m/sec.

5.1.2.2 First Guidance Correction

After the spacecraft has been tracked until its course is determined with sufficient accuracy, a correction is made to decrease the dispersion in the arrival asymptote at Mars. The time at which this correction can be made with the minimum expenditure of propellant may occur at twenty or thirty days after launch; however, the difference between the propellant required at that time and that required immediately after launch

is small. There is some accuracy to be gained by performing the maneuver as early as possible since near earth tracking of the vehicle after the maneuver will permit more accurate measurement of the execution errors. Consequently, it is assumed that the first correction is performed as soon as possible after launch. It is estimated that three days will be required to attain sufficient tracking accuracy to make the maneuver.

After the maneuver the tracking error of 0.1 m/sec and the maneuver execution error of 0.1 m/sec result in an elliptic dispersion of the impact parameter at Mars with semi major and minor axes of the 1σ ellipse of 9060 km and 705 km for launch on January 29, 1969. The semimajor axis is inclined at 25.1 deg to the ecliptic, Fig. 5-2. The ellipse varies from 6850 by 790 km at an inclination of 34.9 deg for launch on January 15, 1969, to 11,050 by 639 km at an inclination of 16.6 deg for launch on February 14, 1969.

Guidance of the vehicle must be accomplished such that the probability of impact on the surface is less than 10^{-4}. Since the probability of failure of the guidance system after the first correction and before another can be made is considerably larger than 10^{-4}, the nominal arrival asymptote after the first correction must be selected so that the probability of entry is less than 10^{-4}. This is satisfied approximately if the entry corridor at Mars falls outside of the ellipse of 4σ dispersion.

The distance of the nominal arrival asymptote from the selected point of orbit injection is smallest with the aiming point located as shown in Fig. 5-2. Thus the distance of the arrival asymptote from the center of the planet for the January 29 launch date is 11,200 km, and the aiming point is inclined at 51 deg to the direction of the impact parameter required for orbit injection. This distance remains relatively constant through the launch window.

5.1.2.3 Second Guidance Correction

The dispersion in the position and time of arrival at Mars after the first guidance correction is so great that a planetary orbit cannot be established without another

correction. After tracking at intervals during the trip, the location of the vehicle relative to earth is predictable to within 220 km in directions normal to the line of sight. This uncertainty together with the uncertainty in the Mars ephemeris results in a standard deviation of 225 km in the predicted location of a vehicle at Mars. The uncertainty in the AU and the tracking error result in a standard deviation of nearly the same magnitude in the direction of the line-of-sight from earth.

The second correction will leave the arrival asymptote with a residual error due to its execution. By waiting to make the correction until the distance to the planet is very small, the effect of the execution error becomes negligible; however, the propellant required is excessive. On the other hand, if the correction is made too early, the errors in performing it will far exceed the tracking errors. As a compromise, the second correction is made at the time when its execution contributes approximately the same errors to the impact parameter as does the uncertainty in radio tracking. This occurs at 26 days prior to arrival at Mars.

The aiming point for the second correction must also be such that the probability of landing on Mars is less than 10^{-4}. The net dispersion in the impact parameter due to tracking and maneuver execution has a 1σ value of 315 km in either direction. To keep the entry corridor at the planet outside of the circle of 4σ dispersion, the nominal asymptote must be aimed a distance of 7120 km from the center of Mars. The nominal periapsis altitude then becomes 1500 km. Minimum altitude is taken as 300 km above the surface to insure orbits of 50 yr lifetime. Figure 5-3 illustrates the dispersion in the arrival asymptote that will exist after the second correction. With the dispersion in the first correction shown in Fig. 5-2, the impulse required for the second correction will fall between 3 and 13 m/sec for more than 99 percent of the trajectories. The 3σ value for computing propellant requirements is 13 m/sec.

5.1.2.4 Orbit Dispersions

The dispersion in the impact parameter and the error in determining the time of periapsis of the approach hyperbola cause a dispersion in the parameters of the orbit

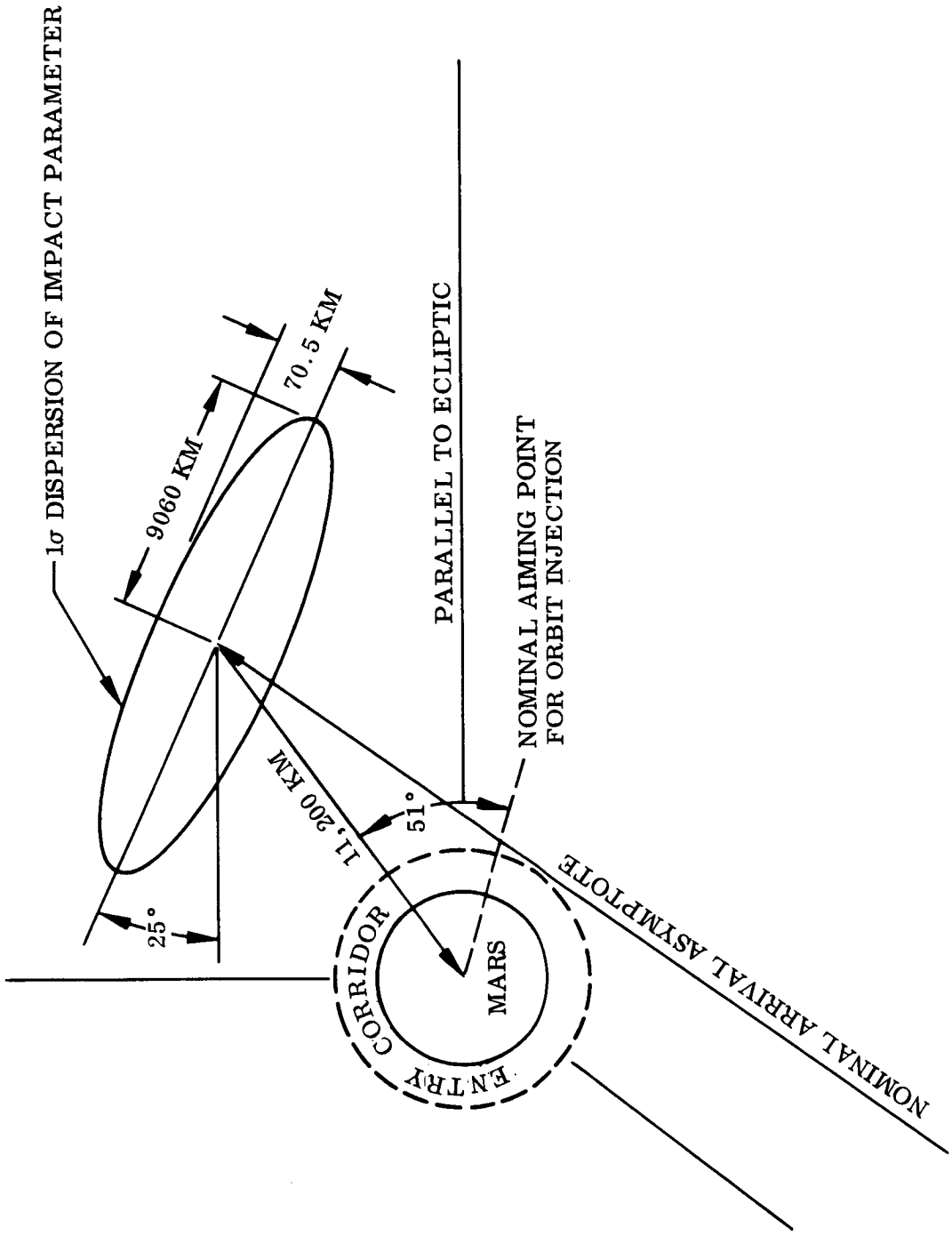


Fig. 5-2 Dispersion of Impact Parameter After First Correction – Mars 1969

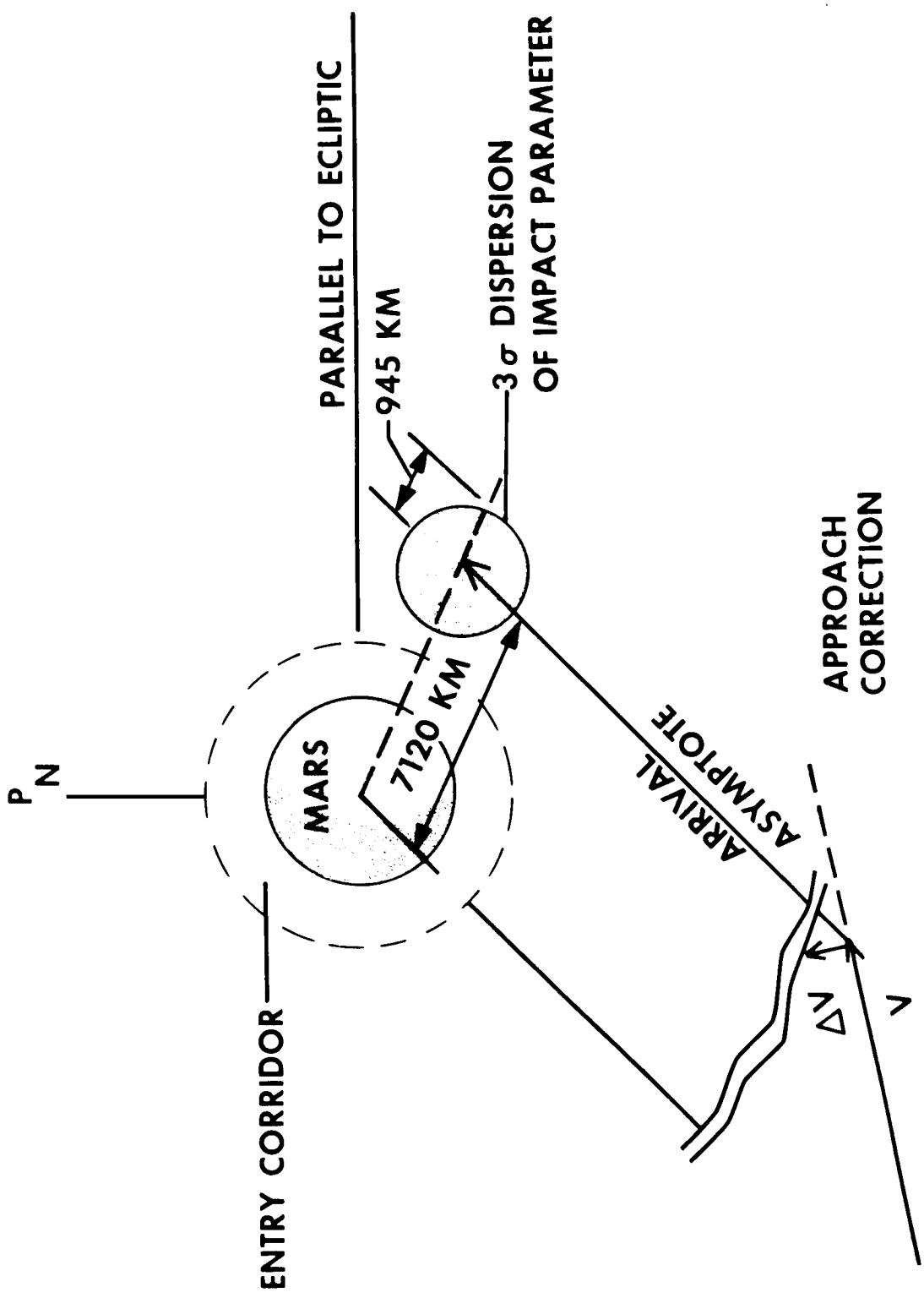


Fig. 5-3 Dispersion of Impact Parameter After Second Correction – Mars 1969

that is established about Mars after the injection maneuver has been performed. The more important of these are shown in Fig. 5-4 as a function of launch date. The nominal aiming point is selected to give the minimum value of periapsis, thereby using the minimum energy for orbit injection, while retaining a probability of 10^{-4} that periapsis will remain more than 300 km above the surface. This varies slightly through the launch window because of the variation in hyperbolic excess velocity at Mars.

The 3σ limits on the parameters give the boundaries outside of which the probability of occurrence is no more than 0.0027. Rather large dispersions in the radius of apoapsis and in the orbit period occur. The dispersions generally become greater in the latter portion of the launch window.

5.1.2.5 Orbit Selection

From the dispersions given in the preceding section, limits on those orbits which may be achieved can be set. A primary consideration is that the line-of-sight to the sun, required for attitude control and power, not be occulted by Mars. Figure 5-5 shows the relative directions of the Sun and the approach asymptote for the nominal arrival date. Periapsis of the nominal approach hyperbola will be rotated 21.5 deg around the planet from the normal to the approach asymptote which passes through the center of Mars. Periapsis of the orbit around Mars will nearly coincide with this, and thus will fall approximately in the plane normal to the ecliptic which contains the Sun and Mars. Therefore, the dispersion of apoapsis with limits of three standard deviations might appear as illustrated in Fig. 5-6. To avoid occulation within this boundary, the angle between the directions of periapsis and the Sun must be greater than 13 deg.

The attitude control system also requires a line-of-sight to Canopus for its operation. With periapsis south of the ecliptic parallel through the center of Mars, this condition is satisfied except for orbits of exceedingly high inclination. Because of the direction of Mars' pole, polar orbits can be achieved without occultation of Canopus. For periapsis more than 13 deg north of the ecliptic parallel, the orbit plane approaches Mars equatorial plane. This condition is not desirable because observation of the surface is

restricted to a zone about the equator and does not permit acquisition of information about the temperate zones. If periapsis is not on the sunward side of Mars, the orbit is further restricted; however, since the most information will be acquired during the time of closest approach it is considered essential to select an orbit so that the surface is sunlit at this time.

A further consideration in selecting the orbit is the line of sight to Earth. One means of measuring the diameter of Mars involves occultation of the orbiter by Mars. Figure 5-7 shows the trace of the nominal orbit for which the line-of-sight to Earth, the center of Mars and the orbiter are colinear on the nominal date of arrival. Periapsis is declined 22 deg below the ecliptic parallel through Mars and rotated 5.5 deg past the Mars-Sun line. The nominal orbit plane contains the approach asymptote and is chosen to contain the line-of-sight to Earth.

The shaded area is that part of the celestial sphere which will be occulted from view of the orbiter by Mars at some time during the orbit. With this selection of an orbit the line-of-sight to Earth will be occulted for all guidance dispersions within the 3σ limit although the trace of the line of sight will not necessarily cross a diameter of Mars on the first pass. As time passes after injection into orbit, the Sun and Earth vectors rotate counterclockwise along the ecliptic parallel. Thus, the Earth eventually comes out of the area of occultation and the Sun enters it. However, it is nearly a year after injection before occultation of the Sun occurs.

Since the vector to Mars' pole is inclined 26.6 deg in a direction nearly opposite to that of perapsis the inclination of the orbit is about 55 deg relative to the Martian equator. The ascending node between the orbit and equatorial planes is rotated about 110 deg from periapsis of the orbit.

5.1.2.6 Capsule Guidance

For mission concepts involving a direct landing capsule, a separation maneuver is made after the second guidance correction. Because of the small amount of propellant

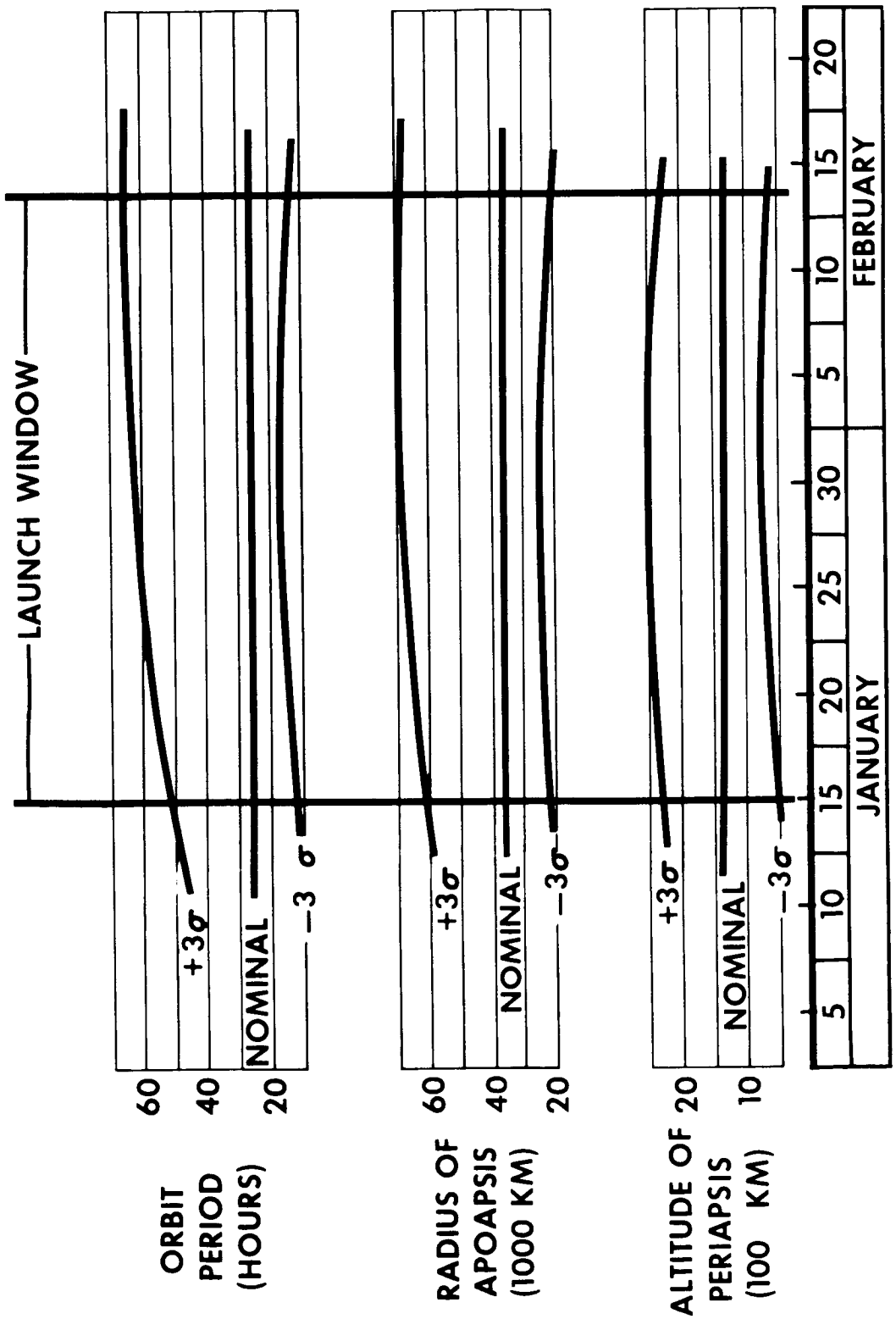


Fig. 5-4 Orbit Dispersion – Mars 1969

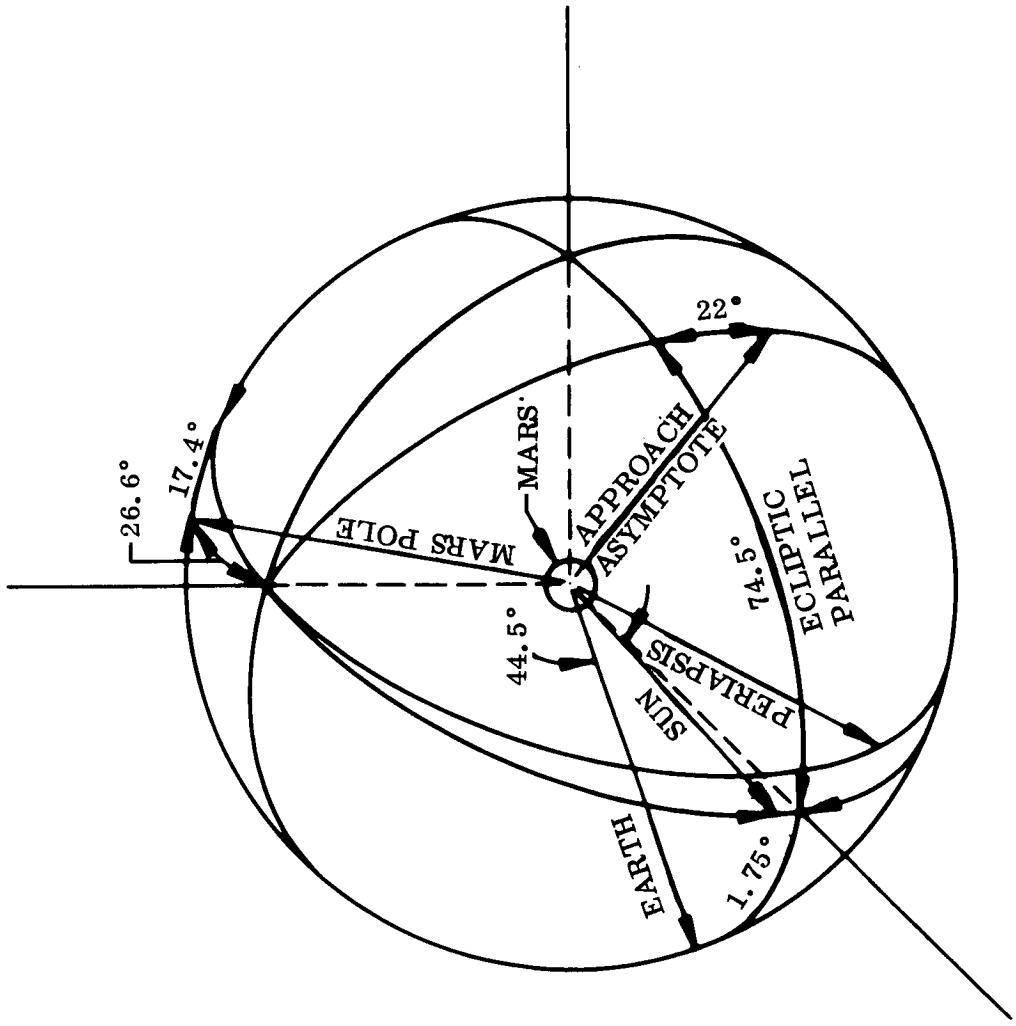


Fig. 5-5 Nominal Approach Conditions – Mars 1969

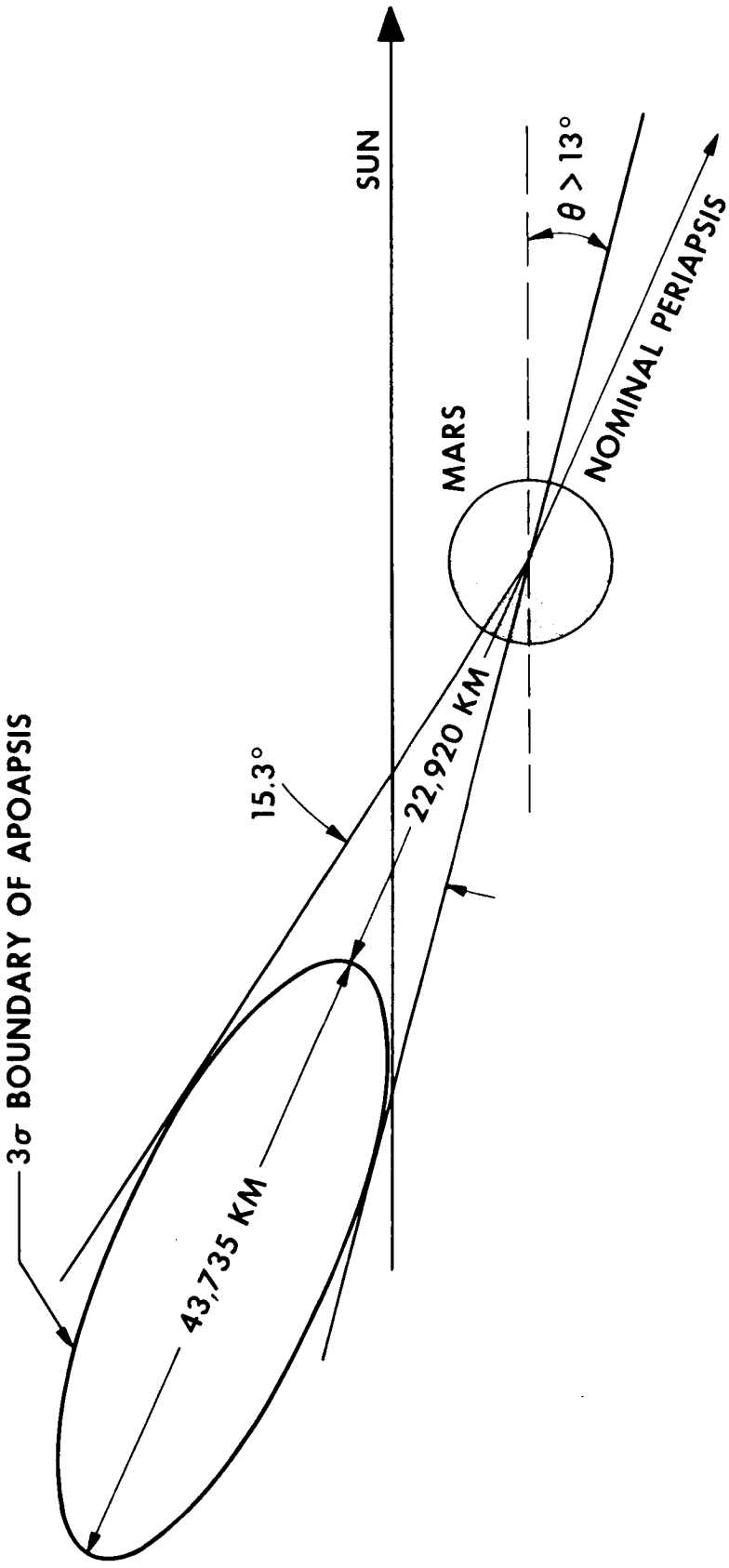


Fig. 5-6 Dispersion of Apoapsis – Mars 1969

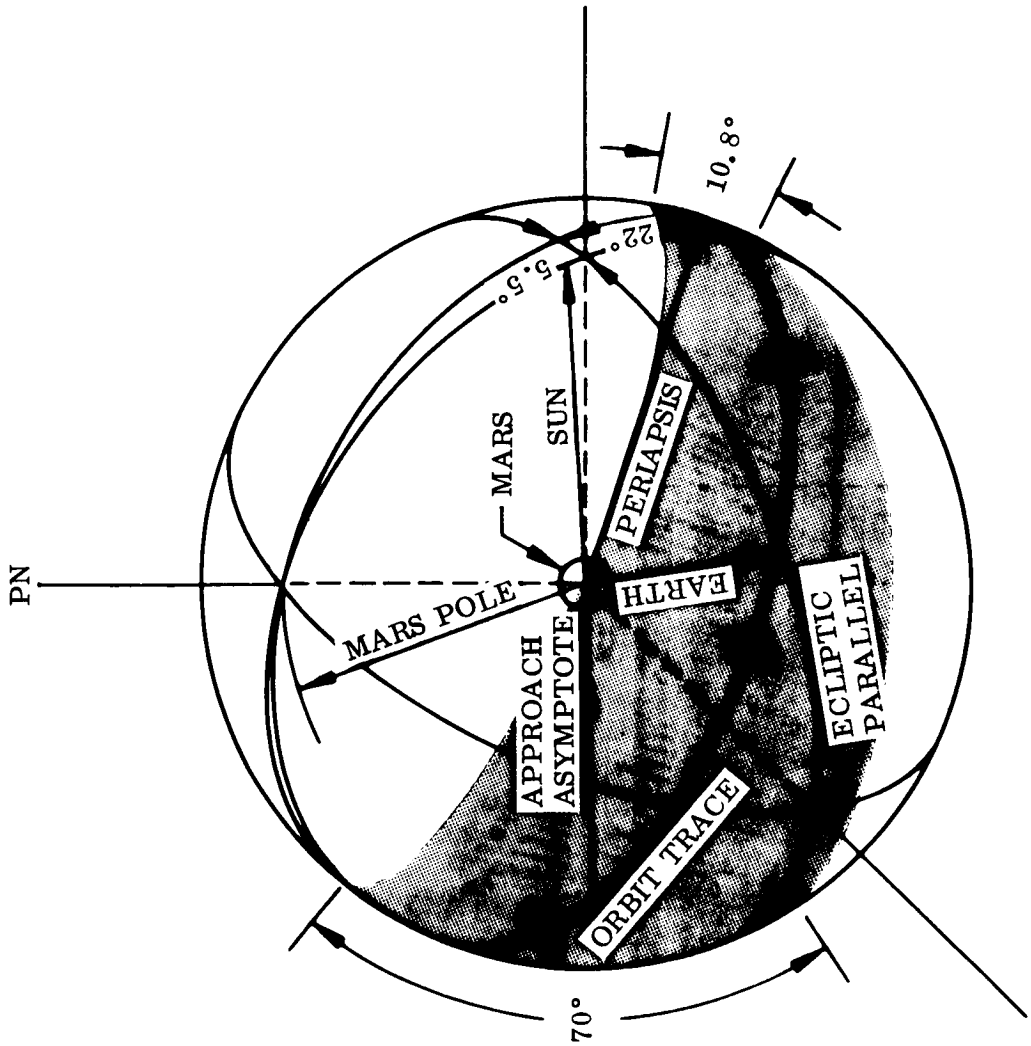


Fig. 5-7 Earth Occultation – Mars 1969

required to deflect the capsule to impact on the planet, the maneuver can be made sufficiently close to Mars that errors in its execution are negligible compared to the radio tracking errors. A time of two days before arrival has been selected for this event. The spacecraft is reoriented to an angle of 32 deg to the flight path, the capsule is separated, spun to 50 rpm and given a velocity of 50 m/sec by firing a solid rocket engine. It thus arrives at Mars some time before the orbiter at a nominal entry angle of 46 deg.

The 3σ dispersion of 945 km due to errors in tracking and execution of the second correction will cause the entry angle to be dispersed between 58 deg and 32 deg. The nominal entry is chosen to restrict the velocity at parachute deployment to Mach 2.5 and to restrict the thermal impulse during descent to that given by entry above 30 deg. The landing point is dispersed between 5 and 30 deg of latitude in the southern hemisphere of Mars.

5.2 EXPERIMENTAL TECHNIQUES AND INSTRUMENTATION

Scientific payload packages were suggested in the Mariner orbiter study in order to generate spacecraft design requirements and to provide measures of mission capability.

The assemblages of scientific instruments proposed here were thoughtfully selected to aid the designers in arriving at a well-proportioned system capable of achieving the prescribed mission objectives with as much reliability as possible through functional redundancy. At the same time the unique opportunities for correlated observations of various phenomena for an extended period afforded by a long-life orbiter led to the selection of a more diversified array of scientific instruments than is required by the primary mission objectives. It is believed that the final selections of scientific payloads described here have much to offer in regard to capability for achieving the primary mission objectives as well as diversity relative to the acquisition of important information beyond the minimum requirements of the missions.

5.2.1 Scientific Objectives

In compliance with instructions from JPL in Ref. 2 concerning the prime objectives of the Mariner Mars 1969 Orbiter, attention was directed mainly to examining the capabilities of the orbiter in relation to the following scientific objectives:

- Size and shape determination of Mars
- Television observation of surface of Mars
- Acquisition of biological and surface environmental data with a landing capsule

Performance of interplanetary experiments during the flight from Earth to Mars is also required insofar as such experiments do not interfere significantly with the prime objectives.

5.2.2 Initial Selection of Scientific Payloads

It was necessary early in the study to indicate tentative scientific payload requirements so as to provide a basis for the design of supporting subsystems. A "shopping list" of experimental instruments was prepared specifying size, weight, power and data output rates for each instrument as shown in Table 5-1. Specifications were obtained, for the most part, from a preferred list supplied by JPL in Ref. 2. Some items, such as radar altimeters, accelerometers, and rate gyros, are represented in accordance with data supplied by vendors and two instruments (the planet diameter scanner and the star deflectometer) are entirely conceptual at present.

A choice of possible payloads was offered to the subsystem designers by selecting from the list four different assemblages of instruments ranging in total weight from 18 to 244 lb for the orbiter alone. In view of the smaller payload capability of the orbiter with capsule compared to the oribiter alone, a somewhat smaller range of optional scientific payload weights was devised for the orbiter with capsule.

5.2.3 Orbiter Capabilities

Determination of Mars Size and Shape. It appears feasible to determine the size and shape of Mars in a number of ways with the aid of the orbiter. Accuracies should be considerably better than are likely to be achieved by instrumentation on Earth. The accuracy to which the diameter of Mars is now known is indicated by the following considerations.

The angular resolving power of a telescope is expressed by the formula $1.22\ \lambda/d$, in which λ is the wavelength of light and d is the diameter of the telescope aperture. In the case of the Palomar 200-in telescope, using light of wavelength 0.6 micron, the resolving power is 1.44×10^{-6} radians. Mars nearest approach to Earth is about 55×10^{6} km. Hence, at best the visual limit of resolution is about 80 km. Because of atmospheric shimmer, photographic resolution is only about half as good as visual

Table 5-1

EXPERIMENTAL INSTRUMENT SHOPPING LIST

Orbiter Instruments	Size (in)	Weight (lb)	Power (watts)	Sample (bits)
Ion Gage	5 diam	1.3	0.1	14
Particle Flux Meter	4 × 5 × 6	2.5	0.35	42
Medium Energy Proton Monitor	4 × 5 × 5	3	1	84
High Energy Proton Monitor	3 × 4 × 4	4	0.5	84
Cosmic Ray Spectrum Analyzer	6 × 6 × 18	18	2.5	98
Low Energy Plasma Monitor	6 × 8 × 8	7	1.25	56
High Energy Plasma Monitor	8 × 8 × 12	20	4	98
Cosmic Dust Detector (A)	4 × 4 × 4	2.5	0.2	56
Cosmic Dust Detector (B)	3 × 4 × 4	2	0.25	28
Micrometeoroid Detector (A)	8 × 8 × 8	8	0.5	56
Micrometeoroid Detector (B)	3 × 8 × 8	4	0.3	28
X-Ray Telescope	4 × 5 × 6	5	3	56
Neutron Spectrometer	5 × 6 × 6	8	3	35
Magnetometer	4 × 4 × 6	5	5	21
Trapped Radiation Detector	4× 5 × 5	4	0.7	28
Microwave Spectrometer (A)	10 × 10 × 12	30	13	210
Microwave Spectrometer (B)	12 × 12 × 12	35	15	420
UV Spectrometer	9 × 10 × 24	22	12	315
IR Spectrometer	15 × 12 diam	29	7	420
UV Photometer (A)	5 × 3 diam	1.5	1.5	21
UV Photometer (B)	5 × 6 × 7	6	5	84
IR Radiometer	4 × 5 × 7	3	3	28
IR Interferometer	7 × 8 × 12	16	5	35
Microwave Radiometer	8 × 8 × 14	24	4	28
Television (A) (low resolution)	2 × 3 × 4	6	15	2×10^5
Television (B) (high resolution)	15 × 7 diam	30	15	1.8×10^6
Television (C) (very high resolution)	24 × 10 diam	130	25	6×10^6

Table 5-1 (Continued)

Orbiter Instruments	Size (in)	Weight (lb)	Power (watts)	Sample (bits)
IR Television	3 × 3 × 5	10	6	2×10^5
Facsimile Television	4 × 6 × 6	10	5	2×10^5
Planet Diameter Scanner	6 × 3 diam	10	5	28
Star Deflectometer	12 × 4 diam	10	2	28
Radar Altimeter	8 × 8 × 14	37	39	14
Bi-Static Radar	4 × 4 × 12	10	5	35
Top-Side Sounder	5 × 5 × 14	25	10	140
Capsule Instruments				
Pressure Gage	2 × 1.6 diam	0.4	0.1	7
Temperature Gage	3 × 1 diam	0.3	0.1	7
Density Gage	2 × 3 × 4	1.5	2	7
Acoustic Velocity Gage	2 × 2.3 diam	0.6	0.3	7
Pitch-Yaw Rate Gyro	5 × 3 diam	2	7	14
Radar Altimeter	4 × 9 × 12	8	25	7
Accelerometer	2 × 2 × 2	2	4	14
UV Photometer	5 × 3 diam	2.5	1.5	21
IR Radiometer	4 × 5 × 7	3	3	28
TV (Surface Scanning)	2 × 3 × 4	5	10	2×10^5
Solar Zenith Angle Indicator	2 × 2 × 4	0.8	2	14
Ionizing Radiation Monitor	4 × 5 × 6	3	0.5	21
Wind Velocity Indicator	24 × 2 diam	2	0.1	14
Gravitometer	6 × 5 diam	10	1	14
Seismometer	5 × 4.5 diam	7.5	0.5	210
Soil Properties Gages	12 × 12 × 24	14	3	35
Mass Spectrometer	3 × 5 × 10	5	6	140
Gas Chromatometer	8 × 8 × 10	14	20	280
Simple Gas Analyzers	6 × 8 × 8	8	6	42
Optical Polarimeter	6 × 3 diam	5	2	21

Table 5-1 (Continued)

Capsule Instruments	Size (in)	Weight (lb)	Power (watts)	Sample (bits)
X-Ray Diffractometer	8 × 10 × 12	16	15	280
Alpha Scattering Analyzer	6 × 6 × 8	7	2	21
Neutron Activation Analyzer	6 × 8 × 10	14	6	98
X-Ray Spectrometer	5 × 6 × 6	8	3	280
Fluorescent Spectrometer	4 × 12 × 15	40	30	280
Gulliver	6 × 8 × 10	6	3	98
Wolf Trap	6 × 6 × 6	4	1	98
Multivator	10 × 3 diam	4	2	140
Optical Rotation	4 × 6 × 6	5	1	98
J-Band Detector	3 × 8 × 10	5	5	210
Organic Gas Chromatometer	5 × 5 × 8	7	4.5	140
Vidicon Microscope	10 × 3 diam	5	2	10^6

capability. Thus, the uncertainty in the dimensions of Mars determined by photographic techniques is about 160 km, which is more than 2 percent of the diameter.

Table 5-2 lists eight combinations of basic information, obtainable with the aid of an orbiter, from which the dimensions of Mars can be deduced. All but one of the combinations require accurate data concerning the orbit parameters of the orbiter. The additional weight and power associated with the experimental technique implied by each combination and the estimated uncertainties in the results are indicated in the bottom rows of Table 5-2. All of the techniques offer considerable improvement in our knowledge of the dimensions of Mars, and two require no additional equipment weight or power.

Table 5-2

DETERMINATION OF MARS RADIUS

Basic Information	Technique							
	1	2	3	4	5	6	7	8
Orbit Parameters	x	x	x	x	x	x	x	
Radio Occultation Time	x							
Star Occultation Time		x						
Planet Angular Diameter			x					x
Radar Altitude				x				x
TV Location of Surface Features					x			
Surface Transponder Doppler Signals						x		
Surface Gravity							x	
Added Weight, lb	0	10	10	37	0	20	26	47
Added Power, Watts	0	2	2	39	0	10	4	41
Estimated Uncertainty, KM	3.5	2.4	1.2	1.3	4	1.4	0.4	3.7

Some of the techniques yield more information than others; e.g., angular measurements of the equatorial and polar diameters of Mars will immediately determine the degree of oblateness, whereas radar altitude measurements cannot yield data about the dimensions of Mars beyond the range of latitudes covered by the orbit. A brief examination of the operational details behind the various techniques will aid in evaluating their relative merits.

Technique No. 1, Radio Occultation. Occultation of the orbiter by Mars with respect to Earth will interrupt communication between Earth and the orbiter. Accurate knowledge of the orbiter's position at the time communication is interrupted will permit the radius of Mars to be inferred. It is estimated the DSIF tracking can establish the orbiter's position within 1 km relative to Mars' center of mass. This would indicate the feasible accuracy in determining the radius of Mars if orbiter position were the only source of error. Reflection and refraction of the radio beam by the ionosphere of Mars (if Mars has an ionosphere) and confused diffraction of the wave pattern by surface irregularities around the limb of Mars will add to the uncertainties in the occultation measurement. Present ignorance of Martian conditions does not permit quantitative estimates of the effects attributable to the ionosphere and surface features.

Refraction of the radio beam by the atmosphere of Mars will delay radio occultation relative to the instant of "geometrical" occultation corresponding to the point where the orbiter enters the "geometrical shadow" of Mars as viewed from Earth. If the composition and density of the atmosphere of Mars were accurately known, the refractive effect could be precisely calculated. For the purposes of the present study, the range of uncertainty concerning Mars' atmosphere is assumed to be bracketed by JPL Mars atmospheric models "H" and "J", respectively representing the least and greatest surface densities among the more recent models.

The refractive indexes of non-polar gases, such as nitrogen, carbon dioxide and argon, which presumably comprise the bulk of the atmosphere of Mars are practically the same for radio-frequency electromagnetic waves as for visible light. The

only polar gas present in detectable amounts with anomalous refractive properties at radio frequencies is water vapor, and its concentration is believed to be too small to exert a significant effect.

The refractive index of a mixture of gases is given by the following expression:

$$n = 1 + \frac{\rho}{\rho_s} \sum_i N_i (n_{si} - 1) \tag{5.1}$$

in which

- n = refractive index
- N = Mole fraction
- ρ = density
- i designates the ith component
- s signifies value for standard conditions (0°C, 1 atm)

The density of the Martian atmosphere at altitudes below 60 km, where most of the refraction occurs, is represented well enough for present purposes by

$$\rho = \rho_o e^{-z/H} \tag{5.2}$$

where

- ρ_o = density at ground level
- H = scale height
- z = altitude

Small-angle approximations and rectangular coordinates can be used to analyze the situation because the refractive deflection of the radio beam is very small and nearly all of the deflection occurs within a distance parallel to the surface that is small compared to the radius of Mars. The curvature of the ray path is proportional to the

gradient of the refractive index normal to the ray path in accordance with the following relation:

$$C = \frac{1}{n} \frac{dn}{dz} \tag{5.3}$$

in which the factor 1/n is unity for all practical purposes. Hence, the ray path deflection angle is given by

$$\alpha = \int C dx = \int \frac{dn}{dz} dx \tag{5.4}$$

in which x is the distance measured along the ray path. The situation is represented schematically in Fig. 5-8. The relation between z and x is given approximately by

$$z = z_o + \frac{x^2}{2r} \tag{5.5}$$

in which r is the radius of Mars and z_o is the altitude of the ray path at closest approach to the surface

The foregoing relations can be combined to obtain

$$\alpha = \frac{-\rho_o}{H\rho_s} \sum_i N_i \quad (n_{si} - 1)\, e^{-\frac{z_o}{H}} \int e^{-\frac{x^2}{2Hr}} dx \tag{5.6}$$

The physical limits of the integral need extend over only that portion of the ray path where the gradient of the refractive index normal to the ray is significantly different from zero. However, it is permissible and simpler to let the integration limits be

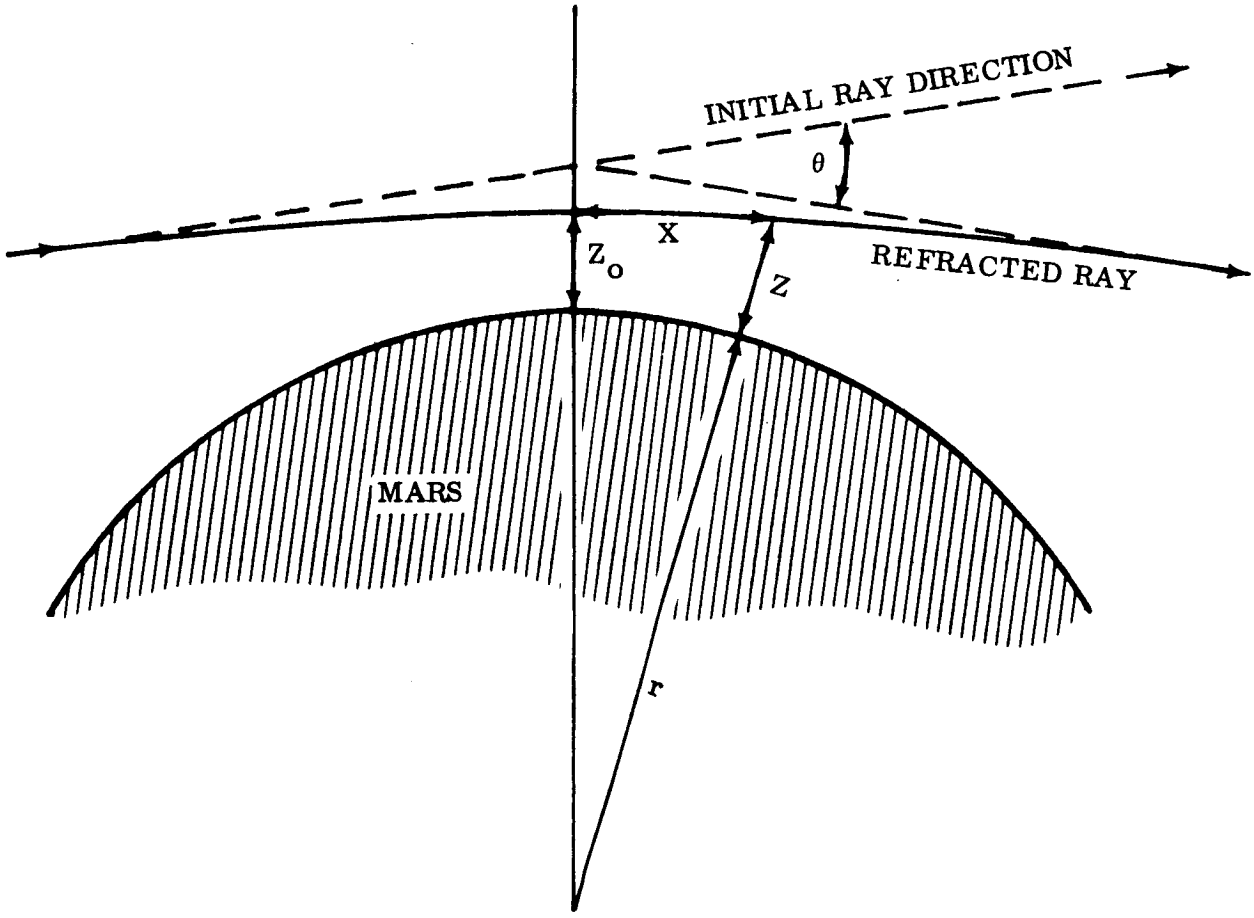


Fig. 5-8 Refraction by Mars Atmosphere

$\pm\infty$ in which case the following is obtained:

$$\alpha = -\frac{\rho_o}{\rho_s}\sqrt{\frac{2\pi r}{H}}\; e^{-\frac{z_o}{H}} \sum_i N_i \cdot (n_{si} - 1) \tag{5.7}$$

The deflection is obviously greatest at grazing incidence, i.e., when $z_o = 0$. Hence, the maximum angle of deflection of the radio beam by refraction in the atmosphere of Mars is

$$\alpha \text{ max} = -\frac{\rho_o}{\rho_s}\sqrt{\frac{2\pi r}{H}} \sum_i N_i \cdot (n_{si} - 1) \tag{5.8}$$

The following date in Table 5-3 were used:

Table 5-3

ATMOSPHERIC DATA FOR MARS

	Index of Refraction	Atmosphere "H"	Model "J"
Nitrogen	1.000296	0	76%
Carbon Dioxide	1.000448	65%	13%
Argon	1.000281	35%	11%
$\sum_i N_i(n_{si} - 1)$		3.89×10^{-4}	3.11×10^{-4}
H, km		12	19
ρ_s, gm/cm^3		1.90×10^{-3}	1.40×10^{-3}
ρ_o, gm/cm^3		2.17×10^{-5}	5.37×10^{-5}

Assuming that the diameter of Mars is 6780 km, we find the maximum deflection angles to be 39 and 82 sec of arc, respectively, for atmosphere models "H" and "J". The correction to be added to the apparent radius of Mars indicated by radio occultation is

$$\Delta r = \alpha T \tag{5.9}$$

in which T is the tangential distance from the orbiter to Mars' surface at the time of occultation (see Fig. 5-9). The uncertainty in α corresponding to the difference between atmospheric models "H" and "J" is 43 seconds of arc. The initial value of T may be anywhere from 8000 to 22,000 km depending upon which of the possible orbits, ranging in period from 12 to 65 hr, the orbiter is injected into upon arriving at Mars. Thus, the uncertainty in Δr may be anywhere from 1.7 to 4.6 km. Because of changes in the relative positions of Mars and Earth, the value of T increases with each cycle of the orbiter, so the most accurate determinations of Mars' radius by radio occultation are obtained early in the orbiter mission.

Except for the possibility that Mars might have an extremely potent ionosphere, the uncertainty in estimating the ordinary refractive effect of the atmosphere is the major source of error in determining Mars' radius, and this source of error will be obviated by acquisition of accurate information about Mars atmosphere. However, with our present state of knowledge, if we assume an uncertainty of 1 km in the location of the orbiter and attribute an uncertainty of 1 km to effects arising from irregularities in the surface of Mars, the resultant uncertainty in measuring the radius of Mars by radio occultation ranges from 2.2 to 4.7 km, depending upon whether we obtain a short or a long-period orbit.

In general, the plane of the orbit about Mars will be tilted at some angle relative to the line of sight from Earth. The guidance and navigation specialists state that we can choose the orbit plane so that the orbiter initially passes behind Mars below the line of sight from Earth. After a while the relative motions of Earth and Mars will

present an edgewise view of the orbital plane after which the orbiter will pass behind Mars above the Earth line of sight. Eventually, the view of the orbit as seen from Earth will be such that occultation no longer occurs. In this way, it will be possible to delineate the shape of Mars by obtaining a series of radius measurements at various latitudes encompassing more than half of one limb of the planet.

It has been suggested that radius measurements on the other half of Mars' limb might be obtained by noting when communication is restored after the orbiter comes out from behind Mars. However, because of frequency drift in the crystal oscillator that controls the signal from the orbiter and because of the narrow bandwidth of the receivers on Earth, a systematic search over a finite interval of the frequency spectrum must be maintained to reacquire the signal from the orbiter. This introduces an uncertainty of about one minute in determining precisely when radio occultation has ceased. It is estimated that proper use of a few additional lb and watts, to reduce the frequency drift of the orbiter signal, might reduce the uncertainty in reacquiring the signal to about 6 sec, but this still represents an uncertainty of about 10 km in addition to other errors in determining the radius. No new or better data concerning the radius of Mars are obtained from measurements based upon reacquiring the orbiter signal, so that technique has little to recommend it.

We summarize the advantages and disadvantages of the radio occultation technique for the 1969 orbiter as follows:

Advantages.

- It permits determination of the radius of Mars with uncertainties ranging from 2.2 to 4.7 km
- The accuracy will improve with improved knowledge of the atmosphere of Mars
- It permits determination of the shape of Mars
- It depends only upon the capabilities of the DSIF communication system, requires no additional equipment or power, and requires no additional capability in the command or data transfer system.
- It is not affected by dust or haze in the atmosphere of Mars

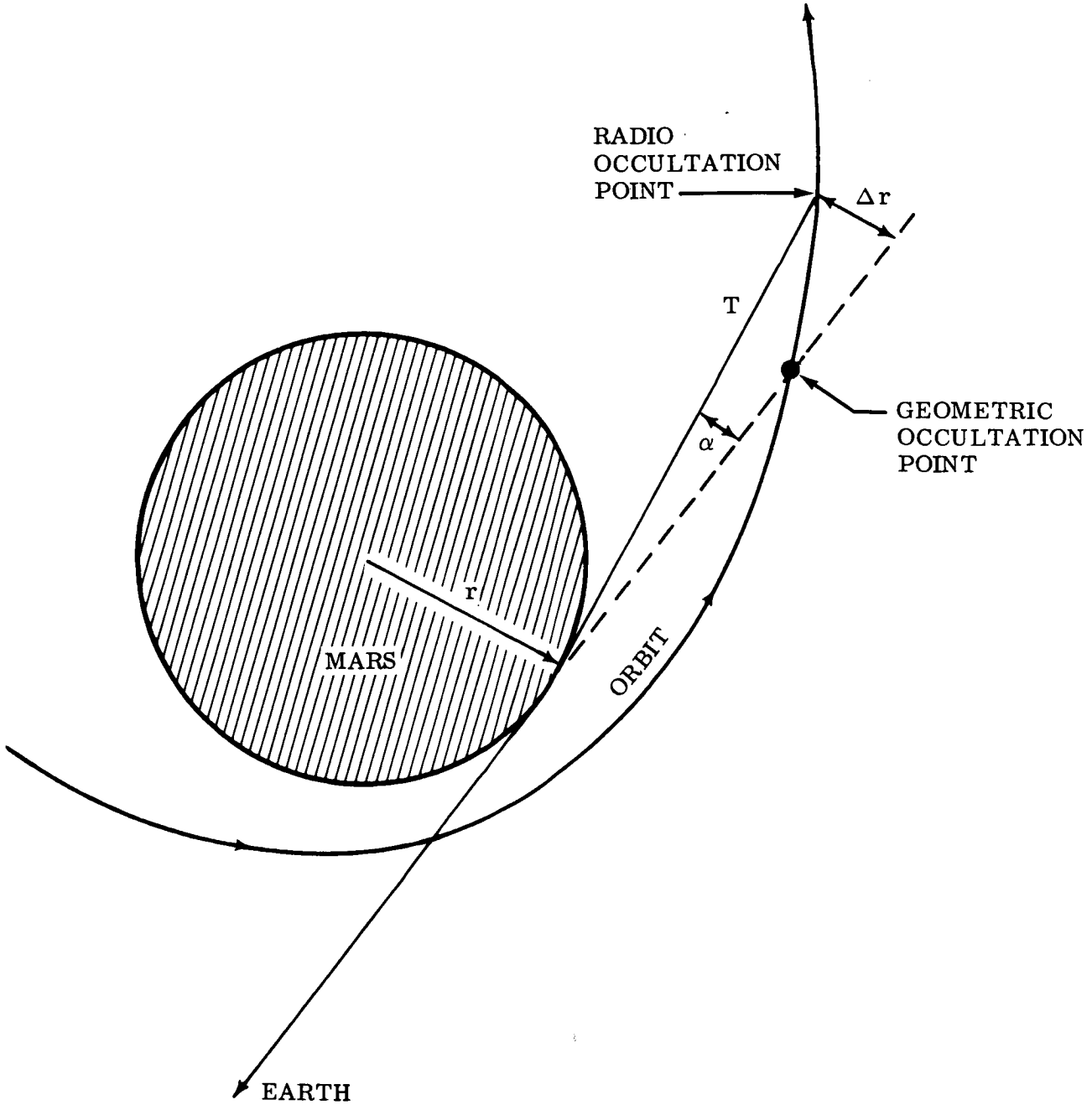


Fig. 5-9 Effect of Atmospheric Refraction on the Radio Occultation Point

Disadvantages.

- It is an available technique only during the first few weeks after injection into orbit.
- It may be adversely affected by the ionosphere of Mars.

Technique No. 2, Star Occultation. As the orbiter circulates around Mars, a very large portion of the celestial background will be obscured by Mars when viewed from the orbiter. Thus, the orbiter will have many opportunities to observe the occultation of bright stars by Mars, an exceedingly rare event when viewed from Earth.

If the orbiter is equipped with a star tracker, gimballed so as to permit alignment with any of a number of appropriate stars, the occultation of a star will provide a measure of the radius of Mars based upon the same principles underlying the radio occultation technique. The same uncertainties associated with atmospheric refraction apply to star occultation as to radio occultation. However, the star occultation technique enjoys a possible advantage in being free from ionospheric confusion. On the other hand, dust or haze in the Martian atmosphere may obscure the horizon and give a false indication of the desired occultation point.

It is probable that the star tracker will be useful for observing star occultations only on the dark limb of Mars because tracking even a bright star as it approaches the sunlit limb of the planet may be difficult. If the star tracker is located on the side of the orbiter facing away from the sun, the dark limb of Mars on the approaching branch of the orbit will be in the field of view at tangential distances ranging from 3000 to 14,000 km, depending upon which orbit the orbiter is in, (see Fig. 5-10. Hence, based upon the 43-sec of arc uncertainty in atmospheric refraction derived in connection with the radio occultation technique, the corresponding uncertainty in the radius of Mars determined by star occultation ranges from 0.6 to 2.9 km. The approaching branch of the orbit is probably favorable for star occultation experiments because the morning side of the planet is then in view, and dust and haze will have had all night to settle.

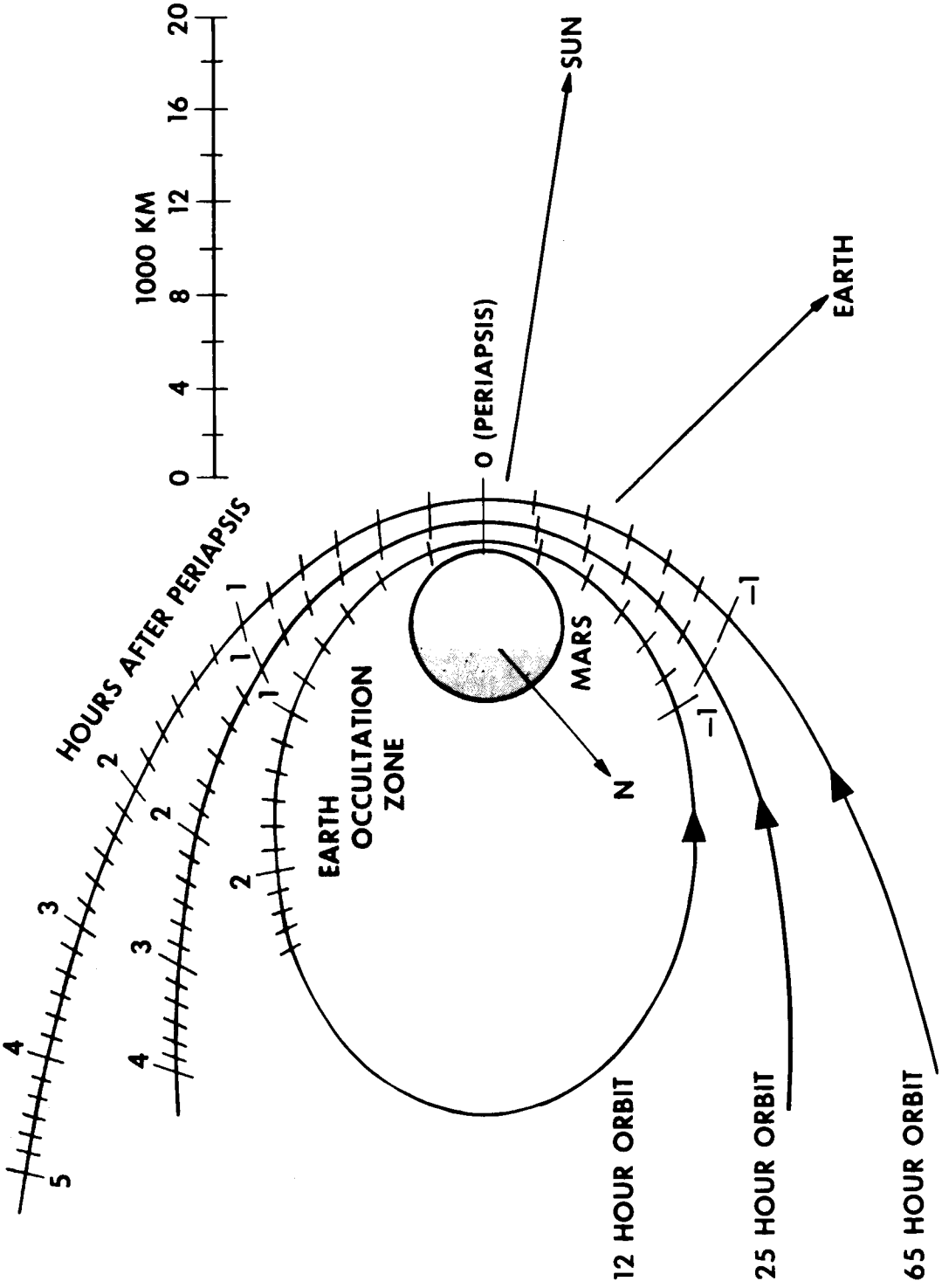


Fig. 5-10 1969 Mariner – Earth Occultation Zone for Mars Orbits

If we assume a 1-km uncertainty in the position of the orbiter and assign a 1-km uncertainty to irregularities in the topography of Mars and combine these uncertainties orthogonally with the atmospheric refraction effect, the resultant uncertainty in determining the radius of Mars by observing star occultations ranges from 1.5 to 3.2 km. This is slightly better than the radio occultation technique because the orbiter is generally closer to the planet when observing star occultations than when involved with radio occultations.

The star occultation technique permits determining Mars' shape by a judicious selection of stars that are occulted at various latitudes on Mars' dark limb, thus providing a number of radius determinations at different latitudes. We conclude this discussion of the star occultation technique by listing its advantages and disadvantages as follows:

Advantages.

- For the particular orbital conditions of the 1969 mission it appears slightly more accurate than the radio occultation technique. With present knowledge of the atmosphere of Mars, the uncertainty in the determination of the radius of Mars varies from 1.5 to 3.2 km.
- The accuracy is subject to improvement with improved knowledge of the atmosphere of Mars.
- It permits determination of the shape of Mars.
- It is an available technique throughout the life of the orbiter.

Disadvantages.

- It adds to the burden of the orbiter command and data transfer system. Upon command from Earth, the star tracker should be able to locate and lock on to any one of a number of stars that will be occulted by Mars when viewed from the orbiter.

Technique No. 3, Angular Diameter. If the angular diameter and distance from the center of a spherical object are known, the radius of the object is

$$r = R \sin \beta/2 \qquad (5.10)$$

in which R is the distance of an external point P from the center of the sphere and B is the angular diameter of the sphere viewed from P. The uncertainty in determining r may be expressed as follows:

$$\delta r = \frac{r}{R}\,\delta R + \frac{1}{2}\sqrt{R^2 - r^2}\;\delta\beta \qquad (5.11)$$

in which the symbol δ designates the uncertainty in the accompanying quantity.

We could assume the uncertainties in R and β are independent, in which case the resultant uncertainty in r would be the orthogonal sum of the two components on the right-hand side of Eq. (5.11). However, to be conservative, we shall assume the worst case and treat the uncertainties as directly additive. The DSIF uncertainty in R is taken to be 1 km. Lockheed optical specialists estimate that the proper choice of a wavelength interval in the red or near infrared portion of the spectrum that avoids carbon dioxide and water emission and absorption bands will permit detection of the true limb of the planet with an angular resolution of about 0.5 min of arc at the standoff distances of concern here. Hence, the uncertainty in measuring the angular diameter of Mars is about 1 min of arc.

The range of radial distances from center of Mars in which the field of view from the orbiter's planetary instrument platform permits observation of the angular diameter of Mars is between 4000 and 10,000 km. Hence, according to Eq. (5.11), the uncertainty in determining the radius of Mars varies from 1.2 to 1.7 km, the smaller value being associated with measurements near periapsis.

The foregoing analysis treats Mars as a sphere. However, the angular measurement technique need not be so restricted. Figure 5-11 illustrates a situation with the oblateness of Mars represented by an ellipse with an eccentricity of about 0.5, which is a gross exaggeration of Mars' actual oblateness. Since DSIF can give the location of the orbiter with great precision relative to the center of mass of Mars, the direction of the radial distance vector R is known relative to the orbiter's frame of reference.

Therefore, the tangent angles, β_1' and β_2' can be determined, in which case the apparent radii of Mars are given by

$$r_1' = R \sin \beta_1'$$

$$r_2' = R \sin \beta_2'$$

The true radii, r_1 and r_2 corresponding to the actual points of tangency from the orbiter to the surface of Mars are slightly greater than the apparent radii for the situation shown in Fig. 5-11. It is obvious by inspection of the diagram that the differences between the apparent and the true radii will be imperceptible for the actual case in which the oblateness of the Mars is relatively quite small. However, the difference between the radii r_1 and r_2 is expected to be easily observable from the orbiter since even Earth-based measurements of the polar and equatorial diameters of Mars indicate a detectable difference.

In addition to observational difficulties, such as haze or dust in the atmosphere of Mars, it might be expected that some uncertainty in the accuracy of the angular measurement technique will be introduced by uncertainties related to optical refraction in the atmosphere of Mars. The effect of refraction is to magnify slightly the apparent radius of Mars. The amount of magnification can be precisely computed if the composition and density distribution of the atmosphere are known.

The situation is described schematically in Fig. 5-12 with considerable exaggeration of the angular magnitudes involved. Curvature of the refracted light ray PO from a point on the surface of Mars to the orbiter results in an apparent increase Δr in the radius of Mars. Using small-angle approximations, the following relationship can be derived:

$$\Delta r = x\alpha - \Delta s \qquad (5.12)$$

in which

x = distance from P measured along the ray

Δs = linear displacement of a point on the refracted ray relative to the tangent at P

α = angle of refraction of the ray relative to the tangent P

The angle of refraction α is given by Eq. (5.6) with $z_o = 0$. The quantity Δs is expressed by

$$\Delta s = \int_0^x \frac{\rho_o}{H\rho_s} \sum_i N_i (n_{si} - 1) \left[\int_0^\zeta \exp - \left(\frac{\eta^2}{2Hr} \right) d\eta \right] d\zeta \qquad (5.13)$$

In which η and ζ are merely dummy variables for purposes of integration.

It is not permissible to let x approach infinity, as was done in the analysis of the first technique, because Δs then becomes infinitely large. Therefore, a value for x is chosen large enough to include substantially all of the refractive effects of the atmosphere of the Mars yet small enough to retain the validity of the small-angle approximations. In the case of atmosphere J , which because of its greater density will exhibit the greater refractive effects, a suitable value for x is 700 km, corresponding to a point about 72 km above the surface of Mars. Using the data from Table 5-3 in the analysis of the first technique, we find Eq. (5.13) yields a value of 0.103 km for Δs. Hence, Eq. (5.12) indicates the value of Δr is 0.036 km. The uncertainty in Δr due to the uncertainty in the properties of Mars' atmosphere is about half of Δr.

We conclude in relation to angular diameter measurements the effects of atmospheric refraction are negligible compared to other sources of error.

Presently available Earth horizon scanners are not suited to the measurement of the diameter of Mars from an orbiter because they operate on the gradient of the infrared

emission that is found to have a fairly reproducible profile corresponding to emission from an altitude of about 35 km in the Earth's atmosphere. There is probably an analogous situation on Mars, but it represents only an imponderable uncertainty so far as the present application is concerned.

It appears, therefore, the angular diameter technique for measuring the dimensions of Mars will require development of a special instrument. The basic principle seems simple enough to leave little doubt about the immediate feasibility of such a development. Existing scanning techniques may be used with the principal problem being the selection of radiation sensors with optimum capability for detecting the required optical discontinuity at the limb of Mars. Lockheed instrument design specialists have estimated that a device with the required capabilities would weigh about 10 lb and require about 2 w.

The status of the angular diameter technique is estimated to be as follows:

Advantages.

- Permits determination of the radius of Mars with uncertainties ranging from 1.2 to 1.7 km, which is considerably better than the two preceding techniques.
- Accuracy is not significantly affected by present ignorance about the composition and density of the atmosphere of Mars.
- Permits determination of the shape of Mars.
- Is an available technique throughout the life of the orbiter.

Disadvantages.

- Requires additional equipment weight and power, estimated 10 lb and 2 w.
- Requires development of a new instrument.
- Adds to the burden of the data handling system; readout precision should be at least 13 bits per measurement.
- May be adversely affected by dust or haze in Mars' atmosphere.

Technique No. 4 Radar Altitude. Conceptually, the simplest, most direct way to determine the radius of Mars is to measure the altitude of the orbiter and subtract the

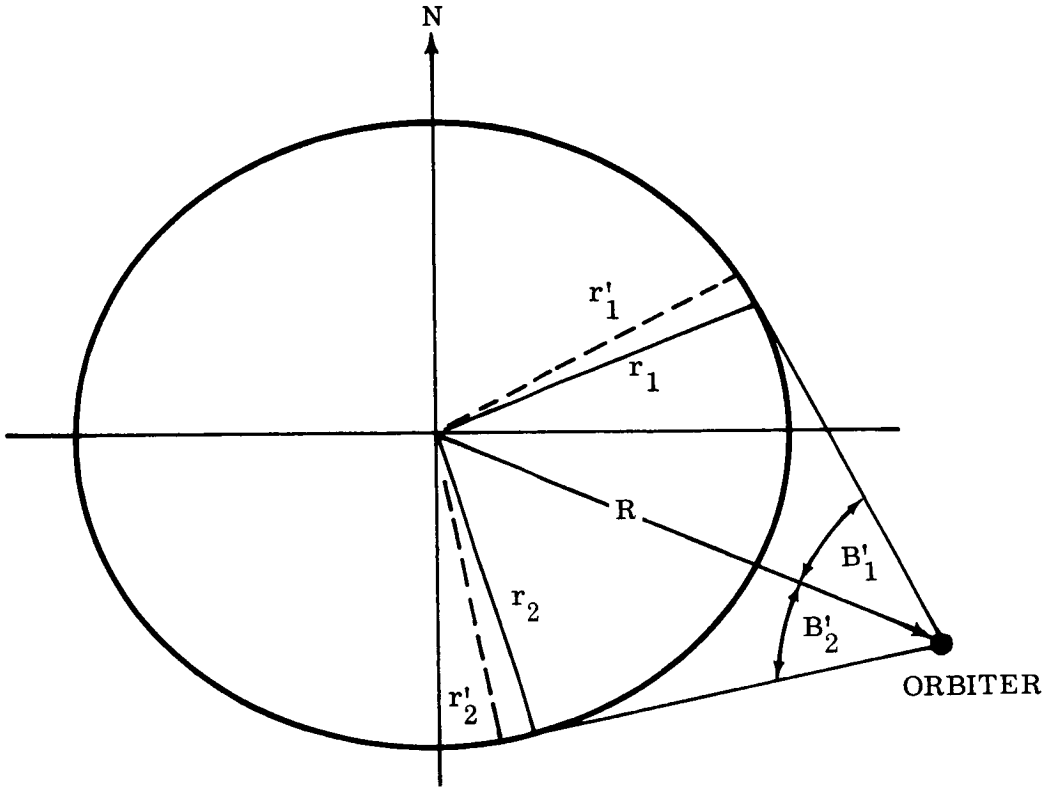


Fig. 5-11 Relation Between True and Apparent Radii Measurements for an Oblate Ellipsoid

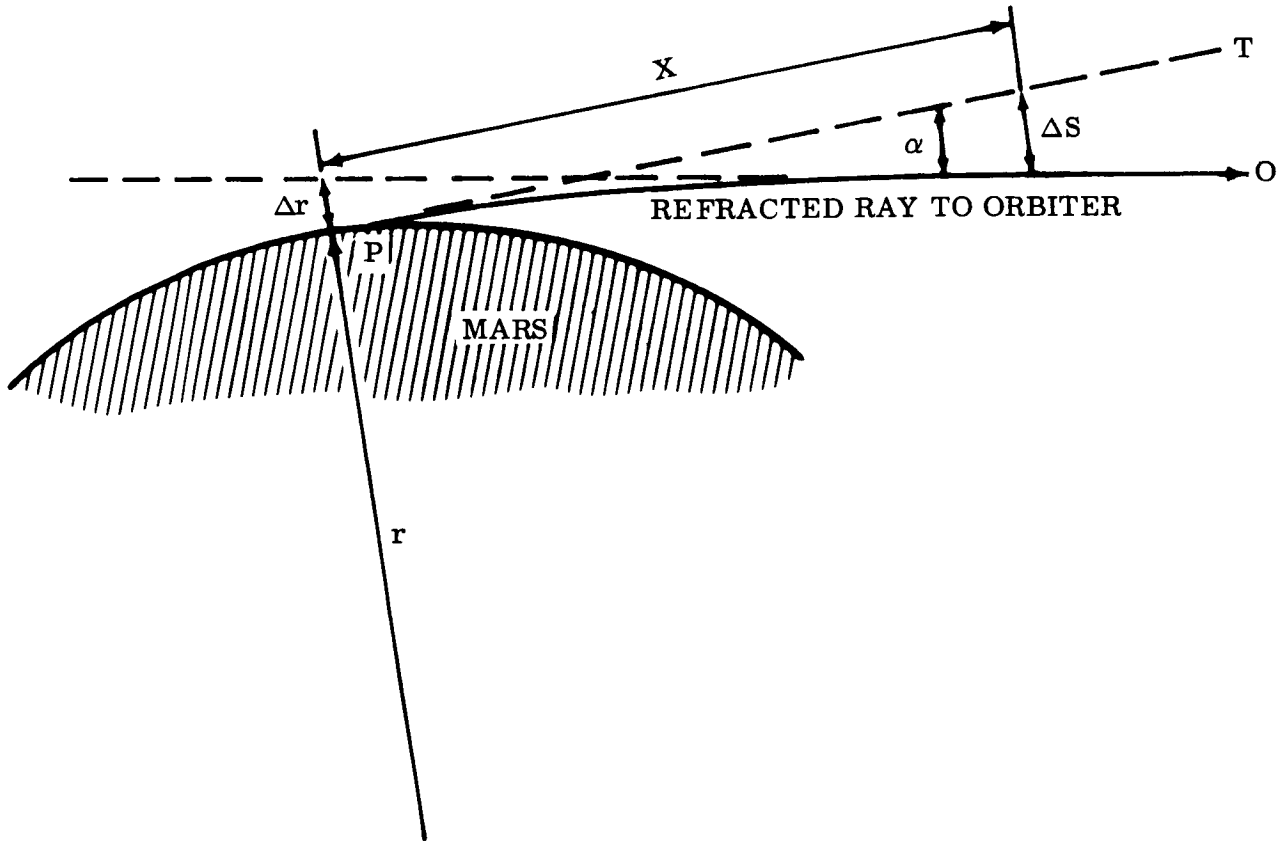


Fig. 5-12 Effect of Atmospheric Refraction on Angular Diameter Measurement

altitude from the known distance or the orbiter from the center of Mars. A radar altimeter with an estimated range of 4000 km and a range accuracy of 0.3 km would weigh about 37 lb, including a 4-ft dish antenna and all the requisite electronics, and would require a peak power input of about 39 w. The resultant uncertainty in measuring the radius of Mars is 1.3 km.

The amount of surface available on Mars for measurement by the radar technique will depend upon the orientation of the orbit. With the highly elliptical orbits proposed in the present study, the limited range of radar will confine the measurements to the vicinity of periapsis. It is estimated that radius determinations ranging in latitude from about 40 deg south to about 20 deg north of the Martian equator may be obtained. This should be sufficient to give a good measure of the oblateness of Mars.

The principal uncertainty, so far as the theoretical feasibility of the radar altimeter technique is concerned, is the question of the reflectivity of Mars at radar frequencies. Sperry Corporation engineers supplied the weight, power range and accuracy specifications quoted here, based upon an assumed radar reflectivity similar to the Moon. A prototype system has been developed. The status of the radar altimeter technique for measuring the radius of Mars is somewhat as follows:

Advantages.

- Permits determination of the radius of Mars with an uncertainty of 1.3 km, which is comparable to the best of the preceding techniques.
- Does not depend upon knowledge of the atmospheric composition and density of Mars.
- Is not affected by dust or haze in the atmosphere of Mars.
- Is an available technique throughout the life of the orbiter.

Disadvantages.

- Is heavy and requires a relatively large amount of power.
- Is electronically complex and correspondingly subject to failure.
- Adds to the burden of the control and data handling system.
- Range of latitudes over which it can make radius measurements depends upon the orientation of the orbit.

Technique No. 5, Television. During the anticipated 6-mo lifetime of the orbiter, there is some likelihood of seeing the same areas more than once and from different points of view. In particular, if a well-defined feature on the surface of Mars is seen from two very different points of view, e.g., on the morning side and the evening side, an opportunity is afforded to determine the radius of Mars at the feature in question with considerable precision.

Figure 5-13 represents the situation as a problem in plane geometry though it should be realized a three-dimensional configuration of points and lines will generally be involved. Suppose an identifiable object is seen at P_1 in a TV picture taken at time t_1. From the known position of the orbiter relative to the center-of-mass of Mars and the known orientation of the camera relative to coordinates fixed by the Sun and Canopus, we can determine the line L_1 on which the object was known to be at time t_1. Suppose at some later time t_2 on another pass around Mars, the same object is seen again in a TV picture but at a different location P_2 because Mars will meanwhile have rotated. Again we can establish a line L_2 on which the object was known to have been at time t_2. Since the angular rate of rotation of Mars is accurately known, the angular separation θ of the points P_1, P_2 is accurately determined by

$$\theta = \omega(t_2 - t_1) - 2\pi k \tag{5.14}$$

in which

ω = angular rate of rotation of Mars

k = an integer representing the number of revolutions Mars completed between t_1 and t_2

By inspection of Fig. 5-13 it is not difficult to convince oneself intuitively that the positions of P_1, P_2 on the lines L_1, L_2 are uniquely determined by the requirements that they be equidistant from the center of Mars and separated by the angle θ. The analytical problem is a bit sticky, particularly in three dimensions, but should offer no serious difficulty with the aid of an automatic computer.

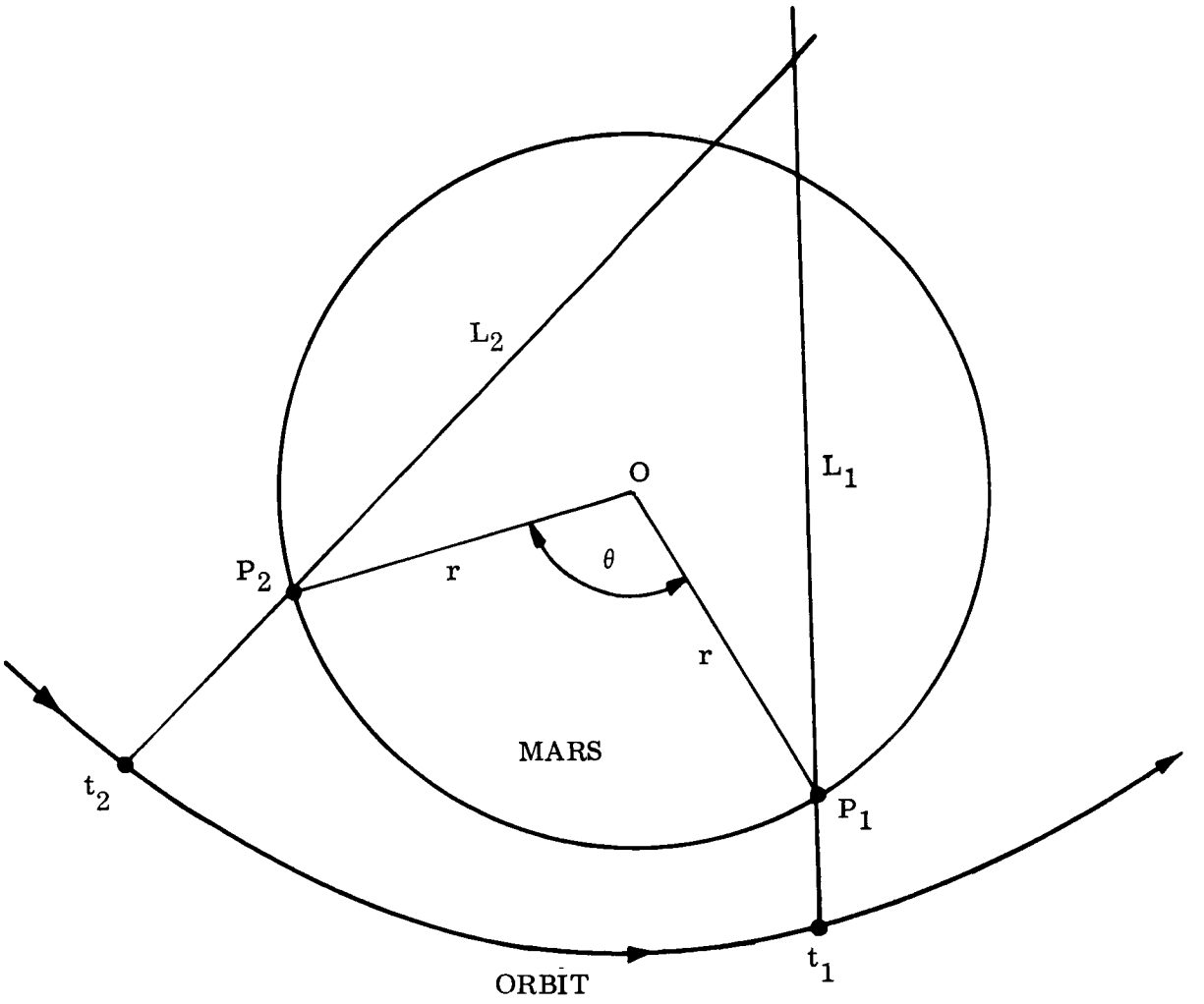


Fig. 5-13 Determination of Mars Radius With Television Data

The resolving power of the wide-angle TV is assumed to be 1 km. The location of the orbiter is assumed to be known within 1 km. The times t_1 and t_2 should be known to 0.1 sec. Hence, the uncertainty in determining the radial distance of the points P_1, P_2 from the center of the Mars is estimated to be about 4 km provided the intersection of the lines L_1, L_2 (if they are coplanar) is not too close to the center of Mars. If the lines should happen to intersect near the center of Mars, the uncertainty in determining the radius becomes very large, and the particular pair of TV observations in that case are not useful. Hence, at least one of the TV observations in each pair should present a line of sight that misses the center of Mars by a wide margin.

The TV technique for measuring the radius of Mars depends to some degree upon unpredictable factors. First, it is necessary to discover at least one well defined object that can be recognized from two widely separated viewpoints of the surface of Mars. Second, TV pictures of the object must be obtained from viewpoints satisfying the geometrical requirements of the problem. Unless some means are provided to adjust the period of the orbit after the first pass around the planet, it may happen that the required observations of the same object from different viewpoints will not be feasible within the lifetime of the orbiter, particularly if suitable objects on the surface of Mars are scarce. The determination of the oblateness of Mars by this method requires that there be two or more suitable objects at somewhat different latitudes.

A favorable aspect of the TV technique is the fact that it involves observations through the atmosphere of Mars at reasonably acute angles relative to the vertical. Therefore, it should be affected by the atmospheric conditions of Mars to a lesser degree than techniques No. 1 and No. 2, which require observation of the surface of Mars at tangential incidence through the thickest possible layer of atmosphere.

The TV technique requires a capability for precise correlation of the TV field of view with angular coordinates determined by the Sun and Canopus so that the lines L_1 and L_2 can be established. The uncertainty needs to be less than 1 min of arc. It is estimated that the present Mariner C attitude sensors can be modified with no appreciable increase in weight and power so as to read out the instantaneous degree of misalignment

relative to the Sun and Canopus with the desired precision. This information would, of course, have to be transmitted along with each TV picture. Hence, a slight additional load on the data transfer system is implied by the TV technique for measuring the radius of Mars.

The advantages and disadvantages of the TV technique are summarized as follows:

Advantages.

- Probably involves no appreciable increase in weight or power and only a slight addition to the data handling capacity, e.g., three 10-bit words indicating the magnitudes of the error signals from the solar sensors and the star tracker.
- Compared to other optical techniques, it is less susceptible to Martian atmospheric conditions.
- Capable of determining the shape of Mars.
- An available technique throughout the lifetime of the orbiter.

Disadvantages.

- Depends upon a fortuitous occurrence of well-defined objects suitably located on the surface of Mars.
- Present estimates do not give it quite as much accuracy as other techniques, but this is not an inherent limitation. The accuracy can be improved by use of high-resolution TV and greater precision in determining the TV frame of reference.

Technique No. 6, Surface Transponder. It is estimated that a two-way doppler link between the orbiter and a transponder on the surface of Mars could indicate the velocity of the transponder relative to the orbiter with an uncertainty of 0.1 m/sec. Possibly even better performance could be obtained by locking the carrier frequency of the orbiter through DSIF to a superstable oscillator on Earth. It is claimed that DSIF can determine the orbiter's velocity relative to the center-of-mass of Mars with an uncertainty somewhat less than 0.1 m/sec. Hence, from the vector difference of the velocities, the velocity of the surface transponder relative to the center of Mars may be determined within 0.1 m/sec.

The velocity of a point on the surface of Mars relative to the axis of rotation of the planet is expressed by

$$\nu = \omega r \cos \varphi$$

in which

ω = angular rate of rotation
φ = latitude

Hence,

$$r = \frac{\nu}{\omega \cos \varphi} \qquad (5.15)$$

If the transponder is on the equator of Mars, then according to Eq. (5.15), an uncertainty of 0.1 m/sec in ν represents an uncertainty of about 1.4 km in r.

In general, it is not to be expected that the transponder will land on the equator. However, the doppler data obtained by tracking the surface transponder for an extended time (e.g., several hours) with the orbiter will contain enough information to locate the transponder both in latitude and longitude. In fact, the doppler data permit a determination of the radius of Mars even though the transponder were to land on one of the poles, a situation outside the range of applicability of Eq. (5.15) because $\cos \varphi = 0$ at the poles.

The surface transponder technique does not merit a more detailed analysis here because its disadvantages relative to the preceding techniques far outweigh its advantages. The merits and demerits of the technique are as follows:

Advantages.

- Not likely to be affected by the atmospheric or ionospheric conditions on Mars.
- Potentially quite accurate; estimated uncertainty is 1.4 km.

Disadvantages.

- Requires landing a surviving capsule on Mars.
- Requires power, weight and data handling capability in a surviving capsule that preferably would be used for other kinds of experiments.
- Requires placing two or more transponders at different latitudes to determine the shape of Mars.
- Requires additional capability in the orbiter; i. e., a two-way doppler link between orbiter and lander.
- Could fail through an adverse timing relationship between the period of the orbiter and the location of the transponder on Mars such that communication within the lifetime of the lander's batteries is not accomplished.

Technique No. 7, Surface Gravity. The radial acceleration field outside a spherically symmetrical mass is given by

$$g = \frac{Gm}{r^2}$$

Hence,

$$r = \sqrt{\frac{Gm}{g}} \qquad (5.16)$$

in which

g = gravitational acceleration
G = 6.670×10^{-8} dyne cm^2/gm^2
m = mass

The value of the product Gm can be determined from orbital data with an uncertainty of about 1 part in 10^4. If a gravitometer with sensitivity sufficient to measure acceleration to one part in 10^4 is placed on Mars' surface, then Eq. (5.16) indicates the radial distance from the center of mass can be determined with comparable precision; i. e.,

$$\frac{\delta r}{r} = \frac{1}{2}\left(\frac{\delta(Gm)}{Gm} + \frac{\delta g}{g}\right)$$

The resultant uncertainty in r is about 0.7 km.

The situation is actually a little more complicated than the above remarks indicate. Allowance must be made for acceleration effects associated with the rotation of Mars, for deviation from spherical symmetry in the distribution of the mass of Mars and for the variation of gravitational acceleration with altitude, assuming Mars has topographical features with significant differences in altitude. The first correction requires knowledge of the location of the gravitometer so that allowance can be made for the latitude dependence of rotational acceleration. The second requires information about the oblateness of Mars which is known with moderate accuracy from the precession of the orbits of the moon of Mars. The altitude data needed for the third correction might be determined from atmospheric pressure measurements, though this implies more knowledge about the average surface conditions of Mars than is now available.

A variation in altitude of one-third of a kilometer would register as a measurable effect on a gravitometer with a sensitivity of one part in 10^4. Thus, the gravitometer might be regarded as a kind of absolute altimeter, if other factors such as the location of the gravitometer and the oblateness of the mass distribution of Mars are known with sufficient accuracy.

Transmission of the gravitometer data directly to Earth via DSIF would permit the latitude and longitude coordinates of the gravitometer to be determined through doppler data. That is, the experiment is not dependent upon establishing a communication link between the surface of Mars and the orbiter.

For very much the same reasons as the surface transponder technique, the disadvantages of the gravitometer technique outweigh its merits relative to other ways of measuring the radius of Mars even though the present rather superficial analysis indicates it is

potentially one of the more precise techniques. Its relative merits and faults are as follows:

Advantages

- Not likely to be affected by the atmospheric or ionospheric conditions on Mars.
- Potentially quite accurate; estimated uncertainly 0.4 km if other data such as latitude, deviation from the mean altitude and magnitude of Mars' oblateness are known.

Disadvantages

- Requires landing a surviving capsule on Mars.
- Requires power, weight and data handling capability in a surviving capsule that preferably would be used for other kinds of experiments.
- It requires two or more gravitometers at different latitudes to determine the shape of Mars.

Technique No. 8, Radar Altitude Plus Angular Diameter

All of the preceding techniques for measuring the radius of Mars depend in some way upon precise knowledge of the orbit parameters which depend upon acquiring adequate DSIF doppler tracking data. If communication with the orbiter should permanently fail before the orbit has been tracked long enough to yield the requisite precision (i.e., within a few hours after injection into orbit) a measurement of the diameter of Mars before failure of the communication link and by a method independent of orbit data would be most welcome. Such a method is represented by a combination of radar altimeter and optical angular diameter measurements.

The required diameter is given by

$$D = \frac{2z \sin \beta/2}{1 - \sin \beta/2} \qquad (5.17)$$

in which

z = altitude above Mars' surface

β = angular diameter

If the uncertainties in the altimeter and angular diameter measurements are assumed to be 0.3 km and 2 minutes of arc, respectively, it is not difficult to show that Eq. (5.17) indicates an optimum altitude of about 3000 km at which to perform the measurement, the resultant uncertainty in the diameter having a minimum value of 7.4 km. According to Fig. 5-10, the optimum time for measuring the diameter varies from a half-hour before or after periapsis for the smallest orbit to 15 min before and after periapsis for the largest orbit. However, before orbit injection it is not likely that the particular orbit to be acquired will be accurately known.

It should be realized that because of the oblateness of Mars, the present technique actually measures the sum of the radii to two different points on the surface, but it is not feasible to resolve the measurement into the separate radii without additional data concerning the position of the orbiter relative to the center of Mars. Hence, as a means of determining the oblateness of Mars, the best measurements will be obtained as the orbiter crosses the equator, for the radii in the equatorial plane are expected to be practically equal, and likewise for symmetrically located radii in a plane through the poles.

The main objection to the present technique for determining the dimensions of Mars is the weight, power and complexity of the required equipment. This is offset somewhat by the fact that it represents a four-fold redundancy in means for measuring Mars if the DSIF communication link does not fail (i.e., Techniques No. 1, 3, 4, and 8), as well as providing a likelihood of delivering the desired data even if the DSIF link fails shortly after orbit injection. If the need for the measurement is very great, this technique should be given serious consideration.

single TV picture frame contains of the order of 2×10^6 bits. Hence, almost two hours are required to transmit one complete picture to Earth. Other factors that complicate the situation are the eccentricity of the orbit, the wide range of possible orbital periods (12 to 65 hours), and the varying intervals during which occultation by Mars interrupts the transmission of data to Earth.

It is desirable to view Mars at minimum range to obtain maximum resolution of surface detail. Hence, TV data are acquired and stored on tape while the orbiter is near periapsis, and the remainder of the orbit period is used to transmit the data to Earth.

The tape storage capacity of 66×10^6 bits was chosen to accommodate the total data transfer requirement of one cycle of the longest period orbit, i.e., the 65-hour orbit. If the orbital period is appreciably less than 65 hours, it is possible either to use more than one orbit cycle to transmit the data to Earth or to load only the amount of data into the storage unit that can be transmitted in one orbit cycle.

The estimated area of Mars available for observation by the orbiter is about 10^8 km^2. The anticipated amount of data to be transmitted to Earth during the 6-month lifetime of the orbiter is about 10^9 bits, which implies that only a very small fraction of the surface of Mars can be viewed in great detail.

TV Camera Characteristics. The recommended TV system comprises three cameras. Two cameras are sensitive primarily to visible light (0.4 to 1.0 micron) and the third responds to infrared (1.0 to 10 microns). Filters in each camera provide for color discrimination in the visible region and selection of particular bands of interest in the infrared. The two visible-light cameras have identical characteristics and each can operate in either a high-resolution or a low-resolution mode. The infrared camera is provided with only low-resolution capability.

The three cameras are mounted on the planet-oriented instrument platform with their optical axes aligned in the same direction. Pictures are taken simultaneously by all

three cameras with one of the visible-light cameras in the high-resolution mode and the other in the low-resolution mode. Two-minute intervals between successive frames provide time for the slow-scan system to transfer the picture data to tape storage.

The high-resolution optical system comprises an f/5.7 lens with a 40-in. focal length. The resultant image intensity is more than sufficient to permit present high-sensitivity vidicon systems to observe scenes near the terminators, even though the average brightness of the Martian surface is estimated to be only one-sixth that of Earth. The very large variation of surface brightness from the terminators to the noon meridian is accommodated by neutral filters in the optical system and automatic gain control in the image-scanning circuit.

A 600-line raster with a line density of 30 lp/mm is used in the high-resolution mode. The resultant angular field of view is 0.57 deg. The same number of lines is used in the low-resolution mode but with a shorter focal length and a larger raster so as to obtain a 5.7 deg angular field of view. The infrared camera also has a 5.7 deg angular field of view but uses only a 200-line raster. The corresponding linear dimensions of the fields of view on the surface of Mars are respectively one hundredth and one tenth of the altitude of the orbiter for the high and low resolution cameras.

The resolving power of the TV cameras relative to surface details on Mars is inversely proportional to the altitude of the orbiter, which may be anywhere from 6000 km while observing the sunrise terminator from a 65-hr orbit to 600 km at periapsis of a 12-hr orbit. Table 5-4 gives the resolving power in meters per line pair projected on the surface of Mars from various altitudes. For a nominal periapsis altitude of 1500 km the resolving power of the high-resolution camera is 50 m while the low-resolution visible light camera and the infrared camera, respectively, have resolving powers of 500 and 1500 m.

The pro's and con's of the radar altitude angular diameter technique are as follows

Advantages:

- Promises a measurement of the dimensions of Mars without depending upon prolonged tracking of the orbiter after injection into orbit; i.e., it does not depend upon accurate orbit data.
- Provides a 4-fold redundancy; i.e., high reliability, in getting the desired measurement.
- Not sensitive to present lack of exact information about the atmosphere of Mars; i.e., refractive effects do not introduce appreciable uncertainty.
- Not expected to be affected by the ionosphere of Mars (if such exists).
- Can provide a measure of the oblateness of Mars.
- An available technique throughout the life of the orbiter.

Disadvantages:

- Adds considerably to the payload weight and power; estimate 47 lb., 41 w.
- Electronically complex.
- May be adversely affected by dust or haze in Mars' atmosphere.
- Angular diameter instrument is still a conceptual device requiring development.

Conclusions Concerning Determination of Mars' Size and Shape. The foregoing discussion does not exhaust the subject, though it is believed to present a fairly comprehensive survey of techniques that might be used. The most attractive techniques are those that require no weight or power in addition to what is expected to be part of the payload anyway. However, these Techniques (No. 1 and 5) appear to be the least accurate. Technique No. 1 (radio occultation) is subject to considerable improvement in accuracy when better information about the atmosphere of Mars becomes available, provided no unusual ionospheric effects are discovered. With highly precise orientation sensors relative to the Sun and Canopus, the accuracy of Technique No. 5 would be improved by an order of magnitude if a suitable object on the surface of Mars were to be observed with high resolution TV (0.1 km resolution) at two different times.

The next most attractive techniques are No. 2 (star occultation) and No. 3 (angular diameter). With more exact information about the atmosphere of Mars, Technique No. 2 could very well be the most accurate of all since most of the uncertainty is in the atmospheric refraction effect. Technique No. 3 has rather poor potential for improved accuracy unless it proves feasible to detect the true limb of Mars with considerably greater precision than the present estimate assumes. However, it is recommended because it is not sensitive to our lack of exact information about Mars' atmosphere.

Technique No. 4 (radar) and No. 8 (radar and angular diameter) rank next in order of preference because of their weight and power requirements. Finally, the least attractive Techniques are No. 6 (surface transponder) and No. 7 (surface gravity) because they require landing instruments on Mars in surviving capsules. It is unlikely that they could compete successfully with obviously more significant chemical and biological experiments to be performed on Mars' surface.

Techniques No. 1, 3, and 5 have been assumed for the basic instrument package for the 1959 orbiter mission.

5.2.4 The Orbiter Television System

The television system described here is intended to provide a measure of the 1969 orbiter's picture acquisition capability based upon a conservative application of present state of the art. The orbiter TV system differs from conventional commercial TV in that the individual picture frames are taken at widely spaced instants of time (2 minutes between frames), a slow scan rate of about 11 lines/sec is used to read out the picture information, and the picture information is read out, stored and transmitted in digital form.

The main factor limiting the TV capability is the capacity of the data transfer link to Earth. The maximum rate of data transfer to Earth is 300 bits/sec, whereas, a

Table 5-4

RESOLVING POWER OF THE ORBITER TV SYSTEM

Altitude (km)	Resolution Mode High (m/lp)	Resolution Mode Low (m/lp)	Infrared Camera (m/lp)
600	20	200	600
1500	50	500	1500
2400	80	800	2400
6000	200	2000	6000

At the nominal periapsis altitude of 1500 km, the speed of the orbiter is about 4 km/sec. The distance traversed in the 2-min interval between TV frames is about 480 km, which is more than three times the low-resolution field of view. Hence, TV coverage at periapsis provides no overlap of successive pictures. However, when the altitude of the orbiter is 3400 km on the approach to or departure from nominal periapsis, the orbital speed has decreased and the field of view has increased just enough to permit some overlap. At an altitude of 6000 km the overlap is about 60 percent. This is the altitude at which observations of the sunrise and sunset terminators would be made in the early part of the orbiter mission. Near the end of the 6-mo orbiter mission, the sunrise terminator will have moved almost to a point below periapsis so that pictures with maximum resolution at very oblique incidence of sunlight may then be obtained.

It is more desirable to obtain a 2-color picture of each scene than alternate colors with successive frames. A beam splitter can be used to produce two identical images thus permitting a different filter for each image. If the images have a 2 to 1 ratio of height to width, they can be projected beside one another on the vidicon target so as to present a square format. The result is scanned and transmitted as a single picture.

Each frame of the visible-light cameras represents 1.8×10^6 data bits, while a frame of the infrared camera requires 2×10^5 bits. Firing all three cameras simultaneously

involves 3.8×10^6 bits. The total data transfer capability of 10^9 bits throughout the 6-mo life of the orbiter provides for sending to Earth about 600 pictures representing 200 different scenes.

The orbiter offers the possibility of observing the same scene more than once from different view angles and different solar illumination angles, but the probability of this occurring accidentally with the high-resolution camera is exceedingly small. To exploit this possibility, means must be provided to command from Earth the time at which a picture is taken within ± 0.5 sec and to control the angular orientation of the camera relative to celestial coordinates within ± 0.1°. Control of the camera's angular orientation could be performed relative to the orbiter's framework provided the orbiter's angular attitude is suitably monitored. A further requirement is that the desired scene shall come within camera range more than once. This may involve a small adjustment of the orbital period after injection into orbit.

The main reason for desiring pictures of the same scene from different view angles is to obtain a stereoscopic measure of the variation in elevation of surface irregularities. Presumably the two visible-light cameras could both be operated in the high-resolution mode, offset a few degrees relative to one another in the plane of the orbit, and separately timed to take pictures with just the proper delay to get the same scene at different angles. However, this procedure requires versatility and sophistication in the command system to a degree that should be viewed with skepticism so far as the first orbiter mission is concerned.

5.2.5 Other Orbiter Experiments

The emphasis on TV leaves little room for other heavy instruments such as spectrometers for microwave, infrared, or ultraviolet radiation. Omission of any kind of high-resolution spectrometer may be regarded as a deficiency that is sufficiently serious to force a compromise on the weight allotted to TV. On the other hand, it may equally well be argued that the only way an orbiter can get really significant data

about the physical character of the Martian surface is by use of an even more sophisticated (and heavier) TV system with image motion control permitting surface resolution down to a meter or less.

The bi-static radar experiment proposed by the Stanford University Radioscience Laboratory is attractive for several reasons. In addition to providing a measure of the electron distribution in interplanetary space, it is expected to measure the electron concentration in the Martian ionosphere and Van Allen belts, if such exist. Variations in the distribution of interplanetary electrons can significantly affect the accuracy of interpreting DSIF range and velocity data. The measurement of the radius of Mars by the radio occultation technique may be affected by a Martian ionosphere. The presence of Van Allen belts around Mars may be indicated by the bi-static radar experiment even though the trapped radiation detectors fail to register any measurable effect because of an unfavorable orbit.

A magnetometer for observing interplanetary fields is a nuisance because of the severe restriction it places on all other components of the spacecraft in regard to residual DC magnetic fields. The somewhat dubious feasibility of reducing all of the local magnetic disturbances to an acceptable level (about 0.1 gamma) for interplanetary measurements is a strong argument for dropping the interplanetary magnetometer from the present mission. Provision need then be made only for the measurement of planetary magnetic fields with expected intensities much greater than the interplanetary background.

To round out the interplanetary experimental capability so as to provide an adequate measure of the interplanetery background with which to compare space environmental conditions in the neighborhood of Mars, it is highly desirable to include an assortment of charged-particle detectors covering a wide spectrum of energies (from 10^1 to 10^9 ev). Instrumentation for measuring the flux of cosmic dust and micrometeoroids between Earth and Mars is also indicated.

5.2.6 Capsule Capabilities

Biological Capsule. The results of the present study indicate that the capability for landing even a very small biological package on Mars, as a part of the 1969 orbiter mission is in doubt. Nonetheless, a small biological instrumentation package is proposed for use in design studies. This package weighs about 12 pounds and consists of a life experiment, a mass spectrometer, an accelerometer, and pressure and temperature gages as shown in Table 5-5.

Atmospheric Capsule. The situation in regard to an atmospheric capsule is quite attractive. Impact survival is not required. The duration of the experiments involves only the relatively brief time of descent through Mars' atmosphere. The data link from the capsule to the orbiter is short compared to direct transmission of data to Earth required by the biological capsule. The weight allowance of scientific instruments for the atmospheric capsule is therefore somewhat more generous than for the biological capsule.

An atmospheric instrumentation package weighing about 18 lb is suggested in Table 5-5. These instruments include accelerometers, pressure gages, temperature gages, a mass spectrometer, an ultraviolet photometer and an infrared radiometer.

5.2.7 Recommended Instrumentation for Mars 1969 Missions

While imposing some severe requirements upon the subsystem designers, an effort has been made here to devise scientific payloads providing well-balanced capabilities for performing both interplanetary and orbiter experiments, in addition to satisfying the primary objectives of the missions. The entire emphasis of the orbiter missions is on planet-oriented experiments, so the instruments for interplanetary measurements have been selected for their ability to contribute to the study of the planetary space environment.

Table 5-5

RECOMMENDED EXPERIMENTAL INSTRUMENTATION

	Weight (lb)	Power (w)	Orbiter Only	Orbiter (with Capsule)
Bus Instruments				
Fixed Mount				
Ion Chamber	1.3	0.1	x	x
Particle Flux Meter	2.5	0.35	x	x
Low Energy Plasma Monitor	7	1.25	x	
Medium Energy Proton Monitor	3	1	x	
High Energy Proton Monitor	4	0.5	x	
Trapped Radiation Detector	4	0.7		x
Magnetometer	5	5	x	x
Bi-Static Radar	10	5	x	
Cosmic Dust Detector	2.5	0.2	x	x
Micrometeoroid Detector	8	0.3	x	x
Planet Oriented				
Visual TV (2 cameras)	60	30	x	x
Infrared TV	10	6	x	
Ultraviolet Photometer	6	5	x	x
Infrared Radiometer	3	3	x	x
Planet Diameter Scanner	10	5	x	
		Total Weight	132 lb	92 lb

			Capsule (Bio)	Capsule (Atm)
Capsule Instruments				
Multivator	4	2	x	
Accelerometer (single axis)	2	4	x	
Accelerometer (3-axis)	6.1	6		x
Pressure gages (2)	0.8	0.2	x	x
Temperature gages (2)	0.6	0.2	x	x
Mass Spectrometer	5	6	x	x
Ultraviolet Photometer	2.5	5		x
Infrared Radiometer	3	3		x
		Total Weight	12.4 lb	18 lb

Relative to an orbiter alone, the inclusion of a biological or an atmospheric capsule reduces the total scientific instrument payload of an orbiter mission. The reduction is justified by the ability of a capsule to acquire data not otherwise obtainable.

Table 5-5 presents the recommended experimental instrumentation for the Mars 1969 orbiter missions. For the orbiter only, 70 lb of the total scientific instrument payload of 132 lb is assigned to TV. The ultraviolet photometer and the infrared radiometer comprise the capability of the planet-oriented instruments for analyzing the physical and chemical properties of the Martian atmosphere and surface. With polarizing filters, it is expected that these instruments will obtain valuable data about the nature of the atmospheric haze and the Martian surface by observation of scattered and reflected light at very oblique angles. A planet diameter scanner is included to insure getting a quick accurate measure of the size and shape of Mars during the first pass just in case the communication link should fail before a satisfactory measure of the dimensions of Mars is obtained by the radio occultation technique.

The effect of adding a capsule is to reduce the permissible orbiter scientific payload from 132 to 92 lb. To accommodate this reduction, Table 5-5 shows that a trapped radiation detector package is substituted for some of the more discriminating charged-particle detectors while the bi-static radar, the infrared TV, and the planet diameter scanner are sacrificed. In exchange we get either a biological capsule with some capability for measuring environmental properties or an atmospheric capsule especially designed to determine the chemical composition and the pressure-temperature-density profile of the Martian atmosphere as a function of altitude up to the height where parachute deployment occurred.

The restriction on payload weight requires that the environmental instrumentation of the biological capsule consist of an abridged version of the corresponding instrumentation in the atmospheric capsule. Thus, the former has only a single-axis accelerometer, which is useful for estimating the maximum deceleration during entry but tells

nothing about the angle of attack at any time during entry and descent. The atmospheric capsule uses a 3-axis accelerometer to determine angle of attack during entry, thus permitting a detailed computation of the precise entry trajectory.

5.2.8 Mars 1971 and Venus 1970 Missions

The payload capability of the Mars 1971 mission opportunity is significantly better than that of the 1969 mission. This suggests that emphasis should be placed upon developing an acceptable biological capsule for 1971. It seems likely that communication by modulated LASER beams will by that time greatly increase the capacity for interplanetary data transfer so that the quantity and quality of TV coverage can be correspondingly improved. In any event an increase in TV resolving power by at least an order of magnitude over that proposed in the present study should be undertaken. The possibility of soft landing a TV camera for close inspection of the surface of Mars should be examined.

As for Venus orbiter missions, the perpetual cloud cover shifts the emphasis from visible-light TV to the far infrared and microwave radiometry and radar. Probably a narrow-field scanning microwave radiometer or radar will reveal some of the topological details of the surface. An atmospheric capsule offers the best means of determining atmospheric composition. Presumably high ambient temperatures make the concept of a surviving capsule on the surface of Venus plausible only for a relatively short time after landing. However, such a capsule could perform a number of meaningful analytical experiments on surface materials before expiring. It would be of interest also to lower a TV system by parachute in an attempt to discover whether the opaque cloud cover extends down to the surface. A major difficulty with the TV-parachute experiment is the transmission of data at a rate sufficiently great to permit acquisition of one or more pictures before the system is destroyed by impact on the surface.

In general, Venus orbiter missions do not present any essentially new operational problems. The de-emphasis of TV represents a considerable reduction in the load on the data link to Earth.

5.3 ELECTRONICS SUBSYSTEMS

The design of the 1969–1971 Mariner electronics subsystems discussed in the following sections is based on the following general criteria:

- The primary objective of the program is success in gathering scientific data and transmitting this data back to Earth.
- Proven techniques and components should be utilized wherever possible to assure the success of the mission.
- All spacecraft–Earth links should be compatible with Deep Space Instrumentation Facility (DSIF) capabilities.
- The DSIF will carry the burden of all spacecraft control, computation, and data processing functions where possible in order to maximize the available spacecraft weight which can be utilized for scientific payload and redundancy.

In addition to the above general criteria, a number of assumptions have been used in the study regarding the expected capabilities and availability of the DSIF communication facilities.

- Commands originating from the Goldstone facility will be sufficient for mission control. The Goldstone facility will have available a 100 kw transmitter with an 85 ft antenna for command transmission. The command frequency will be in the 2110 to 2120 Mc band.
- The three DSIF installations will each employ a 210 ft antenna with a maser preamplifier for signal reception. In addition to the three fixed DSIF installations, the Mobile Tracking Station (MTS) may be used for tracking during launch. The MTS will have a 10 ft antenna with a receiver system excess noise temperature of 1000°K. The received frequencies from all spacecraft, through the mission, will be between 2290 and 2300 Mc.
- The DSIF will not be available continuously throughout the mission. The availability schedule assumed for the study is:
  (1) Continuous for up to 35 days after launch.
  (2) A schedule of 3 days off and 1 day on until the first vehicle is 1 mo from planetary encounter.

(3) Continuous for the following 2 to 3 mo depending on whether one or both vehicles are still operating and the time interval between arrivals at the planet. The first month in orbit, therefore, the DSIF will be available continuously.

(4) During the remainder of the mission, the DSIF will be available 8 hr out of every 24-hr period.

- At planetary encounter (172×10^8 km range), the DSIF acquisition time for angle, two-way doppler, and subcarrier lock may be as long as 26 min based on a round trip signal propagation time of 19 min.

The following paragraphs present, for each mission concept, the basic mission requirements and constraints (Section 5.3.1), the trade-off and decision rationales (Section 5.3.2) and a recommended electronic system configuration (Section 5.3.3).

5.3.1 Mission Requirements

Three possible missions were considered in the study: (1) an orbiter only, (2) an orbiter plus a biological probe, and (3) an orbiter plus a non-surviving atmospheric probe. Since the orbiter-only mission is of primary concern, the requirements for such a mission will be discussed first. Then the additional requirements for the other two missions will be discussed in terms of their effect on the orbiter-only mission.

5.3.1.1 Orbiter-Only Mission

In order to establish a proper framework for the ensuing discussion, a detailed sequence of events for the nominal orbiter mission is presented in Table 5-6 . Some elaboration and definition of this table is necessary to fully understand its contents.

- Spacecraft maneuvers are referenced to body axes. High gain antenna maneuvers are referenced approximately to the spacecraft's heliocentric orbit plane; i.e., the yaw axis is approximately perpendicular to the orbit plane and the roll axis (orbiter-Sun line) lies approximately in the orbit plane as would the pitch axis. The science platform axes are defined similarly to the antenna axes.

- The time of occurrence of events 54 to 59 and 66 to 70 are only for reference. Because these events are initiated by commands from Earth, they must be timed to coincide with Goldstone coverage of the mission. Thus, the two groups of events are nominally separated by 24 hr. The absolute time of these events is not critical, and accurate definition would require detailed trajectory computations beyond the scope of the present study.
- The telemetry modes of operation may be defined as follows:

  Mode 1: The transmitted data will include only engineering performance information at a data rate of 9.375 bits/sec.

  Mode 2: Data includes interplanetary science and limited engineering performance information at a data rate of 9.375 bits/sec.

  Mode 3: Data includes orbit science and engineering performance information at a data rate of 300 bits/sec.

  Mode 4: This mode is identical to Mode 3 with the data rate reduced to 150 bits/sec.

  Mode 5: This mode is identical to Mode 4 with the data rate reduced to 75 bits/sec.

Table 5-6

SEQUENCE OF EVENTS – ORBITER ONLY

Abbreviations

LCE	Launch Complex Equipment
Power	Orbiter Power Subsystem
CC	Orbiter Central Controller
Pyro	Orbiter Pyrotechnics Subsystem
A/C	Attitude Control Subsystem
SIT	Separation Initiated Timer
Comm	Communications Subsystem
Q.C.	Quantitative Command
D.C.	Direct Command
Prop	Propulsion Subsystem
DAS	Data Acquisition System

Table 5-6 (Continued)

No.	Event	Time	Source	Destination	Comment
1	Switch to Internal Power	T - 5 min	LCE	Power	
2	Release Central Controller Inhibit	T - 3 min	LCE	CC	
3	Umbilical Release	T - 20 sec	LCE		
4	Liftoff	T	Event		
5	Atlas Separation	T + 6 min	Event		
6	Shroud Separation	T + 6 min	Centaur		
	A. RF Power Up	+ 5 sec	Timer	Power	T/M Mode 1
	B. Cruise Science On			Power	
7	Orbiter Separation	S = T + 12 min	Centaur Timer		
	A. Enable Central Controller		Separation Connector	CC	
	B. Arm Pyrotechnics			Pyro	
	C. Activate Separation Timer			CC	
	D. Turn On Attitude Control System			A/C	
8	Arm Pyrotechnics	S + 1 min	CC (SIT)	Pyro	
9	Deploy Solar Panels, High Gain Antenna. Unlatch Science Platform.	S + 2 min	CC (SIT)	Pyro	
10	Initiate Celestial Reference Acquisition Sequence. Turn off Timer.	S + 6 min	CC (SIT)	A/C	
			CC	CC	
11	Complete Sun Acquisition	Event 10 +0 to 20 min			

LOCKHEED MISSILES & SPACE COMPANY

Table 5-6 (Continued)

No.	Event	Time	Source	Destination	Comment
12	Solar Array Power Up	Event 11			
13	Complete Canopus Acquisition	Event 11 +0 to 75 min			
14	Turn off Gyros. Switch to T/M Mode 2. Charge Batteries.	Event 13	CC CC CC	A/C Comm, DAS Power	
15	Command Pitch Turn Duration and Polarity	T + 3 days	Q.C.	CC	
16	Command Roll Turn Duration and Polarity	T + 3 days	Q.C.	CC	
17	Load Velocity Meter	T + 3 days	Q.C.	CC	
18	Initiate Midcourse Maneuver Sequence	M	D.C.		M = T + 3 days
	A. Warm up Gyros.			A/C	
	B. Switch to T/M Mode 1			Comm, DAS	
	C. Activate Maneuver Timer			CC	
19	Begin Maneuver	M + 60 min	CC		
	A. Orbiter to Inertial Control			A/C	
	B. Set Pitch Turn Polarity	M + 60 min + 2 sec	CC	A/C	
	C. Start Pitch Turn	M + 60 min + 4 sec	CC	A/C	
20	A. Stop Pitch Turn	Event 19C	CC	A/C	
	B. Reset Turn Polarity	+ 0 to 10 min	CC	A/C	

Table 5-6(Continued)

No.	Event	Time	Source	Destination	Comment
21	A. Set Roll Turn Polarity	M + 71 min	CC	A/C	
	B. Start Roll Turn	M + 71 min + 2 sec	CC	A/C	
22	A. Stop Roll Turn	Event 21B	CC	Prop	
	B. Reset Turn Polarity	+ 0 to 10 min			
23	Ignite Engine	M + 82 min	CC	Prop	
24	Terminate Engine Burn	Event 23 + 1 to 100 sec	CC	Prop	Burn terminated by velocity meter
25	Initiate Celestial Acquisition Sequence	M + 84 min	CC	A/C	
26	Complete Sun Acquisition	Event 25 + 0 to 20 min			
27	Solar Array Power Up	Event 26			
28	Complete Canopus Acquisition	Event 26 + 0 to 75 min			
29	Turn off Gyros. Switch to T/M Mode 2. Charge Batteries.	Event 28	CC CC CC	A/C Comm, DAS Power	
30	Turn off Maneuver Timer	M + 180 min	CC	CC	The timer turns itself off.

Complete Tracking and Repeat Events 15 Through 30, If Required, Before T + 6 days.

LOCKHEED MISSILES & SPACE COMPANY

Table 5-6 (Continued)

No.	Event	Time	Source	Destination	Comment
31	Command High Gain Antenna Yaw Position #1	T + 175 days	D.C.	Comm	
32	Command High Gain Antenna Roll Position #1	T + 175 days	D.C.	Comm	
33	Initiate Antenna Maneuver	A	D.C.	Comm	A = T + 175 days
	A. Activate Antenna Servo				Communication Range = 66×10^6 km
	B. Start Yaw Turn				
34	Stop Yaw Turn Deactivate Yaw Servo	A + 128 sec	CC	Comm	
35	Start Roll Turn	Event 34	CC	Comm	
36	Stop Roll Turn Deactivate Roll Servo	Event 35 + 3 sec	CC	Comm	
37	Switch Transmitter/Receiver to High Gain Antenna	Event 36	D.C.	Comm	
38	Repeat Event 15	E - 26 days	Q.C.	CC	For Approach Maneuver
39	Repeat Event 16	E - 26 days	Q.C.	CC	
40	Repeat Event 17	E - 26 days	Q.C.	CC	
41	Initiate Approach Maneuver Sequence	C	D.C.	CC	C = E - 26 days
	A. Warm up Gyros			A/C	
	B. Activate Maneuver Timer			CC	
42	Repeat Event 19	C + 60 min	CC	A/C	Event 19B = C + 60 min + 2 sec Event 19C = C + 60 min + 4 sec

Table 5-6 (Continued)

No.	Event	Time	Source	Destination	Comment
43	Repeat Event 20	Event 42C to + 0 to 10 min	CC	A/C	Events 20A and 20B
44	Repeat Event 21	C + 71 min	CC	A/C	Event 21B = C + 71 min + 2 sec
45	Repeat Event 22	Event 44B + 0 to 10 min	CC	A/C	
46	Repeat Event 23	C + 82 min	CC	Prop	
47	Repeat Event 24	Event 46 + 0 to 100 sec	CC	Prop	Burn terminated by velocity meter
48	Repeat Event 25	C + 84 min	CC	A/C	
49	Repeat Event 26	Event 48 + 0 to 20 min			
50	Repeat Event 27	Event 49			
51	Repeat Event 28	Event 49 + 0 to 75 min			
52	Turn off Gyros Charge Batteries	Event 51	CC CC	A/C Power	
53	Turn off Maneuver Timer	C + 180 min	CC	CC	The timer turns itself off
54	Command Science Platform Yaw Turn	E - 4 hours	Q.C.	CC	
55	Command Science Platform Roll Turn	E - 4 hours	Q.C.	CC	
56	Initiate Platform Turn	P	D.C.	DAS	P = E - 4 hours
	A. Activate Platform Servos				
	B. Start Yaw Turn				

Table 5-6 (Continued)

No.	Event	Time	Source	Destination	Comment
57	Stop Yaw Turn Deactivate Yaw Servo	Event 56 + 0 to 2 min	CC	DAS	
58	Start Roll Turn	Event 57	CC	DAS	
59	Stop Roll Turn Deactivate Roll Servo	Event 58 + 0 to 1 min	CC	DAS	
60	Load Velocity Meter	E - 3 hours	Q.C.	CC	For orbit injection. No maneuver required.
61	Initiate Maneuver Sequence	E - 82 min	D.C.		
	A. Warm up Gyros			A/C	
	B. Activate Maneuver Timer			CC	
	C. Switch to T/M Mode 3			Comm, DAS	
62	Orbiter to Inertial Control	E - 22 min	CC	A/C	
63	Ignite Engine Warm up DAS	E	CC CC	Prop DAS	
64	Terminate Engine Burn	Event 63 + 5 to 6.5 min	CC	Prop	
65	Turn off Gyros Remove Science Inst. Cover Start DAS Deactivate Maneuver Timer	Event 64	CC CC CC CC	A/C Pyro DAS CC	Data can be obtained even if orbit is not achieved.

Complete Tracking to Determine Orbit Parameters

Table 5-6 (Continued)

No.	Event	Time	Source	Destination	Comment
66	Program Science Platform Position for Sunrise Data	E + 20 hours	Q.C.	CC	
67	Program Science Platform Position for Noon Data	E + 20 hours	Q.C.	CC	
68	Program Science Platform Position for Sunset Data	E + 20 hours	Q.C.	CC	
69	Program DAS Sequence Timer	E + 20 hours	Q.C.	CC	
70	Activate DAS Timer	Event 69	D.C.	CC	
71–75	Repeat Events 66 through 70	E + 12 days	Q.C.	CC	
76	Transfer to T/M Mode 4	E + 12 days	D.C.	Comm, DAS	Communication Range = 187×10^6 km
77–81	Repeat Events 66 through 70	E + 31 days	Q.C.	CC	Read Out Time reduced to 8 hours/day
82–86	Repeat Events 66 through 70	E + 75 days	Q.C.	CC	
87	Transfer to T/M Mode 5	E + 75 days	D.C.	Comm, DAS	Communication Range = 240×10^6 km
88	Turn off Transmitter	E + 180 days	D.C.	Comm	End of Mission

Notes:

A. Events 31, 33 and 34 will be repeated 11 times at preset intervals after T = 175 days on the 1969 mission.
B. Events 32, 35 and 36 will be repeated 10 times at preset intervals after 175 days.
C. The Canopus tracker cone angle will be updated about 8 times throughout the mission by direct command to the attitude control subsystem.
D. During the 1971 mission, Events 31 through 37 will occur nominally at time T + 130 days.
E. During the 1971 mission, Event 76 will be eliminated. Events 82 through 87 will occur at time E + 84 days.
F. No individual back-up events have been considered in the preceding sequence of events.

There are eight basic series of events presented in Table 5-6 . They include launch, primary, and backup midcourse maneuvers, the Mars approach maneuver, Mars orbit injection, on-orbit operation, high gain antenna position updating, and Canopus tracker cone angle updating. The majority of events presented are selfexplanatory but others require further explanation. The rationale employed in the development of these events is more properly deferred to following sections for elaboration. The main purpose for introducing the sequence of events at this point is only to place further discussions in the proper context.

There are several geometrical factors which significantly affect the design of a spacecraft for the anticipated mission. One of these factors is the look-angle coverage required for a low gain antenna system. The desire for uninterrupted communications throughout the midcourse and approach maneuvers is the most significant factor in establishing the look angle requirements for the low gain antenna. In fact, an omnidirectional antenna pattern is required because of the spherically random distribution encountered for corrective spacecraft thrust attitudes as indicated in Section 5.1. Even if communications were not desired during the trajectory correction maneuvers, an essentially omnidirectional radiation pattern would still be required for communications during the initial celestial reference acquisition period (Events 10 through 13). However, the depth of tolerable pattern nulls could be much greater during this acquisition phase because of the shorter communication range involved.

The high gain antenna look angles which will be encountered throughout the mission are defined by four major parameters:

- Attitude stabilization of the spacecraft which results in a random antenna positioning tolerance of ±1 deg.
- Relative motion of the Earth and spacecraft which results in antenna look-angle variations parallel to the plane of the ecliptic.
- Inclination of the spacecraft trajectory to the plane of the ecliptic combined with the distance between the spacecraft and Earth which results in antenna angle variations in a plane perpendicular to the ecliptic plane.

- Relative motion of the Sun-oriented spacecraft and Canopus in conjunction with a single-degree-of-freedom Canopus tracker results in antenna angle variations perpendicular to the ecliptic plane.

The variation of antenna look-angle components as a function of the last three predictable parameters is illustrated in Figs. 5-14 and 5-15 for the nominal 1969 and 1971 missions, respectively. Assuming that the antenna is pointed directly at Earth (within ± 1 deg) at orbit injection and neglecting the relatively minor effects of cross-coupling terms created by spacecraft rolling with a subsequent rotation of the coordinate axes, the required antenna look-angle components parallel and perpendicular to the ecliptic plane can be established as presented in Figs. 5-16 and 5-17 for 1969 and 1971 missions, respectively.

It is readily apparent from Figs. 5-16 and 5-17 that the actual high gain antenna system requirements can only be defined when the dates for initial turn on and mission completion have been specified. This represents a major design tradeoff which will be described in detail in Section 5.3.2.

Another constraint on the system design is the variation in communication range between the spacecraft and Earth throughout the duration of the mission. This variation is presented in Fig. 5-18 for the nominal 1969 and 1971 trajectories.

The final constraint that will be considered in this section is the variation of the solar constant which is of prime importance in the determination of solar array characteristics. The variation of the solar constant during the 1969 and 1971 missions is illustrated in Fig. 5-19.

A discussion of several other pertinent constraints on the design of the spacecraft electronics subsystems is deferred to later sections for reasons of clarity.

5.3.1.2 Orbiter-Plus-Biocapsule Mission

The basic sequence of events presented for the orbiter-only mission must be modified as shown in Table 5-7 for a biocapsule mission. The number of each event refers to its position in time relative to the events in Table 5-6 . The primary operational requirement for the electronics systems design is that capsule data will be measured and transmitted during three phases of the mission: (1) during the capsule-orbiter separation phase, (2) during atmospheric descent and (3) after impact. In addition, a pre-separation checkout operation is required in order to avoid planet impact if the capsule is not expected to function properly.

Based on the trajectory information in Section 3, there are several communication system constraints illustrated in Table 5-8 which significantly affect the proposed system design.

Other factors impose constraints on the design of the capsule electronics systems. For clarity these constraints will be discussed in later sections as required.

5.3.1.3 Orbiter-Plus-Atmospheric Capsule Mission

For the orbiter-plus-atmospheric capsule mission, a few minor modifications are required to the sequence of events presented in Table 5-7 . In fact, deletion of Events 62D, 62G, and all events following 62H, and changing the time of impact to E-5 minutes minimum are the only modifications required.

The basic constraints on the atmospheric capsule electronics system design are similar to those required for a biocapsule prior to impact. The only real differences from Table 5-8 are the maximum atmospheric descent time (17.5 min) and subsonic readout time (70 sec). Other constraints on the design of the electronic systems for an atmospheric capsule mission will be considered in subsequent sections as required.

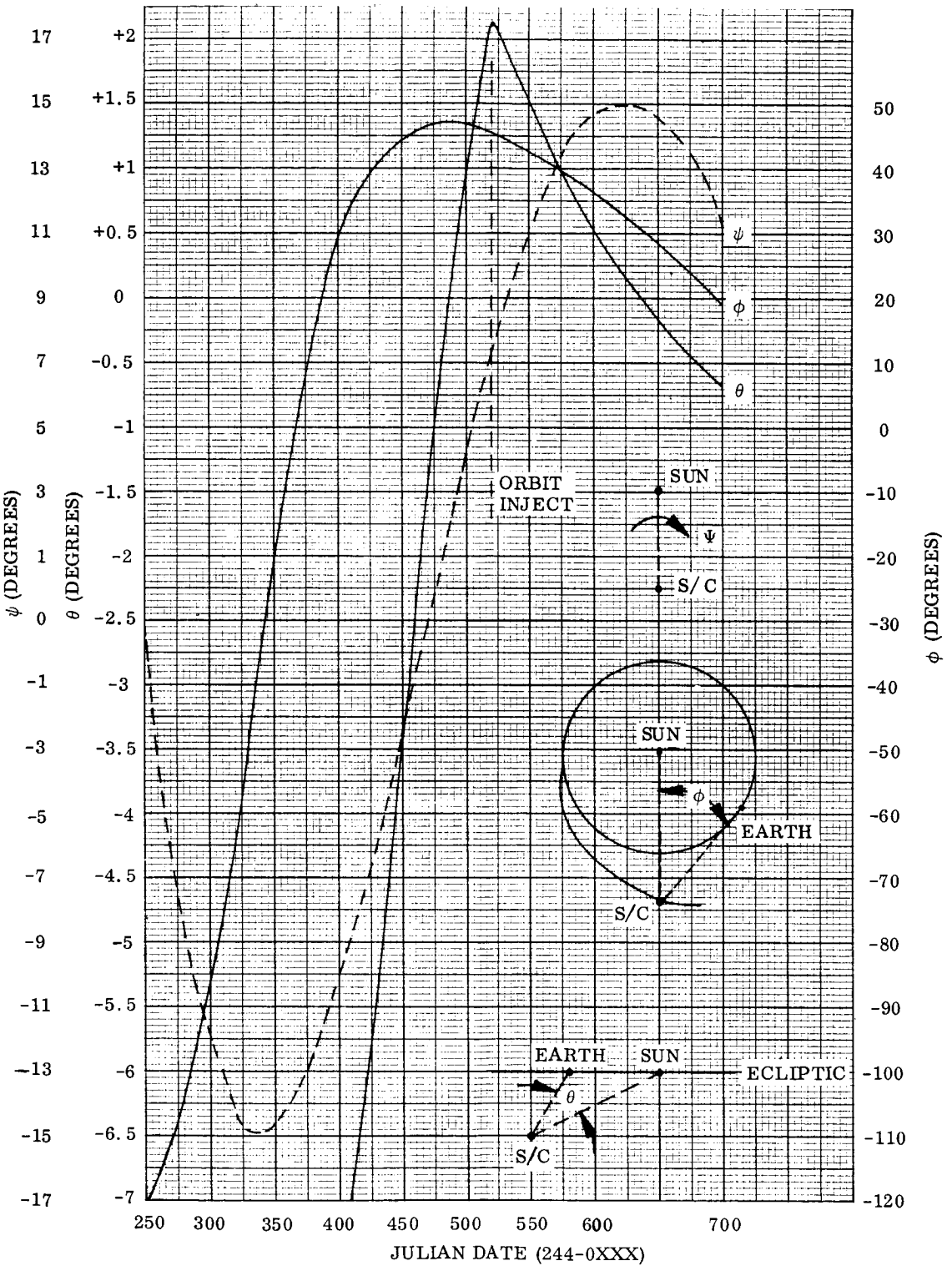


Fig. 5-14 Antenna Look Angle Parameters – 1969 Mission

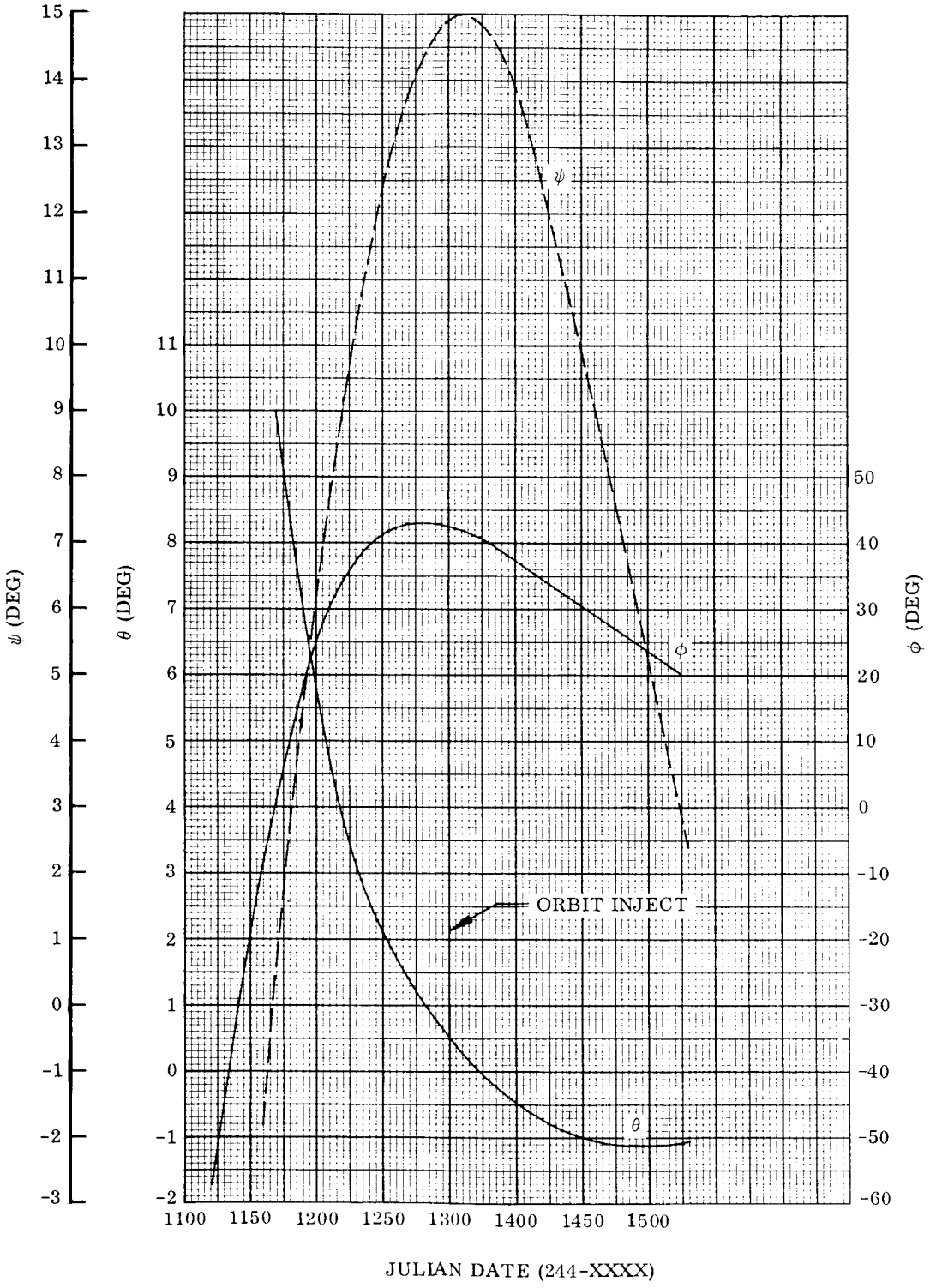


Fig. 5-15 Antenna Look Angle Parameters – 1971 Mission

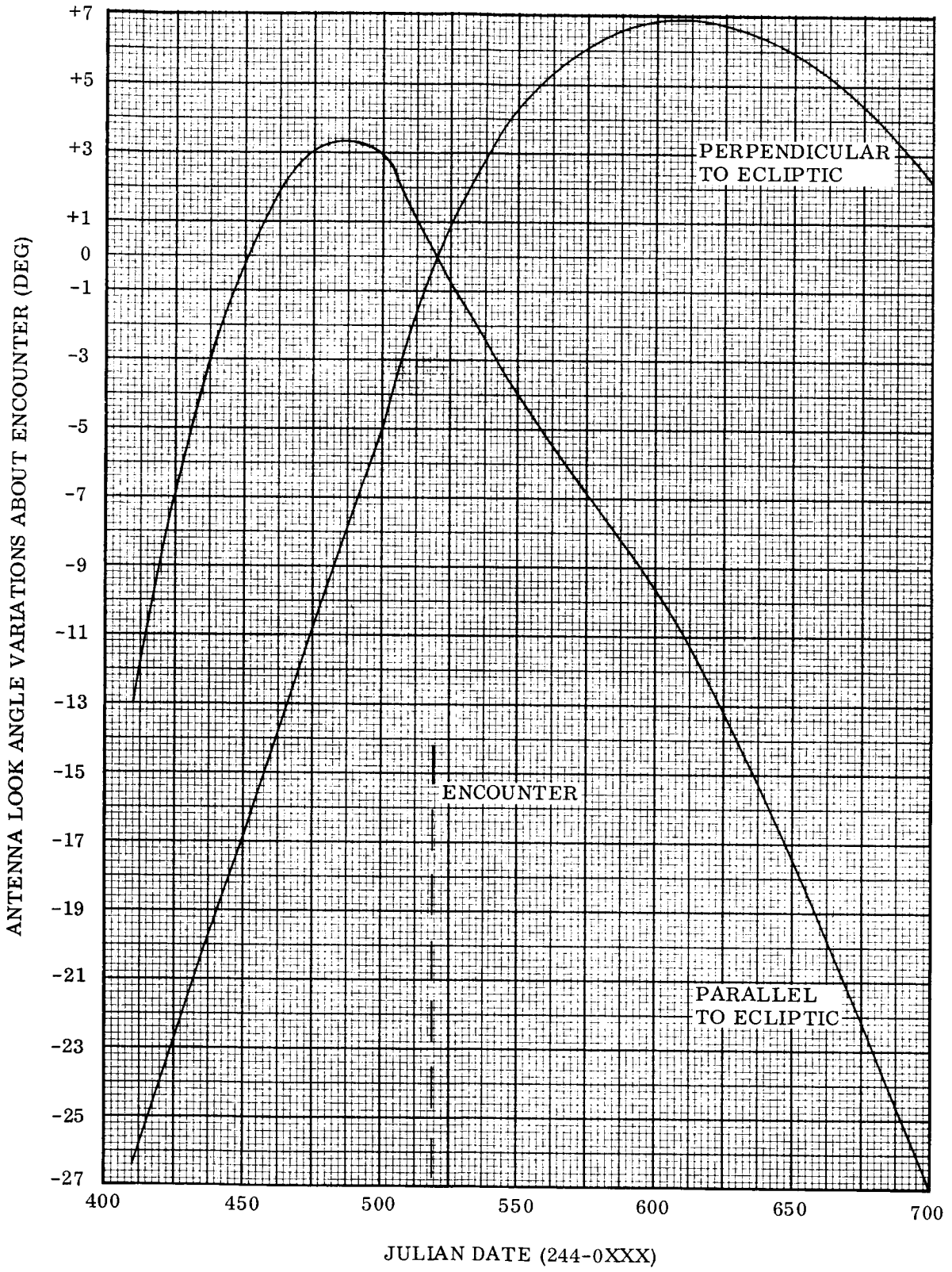


Fig. 5-16 Required Antenna Look Angles Referenced to Look Angle at Encounter – 1969 Mission

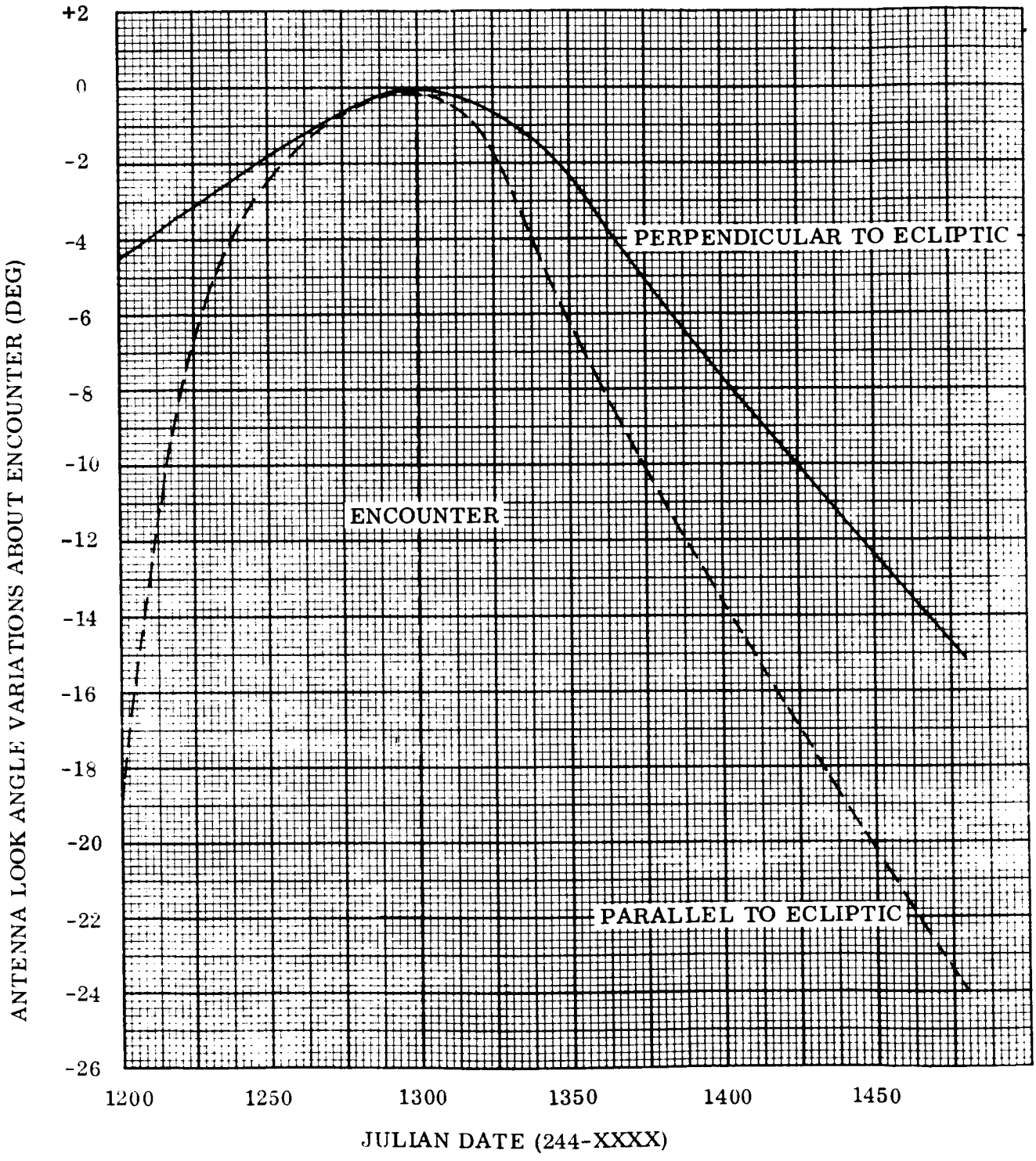


Fig. 5-17 Required Antenna Look Angles Referenced to Look Angle at Encounter – 1971 Mission

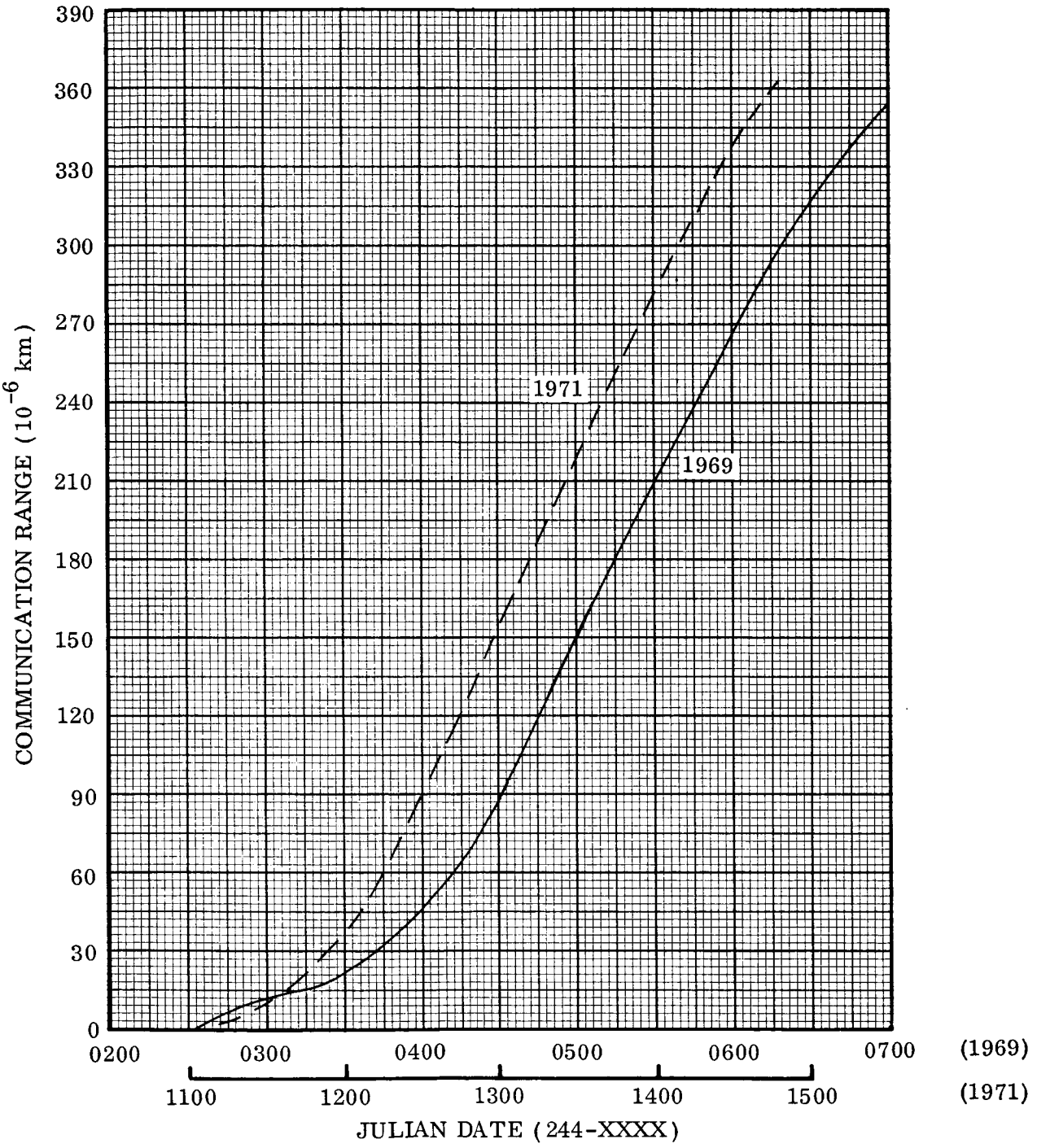


Fig. 5-18 Spacecraft-Earth Communication Range – 1969 and 1971 Missions

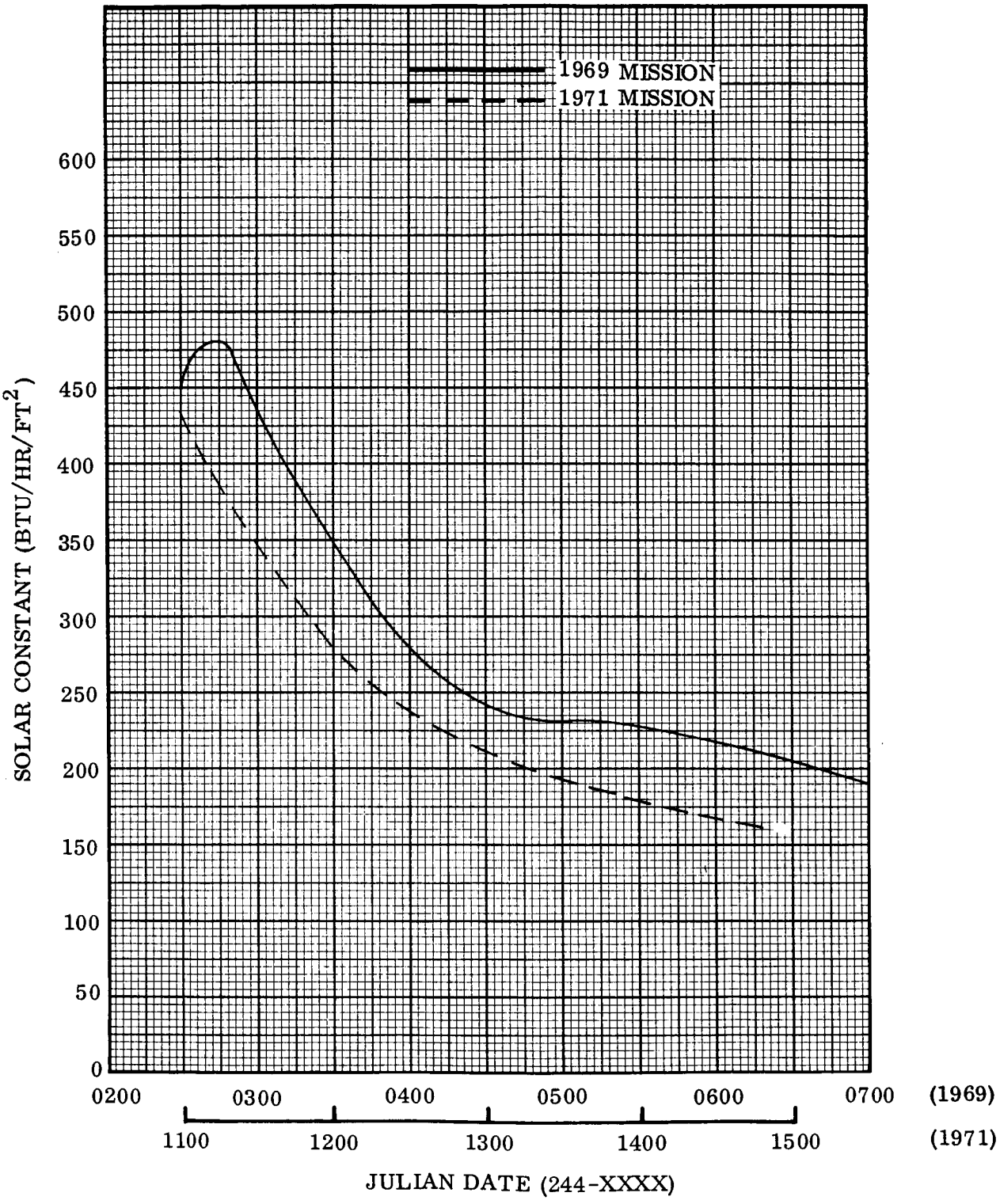


Fig. 5-19 Solar Constant – 1969 and 1971 Missions

Table 5-7

SEQUENCE OF EVENTS-ORBITER PLUS BIOCAPSULE

Abbreviations	
	Orbiter
1. Pyro	Pyrotechnics Subsystem
2. Comm	Communications Subsystem
3. CC	Central Controller
4. A/C	Attitude Control Subsystem
5. SUP	Capsule Mission Support Equipment
6. Power	Power Subsystem
	Capsule
1. C-Prop	Propulsion Subsystem
2. C-ST	Sequence Timer
3. C-Pyro	Pyrotechnics Subsystem
4. CAPSULE	All Subsystems
5. C-DAS	Data Acquisition System
6. C-Comm	Communications Subsystem
7. C-Thermal	Thermal Control Subsystem
8. Switch	"g" - switches
1. D.C.	Direct Command
2. Q.C.	Quantitative Command
3. DSIF	Deep Space Instrumentation Facilities

Note:

Sequence of event numbers indicate relative position of the event referred to in Table .

Table 5-7(Continued)

No.	Event	Time	Source	Destination	Comment
53A	Activate Capsule Battery	X - 24 hours	D.C.	Pyro	X = E - 2 to 4 days
53B	Switch Orbiter to T/M Mode 2A	Event 53A + 5 min	D.C.	Comm	All capsule subsystems are activated when this command is received.
53C	Switch Orbiter to T/M Mode 2	Event 53B + 5 min	D.C.	Comm	Capsule subsystems are deactivated by this command.
53D	Inhibit Propulsion System	X - 3 hours	D.C.	C-Prop	If "go-no go" check was negative, capsule engine will not ignite.
53E	Load Orbiter and Capsule Cruise Sequence Timers	X - 1 hour	Q.C.	CC C-ST	Place Flight Time into Orbiter and capsule sequence timers.
53F	Command Pitch Turn Duration and Polarity	X - 1 hour	Q.C.	CC	Capsule Separation Maneuver
53G	Command Roll Turn Duration and Polarity	X - 1 hour	Q.C.	CC	
53H	Initiate Separation Maneuver Sequence	X	D.C.		
	A. Warm up Gyros			A/C	
	B. Activate Maneuver Timers			CC	
	C. Arm Pyrotechnics			Pyro, C-Pyro	
53J	Begin Maneuver	X + 60 min	CC		
	A. Orbiter to Inertial Control			A/C	
	B. Set Pitch Turn Polarity	X + 60 min + 2 sec	CC	A/C	
	C. Start Pitch Turn	X + 60 min + 4 sec	CC	A/C	

Table 5-7 (Continued)

No.	Event	Time	Source	Destination	Comment
53K	A. Stop Pitch Turn	Event 53JC	CC	A/C	
	B. Reset Turn Polarity	+ 0 to 10 min	CC	A/C	
53L	A. Set Roll Turn Polarity	X + 71 min	CC	A/C	Activate all capsule and orbiter support equipments also.
	B. Start Roll Turn	X + 71 min + 2 sec	CC	A/C	
53M	A. Stop Roll Turn	Event 53LB	CC	A/C	
	B. Reset Turn Polarity	+ 0 to 10 min	CC	A/C	
53N	Separate Capsule	Z	CC	Pyro	Z = X + 82 min
53P	Ignite No. 1 Spin Rockets	Z + 0.5 sec	C-ST	C-Pyro	
53R	Ignite No. 2 Spin Rockets	Z + 1 sec	C-ST	C-Pyro	Back-up to Event 53P
53S	Jettison Sterilization Shroud	Z + 40 sec	C-ST	C-Pyro	
53T	Ignite Capsule Engine	Z + 50 sec	C-ST	C-Prop	Unless Event 53D occurs
53U	Turn Off Capsule Equipment	Z + 65 sec	C-ST	CAPSULE	Except Cruise Sequence Timers
	Turn Off Orbiter Support Equipment	Z + 70 sec	CC	SUP	
	Initiate Celestial Acquisition Sequence	Z + 70 sec	CC	A/C	
53V	Complete Sun Acquisition Solar Array Power Up	Event 53U + 0 to 20 min			
53W	Complete Canopus Acquisition	Event 53V + 0 to 75 min			
53X	Turn Off Gyros	Event 53W	CC	A/C	Read out stored capsule data as soon as communication system is "in-lock."
	Transfer to T/M Mode 2A		CC	Comm	
	Charge Batteries		CC	Power	

Table 5-7(Continued)

No.	Event	Time	Source	Destination	Comment
53Y	Transfer to T/M Mode 2 Turn Off Maneuver Timer	Event 53X + 30 min	CC CC	Comm CC	
61A	Turn on Orbiter Receiver Activate Capsule	E-38 min	CC C-ST	SUP CAPSULE	Transfer Orbiter T/M to Mode 3A. Inititate Capsule C/O Routine
62A	Initiate Supersonic Experiments	See Comment	Switch	C-DAS	Data is stored on capsule for readout at a later time. Event starts at 5g deceleration.
62B	Arm Drogue Chute Mortar	See Comment	Switch	C-Pyro	Event occurs at 50g deceleration
62C	Jettison Capsule Engine Fire Drogue Chute Mortar	See Comment	Switch	C-Pyro	Event occurs at 3.5g deceleration
62D	Deploy Main Chute Release Drogue Chute Stop Supersonic Experiments	See Comment	Switch	C-Pyro C-DAS	Event occurs at g-level equivalent to main chute pressure of 4#/ft^2
62E	Warm Up Subsonic Experiments	Event 61E	Switch	C-DAS	
62F	Initiate Subsonic Experiments Initiate Stored Data Readout	Event 61E + 15 sec	C-ST	C-DAS C-Comm	15 seconds is allowed for communication link synchronization.
62G	Impact. Turn Off Capsule Electronics Deploy Biological Specimen Acquisition Mechanism	I	Switch	CAPSULE C-Pyro	I = E-2 min (minimum) Specimen Acquisition Mechanism is Activated.
62H	Turn Off Orbiter Receiver Switch to T/M Mode 3	E-1 min	CC	SUP Comm	

Table 5-8

BIOCAPSULE COMMUNICATION CONSTRAINTS

Mission Phase		Constraint
Separation	Range:	$0 < R < 1000$ feet
	Operating Time:	6 min
Atmospheric Descent	Range to Orbiter:	10^4 km Maximum
	Capsule Antenna Beamwidth:	≥ 104 deg
	Orbiter Antenna Beamwidth:	≥ 14.5 deg
	Entry Velocity:	21,000 ft/sec
	Peak Deceleration:	150 g's
	Maximum Descent Time:	20.5 min
	Subsonic Read Out Time:	4 min
Post-Impact	Range to Earth:	172×10^6 km
	Impact Shock:	< 900 g's
	Data Acquisition Time:	≥ 20 hr
	Data Transmission Time:	Sufficient to read out data once

Table 5-7 (Continued)

No.	Event	Time	Source	Destination	Comment
C1	Activate Post-Impact Timers Activate Biological DAS Activate Thermal Control	Event 62G	Switch	C-ST C-DAS C-THERMAL	
C2 thru C21	Sample and Store Biological Data	I + η hours	C-St	C-DAS	η = 1, 2, 3, ...20
C22	Activate Receiver	I + 20 hours	C-ST	C-Comm	
C23 thru C26	Repeat C2	I + N hours	C-ST	C-DAS	N = 21, 22, 23, 24
C27	Acquire Earth Transmission	I + 20 to 24 hours	DSIF	C-Comm	
C28	Initiate Data Read Out	Event C27 + 20 min	C-Comm	C-Comm	Allow 20 minutes for DSIF to acquire Capsule signal
C29	Capsule Mission Complete	I + 28 hours			

5.3.2 System Tradeoffs

Several of the system tradeoffs considered in the study are applicable to all three of the missions investigated. Therefore, the tradeoffs will be presented for the orbiter-only mission first since these tradeoffs are common to all missions. Then the following sections will be devoted entirely to mission-peculiar tradeoffs.

5.3.2.1 Orbiter-Only Tradeoffs

Telecommunication System Modulation. There is a basic requirement that the orbiter Communication system must be compatible with the DSIF. This requirement immediately limits the modulation on the link to coherent phase shift keying (PSK). However, some latitude was considered available in the implementation of the coherent PSK technique. That is, a selection is permissible between the double subcarrier implementation employed on Mariner R and Mariner C and the single subcarrier "post 1965" design presently under development. The most obvious advantages of the double subcarrier system is that it is fully flight-qualified and has flown very successfully on a relatively short (3 1/2 mo) mission, and that the DSIF has been equipped to operate with such a system at data rates of 33 1/3 bits/sec or 8 1/3 bits/sec.

The advantages of the single subcarrier system appear to be increased data efficiency (30 percent), less complexity, slightly lower weight and, clock regeneration at the receiver is simpler and more accurate.

The prime disadvantages of this system are that it has not been flight-qualified and the DSIF has not yet been equipped to support it. However, it was felt that the modifications of the double subcarrier system for the higher data rates that can be achieved on the 1969 mission, the possibility that the package must be redesigned, and the two to three year period available for qualification of the post-1965 system provide sufficient justification for attempting to obtain the benefits of the single subcarrier system.

It is realized that the preceding rationale is very subjective and the interpretation of the JPL Space Program Summaries concerning the development status of the post-1965

system may be optimistic. However, the overall feasibility of the 1969 and 1971 orbiter mission does not depend critically on the implementation of the coherent PSK system which will ultimately be flown. Therefore, only the single subcarrier system was used to determine the data rate capability, system weight, etc, in the remainder of the study.

Mission Design Lifetime. One of the many goals of the study was to establish a rationale which could be helpful in defining a design goal for on-orbit mission lifetime. The first step in the rationale is to define the system parameters that are sensitive to on-orbit lifetime. The variation of such parameters as increased communication range, lower solar constant, etc, are reflected in the spacecraft design by increased weight requirements. Therefore, an effective measure of the payload penalty incurred for increased on-orbit operational lifetimes is the additional weight requirement of the spacecraft support subsystems. However, other factors such as increased system complexity must also be evaluated against the enhanced data-gathering capability of an extended mission. Since a reliability analysis could not be included in the scope of the present study, it was necessary that these latter evaluations be subjective in nature.

Neglecting the possible need for more redundancy to achieve a given reliability on extended missions, the high gain antenna is the only electronic system component which will greatly enhance the data-gathering capability of the mission at some cost in complexity. Therefore, the first tradeoff considered is the use of a fixed position antenna (as on Mariner C), a single axis steerable antenna, or a two axis steerable antenna.

Referring again to Fig. 5-16 and 5-17 which present the antenna look-angle variations about the look angle at encounter for 1969 and 1971 missions, respectively, the beamwidth requirements for a fixed antenna can be calculated as a function of the mission design lifetime on-orbit. However, if communications are required throughout the transfer trajectory, the lifetime on-orbit may not be the real determining factor in specifying the required antenna beamwidths.

It will be shown in a later section that the maximum communication range at a data rate of 9-3/8 bits/sec that can be expected using the spacecraft's low gain antenna

is about 66×10^6 km. If it is assumed that, at this range, data transmission will be transferred to the high gain antenna, the beamwidth requirements for a fixed antenna as a function of mission design lifetime on-orbit are illustrated in Fig. 5-20. There are three main factors which should be noted about these results:

- Design lifetimes greater than 6 mo in orbit were not considered because at this time sun occultation can be expected during a portion of each orbit, making attitude control battery-supplied power requirements untenable.
- The antenna axis with the largest beamwidth requirement for a 1969 mission is perpendicular to the ecliptic, but in 1971 this axis is parallel to the ecliptic.
- A fixed antenna tailored to the 1969 mission will provide suboptimum performance on a 1971 mission.

Using the standard equation for approximation of the gain of a rectangular aperture antenna, estimates of the peak antenna gains (obtained only at encounter) can be determined.

$$G = \frac{30,000}{W_H W_E}$$

where

G = peak antenna pattern gain
W_H = H-plane half-power beamwidth
W_E = E-plane half-power beamwidth

The results of this estimation are presented in Fig. 5-21 and 5-22 for a fixed and single-degree-of-freedom antenna. For reference, the peak gain of a two-degree-of-freedom antenna is also indicated. For simplicity, the antennas were assumed to be physically constrained to a maximum reflector dimension of 4 ft. If the 4 ft restriction were deleted, the gains of the single and double-axis antennas could be increased, but the gain of the latter would increase more rapidly. Emphasizing

the four basic assumptions used in deriving these figures; (i.e., (1) continuous, low data rate communications throughout the entire transfer period, (2) peak gain will be designed to occur at encounter, (3) communications will always occur within the half power beamwidth for each axis, and (4) the maximum antenna dimension must be no greater than four feet) the data rate penalty incurred at encounter by restricting the freedom of the antenna can be determined directly from the figures.

As a typical example, assume the mission design lifetime is to be 3 mo on-orbit for the 1969 mission and the data rate attainable at encounter with a two-degree-of-freedom antenna is 300 bits/sec (this will be shown to be the capability of the system design example in a later section). Then the data rate at encounter using a single-degree-of-freedom antenna would be reduced to about 110 bit/sec and using a fixed antenna, the data rate would be reduced further to about 20 bits/sec.

As a further example assume the mission design lifetime is selected to be 6 mo on-orbit. Then the data rate at encounter is further reduced to about 45 bits/sec using a single-degree-of-freedom antenna and 7.5 bits/sec using a fixed antenna.

Referring to Fig. 5-22 for results pertaining to the 1971 mission, the data rate penalty incurred by restricting the antenna freedom will be much less than that incurred on the 1969 mission. For example, a single-degree-of-freedom antenna employed for a 3 mo on-orbit mission would suffer a data rate loss at encounter of about 1.8 db instead of the 4.2 db loss incurred on the 1969 mission.

The real significance of the preceding discussion is demonstrated in Fig. 5-23 which shows the relative data rate penalty, throughout the orbit life of the spacecraft, incurred for a 1969 mission by restricting the antenna freedom entirely or partially for typical mission design lifetimes. The apparently random behavior of gain for the steerable antennas is due to the assumption that the antenna positions will be updated in 3-deg incremental steps. These curves would be smooth if the antenna position was continuously variable. In any event it is readily apparent from this

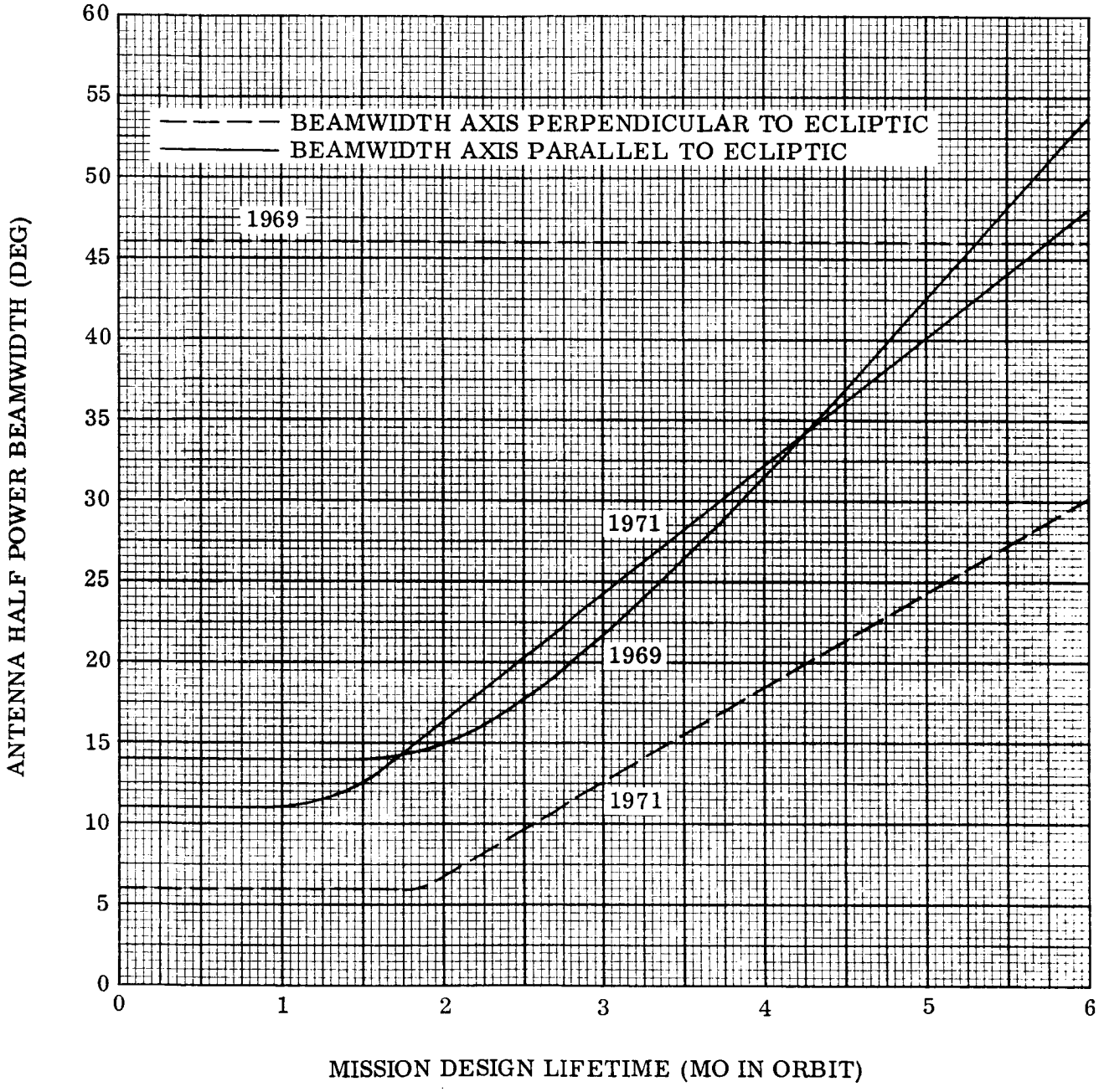


Fig. 5-20 Fixed Antenna Beamwidth Required vs. Mission Designed Lifetime

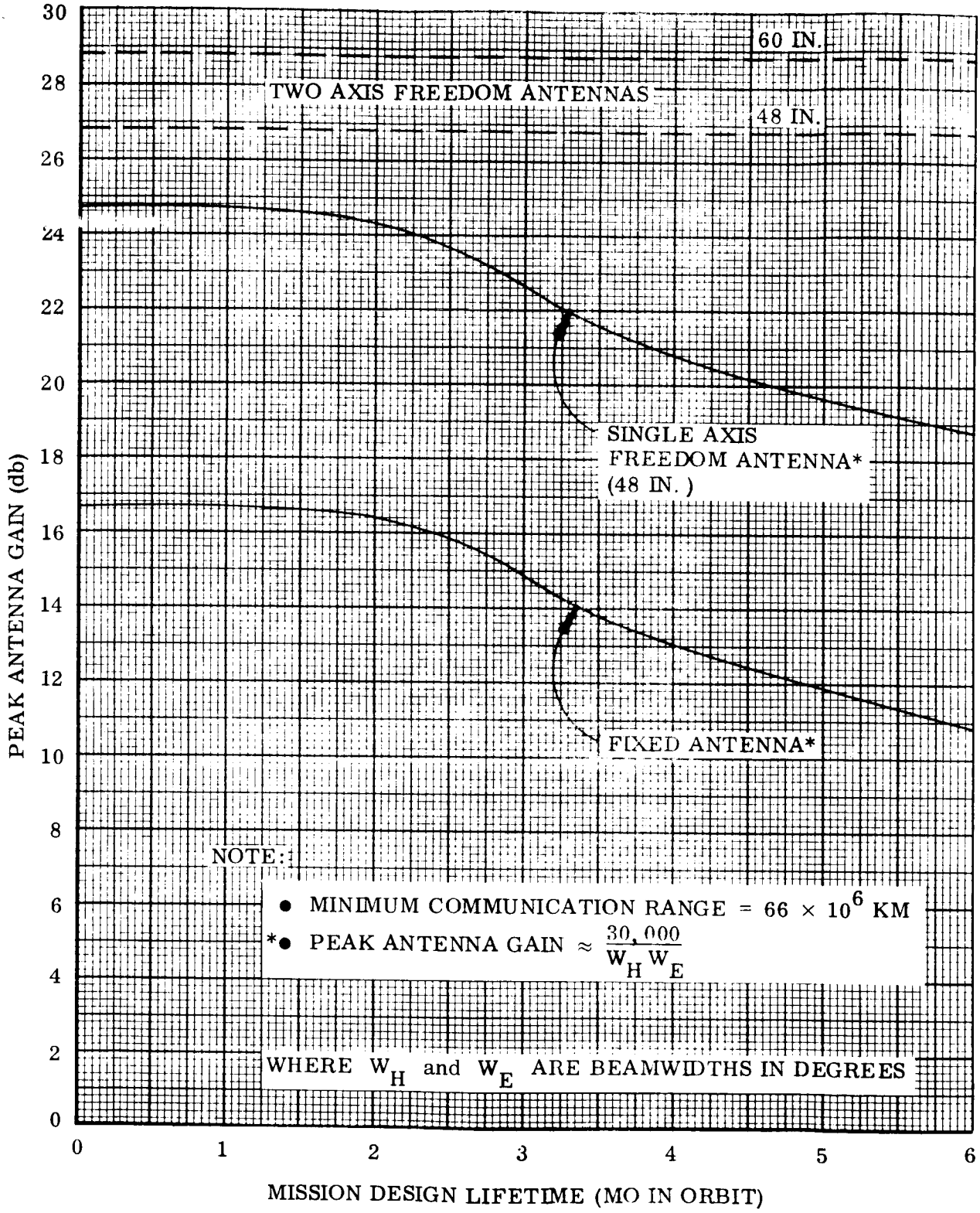


Fig. 5-21 Antenna Gain at Encounter vs. Mission Design Orbit Lifetime – 1969 Mission

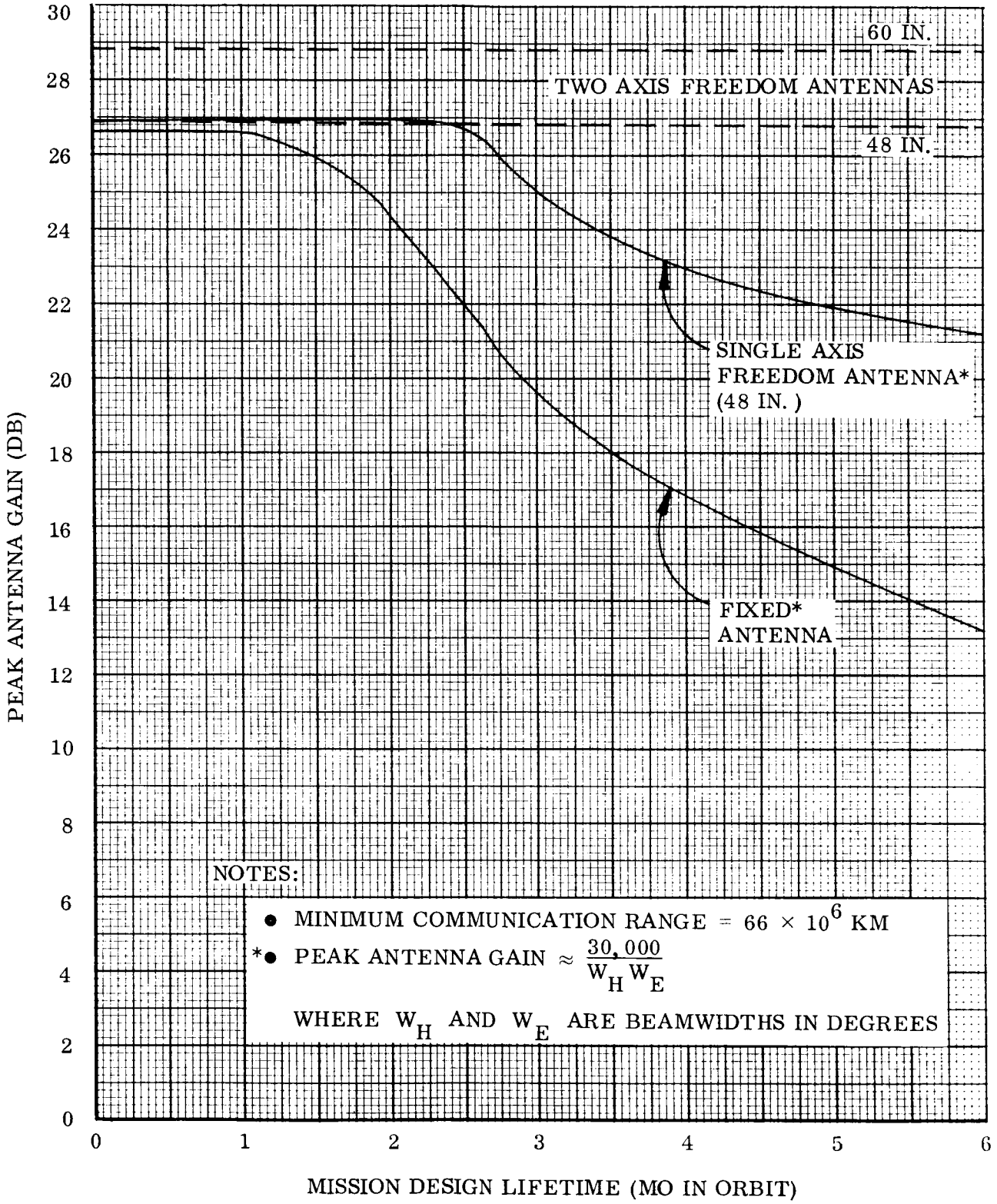


Fig. 5-22 Antenna Gain at Encounter vs. Mission Design Orbit Lifetime – 1971 Mission

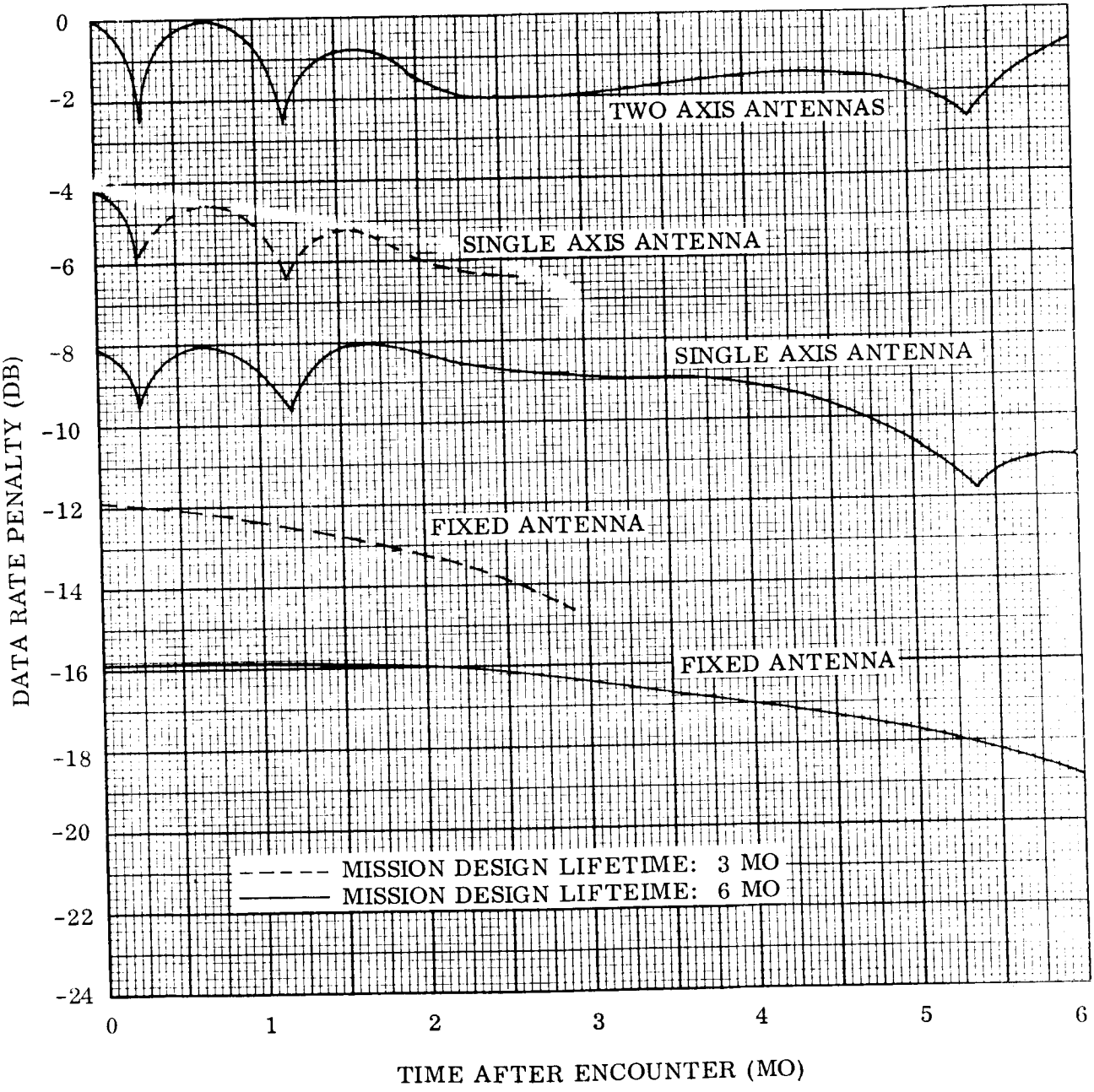


Fig. 5-23 Data Rate Penalty of Limited Freedom Antennas Vs. Time in Orbit 1969 Mission

graph that the data rate penalty incurred after encounter is even greater than the penalty incurred at encounter if the antenna has a restricted motion.

Figure 5-24 presents the data similar to Fig. 5-23 for a 1971 mission. However, the steerable antenna curves have been smoothed for simplicity, as though their positions were continuously variable.

In both Fig. 5-23 and 5-24 the effect of increasing communication range as a function of time in orbit has not been shown, since it is independent of antenna freedom.

If the constraint that communications must be maintained continuously throughout the transfer trajectory is discarded, the antenna gain at encounter as a function of mission design lifetime on-orbit is illustrated in Fig. 5-25 for the 1969 and 1971 missions.

In this case the data rate penalties incurred at encounter by using a restricted motion antenna are much less than the penalty incurred in the previous examples (see Fig. 5-23 and 5-24. Since the required antenna gain at a communication range of 66×10^6 km and a data rate of 9-3/8 bits/sec is only about three db, communications throughout the transfer trajectory can probably be maintained on the 1969 mission with a single-degree-of-freedom antenna by operating on the edge of the main lobe of the pattern ($\leq$ 21 db below peak gain). On the 1971 mission, communication throughout the transfer trajectory is much more certain than for the 1969 mission if a single-degree-of-freedom antenna is used.

All of the preceding calculations were based on the assumption that the Mariner C single-degree-of-freedom Canopus tracker will be used in the spacecraft guidance and control system. If a second-degree-of-freedom is provided for the Canopus tracker, the inherent rolling of the spacecraft would be eliminated. Then the data rate penalty incurred using a single-degree-of-freedom antenna is nearly zero for the 1971 mission and only about 2 db at the conclusion of a 6-mo on-orbit mission in 1969. However, this approach would not reduce the system complexity, while it

would require considerable development efforts to modify an existing, flight-qualified Mariner C component. This approach does not appear to be a logical solution to the problem.

From the preceding discussion a fixed high-gain antenna appears unreasonable for both the 1969 and 1971 missions. A brief summary of the major advantages and disadvantages of the single and double-degree of freedom antennas is presented in Table 5-9 . Based on this summary, it is recommended that a two-degree-of-freedom antenna be incorporated in the design of the spacecraft. Throughout the remainder of the report it is assumed that a two-axis high-gain antenna system will be used.

Table 5-9

SUMMARY OF ANTENNA TRADE-OFFS

Single Axis	Two Axis
	More complexity
	About 5 lb heavier
	3 db more data in 1969 3 to 6 db more data in 1971
New development required for 1971 mission	1969 mission antenna will be used in 1971
Communications may be maintainable throughout transfer trajectory	Communications can be maintained throughout transfer trajectory
Large unfurlable antennas cannot increase the data rates on-orbit comparable to a two-axis antenna	Large unfurlable antennas can be used to increase the data rate significantly

Having made the decision to use a two-degree-of-freedom antenna on the spacecraft, it is possible to investigate the increase in weight requirements of the electronic system as a function of mission design lifetime on-orbit (neglecting redundancy effects).

Only the communication system and solar array weights are directly affected by extended mission lifetimes. The solar array weight increase to provide a fixed output power independent of time in orbit will be considered first.

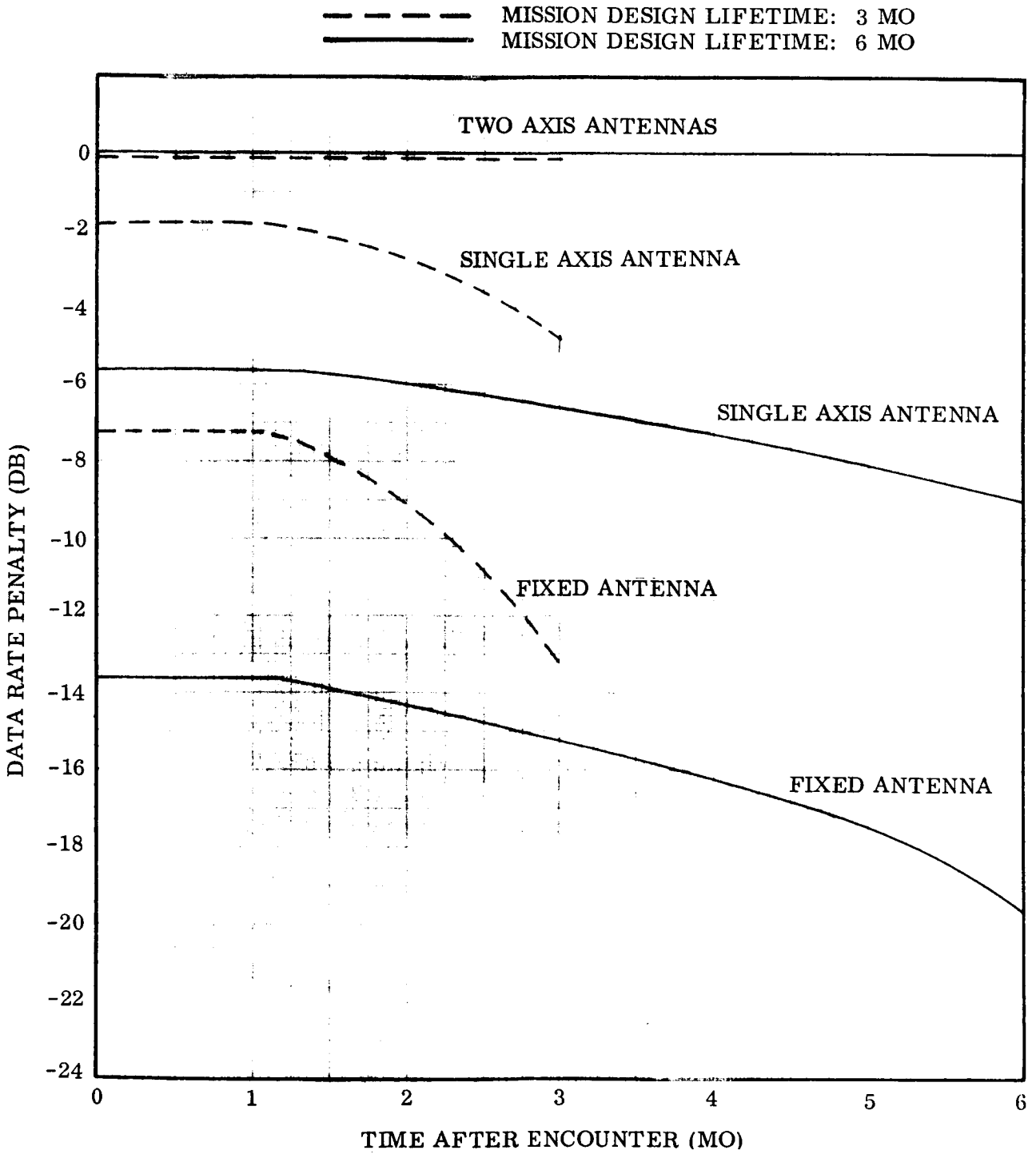


Fig. 5-24 Data Rate Penalty of Limited Freedom Antennas vs. Time in Orbit – 1971 Mission

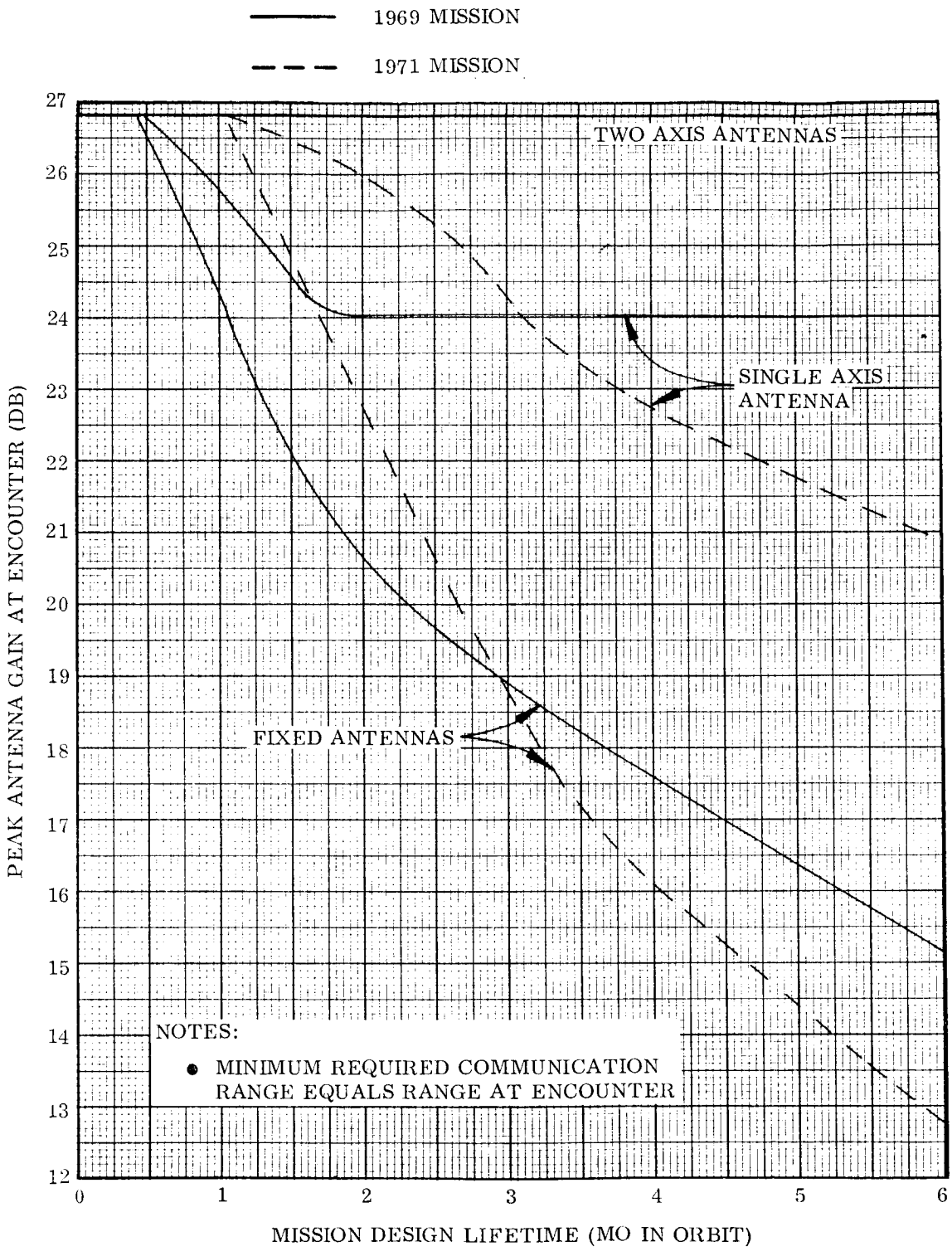


Fig. 5-25 Antenna Gain at Encounter vs. Mission Design Lifetime – 1969 and 1971 Missions

Assume that the Mariner C solar array was used on the spacecraft for the 1969 mission. Then the solar constant, array temperature and array power output would be expected to vary as indicated in Fig. 5-26. Based on the array area of 70.4 sq ft and a specific weight of about 1.1 lb/ft^2, it can be shown as an example that the additional solar array weight required for a 6 mo on-orbit mission instead of a 3 mo mission is about 13 lb if the system requirements are held constant. It will be shown in a later section that the existing Mariner C array is sufficient for a 6 mo mission and is recommended for use since it is a fully qualified system. Thus there is no real solar array weight penalty incurred by prolonging the mission lifetime to 6 mo on-orbit.

The required communication system weight is not only a function of lifetime in orbit but also a function of the transmitted data rate required at completion of the mission. There are three components which are responsible for the primary weight variations as a function of data rate: the antenna, the transmitter, and the portion of the solar array required to supply power for the transmitter. The antenna considered in this portion of the study was a "flex-rib" antenna presently under development at LMSC. This antenna is being developed as an unfurlable parabolic device using a contoured wire mesh as the reflector. Several models of this antenna have already been successfully fabricated and tested at LMSC and one is scheduled for flight test within a few months. The expected physical characteristics of this type of antenna are shown without need for further explanation in Fig. 5-27 and 5-28. In this phase of the study it was assumed that the antenna size might be variable between 3 ft and 16.5 ft in diameter and that an antenna with an aperture in excess of 5 ft would be unfurlable; if less than 5 ft it could be launched in an open position.

The pertinent characteristics of the transmitters considered in this phase of the study are shown in Table 5-10. These transmitters are representative of the state-of-the-art in satellite-borne units with a premium on weight, volume, and efficiency.

Table 5-10

TRANSMITTERS FOR 2.3 G TELEMETRY

	Output Power	Raw Input Power	Weight (lb)	Volume (in^3)	Manufacturer
1.	2.5 (Solid State)	32	2.5	100	Space Technology Labs
2.	5 (Triode)	35	5	100	Radiation at Stanford*
3.	10 (Triode)	64	10	170	Resdel
4.	20 (Amplitron)	50	10	200	—**
	(TWT)	65	10	200	—***
5.	40 (VTM)	140	12	190	Eitel-McCullough
6.	70 (Amplitron)	175	12	250	—**

*Availability uncertain since Radiation at Stanford no longer exists.
**Amplitron built by Raytheon.
***TWT built by Watkins-Johnson.

Using the preceding constraints and estimates, a curve of antenna, transmitter, and directly chargeable solar array weight versus data rate for 3 and 6 mo on-orbit missions was established with the results shown in Fig. 5-29. As an example, assume the transmitted data rate is 300 bits/sec. Then the weight penalty incurred for an extra 3 mo in orbit would only be about 6 lb.

The other set of curves shown in Fig. 5-29 assume that the Mariner C transmitter is used on the mission. Thus, only the antenna size is allowed to vary as a function of data rate and communication distance. These curves indicate similar results to the situation considered in the preceding paragraph. It may also be seen from this graph that the Mariner C transmitter is not state-of-the-art on the basis of weight. However, the long-life requirement for this type of mission is an overriding factor and the status of the Mariner C transmitter is such that it will probably be used on the 1969 mission. The only other transmitter which appears very promising is the 20-w

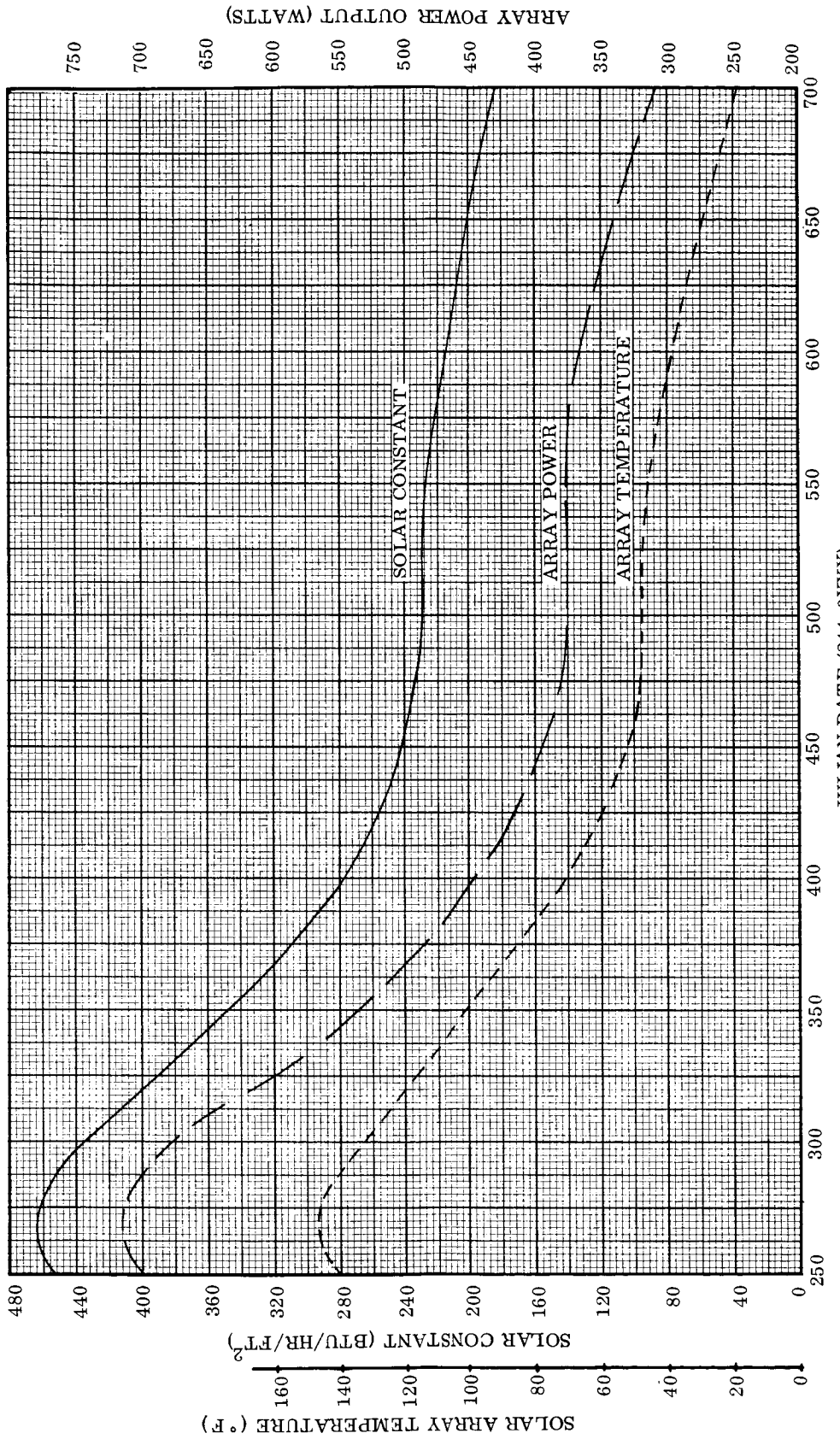


Fig. 5-26 Solar Array Characteristics Using Mariner C Panels – 1969 Mission

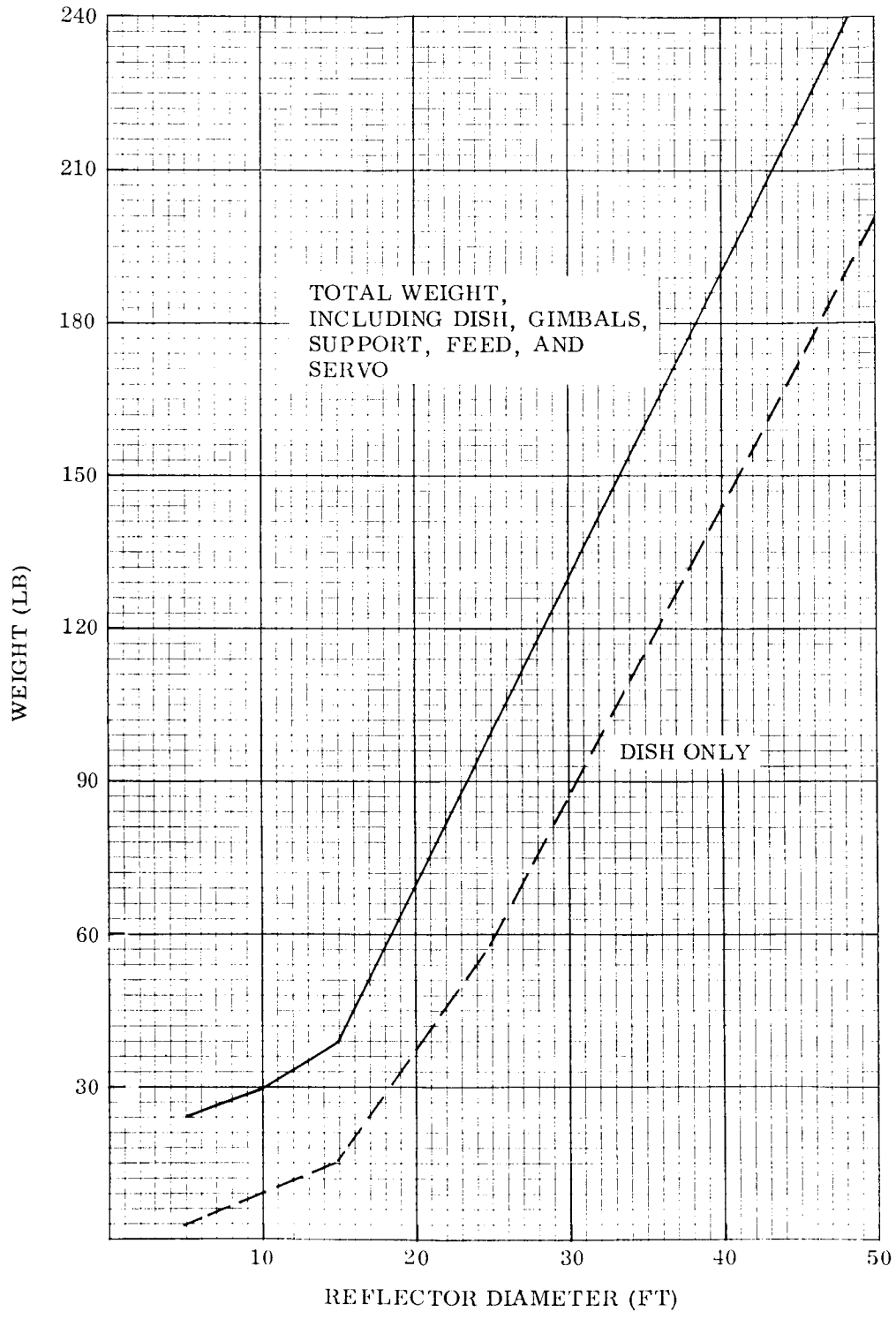


Fig. 5-27 LMSC Flex-Rib Unfurlable-Steerable Antenna – Weight vs. Diameter of Parabolic Reflector

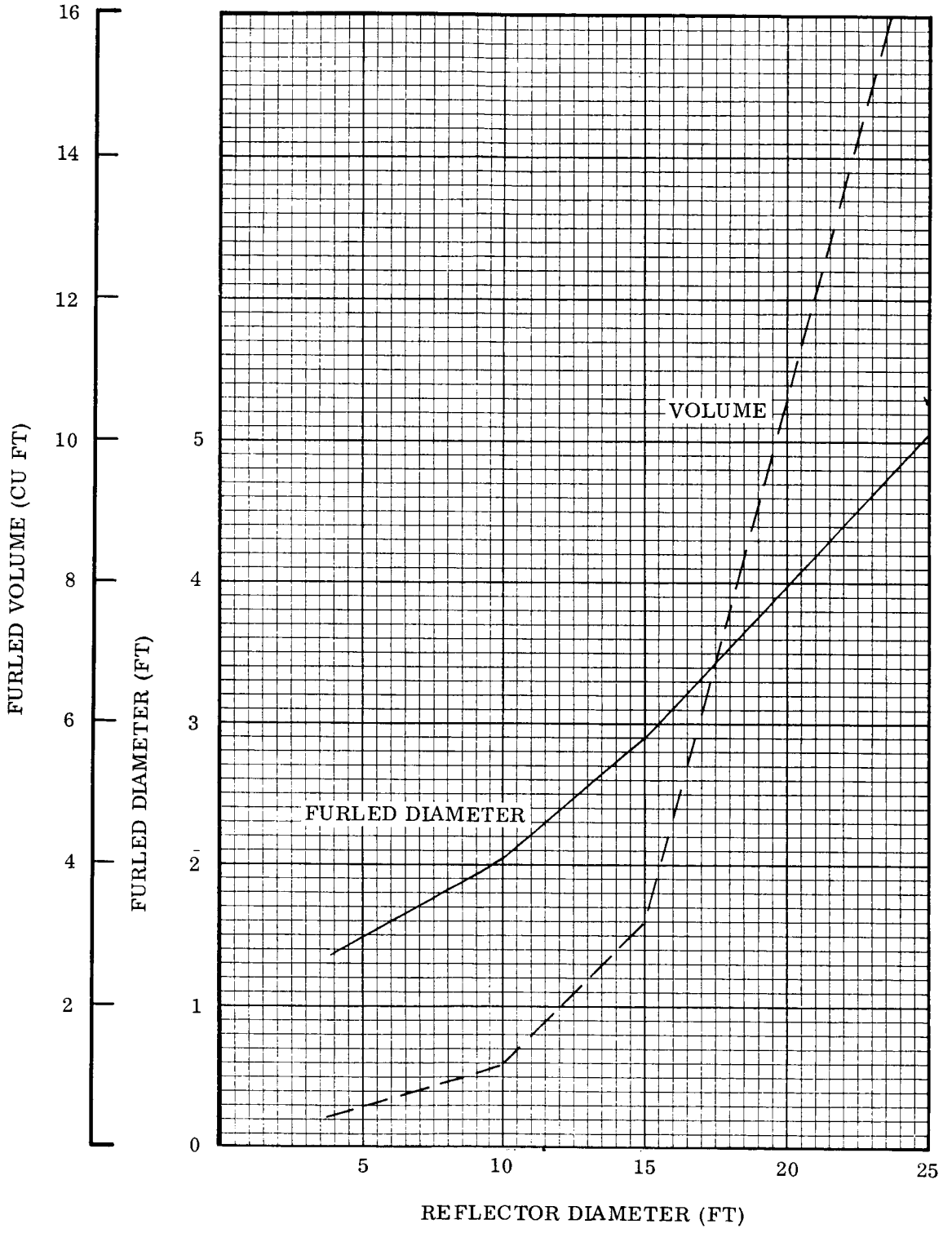


Fig. 5-28 LMSC Flex-Rib Unfurlable Reflector – Furled Diameter and Volume vs. Reflector Diameter

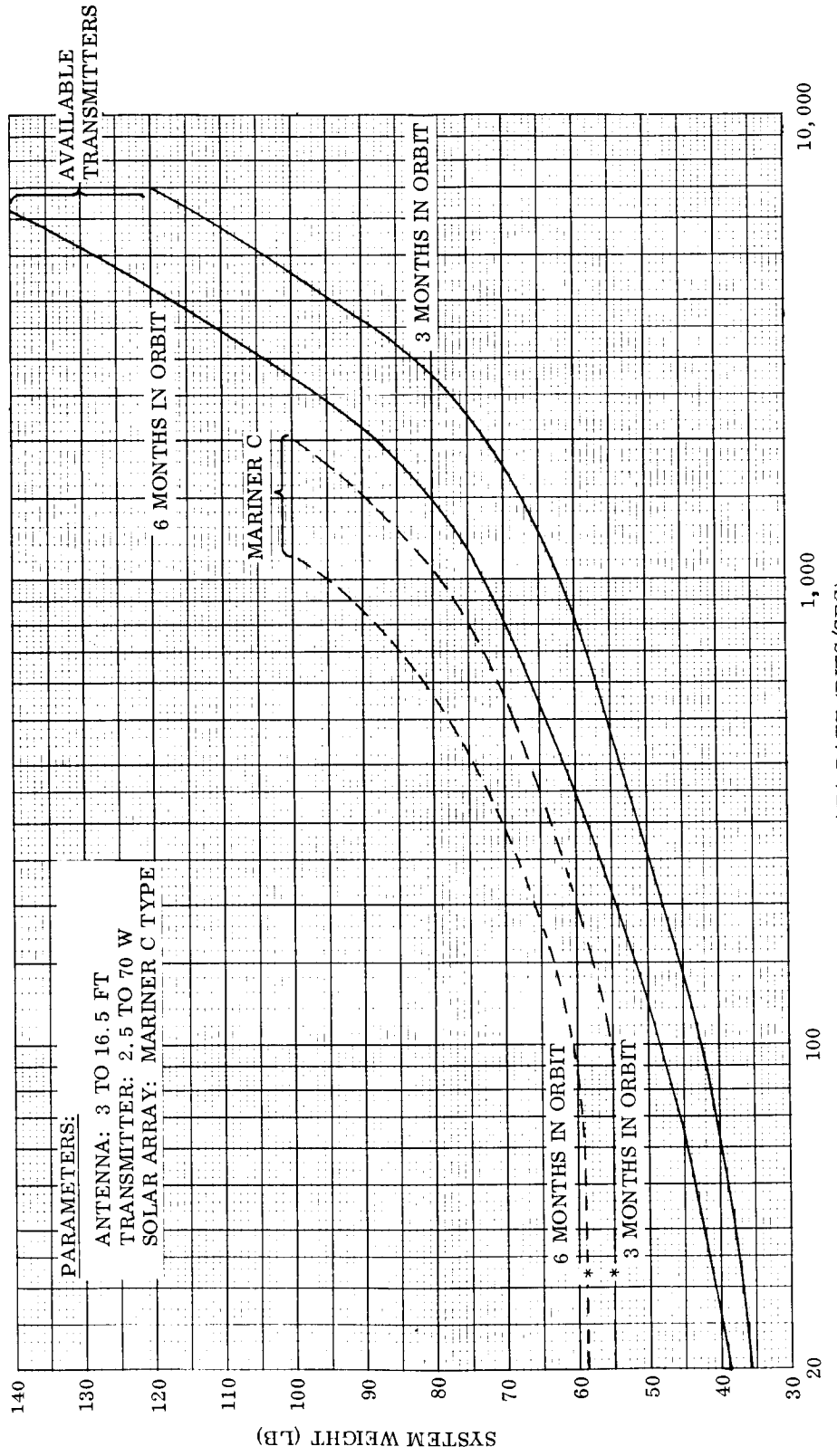


Fig. 5-29 Electronics Systems Weight Variation vs. Time in Orbit and Data Rate

traveling-wave-tube unit being developed by Watkins-Johnson. A design goal for this power amplifier is a tube life of 50,000 hr which, combined with its relatively high efficiency (40 percent for the tube alone), makes this transmitter look very attractive. The qualification and development testing requirements for any new transmitter makes this a long leadtime development item. For the remainder of the study, a conservative approach has been used and the Mariner C transmitter is used for later estimates and calculations.

Since the weight penalties incurred for a 6-mo on-orbit mission are so small (refer to Section 5.1 for attitude-control/gas weight penalties), the 6 mo mission has been selected as the nominal goal.

5.3.2.2 Orbiter Plus Biocapsule

There are two basic concepts which must be defined for a biocapsule mission, prior to any discussion of the most suitable system configuration. These concepts concern: (1) The communication path for transmission between the capsule and Earth during each phase of the mission and (2) the length of time which the capsule must survive on the planet surface.

Communication Path – Post Impact Phase. In deciding whether communication with the biocapsule should be via a direct Earth-capsule link or relayed through the orbiter, it is best to consider the last phase of the mission first, that is, communication to and from the surface of the planet. If a direct Earth-capsule link is considered, the frequency and modulation are required to be S-band and coherent PSK, respectively. If a relay link via the orbiter is considered, there is no frequency or modulation constraint on the capsule-orbiter segment of the link.

Several of the primary considerations for determining the best communication path for the biocapsule link are based on simple geometrical factors. Of prime importance is the fact that the anticipated orbiter guidance dispersions may result in orbital

periods varying from about 11 hr to 62.5 hr. In addition, the biocapsule will have a tendency to land in the southern hemisphere on Mars while the orbiter will spend most of its time above the northern hemisphere. Since the biocapsule rotation period is fixed at about 24.5 hr, determination of available line-of-sight communication periods presents a straightforward but lengthy computation problem which was beyond the scope of the study. In addition, the local obscura in the vicinity of the capsule landing point will be unknown and may further limit communication periods with the orbiter.

This brief introduction to the problem is sufficient to conclude that the capsule survival time on the planet surface before its first line-of-sight contact with the orbiter may vary from only a few hours to several days. It should also be noted that the length of time that the orbiter and capsule will remain within line-of-sight is uncertain, but it may vary from seconds to many hours.

Using a direct capsule-to-earth communication link, the nominal readout periods available occur at 24.5 hr intervals and, neglecting local capsule obscura, available line-of-sight periods will last at least 10 hr. Therefore, the required capsule survival time may be well defined with a minimum requirement of at least 28 hr.

If it is assumed that the capsule requires a minimum of electrical power (8 w) during its dormant, data acquisition, or incubation phase, and that heat sterilized batteries must supply this power, the battery weight required in the capsule for each hour of dormant life will be about 1/2 lb. Apparently the biological experimenters would like a minimum incubation period of about 20 hr for which the direct communication link concept is well-suited. Using the relay concept it may be necessary to provide the capsule with two or more days of survivial capability with an attendant battery weight penalty of at least 12 lb. The design survival period has been selected as one day to minimize capsule weight.

Another advantage of the direct link concept is that the success of the biocapsule mission is independent of the success of the orbiter mission after separation.

Other advantages of the direct link concept can be noted by considering the system antenna design problems. Providing capsule antennas with a sufficiently large look-angel capability is a problem common to both the direct and relay concepts. However antenna size, and hence physical location difficulties, decrease as their operating frequency increases. The use of S-band frequencies, or even higher frequencies, is desirable. A relay link concept poses an additional constraint on the design of the orbiter which must be capable of receiving data at any position in its orbit; its antenna must have a near omnidirectional pattern because the orbiter is stabilized with respect to the Sun and Canopus. This requirement presents additional design problems especially if relatively low frequency (VHF for example) operation is required.

It may also be necessary to provide additional temporary storage capability in the orbiter to avoid undesirable interruptions in the normal orbiter-Earth data transmission if the relay concept is used.

It might also be concluded that an orbiter weight saving on the order of about 13 lb could be achieved by eliminating the capsule-to-orbiter relay equipment. However, this is only true if there is no requirement for communications with the capsule after separation from the orbiter and prior to landing. Such a condition is unlikely

The only question remaining before discarding the relay communication concept concerns the data rate attainable (if any) using a direct capsule-to-Earth link. Tables 5-11 and 5-12 present typical calculations for both the capsule-to-Earth link and the Earth-to-capsule link respectively. The conclusion based on these calculations is that a data rate of about 1 bit/sec can be achieved using a 20-w transmitter on the capsule, and the capsule can sync to Goldstone. Further investigation is required to determine whether voltage breakdown problems will be encountered at this power level and to determine solutions to such problems if they exist. Tabel 5-13 presents the calculations for a biocapsule-to-orbiter link at a frequency of 125 Mc using a 20-w transmitter. This calculation indicates that a data rate of about 33 bits/sec could be achieved on such a link.

Table 5-11

BIOCAPSULE-TO-EARTH LINK CALCULATION

No.	Parameter	Value (db)	Tolerance (db)
1	Total Transmitter Power	+13 dbw	±1
2	Transmitting Circuit Loss	-2	±0.5
3	Transmitting Antenna Gain	-3	+6, -3
4	Transmitting Antenna Pointing Loss	incl. in 3	
5	Space Loss at 2290 Mc, R = 175×10^6 km	-264.5	
6	Polarization Loss	incl. in 7	
7	Receiving Antenna Gain	+61	+0, -1
8	Receiving Antenna Pointing Loss	incl. in 7	
9	Receiving Circuit Loss	incl. in 7	
10	Net Circuit Loss	-208.5	+6.5, -4.5
11	Total Received Power	-195.5 dbw	+7.5, -5.5
12	Receiver Noise Spectral Density (N/B) at T_e = 30° ± 10° K	-213.6 dbw	+1, -2
13	Carrier Modulation Loss	-2	±0.5
14	Received Carrier Power	-197.5 dbw	+8, -6
15	Carrier APC Noise Bw($2B_{LO}$ = 4 ± 1 cps)	+6	+1, -1.2
	Carrier Performance – One Way Tracking		
16	Threshold SNR in $2B_{LO}$	0	
17	Threshold Carrier Power	-207.6 dbw	+2, -3.2
18	Performance Margin	+10.1	+11.2, -8
	Carrier Performance – Two Way Tracking		
19	Threshold SNR in $2B_{LO}$	+1	
20	Threshold Carrier Power	-206.6 dbw	+2, -3.2
21	Performance Margin	+9.1	+11.2, -8

Table 5-11 (Continued)

No.	Parameter	Value (db)	Tolerance (db)
	Data Channel		
22	Modulation Loss	-4.9	±0.3
23	Received Subcarrier Power	-200.4 dbw	+7.8, -2.8
24	Bit Rate (1/T)	0	
25	Required ST/N/B	+6.5	+0.8, -0
26	Threshold Subcarrier Power	-207.1 dbw	+1.8, -1.2
27	Performance Margin	+6.7	+9, -4.6
	Sync Channel		
28	Modulation Loss	-4.9	±0.3
29	Received Subcarrier Power	-200.4 dbw	+7.8, -2.8
30	Sync APC Noise BW ($2B_{LO}$ = 4 ± 1 cps)	+6	+1, -1.2
31	Threshold SNR in $2B_{LO}$	0	
32	Threshold Subcarrier Power	-207.6 dbw	+2, -3.2
33	Performance Margin	+7.2	+11, -4.8

Table 5-12

EARTH-TO-BIOCAPSULE LINK CALCULATION

No.	Parameter	Value (db)	Tolerance (db)
1	Total Transmitter Power	+50 dbw	±1
2	Transmitting Circuit Loss	-0.4	+0.1, -0.3
3	Transmitting Antenna Gain	+51.4	±0.5
4	Transmitting Antenna Pointing Loss	-0.5	+0.5, -0
5	Space Loss at 2115 Mc, R = 175×10^6 km	-263.9	
6	Polarization Loss	incl. in 7	
7	Receiving Antenna Gain	-3	+6, -3
8	Receiving Antenna Pointing Loss	incl. in 7	
9	Receiving Circuit Loss	-1	+0.2, -0.5
10	Net Circuit Loss	-217.4	+7.3, -4.3
11	Total Received Power	-167.4 dbw	+8.3, -5.3
12	Receiver Noise Spectral Density (N/B) at T_e = 700° ± 100°K	-200.1 dbw	+0.5, -0.7
13	Carrier Modulation Loss	-4	±0.5
14	Received Carrier Power	-171.4 dbw	+8.8, -5.8
15	Carrier APC Noise BW ($2B_{LO}$ = 20 ± 4 cps)	+13	+0.8, -0.6
	Carrier Performance – One Way Tracking		
16	Threshold SNR in $2B_{LO}$	0	
17	Threshold Carrier Power	-187.1 dbw	±1.3
18	Performance Margin	+15.7	+10.1, -7.1
	Carrier Performance – Two Way Tracking		
19	Threshold SNR in $2B_{LO}$	+1	
20	Threshold Carrier Power	-186.1 dbw	±1.3
21	Performance Margin	+14.7	+10.1, -7.1

Table 5-12 (Continued)

No.	Parameter	Value (db)	Tolerance (db)
	Sync Channel		
22	Modulation Loss	-3	±0.5
23	Received Subcarrier Power	-170.4 dbw	+8.8, -5.8
24	Sync APC Noise BW ($2B_{LO}$ = 20 ± 4 cps)	+13	+0.8, -0.6
25	Threshold SNR in $2B_{LO}$	0	
26	Threshold Subcarrier Power	-187.1 dbw	±1.3
27	Performance Margin	+17.7	+10.1, -7.1

Table 5-13

BIOCAPSULE-TO-ORBITER LINK CALCULATION (COHERENT PSK)

No.	Parameter	Value (db)	Tolerance (db)
1	Total Transmitter Power	+13 dbw	±1
2	Transmitting Circuit Loss	-1	±0.3
3	Transmitting Antenna Gain	-3	+6, -3
4	Transmitting Antenna Pointing Loss	incl. in 3	
5	Space Loss at 125 Mc, R = 65×10^3 km	-171	
6	Polarization Loss	incl. in 7	
7	Receiving Antenna Gain	0	+6, -3
8	Receiving Antenna Pointing Loss	incl. in 7	
9	Receiving Circuit Loss	-1	±0.2
10	Net Circuit Loss	-176	+12.5, -6.5
11	Total Received Power	-163 dbw	+13.5, -7.5
12	Receiver Noise Spectral Density (N/B) at T_e = 800° ± 400°K	-199.6 dbw	+2, -3
13	Carrier Modulation Loss	-7	±0.5
14	Received Carrier Power	-170 dbw	+14, -8
15	Carrier APC Noise BW ($2B_{LO}$ = 20 ± 4 cps)	+13	+0.8, -1
	Carrier Performance – One Way Tracking		
16	Threshold SNR in $2B_{LO}$	0	
17	Threshold Carrier Power	-186.6 dbw	+2.8, -4
18	Performance Margin	+16.6	+16, -10.8
	Data Channel		
19	Modulation Loss	-2.4	±0.5
20	Received Subcarrier Power	-165.4 dbw	+14, -8
21	Bit Rate (1/T) 33-1/3 bps	+15.2	
22	Required ST/N/B	+6.5	+0.8, -0

Table 5-13 (Continued)

No.	Parameter	Value (db)	Tolerance (db)
23	Threshold Subcarrier Power	-177.9 dbw	+2.8, -3
24	Performance Margin	+12.5	+17, -10.8
	Sync Channel		
25	Modulation Loss	-2.4	±0.5
26	Received Subcarrier Power	-165.4 dbw	+14, -8
27	Sync APC Nose (Bw ($2B_{LO}$ = 10 ± 2 cps)	+10	+0.8, -1
28	Threshold SNR in $2B_{LO}$	0	
29	Threshold Subcarrier Power	-189.6 dbw	+2.8, -4
30	Performance Margin	+24.2	+18, -10.8

Communication Path-Atmospheric Entry Phase. Using the calculations in Table 5-11 which indicate a data rate of 1 bit/sec may be achievable on a direct capsule-to-Earth communication link, it is readily apparent that such a link is insufficient during atmospheric entry due to reacquisition time after entry blackout and the small amount of data which can be transmitted during a subsonic descent period of about 240 sec.

Therefore the only method of communicating during atmospheric entry is to relay data to Earth via the orbiter. Since this is the only possible communication path, the presentation of its characteristics will be deferred to Section 5.2.3.3. However it is appropriate to state that an atmospheric phase capsule-to-orbiter link can provide a data rate capability of 50 bits/sec after blackout using an S-band, coherent PSK system.

Communication Path-Capsule Separation Phase. Once it has been decided that a relay link is required for communications during the atmospheric entry phase of the biocapsule mission, it becomes obvious that a similar relay link should be used during the separation phase where the maximum communication range to the orbiter is only 1000 ft.

Relay Link Implementation. The capsule-orbiter communication link required during the separation and atmospheric entry phases should be compatible with the capsule-Earth link used after landing to minimize the complexity and weight of the capsule. Therefore, an S-band, coherent PSK system is required. Two implementation concepts for this type of system must be considered. The first concept would close the communication link by transmission from capsule to orbiter to Earth using the orbiter only as a repeater, i. e., frequency translator and power amplifier. This concept has the advantage that no PN code generator or demodulation equipment is required in the orbiter specifically for support of the capsule. It does however, have three overwhelming disadvantages.

- The reacquisition time after blackout may take several minutes, thus practically eliminating the chance to obtain entry data before impact.

- The orbiter high gain antenna must be pointing at Earth throughout the separation phase, adding complexity to the mission.
- This concept requires switching in the orbiter-Earth link exciter thereby reducing the reliability of the more important link.

The fate of this concept is obvious.

The second concept, and the most feasible one, is to incorporate a self-sufficient link between the orbiter and capsule. The data received by the orbiter would then be inserted into the orbiter-Earth link in place of normal orbiter data.

5.3.2.3 Orbiter Plus Atmospheric Capsule

The majority of basic tradeoffs pertinent to an orbiter-plus-atmospheric capsule mission have already been discussed in the preceding sections and need not be repeated. However, for this mission, there is no operational constraint on the frequency and modulation used in the capsule-orbiter link. In order to minimize the weight in both the capsule and the orbiter (about 5 lb and 15 lb, respectively) a simple one-way link should be used. It is also desirable to employ a link which can be developed with minimum effort and cost. A PCM-FM system is a very conservative solution to the problem. While the communication efficiency of PCM-FM is poor, relative to coherent PSK and differentially coherent PSK systems, the attainable data rate of about 50 bits/sec appears ample for this mission. As for a choice of frequency, the VHF telemetry band (225−260 Mc) reduces many system problems encountered at higher frequencies and maximizes the availability of componentry. Thus, the link calculations in Section 5.3.3.2 will be based on an operating frequency of 250 Mc.

5.3.3 Electronic System Design

The basic electronic system design concepts for the 1969 Mariner mission to Mars will be presented in this section. The scope of the study did not include a preliminary

design of the vehicle so that only sufficient detail is provided to demonstrate the basic feasibility of the mission and to provide the necessary information for estimating subsystem weight, power and volume requirements. In addition, portions of the system which appear to be compatible with the desired use of Mariner C and other flight qualified components will be specified. Other portions of the system that could employ qualified circuitry will also be delineated (e.g., the Mariner C communication equipments modified to provide different data rates). It is not anticipated that significant modifications will be required for the 1971 mission in any portion of the system with the possible exception of the data acquisition system and its interface requirements with new or modified experiments.

5.3.3.1 Orbiter Only

A functional block diagram of the basic spacecraft is illustrated in Fig. 5-30, a, b and c. Perhaps the simplest manner of explaining these diagrams is to discuss each subsystem separately.

Radio Subsystem

The orbiter radio subsystem must provide three system functions: (1) tracking, (2) command signal reception and demodulation, and (3) telemetry modulation and transmission. As mentioned previously it is expected that this subsystem will employ post-1965 Mariner techniques. To accomplish these general system functions, the orbiter radio subsystem must have the following capability:

- Receive the RF signal transmitted from the DSIF
- Coherently translate the frequency and phase of the received RF signal by a fixed ratio
- Demodulate the received RF signal and send a composite command signal to the orbiter command subsystem

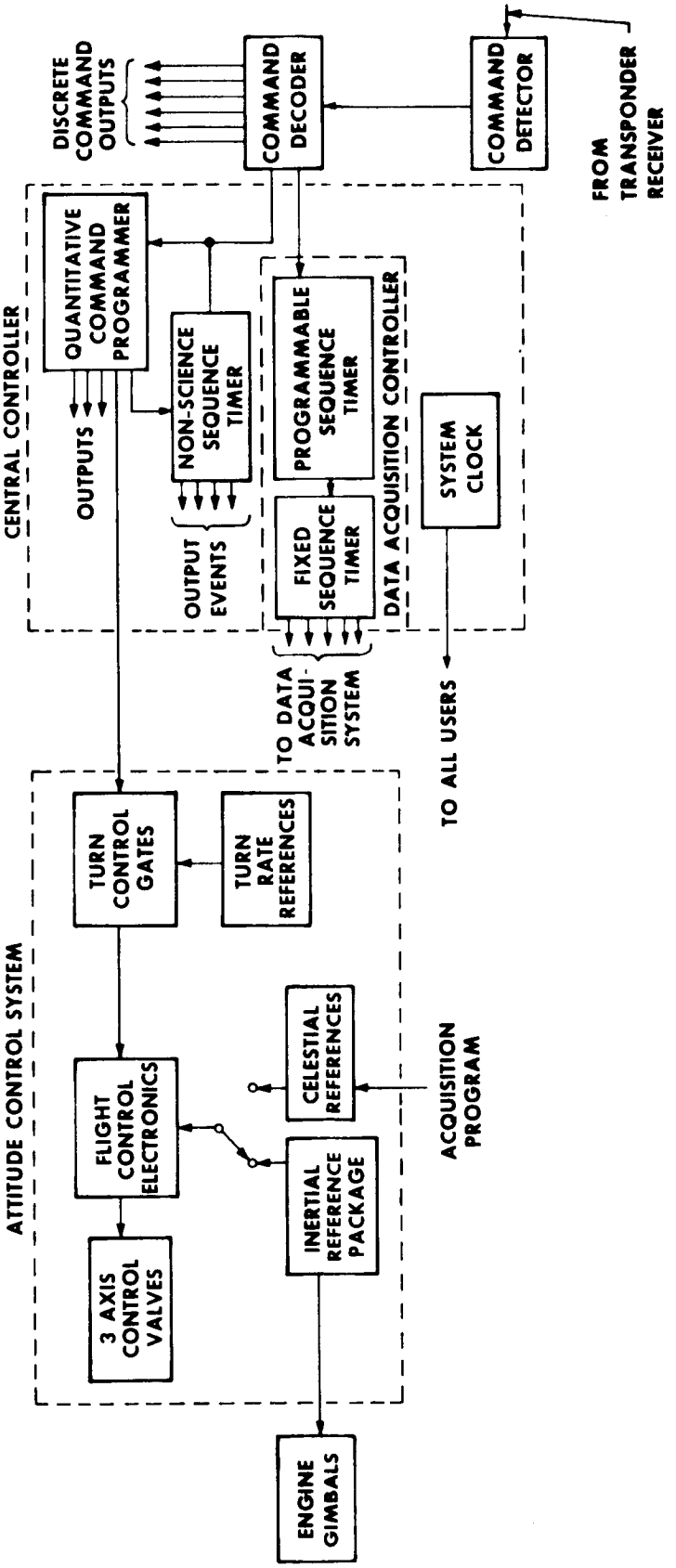


Fig. 5-30 (Continued) Part b

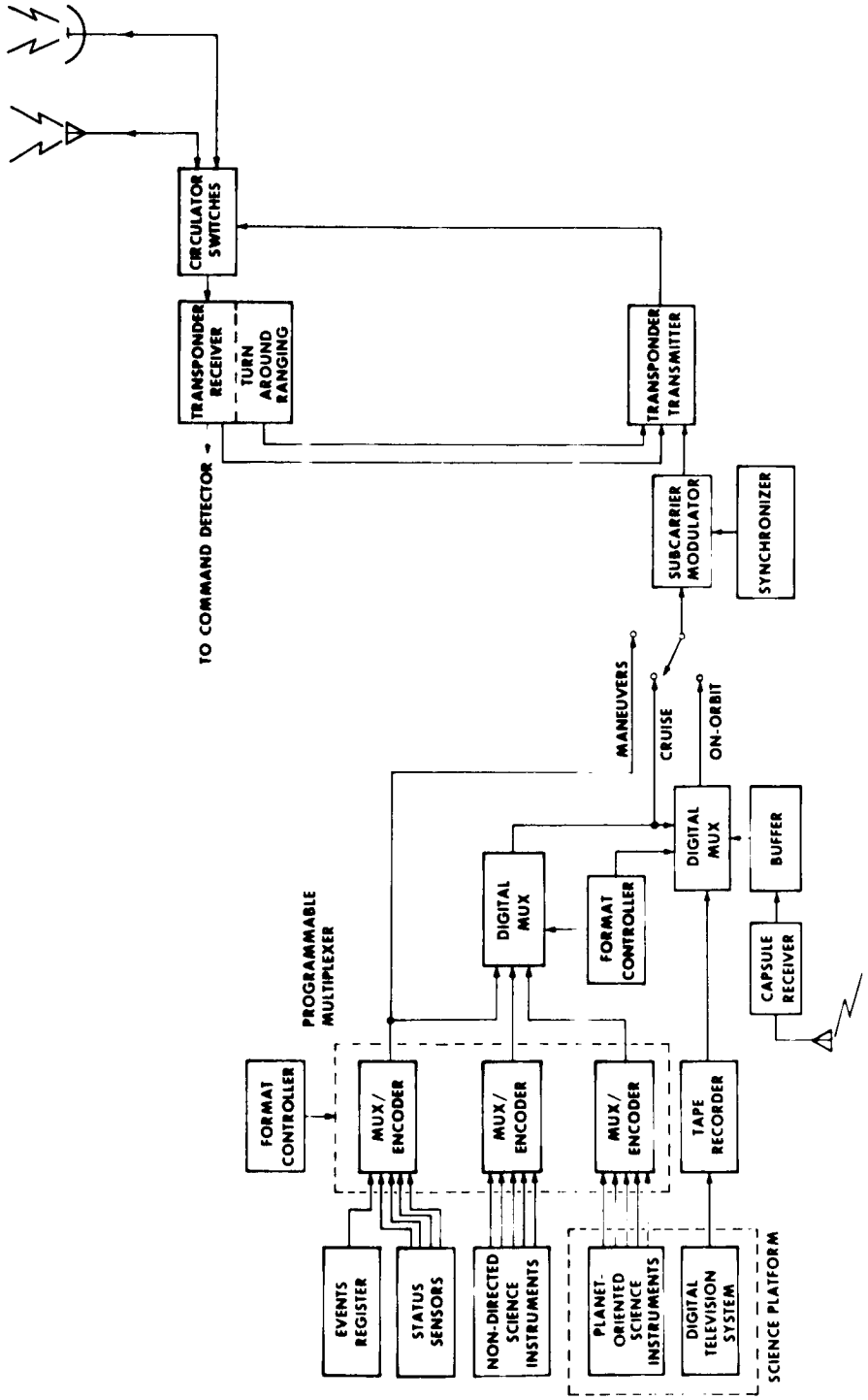


Fig. 5-30 Electronics System Functional Block Diagram Part a

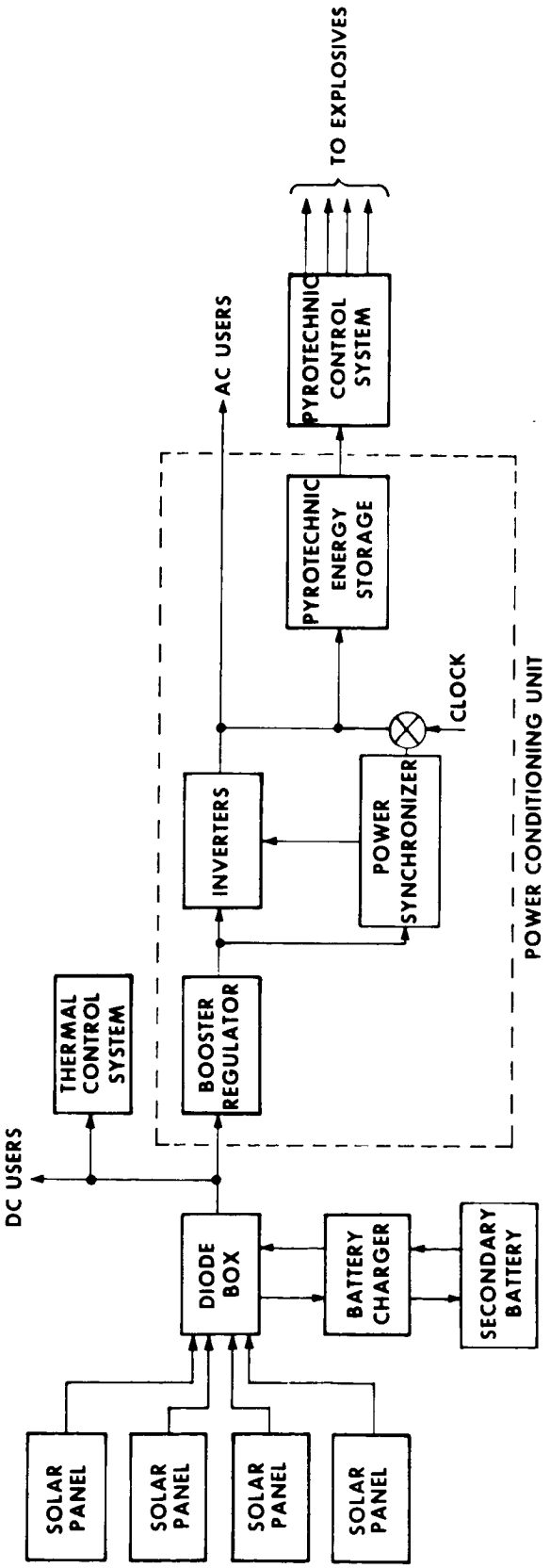


Fig. 5-30 (Concluded) Part c

- If required, demodulate the range code transmitted to the orbiter and subsequently modulate the transmitter with this demodulated ranging signal from the turnaround ranging circuits
- Modulate the transmitted signal with a composite telemetry signal
- Transmit the modulated RF signal to the DSIF

The receiver portion of the transponder will be a double superheterodyne phase coherent circuit employing a tunnel diode preamplifier yielding an effective system noise temperature of 630 degrees Kelvin. The carrier phase-lock loop noise bandwidth at threshold will be 12 cps. The sync subcarrier phase-lock loop noise bandwidth at threshold is 8 cps.

The link calculations for the command link with a command rate of one bit/sec are presented in Table 5-14 using the orbiter's low gain antenna for reception from Goldstone throughout a 1969 mission, including a 6 mo period in orbit about Mars.

Actually the orbiter will use its high gain antenna for reception as long as the spacecraft is in its proper attitude, since even the Goldstone link is marginal through the low gain antenna. It was assumed that the Woomera and Johannesburg stations would only have 10 kilowatt transmitters which are certainly insufficient. The link calculations for these stations using the high gain antenna on the orbiter are presented in Table 5-15.

With the narrow loop noise bandwidths postulated for a receiver, a possible question arises as to whether or not such a receiver can track the doppler shifting signal from the DSIF. The highest rate of change of doppler shifts will naturally be encountered after a Mars orbit has been achieved.

The highest rate of change of doppler shift will occur when the orbiter is near periapsis. It has been estimated that the highest acceleration of the orbiter with respect to Earth will be about 1.5 ft/sec. A second order loop filter with a noise bandwidth of about

Table 5-14

ORBITER COMMAND LINK CALCULATION

No.	Parameter	Value (db)	Tolerance (db)
1	Total Transmitter Power	+50 dbw	±1
2	Transmitting Circuit Loss	-0.4	+0.1, -0.3
3	Transmitting Antenna Gain	+51.4	±0.5
4	Transmitting Antenna Pointing Loss	-0.5	+0.5, -0
5	Space Loss at 2115 Mc, R = 355×10^6 km	-269.5	
6	Polarization Loss	incl. in 7	
7	Receiving Antenna Gain	0	+6, -2
8	Receiving Antenna Pointing Loss	incl. in 7	
9	Receiving Circuit Loss	-1	+0.2, -0.5
10	Net Circuit Loss	-220	+7.3, -3.3
11	Total Received Power	-170 dbw	+8.3, -4.3
12	Receiver Noise Spectral Density (N/B) at T_e = 630° ± 100°K	-200.6 dbw	+0.6, -0.7
13	Carrier Modulation Loss	-4	±0.5
14	Received Carrier Power	-174 dbw	+8.8, -4.8
15	Carrier APC Noise BW ($2B_{LO}$ = 12 ± 2 cps)	+10.8	±0.8
	Carrier Performance – One Way Tracking		
16	Threshold SNR in $2B_{LO}$	0	
17	Threshold Carrier Power	-189.8 dbw	+1.4, -1.5
18	Performance Margin	+15.8	+10.3, -6.2
	Carrier Performance – Two Way Tracking		
19	Threshold SNR in $2B_{LO}$	+1	
20	Threshold Carrier Power	-188.8 dbw	+1.4, -1.5
21	Performance Margin	+14.8	+10.3, -6.2

Table 5-14 (Continued)

No.	Parameter	Value (db)	Tolerance (db)
	Command Channel		
22	Modulation Loss	-2.9	±0.5
23	Received Subcarrier Power	-172.9 dbw	+8.8, -4.8
24	Bit Rate (1/T)	0	
25	Required ST/N/B	+9.6	+0.8, -0
26	Threshold Subcarrier Power	-191 dbw	+1.4, -0.7
27	Performance Margin	+18.1	+9.5, -6.2
	Sync Channel		
28	Modulation Loss	-2.9	±0.5
29	Received Subcarrier Power	-172.9 dbw	+8.8, -4.8
30	Sync APC Noise Bw ($2B_{LO}$ = 8 ± 1 cps)	+9	±0.5
31	Threshold SNR in $2B_{LO}$	0	
32	Threshold Subcarrier Power	-191.6 dbw	+1.1, -1.2
33	Performance Margin	+18.7	+10, -5.9

Table 5-15

DSIF-TO-ORBITER LINK CALCULATION

No.	Parameter	Value (db)	Tolerance (db)
1	Total Transmitter Power	+40 dbw	±1
2	Transmitting Circuit Loss	-0.4	+0.1, -0.3
3	Transmitting Antenna Gain	+51.4	±0.5
4	Transmitting Antenna Pointing Loss	-0.5	+0.5, -0
5	Space Loss at 2115 Mc, R = 355×10^6 km	-269.5	
6	Polarization Loss	incl. in 7	
7	Receiving Antenna Gain	+25	+1, -0.5
8	Receiving Antenna Pointing Loss	-2	+2, -0.5
9	Receiving Circuit Loss	-1	+0.2, -0.5
10	Net Circuit Loss	-197	+4.3, -2.3
11	Total Received Power	-157 dbw	+5.3, -3.3
12	Receiver Noise Spectral Desntiy (N/B) at T_e = 630° ± 100°K	-200.6 dbw	+0.6, -0.7
13	Carrier Modulation Loss	-4 db	±0.5
14	Received Carrier Power	-161 dbw	+5.8, -3.8
15	Carrier APC Noise BW ($2B_{LO}$ = 12 ± 2 cps)	+10.8 db	±0.8
	Carrier Performance – One Way Tracking		
16	Threshold SNR in $2B_{LO}$	0	
17	Threshold Carrier Power	-189.8 dbw	+1.4, -1.5
18	Performance Margin	+28.8	+7.3, -5.2
	Carrier Performance – Two Way Tracking		
19	Threshold SNR in $2B_{LO}$	+1	
20	Threshold Carrier Power	-188.8 dbw	+1.4, -1.5
21	Performance Margin	+27.8	+7.3, -5.2

Table 5-15 (Continued

No.	Parameter	Value (db)	Tolerance(db)
	Sync Channel		
22	Modulation Loss	-2.9	±0.5
23	Received Subcarrier Power	-159.9 dbw	+5.8, -3.8
24	Sync APC Noise BW ($2B_{LO}$ = 8 ± 1 cps)	+9	±0.5
25	Threshold SNR in $2B_{LO}$	0	
26	Threshold Subcarrier Power	-191.6 dbw	+1.1, -1.2
27	Performance Margin	+31.7	+7, -4.9

2 cps for one-way transmission and 4 cps for two-way transmission is required for tracking such an acceleration.* Therefore, the postulated receiver bandwidths should be adequate.

The transponder transmitter will employ a 10 w TWT power amplifier (the tube being used as a backup on the Mariner C vehicle). The link calculations used to compute the attainable telemetry data rate at encounter are shown in Table 5-16. These calculations indicate that a data rate of 300 bits/sec is attainable for up to 12 days on-orbit. To keep the complexity of the system to a reasonable minimum, the data rate will only be reduced twice during the remainder of the mission. The data rate will be reduced after 12 days on-orbit to 150 bits/sec. This data rate can be maintained until 75 days after orbit has been achieved. After 75 days on orbit the data rate will be further reduced to 75 bits/sec for the remainder of the mission.

Using the orbiter's low gain antenna, a telemetry data rate of 9-3/8 bits/sec can be maintained during the interplanetary trip over a communication range from Earth of about 66 million km. The unique data rate of 9-3/8 bits/sec is used because it is a binary factor (8) of the next lowest data rate (75 bits/sec), which makes the implementation of the data rate conversions as simple as possible. The link calculations for this case are presented in Table 5-17. For completeness, the link calculations for the use of the mobile tracking station to enhance the tracking station capability to a range of 20,000 km are presented in Tables 5-18 and 5-19.

Having specified the capability of the communication links it is pertinent to consider the operation of the link. After the Surveyor shroud is separated from the Centaur, the orbiter's RF power is turned on and will operate continuously thereafter. The spacecraft low gain antenna is used for both reception and transmission until about 175 days after launch when the communication range reaches about 66 million km. During this phase of the mission, the transmitted data rate will be continuous at

*"Principles and Applications of Phase-Lock Detection in Phase Coherent Systems", C. L. Nielson, Hallamore Electronics Co., 1957

Table 5-16

ORBITER-TO-DSIF LINK CALCULATION

No.	Parameter	Value (db)	Tolerance (db)
1	Total Transmitter Power	+10 dbw	±1
2	Transmitting Circuit Loss	-2	±0.5
3	Transmitting Antenna Gain	+26.3	+0.5, -1
4	Transmitting Antenna Pointing Loss	-2	+2, -0.5
5	Space Loss at 2295 Mc, R = 175×10^6 km	-264.5 dbw	
6	Polarization Loss	incl. in 7	
7	Receiving Antenna Gain	+60	+1, -2
8	Receiving Antenna Pointing Loss	incl. in 7	
9	Receiving Circuit Loss	inc. in 7	
10	Net Circuit Loss	-182.2	±4
11	Total Received Power	-172.2 dbw	±5
12	Receiver Noise Spectral Density (N/B) at $T_e = 30° \pm 10°K$	-213.6dbw	+1, -2
13	Carrier Modulation Loss	-5	±0.5
14	Received Carrier Power	-177.2 dbw	±5.5
15	Carrier APC Noise BW ($2B_{LO} = 5 \pm 1$ cps)	+7	+0.8, -1
	Carrier Performance – One Way Tracking		
16	Threshold SNR in $2B_{LO}$	0	
17	Threshold Carrier Power	-206.6 dbw	+1.8, -3
18	Performance Margin	+29.4	+8.5, -7.3
	Carrier Performance – Two Way Tracking		
19	Threshold SNR in $2B_{LO}$	+1	
20	Threshold Carrier Power	-205.6 dbw	+1.8, -3
21	Performance Margin	+28.4	+8.5, -7.3

Table 5-16 (Continued)

No.	Parameter	Value (db)	Tolerance (db)
	Data Channel		
22	Modulation Loss	-2.4	+0.2, -0.3
23	Received Subcarrier Power	-174.6 dbw	+5.2, -5.3
24	Bit Rate (1/T) 300 bps	+24.8 db	
25	Required ST/N/B	+6.5	+0.8, -0
26	Threshold Subcarrier Power	-182.3 dbw	+1.8, -2
27	Performance Margin	+7.7 db	+7.2, -7.1
	Sync Channel		
28	Modulation Loss	-2.4	+0.2, -0.3
29	Received Subcarrier Power	-174.6 dbw	+5.2, -5.3
30	Sync APC Noise BW ($2B_{LO}$ = 10 ± 2 cps)	+10	+0.8, -1
31	Threshold SNR in $2B_{LO}$	0	
32	Threshold Subcarrier Power	-203.6 dbw	+1.8, -3
33	Performance Margin	+29	+8.2, -7.1

Table 5-17

CRUISE PHASE ORBITER-TO-EARTH LINK CALCULATIONS

No.	Parameter	Value (db)	Tolerance (db)
1	Total Transmitter Power	+10 dbw	±1
2	Transmitting Circuit Loss	-2	±0.5
3	Transmitting Antenna Gain	+3	±3
4	Transmitting Antenna Pointing Loss	incl. in 3	
5	Space Loss at 2295 Mc, $R = 66 \times 10^6$ km	-256	
6	Polarization Loss	incl. in 7	
7	Receiving Antenna Gain	+60	+1, -2
8	Receiving Antenna Pointing Loss	incl. in 7	
9	Receiving Circuit Loss	incl. in 7	
10	Net Circuit Loss	-195	+4.5, -5.5
11	Total Received Power	-185 dbw	+5.5, -6.5
12	Receiver Noise Spectral Density (N/B) at $T_e = 30° \pm 10°K$	-213.6 dbw	+1, -2
13	Carrier Modulation Loss	-5	±0.5
14	Received Carrier Power	-189 dbw	+6, -7
15	Carrier APC Noise BW ($2B_{LO} = 4 \pm 1$ cps)	+6	+1, -1.2
	Carrier Performance – One Way Tracking		
16	Threshold SNR in 2 B_{LO}	0	
17	Threshold Carrier Power	-207.6 dbw	+2, -3.2
18	Performance Margin	+18.6	+9.2, -9
	Carrier Performance – Two Way Tracking		
19	Threshold SNR in $2B_{LO}$	+1	
20	Threshold Carrier Power	-206.6 dbw	+2, -3.2
21	Performance Margin	+17.6	+9.2, -9

Table 5-17 (Continued)

No.	Parameter	Value (db)	Tolerance (db)
	Data Channel		
22	Modulation Loss	-2.4	+0.2, -0.3
23	Received Subcarrier Power	-187.4 dbw	+5.7, -6.8
24	Bit Rate (1/T) 9-3/8 bps	+9.7	
25	Required ST/N/B	+6.5	+0.8, -0
26	Threshold Subcarrier Power	-197.4 dbw	+1.8, -2
27	Performance Margin	+10 db	+7.7, -8.6
	Sync Channel		
28	Modulation Loss	-2.4	+0.2, -0.3
29	Received Subcarrier Power	-187.4 dbw	+5.7, -6.8
30	Sync APC Noise BW ($2B_{LO} = 4 \pm 1$ cps)	+6	+1, -1.2
31	Threshold SNR in $2B_{LO}$	0	
32	Threshold Subcarrier Power	-207.6 dbw	+2, -3.2
33	Performance Margin	+20.2	+8.9, -8.8

Table 5-18

MOBILE TRACKING STATION-TO-ORBITER LINK

No.	Parameter	Value (db)	Tolerance (db)
1	Total Transmitter Power	+14 dbw	±1 db
2	Transmitting Circuit Loss	incl. in 3	
3	Transmitting Antenna Gain	32	+1, -2
4	Transmitting Antenna Pointing Loss	incl. in 3	
5	Space Loss at 2115 Mc, R = 20×10^3 km	-185	
6	Polarization Loss	incl. in 7	
7	Receiving Antenna Gain	-3	+9, -6
8	Receiving Antenna Pointing Loss	incl. in 7	
9	Receiving Circuit Loss	-1	+0.2, -0.5
10	Net Circuit Loss	-157	+10.2, -8.5
11	Total Received Power	-143 dbw	+11.2, -9.5
12	Receiver Noise Spectral Density (N/B) at T_e = 630° ± 100°K	-200.6 dbw	+0.6, -0.7
13	Carrier Modulation Loss	-4	±0.5
14	Received Carrier Power	-147 dbw	+11.7, -10
15	Carrier APC Noise BW ($2B_{LO}$ = 12 ± 2 cps)	+10.8	±0.8
	Carrier Performance — One Way Tracking		
16	Threshold SNR in $2B_{LO}$	0	
17	Threshold Carrier Power	-189.8 dbw	+1.4, -1.5
18	Performance Margin	+42.8	+13, 2. -11.4
	Carrier Performance — Two Way Tracking		
19	Threshold SNR in $2B_{LO}$	+1	
20	Threshold Carrier Power	-188.8 dbw	+1.4, -1.5
21	Performance Margin	+41.8	+13.2, -11.4

Table 5-18 (Continued)

No.	Parameter	Value (db)	Tolerance (db)
	Sync Channel		
22	Modulation Loss	-.29	±0.5
23	Received Subcarrier Power	-145.9 dbw	+11.7, -10
24	Sync APC Noise BW ($2B_{LO}$ = 8 ± 1 cps)	+9	±0.5
25	Threshold SNR in $2B_{LO}$	0	
26	Threshold Subcarrier Power	-191.6 dbw	+1.1, -1.2
27	Performance Margin	+45.7	+12.9, -11.1

Table 5-19

ORBITER-TO-MOBILE TRACKING STATION LINK

No.	Parameter	Value (db)	Tolerance (db)
1	Total Transmitter Power	+10 dbw	±1
2	Transmitting Circuit Loss	-2	±0.5
3	Transmitting Antenna Gain	-3	+9, -6
4	Transmitting Antenna Pointing Loss	incl. in 3	
5	Space Loss at 2295 Mc, R = 20 ± 10^3 km	-185.7	
6	Polarization Loss	incl. in 7	
7	Receiving Antenna Gain	31	±2
8	Receiving Antenna Pointing Loss	incl. in 7	
9	Receiving Circuit Loss	incl. in 7	
10	Net Circuit Loss	-159.7	+11.5, -8.5
11	Total Received Power	-149.7 dbw	+12.5, -9.5
12	Receiver Noise Spectral Density (N/B) at T_e = 1000 ± 100°K	-198.6 dbw	+0.4, -0.5
13	Carrier Modulation Loss	-5	±0.5
14	Received Carrier Power	-154.7 dbw	+13, -10
15	Carrier APC Noise BW ($2B_{LO}$ = 20 ± 2 cps)	+13	+0.4, -0.5
	Carrier Performance – One Way Tracking		
16	Threshold SNR in $2B_{LO}$	0	
17	Threshold Carrier Power	-185.6 dbw	+0.8, -1
18	Performance Margin	+30.9	+14, -10.8
	Carrier Performance – Two Way Tracking		
19	Threshold SNR in $2B_{LO}$	1	
20	Threshold Carrier Power	-184.6 dbw	+0.8, -1
21	Performance Margin	+29.9	+14, -10.8

Table 5-19 (Continued)

No.	Parameter	Value (db)	Tolerance (db)
	Sync Channel		
22	Modulation Loss	-2.4	+0.2, -0.3
23	Received Subcarrier Power	-152.1 dbw	+12.7, -9.8
24	Sync APC Noise BW ($2B_{LO}$ = 20 ± 2 cps)	+13	+0.4, -0.5
25	Threshold SNR in $2B_{LO}$	0	
26	Threshold Subcarrier Power	-185.6 dbw	+0.8, -1
27	Performance Margin	+33.5	+13.7, -10.6

9-3/8 bits/sec. During the midcourse maneuvers the transmitted data will consist entirely of engineering performance measurements. Throughout the remainder of this phase of the mission, transmitted data will consist of a mixture of performance measurements and cruise science measurements (Mode 2). At 175 days after launch, the steerable high gain antenna will replace the low gain antenna.

During the approach maneuver which occurs about 26 days before encounter (about 142 million km communication distance) communications will be lost for a period of time extending up to two hours.

After the cruise altitude has been re-acquired, transmission will continue in Mode 2 until about 82 minutes before the initiation of the engine burn for injection into orbit around Mars. At this time the system switches to telemetry Mode 3 in which the data rate is 300 bits/sec. Transmission of data at this high rate will be maintained through orbit injection and for about 12 days thereafter. Telemetry mode 4 will be initiated at encounter plus 12 days and will continue through encounter plus 75 days. Telemetry mode 5 will be initiated after 75 days in orbit and the system will operate in this mode until the mission is complete.

Turnaround ranging, if used at all, will only be used for a brief interval shortly prior to the approach maneuver.

Command Subsystem. The function of the command subsystem is to detect the sub-carrier command information passed on by the receiver, decode these commands and distribute them according to the address function. The majority of commands received will be direct commands; i.e., the commanded events will occure immediately. Several commands, however, will be quantitative commands; i.e., they will contain information concerning the future time of an event, or the desired magnitude of an event. These commands will be forwarded to the Central Controller for storage in its command programmer. A tentative list of the commands required for this mission are presented in Table 5-20. It is anticipated that single bit error detection and correction logic will be incorporated into the system although the average bit error rate is less than 10^{-5} based on the expected receiver signal-to-noise ratios.

Table 5-20

SYSTEM COMMANDS

No.	Command	Destination	Comments
	Direct Commands		(Orbiter Only Mission)
1	T/M "off"	Comm	
2	T/M Mode 1	Comm, DAS	Status Data Only at 9-3/8 bits/sec
3	T/M Mode 2	Comm, DAS	Status Plus Cruise Science Data at 9-3/8 bits/sec
4	T/M Mode 3	Comm, DAS	Status Plus Planetary Science Data at 300 bits/sec
5	T/M Mode 4	Comm, DAS	Status Plus Planetary Science Data at 150 bits/sec
6	T/M Mode 5	Comm, DAS	Status Plus Planetary Science Data at 75 bits/sec
7	Switch Transmitter to High Gain Antenna	Comm	
8	Switch Transmitter to Low Gain Antenna	Comm	
9	Switch Receiver to High Gain Antenna	Comm	
10	Switch Receiver to Low Gain Antenna	Comm	
11	Initiate Midcourse Maneuver Sequence	CC	
12	Initiate Approach Maneuver Sequence	CC	
13	Initiate Orbit Injection Sequence	CC	
14	Initiate Science Platform Maneuver	DAS	
15 thru 24	Update Antenna Position	Comm	Roll Only

LOCKHEED MISSILES & SPACE COMPANY

Table 5-20 (Continued)

No.	Command	Destination	Comment
25 thru 35	Update Antenna Position	Comm	Yaw Only
36 thru 43	Update Canopus Sensor Cone Angle	A/C	
44	Reset Data Acquisition Timer	CC	
45	Reset High Gain Antenna Position to Zero	Comm	
46	Initiate Canopus Acquisition Sequence	CC	In event wrong star is acquired
47	Isolate Battery from Power System	Power	
48	Re-insert Battery into Power System	Power	
49 thru 51	Television System Dynamic Range Selection	DAS	Three Ranges
52	Optics System Selection	DAS	Narrow Angle Optics, Camera #1; Wide Angle Optics, Camera #2
53	Optics System Selection	DAS	Narrow Angle Optics, Camera #2; Wide Angle Optics, Camera #1
54	Alternate Optics from Narrow Angle to Wide Angle	DAS	Switch Between Frames
55 thru 63	Command Back-Up for Spacecraft Originated Events		This is an estimate. No attempt was made to allocate these commands.
64 thru 70	Redundancy Switching		This is an estimate. No attempt was made to allocate these commands

Table 5-20 (Continued)

No.	Command	Destination	Comment
	Quantitative Commands		(Orbiter Only Mission)
1	Pitch Turn Duration and Polarity	CC	Capacity: 10 bits Resolution: 1 sec
2	Roll Turn Duration and Polarity	CC	Capacity: 10 bits Resolution: 1 sec
3	Maneuver Velocity Increment	CC	Capacity: 8 bits Resolution: 0.1 meters/sec
4 thru 7	Science Platform Yaw Turn Angles #1 – #4	CC	Capacity: 10 bits Resolution: 15 minutes of arc
8 thru 11	Science Platform Roll Turn Angles #1 – #4	CC	Capacity: 10 bits Resolution: 15 minutes of arc
12 thru 15	Program Science Sequence Timer; Events #1 – #3	CC	Time Between Sunset and Sunrise Terminators. Time Between Sunrise Terminator and High Noon. Time Between Noon and Sunset Terminator. Capacity: 18 bits Resolution: 1 sec

LOCKHEED MISSILES & SPACE COMPANY

Table 5-20 (Continued)

No.	Command	Destination	Comment
	Direct Commands		(Orbiter Plus Capsule Mission)
1 thru 70	Same as for Orbiter Only Mission		
71	Activate Capsule Battery	Pyro	
72	Orbiter to T/M Mode 2A	Comm	Capsule Data only at 9-3/8 bits/ sec
73	Inhibit Propulsion System	C-Prop	
74	Initiate Separation Maneuver Sequence	A/C, CC, Pyro, C-Pyro	

LOCKHEED MISSILES & SPACE COMPANY

Table 5-20 (Continued)

No.	Command	Destination	Comment
	Quantitative Commands		(Orbiter Plus Capsule Mission)
1 thru 15	Same as for Orbiter Only Mission		
16	Time from separation before capsule enters atmosphere	CC, C-ST	This command will activate the Orbiter receiver and Capsule transmitter prior to atmosphere entry Capacity: 13 bits Resolution: 1 min

LOCKHEED MISSILES & SPACE COMPANY

Central Controller. The Central Controller must perform the following functions:

- Provide system clock and timing information for all orbiter subsystems
- Initiate all quantitative commands at the proper time and of the proper magnitude
- Control all fixed sequential activity
- Control data acquisition system sampling and data storage componets
- Adjust individual instrumentation sensor characteristics via command for DSIF

The basic system clock might be a crystal controlled circuit operating at a frequency of about 130 kc/sec. Even without an oven, it is expected that the clock stability will be about 1 part/one hundred thousand over relatively wide temperature ranges which should be sufficient for all orbiter subsystems.

The capacity and resolution requirements for the command programmer were indicated in Table 5-20. The memory of this programmer will be implemented using nondestructive readout techniques to provide permanent storage of such programs as the celestial reacquisition sequence, etc. The activation of timing events will be accomplished through the use of simple counters; i.e., the commanded time of an event transmitted from Earth will be equal to the capacity of the counter less the time of activation after receipt of the command. Thus, the event will be initiated when the counter overflows. The thrust termination velocity meter can be implemented in a similar manner except that velocity increment pulses are derived from an integrating accelerometer rather than the system clock.

The required sequence timer events are indicated in Table 5-21 for appropriate mission phases. It is evident from the table that only one sequence timer is required for the midcourse maneuver(s) and the approach maneuver. By the addition of straightforward inhibiting circuitry, the same timer may also be used to control the orbit injection maneuver sequence.

Table 5-21

SEQUENCE TIMER REQUIREMENTS

SEPARATION INITIATED TIMER

No.	Event	Time	Resolution	Destination	Comment
0	Start	0			Centaur Separation
1	Close Pyro Arming Switch	1 min	1 min	Pyro	
2	A. Activate Solar Panel Deployment Mechanism	2 min	1 min	Pyro	
	B. Unlatch High Gain Antenna				
	C. Unlatch Science Platform				
3	Initiate Celestial Reference Acquisition Sequence. Turn off Timer.	6 min	1 min	A/C	

MIDCOURSE & APPROACH MANEUVER TIMER

No.	Event	Time	Resolution	Destination	Comment
0	Start Event	0			
1	Switch to Gyro Control of Attitude	60 min	1 min	A/C	
2	Set Pitch Turn Polarity	60 min + 2 sec	1 sec	A/C	
3	Start Pitch Turn	60 min + 4 sec	1 sec	A/C	

LOCKHEED MISSILES & SPACE COMPANY

Table 5-21 (Continued)

No.	Event	Time	Resolution	Destination	Comment
4	Set Roll Turn Polarity	71 min	1 min	A/C	
5	Start Roll Turn Polarity	71 min + 2 sec	1 sec	A/C	
6	Ignite Engine	82 min	1 sec	Prop	
7	Initiate Celestial Reference Acquisition Sequence	84 min	1 min	A/C	
8	Turn off Timer	180 min	1 min	CC	

ORBIT INJECTION TIMER

No.	Event	Time	Resolution	Destination	Comment
0	Start	0			
1	Switch to Gyro Control of Attitude	60 min	1 min	A/C	
2	Ignite Engine	82 min	1 sec	Prop	
3	Turn off Timer	180 min	1 min	CC	

DATA ACQUISITION SYSTEM SEQUENCE TIMER

No.	Event	Time	Resolution	Destination	Comment
1	A. Acquire TV Frame Set # 1	0		Payload	Set #1
	B. Start Tape Recorder (Record Mode)				
2	Record Frame Set	1 sec	1 sec	Payload	Set #1
3	Acquire Frame Set	2 min	1 sec	Payload	Set #2

Table 5-21 (Continued)

No.	Event	Time	Resolution	Destination	Comment
4	Record Frame Set	2 min + 1 sec	1 sec	Payload	Set #2
5	Repeat 3	4 min	1 sec	Payload	Set #3
6	Repeat 4	4 min + 1 sec	1 sec	Payload	Set #3
7	Repeat 3	6 min	1 sec	Payload	Set #4
8	Repeat 4	6 min + 1 sec	1 sec	Payload	Set #4
9	Repeat 3	8 min	1 sec	Payload	Set #5
10	Repeat 4	8 min + 1 sec	1 sec	Payload	Set #5
11	Repeat 3	10 min	1 sec	Payload	Set #6
12	Record Low Resolution TV	10 min + 1 sec	1 sec	Payload	Set #6 (Dump High Resolution & IR Data)
13	Stop Tape Recorder	11 min	1 sec	Payload	

AFTER THREE SETS OF 13 EVENTS, AN EVENT COUNTER INITIATES TAPE RECORDER PLAYBACK MODE

LOCKHEED MISSILES & SPACE COMPANY

The data acquisition sequence timing system is unique in that a fixed sequence of events must be repeated three times whenever TV data is being acquired. However, the time interval between these three sequences is programmable from DSIF through the command programmer. An events counters can be used to inititate the playback mode on the tape recorder and to reset the command programmer sequence timer. An additional sequencer, switching one television camera alternately between high and low resolution settings, may consist of a simple bi-stable flip-flop multivibrator Eccles-Jordan Trigger Circuit. This sequencer would be useful in the event one of the television cameras fails to operate properly.

Data Acquisition System. The data acquisition system is easily the most nebulous portion of the vehicle equipment since the experiments that are flown will undoubtedly differ from those presented in Section 5.2. For this reason it is impossible to define the electronics which are required to support the experiments, such as counters, individual encoders, etc. However, it will be noted in the vehicle weight statement in Section 4.9 that 15 lb have been allotted for this equipment. However, the television system provides the majority of telemetry data on-orbit, and therefore it will largely define the tape recorder characteristics and data format.

The television system discussed in Section 5.2 consists of a 600 by 600 line low-resolution camera, a 600 by 600 line high-resolution camera and a 200 by 200 line infrared camera. Assuming each element is encoded into 5 bits, the number of bits in each frame is 1.8×10^6, 1.8×10^6 and 0.2×10^6 respectively. Thus the total number of bits in a television "frame set" is 3.8×10^6. If it is assumed that 95 percent of all on-orbit telemetered data is television information, then 4×10^6 bits of data will be transmitted during the time is takes to read out one television frame set.

In order to maximize the amount of data returned from an orbiter mission, the quantity of data obtained during an orbit period should be as close as possible to the quantity of data that can be transmitted in the same period. Therefore the capacity

of the tape recorder is determined by the longest anticipated orbit period (62.5 hrs) and the maximum data transmission rate (300 bits/sec). No television data will be transmitted during approximately 1.5 hr when pictures are being obtained. Therefore, only about 61 hr of data readout need be stored. The estimated characteristics of a conventional tape recorder for this mission are presented in Table 5-22. For comparison purposes, LMSC presently has an in-house funded development program on a unique tape recording system which for this mission could be expected to have the basic characteristics presented at the bottom of Table 5-22. Of special significance are the extimated weight and volume savings as well as the fact that essentially any record/playback speed ratio is attainable. Conventional tape recorders with speed reduction ratios of 100:1 are difficult to achieve. The only tape recorder with greater reduction ratios unearthed during this study is the Advanced Mariner recorder being developed by the Raymond Engineering Company with a reduction ratio goal of 1000:1. To be conservative the conventional tape recorder estimates have been used in generating spacecraft weight, power, and volume requirements.

It was assumed that during the on-orbit phase of the mission, the data acquisition system might comprise 100 status channels, 21 non-video science channels, and the television system discussed previously. Then a typical data frame might consist of one television line (3000 bits), three non-video science words (30 bits, two status measurements (20 bits) and 110 bits for synchronization and housekeeping functions. Then the time between samples of a given channel would be as shown in Table 5-23. The video repetition rate shown is the time required to transmit one frame set.

During the cruise mode, it was assumed that there might be 15 channels of science data and 100 channels of status data. The data frame format was assumed to consist of all 115 data channels plus 60 bits of sync and housekeeping data. The measurement repetition rates are shown in Table 5-23 for telemetry Mode.

During the maneuvers (Telemetry Mode 1) it was assumed that 115 status channels would be used with the additional 15 channels simply replacing the cruise science measurements. Then the channel repetition rates would be as shown in Table 5-23.

Table 5-22

MARS ORBITER TAPE RECORDER

Capacity:	66×10^6 bits
Record Rate:	33×10^3 bits/second
Record/Playback Speed Ratios:	110 : 1
	220 : 1
	440 : 1
Conventional Recorder:	
No. of Tracks:	6
Record Speed:	11 inches/second
Bit Packing Density:	500 bits longitudinal
Tape Width:	1/2 inch
Tape Length:	1850 feet
Estimated Weight:	36 pounds
Volume:	1200 in^3
Record Power:	15 watts
Playback Power:	3 watts
LMSC Recorder (Development)	
Record/Playback Speed Ratios Obtainable:	Essentially Unlimited
No. of Tracks:	64
Tape Width:	1 inch
Tape Length:	50 feet
Estimated Weight:	11 pounds
Volume:	300 in^3
Record Power:	3 watts
Playback Power:	3 watts
ROM Development Cost:	$180,000
Development Time:	18 months from order
ROM Mfg. Cost:	$15,000 in quantities of 10−20

Table 5-23

CHANNEL REPETITION RATE

T/M MODE	STATUS (sec)	NON-VIDEO SCIENCE (sec)	VIDEO (hr)
1	130	0	0
2	130	130	0
3	525	74	3.7
4	1050	148	7.4
5	2100	296	14.8

A brief description of the television data-acquisition sequence is pertinent at this point. During any orbit period, there are three intervals during which television information will be obtained: (1) near the sunrise terminator, (2) high noon, and (3) near the sunset terminator. During each of these periods, the pictures obtained will consist of six low-resolution, five high-resolution, and five infrared frames. The times at which these pictures are taken is programmed by the DSIF once the orbit parameters have been refined. The system may have to be reprogrammed several times before a proper timing sequence is obtained due to errors in measuring the orbit parameters. Once the proper timing has been established, however, further adjustments will only be required as the orbit appears to precess around the planet.

The multiplexing system should be programmable for an orbiter mission to allow the experimenter some freedom to change the type and quantity of data returned as his knowledge of the scientific environment increases with the processing and reduction of the initial data returns. It will also minimize modifications of the 1971 missions.

Guidance and Attitude Control System. The guidance and attitude control system shown functionally in Fig. 5-29 is basically the Mariner C system. Since the system has already been discussed in Section 5.1, no further consideration will be devoted to it.

Electrical Power System. The electrical power system illustrated functionally in Fig. 5-30 is essentially the Mariner C system. It is expected that the subsequent equipment design will emulate Mariner C developed components almost without modification for the 1969 mission. The only significant modification for the 1971 mission might be the size of the required solar array.

No major equipment development efforts are anticipated other than repackaging and testing of batteries.

The power requirements for the various phases of the Mariner 1969 Mars Orbiter Mission are shown in Fig. 5-31, and summarized in Table 5-24. These power requirements are only for the various subsystem equipments without consideration of the power system inefficiency. No contingencies have been included in these power requirements. The design of the power sources must take these inefficiency contingencies and degradation factors into account. Table 5-25 is a tabulation of the total requirements from the various power sources, with the above factors taken into consideration.

Figure 5-32 presents the block diagram power system configuration design for the 1969 mission. Basically, the following types of power are available to users.

Type of Power	Output Voltage (VAC)	Tolerance Deviation (%)
2400 - - 1 ϕ	50	±2
400 - - 1 ϕ	28	±5
400 - - 1 ϕ	32.5	±5
400 - - 3 ϕ	27 (L-L)	±10
unregulated DC	25 - 50 VDC	N. A.

One exception is that a 50 VDC ±1 percent line will be made available to the power synchronizer.

As stated previously, the power sources for the orbiter section are primarily solar photovoltaic arrays, supplemented by a rechargeable silver-cadmium battery. During

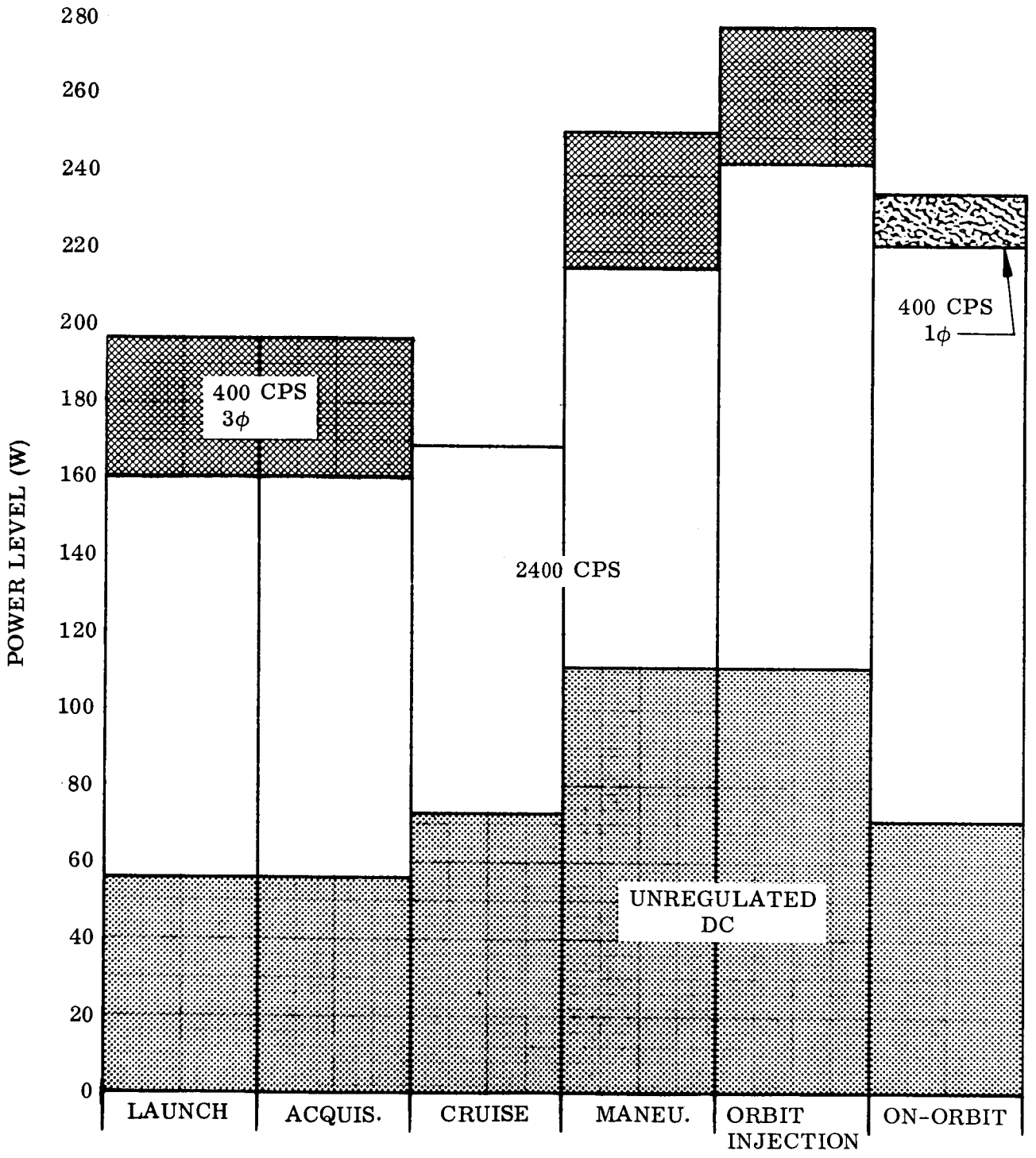


Fig. 5-31 Orbiter-Only Power Profile – 1969 Mission

Table 5-24

ESTIMATED ORBITER ONLY POWER REQUIREMENTS

1969 MISSION

Mission Phase	Subsystem	Power Level (W) 400 ~ 1φ	400 ~ 3φ	2400 ~ 1φ	Unreg. D.C.	Battery Energy (w-hrs)
Launch	Guidance & Control	–	35	26	–	140
	Electronics	–	–	45	56	140
	Science Inst.	–	–	14	–	10
	Thermal Control	–	–	–	–	0
	Battery Charging	–	–	–	–	0
	Status Inst.	–	–	10	–	20
	Failure Sensors	–	–	10	–	20
	Total	0	35	105	56	330
Acquisition	Guidance & Control	–	35	26	–	
	Electronics	–	–	45	56	
	Science Inst.	–	–	14	0	Included
	Thermal Control	–	–	–	–	In
	Battery Charging	–	–	–	–	Launch Phase
	Status Inst.	–	–	10	–	
	Failure Sensors	–	–	10	–	
	Total	0	35	105	56	

Table 5-24 (Continued)

Mission Phase	Subsystem	Power Level (W) 400 ~ 1φ	400 ~ 3φ	2400 ~ 1φ	Unreg. D.C.	Battery Energy (W-hrs)
Orbit Injection (Cont.)	Status Inst.	–	–	10	–	–
	Failure Sensors	–	–	10	–	–
	Propulsion	–	–	–	50	5
	Total	0	35	132	111	85
On Orbit	Guidance & Control	–	–	16	–	–
	Electronics	10	–	52	56	5
	Science Inst.	3	–	63	–	60
	Thermal Control	–	–	–	–	–
	Battery Charging	–	–	–	15	110
	Status Inst.	–	–	10	–	–
	Failure Sensors	–	–	10	–	–
	Total	13	0	151	71	175

For a 1971 mission, an increase in solar panel area of about 20 percent will be required due to variations in the solar constant and panel temperature. This is based on similar orbiter power requirements for 1969 and 1971.

Electrical power distribution for the orbiter mission will follow the same ground rules developed for the Mariner 1964 mission. Electrical distribution harness reliability and electromagnetic interference elimination will be some of the prime considerations for the design of the power distribution system. No foreseeable deviation from the Mariner C power distribution system can be envisioned at this time for the Orbiter missions.

Table 5-24 (Continued)

Mission Phase	Subsystem	Power Level (W) 400 ~ 1φ	400 ~ 3φ	2400 ~ 1φ	Unreg. D.C.	Battery Energy (W-hrs)
Cruise	Guidance & Control	–	–	16	–	–
	Electronics	–	–	45	56	–
	Science Inst.	–	–	14	–	–
	Thermal Control	–	–	–	5	–
	Battery Charging	–	–	–	12	550
	Status Inst.	–	–	10	–	–
	Failure Sensors	–	–	10	–	–
	Total	0	0	95	73	550
Maneuvers	Guidance & Control	–	35	26	–	105
	Electronics	–	–	45	56	120
	Science Inst.	–	–	14	–	24
	Thermal Control	–	–	–	5	5
	Status Inst.	–	–	10	–	18
	Failure Sensors	–	–	10	–	18
	Propulsion	–	–	–	50	5
	Total	0	35	105	111	295
Orbit Injection	Guidance & Control	–	35	26	–	75
	Electronics	–	–	52	56	–
	Science Inst.	–	–	34	–	5
	Thermal Control	–	–	–	5	–

Table 5-25

POWER SOURCE REQUIREMENTS (UNREGULATED)

Power Source	Type	Equipment Requirements	Overall Power System Efficiency	Contingencies	Estimated Degradation	Total Requirements
Solar Photovoltaic System (Mariner C)	Silicon Cells	186 watts	72%	8%	10%	310 watts
Secondary Battery	Silver-Cadmium	330 watt-hours	72%	10%	20%	650 watt-hours

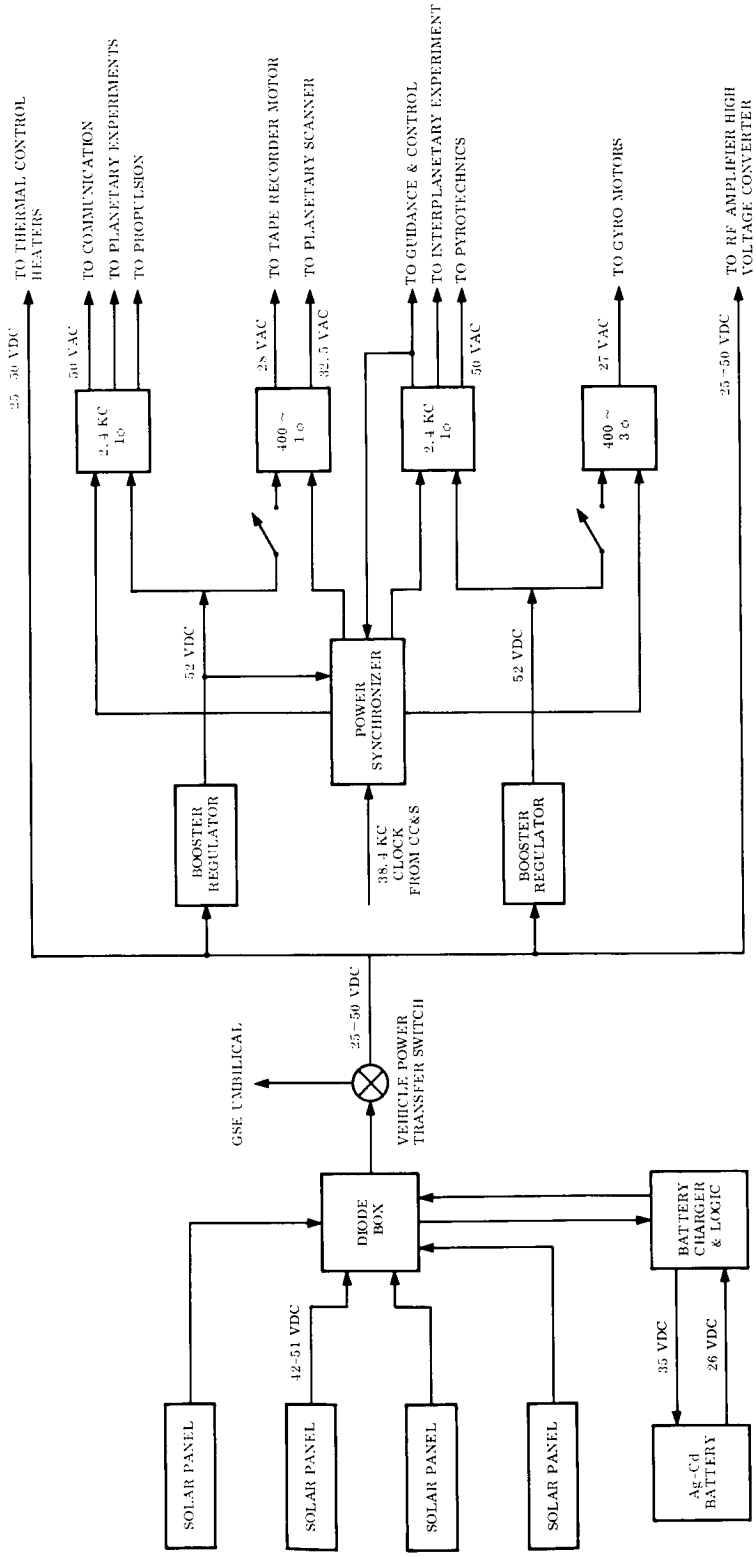


Fig. 5-32 Orbiter Power System

the launch phase of the mission, the orbiter will be powered by the secondary battery until the solar panels are deployed and the sun is acquired by the vehicle. When power becomes available from solar arrays, the system will go into a power sharing mode in which both the battery and the solar arrays will participate in making their power available. Battery participation will depend on booster regulator and battery voltages, which are yet to be determined. During the cruise phase of the mission, the orbiter will draw its power primarily from the solar arrays, at which time, the secondary battery will be recharged. At the end of the predetermined charge cycle, the battery will go into a float charge mode drawing about 20 ma of current and will remain in that state until battery power is needed during the midcourse and Mars approach correction phases. During these two phases, the orbiter will be powered completely by the secondary batter, until solar alignment is re-established by the vehicle. At the initiation of the Mars orbit entry phase and thereafter, which includes the long period of orbiting the planet Mars, the battery and the solar arrays will again go into the power-sharing mode, with the battery recharged between the sharing periods. The orbiter battery can be isolated from the rest of the system by direct command in case of failures or other warranted conditions. This will put the battery into an OFF mode until restored by a second command. This is to insure against the possibility of the battery grounding the system in case of failure.

Table 5-26 is a list of the power system equipment and its characteristics for the 1969 mission. All of the equipment in Table 5-26 are Mariner C components. Only the secondary battery in Table 5-26 is a new unit; however, only repackaging of existing silver-cadmium batteries will be required for the 1969 mission.

The solar photovoltaic arrays on the orbiter are the same as those used in the Mariner C mission except that the output power is higher because of solar constant and array temperature differences caused by the difference in trajectory of the 1969 mission. Figure 5-33 is a plot of the projected photovoltaic system output as a functions of the time from launch. This raw output must be conditioned prior to distribution to power users. The data presented in Fig. 5-33 was derived from Mariner C test data, as shown in Figs. 5-34 and 5-35.

Table 5-26
MISSION POWER SYSTEM EQUIPMENT – 1969

MARINER C EQUIPMENT

Equipment	Est. Wt.	Est. Volume 17.6 ft^2	Input Voltage	Output Voltage	Maximum Power Level (Watts)	Est. Efficiency	Number Required For 1969	Notes
Solar Array	18.7 lbs	(35.5" × 71.4")	Earth Mars	42.5 VDC 51 VDS	172.5 W 81 W	7.3% 8.05%	4	Data for one panel only
Booster Regulator	20.75	16" × 16" × 2-1/2"	25-50 VDC	52 V ± 1% DC	150W	72%	2	Wt. for power regulator package (with 2 boosters)
Power Switchings and Logic Box	–	–	D.C.	D.C.	N.A.	N.A.	1	Wt. and volume included in Power Regulator Package
Power Synchronizer	1.65	6" × 6" × 2-1/2"	50 VAC 52 VDC	N.A.	N.A.	N.A.	1	Additional input of 34.5 Kc signal from CC & S Output: 2400 Ω Signal 400 Ω
Battery Charger	3.0	6" × 6" × 2-1/2"	Unregulated DC	–	30 W	95%	1	Output voltage depends on battery design
2400 cps Inverter	2.65	6" × 6" × 2-1/2"	52V ± 1% DC	50V ± 2% 50V + 5%	80 W	85%	2	Synchronous Square Wave, one phase output – one unit with ±2% tolerance, second unit with +5%, -0% tolerance
400 cps Single Phase	2.01	6" × 6" × 2-1/2"	52V ± 1% DC	28V ± 5% 32.5V ± 5%	8 W	69%	1	Two outputs from same unit square wave
400 cps Three Phase	3.54	6" × 6"× 2-1/2"	52 ± 1% DC	27V ± 10%	18W	78%	2	Output voltage line-to-line measurements

NEW EQUIPMENT

	Type	Est. Wt.	Est. Vol.	Input Voltage	Output Voltage	Capacity	No. of Cells	Est. Efficiency	No. of Cycles	No. Req'd. Per Vehicle
Secondary Battery	Ag-Cd	23 lb	270 in^3	33.6V D.C.	26.4V D.C.	24.6 A. Hrs 650W-Hrs	24	70%	300 (100%~)	1

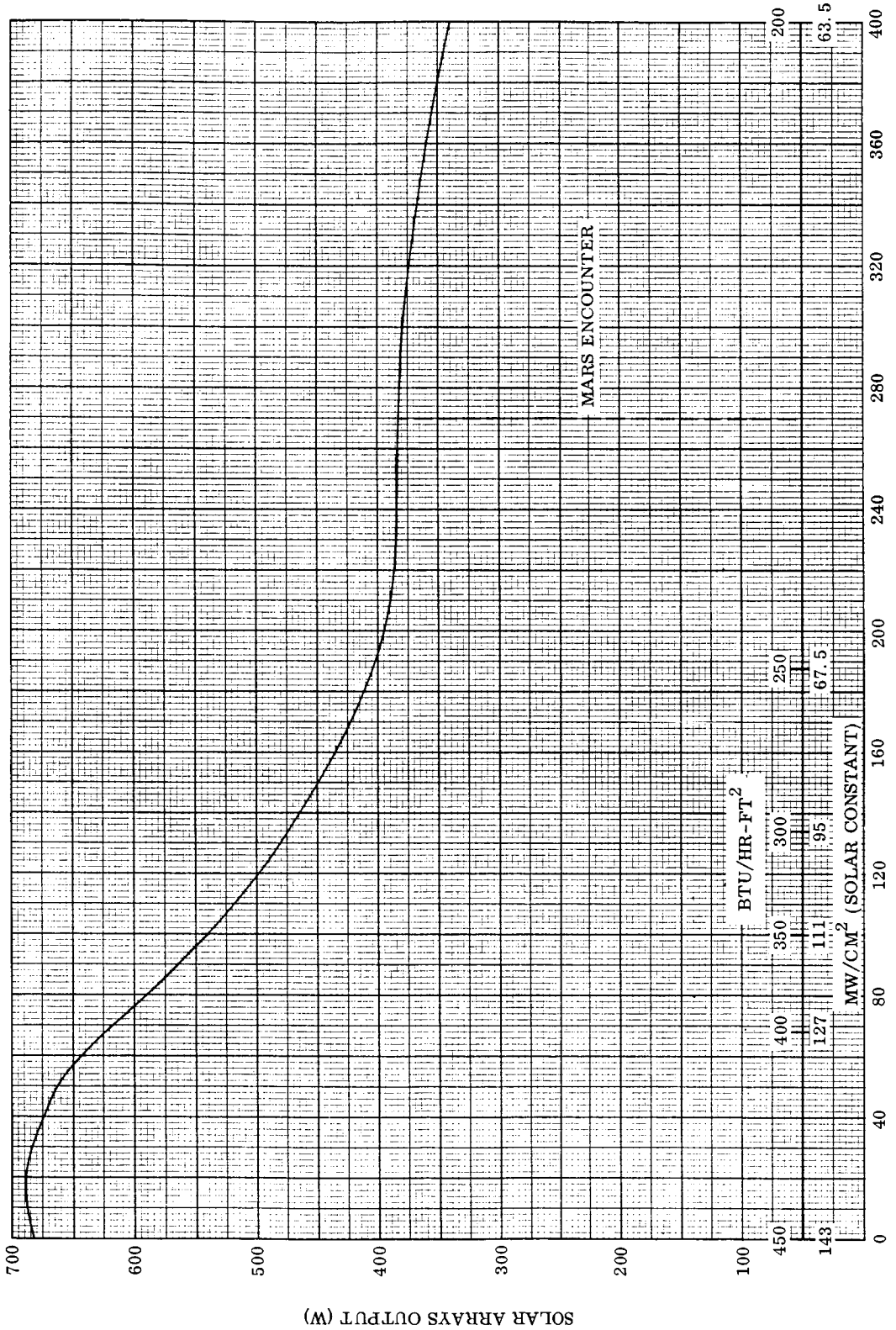


Fig. 5-33 Solar Array Output for Mariner – 1969 Mission

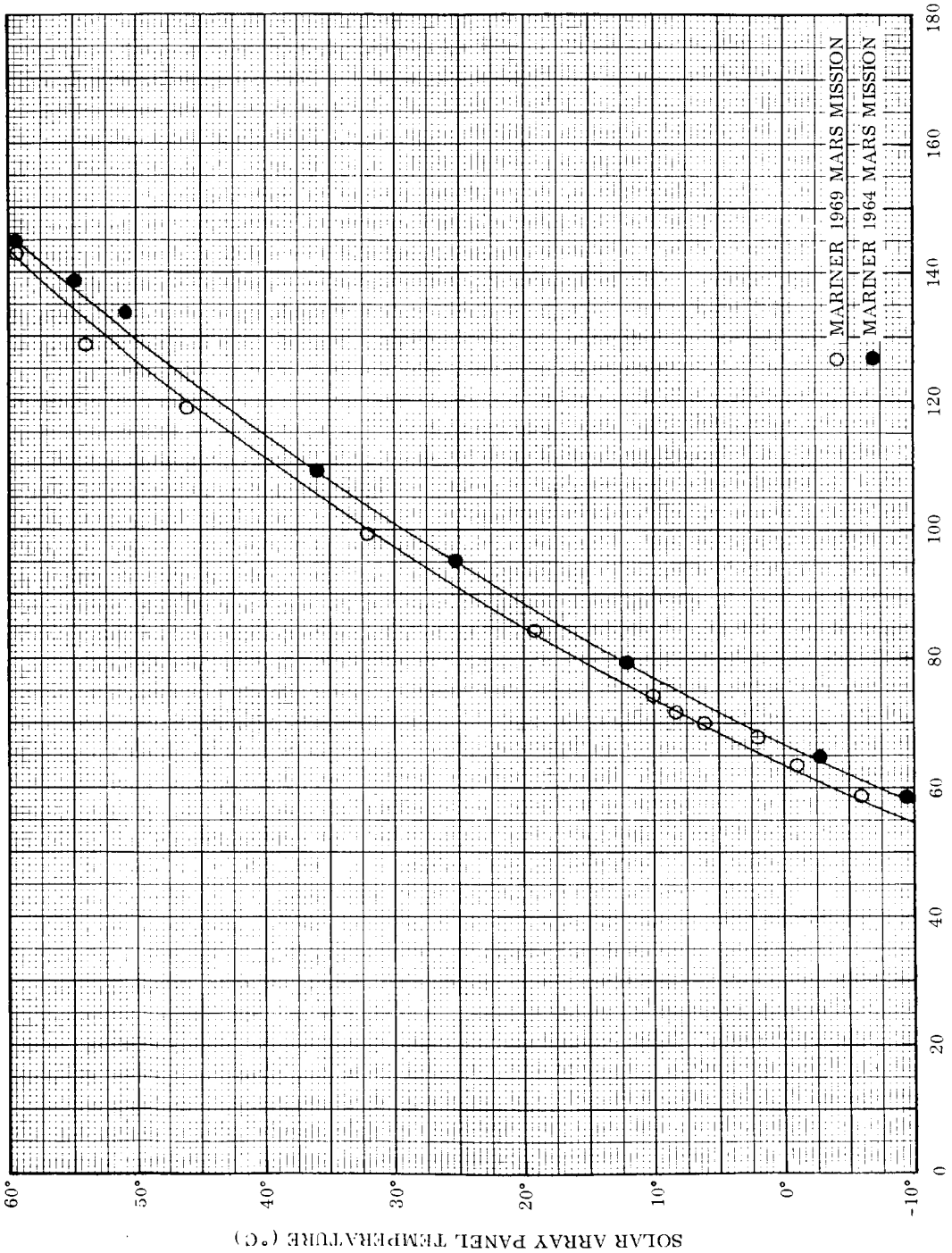


Fig. 5-34 Solar Array Panel Temperature for Mariner C

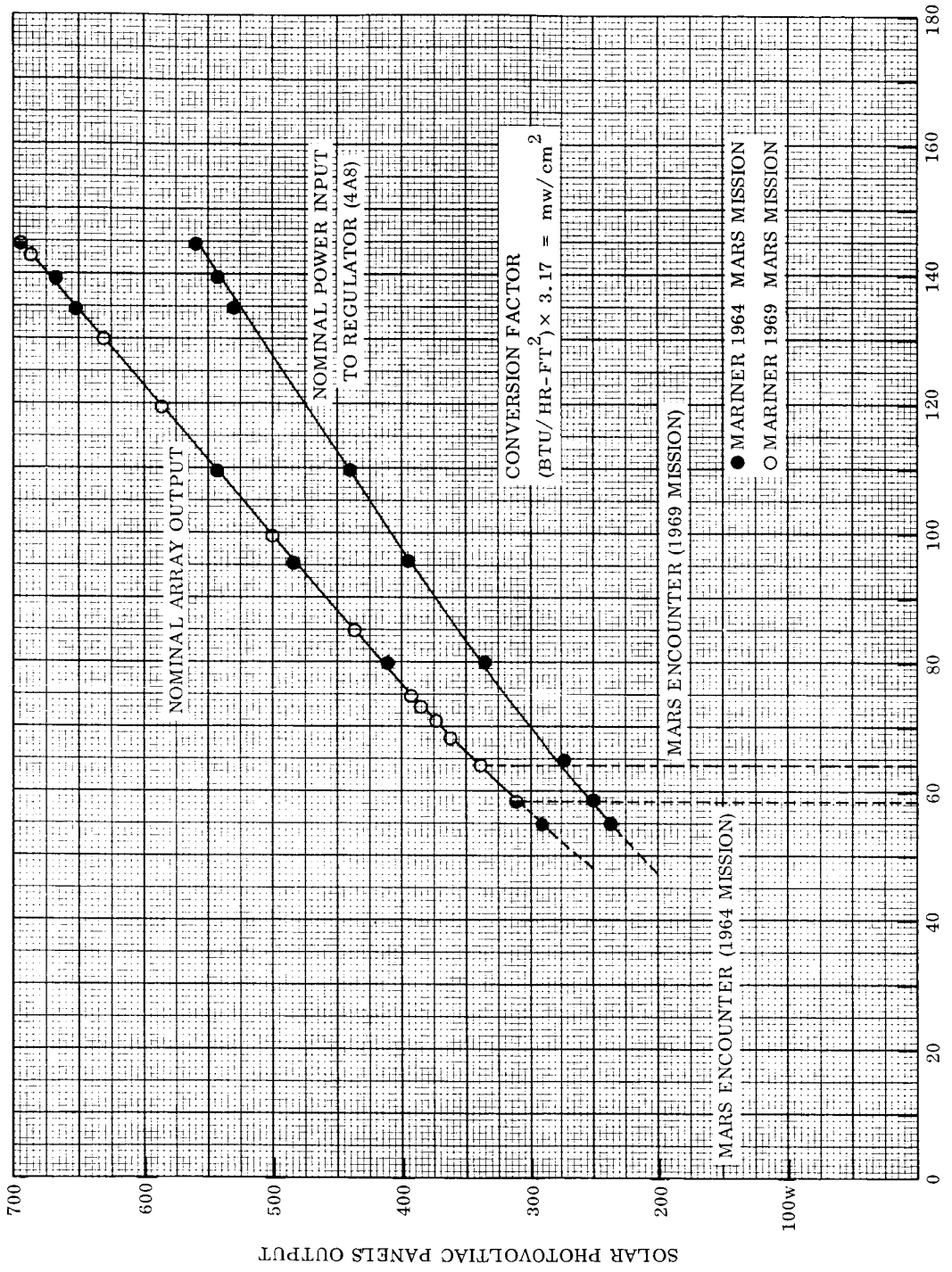


Fig. 5-35 Solar Photovoltaic System Power Output for Mariner C

The pyrotechnic ignition energy storage circuit will basically consist of a bank of capacitors as on Mariner C in order to eliminate harmful transients from propagating through the power supply to other subsystems.

5.3.3.2 Orbiter Plus Atmospheric Capsule

The sequence of events for this mission was presented in Table 5-7 and a functional block diagram of the orbiter was presented in Fig. 5-30. Now Fig. 5-36 presents a functional block diagram of the capsule system and its interface with the orbiter subsystems. The first concept to be considered in this diagram is the need for two transmitters on the capsule and therefore two receivers on the orbiter. This arrangement is a consequence of the requirement for communications during the separation phase and atmospheric entry phase of the mission and the fact that at 250 Mc the free-space attenuation of the link will vary over a range in excess of 160 db. The most obvious solution to a dynamic range problem of this magnitude is to simply reduce the transmitter power output to a sufficient level such that an AGC loop in the receiver can accommodate the remaining variation in signal strength. However, this would require a reduction in transmitted power of about 100 db which is not simple to achieve. However, assume that the orbiter receiver is a three stage superheterodyne circuit with its final IF centered around 500 kc. Then, during the separation phase, capsule signals could be received at this lower frequency. The generation of signals at this frequency in the capsule is simply a problem of translating the modulator output to this lower frequency. In effect, split the receiver in two parts; a mixer in the capsule and the IF amplifier plus the discriminator in the orbiter as illustrated in Figs. 5-37 and 5-38.

The next problem to be considered is the interface between this receiver and the orbiter-earth telemetry link. During the preseparation checkout period and the atmospheric entry period, the received data will be buffered and subsequently inserted into the orbiter-Earth link. During checkout, the data will be inserted in place of normal orbiter measurements. During atmospheric entry, the data will be inserted in the Mode 3 frame in slots allocated for television data. However, since orbit has not yet been achieved, no television data is actually being replaced.

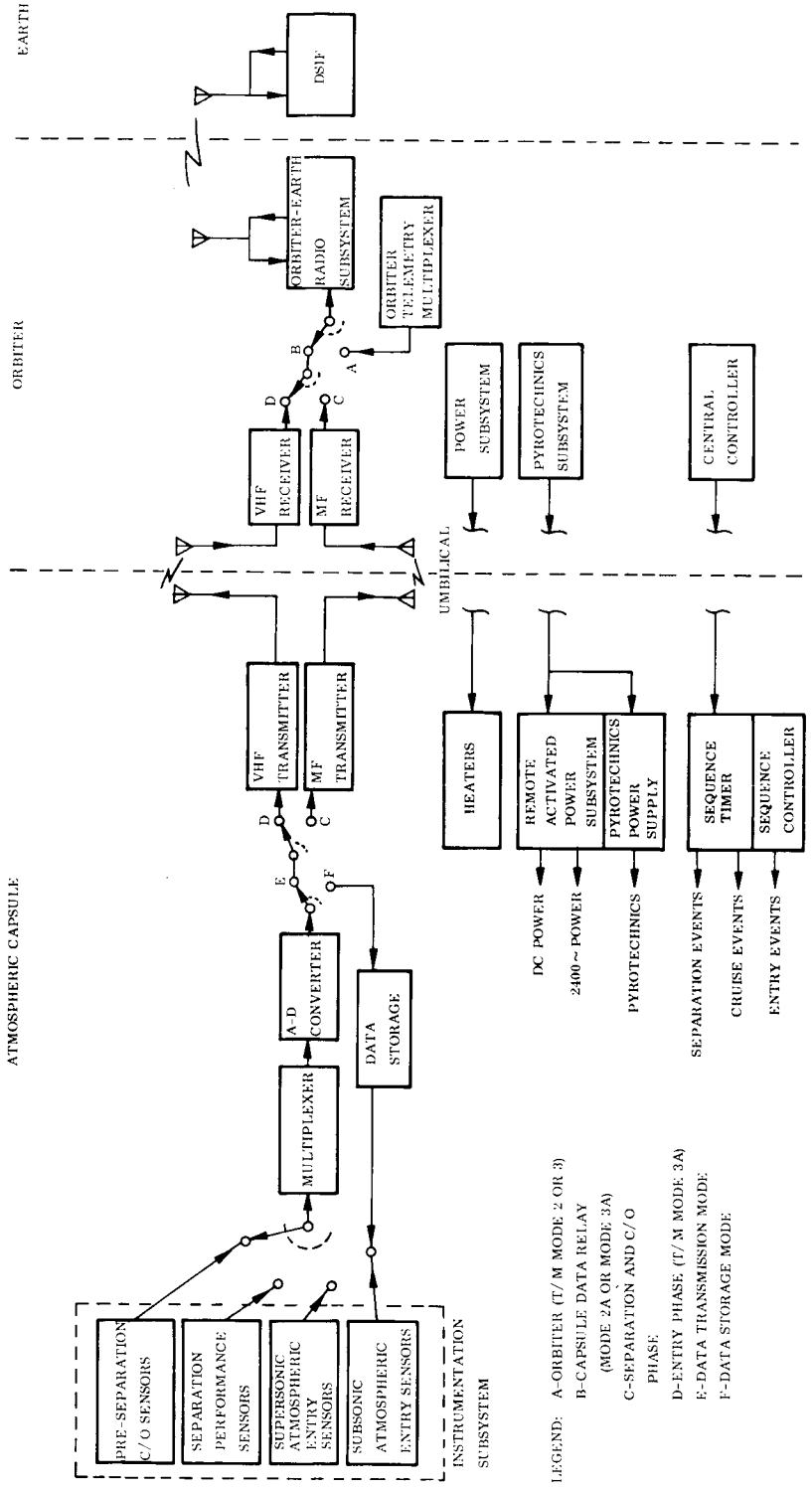


Fig. 5-36 Functional Block Diagram of Atmospheric Capsule System

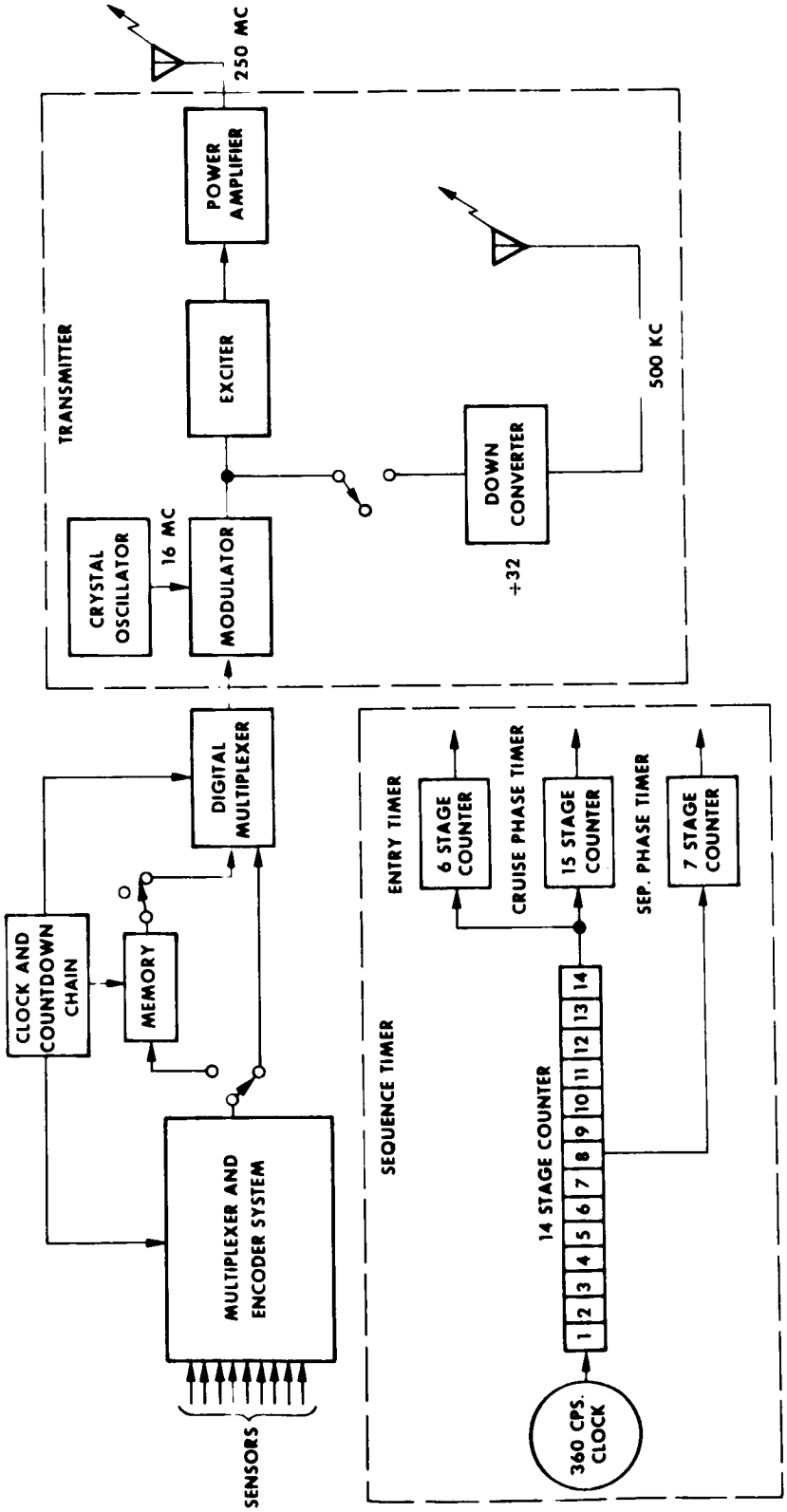


Fig. 5-37 Atmospheric Capsule Data Handling (Capsule)

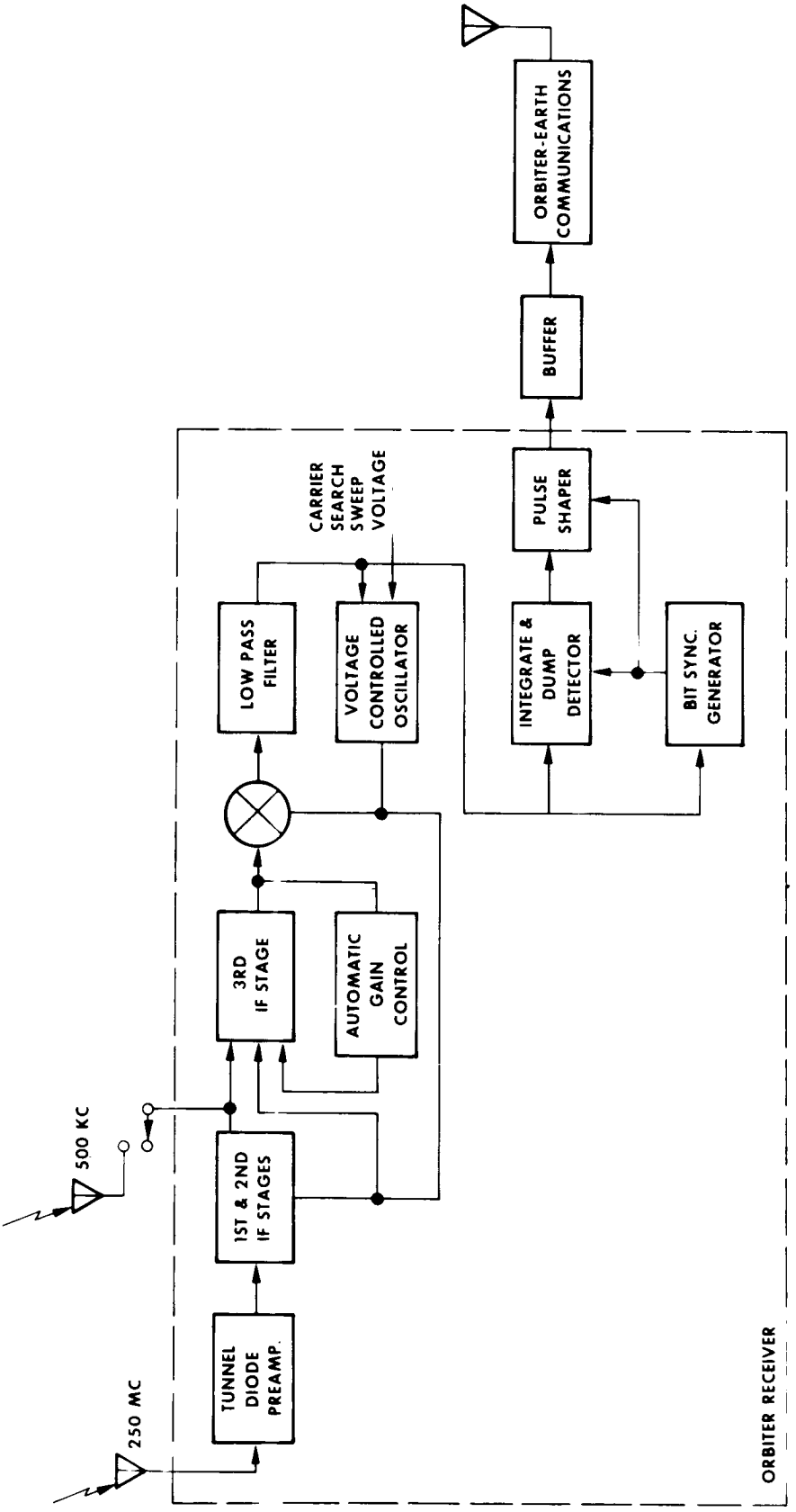


Fig. 5-38 Atmospheric Capsule Data Handling (Orbiter)

During the separation phase however, an additional constraint must be considered; the orbiter has been maneuvered into a noncruise attitude required for release of the capsule, thereby interrupting communications with the DSIF. Therefore, all capsule separation data must be stored in the orbiter for re-transmission after the cruise attitude has been re-established. Since the separation phase is only 1 min and a sufficient capsule-orbiter data rate will not exceed 50 bits/sec, a three-thousand bit core memory will be required to store this data.

The capsule data acquisition system will have four operating modes; checkout, separation, supersonic entry and subsonic entry. During checkout only engineering data will be acquired with science instrumentation checkout data being considered part of this data. During separation, the occurrence of specific events and system status data will be transmitted. During supersonic entry, and especially at velocities in excess of 10,000 ft/sec, it is expected that plasma sheath generation will eliminate all possibility of communicating with the orbiter. Therefore, the data acquired from an accelerometer and various capsule temperature sensors will be stored until the drogue chute is released. Assume that ten measurements are being recorded at this time and the highest sampling rate required for any measurement is one sample/sec from both accelerometer outputs. Also assume that a sample rate of 0.25 samples/sec is adequate for the remaining eight measurements. Then the data storage device will require no greater than 1200 bits capacity.

During subsonic entry only scientific data will be acquired. During one complete multiplexer frame, there may be 25 measurements to be transmitted including 19 from a mass spectrometer. If the sample rate per channel is 0.1 samples/sec, the transmitted data rate (neglecting sync) would be 25 bits/sec. However, the stored supersonic entry data must also be transmitted at this time and the memory should be cleared within 60 sec to ensure transmission before impact. Therefore, the data transmission rate, including a 10 percent allotment for synchronization, should be at least 50 bits/sec. For the nominal subsonic descent time of 70 sec, all stored supersonic data can be cleared and seven data points will be obtained for each subsonic

measurement channel. It is possible to rearrange the sampling format to allow more data points to be obtained from the pressure and temperature sensors for example, by reducing the number of measurements from the mass spectrometer. However, the transmitted data rate of 50 bits/sec appears to be sufficient for a useful mission.

The communication link calculations based on a 50 bit/sec data rate are presented in Tables 5-27 and 5-28 for the separation and atmospheric entry phases respectively. It can be seen from Table 5-27 that even a one mw capsule transmitter is far greater than required. In fact, a 40 db or 50 db attenuator should be inserted in the system.

From Table 5-28 it is apparent that an 8-w solid-state transmitter is satisfactory for the capsule-orbiter relay link. This power capability is well within the state-of-the-art. One of the major concerns of any atmospheric capsule link is the link acquisition time after blackout. Based on JPL External Publication No. 673, it was estimated that the receiver could acquire the transmitted frequency within 6 or 7 sec using a phase lock loop with a loop noise bandwidth at threshold of 75 cps. Allowing another 3 sec (150 bits) to obtain frame synchronization, it is estimated that complete acquisition can be achieved in about 10 sec.

The capsule sequence timer, illustrated with the other electronics equipment in Fig. 5-37, has two phases of operation; the separation phase and cruise phase. The separation phase timer will unitiate five events as indicated in Table 5-7 (Events 53P through 53U). As shown in this table, the resolution of the timer must be 0.5 sec with a capacity of about 64 sec. Therefore, a seven-stage counter will be required.

The cruise sequence timer has only one function and that is to turn on all capsule subsystems nominally 38 min before the oribter engine is ignited to inject the vehicle into orbit. Therefore, the timer must have a capacity of about 96 hrs and a resolution of 1 min is ample. The clock stability required for the capsule sequence timer is only one part in ten thousand which can easily be achieved using crystal controlled oscillators. However, in order to minimize capsule battery weights, the lowest power timer that can be used should be used. The Accutron appears to be very well suited to this mission.

Table 5-27

ATMOSPHERIC CAPSULE-ORBITER LINK (SEPARATION PHASE)

No.	Parameter	Value (db)	Tolerance (db)
1	Total Transmitter Power	-30 dbw	±1
2	Transmitting Circuit Loss	-1	±0.3
3	Transmitting Antenna Gain	-10	+16, -10
4	Transmitting Antenna Pointing Loss	incl. in 3	
5	Space Loss at 500 kc, R = 1,000 feet	-16.3	
6	Polarization Loss	incl. in 7	
7	Receiving Antenna Gain	-10	+16, -10
8	Receiving Antenna Pointing Loss	incl. in 7	
9	Receiving Circuit Loss	-2	±0.5
10	Net Circuit Loss	-39.3	+32.8, -20.8
11	Total Received Power	-69.3 dbw	+33.8, -21.8
12	Filter and Detector Loss	-3	±0.5
13	Net Received Signal Power	-72.3 dbw	+34.3, -22.3
14	Receiver Noise Spectral Density (N/B) at $T_e = (2.5 \times 10^5 \pm 5 \times 10^4)$ °K	-174.6 dbw	+0.8, -1
15	Bit Rate (1/T) 50 bps	+17	
16	Required ST/N/B	+10.6	+1.5, -0
17	Required Received Signal Power	-147 dbw	+2.3, -1
18	Performance Margin	+74.7	+33.8, -26.1

Table 5-28

ATMOSPHERIC CAPSULE-ORBITER LINK (ENTRY PHASE)

No.	Parameter	Value (db)	Tolerance (db)
1	Total Transmitter Power	+9 dbw	±1
2	Transmitting Circuit Loss	-1	±0.3
3	Transmitting Antenna Gain	-3	+6, -3
4	Transmitting Antenna Pointing Loss	incl. in 3	
5	Space Loss at 250 Mc, R = 10^4 km	-160.5	
6	Polarization Loss	incl. in 7	
7	Receiving Antenna Gain	0	+6, -3
8	Receiving Antenna Pointing Loss	incl. in 7	
9	Receiving Circuit Loss	-1	±0.2
10	Net Circuit Loss	-165.5	+12.5, -6.5
11	Total Received Power	-156.5 dbw	+13.5, -7.5
12	Filter and Detector Loss	-3	±0.5
13	Net Received Signal Power	-159.5 dbw	+14, -8
14	Receiver Noise Spectral Density (N/B) at T_e = 800 ± 400°K	-199.6 dbw	+2, -3
15	Bit Rate (1/T) 50 bps	+17	
16	Required ST/N/B	+10.6	+1.5, -0
17	Required Received Signal Power	-172 dbw	+3.5, -3
18	Performance Margin	+12.5	+17, -11.5

The capsule power will be supplied by a single, remote, activated primary battery. This battery will be activated by the bus pyrotechnics system through the capsule umbilical at least 5 min prior to initiation of the preseparation checkout routine. In order to achieve the highest specific energy, and therefore the lowest weight, the batteries will be Ag-Zn-KOH units. The present state-of-the-art in remote activation of silver-zinc batteries is such that they can provide a specific energy for this application of 30 w-hr/lb. However, a heat sterilization unit may suffer a reduction of specific energy to about 14 w-hr/lb.

The estimated power and energy requirements for the atmospheric capsule equipment are presented in Table 5-29. These energy requirements are based on a 4-day cruise period with a 30-min atmospheric entry period. A block diagram of the capsule power system is shown in Fig. 5-39. The philosophy in the design of the capsule power system is similar to that presented for the orbiter power system; i.e., all regulated power will be supplied from a 2400 cps inverter system. If the power system efficiency is assumed to be 85 percent and a 10 percent contingency factor is allowed, the total battery energy requirement is about 170 w-hrs. The characteristics of the power system components are presented in Table 5-30.

Table 5-30

ATMOSPHERIC CAPSULE POWER SYSTEM COMPONENTS

	Type	Est. Wt.	Est. Vol.	Input Voltage	Output Voltage	Capacity	No. Req'd. Per Vehicle
Primary Battery	Remote Activated Ag - Zn	12 lb	120 $in.^3$	N.A.	28V DC	6.1 A-Hr / 170W-Hr	1
2400 cps Inverter	1ϕ	3.2 lb	90 $in.^3$	25-50V DC	50V AC ± 2%	105 w	1

The capsule pyrotechnics will obtain their activation energy from a capacitor bank similar to that used on the orbiter.

Table 5-29

ESTIMATED ATMOSPHERIC CAPSULE POWER/ENERGY REQUIREMENTS

Subsystem	Power Level (w)	Total Energy (w-hr)
Electronics		
Multiplexer/Encoder	7	4
Buffer Storage	1	0.5
Transmitter	62	34
Sequence Timer	0.7	67
Relays, Switches, etc.	2	1
Signal Conditioner	3	1.5
Subtotal	75.7	108
Instrumentation		
Accelerometer	5	2.5
Mass Spectrometer	6	3
Pressure Gauges	0.2	0.1
Temperature Gauges	0.2	0.1
IR Radiometer	8	4
UV Photometer	3.5	1.8
Subtotal	22.9	11.5
Total	~99	~120

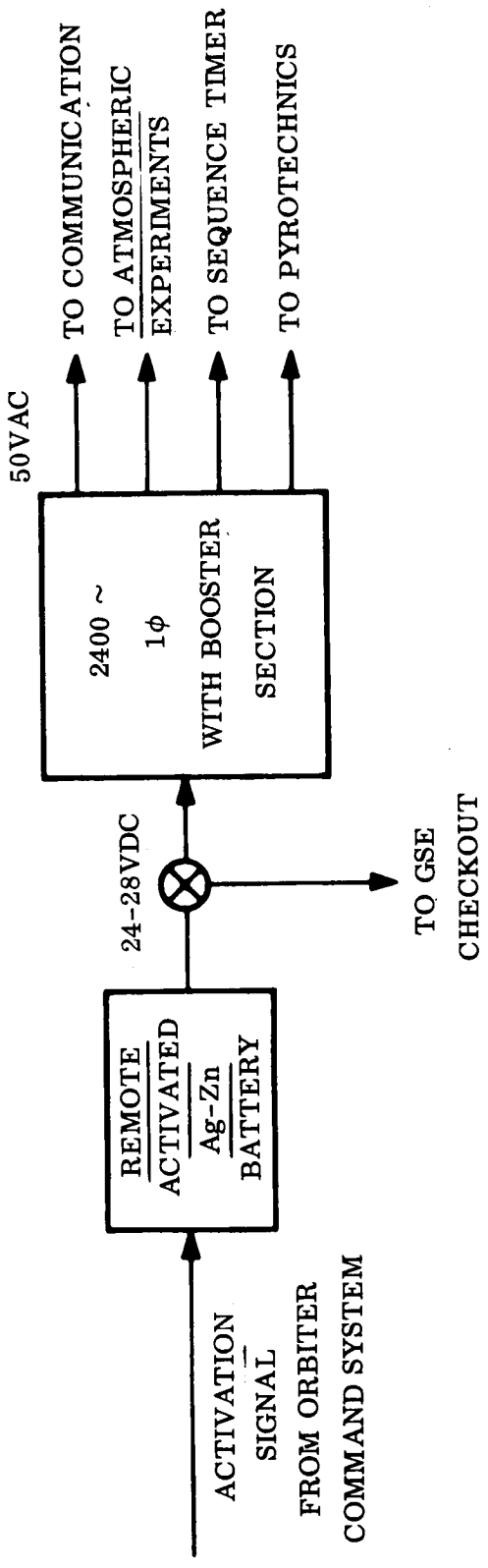


Fig. 5-39 Atmospheric Capsule Power System

Additional equipment must be carried on the orbiter to support the capsule mission, including the following:

- The receiver mentioned previously and illustrated in Fig. 5-38.
- A 3000-bit capacity core buffer/memory.
- A sequence timer with a counter equivalent to that used in the capsule cruise phase timer.
- Slightly additional command capability as indicated in Table 5-20.
- At least two additional pyrotechnic events for activation of the capsule battery and capsule separation.

5.3.3.3 Orbiter Plus Biological Capsule

Functionally, the biological capsule does not differ greatly from the atmospheric capsule except that it must survive impact and operate for about 28 hr after impact. Prior to impact, there is no difference in the operation of the two capsules. There is no operational difference in the orbiter support systems at any time in the mission. However, the implementation of the capsule-orbiter radio subsystem differs significantly and the other biocapsule subsystems differ to varying degrees from the atmospheric capsule systems.

Because the atmospheric and biological capsules are operationally the same prior to impact, there is no need to repeat this portion of the mission operation. Only the operations after impact will be considered in this section.

At capsule impact, the orbiter support systems are turned off permanently. In the capsule, meanwhile, a number of interesting events are occurring.

- The majority of capsule electronics are turned off to conserve energy for the remainder of the mission.
- Before being deactivated, an accelerometer output will be used with simple logic circuits to determine which end is up, so that the capsule antenna system will known which side of the capsule can expect to receive signals from Earth.

- The capsule sequence timer begins a new phase of operation. On the surface of Mars, data acquisition and storage commands will be initiated by the sequence timer at 1-hr intervals for the remainder of the mission. In addition, this timer will be used to activate the capsule receiver after about 20 hr to search for signals from the DSIF representing a read out command.
- Upon receipt of DSIF signals, the capsule transmitter will be energized and after an interval of about 20 min, stored data read out will be initiated. This data will be read out once and repeated until the DSIF signal is lost or the batteries run down.

A functional block diagram of the orbiter-biocapsule interface is shown in Fig. 5-40. Since the only significant difference between this Figure and Fig. 5-36 occurs in the radio subsystem, no further discussion of the diagram is required. However, the more detailed block diagram of the electronics system presented in Figs. 5-41 and 5-42 requires some further explanation.

Recalling the discussion in Section 5.3.2.2 concerning the selection of operating frequencies and modulation for the biocapsule radio subsystem, this system is constrained to use a coherent PSK, S-band link. The addition of a capsule receiver is necessary to determine DSIF readiness for data read out. The one additional antenna shown on the capsule is to ensure that one or the other of the S-band antennas will be facing approximately skyward after impact. This antenna will then be used for subsequent readout to Earth.

It should be noted here that both the atmospheric capsule and orbiter used only near-omni antennas for communications. On a biocapsule mission however, the orbiter's S-band antenna will be a relatively high-gain unit such as a helix or quad-helix array. This gain can be realized by virtue of the fact that the required beamwidth of the orbiter antenna is only 16.5 deg to account for 3σ dispersions in the capsule impact point and orbiter attitude instability. Using the following simplified Eq. 5-18 for a helix antenna, it can be shown that the half-power gain of such an antenna could be as high as 18.6 db.

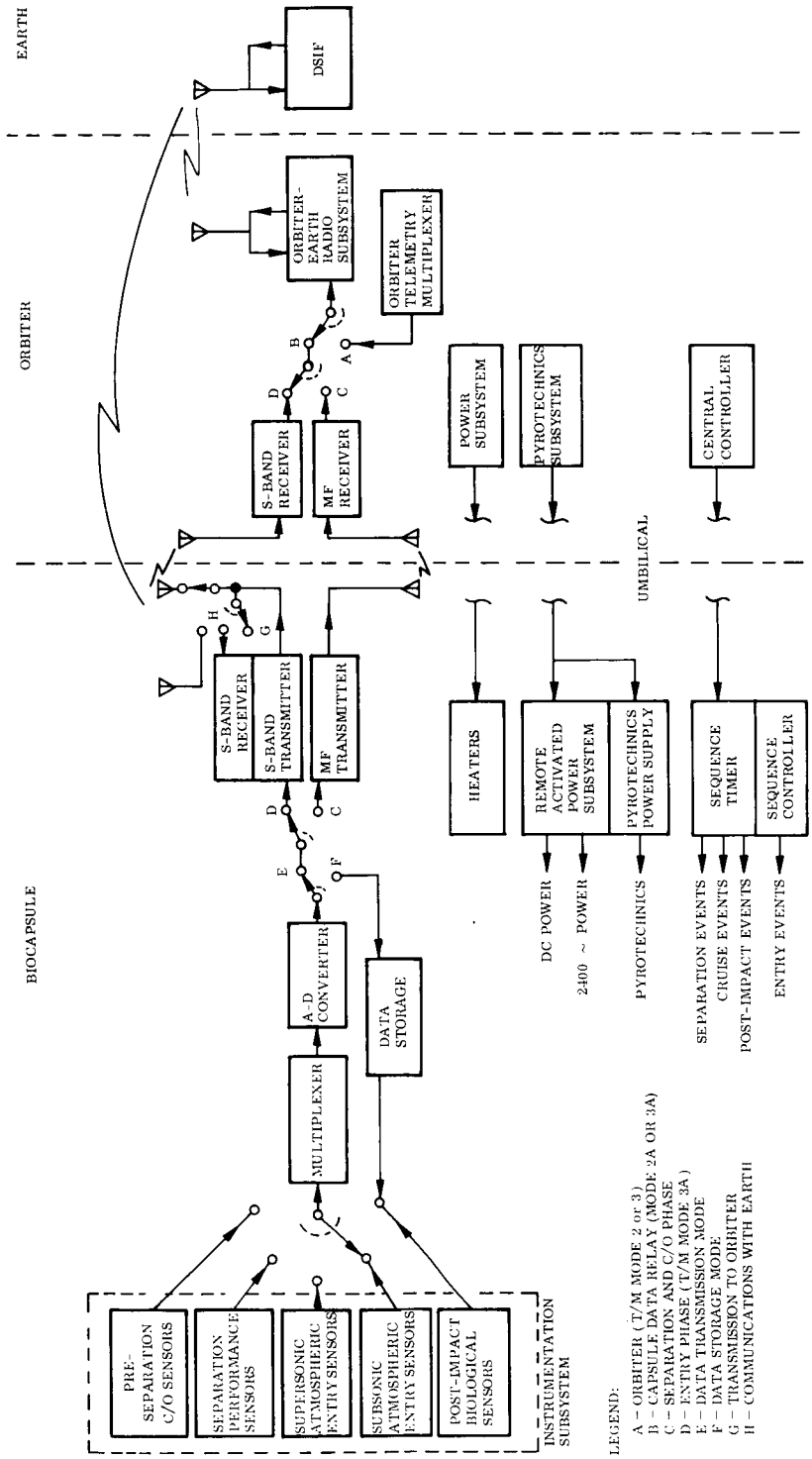


Fig. 5-40 Functional Block Diagram Biological Capsule System

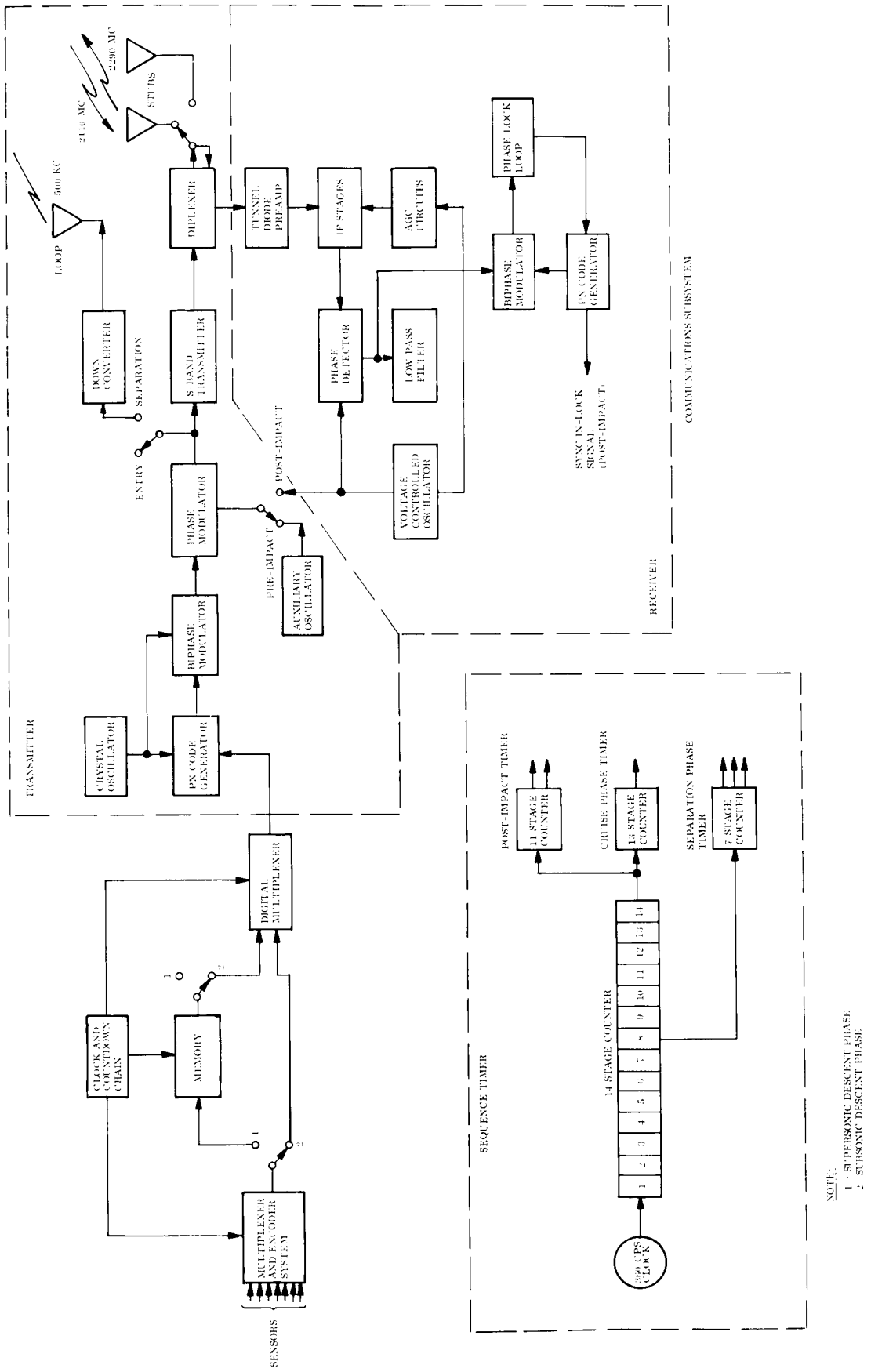


Fig. 5-41 Biocapsule Electronics

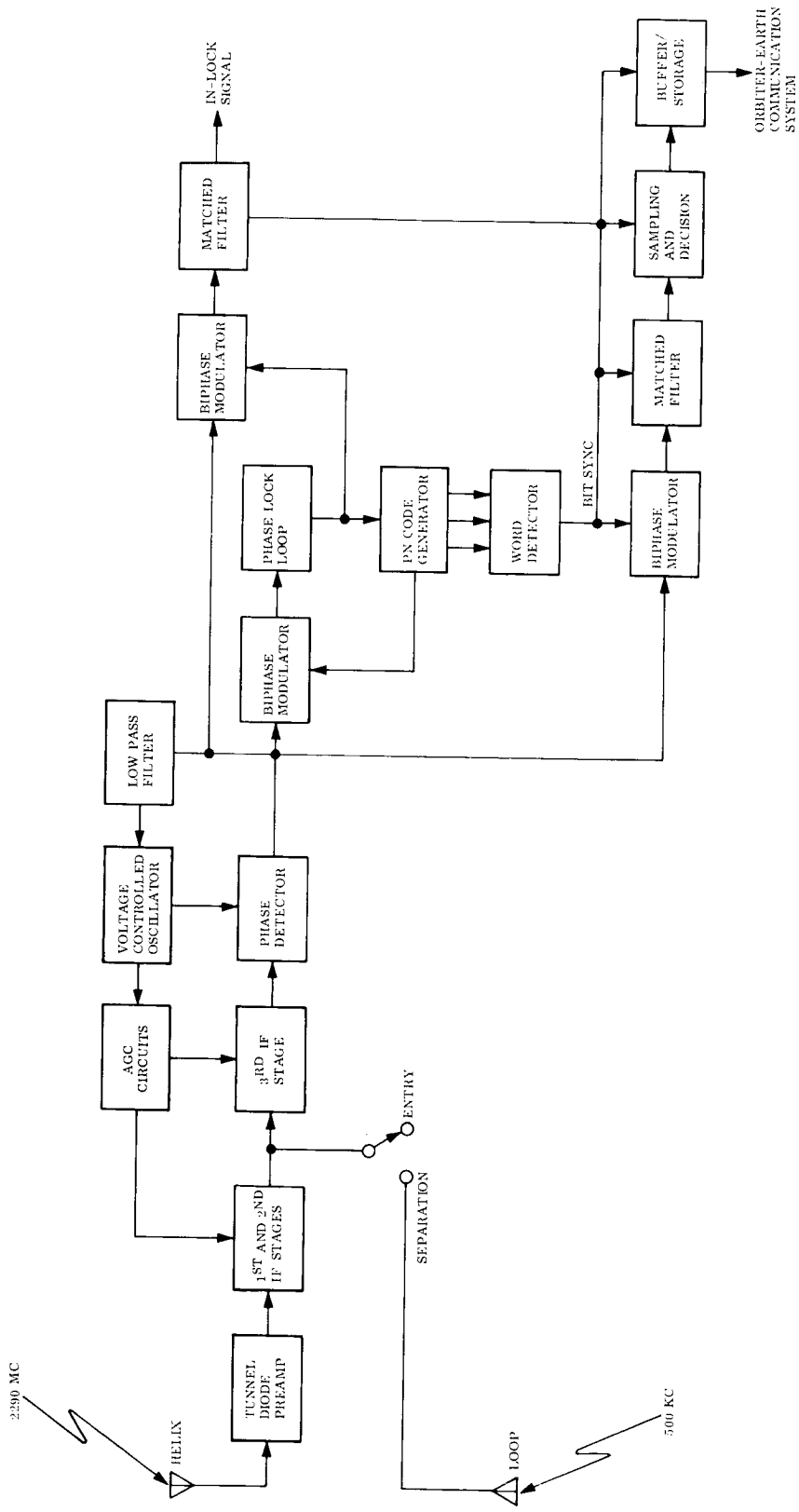


Fig. 5-42 Orbiter Receiver for Support of Biocapsule

$$\text{Peak Gain, } G = \frac{4 \times 10^4}{B^2} \tag{5.18}$$

where

B = half-power beamwidth in deg

However, the length of this helix is given by Eq. (5.19) to be nearly 53 in.

$$\text{Antenna Length} = 0.11\lambda \left(1 + \frac{2.46 \times 10^4}{B^2}\right) \tag{5.19}$$

where

λ = wavelength

Such an antenna is far too long to be properly located in the orbiter designs being considered. However, using an equivalent quad-helix array, the length of the antenna can be reduced to 13 in. The spacing between the helices should be about 13 in. sq. Proper location of the quad-helix antenna was also a problem, so a degradation in capability was accepted through the use of a 1-ft long, single helix antenna yielding a beamwidth at 2290 Mc of 35 deg with a peak gain of about 15 db.

The calculations for the biocapsule-Earth links were presented previously in Tables 5-11 and 5-12 and will not be repeated here. The calculations for the capsule-orbiter entry link are presented in Table 5-31. The separation phase link calculations are not shown because of their basic similarity to the atmospheric capsule separation link calculations. It should be noted that a data rate of 50 bits/sec can be achieved on the atmospheric entry link using a 20-w transmitter in the capsule. The separation link transmitter power requirements are in the microwatt region once again.

Table 5-31

BIOCAPSULE-TO-ORBITER ENTRY LINK

No.	Parameter	Value (db)	Tolerance (db)
1	Total Transmitter Power	+13 dbw	±1
2	Transmitting Circuit Loss	-2	±0.5
3	Transmitting Antenna Gain	-3	+6, -3
4	Transmitting Antenna Pointing Loss	incl. in 3	
5	Space Loss at 2290 Mc, R = 10^4 km	-179.7	
6	Polarization Loss	incl. in 7	
7	Receiving Antenna Gain	+13	+2, -1
8	Receiving Antenna Pointing Loss	incl. in 7	
9	Receiving Circuit Loss	-1	±0.2
10	Net Circuit Loss	-172.7	+8.7, -4.7
11	Total Received Power	-159.7 dbw	+9.7, -5.7
12	Receiver Noise Spectral Density (N/B) at T_e = 600° ± 100° K	-200.8 dbw	+0.7, -0.8
13	Carrier Modulation Loss	-2	±0.5
14	Received Carrier Power	-161.7 dbw	+10.2, -6.2
15	Carrier APC Noise BW ($2B_{LO}$ = 40 ± 8 cps)	+16	+0.8, -1
	Carrier Performance – One Way Tracking		
16	Threshold SNR in $2B_{LO}$	0	
17	Threshold Carrier Power	-184.8 dbw	+1.5, -1.8
18	Performance Margin	+23.1	+12, -7.7
	Data Channel		
19	Modulation Loss	-4.9	±0.3
20	Received Subcarrier Power	-164.6 dbw	+10, -6
21	Bit Rate *1/T) 50 bps	+17	

Table 5-31 (Continued)

No.	Parameter	Value (db)	Tolerance (db)
22	Required ST/N/B	+6.5	+0.8, -0
23	Threshold Subcarrier Power	-177.3 dbw	+1.5, -0.8
24	Performance Margin	+12.7	+10.8, -7.5
	Sync Channel		
25	Modulation Loss	-4.9	±0.3
26	Received Subcarrier Power	-164.6 dbw	+10, -6
27	Sync APC Noise BW ($2B_{LO}$ = 20 ± 4 cps)	+13	+0.8, -1
28	Threshold SNR in $2B_{LO}$	0	
29	Threshold Subcarrier Power	-187.8 dbw	+1.5, -1.8
30	Performance Margin	+23.2	+11.8, -7.5

Either the Amplitron or a traveling wave tube can be used as the power amplifier in the capsule transmitter. However, the ability of either or both of these devices to accept heat sterilization and to withstand 900-g shocks on surface impact is uncertain.

Typical experiments that might be conducted on the surface of the planet are given in Section 5.2 as two pressure sensors, two temperature sensors, a mass spectrometer with sequential output equivalent to 19 channels, and a biological experiment equivalent to 15 channels. If these instruments are sampled once per hr over a 24 hr period, the total storage capacity required is about 10,000 bits. With an acquisition time on the order of 20 min after initial signal reception, and a transmitted data rate of 1 bit/sec, the minimum required transmission time is slightly more than 3 hrs.

Since the capsule antenna pattern may have nulls sufficiently deep to cause a loss of lock for short intervals during this 3-hr readout period, the capsule transmitter will always be turned off when the receiver is out of lock in order to conserve energy. Thus an allowance for at least three interruptions in the data link should be considered in determining the battery energy requirements.

It is expected that the 10,000-bit memory will be a non-destructive readout core device in order to minimize standby power requirements and allow the possibility of multiple readout.

The expected energy requirements for the biocapsule are shown in Table 5-32 along with the characteristics of the power system equipments illustrated in the functional block diagram of Fig. 5-43. The power will be supplied by a silver-zinc, remote-activated primary battery similar to that used in the atmospheric capsule. However, if the assumed heat sterilizable battery specific energy of 14 w-hrs/lb is required to be used, the biocapsule battery alone would weight 58 lb. This weight is intolerable. Radiation sterilization or asceptic assembly techniques must be considered if a biological capsule mission is seriously considered. In this case, the battery weight would still be a relatively high 27 lb.

Table 5-32

ESTIMATED BIOCAPSULE POWER/ENERGY REQUIREMENTS

Subsystem	Power Level (w)	Total Energy (w-hrs)
Electronics		
Multiplexer/Encoder	7	7
Buffer Storage	2	28
Transponder	70	328
Sequence Timer	0.7	84
Relays, Switches, etc.	2	1
Signal Conditioner	3	3
Subtotal	84.7	451
Thermal Control		
Heaters	5	120
Instrumentation		
Mass Spectrometer	6	6
Accelerometer	5	3
Pressure Gauges	0.2	3
Temperature Gauges	0.2	3
Multivator	2	48
Subtotal	13.4	63
Total	103	634

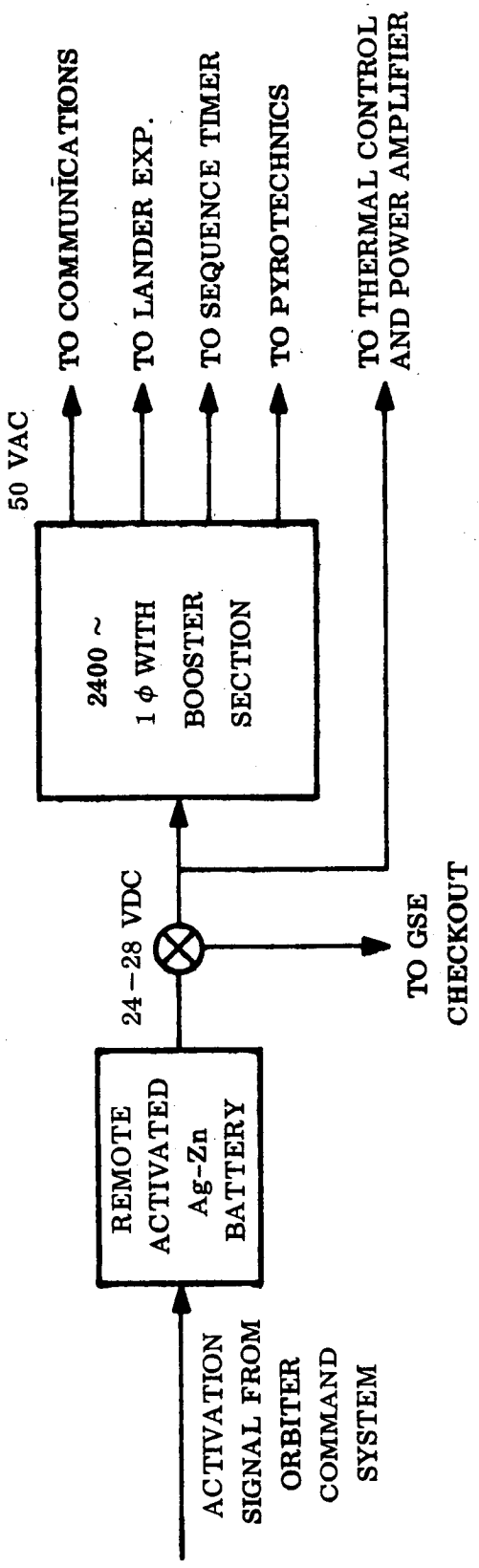


Fig. 5-43 Biocapsule Power System

The additional energy requirements for the capsule support equipment in the orbiter can be obtained from the secondary battery.

5.3.4 System Weight and Volume Summary

The estimated weight and volume requirements are summarized in Table 5-33 with a more detailed breakdown provided in Section 4.9. Since a reliability analysis was far beyond the scope of this study, these estimates do not include an allowance for redundancy or associated failure sensors. Without any analysis on which to base an estimate, an allowance of perhaps 15 percent (50 lb) for redundancy might be required for both the 1969 and 1971 orbiters. The capsules will carry no redundancy because of their short periods of activity and because they are not considered critical to the overall success of the mission.

5.3.5 Long Lead Time Development Items

There were no long-lead time development items, required for the 1969 orbiter-only mission, uncovered during the course of this study. The only component which may require a major development effort at an early date is the tape recorder. The Advanced Mariner tape recorder developed or being developed by Raymond Engineering has a greater capability than that required for the 1969 mission. Whether suitable modifications would be difficult is unknown, but should be investigated.

There were two components mentioned previously which are presently under development and if they are successful they could significantly increase the mission capability -- a non-standard tape recording technique under development at LMSC and a Watkins-Johnson 20-w TWT which should be on the market shortly. These components would both require an early start to qualify them for the planned mission.

Table 5-33
ELECTRONICS WEIGHT AND VOLUME SUMMARY

Mission	Estimated Weight (lb)	Estimated Volume ($in.^3$)
Orbiter Only	355	9020
Orbiter Plus Atmospheric Capsule	368 35	9570 810
Orbiter Plus Biological Capsule	371 73	9720 1230

5.4 PROPULSION

The objectives of the 1969 Mariner Mars propulsion study were to establish propulsion requirements for the vehicle, to select propellants, to develop a propulsion system concept, and to define possible development problems areas. Emphasis was placed on those design and performance aspects having the most impact on the overall spacecraft system. As a result of this study it was found possible to satisfy both the mid-course maneuver and the orbit injection propulsion requirements with a single-engine propulsion unit. The ablative-cooled engine selected to fill these requirements is considered state-of-the-art, and uses storable nitrogen tetroxide (N_2O_4) and monomethyl hydrazine (MMH) as propellants.

Wherever possible, recent advances in propulsion system technology have been incorporated into the propulsion system design. In particular, passive ullage control through the incorporation of propellant containment screens in a tank outlet (sump) have been included.

A cold gas propulsion unit was selected for the vehicle attitude control system. Extensive flight experience at JPL, LMSC, and elsewhere has demonstrated the reliability of such a system. A subliming solid system was critically evaluated. Although it offers a significant reduction in weight and potential improvement in reliability (low pressure storage), the subliming system was not selected because of the lack of flight experience and lack of proven technology. However, use of subliming systems on near-future Air Force and NASA vehicles may allow its reconsideration as a feasible improvement later in the program.

A heat sterilizable solid propellant rocket motor is proposed for propulsion on the capsule. Although present information indicates that off-the-self hardware is not available to fulfill this requirement, it was determined feasible to develop such a system within the required time schedule. Standard, small impulse solid motors were chosen for spin rockets on the capsule.

5.4.1 Primary Propulsion System

Performance Requirements. The launch window for the 1969 Mars orbiter mission extends from January 15, 1969 to February 14, 1969. For injection into a 1,800 by 36,000 km orbit, the ideal required ΔV varies from 5600 fps on January 15, 1969 to 6670 fps on February 14, 1969. The propellant tanks must be designed for capacity to satisfy the last day of the launch window including allowance for gravity losses. For maximum performance the tanks must be partially filled on the first day of the window, and incrementally on-loaded through the window. As discussed under the guidance and control section, two midcourse correction maneuvers are required during the transfer trajectory. Provision is made for an additional midcourse maneuver if required. Finally, sufficient incremental velocity is required to place the orbiter into Mars orbit. In the interest of simplicity and the associated reliability, every effort was made to satisfy all of these requirements with one engine. The midcourse and orbit correction maneuvers have a minimum impulse requirement of 100 lb-sec as determined by the guidance analysis. This minimum impulse capability is available from engines up to 1000 lb thrust, and this value was used as an upper limit of thrust during the optimization analysis.

System Concept Selection. Three candidate propulsion systems were studied for spacecraft primary propulsion:

- A dual system consisting of a bipropellant unit for orbit injection and the Mariner C hydrazine monopropellant thruster for trajectory corrections.
- A solid propellant motor for orbit injection in conjunction with the Mariner C hydrazine monopropellant system for trajectory corrections.
- A single pressure-fed storable liquid bipropellant system for both orbit injection and trajectory corrections.

As previously mentioned, propellant on-loading is required through the launch window for maximum performance. On-loading of solid propellants is not considered feasible. Further, the specific impulse of available solid propellants is considerably less than the proposed 302 sec. The combination of these two considerations yields about a 100 lb payload penalty indicating the choice of a solid propellant would be ill-advised.

The all-liquid dual system is considerably more complex than a single system, requiring three propellants and requiring mounting provisions considered difficult to implement without separate thrust-vector control systems. The dual system is also heavier than a single engine and would be selected only if a single system could not provide the minimum impulse bit required for guidance corrections. As a result of these considerations, the effort was concentrated on the design of a single system which could satisfy all the primary propulsion requirements.

Propellant Selection. The mission feasibility study showed that the mission could be performed with state-of-the-art storable liquid propellants. Nitrogen Tetroxide is a readily available storable oxidizer having extensive test experience in the 300-sec specific-impulse regime. The majority of this testing has been done with either Monomethyl-Hydrazine (MMH) or 50 percent MMH and 50 percent Hydrazine (50-50) as the fuel. The chemical characteristics of these two fuels are very similar, except for their freezing points, with the value for MMH considerably lower than for 50-50. Although theoretically a 1-sec specific impulse advantage is found for the 50-50, rocket engine manufacturers have not been able to demonstrate it in testing. Therefore, to minimize thermal control requirements, MMH was chosen as the fuel.

Engine Selection. The thrust chamber optimization was accomplished by an iterative technique. Based on an assumed chamber pressure and area ratio, the minimum delivered specific impulse was determined from Fig. 5-44 . The data for this figure, which accounts for the low chamber pressure re-combination losses recently quantitized during many small engine test programs, was obtained from Aerojet General Corp. Results from their tests on NASA Contract No. NAS/7-136 are to be documented in the near future. Using this specific impulse, the maximum total propellant weight required for maneuvers (maximum of three totaling no more than 46 m/sec) was calculated. Subtracting this weight, the booster adapter weight, and the capsule weight from the vehicle escape weight (1990 lb) yields the vehicle weight at start of orbit injection. Thrust, chamber pressure and expansion ratio were varied in a tradeoff analysis to optimize nonpropulsive weight in a 1800 by 36,000 km orbit about Mars. The tradeoff

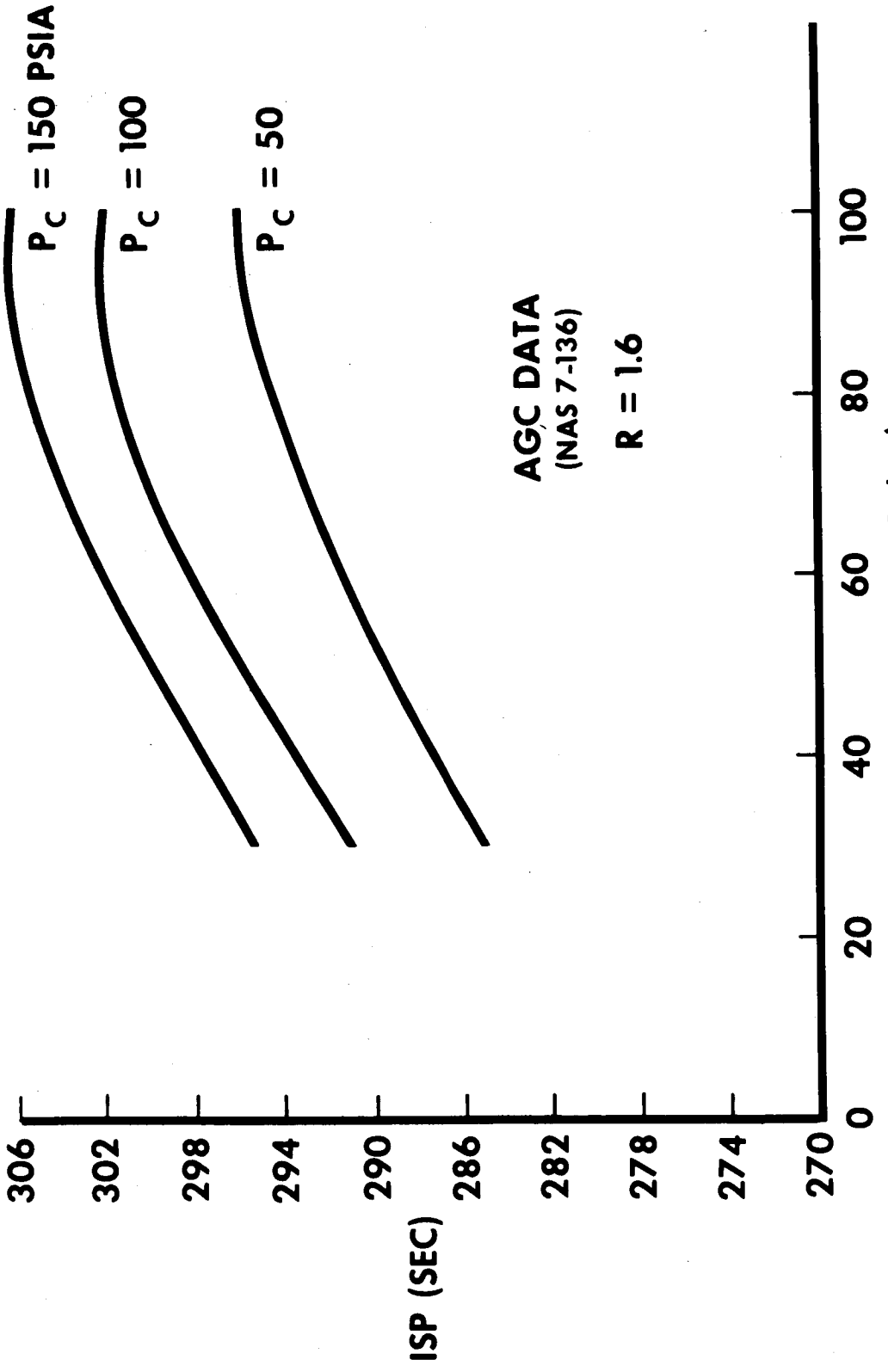


Fig. 5-44 Thrust Chamber Performance ($N_2 O_4$/MMH)

matrix was:

$$\text{Chamber Pressure } (P_c) = 150, 100, 50 \text{ PSIA}$$
$$\text{Expansion Ratio } (\epsilon) = 100{:}1,\ 60{:}1,\ 30{:}1$$
$$\text{Thrust } (T) = 300, 500, 750, 1000 \text{ lb}$$

Total nonpropulsive weight on orbit was determined by subtracting propulsive weight from the burnout vehicle weight. For this exercise, propulsive weight includes the thrust chamber, helium tank, propellant tanks, valves, lines, and residuals. Figure 5-45 presents the results of this procedure. From this figure, and the limited Surveyor envelope restriction, a design point of 750 lb thrust, 150 PSIA chamber pressure, and expansion ratio of 60:1 was chosen.

5.4.2 Details of the Selected Primary Propulsion System

The primary propulsion system is schematically shown in Fig. 5-46 . The preliminary design characteristics are presented in Table 5-34 and the detailed weight breakdown is shown in Table 5-35.

Engine. The performance characteristics of the engine design are provided in Table 5-34 . This engine utilizes an ablation-cooled thrust chamber to an area ratio of 20:1 and a radiation skirt extension from 20:1 out to 60:1. A throat insert is necessary to eliminate throat ablation and consequent thrust decay. This specific engine design is not presently available or under contractual development at any of the manufacturers. However, information from the manufacturers contacted indicates that development program unknowns will be minimized since extensive in-house prototype testing has been accomplished at thrust levels bracketing this design. Since a development program will be required, this is a long-lead time item requiring an estimated 18 mo through qualification. The design shown in Fig. 5-47 was provided unsolicited by Rocketdyne. Rocketdyne indicated that many requests for design confirmation on an engine of this type have been received and that they felt a preliminary design was warranted.

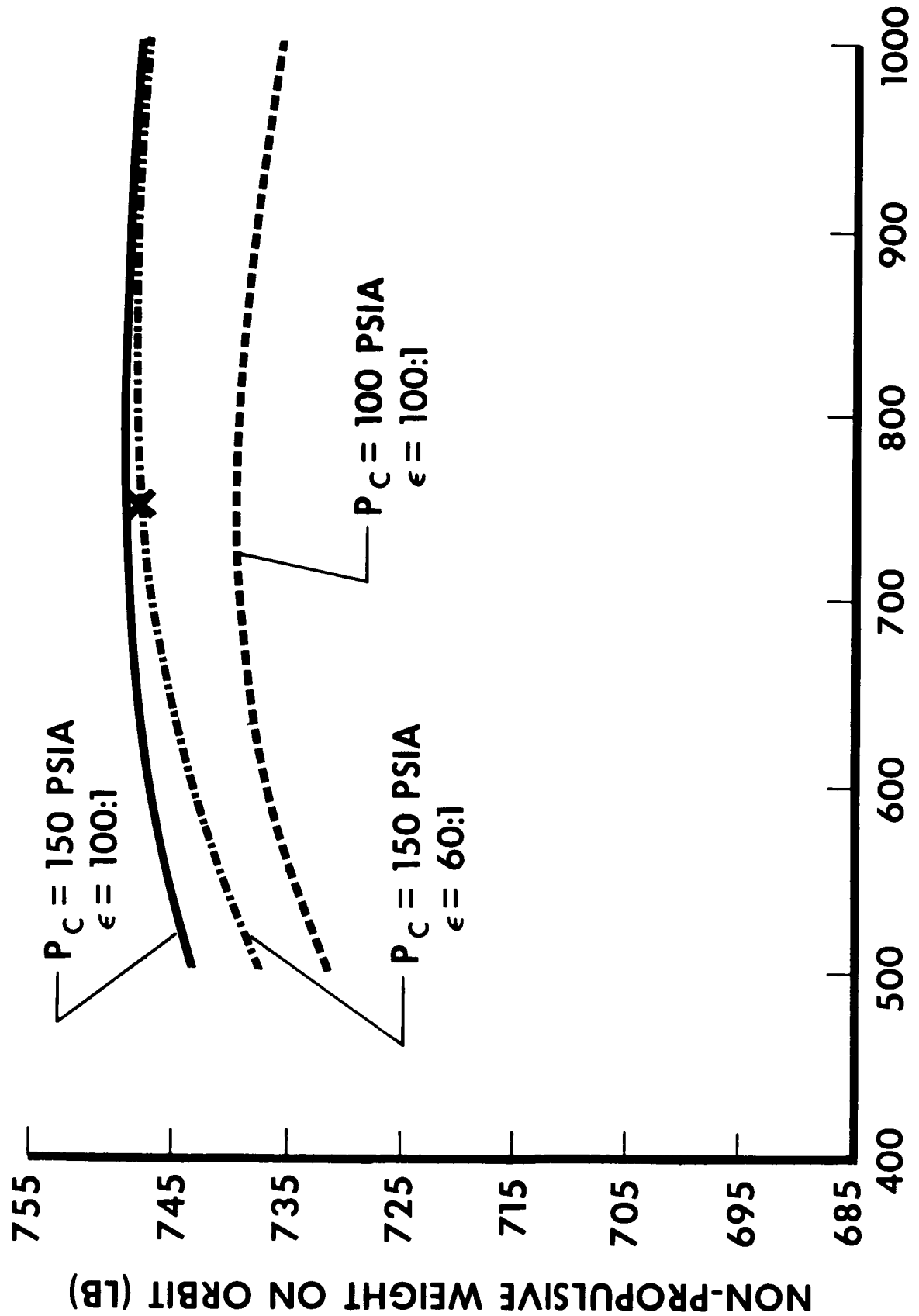


Fig. 5-45 Thrust Chamber Optimization (N_2O_4/MMH)

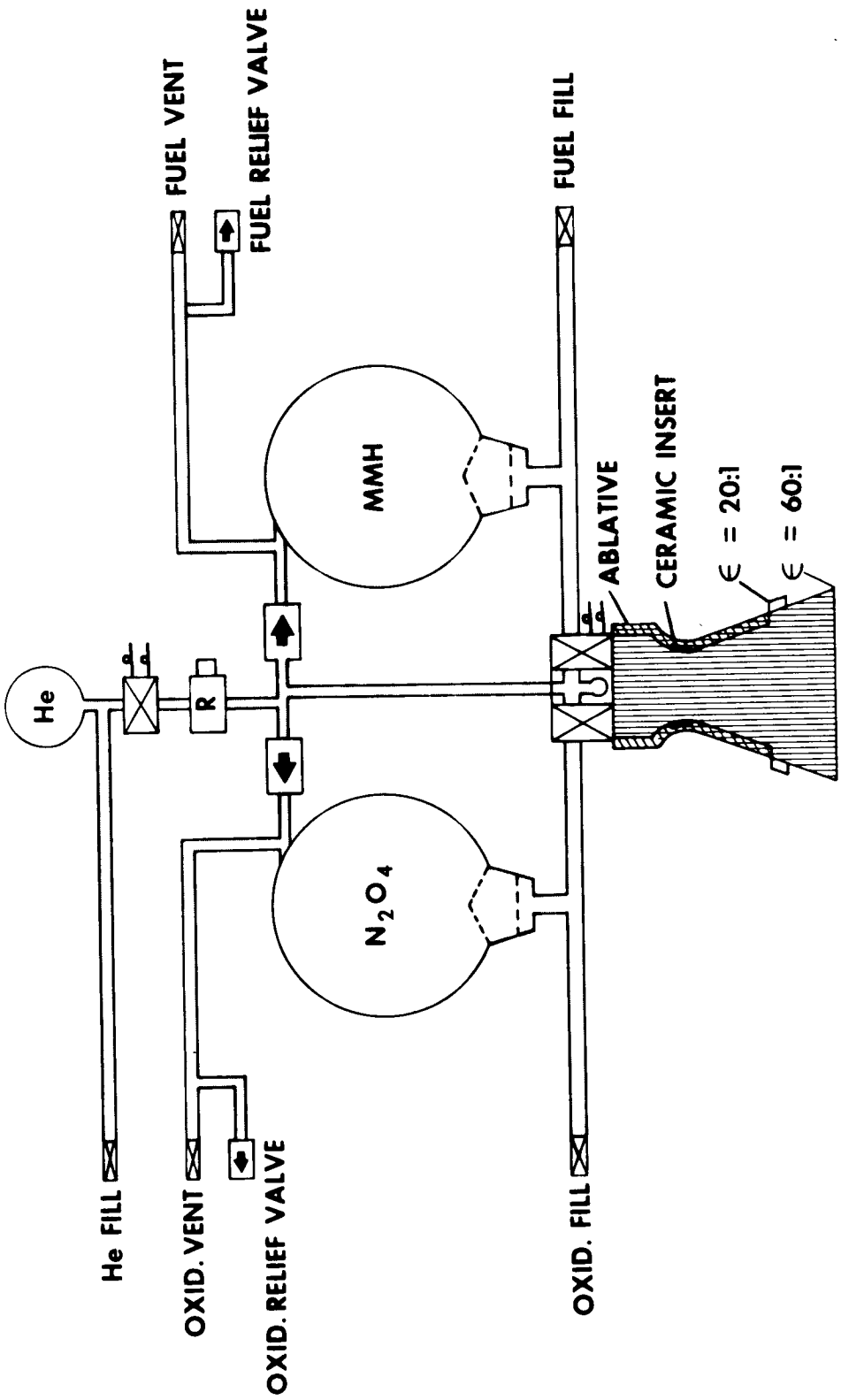


Fig. 5-46 Primary Propulsion System Schematic

Table 5-34

ORBITER PRIMARY PROPULSION SYSTEM CHARACTERISTICS

Parameter	Value
Thrust	750 lb_f
Area Ratio	60:1
Chamber Pressure	150 psia
Mixture Ratio	1.6:1
Minimum Impulse Bit	100 lb_f-sec
Specific Impulse	302 $\frac{lb_f\text{-sec}}{lbm}$
Thrust Duration Time	400 sec
Number of Starts	4
Tank Operating Pressure	250 psia
Helium Load	3.4 lbm
Helium Tank Volume	1.08 ft^3
Oxidizer	Nitrogen Tetroxide
Fuel	Monomethyl Hydrazine
Ox Tank Volume	7.4 ft^3
Fuel Tank Volume	7.4 ft^3

Thrust Vector Control System. Figure 5-47 shows a gimbal ring assembly at the throat of the thrust chamber. This location was selected to provide the longest possible moment arm, thereby minimizing TVC requirements. An electromechanical gimbal assembly attached at this point will provide two-axis attitude control during engine firing. The third axis control will be provided by the reaction control system. The electromechanical system was selected primarily due to the greater innate reliability, compared to a hydraulic system which requires liquid storage during the long mission life.

Pressurization. The pressurization system utilized flight-proven concepts and hardware throughout. Helium was chosen as the pressurant, due to significant weight savings compared to other pressurants. Leak potential is theoretically higher with helium than

Table 5-35

PRIMARY PROPULSION SYSTEM WEIGHT BREAKDOWN

Equipment	Weight (lb)
Engine assembly (including gimbal ring)	21.8
Propellant Tanks*	31.0
Fill valves	0.5
Lines and fittings	4.3
He tank	23.7
He gas	3.4
He fill valve	0.2
He tank support	2.0
Pressure regulator	1.0
Gas filter	0.5
Check valves (2)	2.0
Relief valves (2)	2.0
Thrust structure	3.0
Residual propellants	10.0
Gimbal actuator system	7.0
Start valve	1.5
TOTAL	112.1

*The fuel and oxidizer tank weight is made up as follows:

Tank shell	10.6
Weld lands	0.6
Attached flange	1.2
Sump	1.3
Slosh and vortex baffles	1.8
TOTAL	15.5 lb per tank assy.

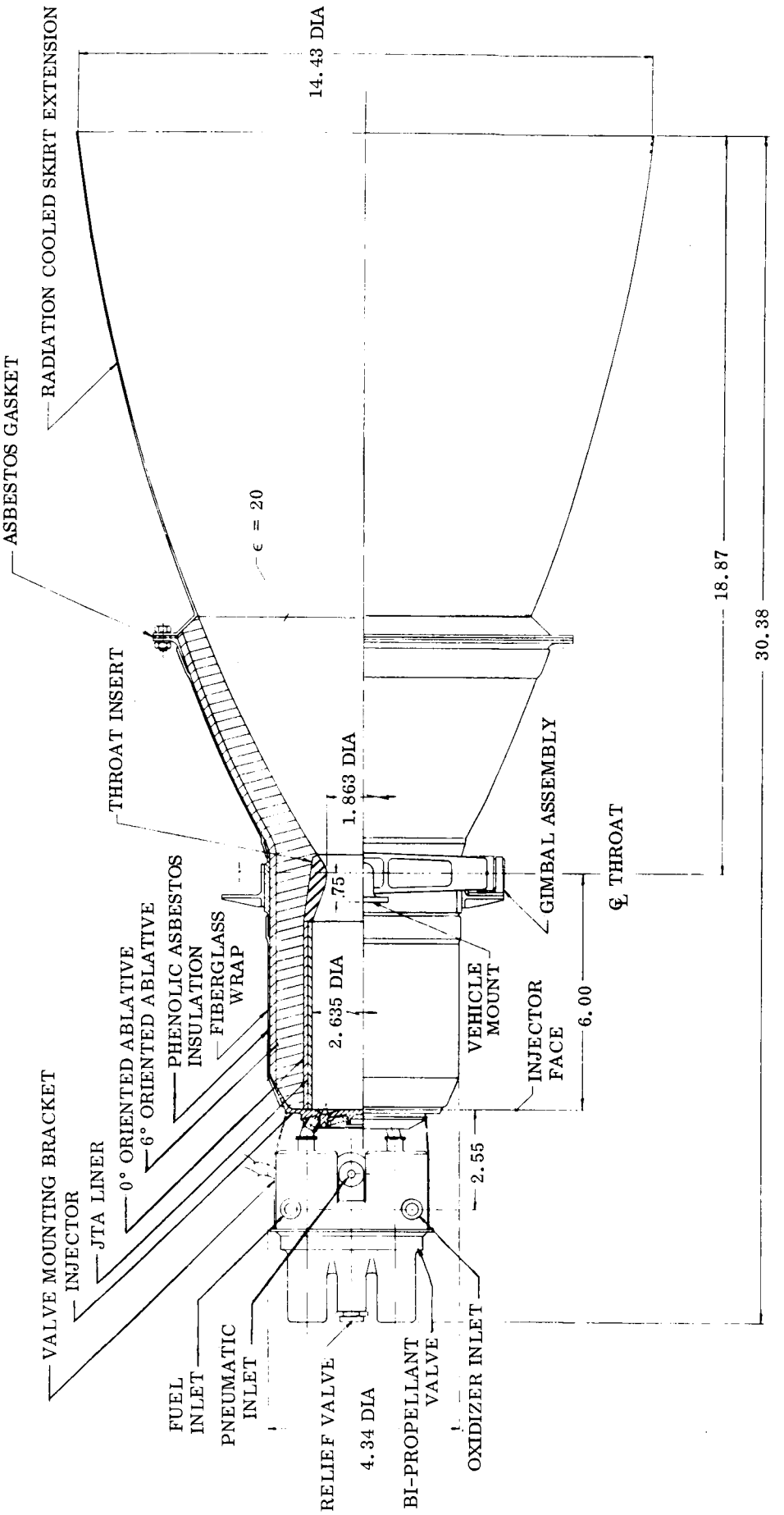


Fig. 5-47 Primary Propulsion System Thrust Chamber

other available gases. The successful experience with helium management and storage on LMSC programs to data, using a maximum of welded joints and stringent check procedures to avoid leaks, indicates that vehicle reliability and life requirements should not be compromised.

Propellant Containment and Scavenging System. The Mars orbiter stage is equipped with equal volume spherical propellant tanks. The shape of the outlet section is modified to minimize residual propellants. This may be accomplished by extensive modification to the hemispheres or minimum hemisphere modification and the addition of propellant sumps.

Since more than one restart is required, either a propellant settling system or passive containment of the restart propellants at the tank outlet must be provided to assure reliable gas-free restart.

A passive propellant containment system with sumps was chosen, based on present Agena containment/scavenging system design, since it provides the following advantages:

- Minimum stage burnout weight
  - Minimum residual propellants
  - Minimum propellant positioning hardware
- Maximum restart reliability
  - Restart propellants positioned over tank outlet at all times (no moving parts)
  - No auxiliary thrust device operation required prior to restart
  - Multiple restart capability
- Minimum stage cost
  - Sumps inexpensive to fabricate
  - Passive containment system fabricated from screen material
  - No auxiliary thrust system required
  - Identical oxidizer and fuel containment and scavenging system parts

After separation from the booster, surface tension forces will shape the ullage bubbles into spheres and aerodynamic drag forces may position them over the tank outlets. The containment screen acts as a "bubble barrier" to prevent gas from entering the sumps. Since there is negligible volume between the propellant valves, and the injector and propellant preflow is small, the ΔP across the containment screen is insufficient to allow penetration of any bubble resting on the screen at first start. At chamber ignition, the resultant buoyant force on the ullage bubbles will immediately eject them to the top of the tanks.

After first and subsequent shutdowns, the ullage bubbles will again assume spherical shapes and stable positions in the tanks. Calculations show that even for minimum propellants at final restart, the ullage bubble will be essentially spherical, will be kept out of the sump by the containment screen, and should not enter the sump during restart.

During coast periods, heat-soak back to the propellant valves will raise the temperature and vapor pressure of adjacent propellants. However, the temperature rise will never be sufficient to allow propellant boiling. Hence, no check valves are required to maintain the sumps full of propellants.

During depletion, the sump acts as a reservoir maintaining flow to the thrust chamber as the terminal quantities of propellants flow into them from the tanks. Further, they are each equipped with a conical screen which dissipates any rotary or vortex motion. Based on these factors and the shape of the sumps, low propellant residuals are assured.

Spacecraft Interface. The forces caused by the impingement of main engine exhaust gases on the solar panels have been estimated for gimbal angles of 0 deg and ±5 deg. For a gimbal angle of zero, the total force on each of the two panels nearest the engine is estimated to be approximately 3×10^{-4} lb. The maximum unbalanced force results when the engine is gimballed to its maximum capability in the direction of one of the panels. In this case the total force on one panel is predicted to be approximately

2×10^{-3} lb. The force on the other panel may be considered negligible in comparison. Because of the high degree of expansion experienced by the exhaust gases before they reach the solar panels, the free-stream temperature will be very low, probably less than 100° R. As the gases impinge on the panels their temperature will increase as kinetic energy is converted into thermal energy. However, since the gas density is very low at this point the total energy involved is extremely small, even for a large gas temperature increase. Hence, the solar panels should experience almost no temperature change during engine burn.

5.4.3 Reaction Control System

It is required that the reaction control system be capable of providing a minimum impulse bit of 2.6×10^{-3} lb_f-sec in a 20 ms pulse. Based on LMSC test experience on similar systems, a square wave approximation of the actual thrust time profile is 0.6 times the product of maximum thrust level and pulse width. The required thrust per jet is therefore 10.84×10^{-2} lb_f. For a complete mission, i.e., Earth to Mars, plus a 6-mo Mars orbit life, the total impulse requirement is about 435 lb_f-sec. A total impulse of 1305 lb_f-sec has been used for this design, as explained in Section 5.1. This philosophy is consistent with the Mariner C reaction control system.

The following four propulsion systems currently under development or in flight status were evaluated for use in the reaction control system:

- Hydrazine monopropellant
- Nitrogen cold gas
- Encapsulated solid propellant
- Subliming solid

The only configuration of the encapsulated solid system which offered a weight advantage over the cold gas system involved the use of a multidirectional motor which was not available in a reliable form. In addition, confidence has not been established in the tape-feed system, particularly regarding tape tear.

The subliming solid system shows a definite weight savings (at least 15 lb) over the nitrogen cold gas system. Although it is less complex and inherently more reliable, it does not have the flight experience of the nitrogen system. Additionally, power is required for thermal control.

The hydrazine plenum system shows a weight advantage about equal to that of the subliming solid system, but it is far more complex, and also has no flight experience. Hence the N_2 cold gas system was chosen for the preliminary design, with the subliming solid system considered as a possible state-of-the-art improvement should reliable experience be gained on forthcoming flights.

The nitrogen cold gas system weight breakdown is given on Table 5-36. This data is based on a nozzle optimization study performed on the present Agena cold gas system. In this study, area ratio was varied while holding thrust, chamber pressure, and total impulse constant. Total system weight was calculated and plotted as a function of area ratio in Fig. 5-48 for a total impulse of 1284 lb-sec, later increase to 1305 lb_f-sec.

Table 5-36

NITROGEN COLD GAS SYSTEM WEIGHT BREAKDOWN

Item	Weight (lb)
Nitrogen gas	19.0
Nitrogen tanks (2)	24.0
4 Jet manifold assembly (2)	2.5
2 Jet manifold assembly (2)	1.5
Plumbing and line fittings	4.0
Gas Regulators (2)	2.0
TOTAL	53.0

Nozzle area ratio	ϵ	= 15:1
Specific impulse	I_{sp}	= 68 sec
Tank pressure	P_t	= 3000 psia

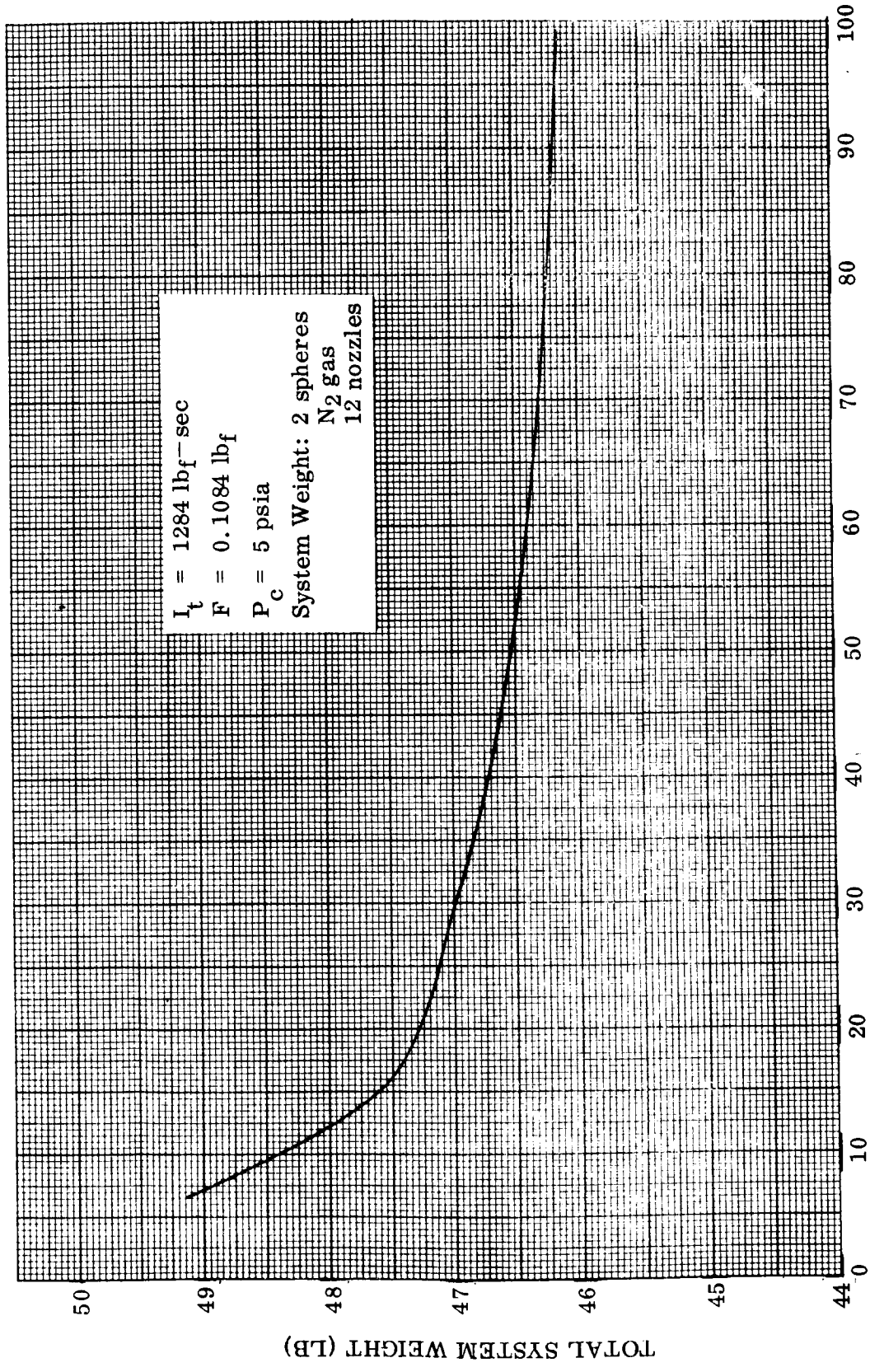


Fig. 5-48 Attitude Control Nozzle Optimization

340

The selected reaction control system is shown schematically in Fig. 5-49. This system design is identical to that used on Mariner C and is completely redundant. The two systems are designed to operate simultaneously. Each unit has a nitrogen gas bottle (standard Agena item), a pressure regulator (Mariner C hardware), six valves and six nozzles with welded joints to minimize leakage possibilities.

The valves and nozzles are clustered at the ends of the solar panels, four on one and two on the adjacent panel. This provides equal pure couple control in 3 deg of freedom. Each nitrogen bottle is loaded with 1.5 times the amount necessary for a complete mission. This assures that if a valve sticks open from the time of booster separation, enough gas will remain in the bottle of the other unit to allow accomplishment of a complete mission, as explained in Section 5.1.

5.4.4 Capsule Guidance Propulsion System Selection

Capsule propulsion system requirements are:

Velocity Increment	50 meters/second
Maximum Total Impulse	765 lb_f-sec
Burn Time	~10 sec
Thrust	~ 75 lb_f
Sterilization	By heat, as defined in Section 5.8
Electromagnetic Interference (EMI)	No metallic components or exhaust products
	No ionized exhaust products

The capsule propulsion system is used to direct the capsule toward the surface of Mars with a single short burn after mechanical ejection from the orbiter. As part of the lander package, the capsule propulsion system is subject to the sterilization requirements. A preliminary survey of heat sterilizable propellants conducted for this study indicated that such motors are not available off-the-shelf. However, results of the survey indicate that sterilizable propellants are presently under development, and a motor for this usage could be developed within the proposed schedule. This is

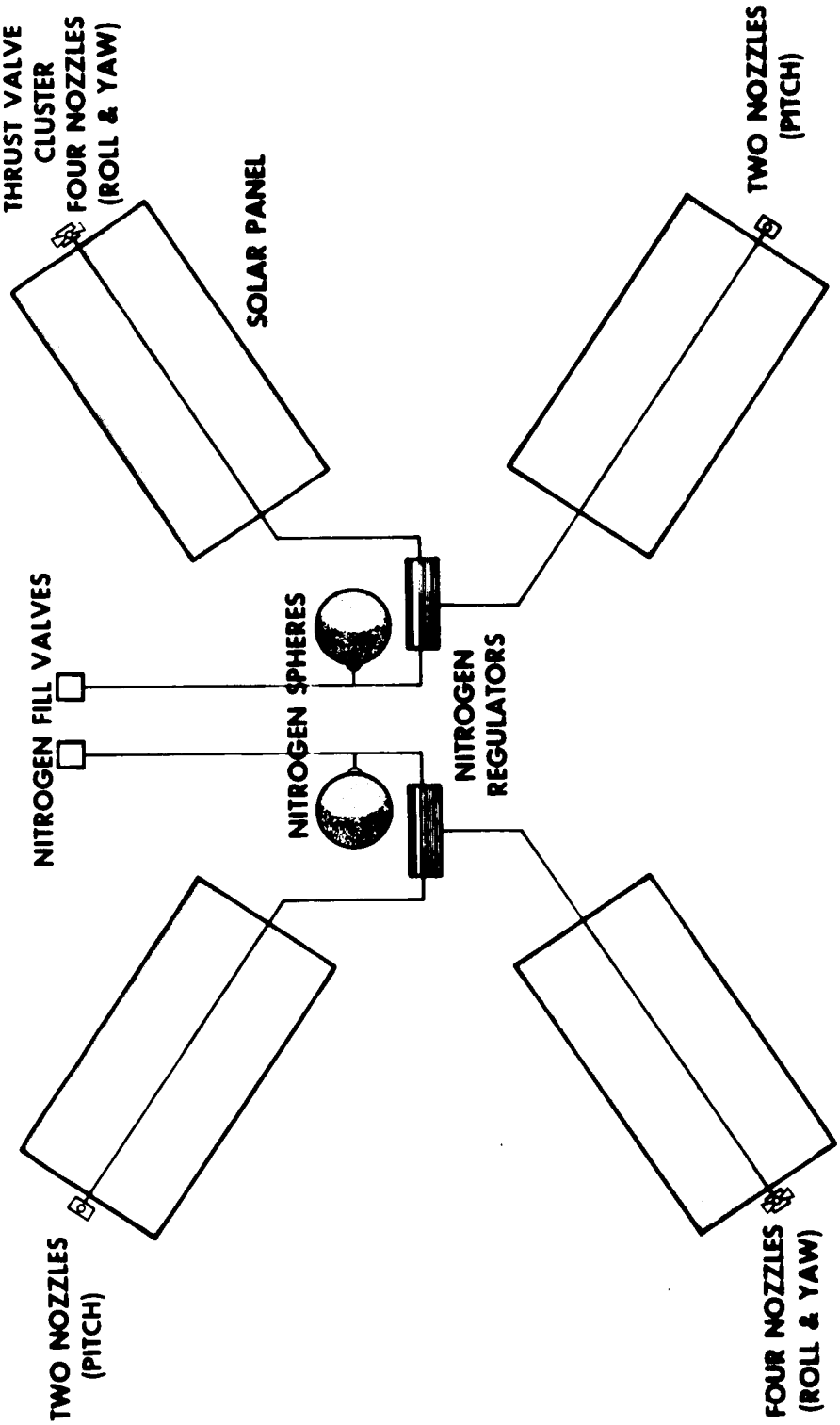


Fig. 5-49 Reaction Control System – Cold Gas

another long lead time item, requiring at least 12 mo through qualification, according to discussion with Aerojet & Atlantic Research Corp. personnel. Sterilizable propellants under development include ARC Arcite 413 and AGC JATO propellant.

Arcite 413, used in the Terrior Weapon System, is cured at a constant temperature of 350° F, illustrating the feasibility of sterilizing solid propellants. A quoted specific impulse of 220 sec yields a system weight of 6 lb. Since total impulse required is low and high reliability is necessary, a solid propellant motor is a good selection.

Presently developed and flown propellants which yield no metallics in the exhaust gases can satisfy at least part of the EMI requirements. Both vendors indicated non-metallic motor uses and thrust chamber nozzles could be readily developed. The exclusion of ionized particles in the exhaust requires further examination.

5.4.5 Capsule Spin Motors Selection

In the proposed design, the capsule, after ejection from the orbiter, is given a spin rate by two small solid motors for thrust vector control during guidance rocket firing. Prior to ignition of the guidance rocket, the spin motors are ejected with the sterilization shroud. Hence the sterilization requirement does not apply to the spin rockets. Since many motors are available off-the-shelf that will fill the requirements, no attempt was made at this time to select any particular one.

5.5 THERMODYNAMIC ANALYSIS

The thermodynamic analyses have been limited to parametric studies and general energy balances to determine steady-state temperature levels of the spacecraft. This method of analysis was the most expedient, due to the various configurations considered and the limited detail available on spacecraft hardware.

Thermal control of the Mars orbiter will most likely be accomplished by some combination of passive and active temperature control. Passive temperature control involves the use of specific surface finishes, insulation, isolators, heat-sinks, and optimum equipment arrangements to properly manage all of the thermal energy. Active temperature control systems may consist of a shutter system which exhibits different effective surface finishes as a function of temperature, variable conductance devices, thermostatically controlled heaters, and circulating liquids or vapors with a space radiator system each by itself or in any combination required to maintain near optimum temperature levels.

The phases of the Mars orbiter mission considered were:

- Prelaunch and Ascent
- Transfer Orbit
- Mars Orbit

5.5.1 Prelaunch and Ascent

During prelaunch operation, normal spacecraft cooling techniques will be used to absorb the external heat loads and any internal power dissipation. The aerodynamic shroud, which protects the spacecraft from the ascent heating pulse, may be exposed to the external environments of solar radiation (direct, reflected, and diffuse), convective heat transfer with the ambient air, and radiation heat transfer with the surroundings depending upon the prelaunch cooling method utilized. Direct internal air conditioning or a shroud cooling blanket, or a combination of the two, may be utilized depending

upon the power dissipation rates and desired spacecraft temperature levels. Direct internal air conditioning is usually the most effective.

During the ascent phase of flight, with the shroud on, shroud insulation will not be required to maintain low back face temperatures; adhesive backed foil may be necessary, however, to reduce radiation exchange with the spacecraft. Maximum internal backface temperature of the honeycomb section has been predicted to be less than 200°F for the OAO mission which utilizes the identical shroud.

5.5.2 Transfer Orbit

During the long transfer orbit (~270 days), the spacecraft remains solar oriented except during midcourse corrections. Due to the transfer orbit trajectory to Mars away from the sun, the solar energy varies from a maximum of approximately 460 $Btu/Hr/Ft^2$ at the time of Mars encounter (Fig. 5-50). The higher values of incident solar energy is due to the Earth being near its perihelion at the anticipated launch time and the spacecraft trajectory which falls inside the Earth's orbit.

Passive Thermal Control. With a passive thermal control system the spacecraft temperatures will reflect the decrease in available solar energy as the spacecraft approaches Mars. Passive thermal control may be feasible, however, depending upon the temperature limits of the critical spacecraft components. Surface finishes can be selected that will result in maximum design temperatures near Earth and temperature levels nearer the lower limits at Mars. Passive thermal control feasibility will then depend upon the Earth to Mars temperature excursion falling within the allowable design temperature range of the sensitive components in the spacecraft.

Specific studies have been conducted to demonstrate the feasibility of passive thermal control. A range of surface finishes was selected for solar oriented portions of the vehicle while low emittance finishes were assumed on the remaining surfaces that radiate to outer space. The variation in surface temperature as a function of surface α/ϵ is shown in Fig. 5-51 for internal power dissipation rates of 100, 150, and 200 w for values of the solar constant near Earth and at Mars encounter. The temperature

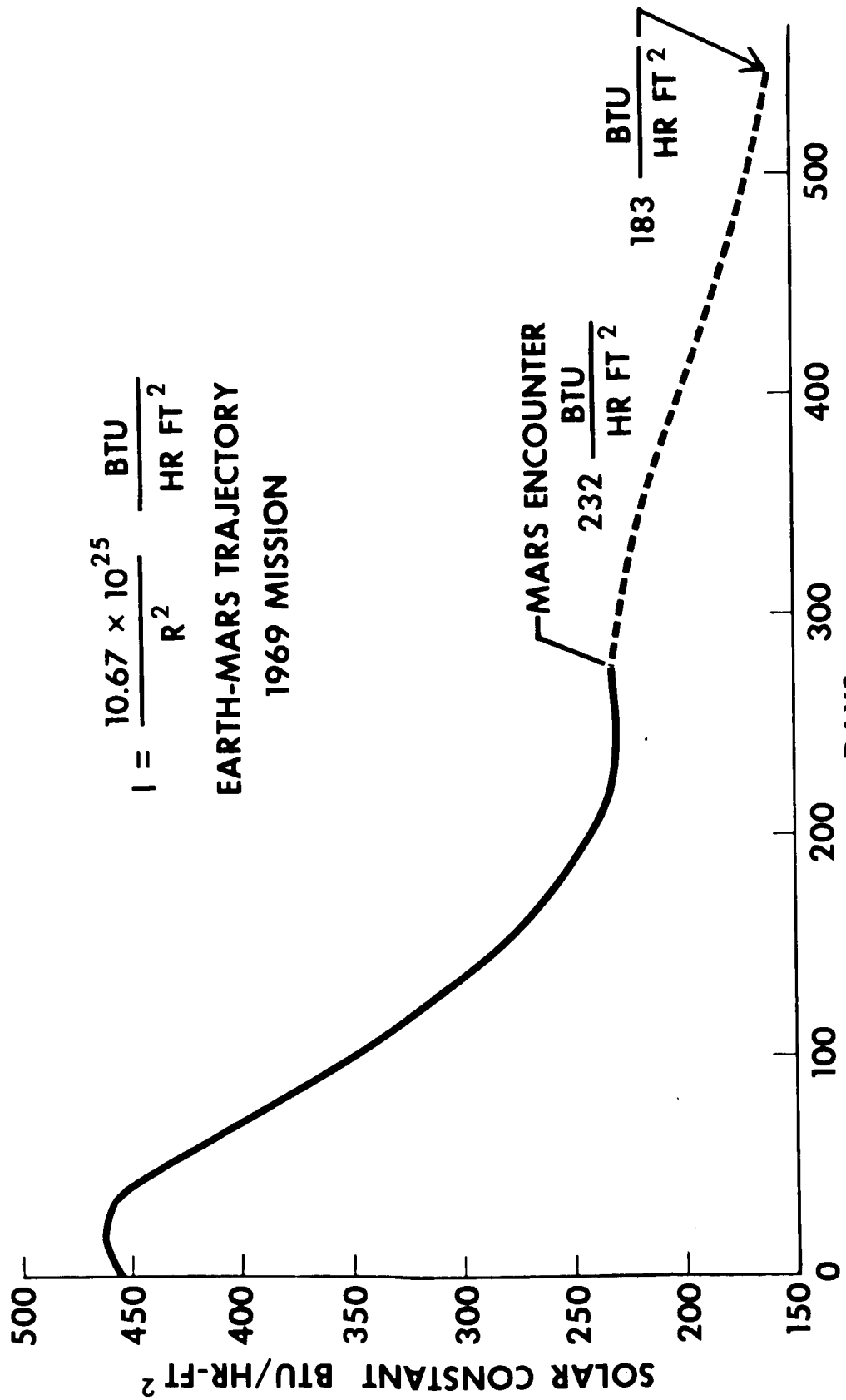


Fig. 5-50 Solar Constant, Earth-Mars 1969 Trajectory

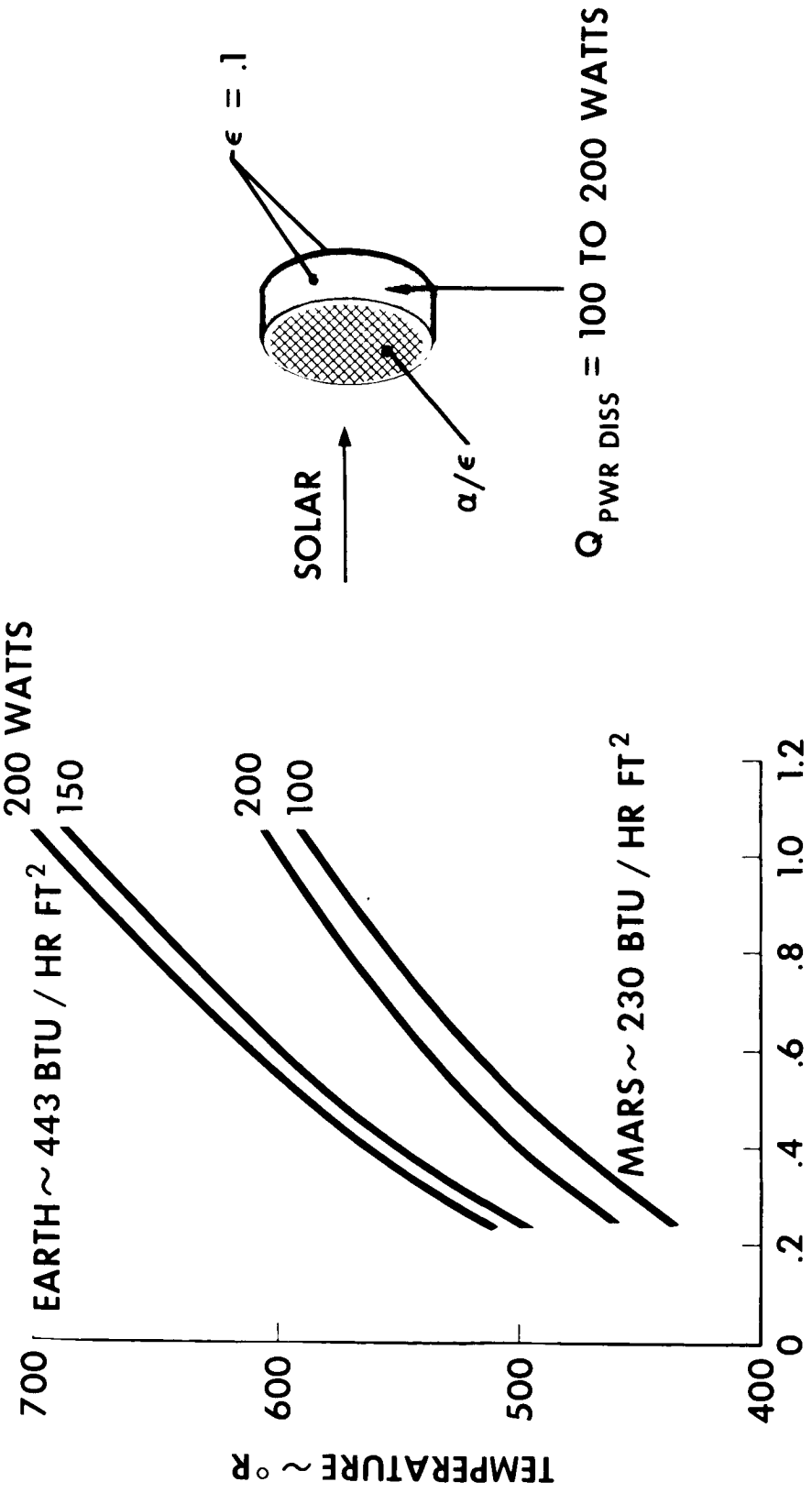


Fig. 5-51 Orbiter Temperatures vs. α/ϵ Ratio

excursions (Earth to Mars) vary from 60° F with an α/ϵ ratio of 0.24 to 100°F with an α/ϵ ratio of 1.06. Considering that most electronic components are qualified to the LMSC 6117B environmental specification temperature range of -30 F to +160°F, the provision of an α/ϵ ratio of 0.55 would result in temperatures below 150°F near Earth and approximately 50°F at Mars.

The possibility of using the increase in solar absorptance (α), that occurs when some paints are exposed to ultraviolet radiation, was considered in order to make better use of the available solar energy at Mars. Figure 5-52 presents the equivalent sun-hours that a solar oriented surface will experience during the transfer orbit. With the sun-hour curve and LMSC Thermophysics Laboratory data of Ref. 9, solar absorptance curves were determined for three white paints as a function of time. Studies of the orbiter were then conducted using both a degrading White Silicone paint and White Skyspar paint on the solar oriented surfaces. Figure 5-53 presents the results of these studies. Assuming that the internal power dissipation rate of the orbiter will be approximately 200 w, the White Silicone front face results in temperatures ranging from 117°F near Earth to 48°F at Mars encounter, whereas the White Skyspar would result in a temperature range from 170°F to 96°F. From the results of the orbiter studies using the degrading white paints, it is evident that the degradation is too rapid to obtain the desired constant temperature during the transfer orbit.

Solar panel temperatures were determined for the mission considering only the effects of incident solar energy. An α/ϵ ratio of .85/.85 for the solar cells and a backside emittance (ϵ) of .90 (JPL values) were used for the analysis. The resultant temperature history of the solar panel is presented in Fig. 5-53. A maximum temperature of 139°F is reached after 20 days and drops to 45°F at Mars encounter and subsequently to 16°F at the end of the Mars mission.

Passive thermal control appears feasible based upon the temperature excursions expected for the mission. Further detailed analyses are required to determine temperature histories of the critical spacecraft components.

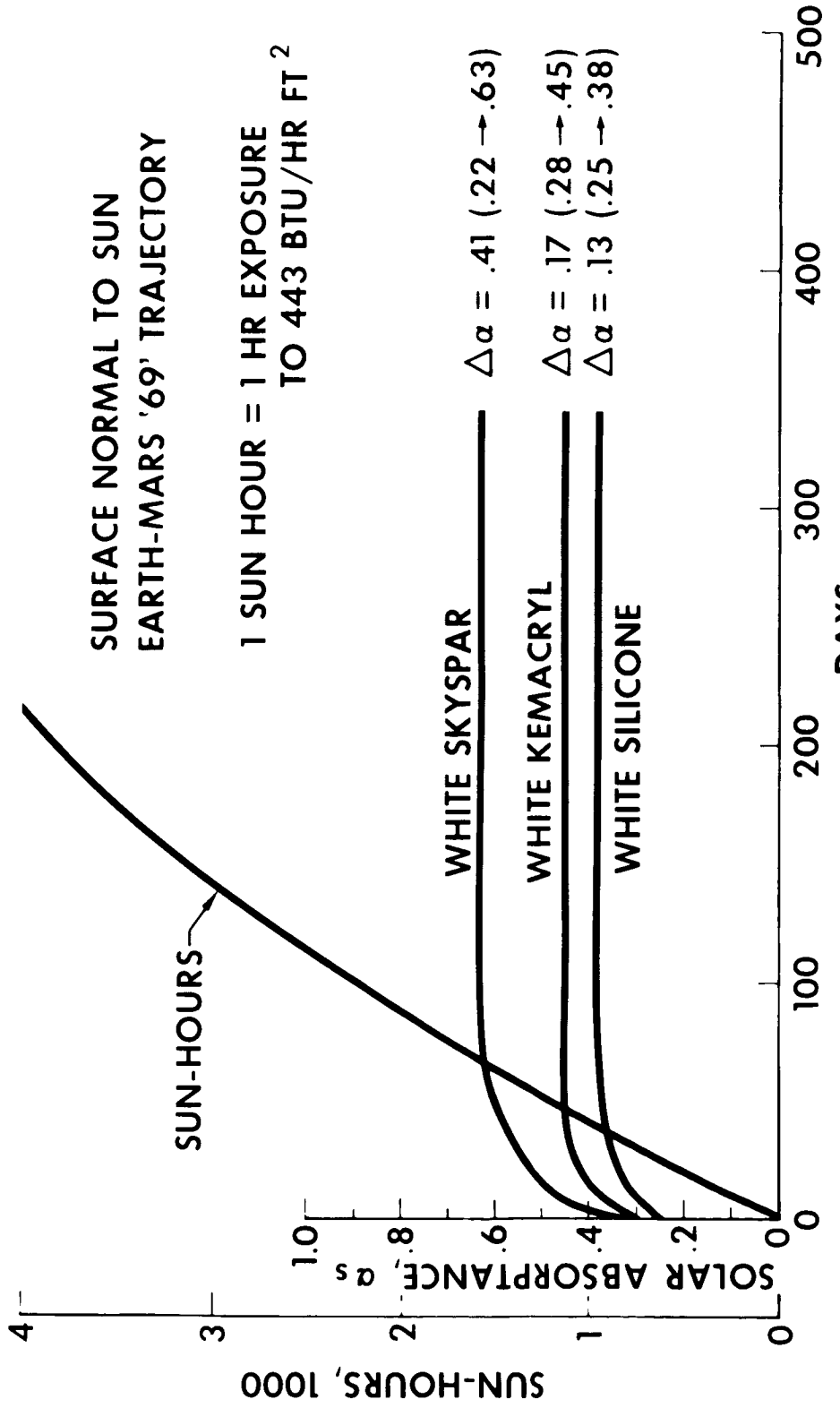


Fig. 5-52 Degradation of White Paints, Surface Normal to Sun, Earth-Mars 1969 Trajectory

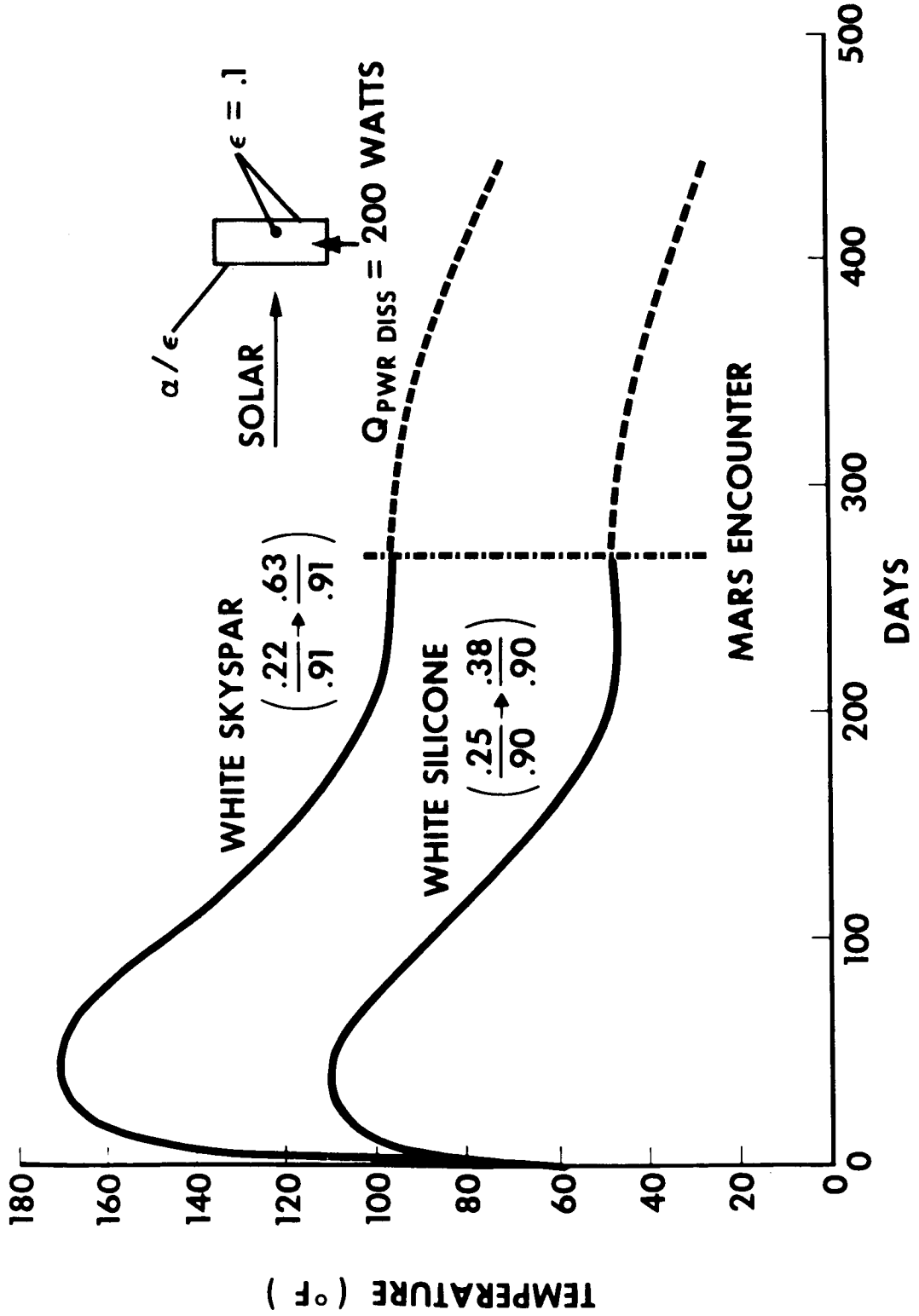


Fig. 5-53 Orbiter Temperatures, Earth-Mars 1969 Trajectory

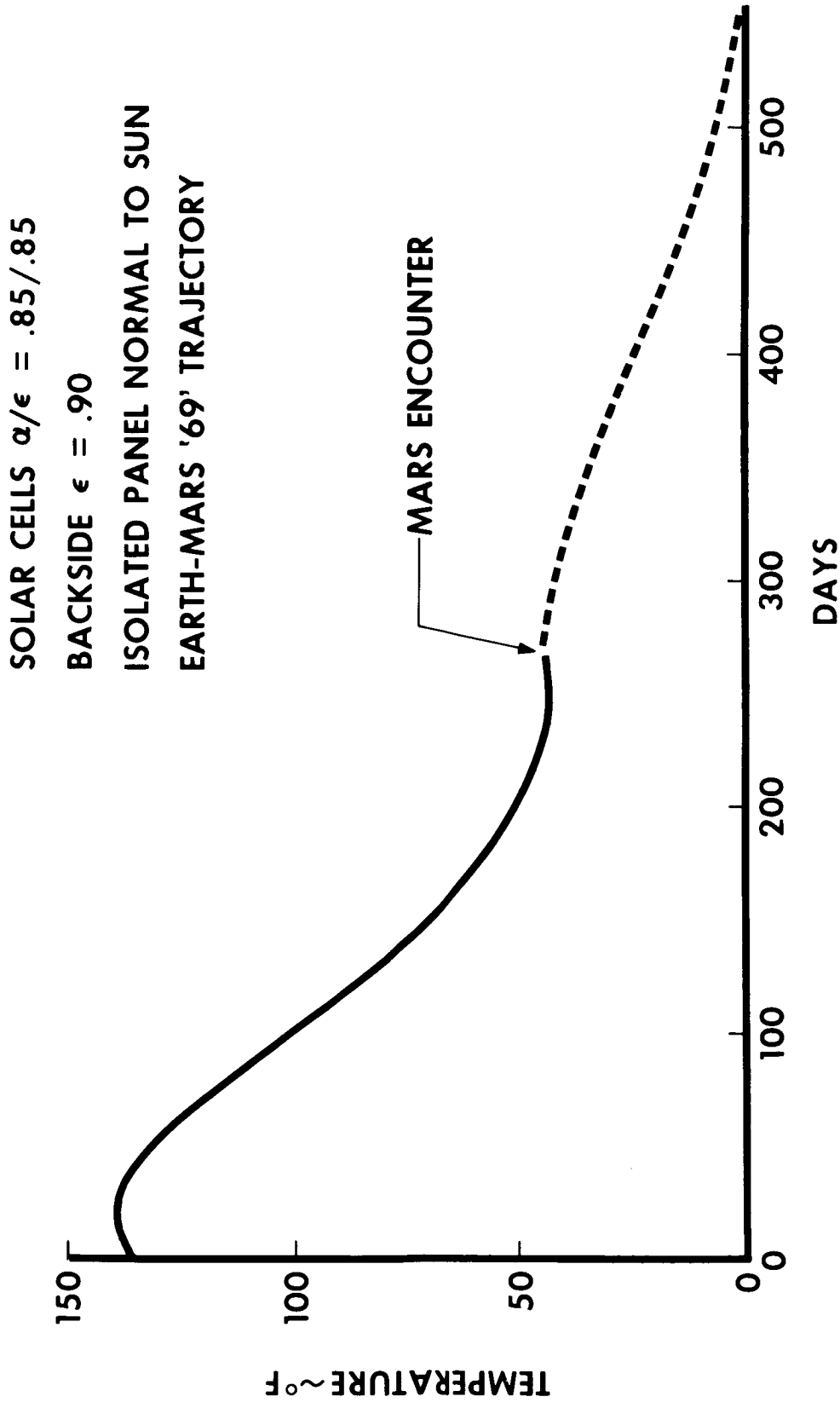


Fig. 5-54 Solar Panel Temperatures, Earth-Mars 1969 Trajectory

The capsule (atmospheric or biological) will be essentially shielded from the sun due to its location behind the orbiter. The thermal control concept for the capsule is to minimize the energy losses by the use of isolators, insulation, low emittance surfaces throughout, and the use of heater power. The equipment section with the scientific instruments will be surrounded with insulation and low emittance surfaces, and thermally isolated from the main structure. Equipment arrangement will locate the temperature-sensitive components in the center surrounded by the less sensitive items. Some solar energy is incident upon the capsule periphery where the spin rockets and separation charges are located, and will be adequate to maintain these components at acceptable levels.

Active Thermal Control. An active thermal control system of shutters as utilized on the Mariner C spacecraft can be used if passive control is inadequate. With the use of shutter systems, it would be possible to dissipate more energy near Earth and less at Mars to result in more uniform temperatures throughout the mission.

5.5.3 Mars Orbit

During the Mars Orbit, the solar constant will decrease from 232 Btu/Hr/Ft^2 to approximately 183 Btu/Hr/Ft^2 after 180 days. The sun remains the most significant energy source to the orbiter along with the internal power dissipation rates.

Typical Mars heat rates were calculated for the nominal orbit using the heat flux program developed for JPL (Ref. 10). Figure 5-55 presents the absorbed heat rates (Btu/Sec) upon one solar panel. The heat fluxes upon the remaining surfaces were also calculated but are not presented. With the maximum absorbed heat fluxes, the resultant solar panel temperature would be 80°F as compared to 45°F with only solar energy incident upon the panel. The Mars heat rates are incident upon the spacecraft approximately 5 percent of the orbit only; therefore, solar energy remains the prime energy source.

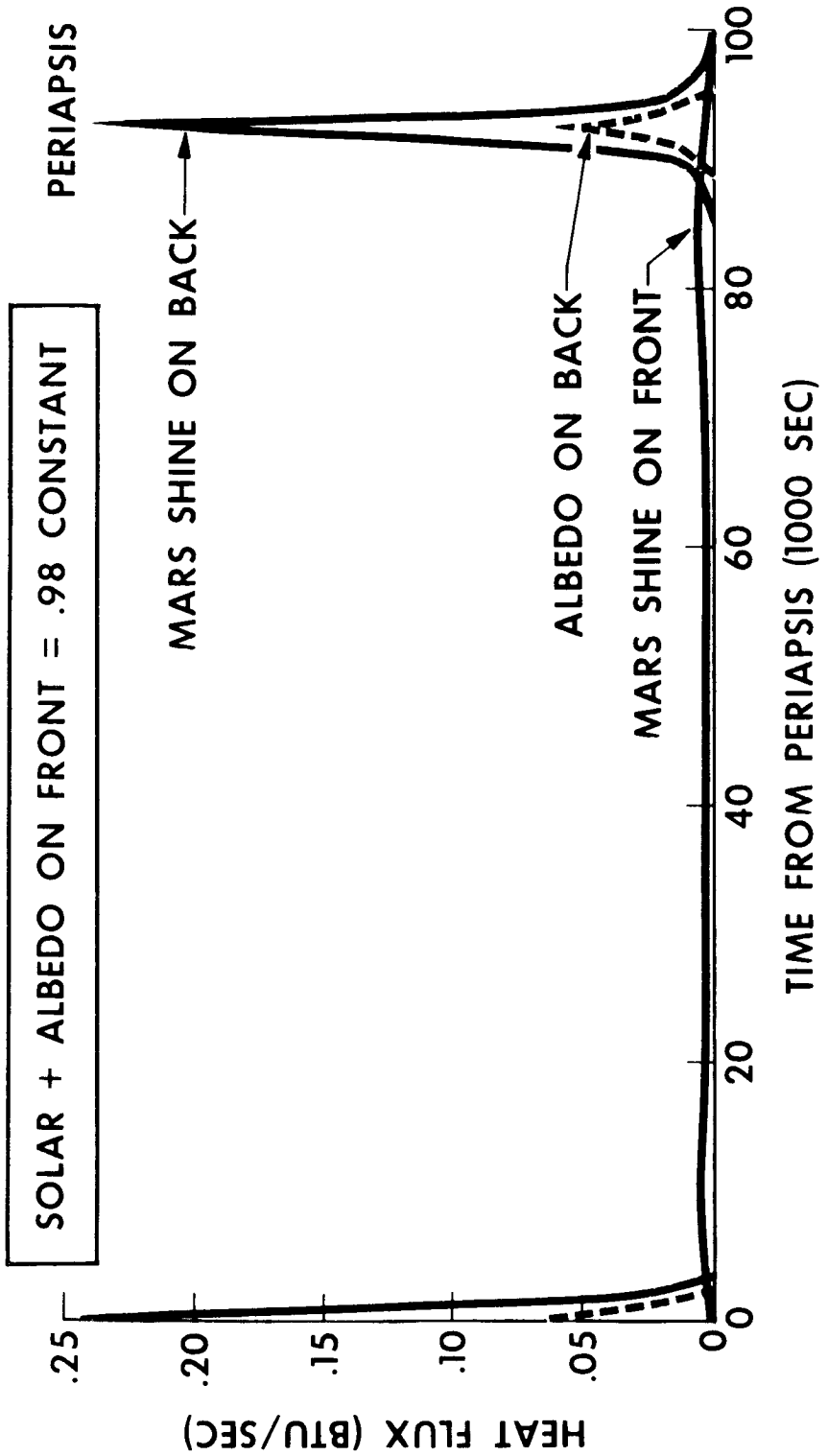


Fig. 5-55 Absorbed Fluxes on Typical Solar Panel

The decrease in solar energy from 232 Btu/Hr/Ft^2 at encounter to 183 Btu/Hr/Ft^2 at the end of the mission results in a 30°F temperature drop of the solar panels and a 20 to 25°F temperature drop for the orbiter. The terminal point of the Mars orbit mission, with its low value of incident solar energy will be the design condition for the thermal control system.

5.5.4 Venus Mission

The Venus mission with its trajectory in toward the sun presents a high temperature problem instead of a low temperature problem as is the case for the Mars mission. The solar constant will increase from 443 Btu/Hr/Ft^2 at Earth to 863 Btu/Hr/Ft^2 at Venus. The effect of the increased solar energy upon a solar panel oriented normal to the sun will raise its temperature from 135° F at Earth to 240° F at Venus. In order to obtain lower temperatures, if desired, the panels may have to be oriented at an angle off of normal from the solar vector. Areas of low α/ϵ surfaces between cells should also be considered. The spacecraft will require a low α/ϵ surface on the front face to minimize energy gains and high emittance surfaces on the remaining faces to radiate sufficient energy away in order to maintain acceptable temperature levels. The thermal control concept will be to design for minimum temperatures at Earth in order to obtain desirable temperature levels at Venus.

5.6 AEROTHERMAL ENVIRONMENT

The lander vehicle will be subjected to a relatively mild aerothermal environment during entry of the Martian atmosphere. This section describes the environmental conditions and associated heat transfer. Also discussed briefly are the prerequisite high-temperature properties and structure of the Martian atmosphere.

5.6.1 Atmospheric Characteristics

Experimental observations of the Martian atmosphere have been insufficient to afford an accurate definition of its characteristics. The major constituents are believed to be carbon dioxide, nitrogen, and argon; their relative concentrations are ill-defined. Surface pressure and atmospheric temperature distribution are known only within relatively large ranges. Several possible atmosphere models were provided by the contracting agency for the conduct of this study (Ref. 2). The models identified as G and K have been utilized in evaluation of the environment; they represent the extremes with respect to both density gradient (in the altitude range of thermal interest) and composition, the factors most affecting heat transfer.

The high-temperature thermodynamic and radiative properties of the Martian-atmosphere gas mixture have been obtained from the results of a separate NASA study conducted by LMSC (Refs. 11 and 12). None of the particular mixtures considered in the LMSC work are identical to those of the adopted model atmospheres; however, the two mixtures described below are representative of the extremes and therefore have been used.

	Volume Concentration	
Constituent	Mixture 1 (≈ K)	Mixture 2 (≈G)
CO_2	0.16	0.64
N_2	0.76	0.28
A	0.08	0.08

References 11 and 12 describe, in addition to the computed properties of these mixtures, the basic techniques and assumptions utilized in generation of the results. It is noted that in the temperature range of interest here, the LMSC steradiancy prediction, shown for a representative pressure in Fig. 5-56, is somewhat less than that observed by James and that predicted by Spiegel and Horton (Ref. 13). The difference between the LMSC predictions and those of Spiegel and Horton arises from two sources. First, Spiegel and Horton employed the Kivel and Bailey prediction of steradiant emissivity per CN particle which is greater than the result obtained by Weisner at LMSC. Second, the CN particle concentration computed by Spiegel and Horton is greater; evidently the heats of formation used for the CN molecule in the two equilibrium-composition calculations differ.

5.6.2 Entry Trajectory

The lander vehicle enters the atmosphere ballistically at a speed of 21,000 ft/sec and at an entry angle in the range from 30 deg to 60 deg. As indicated in Figs. 3-32 and 3-36 the vehicle enters in an asymmetric attitude, but the angle of attack oscillation is rapidly damped.

A typical entry trajectory is shown in Fig. 5-57. The vehicle decelerates at relatively high altitudes as a consequence of its low ballistic coefficient (W/C_DA) of 7 lb/ft^2.

5.6.3 Shock Layer Flow

Thermodynamic conditions immediately behind the shock are simply determined assuming thermodynamic equilibrium by application of the conservation equations. Typical results obtained for conditions behind the normal portion of the shock are described as a function of time in Fig. 5-58; they are for the trajectory shown in Fig. 5-57. The enthalpy decreases monotonically for the time period shown. The enthalpy reference is that of the elements in their standard state at 298° K. The pressure initially rises as the vehicle descends, peaking at a value less than 0.2 atm.

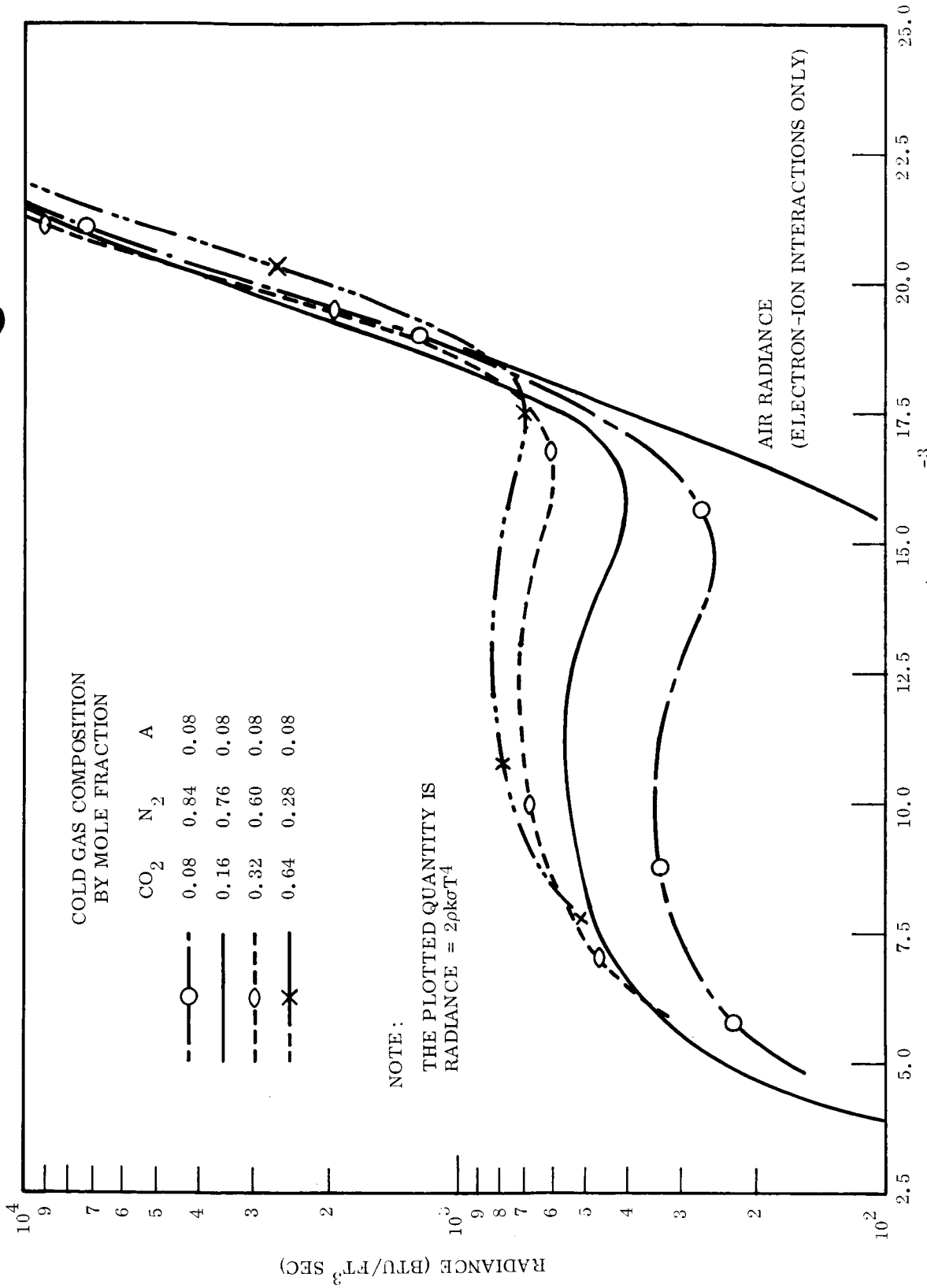


Fig. 5-56 High Temperature Radiance of Several N_2, CO_2, A Gas Mixtures at 1.0 Atmosphere of Pressure

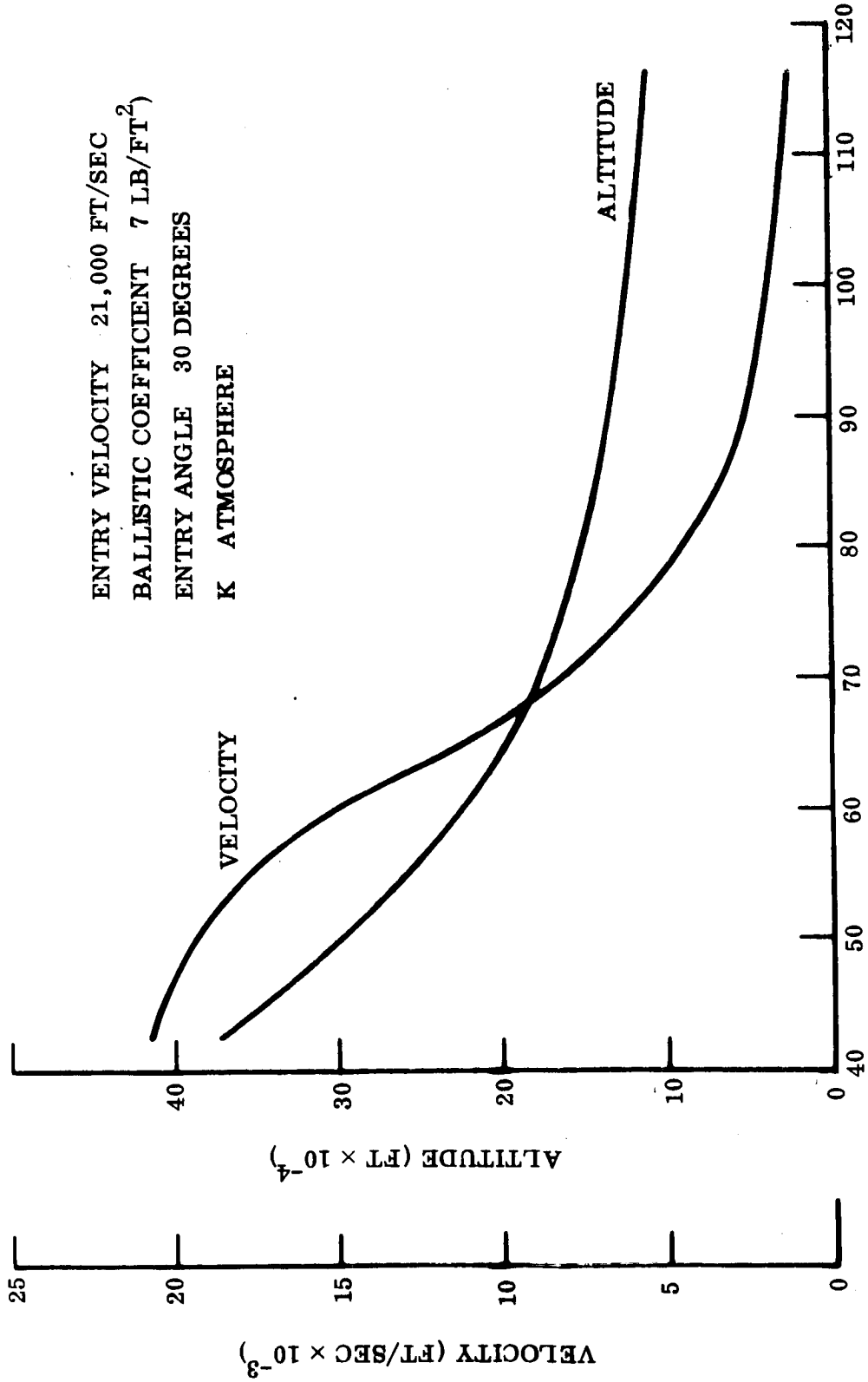


Fig. 5-57 Heat Shield Design Trajectory for Mariner Capsule

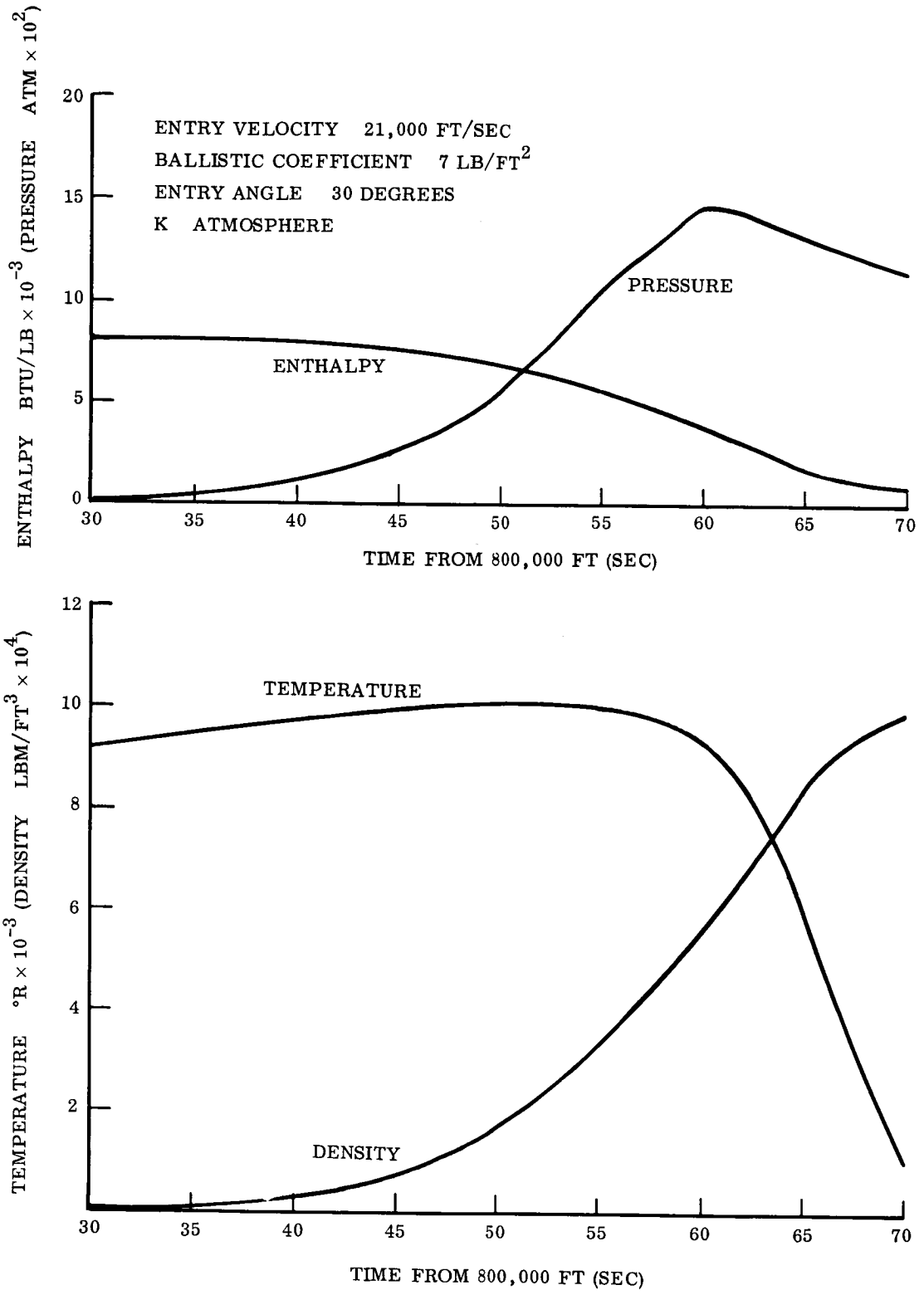


Fig. 5-58 Shock Layer Thermodynamic Conditions

for this trajectory. The maximum temperature in the shock layer is approximately 10,000° R; the density is low during the period of high temperatures, being of the order of 1/100 of earth sea-level density.

The pressure distribution over the surface of the vehicle has been established empirically from the data reported in Refs. 13 and 14. The zero-angle-of-attach distribution is described in Fig. 5-59. For this case the pressures on the large radius sector are somewhat less than predicted by Newtonian theory; even so, the pressure gradient on this sector is much less than that over the small radius corner. At angle-of-attack, the pressure distribution becomes asymmetric. The flow stagnation point (peak pressure location) moves toward the windward corner, reaching the small radius sector at about 30-deg angle-of-attack.

The flow structure within the shock layer has been determined using a stream-tube technique which is discussed in the subsequent section on radiative heat transfer. The shock standoff distance, shown as a function of surface position in Fig. 5-60 for the zero-angle-of-attack case, is a small fraction of the body radius. The velocity and density increase in essentially linear fashion, moving from the surface through the shock layer. The flow velocity immediately behind the shock surface is approximately twice that at the body surface; the density change is comparable. At angle-of-attack the shock-standoff distance is reduced in the windward corner region and increased on the lee side. With increasing angle-of-attack, the flow over the large radius sector changes from subsonic to supersonic.

5.6.4 Heat Transfer

Convective Analysis Techniques. Although the lander vehicle is a very blunt configuration, convection is the dominant heat transfer mechanism for the velocities of interest here. As a consequence, careful consideration must be given to the several phenomena which may affect convective rates. Cross flow, bow-shock-curvature-induced vorticity, mass transpiration, and boundary layer transition are important considerations and will be discussed after a review of the basic convective heat-transfer relations.

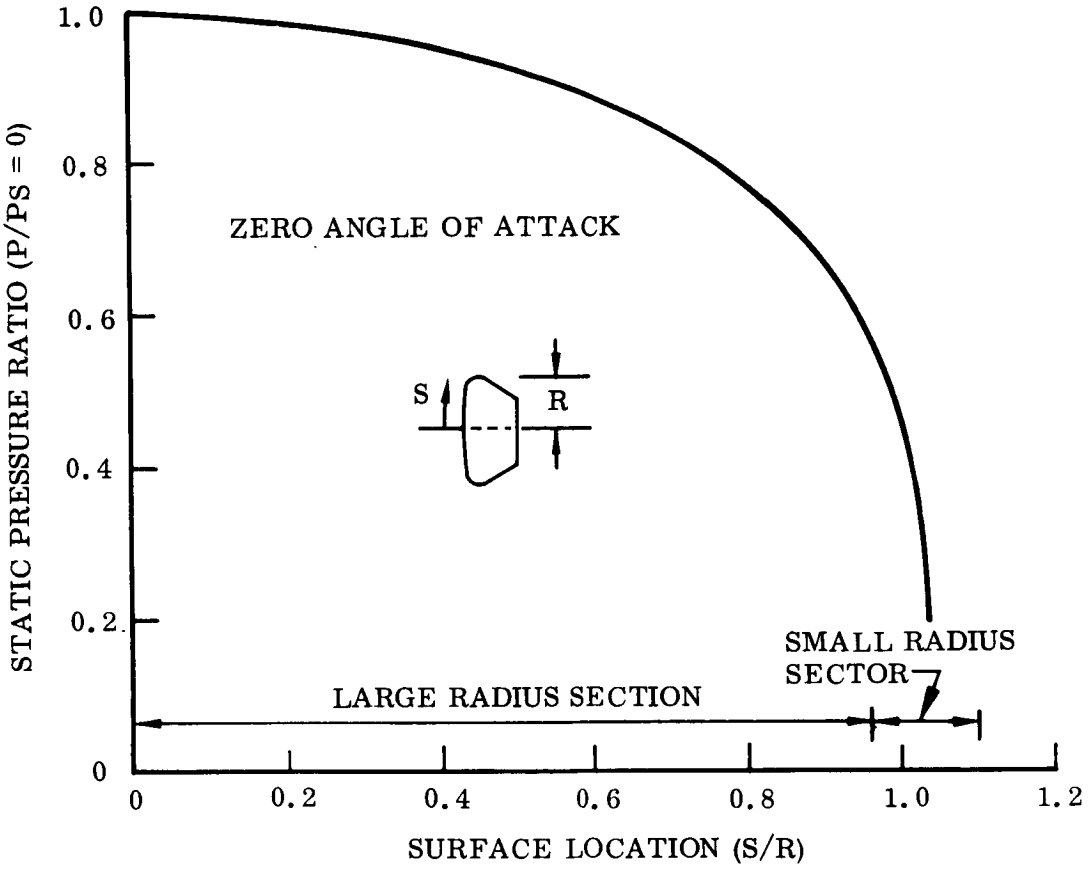


Fig. 5-59 Lander Vehicle Surface Pressure Distribution

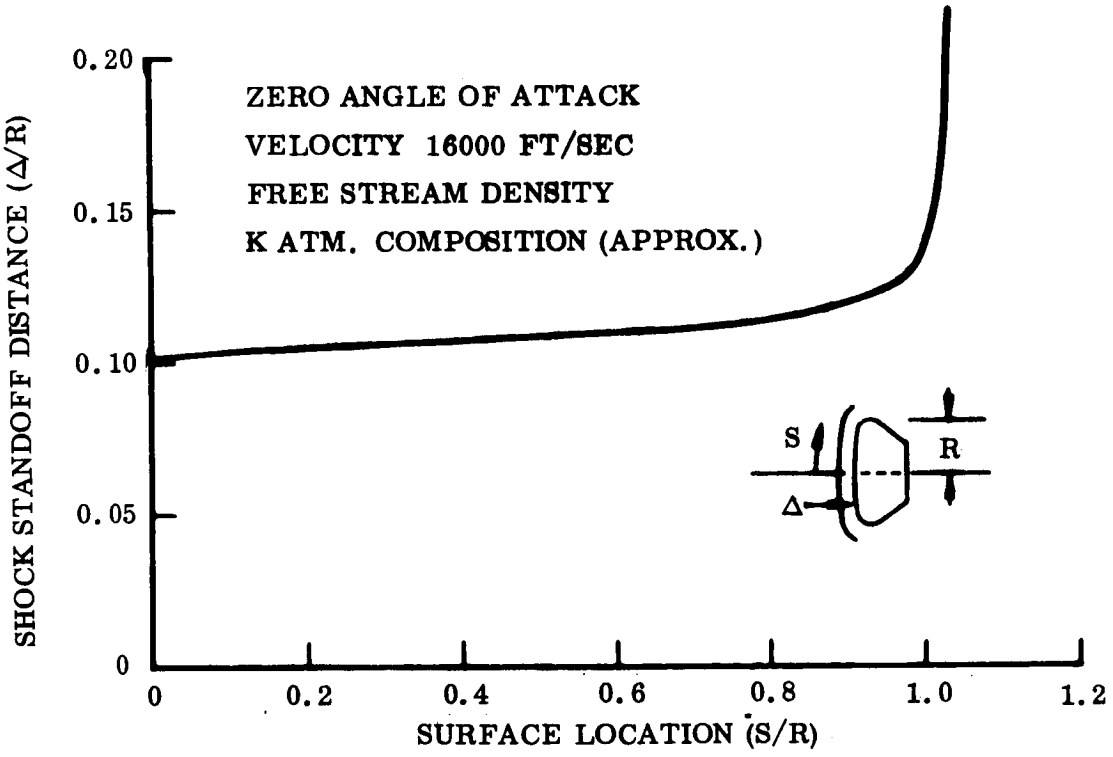


Fig. 5-60 Lander Vehicle Shock Standoff Distance

362

The stagnation-point convective-heat-transfer coefficient has been evaluated using the theoretical correlation obtained by Hoshizaki (Ref. 15) for an equilibrium boundary layer. (Dependence of the heating level on carbon-dioxide/nitrogen ratio is not significant as shown by Hoshizaki, thus the single equation may be applied for the several atmospheres of concern.)

$$(h_0)_{x=0} \sqrt{R_M} = 2.2\, \rho_\infty^{0.5} \left(\frac{u_\infty}{10^4}\right)^{1.19} \left[\frac{R_M}{u_\infty} \left(\frac{du_e}{dx}\right)_{x=0}\right]^{0.5} \qquad (5.20)$$

where ρ_∞ is in lbm/ft^3, u_∞ in ft/sec, r_m in ft, and $(h_0)_{x=0}$ in lb$_m$/ft^2-sec. Nomenclature for Section 5.6 is shown on page 5-272.

The effective velocity gradient is determined in the general, three-dimensioned case from the surface pressure distribution through the relations:

$$\frac{R_M}{u_\infty} \left(\frac{du_e}{dx}\right)_{x=0} = \left[\frac{1}{2}\left(\frac{R_M}{R_{eff}}\right)_x + \frac{1}{2}\left(\frac{R_M}{R_{eff}}\right)_y\right] \left[2 \frac{\rho_\infty}{\rho_o} \left(1 - \frac{1}{2}\rho_\infty/\rho_o\right)\right]^{0.5} \qquad (5.21)$$

and

$$\left(\frac{R_M}{R_{eff}}\right)_x = \left[\frac{(1 - P/P_{x=0})^{1/2}}{x/R_M}\right]_{y=0,\ x\to 0}$$

$$\left(\frac{R_M}{R_{eff}}\right)_y = \left[\frac{(1 - P/P_{y=0})^{0.5}}{y/R_M}\right]_{x=0,\ y\to 0}$$

where the x-coordinate distance is measured from the stagnation point along the axis

of symmetry and the y-coordinate distance is measured in the direction normal to the x-coordinate. It is noted that at zero angle of attack

$$\left(\frac{R_{eff}}{R_M}\right)_x = \left(\frac{R_{eff}}{R_M}\right)_y = 2.10$$

The convection coefficient away from the stagnation point is related to that at the stagnation point by means of Lee's similarity solution

$$\frac{h}{(h_0)_{x=0}} = \frac{\rho_e u_e \mu_e r^{\nu}}{2\left[\int_0^x \rho_e \mu_e u_e r^{2\nu} dx\right]^{0.5}} \left[\rho\mu \frac{du_e}{dx}\right]_{x=0}^{0.5} \qquad (5.22)$$

At non-zero angle-of-attack, the distribution has been predicted for two limiting cases, axi-symmetric and two-dimensional flow. The available experimental data are, for the most part, bracketed by the two predictions. The data are extensive and have been used, in combination with the theoretical results, to define the convective coefficient distributions shown in Fig. 5-61 for the plane of symmetry.

At angle-of-attack, theoretical prediction of the convective heat-flux distribution off the plane of symmetry is difficult as a consequence of the complexity of the cross-flow pattern. Greater reliance must be placed on the experimental data. Two observations are pertinent. The convective flux level varies only slightly over the large radius sector in a direction normal to the plane of symmetry. The flux is maximum at the plane of symmetry.

At the higher altitudes, when convective heating first becomes appreciable the Reynolds number is small and consequently the boundary layer occupies an appreciable portion of the shock-layer. At such conditions, the velocity gradient in the inviscid flow normal to the surface may appreciably increase the heat rate. The magnitude of

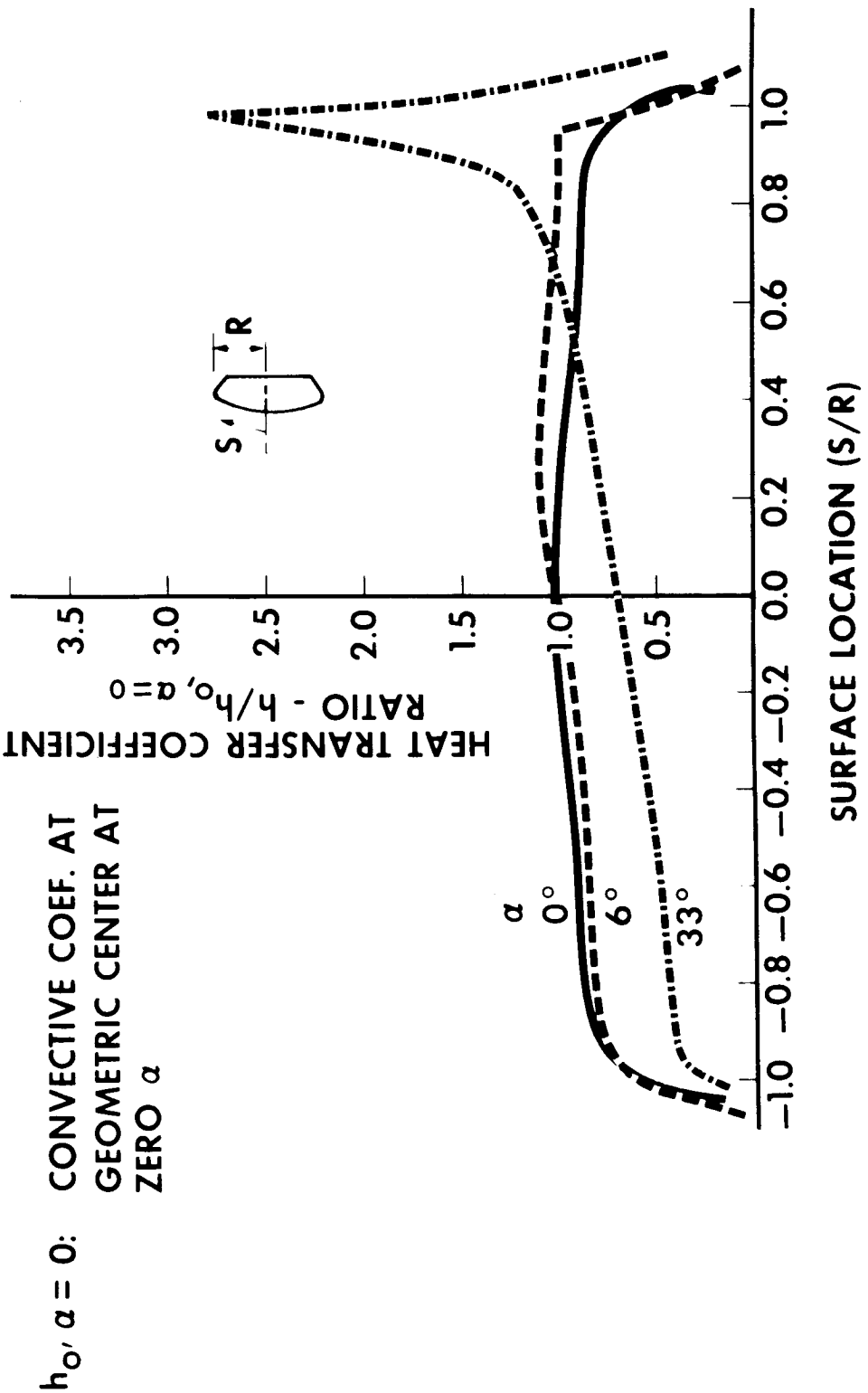


Fig. 5-61 Forebody Convective Heat Transfer Distribution

this bow-shock-curvature-induced vorticity effect has been examined using the results obtained by Van Dyke for the stagnation point (Ref. 16). The influence on total heat transfer is small and hence the vorticity effect may be neglected.

At the lower altitudes the Reynolds number becomes relatively large and the possibility of turbulent boundary-layer flow must be examined. The momentum-thickness Reynolds number has been adopted as a transition criterion for the purposes of this study. The local value is determined using a transformation of the flat-plate incompressible result, which is

$$Re_0 = \frac{0.664 \left[\int_0^x \rho_e \mu_e u_e r^{2\nu} \, dx \right]^{0.5}}{\mu_e r^{\nu}} \qquad (5.23)$$

The computed distribution over the forebody at a representative time in the trajectory of Fig. 5-57 is shown in Fig. 5-62. Available flight test data (Refs. 17, 18, 19) indicate that the boundary layer may transit at a Reynolds No. of approximately 300. Using this value to estimate the occurrence of transition, it is predicted that the boundary layer will remain laminar except for a short period during entry into the G-atmosphere and then only at the steeper entry angles. In these latter cases, turbulence is confined to the small radius corner region immediately upstream of the point of separation. The turbulent heat flux in this region (as determined by the method proposed by Bromberg, Fox and Ackerman, Ref. 20) is somewhat less than the laminar heat flux on the large radius sector; this difference is a consequence of the relatively low pressures near the point of separation.

Convective heating to an ablating surface is appreciably reduced by the injection of gaseous ablation products into the boundary layer. The theoretical results of Libby (Ref. 21) have been used to describe the extent of the reduction. His results are for air injection into air at a stagnation point and have consequently been modified for application. Libby's results are presented in terms of a dimensionless injection

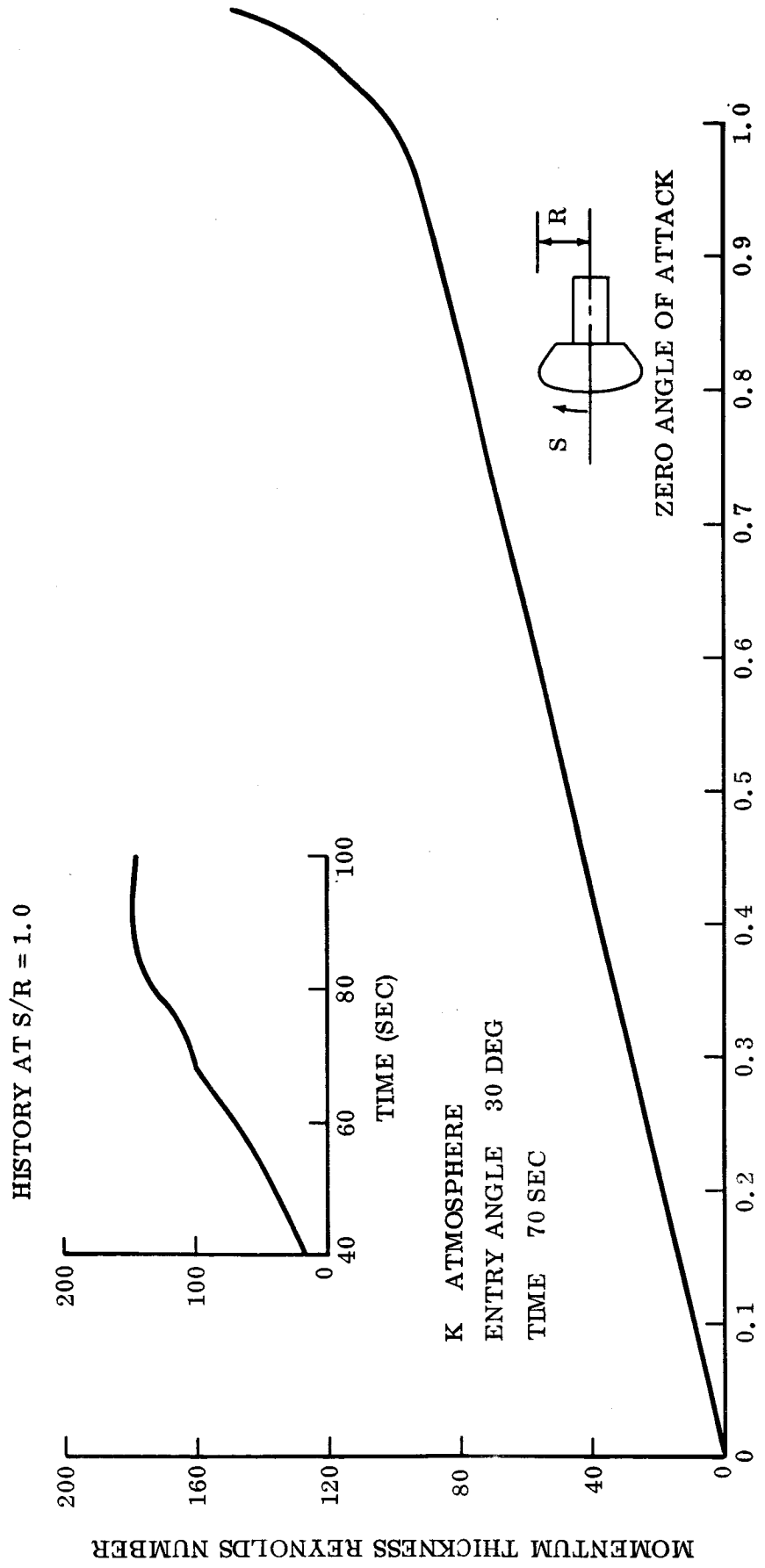


Fig. 5-62 Momentum Thickness Reynolds Number Distribution of Forebody

velocity; this dimensionless velocity is simply transformed to a more convenient parameter, the ratio of the mass injection rate to the non-blowing value of the convection coefficient. The effect of injection of a gas other than air may be accounted for by a multiplying factor $(M_a/M_{inj})^{1/4}$. The assumption of local similarity permits extension to positions away from the stagnation point.

Reaction kinetics in the boundary layer may be sufficiently slow at the higher altitudes such that an appreciable departure from chemical equilibrium occurs. As a consequence a significant reduction of the convective heat transfer may occur depending on the catalicity of the surface. Quantitative investigation of the non-equilibrium affect has not been conducted; such a study is beyond the scope of this work.

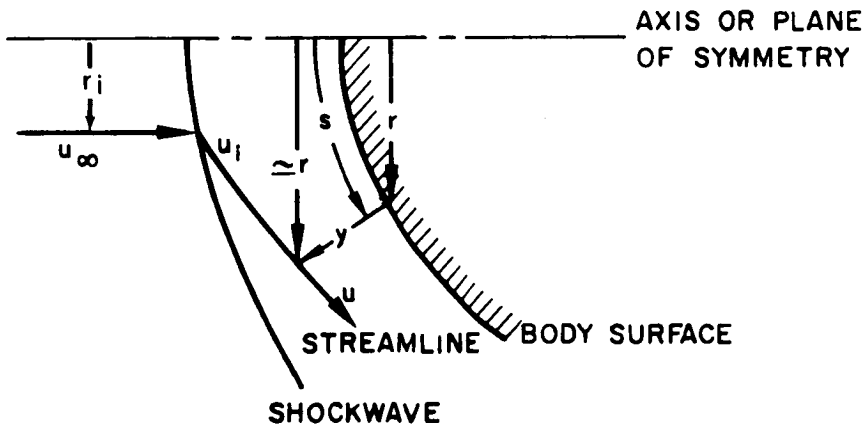
Radiative Analysis Techniques. The radiative heat transfer to the vehicle surface from the shock layer gases may be determined in the general case by definition of the volumetric and spectral emission distributions through the shock layer. Self-absorption and radiative energy loss must be considered. A rigorous evaluation is complex and simplifying assumptions are usually introduced. For the situation of interest, the shock layer is relatively thin in comparison with the body radius of curvature, and the shock layer may be locally approximated as a semi-infinite plane parallel slab whose properties vary only in the direction normal to the vehicle surface. The optical thickness of the shock layer is small and hence self absorption may be neglected. Under these conditions the local radiative flux to the surface is given by

$$q_r = 2 \int_0^{\Delta} \rho k \sigma T^4 dy \qquad (5.24)$$

where k is the Planck-mean mass absorption coefficient which is related to the Planck-mean emissivity per unit length by

$$k = \frac{1}{2}\frac{\epsilon}{L}$$

To solve Eq. 5-24 the density and temperature (or pressure and enthalpy) distributions through the shock layers must be determined. A streamtube technique has been used. The differential conservation equations expressed in terms of the natural (stream-tube) co-ordinate system (s , y) are



$$\rho u r^{\nu} dy = dm \tag{5.25}$$

$$\rho u \frac{du}{ds} = - \frac{dp}{ds} \tag{5.26}$$

$$\rho u \frac{d(H + u^2/2)}{ds} = - 4\rho k\sigma T^4 \tag{5.27}$$

To simplify integration, the approximations are introduced that (1) the local velocity vector is parallel to the surface, (2) the normal pressure variation across the shock layer is small, and (3) the shock layer is then compared with the surface radius. With these approximations

$$\int_0^y \rho u dy = \frac{\rho_\infty u_\infty}{r^{\nu}} \int_0^{r_i} r_i^{\nu} dr_i \tag{5.28}$$

$$\frac{u^2}{2} - \frac{u_i^2}{2} = -\int_{S_i}^{S} \frac{1}{\rho}\frac{dp}{ds}\, ds \tag{5.29}$$

$$H - H_i = -\int_{S_i}^{S} \left(\frac{4k\sigma T^4}{u} - \frac{1}{\rho}\frac{dp}{ds}\right) ds \tag{5.30}$$

Eq. (5.28) determines the locus of the entering streamlines (entering at r_i or S_i) which pass through a point (y, r or S) within the shock layer. Eq. (5-29) and (5.30) are integrated simultaneously by forward finite differnces to determine all pertinent quantities along a given streamline once the surface pressure is given and k, T, and ρ are expressed as functions of H, p. The initial conditions at r_i or S_i are determined from the shock-wave conservation equations. When Eqs. (5-29) and (5-30) are solved, the radiation heat flux to the vehicle surface may be calculated by combining Eqs. (5-24) and (5-28).

$$q_r(S) = \frac{2\rho_\infty u_\infty}{r^\nu} \int_0^{r(S)} \frac{k\sigma T^4}{u}\, r_i^\nu\, dr_i$$

The formulation does not enable consideration of the general three-dimensional flow case but is limited to axi-symmetric and two-dimensional flows.

The radiative heat transfer distribution along the plane of symmetry of the lander vehicle has been obtained for several angles-of-attack assuming rotationally symmetric flow. (Some error is incurred at larger angles of attack due to the asymmetric character of the flow.) Some of the results showing the effect of angle-of-attack on the distribution are described in Fig. 5-63. The maximum radiative heat load occurs at zero angle-of-attack as would be expected from consideration of relative shock layer temperatures. At zero angle-of-attack the peak flux occurs at the stagnation point and the flux is relatively uniform over the large radius sector. At larger angles-of-attack,

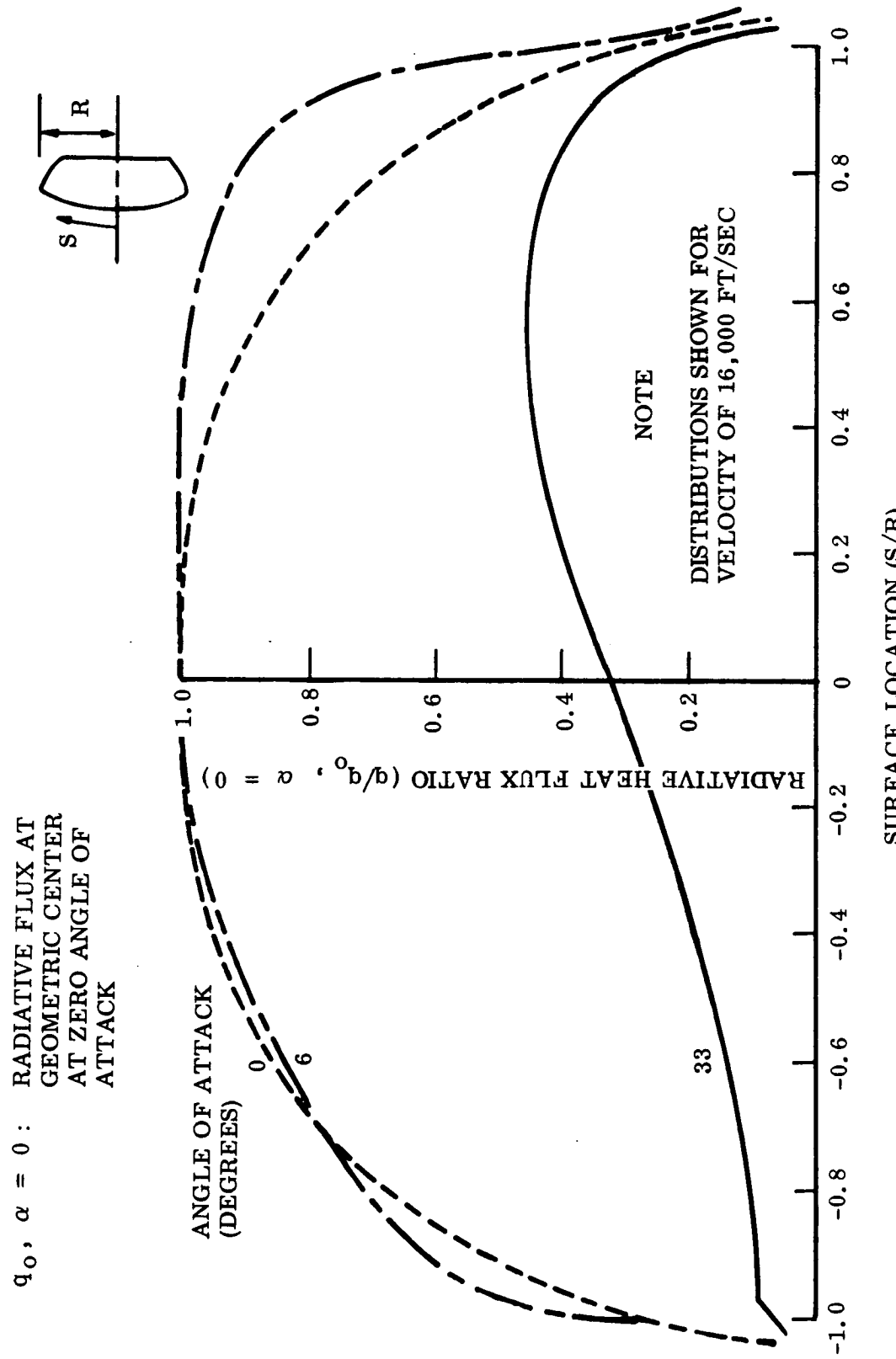


Fig. 5-63 Radiative Heat Transfer Distribution Over Capsule Forebody

the peak radiative heating occurs between the stagnation point and the geometric center; this is a consequence of the relatively rapid shock-layer-thickness growth away from the stagnation point.

The radiative flux distribution exhibits some sensitivity to the flight condition, in particular to the velocity. This behavior is unlike that for an air atmosphere (Ref. 22) and is a consequence of the peculiar variation of the radiation intensity with enthalpy (Ref. 12).

The streamtube technique accounts for radiative energy loss from the flow. It is noted, however, that for the flight conditions of interest the losses are not significant; the shock-layer flow is essentially adiabatic.

The radiative flux to the surface has been determined, neglecting two possibly important contributions. Ablation products injected into the boundary layer may radiate significantly. Appreciable emission may emanate from the non-equilibrium zone immediately behind the shock. Insufficient data are available to afford an accurate assessment of the importance of these phenomena.

Afterbody Heat Transfer Analysis. Definition of the afterbody thermal environment requires consideration of flow phenomena distinct from those of the forebody. Engineering analysis methods are in general poorly developed, and greater recourse to approximation and empiricism is required to predict the heat transfer. Fortunately, an abundance of convective heat transfer data exist for a similarly configured body, the Apollo. Radiative heat transfer to the afterbody because of its relatively low level need not be considered.

Convective heat transfer data, in the form of the ratio of local convection coefficient to stagnation point, have been taken from Refs. 13 and 14 for direct application here. The axial variation of the convection coefficient except in the immediate neighborhood of the separation point is generally small, whereas the peripheral variation at angle-of-attack is large. The experimental data are sufficient to define the windward line (maximum) convection coefficient and an approximate peripheral average convection coefficient.

Convective heating to an aerodynamic stabilizer (right-circular cylinder extending rearward from the main body) has been estimated using a simple flow model in the absence of experimental data. In particular, that portion of the stabilizer extending out of the separated region has been treated as a cylinder in the free stream, swept at an angle $(\pi/2 - \alpha)$. Convective heating to that portion remaining in the separated zone has been assumed to be equal to that on the afterbody. The extent of direct flow impingement was estimated using flow discharge photographs (Ref. 14) of the flow over the Apollo configuration.

The estimated windward line and peripheral average convection coefficient levels are shown in Fig. 5-64, for both the afterbody and aerodynamic stabilizer. The results for the latter section must be considered very approximate. In application of these results to obtain convective heating histories, the peripheral average values have been used since the vehicle is spinning at a relatively rapid rate.

Entry Heating Predictions. The heating experienced by the capsule has been determined for four trajectories, corresponding to entries at the limit entry angles (30 and 60 deg) into the extreme atmospheres (K and G). The computations for the forebody have been made assuming zero angle-of-attack. (Recognizing that the angles-of-attack are moderate and that the vehicle is spinning, and examining the heat transfer distributions of Figs. 5-61 and 5-63, it does not appear that the total heat transfer at any location will differ substantially from that predicted for zero angle-of-attack.) Heat transfer results for the stagnation point, or peak-heating position, are shown in Fig. 5-65 . The convective rate shown is that to a cold wall without mass injection. In every case, convection dominates over radiation. As would be expected, total heat transfer is greatest (about 1100 BTU/ft^2) for the case of shallow-angle entry into the K atmosphere. The maximum heat transfer rate in this case is relatively low, and the heating period is long. The conditions of this trajectory are most severe from a heat shielding consideration and consequently they will be used in determination of heat shielding requirements.

Heat transfer to the capsule afterbody is relatively sensitive to angle-of-attack, as indicated by the results of Fig. 5-64. Vehicle dynamics are, in turn, dependent on

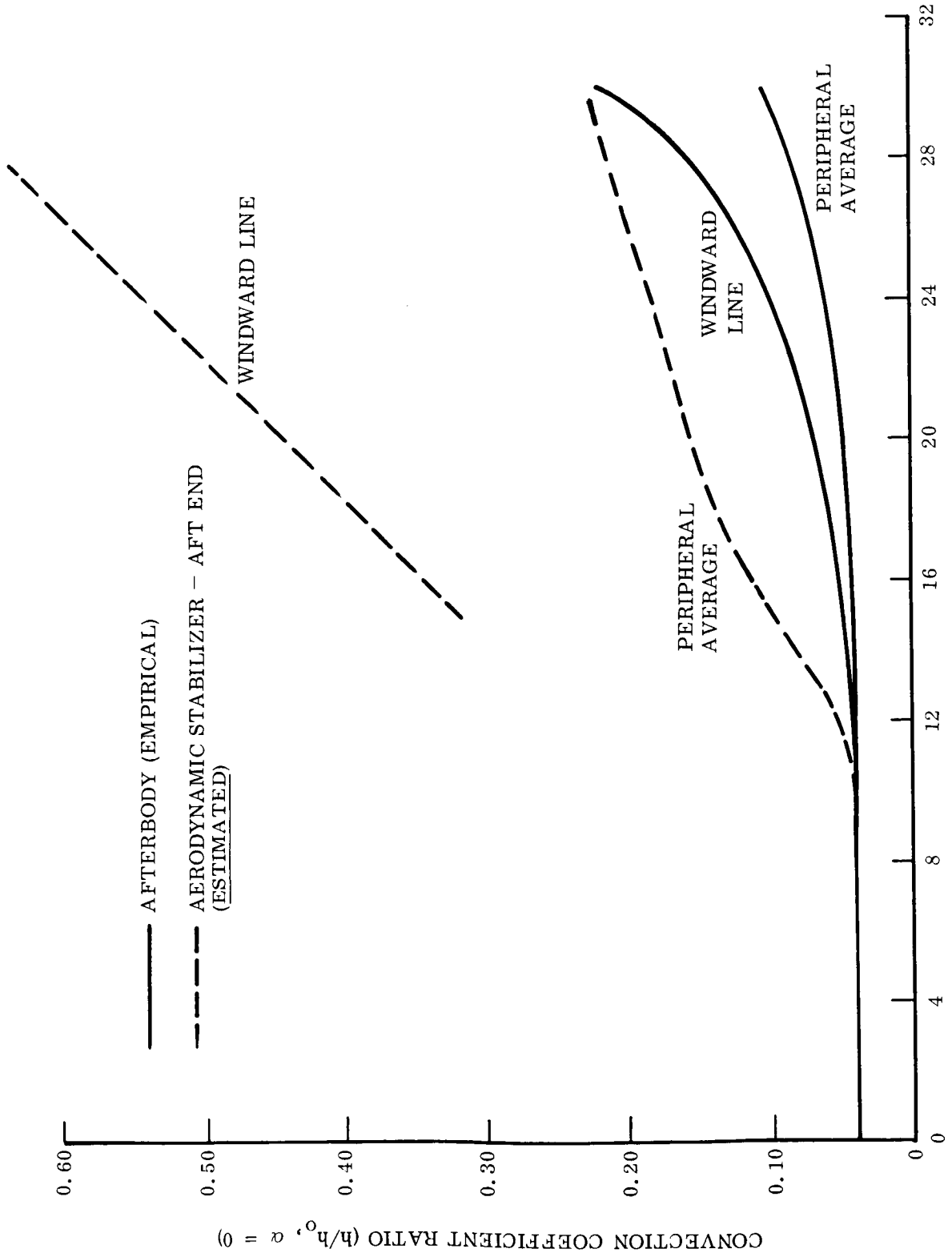


Fig. 5-64 Influence of Angle of Attack on Afterbody and Aerodynamic Stabilizer Convective Heat Transfer Level

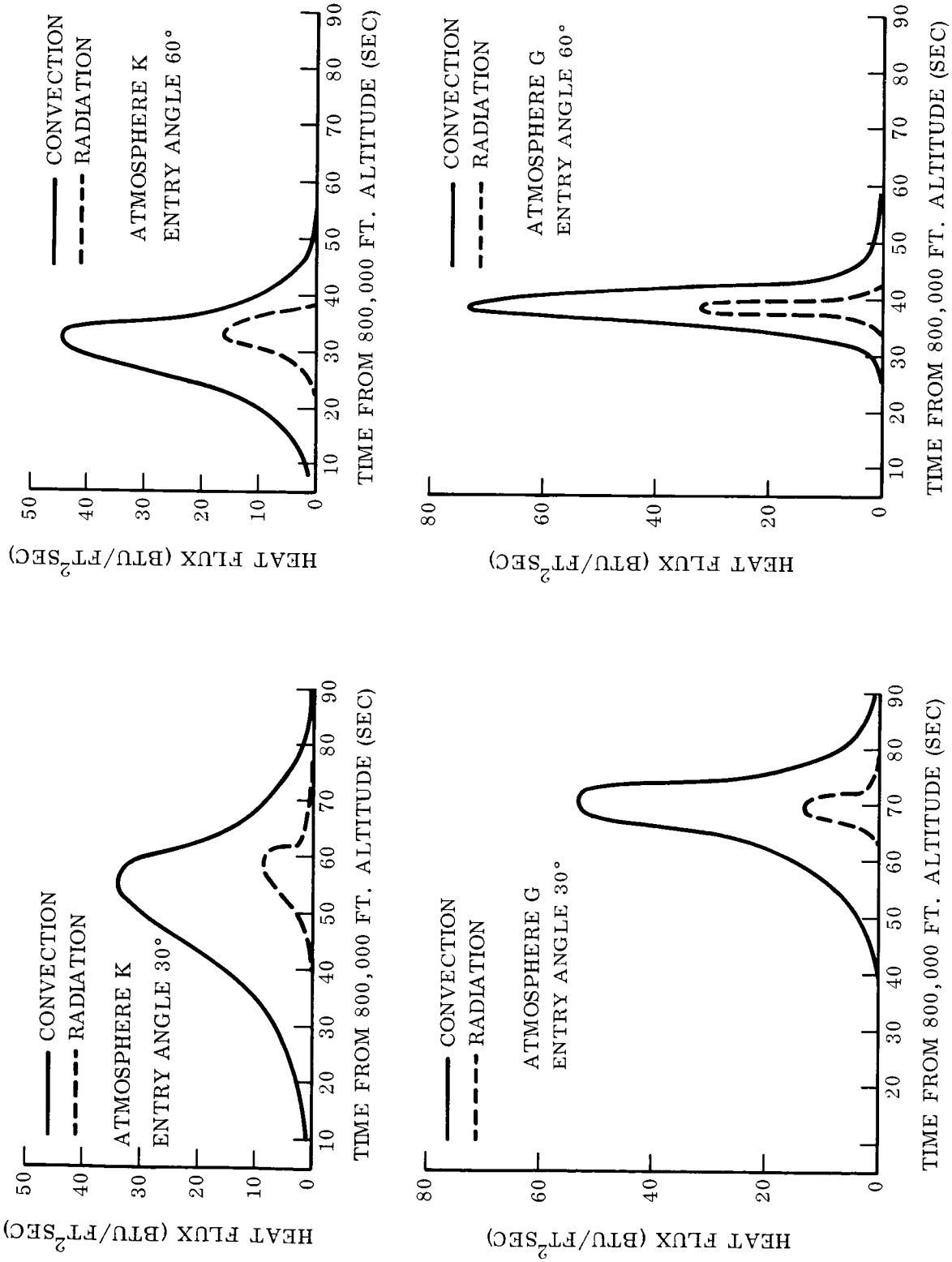


Fig. 5-65 Influence of Atmosphere and Trajectory Uncertainties on Stagnation Point Heating

entry angle (see Fig. 3-32). The trajectory which is thermally most severe for the afterbody is entry at 60-deg angle into the K atmosphere. The estimated angle-of-attack history for this trajectory is shown in Fig. 5-66. The associated convective heat-transfer histories for the afterbody and aerodynamic stabilizer are described in Fig. 5-67. At early times when the angle-of-attack is relatively large, heat transfer to the stabilizer is somewhat greater. Later when the angle-of-attack becomes small and both sections are within the separated flow region, the heating rates are identical. Total heat transfer to the afterbody and stabilizer is small as compared to that to the forebody.

5.6.5 Thermal Protection

There are many materials which can be considered as candidates for thermal protection of the lander vehicle. In this study, microballoon-loaded nylon-phenolic and beryllium have been considered. They are representative of the more efficient ablative and heat-sink type materials. Techniques used for prediction of their performance are briefly reviewed, then shielding requirements are indicated. Protection of the afterbody is discussed separately.

Heat-Sink Thermal Protection. Because the thermal environment by the lander vehicle is relatively mild, there is no large weight penalty associated with the use of an efficient heat-sink-type thermal protection system. The heat-sink system meets sterilization requirements. Because the sink acts as a calorimeter, it affords a simple means of measurement of the incident heat flux. The heat sink has the disadvantage that design uncertainties in the heat load directly influence (in linear manner) the shield weight. Furthermore, in design of the vehicle assembly, the heat shield must be thermally isolated from temperature-sensitive components.

The heat sink accommodates net heat transferred to the surface by sensible enthalpy change (simple temperature rise). As a consequence of its high specific heat, beryllium is an unusually attractive material for the heat-sink application. The techniques for prediction of its temperature response are well known and consequently will not be discussed. Thermal-physical properties of the material have been obtained from

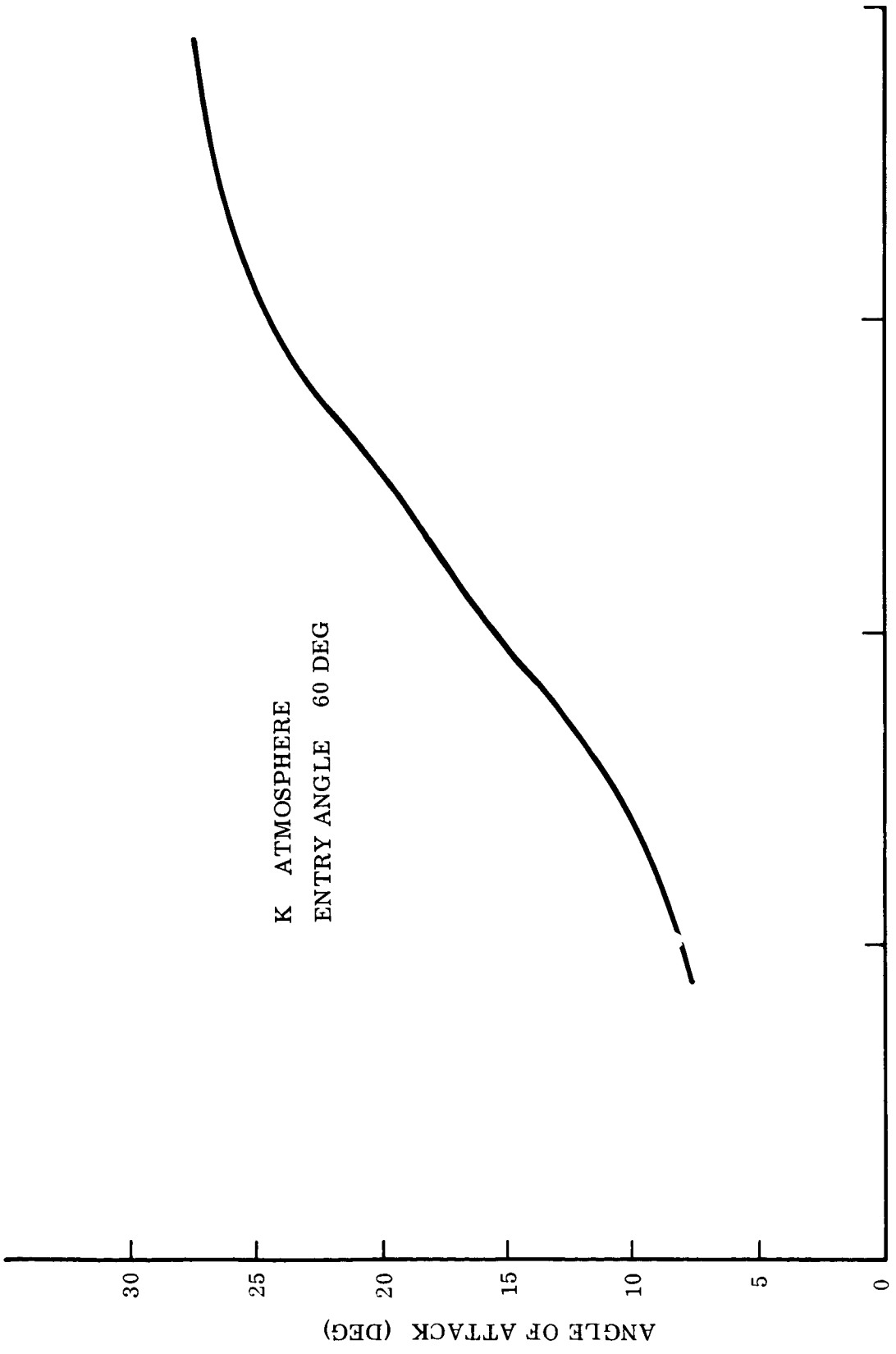


Fig. 5-66 Estimated Angle of Attack History During Entry

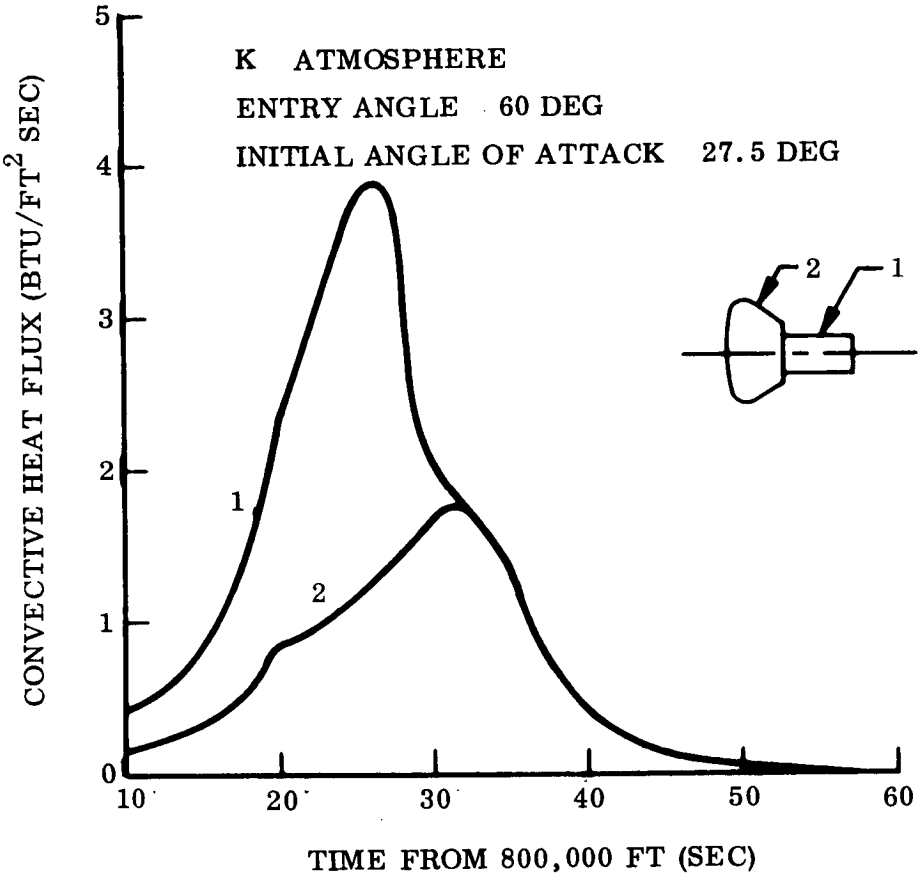


Fig. 5-67 Afterbody Heating Histories

Ref. 23. In this regard, it is noted that the assumed density is 115 lb/ft^2. In evaluation of the surface boundary conditions, the absorption coefficient for radiation incident from the shock layer has been conservatively taken as unity, whereas emission from the surface has been computed using experimentally derived values of the emissivity.

The predicted shield-temperature response at the stagnation point is given in Fig. 5-68 for three different section thicknesses (The temperature distribution through the section being essentially isothermal and consequently only the bulk-or average-temperature is shown). For an allowable temperature of 1500° F the thickness requirement is approximately 0.1 in. The variation of required thickness with position on the forebody is shown in Fig. 5-69. For a given allowable temperature the thickness may be maintained constant over the large radius sector without appreciable weight penalty. Thickness may be rapidly reduced in moving around the shoulder.

Ablator Thermal Protection. Nylon-phenolic may be considered a typical charring ablator. Incident heat is largely absorbed in pyrolysis (decomposition) of the virgin material and by the gaseous pyrolysis products percolating through the residual char layer. Under high heat-flux conditions this class of materials is thermally superior to the heat sink class; however, in a mild environment the amount of ablative material used for insulation of the substructure is relatively large and the two material classes are competitive from a weight standpoint.

Shielding requirements with ablative materials are less affected by perturbations in the heat transfer than are those with heat-sink materials; thus environmental uncertainties are not of as much consequence in heat shield design. Ablative material shield fabrication is usually simpler and less expensive than construction of beryllium shields.

Not all ablative materials will withstand sterilization by temperature soaking. Nylon-phenolic, in particular, is not heat sterilizable. It has been considered here because its performance characteristics are well defined. Other materials with gross performance comparable to nylon-phenolic, such as some members of the silicone rubber

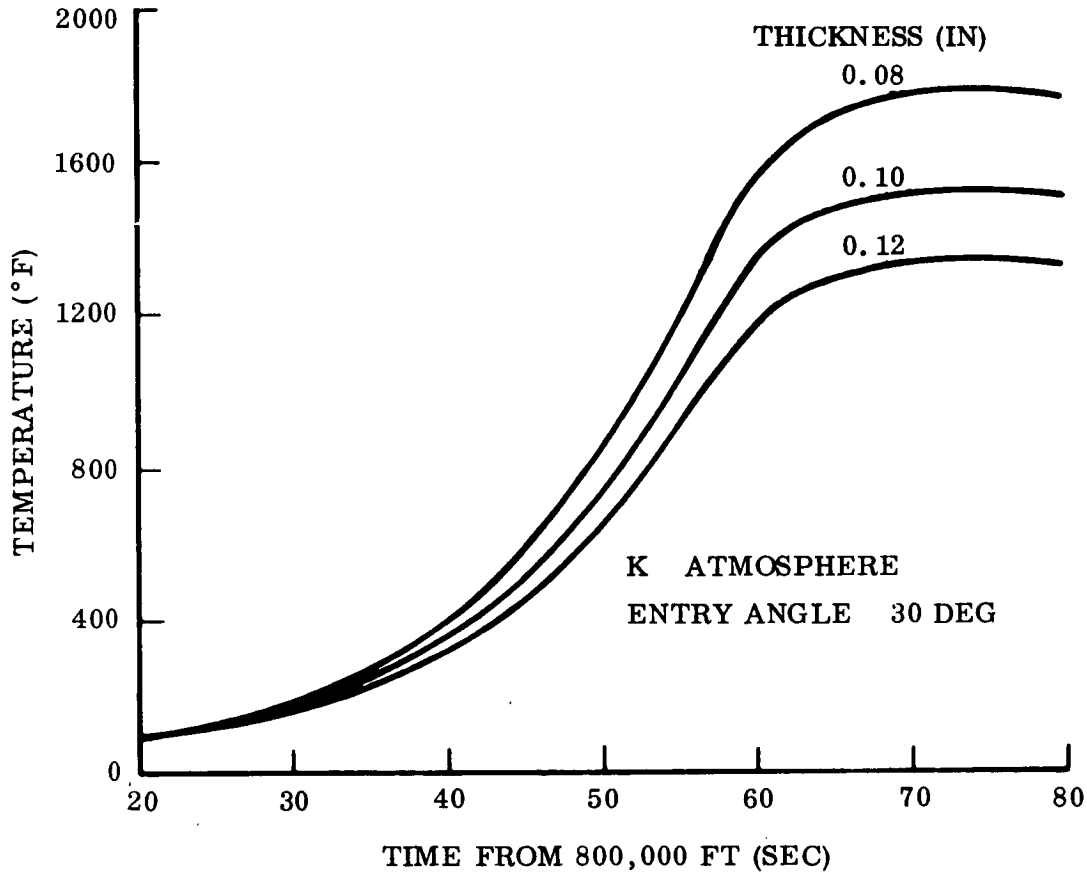


Fig. 5-68 Beryllium Heat Shield Temperature Response at Forebody Geometric Center

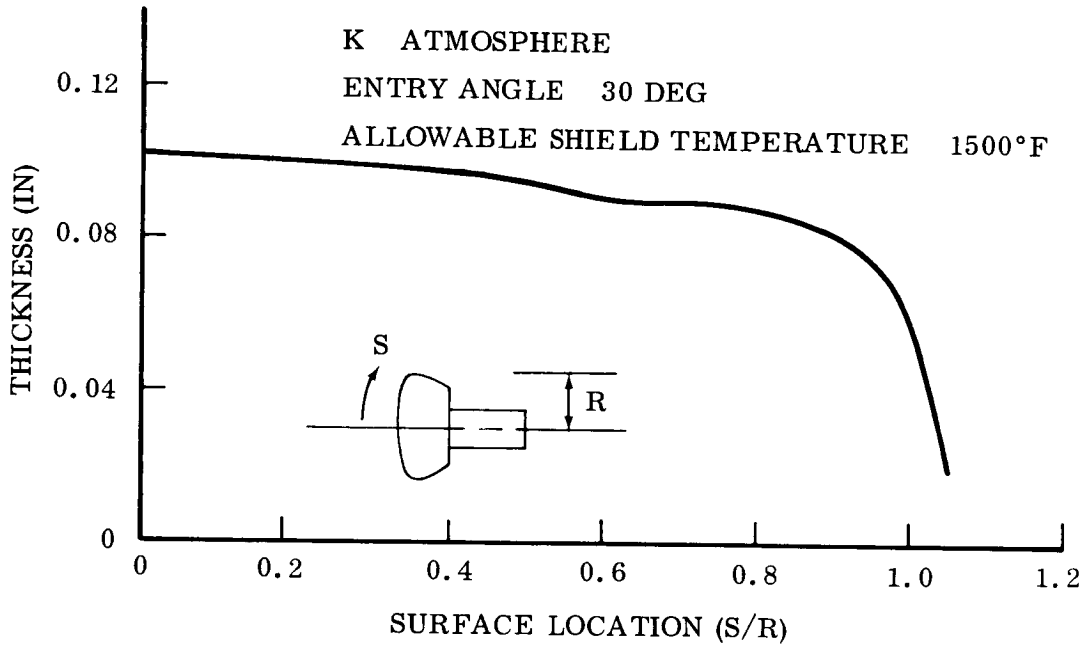


Fig. 5-69 Beryllium Shield Thickness Requirements

family, will withstand high temperature soaking. Thus the end results for nylon-phenolic shield weight requirements are not directly applicable, but may be considered representative of the results which would be obtained for other acceptable charring ablators.

To describe the thermal performance of nylon-phenolic, the theoretical model developed by Kratsch and others (Ref. 24) has been used. The model rigorously accounts for the significant phenomena by mathematically coupling the energy and mass transfer processes. Reference 24 includes all the data required in implementation of the model for nylon-phenolic. In particular, the kinetics of the pyrolysis reaction was defined. Thermophysical properties of the virgin plastic, partially degraded plastic, and char material are provided, and a detailed description of the gaseous pyrolysis products is given. The model has been extended recently for application in Mars-like atmospheres (Ref. 11). The model has been corroborated by correlation of both ground and flight-test data (Refs. 11, 18, and 24).

A rigorous finite difference formulation of the conduction equation for charring materials (Ref. 25) has been used in determination of required heat-shield thicknesses. Initial results indicated that the thickness of nylon-phenolic used for insulation comprises the majority of the section thickness. As a consequence, the inclusion of phenolic micro-balloons to improve insulating capability was considered. The results presented are for a loaded nylon-phenolic material in which the volumetric concentration of micro-balloons is 0.5; the density and conductivity of the loaded material are both about a factor of two less than the unloaded nylon-phenolic.

The predicted temperature response of a nylon-phenolic/substructure composite at the stagnation point is described in Fig. 5-70. The exterior strata of the nylon-phenolic are elevated in temperature to the pyrolysis range (800 − 1100° F) early during the heating period. As time progresses the temperature wave moves slowly across the section. The surface temperature peaks at a value somewhat less than 2000° F and drops rather rapidly. For the nylon-phenolic section thickness considered, 0.15 in. the temperature equilibrates somewhat in excess of 500° F. Very little surface

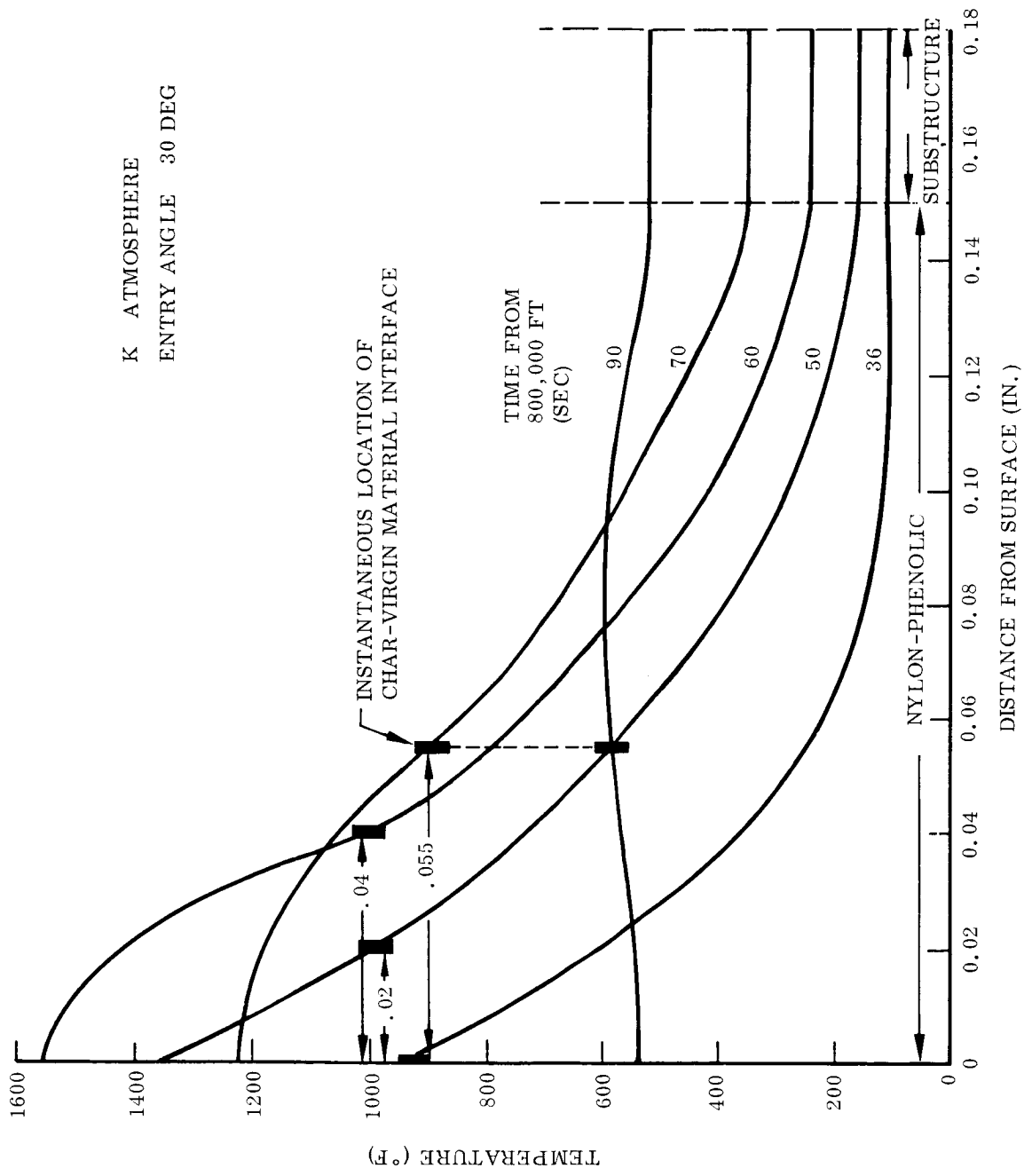


Fig. 5-70 Nylon-Phenolic Heat Shield Temperature Response at Forebody Geometric Center

erosion occurs; however, the pyrolysis zone penetrates to a depth of about 55 mils. Thus, about one-third of the nylon-phenolic is degraded, while two-thirds of the thickness is required for insulation of the substructure.

It is of interest to examine the effect of pyrolysis on the convective heating. Figure 5-71 shows that the injection of gaseous ablation products reduces the convective heat flux by a factor of about two during the peak heating period.

Because the substructure temperature continues to rise well after the cessation of heating, the required nylon-phenolic thickness for a given allowable-substructure-temperature rise will depend on the time at which the heat shield is separated from the instrument package. Shield section weight at the stagnation point is shown in Fig. 5-72 as a function both of the allowable structure temperature and the velocity at shield separation. (Included in the section weight are the nylon-phenolic and substructure contributions; no accounting is made for an adhesive bond.) The section weight requirement varies slowly with both parameters. The figure also shows for comparative purposes section weight for a beryllium shield; the two types of shields are seen to be about equal in weight.

Necessary nylon-phenolic thickness varies very little across the large radius sector of the forebody. As with the beryllium shield, thickness requirements are rapidly reduced in moving around the corner to the afterbody.

Afterbody Heat Shielding. Heat transfer to the afterbody is sufficiently small that thermal protection is not required. The basic structure will accommodate the heat without excessive temperature rise.

Figure 5-73 describes temperature histories of the afterbody and aerodynamic stabilizer by means of a normalized temperature rise parameter. The afterbody skin is magnesium with an effective thickness of 0.054 in. and a thermal capacitance ($\rho c \delta$) of 0.12 Btu/ft^2 ° F; thus its final temperature rise will be only 250° F. The aerodynamic stabilizer will survive sufficiently long so that it has served its purpose.

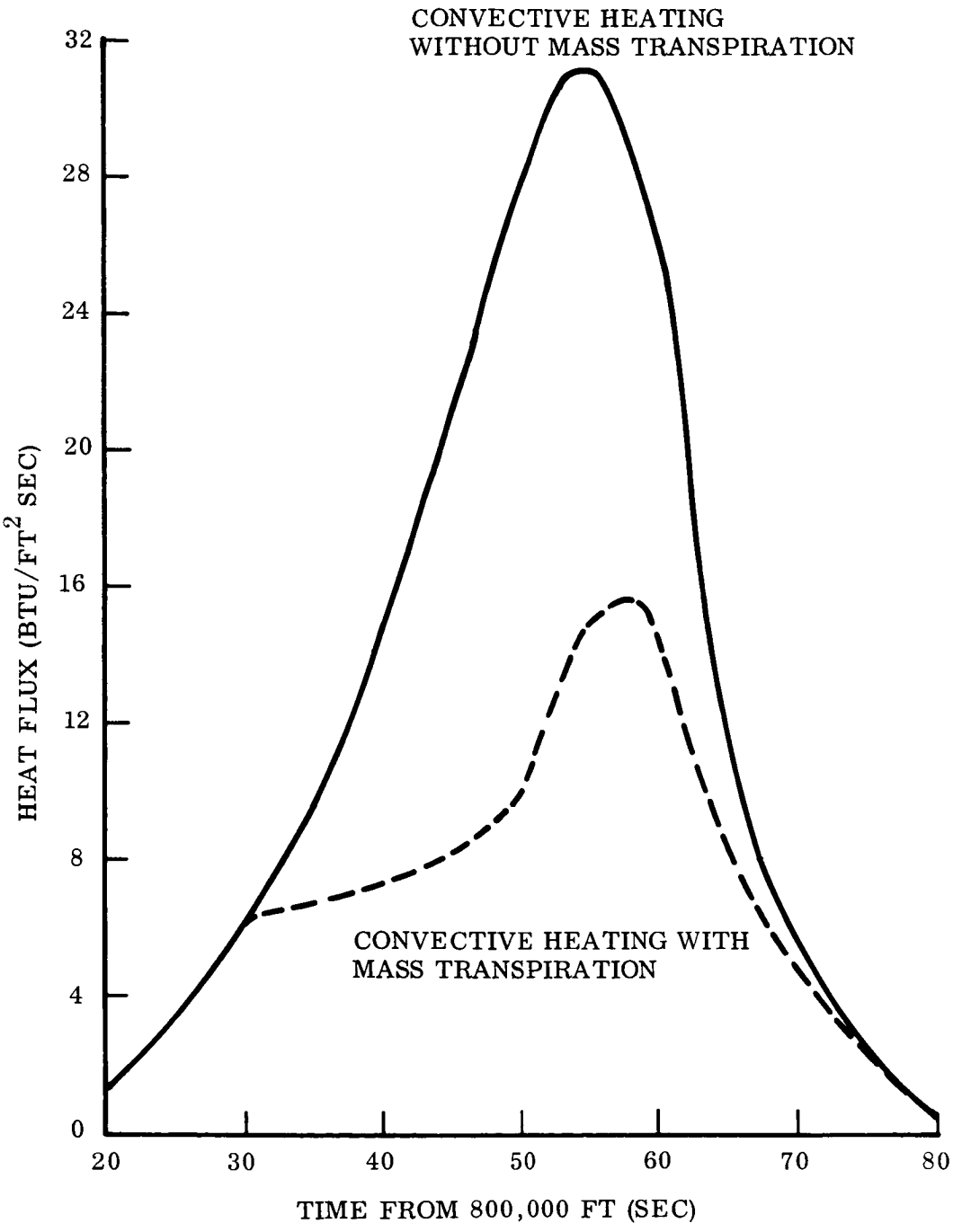


Fig. 5-71 Influence of Injection on Convective Heat Transfer History

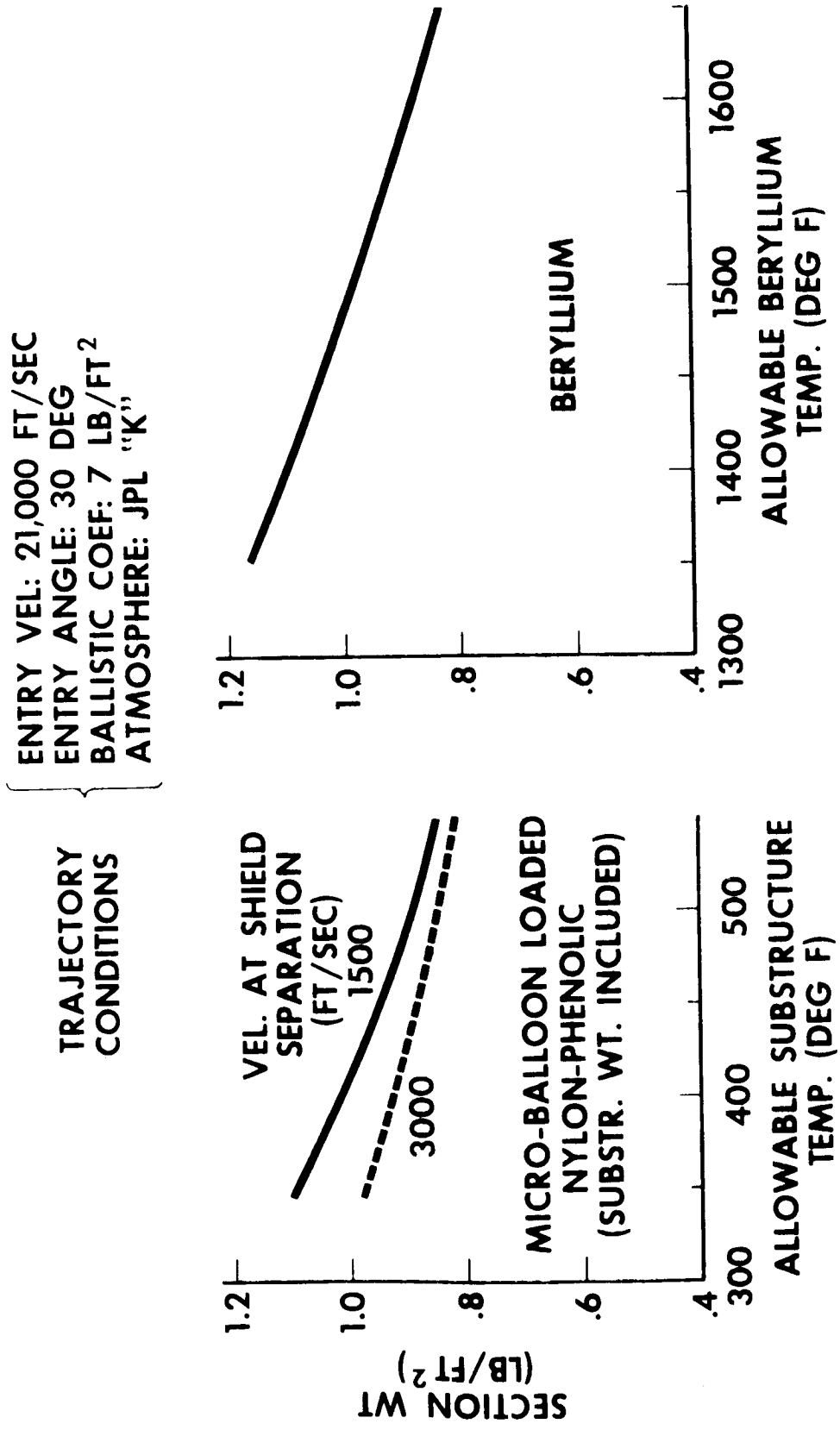


Fig. 5-72 Heat Shielding Requirements at Stagnation Point

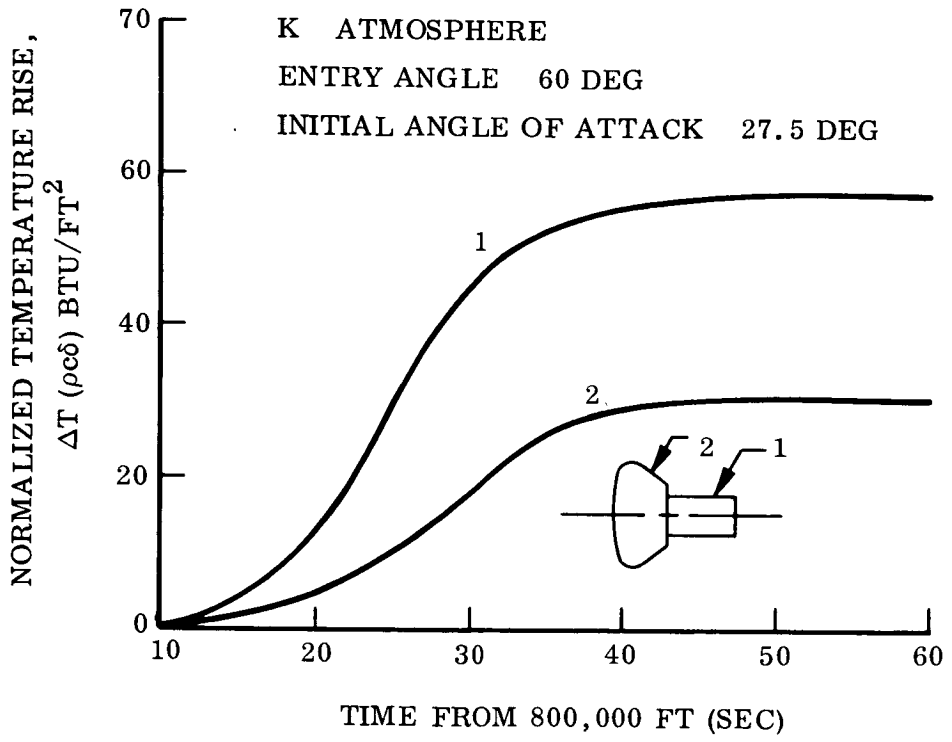


Fig. 5-73 Afterbody Temperature Histories

5.6.6 Conclusions

Preliminary analysis indicates the feasibility of thermally protecting the lander vehicle from the heating experienced during entry of the Martian atmosphere. Ablative or heat sink type shields may be used. Comprehensive material optimization studies should be conducted in subsequent efforts.

The thermal environment is relatively mild. Convective heat transfer exceeds radiative heat transfer. Several environmental phenomena warrant further investigation in subsequent studies. In particular, the influence of uncertainties in the occurrence of boundary layer transition and high temperature emissivity on heat shielding requirements should be assessed. Nonequilibrium effects require definition.

5.7 PARACHUTE DESCENT SYSTEM

Two basic requirements were assumed in the study of parachute deceleration systems designed to lower approximately 100 lb to the surface of Mars. The first requirement was to decelerate an atmospheric (non-surviving) capsule to provide at least 60 sec at subsonic velocity prior to impact. The second requirement was to decelerate a combination atmospheric-biological (surviving) capsule to provide at least 60 sec at subsonic velocity and to reduce the vertical descent velocity to 60 ft/sec at nominal zero elevation.

The environmental characteristics used are shown in Ref. 2 with various atmospheres, Models G through K, considered as appropriate to limiting conditions (i.e., worst cases) for descent system design. The envelope of reentry trajectories for the vehicle prior to initiation of the parachute recovery sequence is as shown in Fig. 5-74, where the boundaries of the envelope are set by the limiting cases of reentry at the shallowest angle in the most-dense Martian atmosphere and reentry at the steepest angle in the least-dense Martian atmosphere.

Other data pertinent to design of the parachute systems are:

- Oscillations of the capsule on the main chute limited to ±20 deg to limit the requirement for distribution of crushable material.
- There may exist Martian surface irregularities of up to 5 km (5 km = 16,405 ft).
- The descent system components/assembly will be required to undergo heat sterilization as defined in Section 5.8.
- At time of initiation of the recovery sequence, the vehicle will be spinning (about the longitudinal axis) at a rate of up to 60 rev/min.

Design criteria for the parachute descent systems are:

- Reliability
- Minimum weight consistent with obtaining the specified times of subsonic descent
- Cost

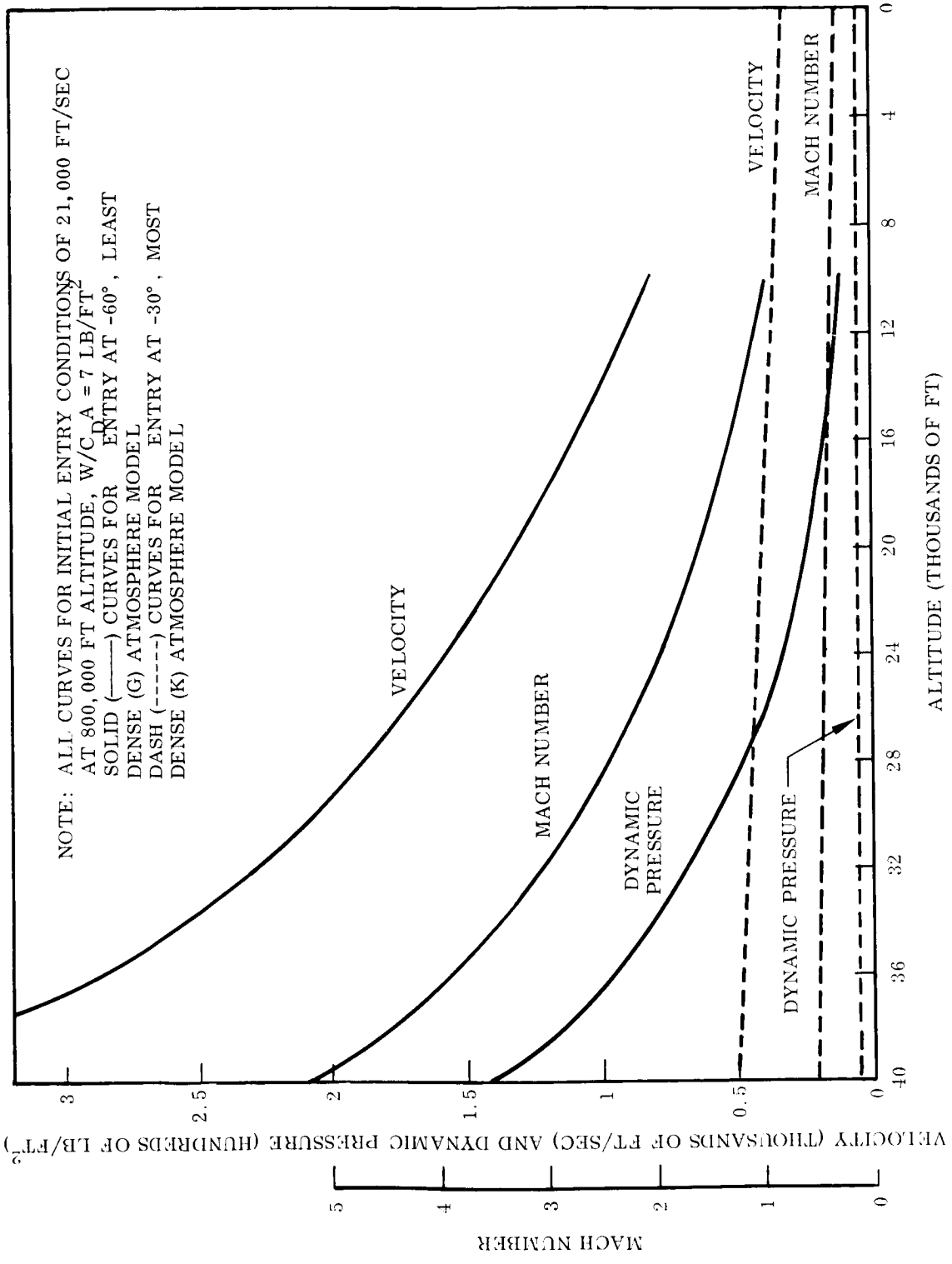


Fig. 5-74 Envelope of Entry Trajectories

5.7.1 Approach to Design

The type of final descent parachute to be used for a biocapsule is selected on the basis of allowable oscillatory amplitude during descent. Once the type of final descent chute is established, its size is fixed by the requirement of 60 ft/sec vertical velocity, the mass to be lowered, and the Martian environment. Since the final descent parachute is the largest single item in overall descent system weight, it is desirable to design this chute from the lightest materials available which are compatible in strength with the loads (mechanical and thermal) to which the chute is to be subjected.

It would be possible to use a single-parachute descent system for the capsule if the aerodynamic drag of the reentry vehicle were of itself sufficient to decelerate the vehicle to a Mach number and dynamic pressure suitable for the deployment of a relatively large, final descent chute* at an altitude of, say, 16,500 ft (16,500 ft is selected as the minimum altitude for deployment of the final descent chute in view of the possibility of Martian terrain elevations of up to 5 km above nominal zero elevation).

However, as seen in Fig. 5-74, the reentry trajectory envelope for the vehicle is such that a single parachute system will not suffice in all cases. It is therefore necessary to use an initial deceleration (drag) parachute to decelerate the vehicle to a Mach-number dynamic-pressure condition safe for deployment of the final stage parachute at an altitude of 16,500 ft. The required drag parachute is sized on the basis of the lightest weight chute required to decelerate the payload to conditions safe for the final descent chute, keeping in mind such factors as drag chute state-of-the-art and the requirement for testing the system in the Earth environment.

Design of the descent system parachutes is therefore relatively straightforward, involving mainly cut-and-try sizing of the drag chute and checking of subsonic descent time.

---

* Where suitable conditions for deployment of large, final-descent type parachutes mean mainly subsonic speeds. Such chutes can be built to withstand high dynamic pressures, but will not inflate reliably in transonic or supersonic flow.

5.7.2 Note on Parachute Textile Materials

Parachute textile materials are selected for ability to withstand mechanical and thermal loads, aerodynamic characteristics (e.g., porosity), and for availability and cost. In this case, the most stringent textile requirements are imposed by the heat sterilization procedure. The proof-test heat sterilization procedure of three, 36-hr cycles at 293°F is too severe for presently available commercial and MIL SPEC Nylon and Dacron parachute textiles. However, the recently-introduced DuPont NOMEX Nylon yarn (Ref. 26), formerly designated as "HT-1" by DuPont, shows less than 5 percent strength loss after more than 1,000 hours exposure to 350°F hot, dry air. Parachute textiles made from NOMEX yarn would therefore be satisfactory for fabrication of the Mars capsule parachutes.

NOMEX yarn has already been made into parachute textiles in pilot quantities. The finished textiles are generally 10 percent higher in weight, substantially lower in breaking elongation, and somewhat lower in porosity than comparable textiles woven from standard Nylon. NOMEX textiles are also much higher in price than comparable standard Nylon textiles.

In this study NOMEX is selected as the primary material for fabrication of the Mars capsule parachutes in view of its very superior heat resistant qualities. For more specific identification of the general types (strength and weave) of materials recommended, following sections of this report will call out a NOMEX material similar to existing commercial and/or MIL SPEC fabrics.

5.7.3 Final Descent Parachute for a Biocapsule

Recovery system weight to a large extent depends on the weight of the final descent parachute, and the first step in weight optimization is, therefore, to make the final descent chute as light as possible. For the Mars capsule, a 10 percent flat, extended skirt-type chute is selected for final descent, since this type of chute provides the best drag-to-weight efficiency of all nonrotating canopy designs within the allowable oscillatory limit of ±20 deg. The size of the final descent chute is fixed at 30.3 ft nominal

diameter (D_o) by the requirement of 60 ft/sec on Mars at a mass density of 4.21×10^{-5} sl/ft^3 for a nominal total lowered weight of 100 lb, using a conventional design drag coefficient (C_{D_o}) of 0.70.

The configuration recommended for the final descent parachute is: 30.3 ft nominal diameter, solid textile, 10 percent flat extended skirt type parachute with a NOMEX fabric similar to 0.88 oz/yd^2 (JAN-P-498) Nylon in the lower two-thirds of the canopy, NOMEX similar to 1.1 oz/yd^2 (MIL-C-7020D Type I) Nylon in the upper third of the canopy, and twenty-eight 300-lb tensile strength NOMEX suspension lines similar to MIL-C-7515B, Type XI, Nylon. The weight of this parachute will be approximately 11.9 lb, including a 10 percent allowance to account for the use of NOMEX rather than standard Nylon, and it will safely withstand deployment at a dynamic pressure of 4.0 lbs/ft^2, using design and safety factors recommended for terminal-stage space vehicle recovery. This configuration represents a 1-lb savings in weight relative to a conventional light-weight chute of the same size and of standard Nylon.

Since appreciable residual spin may remain at the time of final-descent chute deployment, a swivel must be incorporated into the final descent chute attachment rigging.

Also, so that the final descent parachute will not drag the capsule after touchdown, some type of post-impact release fitting must be incorporated into the final descent chute attachment rigging. Several different types of parachute load release fittings have been developed and flight tested on previous drone, missile, and cargo delivery parachute systems.

5.7.4 Drag Parachute

Current state-of-the-art in drag parachutes indicates that there should be no major difficulty in design and development of a ribbon-type parachute to operate reliably at Mach numbers up to, say, 2.5; especially at the relatively low dynamic pressures (order of 30 lb/ft^2) anticipated for the Mars parachute descent system. As an example of technology in this field, a 2.18-ft constructed diameter ribbon-type parachute has

been successfully deployed in a flight test at Mach 2.45, 60,000 ft altitude, and an incompressible dynamic pressure of 520 lb/ft^2. However, in general, the lower the Mach number, the easier and less expensive the development program necessary for a drag chute system.

For service in the Martian environment, a rather large drag parachute (10 to 15-ft diameter range) is required. Since there is at present no high-supersonic flight-test experience with this large a parachute and since obtaining dynamically similar test conditions in the Earth environment becomes a complicated and costly affair for higher Mach numbers, the most practical and reliable approach is to reduce the Mars-descent-system drag-chute Mach number requirement by as much as possible. For these reasons, Mach 2.5 is (somewhat arbitrarily) established as an upper limit for deployment of the Mars descent system drag chute.

As noted before, the final descent parachute should be deployed at subsonic speed, at 16,500 ft altitude or above, and at a dynamic pressure of 4.0 lb/ft^2 or less. These conditions establish the design point for the final descent chute shown in Fig. 5-75. The drag chute is sized so as to decelerate the vehicle to the final descent chute design point when deployed at Mach 2.5 or less. By calculation, it is determined that a 12-ft nominal diameter ribbon-type parachute deployed at Mach 1.75 at 21,800 ft will decelerate the vehicle to the final descent chute design point for the limiting case of reentry at the steepest angle in the least dense atmosphere. The trajectory for the capsule on the drag chute is also shown in Fig. 5-75. Although a smaller drag chute deployed at higher Mach number would also serve to decelerate the capsule to the required final descent chute design point, the 12-ft diameter drag chute has the additional utility of providing a sufficient time of descent (without the use of a final descent chute) between sonic speed and zero nominal elevation (touchdown) to serve as the only chute required for an atmospheric capsule.

The configuration recommended for the drag parachute is a 12-ft nominal diameter, ribbon-type parachute with 100-lb and 200-lb NOMEX ribbons (similar to MIL-T-5608E,

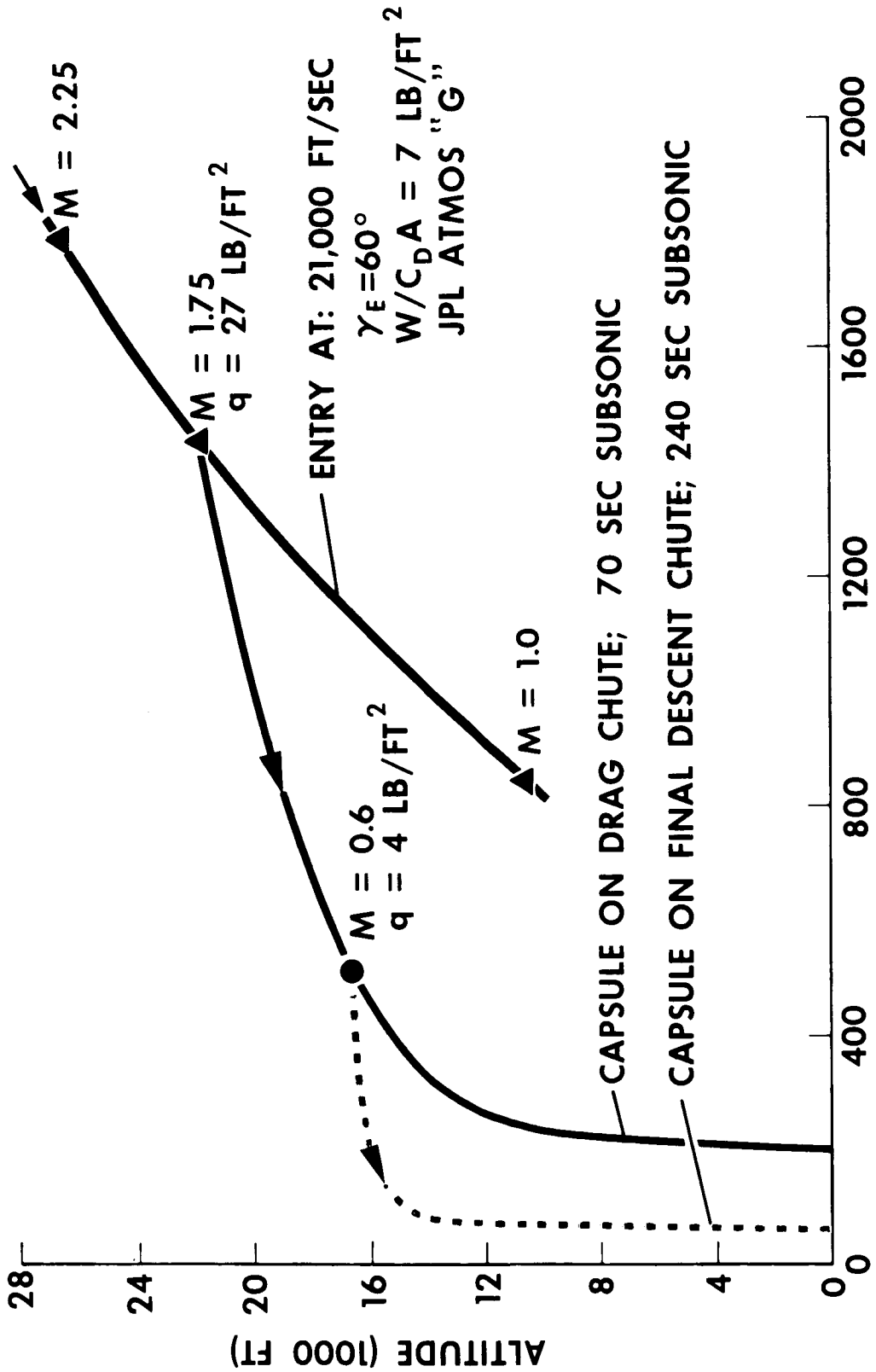


Fig. 5-75 Parachute Design

Type V, Classes A and B, respectively) in the canopy and with twelve 375-lb NOMEX suspension lines (similar to MIL-C-5040B, Type II). The canopy ribbons mentioned might be replaced by other ribbons of equivalent strength in order to secure a canopy grid pattern suitable for supersonic inflation.

The weight of the drag parachute will be approximately 1.9 lb and it would safely withstand deployment at an incompressible dynamic pressure of 27 lb/ft^2, using design and safety factors recommended for space vehicle decleration stage parachutes. Note that the weight estimated for the drag chute includes a 10 percent allowance for use of NOMEX textiles and that the calculated drag chute trajectory in Fig. 5-75 has taken into account the known supersonic drag-area reduction for parachutes.

5.7.5 Recovery System Sequencing

Since the elapsed times from beginning of entry (or from time of de-orbiting) vary widely for the envelope of entry trajectories which must be considered, the most direct manner in which to initiate sequencing of the descent system appears to be use of a "g"-switch. The trajectory data of Fig. 5-76 show that initiation of drag chute deployment at a longitudinal load factor setting of 3.5 would result in deployment conditions varying from Mach 1.75 at 21,800 ft (incompressible dynamic pressure of 27 lb/ft^2) to Mach 2.5 at 131,000 ft (incompressible dynamic pressure of 27 lb/ft^2). Thus, use of a single g-switch has the advantage of simplicity in the instrumentation required to initiate deployment and the disadvantage of exposing the drag chute to a high-Mach environment for a relatively long time for one of the extremes of entry conditions. However, since the drag chute can be qualified for high-Mach performance in development tests, this scheme appears more desirable than use of a multiple-g switch and time-delay deployment scheme which could be used to narrow the Mach number spread in deployment conditions. Since the g-switch circuit is critical to successful deployment of the drag chute, parallel circuitry is mandatory.

Operation of the g-switch at a preselected setting (e.g., longitudinal load factor of 3.5) would actuate a pyrotechnic device which would effect ejection of the aft cover

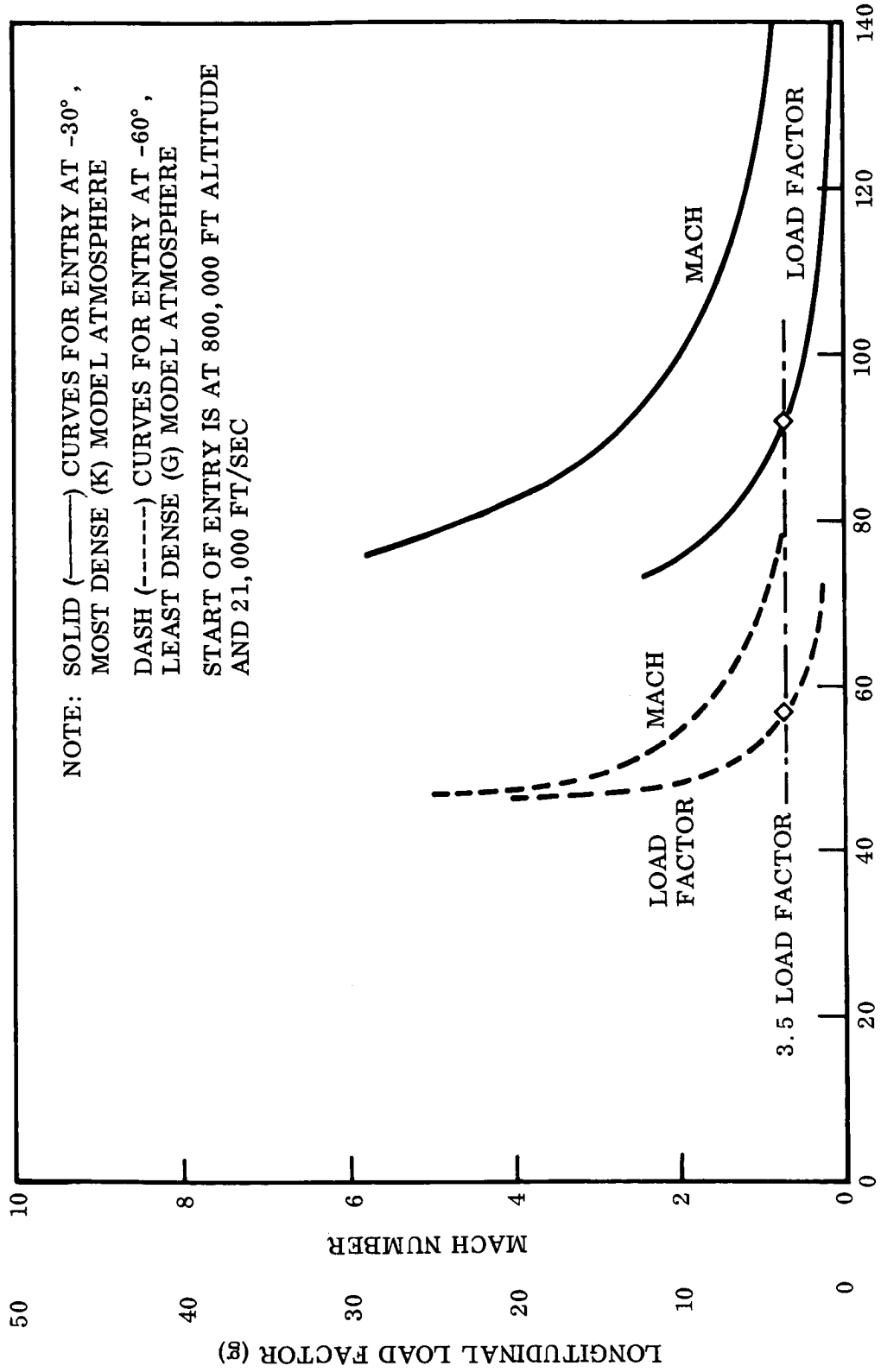


Fig. 5-76 Capsule Entry Time History

from the vehicle, and an intermediate tie-line between the aft cover and the drag chute deployment bag would be used to extract the drag chute pack from its compartment and subsequently to peel the deployment bag from the drag chute. That is, the aft vehicle cover serves as a pilot chute for deployment of the drag chute.

Release of the drag chute (in the case of the descent system configuration requiring also a final descent chute) could also be signalled by a g-switch, with the switch setting selected to deploy the final descent parachute at its design dynamic pressure of 4.0 lb/ft^2. The circuit used for this element of the sequence should be well damped, in view of the wide fluctuations in load which will occur during and following supersonic deployment of the drag chute. An intermediate jumper line from the drag parachute to the final descent chute pack would be used to extract the final descent chute pack from its stowage compartment in the capsule and subsequently to peel the deployment bag from the final descent parachute. Thus, the drag chute serves as a pilot chute for deployment of the final descent chute; a system which has the advantage that the vehicle continues to descend on the drag chute should any element of the drag chute release circuit fail (as contrasted, for example, to a scheme in which the final descent chute is deployed independently following release of the drag chute).

5.7.6 Development Test Program

The approximate development test program recommended for the Mars descent system is summarized in Table 5-37. In the wind tunnel and systems tests, it is particularly important that the flow field which will exist at time of deployment of the drag chute be duplicated insofar as possible, including the effects of vehicle spin and oscillation. Satisfactory ejection and deployment of parachutes at supersonic speeds is a complex problem, particularly in view of the adverse pressure gradient existing in the supersonic wake of a bluff body, and systems tests must therefore be designed to ensure that the design used presents a satisfactory solution to the problem.

In addition to the wind tunnel and free-flight tests shown in Table 5-37, there also should be performed the usual textile, bench, and mockup tests performed for a

Table 5-37

PRELIMINARY DEVELOPMENT TEST PROGRAM – PARACHUTE

Approximate No. of Tests	Purpose of Tests	Type of Test	Components or Article	Test Conditions (Approx.)	Instrumentation
15	Function, strength, & performance at max. q and velocity of descent	Aircraft launch	Final descent chute assembly	Dummy vehicle, W = 38 to 2,200 lbs, deploy at altitudes up to 27,000 ft	1. Range tracking (incl. chute oscillation 2. Color films in vehicle-borne cameras 3. Telemetered accel. & telltales
10	Function, strength, & performance at max. q and Mach number	Wind tunnel	Drag chute assembly	Mach 1.75 to Mach 2.5, dynamic pressure of approx. 27 lb/ft^2, deploy from dummy capsule in tunnel	1. Films of chute deployment and oscillation (vehicle-borne cameras & tunnel cameras) 2. Recorded force data
5	Functional test at low speed, max. q	Aircraft or balloon launch	System	Dummy vehicle with close to actual configuration (incl. ejection of aft cover, spin, and heat shield drop), W = 225 to 1,000 lbs, deploy at altitudes up to 30,000 ft	1. Range tracking (incl. chute oscillation 2. Color films in vehicle-borne cameras 3. Telemetered accel. & telltales
7	Function, strength, & performance at max. q and Mach number	Balloon launch (with possible rocket boost)	System	Mach 1.75 to Mach 2.5 at extreme altitude (approx. q of 27 lb/ft^2); vehicle to simulate actual system	1. Range tracking (incl. chute oscillation) 2. Color films in vehicle-borne cameras 3. Telemetered accel. & telltales
≤ 3	Strength	Thermal (heat sterilization procedure)	Final descent & Drag chute assemblies	Three cycles of 36 hours each at 293°F	1. Textile testing machine 2. Recording thermometer 3. "TempilStik"

parachute recovery system; for example, ground tests of the aft cover ejection mechanism to determine if sufficient kinetic energy is delivered to the aft cover assembly by the mechanism.

5.7.7 Summary of Design Data

Weight. Preliminary design calculations indicate that descent system weight will be:

Item	Weight (lb)	
	Biocapsule	Atmospheric Capsule
Final descent parachute	11.9	0
Final descent chute deployment bag	0.4	0
Final descent chute swivel and release fitting	0.8	0
Drag chute	1.9	1.9
Drag chute riser	1.0	1.0
Drag chute bag	0.3	0.3
Ejection device, etc.	1.5	1.5
Total	17.8	4.7

Packed Volume. Packed volume required for the two parachute assemblies (chute, bag, connecting links, riser) will be approximately:

- Final descent parachute assembly . . . . . 810 cu in.
- Drag parachute assembly . . . . . 190 cu in.

Parachute Loads. Peak loads at deployment of the parachutes will be approximately:

- Drag parachute . . . . . 1,525 lb force
- Final descent parachute . . . . . 3,640 lb force

5.7.8 Time of Descent

The atmospheric capsule system will have a subsonic time of descent of about 71 sec (1 min 11 sec) between 18,600 ft and ground zero. The biocapsule, using the final

descent chute, will have a subsonic time of descent of about 248 sec (4 min 08 sec). Figure 5-77 shows altitude versus time elapsed after reaching sonic speed for the two systems. Note that Fig. 5-77 is for the case of steepest reentry into the least dense (K) atmosphere at the same angle; the times of descent of Fig. 5-77 would be increased by a factor of 1.5 if the parachutes were initially deployed at the same altitude. From Fig. 5-77 it is evident that neither parachute descent system provides sufficient margin for the case of the 5-km (16,405-ft) high mountain; however, such a case is, statistically, of vanishingly small probability. The two-parachute descent system gives ample time (1 min) at subsonic velocity for terrain elevations as high as 12,000 ft.

5.7.8 Tradeoffs

For small changes in total lowered weight, each of the descent system configurations described herein will remain at about the same percentage of total lowered weight, all performance criteria remaining the same. Thus, the single-drag-chute system will weigh about 5 percent of total lowered weight, and the drag chute/final descent chute system will amount to about 18 percent of total lowered weight.

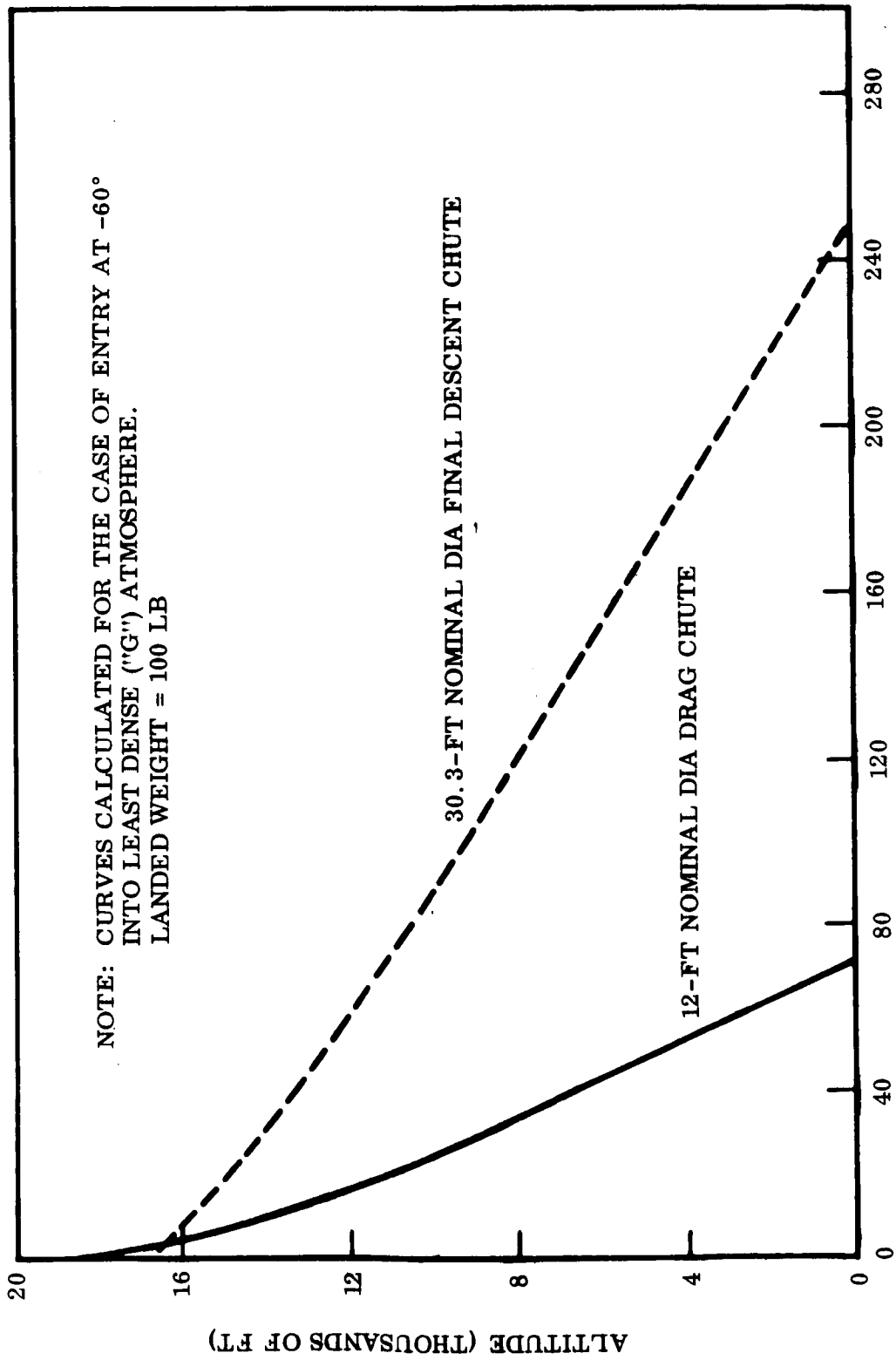


Fig. 5-77 Capsule Subsonic Descent Time History

5.8 STERILIZATION

5.8.1 Sterilization Concept

Necessity. Studies of the Martian atmosphere indicate that conditions are such that life in some form may exist. In light of this, Mars has been declared a biological preserve, and any vehicle destined for entry into the atmosphere must be sterilized to prevent contamination of the planet by terrestrial microorganisms. Sterilization criteria has been established requiring the vehicle to be absolutely sterile in order to achieve a probability of one in 10,000 that no viable earth organism reaches Mars.

Treatments and Methods. The most accepted method for sterilization of spacecraft is by dry heat. Temperature cycles of 145°C for 36 hr, three cycles for certification and 135°C for 24 hr for sterilization, have been established. Thermal sterilization requires heating in an inert atmosphere to minimize oxidation.

Gaseous sterilization using ethylene-oxide has been used for surface sterilization of the Ranger vehicle and as a sterilant in aseptic assembly glove box operations. Aseptic assembly techniques have been proposed for combining with heat sterilization in producing a sterile vehicle containing heat sensitive components.

Other sterilization techniques such as ionizing radiation may be possible; however, insufficient data as to dosage, procedures and vehicle integration technique is available to allow consideration during this study. Liquid wipeon sterilants can be used as a cleansing step prior to other sterilization processes.

Vehicle Integration. The integration of sterilization procedures into spacecraft factory-to-launch sequences requires many precautions to prevent inadvertent re-contamination after the final sterilization treatment. The vehicle or probe to be sterilized must be encapsulated in a biological shroud and a positive pressure maintained within the shroud. The probe or vehicle must remain encapsulated until final separation from the booster

or bus has been accomplished. The minimum distance from earth for ejection of the sterility shroud is 600 km.

For the purposes of this study a heat sterilizable atmospheric probe was considered. A set of sterilization guidelines have been adopted and integrated with vehicle design. Components and materials of construction were selected for compatibility with heat sterilization. The use of organic materials was avoided because of many disadvantages (i.e., incompatibility with heat, a possible bacteria culture medium, raising the vehicle material contamination level).

Assembly of the probe would be performed in a clean-room environment to minimize material contamination levels. All components and systems would be assembled and the completed probe encapsulated in a biological shroud. Umbilical connections to the capsule provide for flowing heated nitrogen through the capsule to perform the heat sterilization cycle. Prior tests with a thermal mockup would provide data as to length of time to achieve thermal stabilization of the largest thermal mass. Filtered sterile nitrogen would be circulated through the capsule for the prescribed sterilization cycle. After-sterilization provisions allow for maintaining a positive pressure within the capsule to retain the sterile condition.

Once mated to the spacecraft, instrumentation can provide a constant monitor of pressure within the capsule. If pressure were to be lost, the capsule would be removed from the vehicle, and a "spare" capsule subsituted; the faulty capsule would have the leakage point diagnosed, and the heat sterilization cycle repeated.

The sterility shroud would be retained until the capsule has been separated from the orbiter bus. Separation of the shroud from the landing capsule can be programmed to prevent the shroud from entering the Martian atmosphere.

5.8.2 Problem Areas

Heat Sensitive Items. Heat sterilization imposes many restrictions on vehicle design. Each component and material of construction must be researched to determine

compatibility with the thermal environment. In most cases, spacecraft components can withstand the sterilization temperature without damage.

Some spacecraft components are classified heat sensitive and cannot withstand the heat sterilization temperature. For the purposes of this study each of the systems considered for use within the entry capsule were analyzed for possible heat sterilization problem areas. Major areas of concern were batteries, propulsion, and parachutes.

Currently available high-energy primary batteries cannot withstand the heat sterilization cycle. The atmospheric probe being considered in this study requires a relatively low amount of electrical power. The Jet Propulsion Laboratory has informed LMSC that a heat sterilizable battery can be made available which will satisfy the power requirements of the probe.

Obtaining a heat sterilizable solid propellant was considered a problem area. One propellant company has successfully tested solid propellants which have been subjected to the sterilization temperature cycles. This propellant has been considered for the propulsion system for the atmospheric probe.

Heat sterilization of the parachute retardation system may be accomplished in an inert atmosphere. Several parachute manufacturers have been conducting tests to determine performance degradation after the temperature cycles.

System Tradeoffs. In selecting components and systems to be compatible with heat sterilization it sometimes becomes necessary to sacrifice performance or weight to obtain an operational vehicle. The atmospheric probe being considered during this study required some alteration of component selection.

- The parachute material will have to be a heavier type than ordinarily necessary to be able to withstand the sterilization process.

- The batteries to be used must be heavier than nominal to withstand the heat sterilization requirement. Estimates of 10 w-hr/pound have been suggested by JPL rather than 30 w-hr/pound for a non-heat sterilizable system.
- The mass spectrometer to be used will employ a Faraday cup rather than a scintillation counter using a crystal. This unit can be heat sterilized whereas the crystal system would deteriorate with heat.

Alternate Sterilization Processes. While this study only considered a heat sterilizable atmospheric probe, the possibility of using alternate sterilization methods exists. Gaseous sterilization using ethylene-oxide gas, radiation, and aseptic assembly all may be used in conjunction with heat sterilization.

A possible step to aid in assurance of a sterile capsule would be to surface sterilize the orbiter bus with ethylene-oxide gas after final assembly of the vehicle. This procedure would require sealing the interior of the bus from the adjacent booster stage.

5.8.3 Support Equipment

Heat Sterilization. Specifications for heat sterilization require heating in an inert atmosphere. Sterilization cycles can be accomplished in an oven containing nitrogen, provided provisions are made to replace the atmosphere within the capsule with nitrogen. Care must also be taken to accommodate the increase in pressure within the capsule. A laboratory-type temperature chamber can be used to perform the sterilization.

The concept proposed during this study is to circulate heated sterile nitrogen through the capsule using quick disconnect couplings for inlet and outlet of the heated gas. Equipment to perform this function will essentially be a closed-loop air-conditioning system. Sterile nitrogen would be introduced to the unit and heated to the sterilization temperature. The heated gas would be circulated through the unit to sterilize components through the gas flow lines. Bacteria filters would be inserted in the inlet and outlet lines of the unit for added sterility confidence.

Procedures. Procedures for performing the sterilization cycles must, by necessity, be carefully detailed. These procedures should be included in specifications to vendors for assembly of subsystems. An outline of sterilization procedures is as follows:

- Structural design to allow maximum surface area for sterilization heat
- Assembly of all components and subsystems in clean rooms to reduce natural contamination levels
- Maximum protection of subassemblies during shipment to protect against undue contamination
- Assembly of the capsule in highest-level clean-room atmosphere
- Biological shielding of capsule after assembly
- Heat sterilization of capsule just prior to mating with the orbiter spacecraft
- Maintenance of positive pressure within the capsule after sterilization to prevent recontamination
- Retention of biological shield until after separation of the capsule from the orbiter.

NOMENCLATURE FOR SECTION 5.6

c	specific heat
H	static enthalpy
h_o	non-blowing value of convection coefficient
k	Planck-mean mass absorption coefficient
m	mass flow between surface and streamline
M_a	molecular weight of atmospheric gas mixture
M_{inj}	molecular weight of injected gas mixture
p	pressure
q_r	radiative heat flux
r	distance from axis or plane of symmetry
Re_Θ	momentum thickness Reynolds number
R_M	maximum body radius
R_{eff}	effective radius of curvature
s	distance along streamline
T	temperature
u	velocity
x	distance along surface in plane of symmetry from stagnation point
y	distance along surface normal to plane of symmetry from stagnation point, or distance from surface through shock layer
δ	material thickness
ϵ	emissivity
μ	viscosity
ρ	density
σ	Stefan-Boltzmann constant
ν	index, zero for two-dimensional flow and unity for axisymmetric flow

SUBSCRIPTS

e	edge of boundary layer
i	entry point
o	s
∞	free stream

Section 6

PROGRAM PLAN FOR MARS ORBITER AND ATMOSPHERIC CAPSULE DEVELOPMENT

As a base for establishment of a reasonable estimate of the eventual cost of system design and development, all phases of the program, from preliminary design to completion of reduction of data from the orbiter, have been reviewed. The proposed program outlined herein establishes milestone dates and has been set down in sufficient detail to allow logical derivation of program requirements and to highlight those areas in which special effort is required. The plan assumes two separate missions: a Mars orbiter launched in 1969, and a Mars orbiter and atmospheric capsule launched in 1971. Additional data is presented to show the effect of adding an atmospheric capsule to the 1969 mission.

To allow derivation of reasonable price data and to arrive at a tangible integrated testing and manufacturing plan, it has been assumed that LMSC would be the Contractor for the orbiter and capsule; however, the plan presented and cost thereof should be approximately the same for any other contractor with comparable capability.

6.1 DEVELOPMENT PROGRAM

Following is a discussion of the ground rules of the proposed plan, an outline of the orbiter and capsule subsystems (as a base for discussion of hardware elements), and a description of the basic pieces of the plan including the Master Schedule and the factory-to-launch sequence.

6.1.1 Program Ground Rules

A preliminary program plan has been prepared for the development, manufacture and test, and launch of Mars orbiters and capsules based on the following ground rules:

- Two launches of orbiter will be planned for the 1969 mission
- Two launches of orbiter/capsule will be planned for the 1971 mission
- Floxed Atlas-Centaur launch vehicle (launch system, launch pads, and modifications not costed)
- Program go-ahead approximately September 1, 1965 for Phase II and hardware
- Utilize maximum proven hardware from Mariner C (solar arrays, etc.)
- Scientific instruments to be "GFE", design integrated by LMSC and installed by JPL
- Capsule sterilization at JPL
- 210 ft. dish DSIF network available
- Six month data acquisition following each Mars encounter

6.1.2 Orbiter/Capsule Subsystems and Functions

The hardware elements of the program comprise the orbiter, the capsule, and support equipment (AGE). Figures 4-5 and 4-6 show the general configuration of the orbiter and capsule; the 1971 orbiter is essentially the same as the 1969 orbiter except that it provides mechanical support for the capsule and embodies rearrangement of the scientific instruments to provide space for the capsule support cone. A single electrical breakaway connector connects the capsule functionally to the orbiter.

The basic subsystems and their major components are listed below.

Orbiter.

Spaceframe – Includes release mechanisms, separation springs, and actuation hardware for solar-array extension and magnetometer boom extension.

Scientific Instruments – Includes the various instruments for both interplanetary and Mars orbit measurements. Includes also the instrument platforms and actuation servos.

Electronics – Includes the antennas, communication and command equipment, and the central controller for all subsystems.

Guidance and Control – Includes the inertial platform, the position-orienting instruments, the control electronics package, and the attitude control elements (gas supply, valves and plumbing, and pitch/yaw/roll gas jets).

Thermal Control – Includes temperature control louvers, heaters, insulation.

Propulsion – Includes the gimballing liquid propellant engine, the propellant tankage (including pressurization gas), plumbing and valving.

Electrical Power – Includes battery, solar arrays, power conditioning equipment, and all electrical interconnect cabling.

Capsule.

Spaceframe – Includes the entry heatshield (jettisonable), the sterility shroud (jettisonable), the separation devices, and payload release mechanism.

Capsule Guidance and Control – Includes the parachute pack and solid-propellant rocket.

Payload Assembly – Includes structural frame which mounts the various scientific instruments and electronic equipment.

Scientific Instruments – Includes instruments for sampling of Mars atmosphere as payload package moves from orbit to Mars impact.

Electronic-Electrical – Includes battery, power conditioning, antenna, and information storage, conditioning, and transmission equipment (for transmission to orbiter).

Support Equipment.

These equipments (AGE) comprise the handling, checkout, and transportation hardware required for supporting the orbiter and capsule from factory to launch. Also included is the sterilization equipment required for sterilizing the capsule at JPL. Three complete sets of AGE (excluding the sterilization equipment) are included, one set each to LMSC, JPL, and MILA.*

* MILA is used to designate the launch pad area whether in NASA or Air Force location.

6.1.3 Basic Plan Outline and Schedule

Quantities of Hardware Required. For the 1969 Mission phase of the program, the following hardware will be required:

3	Flight articles (orbiter) – includes one backup unit
1	Qualification test article (orbiter)
1	Structural test article (orbiter structural elements only)
1	Functional mockup (orbiter)
	Components for development and reliability tests
3	(Sets) AGE
	20 percent spares

The following hardware will be required for the 1971 Mission:

3*	Flight articles (orbiter/capsule) – includes one backup unit
2	Flight articles (capsule) – for additional backup
1*	Qualification test article (orbiter/capsule)
1*	Structural test article (orbiter/capsule structural elements)
1	Sterilization article (capsule)
1*	Functional mockup (orbiter/ capsule)
**	Miscellaneous hardware for development and reliability tests
3***	(Sets) AGE

The Master Schedule. The 1969 mission plan, as illustrated by Fig. 6-1 would result in the delivery of three orbiters to MILA in the fourth quarter of 1968, ready to launch in the first month of 1969. Two launches are planned; the third orbiter would be readied and available as a backup article. Both launches would be performed within the 30-day opportunity and it is expected that two separate launch pads (Launch Complexes 36A and 36B) would be assigned.

---

*Includes "modified" 1969 orbiter elements
**Testing required only for modified or new elements
***Includes modified 1969 AGE elements

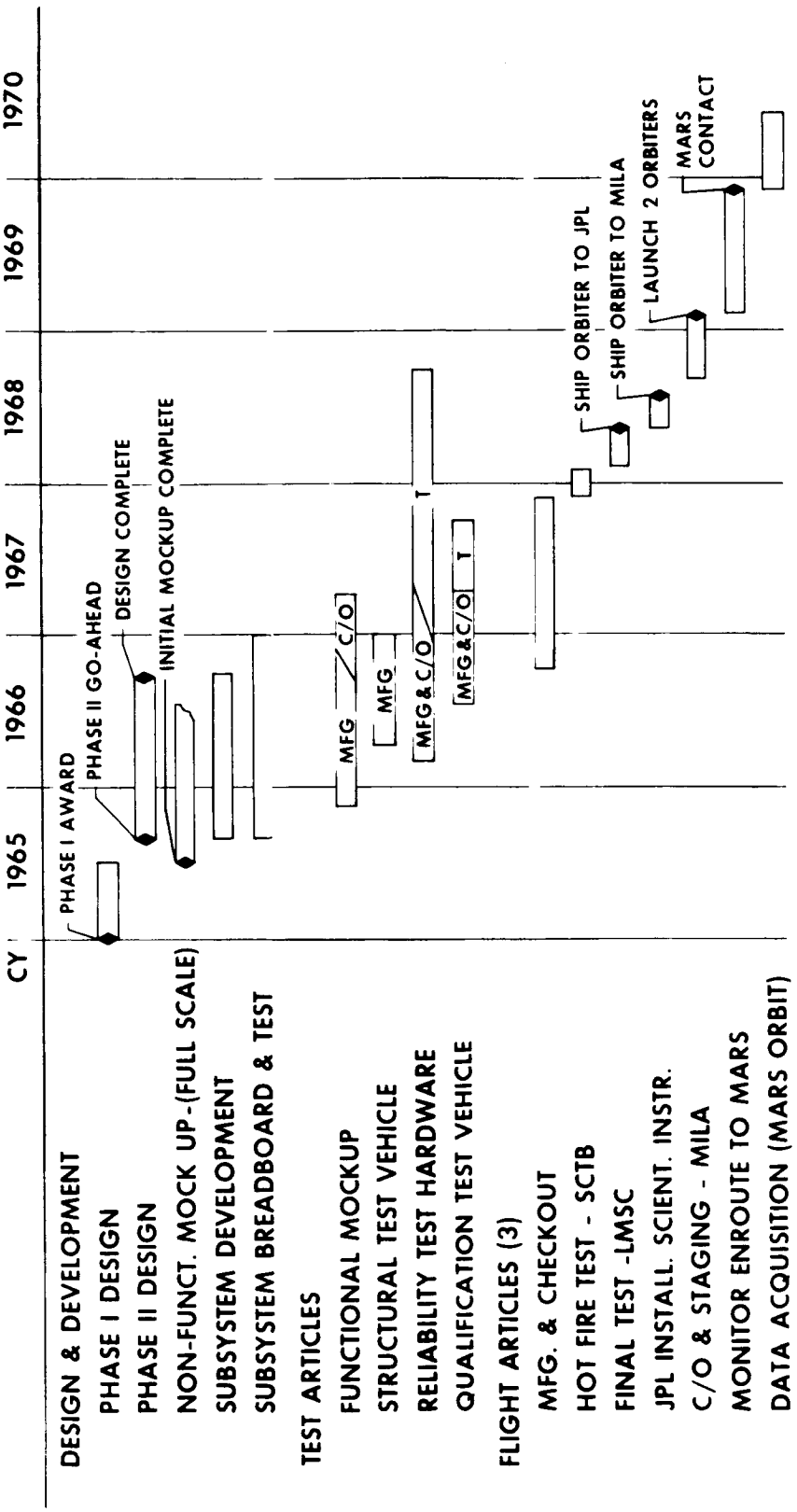


Fig. 6-1 Program Master Schedule – 1969 Mission

Following a Phase II go-ahead in September 1965, subsystem design and development would be initiated in parallel. Design can be completed in the fourth quarter of 1966, allowing sufficient time to complete the qualification and reliability test hardware in early 1967 and providing a reasonable span for building the flight articles and performing preliminary checkout of integrated subsystems. The orbiters (flight articles) would be shipped to JPL in May of 1968 where the scientific instruments would be installed and final checkout (equivalent to launch base checkout) performed prior to shipping to MILA. The 1969 mission effort will terminate with data acquisition and reduction, approximately mid-1970.

The 1971 mission plan illustrated by Fig. 6-2 is quite similar to that for the 1969 mission. Two launches are planned in a 30-day opportunity in May 1971. A third orbiter/capsule vehicle would be readied at MILA for backup to the two launch vehicles; additionally, two complete capsules would be available for replacement on any of the three flight vehicles. A separate capsule would be supplied to JPL for sterilization and sterility assessment during the development and qualification phase (delivery to JPL in fourth quarter of 1969).

All flight articles for a particular mission would be assembled essentially in parallel; therefore, no schedule offsets have been shown for the separate articles. Also, manufacture of AGE would proceed essentially in parallel with equivalent flight articles so that interface tests could be made; for example, the LMSC qualification unit of AGE would be used in conjunction with the qualification tests of the orbiter or capsule.

Factory to Launch Sequence (Flight Articles). It is planned that the orbiter or capsule be assembled in a segregated and environmentally isolated (dust filtration and air conditioning) area at the LMSC Sunnyvale complex. The capsule will be assembed in a "white room" atmosphere and sealed, with the objective of limiting the quantity of spores to be eradicated by the subsequent heat sterilization at JPL. The components of the various subsystems will be manufactured at LMSC or subcontractor's facilities and delivered to the assembly site.

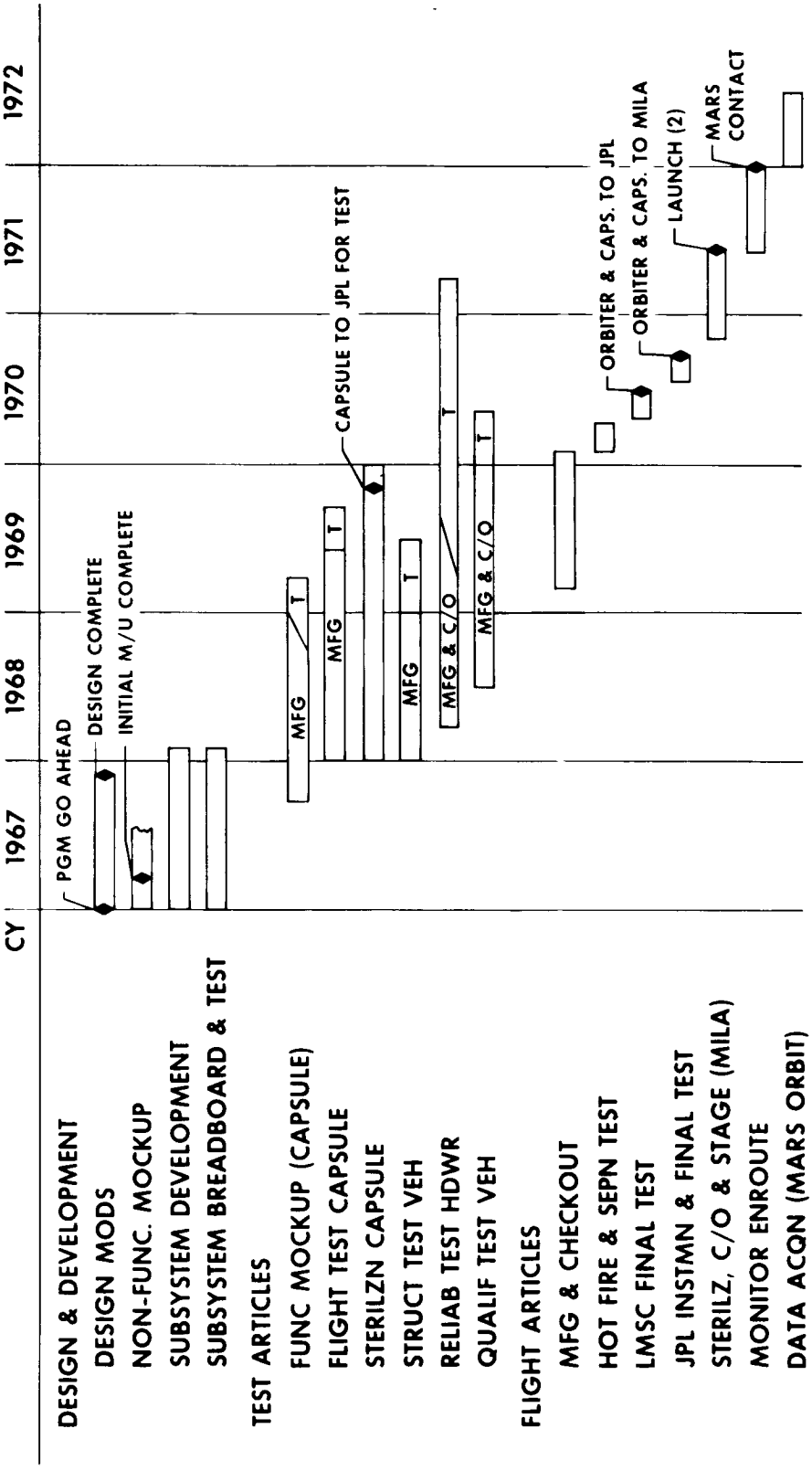


Fig. 6-2 Program Master Schedule—1971 Mission

Acceptance Testing. Acceptance testing of each major element of a subsystem and finally of the preassembled subsystem itself will be conducted at appropriate coordinated test stations. Section 6.2 discusses the overall test plan.

Preliminary Acceptance Test and Hot Fire. The orbiter and capsule would be separately assembled and given a preliminary acceptance test in the assembly area. They would then be mated and shipped to Santa Cruz Test Base (LMSC facility, approximately 30 miles from Sunnyvale) for hot fire test. The main engine would be operated while the other subsystems are exercised through a nominal routine. The various pryotechnic devices would also be activated as practicable and capsule separation from orbiter simulated (in a holding fixture). After test, toxic fuel systems would be drained and purged and refurbishment as necessary accomplished.

Final Acceptance Test at LMSC Assembly Site. The orbiter or orbiter/capsule would then be returned to the LMSC assembly site where a complete final acceptance test would be performed. After complete integrated systems runs, the articles would be given a checkout test identical to that which would be conducted during MILA checkout, using the AGE checkout gear.

Installation and Checkout of Scientific Instruments. The orbiter or orbiter/capsule would be placed in an environmental-isolating transport van (AGE) and shipped to JPL. JPL would install the scientific instruments in the flight articles and check out the installation. Additional checkout of other subsystems is planned to assess maintenance of functional capability; an additional set of AGE would be provided to JPL for purposes of handling and checkout.

Sterilization of Capsule. The complete capsule would be sterilized in the heat-sterilization chamber (AGE) at JPL. The capsule would be reattached to the orbiter and mounted in the transport van (AGE) for shipment to MILA.

MILA Operations – Checkout and Staging. The orbiters and capsules upon arrival at MILA would be completely inspected and checked out, using the AGE checkout equipment, to a predetermined test schedule (part of the integrated test plan and reliability plan). For the 1969 mission, three orbiters would be readied in a launch assembly area assigned to this project. For the 1971 mission, three combined orbiter/capsule vehicles and two separate capsules would be readied. The Launch Operations Support Plan, Section 6.6, provides details of the MILA operations.

If at any time an orbiter or capsule should fail to pass a prelaunch checkout, it would be replaced with a standby article. The faulty unit would be returned to JPL or LMSC for repair or adjustment.

At time of launch vehicle staging, the orbiter or orbiter/capsule would be transported to the launch pad in the transport van and hoisted and erected onto the Atlas-Centaur vehicle. The pressurized gas tanks will have been filled and sealed in the launch assembly building. Propellant would be loaded on the pad, with on-loading occurring at discrete steps through the launch period if delays are experienced. After staging, a countdown of the Atlas-Centaur/orbiter vehicle can be conducted with a simulated launch and flight being completed immediately prior to actual launch.

Test Articles. Various test articles are required to validate the functional characteristics and reliability of the flight articles. These are described in general terms as follows. For a detailed description of the testing involved and the test plan, refer to Section 6.2

Development Test Hardware. Various functional models and breadboards will have to be fabricated and tested during the development engineering phase to verify functional concepts and interfaces. Additionally, test specimens for materials tests, thermal and structural evaluation, and process development will have to be fabricated and tested. This development-test hardware will not necessarily be identical to the final orbiter or capsule but must satisfy all requirements of the development test

program. Previously qualified or standard components can be combined with newly developed items in building up the test breadboards and other test articles required.

Functional Mock-Up. A complete orbiter or capsule would be assembled utilizing prototype units from each subsystem. System interfaces, mounting arrangements, interconnect cabling and plumbing can be determined on this mockup. Additionally, the prototype AGE checkout equipment can be connected to the mockup subsystems and preliminary system checks made. This mockup would be updated as qualified hardware became available, or as changes are made to the orbiter or capsule so that it always represented the latest configuration.

Qualification Articles. One equivalent vehicle is planned for all the qualification tests. Although qualification may be required at the assembly or subsystem level, the final assembled flight article will require functional qualification under the expected environmental and operating conditions. The hardware supplied for the qualification test would be identical to that delivered for the flight articles.

Structural Test Articles. The spaceframe of the orbiter and capsule and those pieces of equipment which affect the structural function of the flight articles would be assembled and tested under various static and dynamic loads. These structural items will be the prototypes of those used on the flight articles. Dummy weights simulating functional subsystem equipment can be utilized in lieu of the subsystem components (electronic, etc.).

Sterility Test Article – Capsule. A complete capsule, including all functional equipment, would be assembled, checked out, and shipped to JPL for sterilization and post-sterilization assessment. This article would include items identical to flight article hardware and would afford final verification that the sterilization process will be effective and will not degrade the functional characteristics of the capsule.

Table 6-1

INTEGRATED TEST PLAN – 1971 MISSION,
ORBITER AND CAPSULE

ORBITER

Test Article Description	Development Tests					Qualification Tests					Reliability Assessment Tests					Acceptance Tests							Launch Base Tests & Reliability Demonstration			
	Envir.	Elec.	Mech.	Struct.	Funct.	Envir.	Elec.	Mech.	Struct.	Funct.	Envir.	Elec.	Mech.	Func.	Life	Envir.	Elec.	Mech.	Func.	F.S.O.	Hot Fire	Elec. C/O	Mech. C/O	F.S.O.	Rel. Dem.
Orbiter Assembly	(2)		(2)	(2)	(2)	(2)		(2)	(2)	(2)				(2)	(2)			(2)	3	(2)	(3)	(3)	(3)	(3)	(3)	
• Space Frame Assembly			2	(2)																						
• Adapter, Centaur			2	(2)																						
• Shell Structure			2	(2)																						
• Separation Spring Assembly			4	(4)																						
• Solar Panel Mechanics			4	(4)																						
• Release Band Mechanics			4	(4)																						
• Struct. Assembly			2	(2)																						
• Outer Shell			2	(2)																						
• Webs Internal			6	(6)																						
• Sc. Plat. Stationary			2	(2)																						
• Sc. Plat. Support			2	(2)																						
• Tank Support			2	(2)																						
• Engine Mount			2	(2)																						
• Antenna Supports			4	(4)																						
• Solar Array Supports			4	(4)																						
• Magnetometer Boom			2	(2)																						
• Brace Struts			6	(6)																						
• Capsule Support Struts			6	(6)																						
• Pin Puller, Capsule Separation			6	(6)	(6)																					
• Ejection Spring Capsule			2	(2)																						
• Pin Puller, Solar Array			6	(6)	(6)																					
Scientific Instruments S/S																(2)	(2)	(2)	4	(4)		(1)	(1)	(1)	(1)	
• Ion Chamber	(1)		(1)	3				(2)	3				(3)													
• Particle Flux Meter	(2)	2	(2)		(2)	2	(2)	(2)		(2)		(2)	(2)	(2)	1							(1)	(1)	1		
• Cosmic Dust Collector			(2)		2			(2)		2			(2)	(2)	1											
• Micrometeoroid Detector		(2)			2		(2)			2				(2)	1											
• Magnetometer		(2)			2		(2)			2				(2)	1							1				
• UV Photometer	(2)	(2)			2	(2)	(2)			2		(2)		2	1							(1)		1		
• I.R. Radiometer	(2)	(2)			2	(2)	(2)			2		(2)		2	1							(1)		1		
• Multivator	(2)	(2)	(2)		2	(2)	(2)	(2)		2		(2)	(2)	2	1							(1)	(1)	1		
• Planet Dia. Scanner	(2)	(2)			(2)	(2)	(2)			2		(2)		2	1							(1)		1		
• Platform & Cover	2		(2)	(2)	(2)	2		(2)		(2)	(2)		(2)	(2)	(2)								1	(1)		
• Servo, Platform	2	(2)	(2)		(2)	2	(2)	(2)		(2)	(2)	(2)	(2)	(2)								1	(1)	(1)		
• T.V. Camera, I.R.	2	(2)	(2)	(2)	(2)	(2)	(2)	(2)		(2)	(2)	(2)	(2)	(2)	1							1	(1)	(1)		
• Trapped Radiation Detector	4	(4)	(4)		(4)	4	(4)	(4)		(4)	(4)	(4)	(4)	(4)	2							1		(1)		
• T.V. Camera (Pictorial)	2	(2)	(2)		(2)	(2)	(2)	(2)		(2)	(2)	(2)	(2)	(2)	2							1	(1)	(1)		

NOTE: F.S.O. – functionally simulated operation
( ) – reusable test article

Modifications for 1971 Mission. It has been assumed that the 1969 orbiter, with certain modifications, can be utilized for the 1971 mission. It is therefore planned that only modifications to the various subsystems be accomplished for the 1971 mission. This approach reduces the effort required for design, development, and testing. Similarly, AGE can be modified for usage for the 1971 mission rather than building completely new equipment. The modification concept is reflected in the cost summary data which are contained in Section 7.

6.2 INTEGRATED TEST PLAN

6.2.1 Integrated Test Matrix

In order to maintain test program costs within reasonable limits, an integrated program approach is required. Such a program permits the acquisition and usage of all test data from the various test sources. The program has the advantage that with computer assistance, demonstration of reliability can be performed with a minimum of additional testing, and redundancy in the types of tests performed can be eliminated.

The numbers of test articles planned to conduct the development, qualification, reliability assessment, acceptance and launch base tests are tabulated in Table 6-1.

Objectives of the Integrated Test Plan are:

- Verification of product design
- Determination of functional and environmental suitability
- Demonstration of design adequacy
- Identification of problem areas
- Demonstration of reliability of all hardware including the final system
- Provision for the acquisition and reduction of all test data

The various testing routines within the program consist of:

- Development Testing. To determine where design revision is required to specification, and to provide data for final design verification. Tests would

Table 6-1 (Concluded)

INTEGRATED TEST PLAN – 1971 MISSION, ORBITER AND CAPSULE

ORBITER (CONT.)

Test Article Description	Development Tests					Qualification Tests				Reliability Assessment Tests						Acceptance Tests						Launch Base Tests & Reliability Demonstration			
	Envir.	Elec.	Mech.	Struct.	Funct.	Envir.	Elec.	Mech.	Struct.	Funct.	Envir.	Elec.	Mech.	Func.	Life	Envir.	Elec.	Mech.	Func.	F.S.O.	Hot Fire	Elec. C/O	Mech. C/O	F.S.O.	Rel. Dem.
Electrical Pwr S/S	2	(2)	(2)	(2)	2	(2)	(2)	(2)		2	2	(2)	(2)	(2)	2		(2)		(2)	2		(1)		1	(1)
• Batteries	(4)	(4)	(4)		4	(2)	(2)	(2)		2	2	(2)	(2)	(2)	2										
• Solar Panels	(4)	(4)	(4)	(4)	4	(2)	(2)	(2)	(2)	2	2	(2)	(2)	(2)	2										
• Elec. Interconnects	(6)	(6)	(6)		6	(2)	(2)	(2)		2	2	(2)	(2)	(2)	2										
• Pyrotech. Energy Supply	(4)	(4)	(4)		4	(2)	(2)	(2)		2	2	(2)	(2)	(2)	2										
• Pwr Conditioning Units	(2)	(2)	(2)		2	(2)	(2)	(2)		2	2	(2)	(2)	(2)	2										
• Pwr TRF Switch	(2)	(2)	(2)		2	(2)	(2)	(2)		2	2	(2)	(2)	(2)	2										
CAPSULE																									
Capsule Assembly	(3)	(3)	(3)	(3)	3	(2)	(2)	(2)		2				(2)	(1)	(1)	(1)	(1)	(1)	5		(5)	(5)	(5)	(5)
• Space Frame Assy	(1)		(1)	(1)	1																				
• Heat Shield	(2)			(2)	2																				
• Thermal Shield	(2)			(2)	2																				
• Separation Devices	(4)		(4)	(4)	4																				
• Sterility Shroud Assy	(2)			(2)	2																				
• Forebody Aft Body				(2)	2																				
Communication & Elec	(2)	(2)	(2)		2	(2)	(2)	(2)		2	(2)	(2)	(2)	(2)	1	(2)	(2)	(2)	(2)	2		(2)	(2)	2	(2)
• Loop Antenna	(2)	(2)	(2)		2	(2)	(2)	(2)		2	(2)	(2)	(2)	(2)	1										
• Whip Antenna	(2)	(2)	(2)		2	(2)	(2)	(2)		2	(2)	(2)	(2)	(2)	1										
• Pwr Conditioner	(2)	(2)	(2)		2	(2)	(2)	(2)		2	(2)	(2)	(2)	(2)	1										
• Batteries	(4)	4			4	(2)	(2)			2	(2)	(2)		(2)	2										
• Multiplexer/Encoder	(2)	2	(2)		2	(2)	(2)	(2)		2	(2)	(2)	(2)	(2)	1										
• Memory	(2)	2	(2)		2	(2)	(2)	(2)		2	(2)	(2)	(2)	(2)	1										
• Transmitter	(2)	2	(2)		2	(2)	(2)	(2)		2	(2)	(2)	(2)	(2)	1										
Parachute Subsystem	(2)				2	(2)				2				(2)	(1)				1						
• Cover Assy					2					2				(2)											
• Separation/Deploy Mechanism	(2)		(4)		4	(2)				2				(2)											
• Descent Chute	(2)				2	(2)				2				(2)											
• Drag Chute	(2)				2	(2)				2				(2)											
Scientific Instruments																(2)	(2)	(2)	3	(3)		(3)	(3)	(3)	(3)
• Pressure Gage	2		(2)		(2)	(2)		(2)		2	(2)	(2)	(2)	(2)	(2)										
• Temperature Gage	2		(2)		(2)	(2)		(2)		2	(2)	(2)	(2)	(2)	(2)										
• UV Photometer	2		(2)		(2)	(2)		(2)		2	(2)	(2)	(2)	(2)	1										
• IR Radiometer	2		(2)		(2)	(2)		(2)		2	(2)	(2)	(2)	(2)	1										
• Mass Spectrometer	2		(2)		(2)	(2)		(2)		2	(2)	(2)	(2)	(2)	1										
Guidance & Control																									
• Spin Rockets	(4)			(4)																	4				
• Guidance Rocket	(2)			(2)																	2				
• Sequence Timer	(2)	(2)	(2)		2	(2)	(2)	(2)		(2)	(2)	(2)	(2)	2	1										
ORBITER PLUS CAPSULE																									
Orbiter plus Capsule Complete Integrated System																(3)	(3)	(3)	(3)	3	1	(3)	(3)	(3)	(3)

Table 6-1 (Continued)

INTEGRATED TEST PLAN – 1971 MISSION, ORBITER AND CAPSULE

ORBITER (CONT.)

Test Article Description	Development Tests					Qualification Tests					Reliability Assessment Tests					Acceptance Tests						Launch Base Tests & Reliability Demonstration			
	Envir.	Elec.	Mech.	Struct.	Funct.	Envir.	Elec.	Mech.	Struct.	Funct.	Envir.	Elec.	Mech.	Func.	Life	Envir.	Elec.	Mech.	Func.	F.S.O.	Hot Fire	Elec. C/O	Mech. C/O	F.S.O.	Rel. Dem.
Communications & Data Handling S/S	(2)	(2)	(2)		2	(2)	(2)	(2)		2	(2)	(2)	(2)	(2)	(1)	(2)	(2)	(2)	(2)	2		(3)	(3)	3	(3)
• Servo, Antenna	(2)	(2)	(2)		2	(2)	(2)	(2)		2	(2)	(2)	(2)	2	(1)										
• Antenna 4 Ft	(2)	(2)	(2)		2	(2)	(2)	(2)		2	(2)	(2)	(2)	2	(1)										
• Loop Antenna	(2)	(2)	(2)		2	(2)	(2)	(2)		2	(2)	(2)	(2)	2	(1)										
• Radio Subsystem	(2)	(2)			2	(2)	(2)			2	(2)	(2)	(2)	2											
• Communications Subsystem	(2)	(2)			2	(2)	(2)			2	(2)	(2)	(2)	2											
• Central Controller	(2)	(2)			2	(2)	(2)			2	(2)	(2)	(2)	2											
• Tape Recorder	(2)	(2)	(2)		2	(2)	(2)	(2)		2	(2)	(2)	(2)	2	(1)										
• Omni Antenna	(2)	(2)	(2)		2	(2)	(2)	(2)		2	(2)	(2)	(2)	2	(1)										
• Command Decoder	(2)	(2)			2	(2)	(2)			2	(2)	(2)	(2)	2	1										
• Power Amplifier	(2)	(2)			2	(2)	(2)			2	(2)	(2)	(2)	2											
• PN Generator	(2)	(2)			2	(2)	(2)			2	(2)	(2)	(2)	2											
• Multiplexer, 128 Channel	(2)	(2)			2	(2)	(2)			2	(2)	(2)	(2)	2											
• Cross Dipole	(2)	(2)	(2)		2	(2)	(2)	(2)		2	(2)	(2)	(2)	2	(1)										
• Orb. Antenna	(2)	(2)	(2)		2	(2)	(2)	(2)		2	(2)	(2)	(2)	2	(1)										
• Multiplexer/Encoder	(2)	(2)			2	(2)				2	(2)	(2)	(2)	2											
Guidance & Control Subsystem	(2)	(2)	(2)		2	(2)	(2)	(2)		2	(2)	(2)	(2)	(2)	(2)		(2)	(2)	(2)	2			(3)	(3)	3	(3)
• Star Tracker	(2)	(2)	(2)		2	(2)	(2)	(2)		2	(2)	(2)	(2)	(2)	(2)										
• Accelerometer	6	(6)	(6)		6	(6)	(6)	(6)		6	(4)	(4)	(4)	(6)	2										
• Control Electronics	4	(4)			4	(4)	(4)			4	(4)	(4)		4	2										
• Sun Sensor	2	(2)			2	(2)	(2)			2	(2)	(2)		(2)	1										
• Tank, Attitude Control Gas				2					2																
• Pitch Gas Jet	4		(4)		4	(4)		(4)		4				4											
• Yaw Gas Jet	4		(4)		4	(4)		(4)		4				4											
• Control Valves, Attitude	(6)	(6)	(6)		6	(6)	(6)	(6)		6	(4)	(4)	(4)	(4)	4										
• Gyros		(8)	(8)		8		(8)	(8)		8		(4)	(4)		(4)										
Thermal Control S/S	(2)				2					2				(2)	2										
• Insulation	(2)				2					2															
• Louvers Assy	(2)				2					2															
Propulsion S/S	(2)	(2)	(2)		2	(2)	(2)	(2)	(2)	2	(2)	(2)	(2)	2	1	(2)	(2)	(2)	(2)	2	(2)	(2)	(2)	(2)	2
• Engine 750 lb thrust	(2)	(2)	(2)		2			(1)	(1)	2				2											2
• Gimbal Support			1	1				(1)	(1)	1															
• Valves, Propellant Control	(4)	(4)	(4)		(4)					4			4	4											
• Tank, Fuel (MMH)	(2)			2					2																
• Tank, Oxidizer (N_2O_4)	(2)			2					2																
• Tank, Pressurization	(2)			2					2																

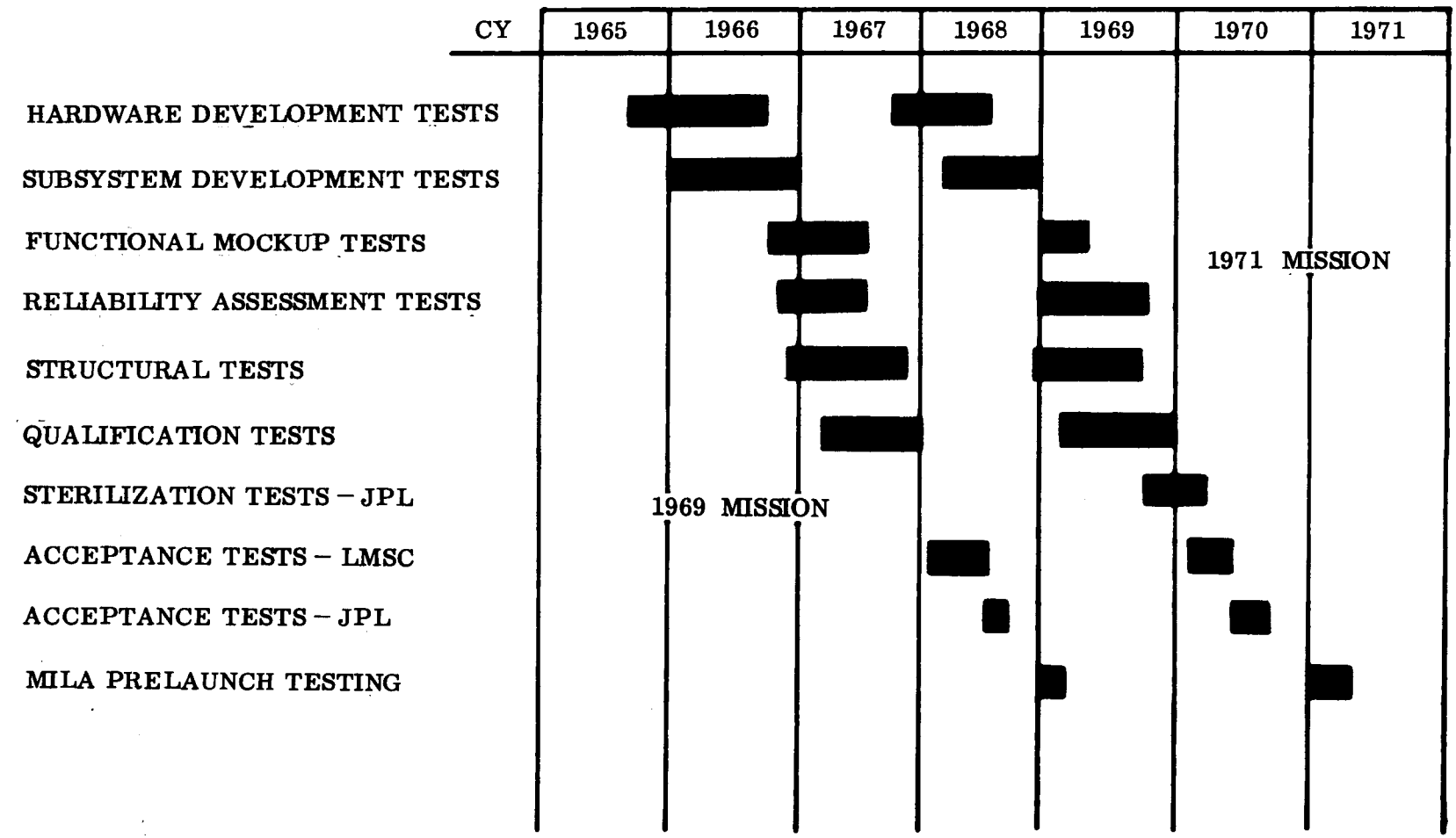


Fig. 6-3 Program Test Schedule–by Mission

begin after completion of preliminary design and would be conducted concurrently with final design.

- Qualification Testing. To assure suitability of spacecraft parts, subassemblies, and assemblies for fabrication. Qualification testing would begin after final design verification.
- Reliability Assessment Testing. Establishes operating life data, and critical failure modes of qualified hardware. This testing would begin after fabrication and testing of breadboard test modules, but would primarily require flight-type hardware.
- Acceptance Testing. Assures that hardware meets established specifications for final flight configuration. Tests would be conducted at LMSC and at JPL prior to final spacecraft delivery to MILA.
- Reliability Demonstration Tests. These tests are conducted as a means of demonstrating reliability of the flight article. Such tests would be few in number (because of verification and data from other previously conducted tests), and serve only to afford additional data not provided by the acceptance or reliability assessment tests.

6.2.2 Program Test Schedule

The outline schedule for the integrated test program is shown in Figure 6-3. The specific tests performed in each of the categories listed are discussed in following sections.

6.2.3 Development Tests

Component and Subsystem Tests. Development tests are functional tests conducted on prototype materials, components, and breadboard assemblies at the subsystem level. The operating and environmental conditions are simulated to obtain design data, verify design assumptions, and improve design configurations by elimination of critical areas and problems discovered.

Full-Scale Functional Mock-Up. In addition to the various other tests performed during the development phase of the program, a full-scale functional mock-up would be constructed. Essentially, this mock-up would simulate the final complex of subsystems except that it would initially be constructed of items in the final breadboard stages.

The various hardware elements would undergo a series of tests and an overall checkout in order to verify that all subsystems can function in sequence as an integrated system. Interface problems between subsystems could be explored and means determined to solve these problems.

6.2.4 Qualification Tests

Qualification tests would be conducted at the completion of development testing to demonstrate final product capability to meet operational requirements under expected environmental conditions. Such tests require a minimum of one each of the end item components, although additional units would be desirable during environmental exposure periods. The result of such tests can then be factored into the reliability test considerations.

In the course of these tests, not only would all specifications, governing the design and employment of say, a star tracker, be ratified by test results, but the tracker would be subjected to simulated launch loads, a long dormant period under vacuum, and finally be expected to function on command by acquiring data and tracking a simulated and collimated celestial body.

6.2.5 Acceptance Tests

Acceptance tests would be conducted in three phases:

- "Black Box" or components tests
- Subsystems acceptance tests
- Final acceptance test

"Black Box" or Component Acceptance Tests are made during the manufacturing process, and are a prerequisite to final installation on the final test vehicle.

Where these equipment items are purchased from vendors outside LMSC, the tests may be carried out at the vendor's facility. However, when this practice is followed, a checkout is performed at LMSC to ensure that the shipping process has not degraded the function of the device. All testing done at vendors' plants would be witnessed by LMSC Quality Assurance personnel.

Subsystems Acceptance Tests follow the same general pattern as the tests described above. In these subsystem tests however, the tests must be designed to reveal the functional capabilities of a complete subsystem. The environments will not be simulated for purposes of these tests as a general rule.

Final Acceptance Test – LMSC. This test requires combined operation of all subsystems, and duplicates as closely as possible the normal pre-flight, launch, and flight-mission functions. The tests would be conducted at the factory for manufacturing release, with simulated engine operation.

The total system test would be repeated at the LMSC Santa Cruz Test Base, with simulated countdown, launch, and flight mission sequence of events included. An actual engine short-duration "hot fire" test would be performed. Use of hardline umbilical and test plug connections would be mandatory throughout this test which would include, but not be restricted to:

- Spacecraft/GSE interface
- Booster/spacecraft interface (with simulators)
- Orbiter, capsule interface
- Orbiter functions and events including
  - Guidance and control
  - Communications
  - Propulsion subsystem
  - Scientific instruments payload (simulated)
  - Electrical subsystem

- Capsule functions and events including
  - Communications
  - Electrical subsystem
  - Scientific instruments payload (simulated)
  - Parachute descent subsystem
- Countdown simulation
- Launch and flight functional simulation

Final Acceptance Test – JPL. The complete orbiter or orbiter/capsule would be shipped to JPL where the scientific instruments would be installed and the capsule sterilized. Following this work, an additional acceptance test would be conducted. This test would include those tests which will be conducted at MILA in the assembly area and on the launch pad, and additional JPL tests to verify the operation of the scientific instrument subsystems.

6.2.6 Reliability Tests

In keeping with the overall ITP (Integrated Test Plan) philosophy, reliability tests-peculiar will not duplicate data obtained from other types of tests; the rationale being that all of the other test programs would afford meaningful data applicable for reliability determinations. However, within the general category of reliability tests there are two sub-categories:

- Reliability Assessment Tests (RATS)
- Reliability Demonstration Tests (RELDEM)

The former category or RAT is performed at the black box level during the development and qualification test phases. These tests are designed to explore areas of criticality in the design, demonstrate and assess failure modes, and by accelerated stress means determine the validity of the MTTF (Mean Time To Failure) predicted for the hardware element in question. As detailed in Section 6.3, all variable data would be continuously acquired; computer data reduction would give a measure of reliability growth against a desired numerical index.

The second category of tests is the Reliability Demonstration, really an extension of the FAT (Final Acceptance Test). Essentially, their purpose is as follows:

> Whereas the FAT is final demonstration of function, the RELDEM follows the philosophy that function must be for a required time in specific environment.

After computer evaluation of all data accrued during the total test program, it is necessary to add sufficient iterations of tests, and sufficient time duration per iteration to permit reliability at a specific confidence level to be demonstrated mathematically. Since all foregoing data tends to build confidence in the reliability of the product at black box and subsystems levels, few iterations for relatively short time periods are necessary at the systems level to complete the picture (accomplished by acceptance and prelaunch tests).

6.2.7 Launch Base Tests

These tests are expected to be conducted within an assembly facility at MILA. The tests would include but not be restricted to:

- Receiving inspection by Quality Assurance to determine damage in transit.
- Subsystems performance checkout tests to determine, by comparison with existing program test data, any major change in performance capability or level.
- Propulsion subsystem and guidance subsystem alignment and checkout tests.
- A final systems checkout, simulating countdown, launch, and mission events and operations to the maximum extent possible.

Tests conducted at the launch pad would include, but not be restricted to:

- Spacecraft systems performance checkout (may be automated checkout)
- Radio communications checkout
- Countdown (including destruct system checkout) and launch

6.3 RELIABILITY PROGRAM – MARINER 1969 MARS ORBITER CAPSULE

6.3.1 General Approach to Hardware Reliability Assurance

The reliability requirements imposed upon the hardware responsible for the success of this mission are extremely rigorous. Not only must all hardware survive the adverse conditions of shock, vibration, etc., during launch, but also it must survive a long dormancy period, and yet function satisfactorily when commands are received to operate in the active mode.

It is apparent that the probability of mission success is divided into several interrelated subordinate probabilities, all of which are directly dependent upon specific hardware elements functioning reliably. It may be written that:

Probable Mission Success = f {
- Probability of successful launch
- Probability of achieving successful transfer phase
- Probability of successful planet orbiting
- Probability of successful ejection of the capsule (1971 mission)
- Probability of successful experiments function
- Probability of successful data transmission and reception

Each of these subprobabilities involves the successful function of many items of hardware, many of which are novel in design, and are end-functionally applied for the first time during the discharge of this mission. In order to achieve the high hardware reliabilities required, it is necessary that test programs be instituted which furnish the desired design proof of adequacy as deep space conditions are simulated during all prelaunch test performance.

Such a program, which is described fully in Section 6.2 would take the maximum advantage of computer assistance so that results may be acquired, reduced, translated, and stored in order to permit meaningful design and procedural decisions to be made.

A computer-assisted approach is considered essential to the successful prosecution of the militant reliability program necessary to assure mission success. The means by which such a program could be implemented are detailed in the following text (a similar approach to that being used on the LMSC Polaris Missile program), in order to establish a sound basis for cost and schedule estimates.

6.3.2 Reliability Goal Determination and Subsystem Reliability Apportionment

The reliability requirements for this mission are determined by the dictates of the mission sequence of events. The time column of Table 6-2 shows the timetable of event occurrence and persistence, and thus sets the active and dormant life requirements and equipment. The time intervals may be translated into Mean Times to Fail (MTTF) for the various subsystems.

Once the subsystem MTTF's are known, a mathematical model may be constructed, and solved by the computer in order to derive the various reliability indices or figures of merit for each equipment element within each subsystem. The model ascribes significance or weighting factors to each equipment element, ranking it in order to express its functional contribution in the terms of

- How probable is failure in a catastrophic mode?
- How deleterious is failure to ultimate mission success?
- The redundancy required to minimize effect of failure of equipment, in areas of critical function.

The mathematical model must take into consideration the reliability indices of the launch vehicle, the orbiter, and the capsule. Since the reliability of the launch vehicle is a vital link in the mission success chain, and since the vehicle would be

Table 6-2

1971 MISSION SEQUENCE OF EVENTS

Orbiter			Capsule		
	Event	Time		Event	Time
1.	Launch Sequence	T	C1.	Pre-Separation Checkout	E-2 days
2.	Midcourse Correction	T + 3 days	C2.	Separation Sequence	E-2 days
3.	Midcourse Correction (Backup)	T + 5 days	C3.	Atmospheric Entry	E - 10 to 33 min
4.	Switch to High Gain Antenna	T + 124 days*	C4.	Impact	I
5.	Mars Approach Correction	E - 26 days	C5.	Data Readout to Earth (Orbiter)	E + 10 min
5A.	Capsule Separation	E - 2 days			
5B.	Atmospheric Capsule Readout	E - 40 min			
6.	Orbit Injection	E - 5 min			
7.	Start Data Acquisition	E			
8.	Mission Complete	E + 6 mo			

* T + 170 days for 1969 mission

E = Encounter = 200 days nominal

LOCKHEED MISSILES & SPACE COMPANY

furnished by a manufacturer other than LMSC, strict attention must be paid to the acquirement of all meaningful reliability data concerning it. Such a task would require close cooperation between LMSC and the launch vehicle supplier, and mutual agreement upon the reliability technology applied throughout the program.

Figure 6-4 depicts the means by which data from outside LMSC would be acquired and resolved, not only from the launch vehicle supplier but also from the suppliers of all purchased subsystems or subsystem elements.

6.3.3 Reliability Data Matrix and Computer Program

Figure 6-5 illustrates the tripartite computer-assisted approach to the entire reliability program.

Program 1, as has been stated, concerns itself with the determination of reliability goals, and apportionment of subsystems reliability indices from analysis of the basic mission requirements.

Program 2 is an assistance to design engineering. In this particular program, circuits are synthesized, and the parameters variation explored. Not only may the optimum stress levels for parts be determined, but also the reliability values for each subsystem circuit element may be derived.

Program 3. This program accepts and reduces all data accruing from the Integrated Test Program (ITP). In order to minimize the monetary value of the total test program for the entire mission, the reliability tests would be held to a minimum, and redundancies in testing eliminated insofar as possible. This approach is possible if use is made of all available data which can contribute to reliability determinations at applicable confidence levels. The detailed means by which such data treatment is effected are described in Section 6.2.

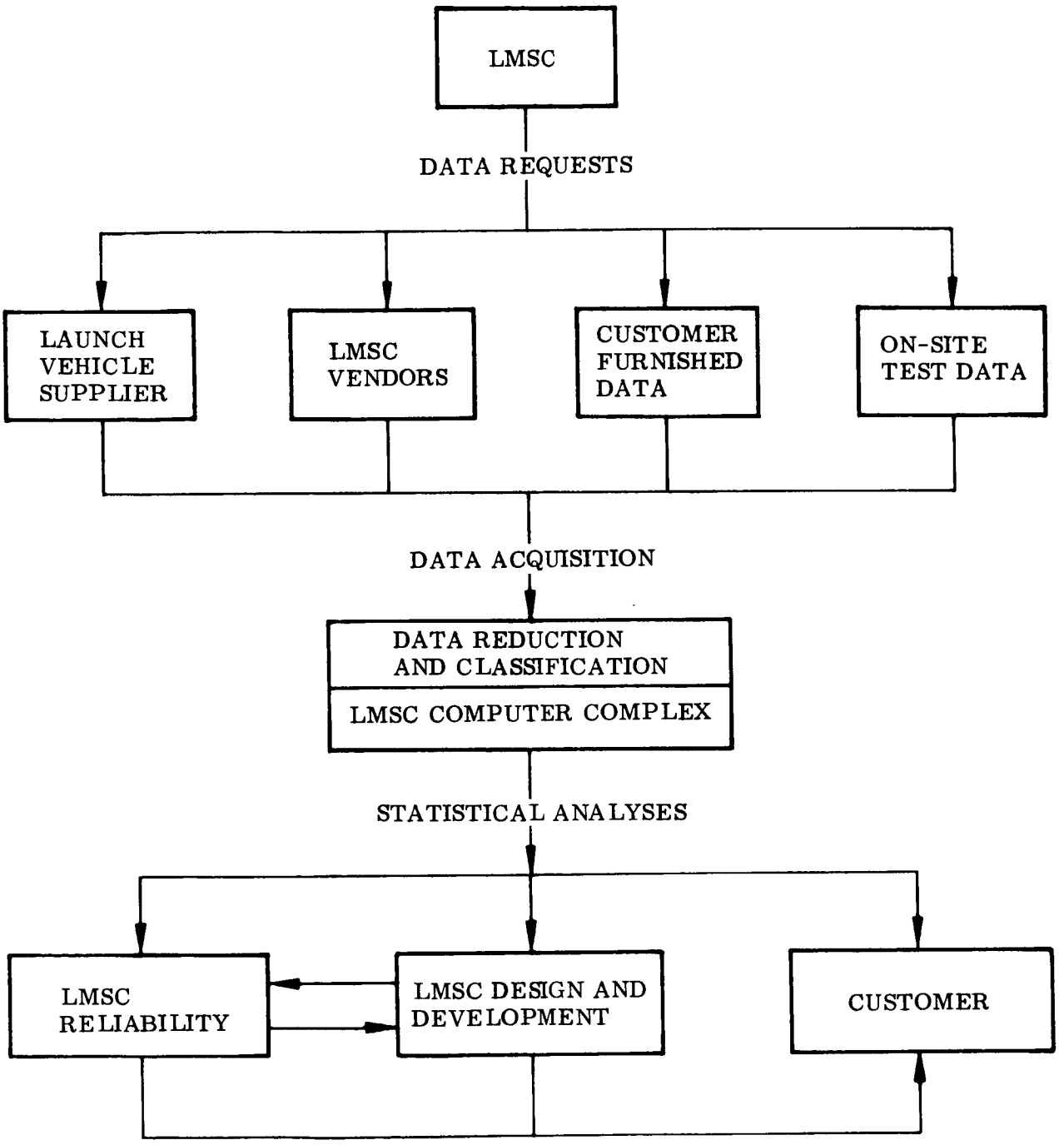
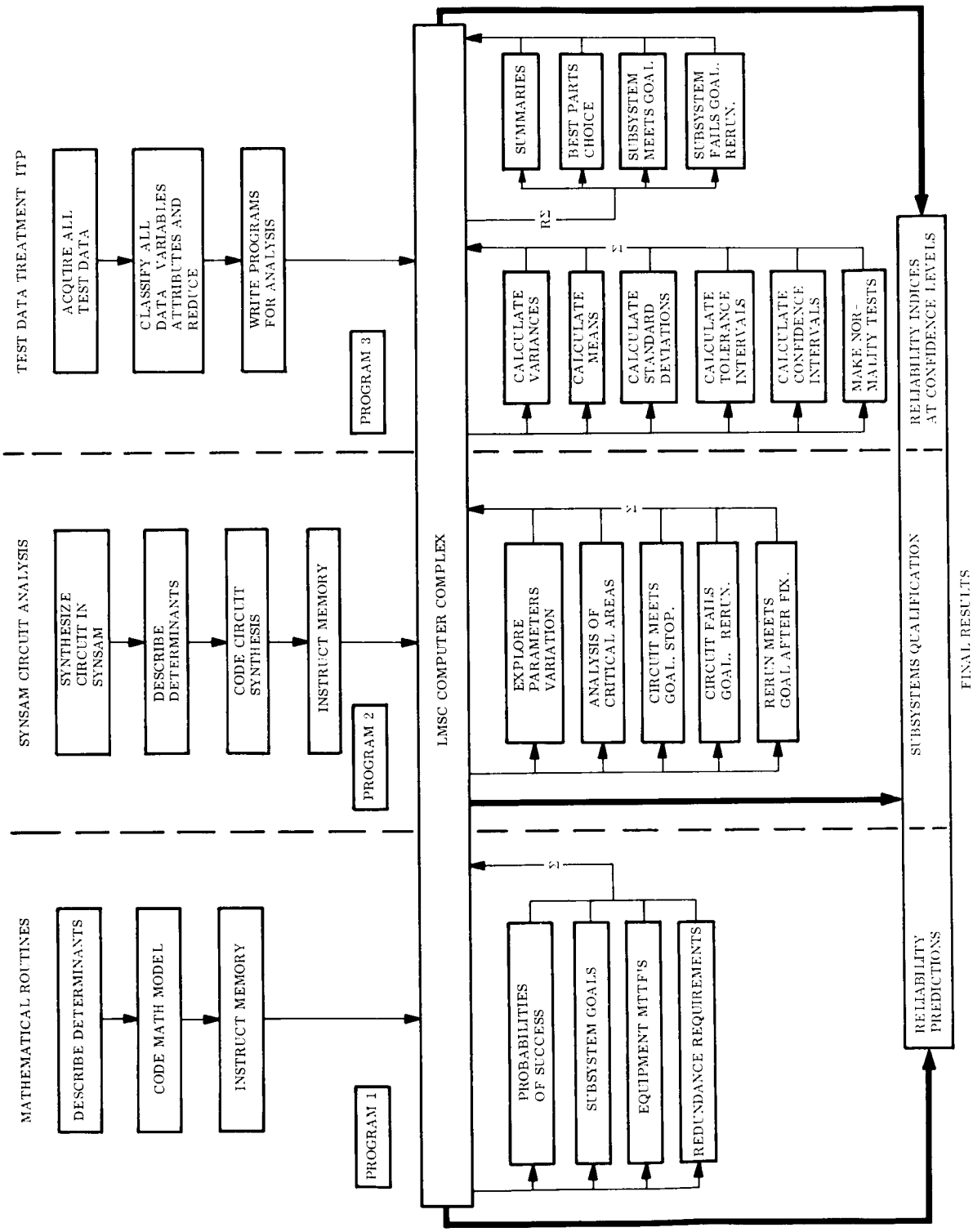


Fig. 6-4 Reliability Data Acquisition and Reduction


TEST DATA TREATMENT ITP
ACQUIRE ALL TEST DATA
CLASSIFY ALL DATA VARIABLES ATTRIBUTES AND REDUCE
WRITE PROGRAMS FOR ANALYSIS
PROGRAM 3
SYNSAM CIRCUIT ANALYSIS
SYNTHESIZE CIRCUIT IN SYNSAM
DESCRIBE DETERMINANTS
CODE CIRCUIT SYNTHESIS
INSTRUCT MEMORY
PROGRAM 2
MATHEMATICAL ROUTINES
DESCRIBE DETERMINANTS
CODE MATH MODEL
INSTRUCT MEMORY
PROGRAM 1
LMSC COMPUTER COMPLEX
SUMMARIES
BEST PARTS CHOICE
SUBSYSTEM MEETS GOAL
SUBSYSTEM FAILS GOAL. RERUN.
RX
CALCULATE VARIANCES
CALCULATE MEANS
CALCULATE STANDARD DEVIATIONS
CALCULATE TOLERANCE INTERVALS
CALCULATE CONFIDENCE INTERVALS
MAKE NORMALITY TESTS
EXPLORE PARAMETERS VARIATION
ANALYSIS OF CRITICAL AREAS
CIRCUIT MEETS GOAL. STOP.
CIRCUIT FAILS GOAL. RERUN.
RERUN MEETS GOAL AFTER FIX.
PROBABILITIES OF SUCCESS
SUBSYSTEM GOALS
EQUIPMENT MTTF'S
REDUNDANCE REQUIREMENTS
RELIABILITY PREDICTIONS
SUBSYSTEMS QUALIFICATION
RELIABILITY INDICES AT CONFIDENCE LEVELS
FINAL RESULTS

As each step in all three programs is resolved by the computer, results are fed back into the memory, after reduction of the information on the first printouts. This recomputed technique permits a final analysis of all available data to produce a set of final results. The feedback loops are designated Σ to denote a summation and digest of first-order results.

6.3.4 Hardware Reliability Analysis

The hardware involved in the Mariner 1969 Mars program falls within two broad generalized categories:

(a) Electrical, Electronic
(b) Mechanical

In order to achieve the very high reliabilities essential to mission success, a departure from the more customery "Worst Case" analysis will be necessary. The method proposed is known as SYNSAM or Synthetic Sampling Analysis, and is particularly advantageous in dealing with hardware in the (a) category above.

SYNSAM differs from "Worst Case" in that a measure of circuit drift reliability may be predicted, whereas no such measure of reliability is possible with "Worst Case." Assuming component parameter distributions, a determination of the circuit output distribution and the predicted reliability may be computed. By adjustment of the various parameter values of a given component, it is possible to alter the output distributions and improve the functional reliability of the circuit. SYNSAM is particularly valuable in reliability analysis for Mariner circuits, since it permits at least predictive answers to the questions: "If output of a circuit is x and reliability is y and if we know the measure of component parametric drift with time, what will be the reliability of the circuit after a dormancy period of 200 plus days in deep space environment?" If such a prediction can be made, design can allow for such drifts and produce a more reliable circuit. SYNSAM is a statistical technique easily resolvable by the computer.

Analysis of all items falling into the broad category (b) would employ another computer assisted technique. Parametric variation for mechanical devices does not lend itself readily to such mathematical routines as "Monte Carlo." However, variables may be treated, and reliability results obtained, by means of a routine known as MESTAN.

MESTAN, or Means and Standard Deviations Analysis relies on the Theorem of Propagation of variance. The routine is statistical and permits of the collation and reduction of parameters into distributions, the mean and standard deviations of which may be described. If determinations are made that X percent of cases falls within $\pm Y\sigma$ limits about a mean, then KOLMOGOROV SMIRNOV tests for Normality may be made, and the conclusions drawn, that the reliability imposed in the sample, possesses a given confidence interval. These technniques are well suited to the determination of the reliability of mechanical structures and/or devices.

6.3.5 Reliability Design Review

Design reviews for the Mariner program would be on a formal basis. At the outset of the program, a Design Review Commitee would be convened, comprised of:

- The Program Manager, who would act as chairman
- The Reliability Manager
- The Quality Assurance Manager
- The several cognizant design managers
- Specialists in design as designated
- Representatives of marketing and contracts as applicable
- Customer liaison personnel as designated

There would be at least three formal Design Reviews:

- Initial or conceptual, where the various design concepts are critiqued exhaustively and recommendations for early design changes are made.
- Interim or breadboard review. This review will be conducted at the early breadboard stage, as design undergoes translation into early hardware.

- Final, or preproduction design review. This review represents the final critique by all parties, and furnishes recommendations for last-minute design changes, before production phases begin.

There would be as many informal reviews as the committee considers necessary, but such reviews would be held to a minimum in the interests of time and cost savings.

The purpose of all design reviews is to survey the progress of the program, highlight troublesome areas, recommend fixes and changes, review reliability growth, and monitor costs and schedule compliance.

As these factors are considered, the Reliability Manager would be responsible for determining the impact of design changes proposed upon reliability growth by means of having the computer reduce the new data and deliver a numerical solution.

All minutes and proceedings of the committee would be entered in a Design Review Log, which would form a complete history of the design review program, and excerpts from which would be included in the scheduled reports to the customer.

6.3.6 Reliability Documentation

A "major milestone" chart would be compiled to depict significant reporting dates for reliability events. Such events would take the form of but not be restricted to:

Reports of
- Preliminary design reviews
- Interim design reviews
- Final design review
- Regular progress reports as necessary
- Trouble and failure report summaries
- Recommendation for corrective action reports
- Reliability growth curves

A corrective action committee would be formed to rule upon the reliability implications of all corrective actions recommended, and this committee would issue reports, at the regularized intervals as prescribed by the major milestones report.

Since much of the reliability reporting would be in the form of computer runoffs, the volume of reportage would be too voluminous to transmit each first-order run, or subroutine run. Regular summaries would be used instead with the computer performing the summation and digest and releasing a printout on a scheduled basis.

6.4 PROGRAM MANUFACTURING PLAN

6.4.1 Basic Plan and Approach

A proposed manufacturing plan for the orbiter and orbiter/capsule is described in this section. The plan provides flexibility of manufacturing operations and quick response to design changes which may occur as design progresses toward the flight hardware phase.

The basic objective of the manufacturing effort is to furnish a product at minimum cost which satisfies the design and reliability requirements; this can be accomplished through the following:

- Project Type Organization. Segregated manufacturing areas for final assembly and test; close coordination with Engineering, Procurement, Quality Assurance, and Test Operations
- Development Shop Approach. Extensive use of development technicians and skilled mechanics in experimental shop to assure efficient tooling and minimum shop operations
- Integrated Reliability. Special training of personnel in "Hi-Rel" packaging, handling, and assembly; integration of manufacturing tests with master program plan (Integrated Test Plan)

- Control of Processes. Continuous monitoring and recording of critical processes and testing

The basic areas of interest discussed herein are:

- Product Requirements. Special materials, processes, manufacturing techniques
- Manufacturing Sequence. General plan of assembly breakdown
- Manufacturing Schedule. Milestones and schedules for 1969 and 1971 missions
- Fabrication/Test Plan. Product flow from vendor to launch base

6.4.2 Product Requirements

The general configuration of the orbiter for the 1969 mission is shown in Fig. 4-5. The orbiter/capsule configuration is shown on Fig. 4-6.

Orbiter. The materials utilized in the orbiter are within the state-of-the-art of existing technology. A basic structural shell which allows internal mounting of subsystem equipment is readily built up of sheet metal, machined fittings, and tubing elements. Thermal insulation and micrometeorite shielding (as required) will be applied to the structural shell or directly to the equipment. The servicing and handling equipment required to support the orbiter is conventional (handling dollies, slings, etc.). The liquid-propellant engine of the orbiter requires hot-fire facilities for subsystem testing and for final integrated system hot-fire test. The propellant tanks are conventional, representing small-scale duplicates of those used on Agena and other space vehicles.

Capsule. The primary requirement is the sterilization requirement. It is assumed that heat sterilization of the completed capsule is required. Assembly operations would be a "white room," but not sterile, atmosphere; the capsule would then be installed in the sterility shroud and sealed and internally pressurized with sterilant, ethylene oxide.

The capsule heat shield forebody would require new process development, as would sterility shroud sealing techniques; however, no new engineering concept is required to accomplish this development.

Support Equipment (AGE). The sterilization chamber (proposed to be built at LMSC and delivered to JPL) is the only advanced state-of-art item in the AGE list. The checkout equipment would be conventional and tailored to integration with existing equipment at MILA. The handling equipment would be simple support frames and hoists to allow manipulating the orbiter or capsule or orbiter/capsule combination and storing them in ready condition. Servicing equipment would be conventional and comprise only those elements required to service the propellant/pressurization tankage and the cold-gas pressure bottles on the orbiter.

Make or Buy Items and GFE. It is assumed that 40 to 50 percent of the equipment items on the orbiter and capsule will be "buy" items; included would be certain communication equipment, the engine, the batteries, and parachute pack. The scientific instruments are assumed to be GFE.

6.4.3 Manufacturing Schedule

Figure 6-6 shows in outline form the manufacturing schedule and milestones for the 1969 and 1971 missions. The schedule indicates a rather rapid buildup in 1966 and 1967 with tapering off until a second buildup starting in the latter half of 1968. This "lull" would create a problem of maintaining a staff of experienced personnel which could be assigned to the 1971 program.

The detail scheduling of miscellaneous test articles (for development test, etc.) is not shown. These articles will be integrated into the manufacturing schedule without affecting the established flight article delivery.

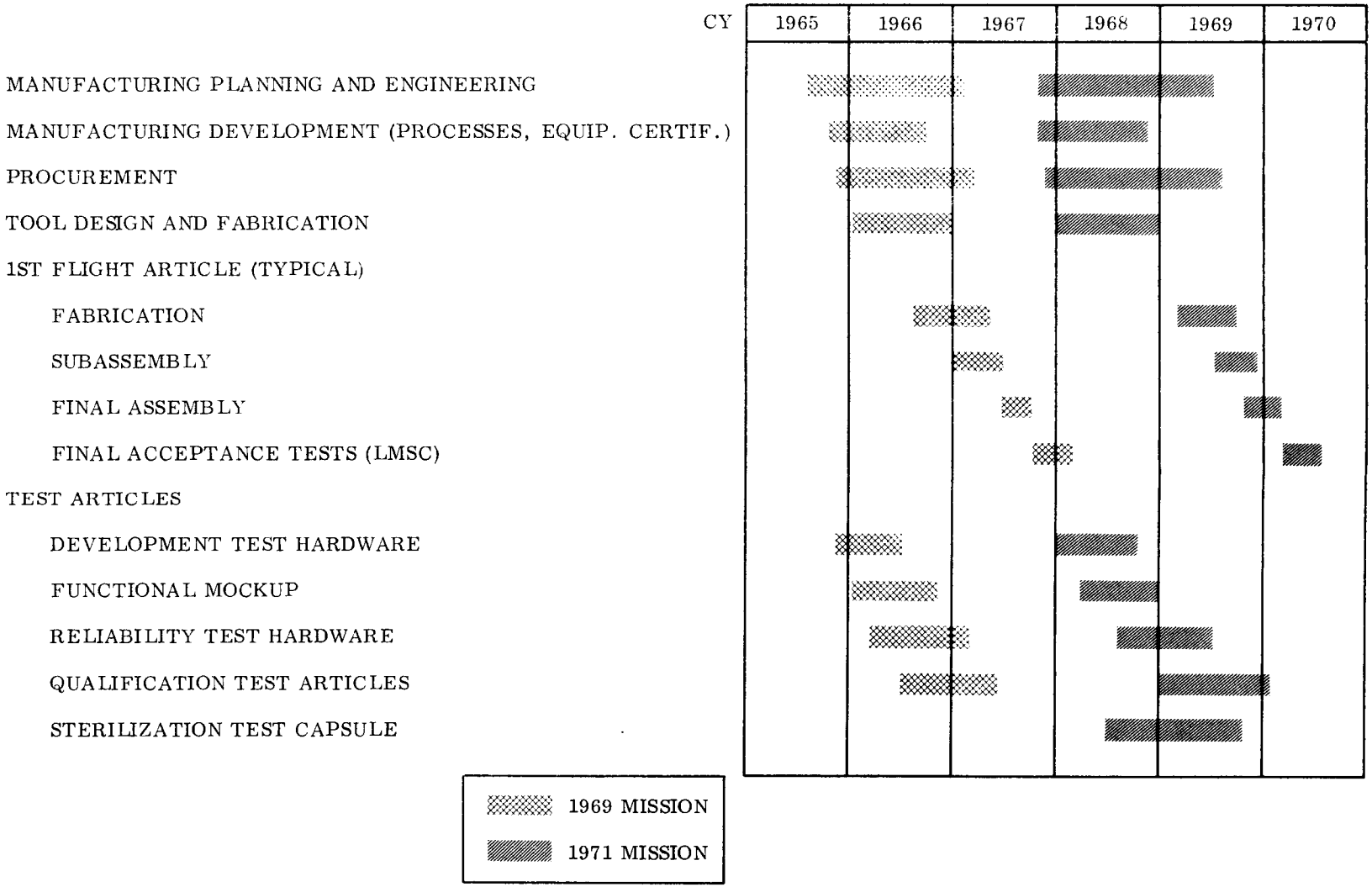


Fig. 6-6 Manufacturing Schedule

6.4.4 Fab/Assembly/Test Plan

The product flow plan from vendor through final acceptance test of orbiter and capsule at LMSC and JPL is shown on Figs. 6-7 and 6-8 respectively.

All tooling would be of the soft type with master gage control on the following interfaces:

- Orbiter adapter to Centaur mounting
- Orbiter adapter to orbiter mounting
- Orbiter to capsule mounting
- Scientific instruments mounting on orbiter and capsule

Fabrication tooling would be held to a minimum and would be duplicated as required to support the product flow rates.

The manufacturing tests performed in the product line would be a portion of an overall integrated test plan (see Section 6.2 for detail). This will provide not only the go/no go acceptance or rejection of the component, subsystem,or vehicle, but will accumulate data into the master test data bank to become part of the total reliability assessment program.

Because of the need to install the pyrotechnic devices before the sterilization shroud is installed (parachute release device and the guidance rocket motor), final assembly of the capsule, and acceptance testing, may require an isolated facility such as at SCTB. Figure 6-8 illustrates the product flow for this condition and shows SCTB as the place of assembly and test. If it were found later that this minor explosives handling could be done at the main assembly plant area, a change would be made to the plan. JPL would require evaluation of this problem relevant to the capsule sterilization operation.

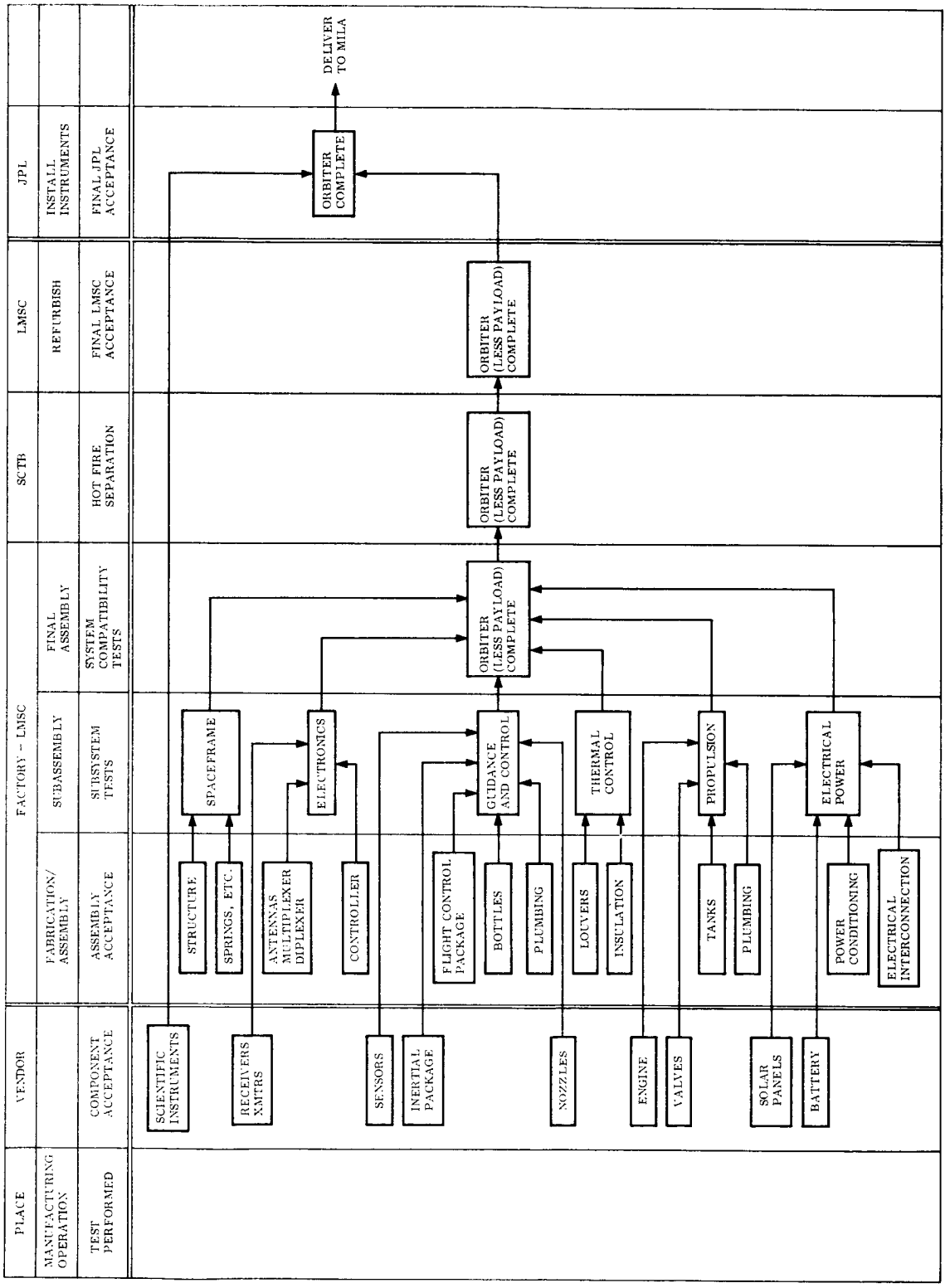


Fig. 6-7 Orbiter Product Flow Plan

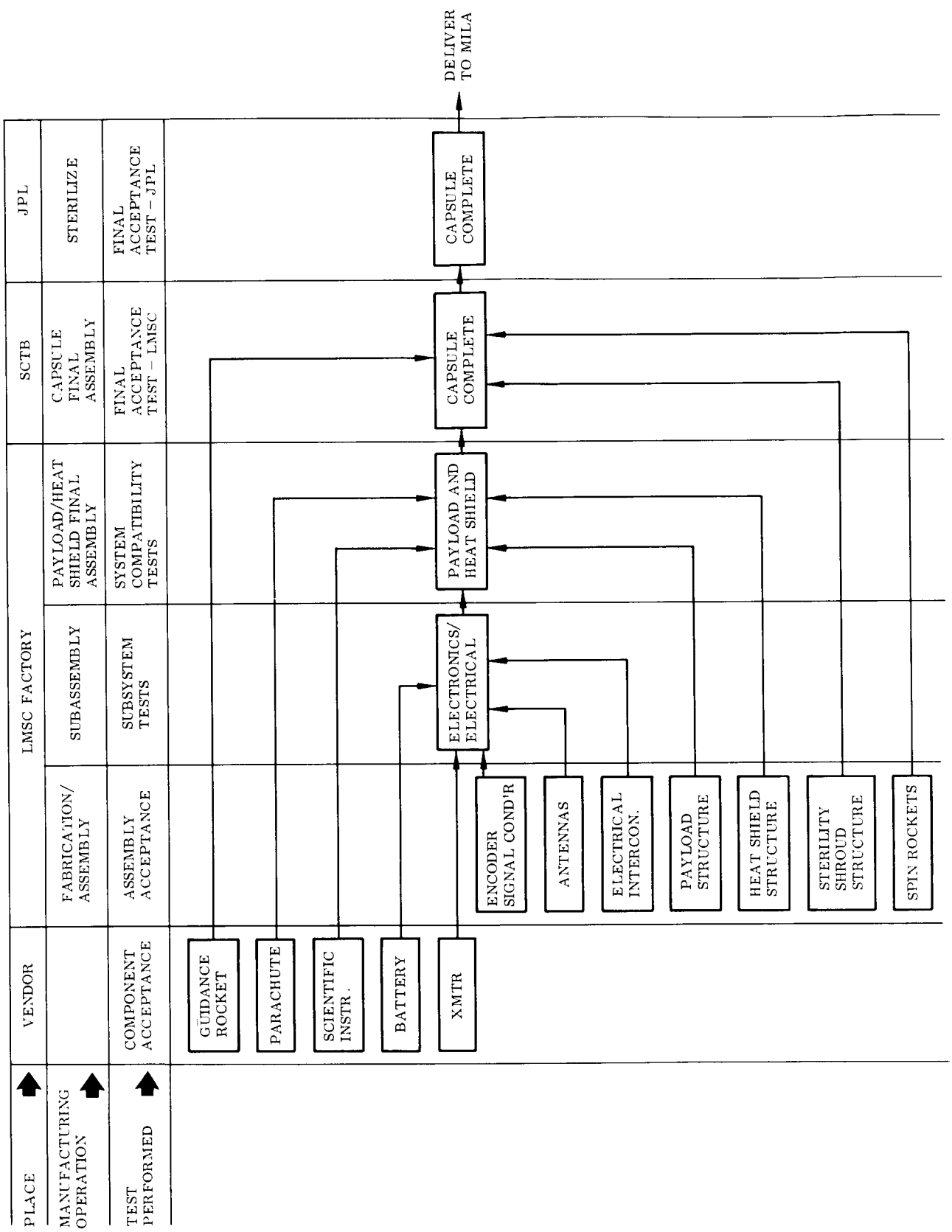


Fig. 6-8 Capsule Product Flow Plan

6.5 FACILITIES PLAN

The development and manufacture of the orbiter and capsule will require certain special facilities. In the following discussion, major items are outlined in four categories:

- Development test facilities
- Assembly plant and test facilities
- JPL facilities
- Launch base facilities

6.5.1 Development Test Facilities

Special facilities will be required for testing at the subsystem or vehicle level. Examples are as follows:

High Vacuum Orbital Simulator (HIVOS). A chamber large enough to accept the total orbiter or capsule, simulate space vacuum, and provide simulated solar energy and space cold. (This chamber exists at LMSC and has not been included in the "additional facilities" requirements.) Solar array extension, solar array operation in space environment, antenna and instrument servo actuation, and similar functional tests would be performed in this or a similar chamber.

Hazardous Tests in Vacuum. A smaller vacuum chamber with space heat/cold simulation equipment and "boiler-plated" to allow detonation of pyrotechnic devices (pin pullers, linear shaped charges, spin rockets, etc.) would also be required. The various pyrotechnic devices would be tested in this chamber to check effect of long time soak at various temperatures prior to ignition. (Santa Cruz Test Base has such an installation and therefore this item is not listed in additional equipment).

Hot-Fire Test Facility. A test facility for testing both the liquid-fueled orbiter engine and the capsule guidance rocket motor, attached to the spaceframe would be required. In addition to the early engine development tests, final acceptance hot-fire tests on the assembled orbiter would be accomplished, simulating booster vibrational inputs.

Also, spaceframe separation tests would require fixturing and hazardous testing area to test structural and functional system reaction to explosive charges used for separation. These areas are available at SCTB but project tooling is needed for vehicle and subsystem support during the testing (the costs for these items have been included in "special tooling and equipment").

Parachute Test. In addition to flight tests wherein the chute would be deployed under conditions simulating Mars entry (by changing altitude, payload weight, etc.), it is planned to perform a vacuum wind-tunnel test on chute deployment. Arnold Engineering Development Center would probably be used for this type of test and test priority would have to be arranged.

Numerous other tests on electronic components, antennas, mechanisms, electrical power, and similar orbiter or capsule hardware must be accomplished under simulated operating conditions. It was assumed that a typical large aerospace company would have the various facilities and equipment necessary to perform these tests and no special listing nor cost has been derived for this report. The special equipment required for acceptance testing of the orbiter or capsule and the various components/subsystems thereof is essentially tailored to the Mariner requirements and has been costed as project or special tooling and test equipment.

6.5.2 Assembly Plant and Test Facilities

A centralized assembly facility would be required for the orbiter and the capsule. Because of the need to control the bacterial count on and within the capsule, a white-room facility is planned for its assembly. To provide a good background for the orbiter assembly, a clean room with filtered and air-conditioned air is planned.

Because of the limited-quantity production, separate detail fabrication areas are not planned. The Mariner program would be supported by existing sheet metal, machine, and processing shop areas. However, all final assembly and testing would be

accomplished in the aforementioned clean areas. No new manufacturing building would be required for this program, but modification to install the white-room area for the capsule would be required. If it were found undesirable to assemble the pyrotechnic assemblies of the capsule in the main plant area, final installation of these devices and sterility shroud sealing would be accomplished at SCTB. This approach would require an additional white-room at SCTB. Because of the smallness of the items involved (the guidance rocket motor and the pin pullers), it has been assumed that this work can be done at the main assembly plant and no costs have been added for the SCTB installation.

The equipment required for acceptance of the flight articles would be in one of two categories: (a) special project tooling and test equipment (and therefore not accruing cost to the facilities/equipment area) or (b) capital equipment. LMSC has the necessary shakers, vacuum chamber, hot-fire test stands, and other capital equipment required; a general assumption has been made that other qualified contractors would also have this equipment or facilities and not require new installations.

6.5.3 JPL Facilities Requirements

The plan described in this report assumes that capsule sterilization would be accomplished by JPL. Also, installation of the scientific instruments in the orbiter would be accomplished by JPL. It is planned that a sterilization chamber would be furnished as AGE to JPL. This chamber would require certain venting and power which would accrue as facility modifications. In addition, a clean room area, filtered and air-conditioned air, would be required for the orbiter during installation and final checkout operations. It is assumed that JPL would use orbiter and capsule AGE for any handling and checkout of the vehicles at JPL.

6.5.4 Launch Base Facilities

The launch base facilities would consist of a spacecraft (orbiter or orbiter/capsule checkout-assembly building and the launch complex 36A and 36B. The checkout-assembly

building is assumed available for the period required. It will require filtered and air-conditioned air (presumed already available). The launch complex consists of:

- Launch pad (36A or 36B)
  - Launch pad service building
  - Umbilical tower
- Launch control building
- Gantry service tower
- Cableways to pad A or pad B

Both pads 36A and 36B would be required for the 1969 Mariner Mars mission. The orbiter would be assembled or checked out in the launch control building, transported to the launch pad in the transport van (AGE), and erected atop the booster vehicle. No modification would be required to the existing umbilical tower. The cabling from the launch control building to the launch pads would be supplied as AGE cable assemblies.

6.6 LAUNCH OPERATIONS PLAN

The launch operations activity would include those efforts which are required to transport the orbiter or capsule from the assembly plant (Sunnyvale, Calif.) to JPL, transport the orbiter or capsule to the launch base at MILA, checkout the orbiter and capsule at the launch base, transport the orbiter or capsule to the launch pad, assist in erection atop the launch vehicle, and accomplish a prelaunch checkout of the orbiter and capsule in the launch-ready condition. Manpower has been allotted to these efforts and cost of support equipment (AGE) has been included.

6.6.1 Support to JPL

After acceptance by the customer of the orbiter and capsule at Sunnyvale, Calif., it would be transported in the transport van (AGE) to JPL for installation of the scientific instruments and sterilization of the capsule. The transport van would

be equipped with air conditioner, pressure regulator, and would be instrumented for recording shock loads imposed on the spacecraft during transit. An LMSC engineer would accompany the spacecraft to JPL and thence to the launch base to insure status. A spacecraft log book would accompany each vehicle and would be maintained with entries by the LMSC engineers and JPL personnel. The capsule, after sterilization at JPL and following installation of scientific instruments would be reassembled to the orbiter and a checkout performed using AGE checkout equipment. The spacecraft will then be loaded into the transport van for movement to Cape Kennedy.

6.6.2 Support to Cape Kennedy

The spacecraft checkout building would be the receiving area for the orbiter and capsule. This building is located in the industrial area at Cape Kennedy. It would also be utilized for storage area for this program and for administrative offices.

Personnel support is planned for loading and unloading the spacecraft, checkout of the spacecraft, transporting the spacecraft from the checkout building to the launch pad, and checkout of the spacecraft (after its erection atop the launch vehicle) remotely from the launch control building.

6.6.3 Launch Base Test Plan

The launch base test plan has been developed as the final part of the factory-to-launch testing sequence. All testing at the launch base is based upon the following:

- No testing at the launch base would invalidate a previous test
- Prime purpose of testing at launch base would be to verify the integrity of the overall system; therefore, qualitative type test equipment would be utilized.
- There would be no replacement nor rework of spacecraft. All failed articles would be replaced en toto and failed articles shipped back to JPL or LMSC. Only complete orbiters or capsules would be handled at the launch base.

An outline of the launch base test plan follows:

1. Industrial area – spacecraft checkout building
   a. Receiving inspection of orbiter and capsule (visual for damge, etc.)
   b. Qualitative functional checks
      (1) Magnetometer boom extension
      (2) Antenna extension
      (3) Solar panel extension, circuit continuity
      (4) Guidance and control, passive
      (5) Transmitter (capsule)
2. Launch pad assembly
   a. Install Centaur adapter
   b. Mate orbiter/capsule to Centaur adapter
   c. Install pyrotechnics
   d. Conduct telemetry system check
   e. Final level all tankage (helium, nitrogen, etc.)
   f. Install external shroud

6.6.4 Support Equipment (AGE)

The following equipment would be utilized in handling and transporting the orbiter and capsule and in accomplishment of checkout and launch operations. One set each of the handling, servicing, and checkout equipment is planned for LMSC, JPL, and the launch base; the launch control equipment is planned as one set for the launch base only. Additional pieces would be planned for shop handling aids and for required quantities of orbiter or capsule-peculiar items.

Handling Equipment

- Transport van – for orbiter or capsule or combined
- Orbiter handling dolly – horizontal
- Orbiter checkout dolly – vertical (supports solar panels during extension)
- Capsule dolly

- Orbiter handling tilt sling
- Capsule sling
- Orbiter protective cover
- Capsule protective cover

Servicing Equipment

- Propellant loading equipment, fuel (MMH) and oxidizer (N_2 O_4)
- Gas pressurization equipment, Helium and nitrogen

Checkout Equipment

- Electrical umbilical coupling
- Mass spectrometer leak detector
- Orbiter propulsion checkout console
- Solar collector portable checkout unit
- Battery load tester
- External orbiter power supply
- Battery charger
- Guidance checkout console
- Communication/decoder checkout
- Antenna coupler

Launch Control Equipment

- Cable assembly (launch pad to control building)
- Orbiter checkout console
- Capsule checkout console

Section 7
PROGRAM COSTS

The estimated program costs have been based upon the various plans and hardware systems described herein and within certain ground rules:

- 1969 mission to require 3 orbiter vehicles as flight articles
- 1971 mission to require 3 orbiter/capsule vehicles and 2 backup capsules as flight articles
- Utilize maximum proven hardware from Mariner (solar arrays, etc.)
- JPL to install scientific instruments, sterilize capsules (estimated costs included for these operations)
- Scientific instruments to be GFE (estimated costs included)
- Launch vehicle to be Atlas-Centaur (costs for vehicle, vehicle modification, and launching not included)
- Data acquisition and analysis to continue 6 mos after Mars contact for each mission (costs included for data analysis and reduction but not for acquisition)
- Launch operations for orbiter and capsule (assembly, checkout, servicing, and prelaunch countdown) will be accomplished and costs accruing from these are included.

This cost estimate is considered to be a bare minimum. The program costs to be expected may be higher, depending on the degree of usage of existing hardware.

7.1 SUMMARY OF COSTS

Table 7-1 itemizes the program costs in three categories:

1969 Mission – orbiter only	$58.9 Million
1969 Mission – capsule added cost	$19.9 Million
1971 Mission – orbiter and capsule	$51.8 Million

Table 7-1

SUMMARY – PROGRAM COSTS

Cost Segment	1969 Mission (Orbiter Only)	1969 Mission (Capsule Added Cost)	1971 Mission (Orbiter & Capsule)
Technical Direction & Documentation	$ 4.5	$ 2.5	$ 6.1
Engineering & Development (Incl. Devel. Test Equip. Hardware)	21.8	9.9	17.6
Reliability & Qualification Testing (Incl. Test Equip. & Hardware)	12.4	3.6	6.8
Manufacturing (Flt. Articles & AGE) (Incl. Spec. Tooling)	12.0	3.6	13.3
Spares	1.2	0.3	1.7
Support of Launch Operations (Incl. Data Reduction)	6.4	–	6.3
Special Facilities	0.6	–	–
Total Costs	$58.9	$19.9	$51.8

The lower total for the 1971 mission assumes that much of the technology developed in the 1969 mission is reusable (modified) and that certain hardware elements (such as AGE) can be modified and reused.

7.2 DISTRIBUTION OF COSTS BY TIME

Figure 7-1 illustrates the funding requirements for the 1969 mission, the 1971 mission, and the total distributed by calendar and fiscal year. The rather sharp buildup in CY 1966 indicates a problem area which can be helped by initiating the program earlier, relevant to development. Funding is rather constant for the years 1966 thru 1969 if programs are planned as outlined herein.

Figure 7-2 illustrates separately the funding requirements for engineering/development, manufacturing, and reliability/qualification testing. For the former two, a comparatively large "sag" occurs in funding (and manning level) between the 1969 and 1971 missions. The engineering sag is in CY 1967, the manufacturing sag in CY 1968. Both conditions would contribute to problems in maintaining skilled manpower during these periods. Some improvement could be attained by moving the 1971 program upstream, but this would lessen the probability that maximum advantage was to taken of the data from the 1969 mission testing, flight, and data acquisition. Further analysis of these areas is required.

The sag in the reliability/qualification testing area is not severe; the largely reduced amount of testing required in the 1971 mission results from the assumption that requalification of many items within the orbiter will not be necessary, and considerable reliability confidence and experience will be available from the 1969 mission.

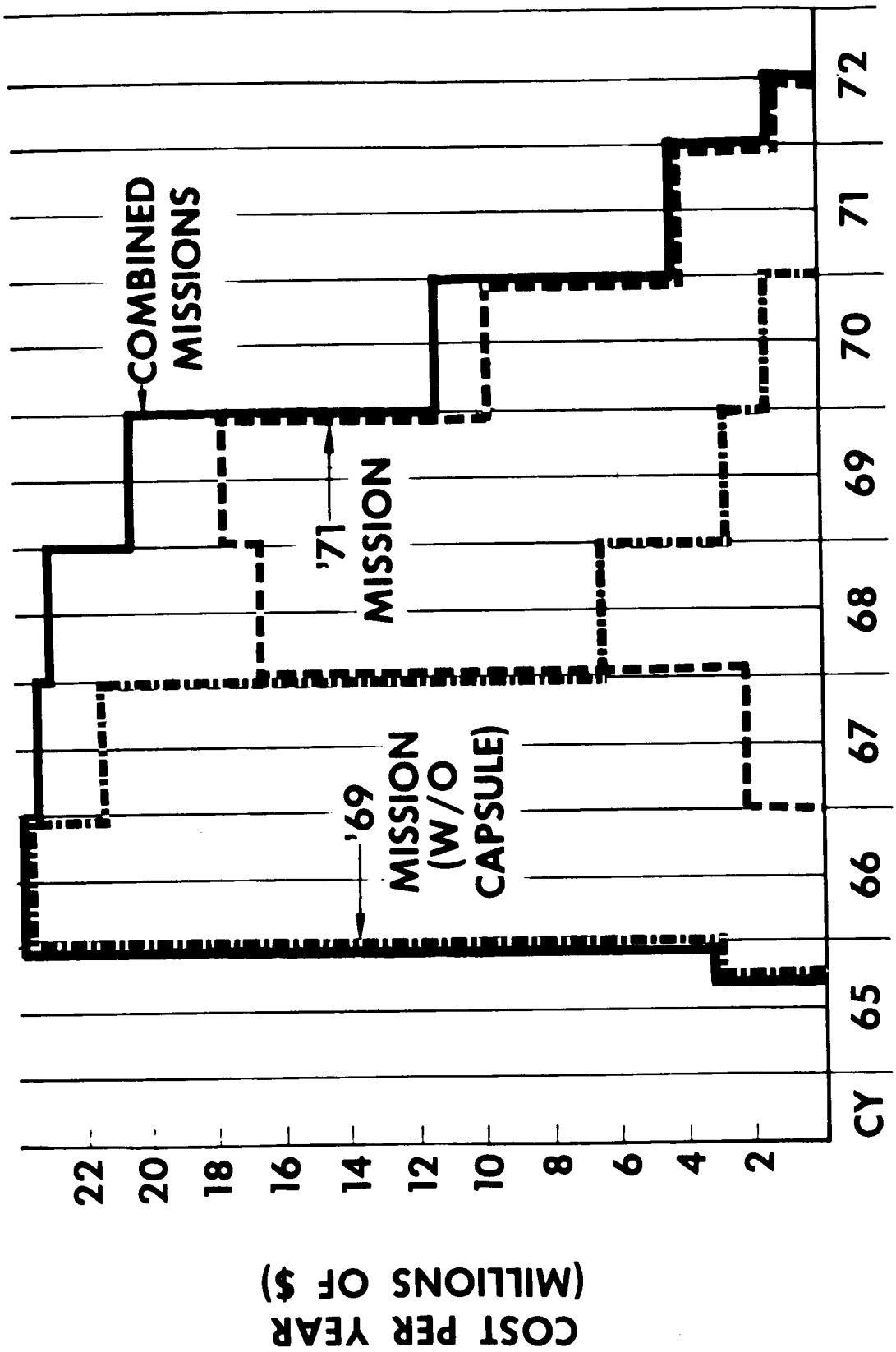


Fig. 7-1 Program Cost Distribution

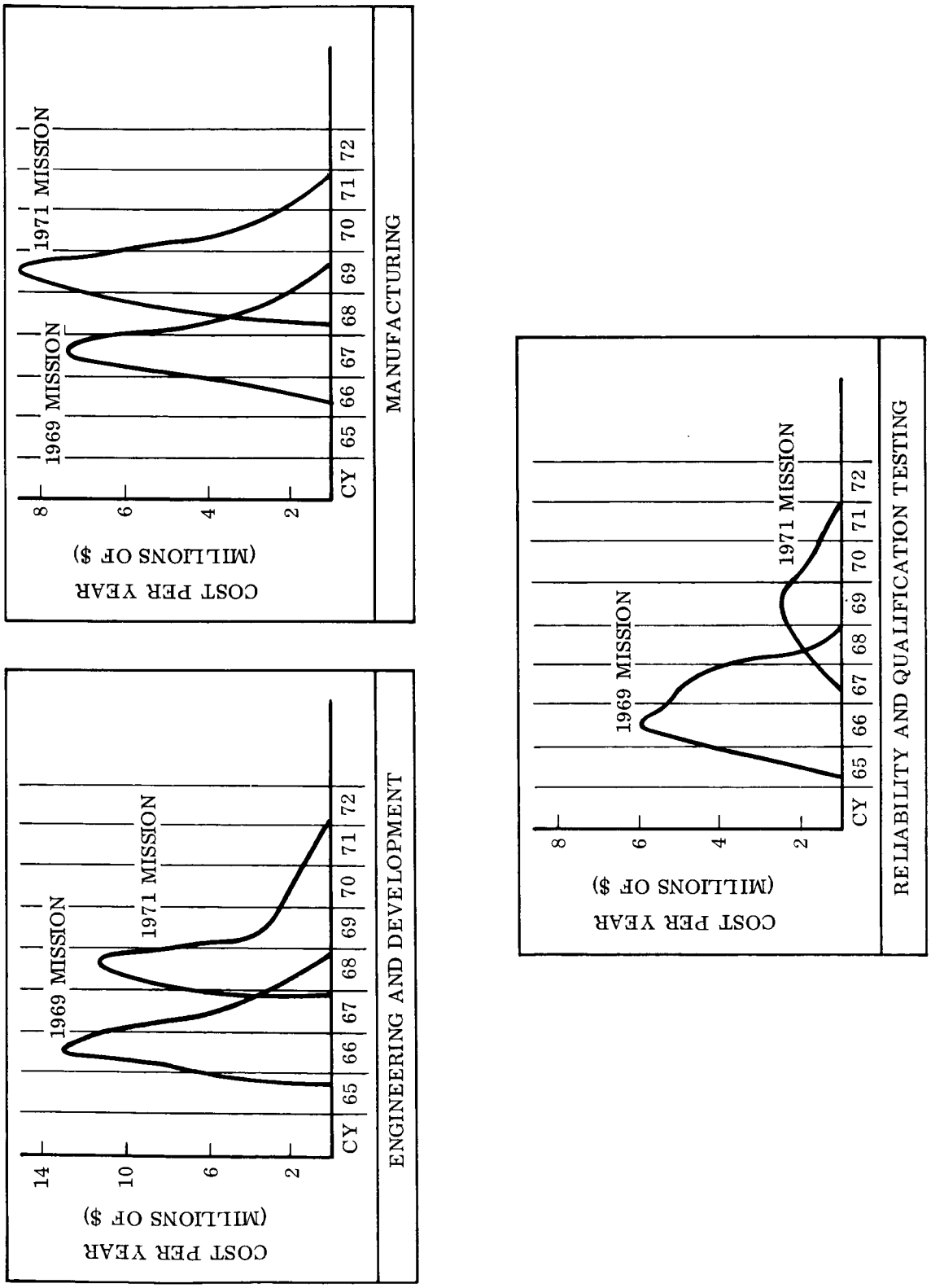


Fig. 7-2 Program Cost Distribution for Developing, Manufacturing, and Testing

456

Section 8
REFERENCES

1. Lockheed Missiles & Space Company, Proposal for Mariner Mars Orbiter 1969–1971, Volume I, LMSC A304797-1, 21 Feb 1964

2. Jet Propulsion Laboratory, JPL Inputs to Lockheed Study Contract 950877, T.M. 161-1, 27 Mar 1964

3. Lockheed Missiles & Space Company, Interim Report, Voyager Program Study, Period Ending 15 September 1963, LMSC 5-53-63-4, 4 Oct 1963

4. Jet Propulsion Laboratory, Design Parameters for Ballistic Interplanetary Trajectories, Part I, One-Way Transfer to Mars and Venus, by V. C. Clarke, Jr., et al., TR No. 32-77, Jan 1963

5. -----, Earth-Mars Trajectories, 1969 and 1971, TM No. 33-100, by V. C. Clarke, Jr., et al., 1964

6. Lockheed Missiles & Space Company, Trajectory Handbook (IBM printout data), prepared for NASA Marshall Space Flight Center Under Contract LMSC-895119

7. -----, 7090 Interplanetary Trajectory Program User's Manual, IDC-57-14-31, M. A. Krop, to R. L. Nelson, 18 Jul 1961

8. Jet Propulsion Laboratory, Oral Communication with R. V. Morris, Guidance and Control Analysis and Integration, Sec. 343, JPL

9. Lockheed Missiles & Space Company, Thermophysics Design Handbook, LMSC 8-55-63-3, Jul 1963

10. -----, Heat Flux Study, T. Newby, R. Eurich, and D. Ow, LMSC M-16-64-1, 15 Jul 1964

11. -----, Study of Heat Shield Requirements for Manned Mars Landing and Return Missions, Quarterly Progress Report – Contract NAS 2-1798, LMSC 804000, 17 Mar 1964

12. -----, Study of Heat Shield Requirements for Manned Mars Landing and Return Missions, to Monthly Progress Report – Contract NAS 2-1798, 16 Jun 1964

13. NASA, Ames Facility, Apollo Forebody Pressure and Heat Transfer Distributions in Helium at $M_\infty = 20$, by J. G Marvin, Thorval Tendeland, and Marvin Kussay, X-854, Nov 1963

14. -----, Pressure and Heat Transfer Distribution on the Afterbody of a Lifting Mercury-Type Capsule at Mach Number 15 in Helium, by Joseph G. Marvin, TM X-783, Apr 1963

15. H. Hoshizaki, "Heat Transfer in Planetary Atmospheres at Super-Satellite Speeds," ARS Journal, Vol. 32, No. 10, Oct 1962

16. M. VanDyke, "Second-Order Boundary-Layer Theory for Blunt Bodies in Hypersonic Flow," Proc. ARS International Hypersonic Conference at MIT, 16–18 Aug 1961

17. Lockheed Missiles & Space Company, Summary Analysis of X-17 RTV Program – Aerodynamic Heating and Boundary Layer Transition, by D. M. Tellep and H. Hoshizaki, 2161

18. L. F. Hearne, W. D. Coleman, and S. R. Foiles, "Flight Test Corroboration of an Analytical Model for the Thermophysical Behavior of Char-Forming Organic Polymers," Sixth BOWACA Symposium on Aeroballistics, Washington, D. C., 31 Oct – 1 Nov 1963

19. T. E. Shaw and J. D. Stewart, "Summary Analysis of G. E. – MSVD RVX-1 Thermodynamic Data, Flights 3 and 5," Trans. 4th Symposium on Ballistic Missile and Space Technology, Vol. II, Aug 1959

20. Ramo Wooldridge Corporation, A Summary of Several Techniques Used in the Analysis of High Enthalpy Level, High Cooling Ratio Turbulent Boundary Layers on Blunt Bodies of Revolution, by R. L. Phillips, GM-TM-194, Sep 1957

21. Paul A. Libby, "The Homogeneous Boundary Layer at an Axisymmetric Stagnation Point With Large Rates of Injection," JAS, Vol. 20, No. 1, Jan 1962

22. K. H. Wilson and H. Hoshizaki, "Inviscid, Non-Adiabatic Flow About Blunt Bodies," LMSC 6-90-64-1, Jan 1964; also AIAA Preprint 64-70, Jan 1963

23. Lockheed Missiles & Space Company, Beryllium Design Data, LMSD-48472, 29 Apr 1959

24. -----, Theory for the Thermophysical Performance of Charring Organic Heat Shield Composites, by K. M. Kratsch, L. F. Hearne, and H. R. McChesney, LMSC 803099, 18 Oct 1963

25. -----, Charring in Reinforced Plastics (CHIRP) – An IBM 7094 Digital Computer Program, by M. G. Meyer, (Internal Report), Nov 1963

26. E. I. DuPont DeNemours & Company, Properties of NOMEX High Temperature Resistant Nylon Fiber, Bulletin NP-33, Wilmington, Del., Oct 1963